CISBAT

PROCEEDINGS VOL. I

INTERNATIONAL CONFERENCE

FUTURE BUILDINGS & DISTRICTS

SUSTAINABILITY FROM NANO TO URBAN SCALE

9 - 11 SEPTEMBER 2015 EPFL

LAUSANNE - SWITZERLAND

LESO-PB
EPFL
ÉCOLE POLYTECHNIQUE FÉDÉRALE DE LAUSANNE

Schweizerische Eidgenossenschaft
Confédération suisse
Confederazione Svizzera
Confederaziun svizra
Swiss Federal Office of Energy SFOE

sccer | future energy efficient buildings & districts

Cambridge University

Massachusetts Institute of Technology

IBPSA CH

CISBAT 2015

FUTURE BUILDINGS & DISTRICTS SUSTAINABILITY FROM NANO TO URBAN SCALE

International Scientific Conference
9-11 September 2015, EPFL, Lausanne, Switzerland

PROCEEDINGS VOL. I

Schweizerische Eidgenossenschaft
Confédération suisse
Confederazione Svizzera
Confederaziun svizra

Swiss Federal Office of Energy SFOE

IBPSA-CH

Cambridge University

Massachusetts Institute of Technology

CISBAT 2015

International Scientific Conference
9-11 September 2015, EPFL, Lausanne, Switzerland

FUTURE BUILDINGS & DISTRICTS –
SUSTAINABILITY FROM NANO TO URBAN SCALE

ISBN Electronic version: 978-2-9701052-2-0
ISBN Print-version: Vol.I 978-2-9701052-0-6 Vol.II 978-2-9701052-1-3

Conference Host / Editor
Solar Energy and Building Physics Laboratory (LESO-PB)
Ecole Polytechnique Fédérale de Lausanne (EPFL)
Station 18, CH - 1015 Lausanne / Switzerland, leso@epfl.ch , http://leso.epfl.ch
Conference Chair: Prof. J.-L. Scartezzini
Conference Manager: Barbara Smith

Scientific partners
Cambridge University, United Kingdom
Massachusetts Institute of Technology, USA
Swiss Chapter of International Building Performance Simulation Association, Switzerland

Under the patronage of
Swiss Federal Office of Energy (SFOE)
Ecole Polytechnique Fédérale de Lausanne (EPFL)

Schweizerische Eidgenossenschaft
Confédération suisse
Confederazione Svizzera
Confederaziun svizra

Swiss Federal Office of Energy SFOE

Cambridge University

Massachusetts Institute of Technology

IBPSA-CH

sccer | future energy efficient buildings & districts

PREFACE

"Future Buildings and Districts – From Nano to Urban Scale" was the topic of the international scientific conference CISBAT 2015, which took place in the Swiss lakeside city of Lausanne from 9 to 11 September 2015.

Designed as a platform for interdisciplinary dialog and presentations of innovative research and development in the field of sustainability in the built environment, the conference covered a wide range of subjects from solar nanotechnologies to the simulation of buildings and urban districts.

CISBAT 2015 was the 13th edition of CISBAT, whose vocation is to present new perspectives offered by renewable energies in the built environment as well as the latest results of research and development in sustainable building technology, in a setting that encourages networking at the international level. The conference assembled building scientists, engineers, urban planners and building designers from all over the world in an effort to promote clean technologies for sustainable buildings and cities. Close to 170 scientific papers were presented during three intense days of conference.

CISBAT 2015 was organized in scientific partnership with the Massachusetts Institute of Technology (MIT) and Cambridge University. Furthermore, the organizing committee was proud to be able to count on an international team of renowned scientists to ensure the quality of presented papers. The conference also teamed up for the third time with the Swiss Chapter of the International Building Performance Simulation Association (IBPSA-CH) to strengthen the subject of “Building Simulation”, one of the conference's leading topics.

Finally we were proud to host an outreach event of the Swiss Competence Centre for Energy Research “Future Energy Efficient Buildings and Districts” (SCCER FEEB&D) as well as a Workshop on Grid-Supportive Buildings organised by Fraunhofer IBP and E.ON Energy Research Center, RWTH Aachen.

Organised under the auspices of the Swiss federal Office of Energy (SFOE) and the Federal Commission for Technology and Innovation (CTI), CISBAT 2015 connected researchers and projects and gave an exciting insight into current research and development in the field of sustainable buildings and cities. It is our greatest wish that the conference will have led to a better understanding of the issues at stake and to fruitful, creative collaboration between its participants.

Prof. Dr J.-L. Scartezzini

Chairman of CISBAT 2015
Head of Solar Energy and Building Physics Laboratory (LESO-PB), Swiss Federal Institute of Technology Lausanne (EPFL)

CONTENTS VOL. I

Author index see back of book

Nanostructured Materials for Renewable Energies

Sustainable Building Envelopes

Daylighting and Electric Lighting

Indoor Environment Quality

Model Predictive Control

Urban Ecology and Metabolism

CONTENTS VOL. II

Integration of Renewable Energy in the Built Environment

Building Simulation (IBPSA Special Session)

Urban Simulation

Information Technologies and Software

Nanostructured Materials for Renewable Energies

PLASMONIC COUPLING CONTROLLED ABSORPTION AND EMISSION IN LIQUID LUMINESCENT SOLAR CONCENTRATOR

S. Chandra[1]*, J. Doran[2], S. J. McCormack[1]

[1] *School of Engineering, Trinity College Dublin, The University of Dublin , Ireland*
[2] *School of Physics, Dublin Institute of Technology,*
Kevin Street , Dublin 08, Ireland
**Corresponding author email: schandra@tcd.ie, Phone: + 353 1 896 3321*

ABSTRACT

Quantum dot (QDs) absorption and emission were studied in the presence of gold nanorods (Au NRs) for liquid quantum dot luminescent solar concentrator (QLSC) of 40×25×2 mm. The plasmonic coupling between QDs and Au NRs in the LSCs was manipulated by spacing between QDs and Au NRs through concentration distribution and orientation & aligning the Au NRs through applying an external electric field. The electric field controlled plasmonic interaction increased absorption of QDs by 10-13 % and corresponding emission enhancement is 6-14 %. The response of change in QDs absorption and emission has been categorized in three regions. Unresponsive; for a field strength of 0 - 2.5×10^4 Vm^{-1}, active; in the range of 2.5×10^4 Vm^{-1} - 7.5×10^4 Vm^{-1}, and above 7.5×10^4 Vm^{-1} fall in saturation region. The results have shown significant enhancement in absorption, fluorescence emission for liquid QLSC.

Keywords: Quantum Dot, Plasmonic Coupling , LSC.

INTRODUCTION

Luminescent solar concentrator (LSCs) technology was proposed in the late 1970s [1, 3] as a means to concentrate solar radiation on a smaller area of solar cell to enhance their output. The main objective of this technology is to replace the large area of solar cells in a standard flat-plate PV panel by an inexpensive polymeric collector, thereby reducing the cost of the module and consequently solar power. A LSC system has advantages over other alternative concentrating systems: concentrates both direct and diffuse radiation, not subjected to a concentration ratio limitation [4, 5], and is static. An LSC plate consists of a transparent polymer sheet doped with a luminescent species (*organic dyes, quantum dots*), as illustrated in Figure 1a with a cross-sectional view in Figure 1b.

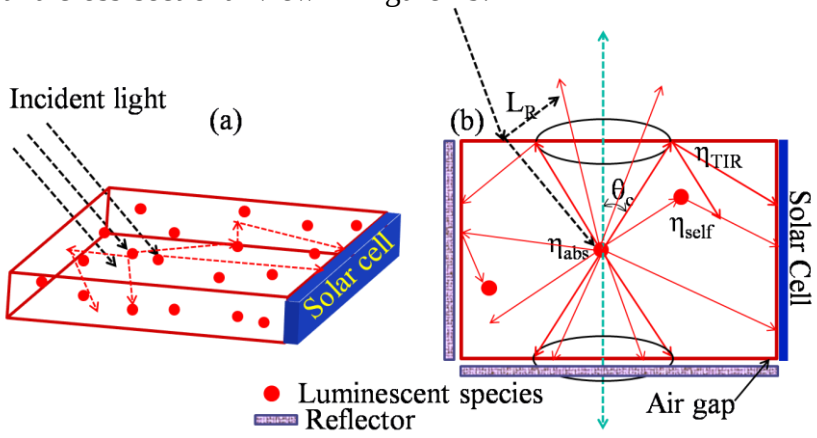

Figure 1: a) Schematic of LSC device without attached external reflectors, b) external reflectors attached LSCs cross- sectional view [6].

LSCs absorb incident solar radiation, and subsequently, re-emit light over all solid angles. The re-emitted light which falls within the critical angle is guided via total internal reflection (TIR) to the sheet edges where solar cells are attached. In a quantum dot solar concentrator (QDSC) [7] the organic dyes are replaced by QDs. QDs have some potential advantages over organic dyes such as wavelength tunability [8, 9]. The conversion efficiency of QDSCs developed to–date [10] has been limited by; re-absorption and scattering losses [11], overlap of the absorption and emission spectra, and escape cone losses. Some of these problems could be addressed by exploiting plasmonic interaction between QDs and metal nanoparticles (MNPs). The plasmonic interaction has potential to increase the excitation and emission rate of QDs, direct the emission, and consequently improve the efficiency of QDSCs.

PLASMONIC INTERACTION

MNPs (particularly gold and silver) possess unique optical properties of a localized surface plasmon resonance (LSPR) which is a collective oscillation of conduction band electrons, induced by excitation light. MNPs behave like a nanoscopic antenna [12] giving rise to strong enhancements of the local electromagnetic field intensity close to the NPs [13, 14]. When a fluorescent emitter (e.g. QDs, organic dye) is placed in the range of enhanced local electric field intensity, plasmonic interaction takes place which can enhance light absorption, the excitation rate, and radiative and non-radiative decay rates of the optical emitter. The emission can be controlled through the modification of the local electromagnetic boundary condition (or PMD) near the optical emitter. Plasmonic coupling depends on several parameters: spacing between optical emitter and MNPs; orientation of MNPs with respect to optical emitter; and overlap of surface plasmon resonance (SPR) frequency of MNPs and absorption and emission of optical emitter.

This work has examines: the control of the plasmonic interaction through orienting Au NRs with respect to QDs in ethanol media. The spacing was controlled by the concentration distribution of QDs and Au NRs in the composite. The plasmonic interaction was studied through measured absorption and fluorescence emission of QDs in QD/Au NR composites.

METHOD

Spheroid Au NRs synthesis: A two-step continuous process was used to synthesize an aqueous colloidal suspension of spheroid Au NRs of aspect ratio ~1.85. Firstly, the gold precursor (*gold (III) chloride trihydrate (*$HAuCl_4.3H_2O$) was reduced to seed-like particles in the presence of polyvinylpyrrolidone (PVP) by ascorbic acid (AA). In a continuous second step the following were added; silver nitrate ($AgNO_3$), AA, and sodium hydroxide (NaOH) which led to the growth of spheroid Au NRs and spherical NPs. The gold precursor concentration was fixed throughout synthesis process, and 1.35 weight ratio of AA to $AgNO_3$ formed the spheroid shape of Au NRs. PVP protected Au NRs were extracted from the parent solution by centrifuging 8000 rpm for 30 minutes at 10 ^oC, and re-dispersed in ethanol. Their extinction spectra is presented in Figure 2.

A red-shift of ~5 nm was observed in the longitudinal SPR band, which is due to the difference in refractive index of water and ethanol. Au NRs and their plasmonic coupling with QDs were studied in the ethanol media in liquid LSCs. The core-shell CdSe/ZnS QDs (QD 610) was supplied by Evident Technology, USA, and their absorption and emission peak wavelength 575 and 610 nm, respectively.

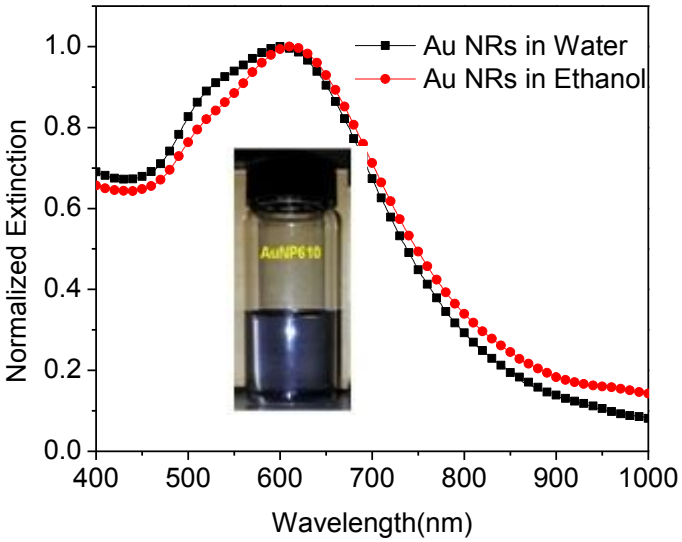

Figure 2: a) Normalized extinction spectra of Au NRs 610 in parent solution (water) and dispersed in ethanol and photograph of their solution in inset (the extinction spectra was measured by UV/Vis/NIR spectrometer)

LIQUID LSC and Au NRs ORIENTING SETUP

The electric field controlled orientation of Au NRs in the QDs/Au NRs was carried out in a custom made transparent conducting electrode mould cell of 40×25×2 mm, as shown in Figure 3a**,** which is similar to liquid LSCs. The electric field controlled Au NRs orientation setup is presented in Figure 3b was constructed to allow the measurement of the absorption and fluorescence emission simultaneously as a function of applied electric field. The composite of Au NR 610 and QD 610 were prepared suspending 0.04 wt% QD 610 and 1 and 3 ppm of Au NR 610 in ethanol . The fluorescence emission was measured at the edge of cell hence the arrangement is similar to the liquid solar concentrator.

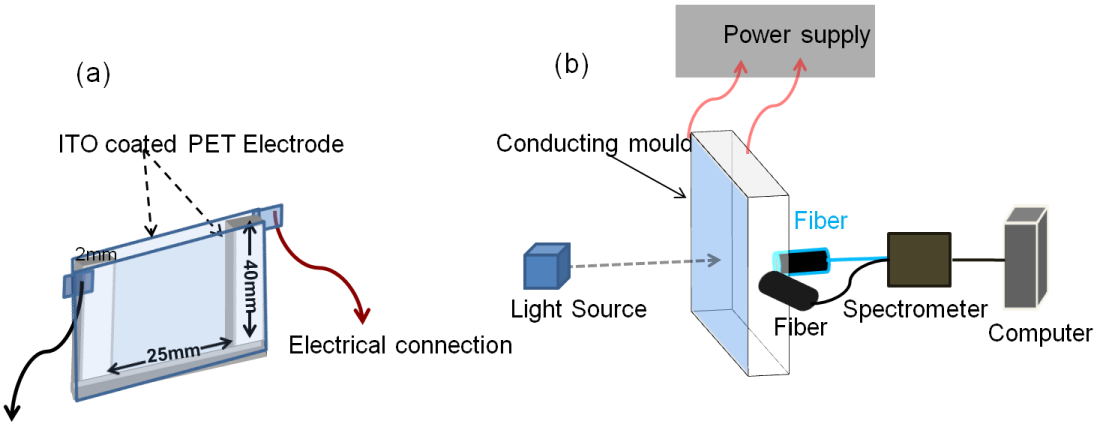

Figure 3: a) Custom made transparent conducting electrode mould cell of 40×25×2 mm cell, and b) block diagram of Au NRs orientation setup and AC electric field of 50 Hz was applied.

RESULTS

The absorption and edge emission of QDs was measured with an applied electric field. The absorption and emission of QDs alone showed less than ±0.5% variation in applied electric field, which can be considered constant. Therefore, change in absorption and emission upon adding Au NRs is solely attributed to plasmonic coupling. Absorption and fluorescence emission were measured simultaneously as a function of applied electric field strength. The absorption of the QDs in composites started responding to the electric field at ~2.5 $\times 10^4$ Vm^{-1} and nearly saturated at ~7.5 $\times 10^4$ Vm^{-1}, as shown in Figure 4a

The response can be divided in three regions of electric field strength (i) unresponsive region from 0 to 2.5$\times 10^4$ Vm^{-1} where the field strength is not enough to overcome Brownian motion of Au NRs in solution; (ii) active region from 2.5 to 7.5 $\times 10^4$ Vm^{-1} is the range where the electric field strength exerts enough rotation moment on Au NR to exceed thermal energy (k_BT) and resistive force of medium. It showed the response to the field which led them to be oriented and aligned [15]; (iii) saturation region from 7.5 $\times 10^4$ Vm^{-1}, illustrating that the orientation and alignment process is completed. The QDs enhanced fluorescence emission follows the absorption in Figure 4b. The enhanced emission contributed by increased absorption of QDs due to plasmonic coupling with Au NRs. The applied electric field controlled the orientation and alignment of Au NR in composites therefore manipulated plasmonic coupling and consequently the absorption and fluorescence emission of QDs in the composites.

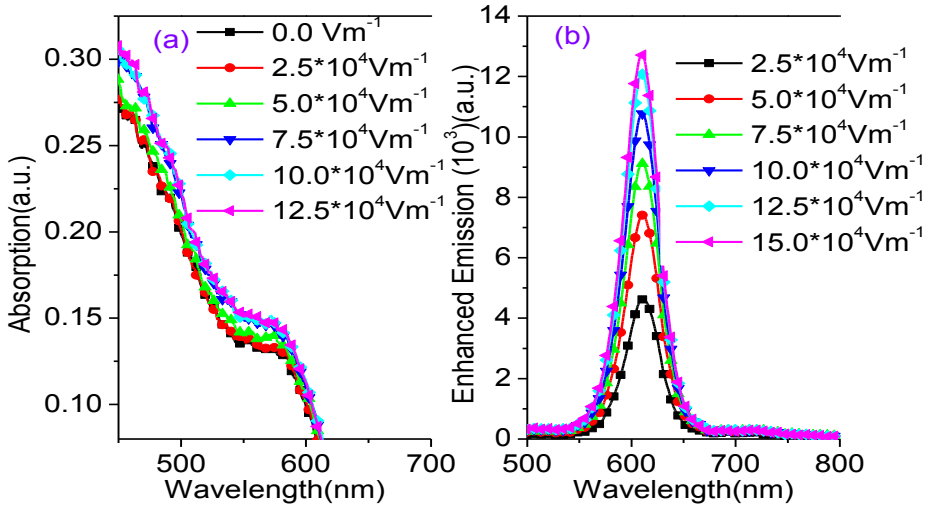

Figure 4: The composite 0.04 wt% QD 610 and 1 ppm of Au NR 610 in applied AC electric field, a) absorption of QDs in composite, b) QDs enhanced emission at edge of conducting cell for composite.

Au NRs concentration was increased from 1 ppm to 3 ppm to study plasmonic coupling dependency on both the spacing and orientation while the QDs were fixed. The increase in absorption is higher compared to 1 ppm of Au NRs in Figure 5a, however, the enhancement in emission is less which is possibly by non-radiative relaxation of excited QDs to Au NRs, due to decreased spacing between QD-Au NRs at higher concentration of Au NRs [16], which compensated the enhanced emission. The higher concentration of Au NRs leads to a background tail at longer wavelengths in the fluorescence emission as in Figure 5b.

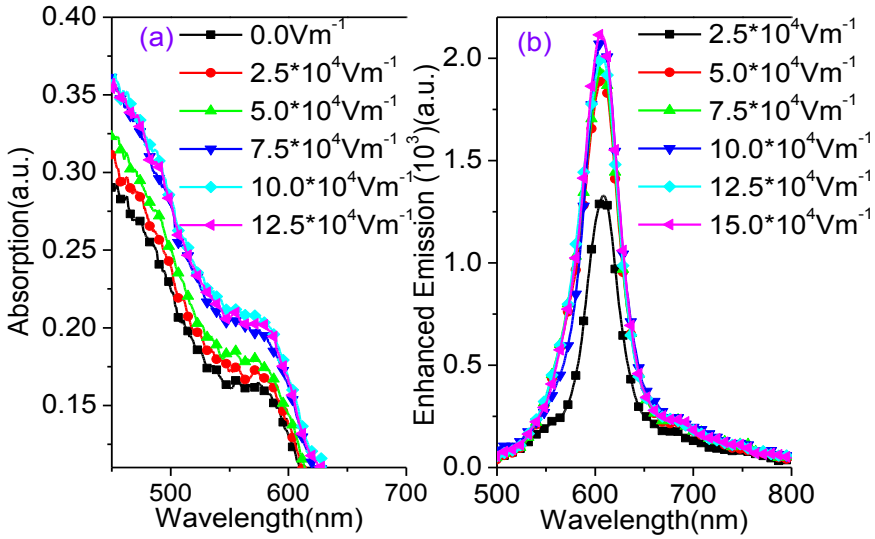

Figure 5: Composite of 0.04 wt% QD 610 and 3 ppm of Au NR 610 in an applied electric field, a) QDs absorption in composite, b) QDs enhanced fluorescence emission at the edge of conducting cell for composite.

The enhancement in absorption and fluorescence for the 1 ppm composite is ≈10% and ≈15%, respectively, presented in the Figure 6a. The 3 ppm composite, absorption and emission enhancement differed compared to 1 ppm composite in the Figure 6b, which may be explained by competition between enhanced emission and non-radiative relaxation of QDs. The enhancement in fluorescence emission can be attributed by two factors; (1) the increased absorption rate of QDs; (2) the possibility that the orientation of the Au NRs controlled the plasmonic interaction between Au NRs and QDs and re-directed the emission of QDs.

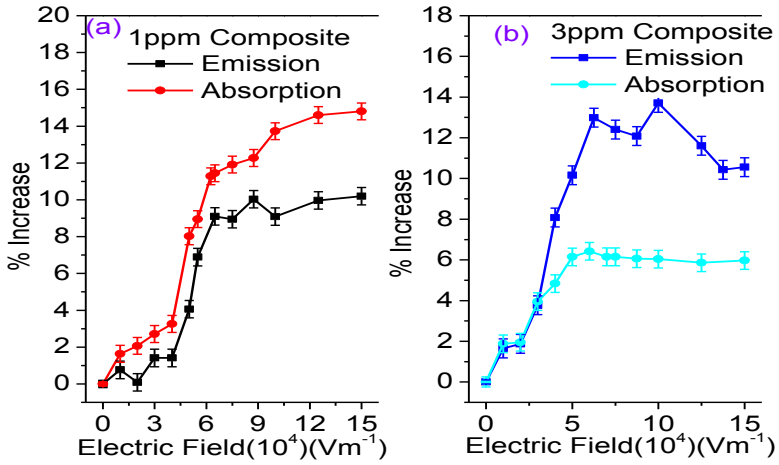

Figure 6: % changes in integrated absorption and emission of QDs in composite 0.04 wt% QD 610 and 1 and 3 ppm of Au NR 610 for the applied electric field.

CONCLUSIONS

The fabricated transparent conducting electrode mould cell was demonstrated as a liquid LSC of 40×25×2 mm. The absorption and emission of QDs alone remained unchanged in applied electric field hence a change in absorption and emission of QDs in the composite of QDs/ Au NRs is solely contributed by the plasmonic coupling between QDs and Au NRs. QDs

absorption and emission in the composite of Au NRs /QDs increased as function of applied electric field strength. The electric field response to orient and align the Au NRs in the composite of QDs/Au NRs is divided in the three region of unresponsive, active, and saturation. The increase in QD absorption in the applied electric field is 13 % for the composite of 3 ppm Au NRs, and 10 % for the 1 ppm composite. However, the corresponding QDs emission enhancement is 14 % greater for the 1 ppm Au NRs composite compared to 6 % for the 3 ppm composite .

REFERENCE

1. Weber WH, Lambe J. Luminescent greenhouse collector for solar radiation. Applied Optics, Vol. 15: pp 2299-2300, 1976.
2. Goetzberger A, Greubel W. Solar energy conversion with fluorescent collectors. Applied Physics, Vol.14, pp123-139, 1977.
3. Rapp CF, Boling NL. Luminescent Solar Concentrator. *Proceedings* of the 13th IEEE Photovoltaic Specialists Conference, pp 690-693, 1978.
4. Smestad GP, Ries R, Winston R, Yablonovitch E. The thermodynamic limits of light concentrators. *Solar Energy Materials*,Vol.21,pp99-111,1990.
5. Richards BS, Shavlav A, Crokish P. A low escape cone loss luminescent solar concentrator. Proceedings of 19th European Photovoltaic Solar Energy Conference, Paris, 2004, pp 113-116, 2004 .
6. Chandra, S. , McCormack, S.J., Kennedy, M., Doran, J.: Quantum dot solar concentrator: Optical transportation and doping concentration optimization. Solar Energy , 2015, Vol. 115, pp552-561, 2015.
7. Barnham, K. , Marques, J. L. , Hassard, J. ,O' Brien, P. : Quantum dot concentrator and thermodynamic model for the global red-shift, Applied Physics Letter, Vol. 76 ,pp 1197−1199, 2000.
8. Alivisatos, A. P. : Perspective on the physical chemistry of semiconductor nanocrystals, Physical Chemistry, Vol. 100 pp 13226−13239 , 1996.
9. Chen, H. Du, C. , Krishnan, R. , Krauss, T. D. , Harbold, J. M. , Wise, F. W. , Thomas, M. G. , Silcox , J. : Optical properties of colloidal PbSe nanocrystal, Nano Letter , Vol. 2, pp1321−1324, 2002.
10. Rowan, B. C. , Wilson, L. R. , Richards, B. S.: Advanced material concepts for luminescent solar concentrator, IEEE, Vol. 14, 1312−1322. 2008 .
11. Chatten, A. J. , Barnham, K. W .J. , Buxton, B. F. , Ekins-Daukes, N. J. , Malik, M. A.: New approach to modelling quantum dot concentrators, Solar Energy Mater and Solar Cells, Vol. 75, pp 363–371, 2003.
12. Schuck, P. J. , Fromm, D. P. , Sundaramurthy, A. , Kino, G. S. , Moerner, W. E.: Improving the mismatch between light and nanoscale objects with gold nanoantennas, Physical Review Letter Vol.94, pp 017402−017405, 2005.
13. Calander, N., Willander, M.: Theory of surface-plasmon resonance optical field enhancement at prolate spheroids, Applied Physics Vol. 92, pp 4878−4884, 2002.
14. Muhlschlegel, P. , Eisler, H. J. , Martin, O. J. F. , Hecht, B. , Pohl, D. W. : Resonant optical antennas, Science , Vol. 308 , pp 1607−1609, 2005 .
15. Zijlstra, P., van Stee, M., Verhart, N., Gu, Z., Orrit, M.: . Rotational diffusion and alignment of short gold nanorods in an external electric field. *Physical Chemistry*, Vol. 14,, 4584-4588, 2012.
16. Chandra, S. , McCormack, S.J., Kennedy, M., Doran, J., Chatten, A. J.: (2012). Enhanced Quantum Dot Emission for Luminescent Solar Concentrators using Plasmonic Interaction. Journal of Solar Energy Materials & Solar Cells,Vol. 98, pp 385-390, 2012 .

Cost-effective pilot-scale demonstration of ambient-dried silica aerogel production by a novel one-pot process

Lukas Huber, Shanyu Zhao, Matthias M. Koebel

Laboratory for Building Energy Materials and Components, EMPA, Überlandstrasse 129, CH-8600 Dübendorf, Switzerland

ABSTRACT

Over the past decade, aerogel based insulation products have established their place in various niche markets, such as thermal insulation for aerospace, apparel, petrochemical pipelines and pumping fluid media in industry applications. In the building industry, aerogel superinsulation enables superior insulation performance compared to conventional insulation materials. This allows putting in place a slimmer insulation layer (and thus space saving) or improving the insulation performance (U-value) of the building envelope. The widespread application of silica aerogels is currently hindered by their poor mechanical properties [1] and high materials cost. Aerogel insulation products have a tremendous growth potential in excess of 20 % by volume per annum [2]. For comparison conventional insulation products grow at an annual rate on the order of 5 %.

One of the cost limiting key challenges in aerogel production is the cumbersome multistep synthesis methodology. Today's aerogel production requires several solvent exchange steps which is not only very time and labor intensive but also costly. Supercritical drying from CO_2 is another major obstacle in the mass production of silica aerogels due to the fact that it is done in high pressure autoclaves. Not only does this process require an additional solvent exchange step into CO_2 but it is also accompanied by a significant energy cost.

Two years ago, a novel one-pot production process for silica aerogels was invented and patented at our laboratory which allows the production of silica aerogel granulate by ambient pressure drying within only 5 hours from start to finish. This simplified chemical synthesis consists of only three steps: gelation, modification and ambient pressure drying. Currently we are able to produce up to 70 liters at a time, following a first successful scale-up study. Our in-house aerogel has a thermal conductivity of 17.9 mW/(m K), which is identical to that of commercially available granulate (e.g. Cabot P300).

In summary, this new process gives access to a new generation of low-cost high-quality aerogel granulate and is expected to substitute today's conventional processes. A significant price reduction of silica aerogel materials is expected to reshuffle the insulation market. In the future we should look forward to seeing new aerogel insulation products and companies appear on the world markets.

Keywords: Aerogel, Thermal insulation, Sol-gel

INTRODUCTION

Silica aerogel was first produced in the early 1930's by Steven Kistler [3,4] from silica gels by replacing the pore fluid with a gas. Due to their extremely low density and outstanding physical properties, especially for thermal and acoustic insulation, they were commercialized a few years later by Mosanto Chemicals in the form of powder. However, the time-consuming and labor-intensive solvent-exchange steps led to a slowdown of their development for the following three decades. In the late 1960's Teichner [5] achieved a major technological breakthrough by the replacement of Kistler's sodium silicate precursors by alkoxysilanes. This eliminated the formation of inorganic salt byproducts from the gels and the need for a water-to-alcohol exchange step. In the late 1990's, Schwertfeger *et al.* [6] described the synthesis of "ambigel" type aerogels, by ambient pressure drying without any use of a supercritical drying equipment. Ambient pressure drying was applied with great success to the synthesis of silica aerogels from alkoxides, as well as from sodium silicate, and today can be viewed as the most promising manufacturing technique for silica aerogels [7].

Figure 1 compares the production flow path of silica aerogels from sodium silicate (which involves many solvent exchange steps) to that from alkoxide precursors using our novel one-pot process. The process starting from sodium silicate precursors requires 7 times more solvent than the volume of the final aerogel whereas our novel one-pot process necessitates only 1.1 times the volume of the final aerogel.

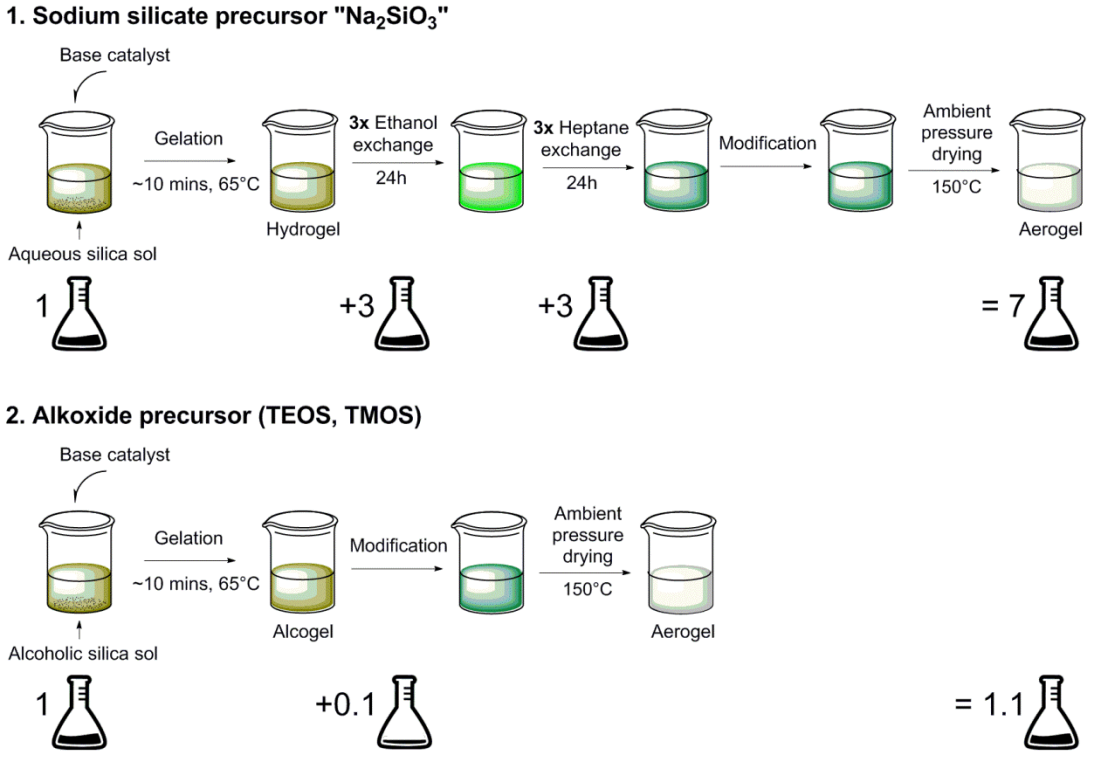

Figure 1: Schematic overview of the two main synthesis paths of silica aerogels from sodium silicate and silicon alkoxides using our novel one-pot process

METHOD

Preparation of the silica aerogel

Scale-up tests of the simplified one-pot production route [8] were carried out in a custom built pilot reactor. Prior to gelation, a silica sol mixture was prepared as follows: A silica sol (prepolymerized tetraethoxysilane, TEOS), water and ethanol were mixed in a drum. To this homogeneous solution, a hydrophobization agent (hexamethyldisiloxane, HMDSO) and 2 M Ammonia solution were added and the mixture homogenized again. This silica sol was poured into a 75 liter reactor (Figure 2) and slowly heated up to 65°C. The gelation onset was about 10 minutes from the point of ammonia addition. After gel aging, the syneresis liquid was removed before a dilute HCl solution was added to catalyze the hydrophobization. After this modification step at 65°C, the gel was removed from the reactor and dried for 3 hours at 150°C.

Figure 2: Reactor used for upscaling experiments

Characterization

The envelope density of the aerogels was measured with a GeoPyc 1360 form Micromeritics with 10 measurement cycles using a consolidation force of 4 N. The measured envelope density was used for the nitrogen sorption/desorption measurements which were carried out at 77 K on a gas sorption analyzer Micromeritics 3flex. Prior to the measurement, approximately 200 mg aerogel granulate was degassed at 250°C for 4.5 hours at a pressure of

1.3×10^{-2} mbar. The Brunauer-Emmet-Teller (BET) method [9] was used to calculate the specific surface area of the materials.

The thermal conductivity of aerogel granulate was determined (in packed bed configuration) using a guarded hot plate device according to the methods described in SN.EN 12667 and ISO 8302 in agreement with the Swiss SIA 279 standard “Thermal insulation material". Prior to the measurements, two frames (490 mm x 490 mm x 50 mm) were filled with approximately 1900 g of aerogel granulate. A square, flat heating element is sandwiched symmetrically between the two test objects, the outer surfaces of which are maintained at a constant temperature by cooling elements (Figure 3). This guarantees maintaining a stationary temperature difference. For highest possible measurement accuracy the hotplate is divided into a central measurement zone which is thermally isolated from the surrounding edge zone, with both zones being maintained at the same temperature. In the measurement zone, the electrical heating power under stationary conditions is measured and the heat flux with respect to the two surfaces is determined. The thermal resistance is given by the quotient of the measured temperature difference and the heat flux. The layout of the test setup is shown schematically in the drawing. The two filled frames with aerogel granulate lie horizontally sandwiched between the hotplate and the two cooling plates, and are surrounded by a thick layer of thermal insulation. Measurements are made automatically using an electronic control and data acquisition system. In order to maintain stable operating conditions deviations from set temperatures, the temperature difference between the core and edge zones, the temperatures within the heating and cooling plates and the input power are all regulated so as to lie within narrow limits. The instrument was calibrated with known standard materials prior to the test measurements.

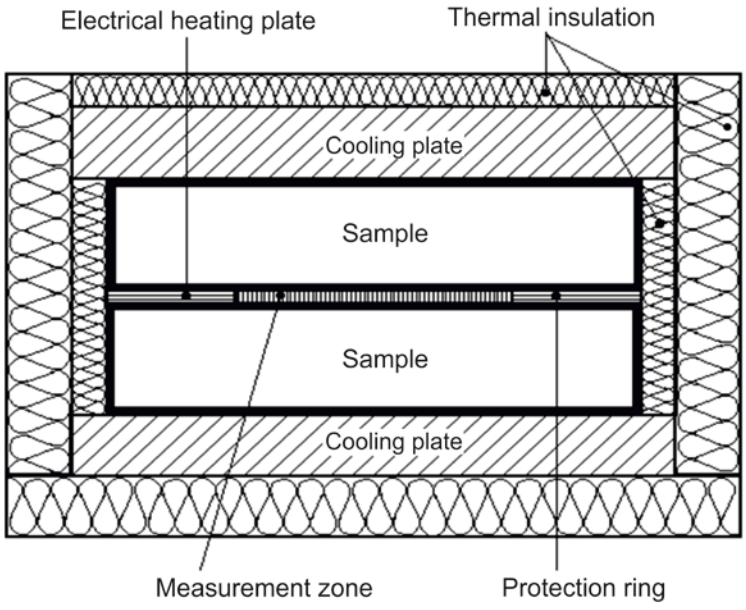

Figure 3: Measurement setup for the thermal conductivity

RESULTS AND DISCUSSION

Figure 4a shows a photograph of silica aerogel granulate produced in-house by the new one-pot method. The scanning electron micrograph of the one-pot aerogel granulate clearly reveals a colloidal particle network structure (Figure 4b). Table 1 summarizes the apparent density, thermal conductivity and BET surface area of commercial and one-pot silica aerogel granulate for comparison. The commercial silica aerogel granulate has a thermal conductivity of 17.9 mW/(m K) at an apparent density of 76 kg/m^3. The one-pot aerogel granulate which was not sieved after drying has a density of 83 kg/m^3 and a thermal conductivity of 17.4 mW/(m K). After sieving, the one-pot aerogel granulate (meshsize: 2 mm) the thermal conductivity increases to 18.7 mW/(m K), due to differences in particle size and packing density [10].

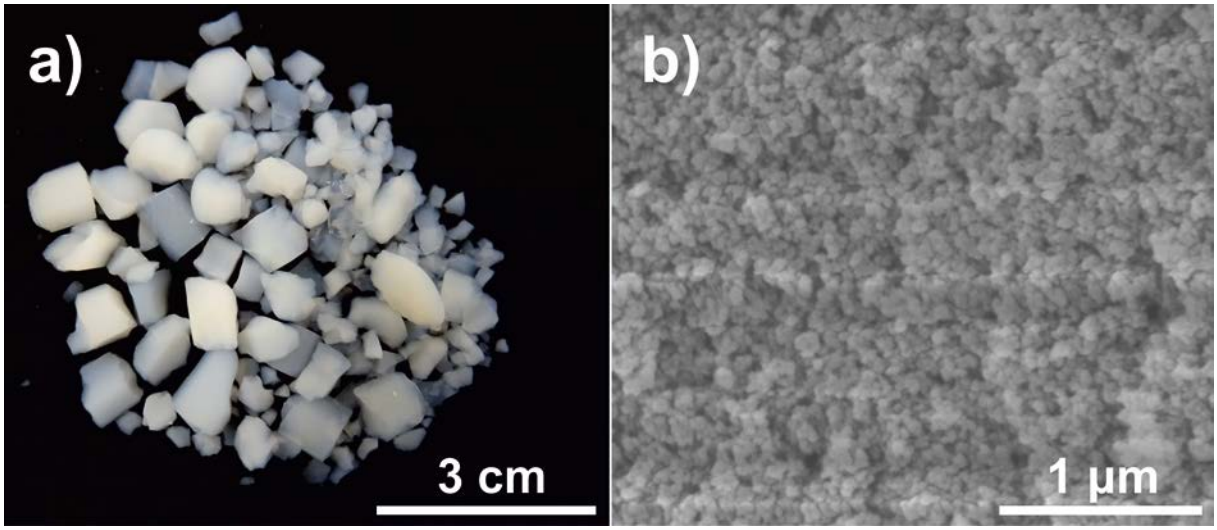

Figure 4: (a) Aerogel granulate after drying at 150°C for 3h and (b) scanning electron micrograph of silica aerogel granulate

Table 1: Apparent density, thermal conductivity and BET surface area of commercial and one-pot aerogel granulate

	Apparent density [kg/m^3]	λ_{10} [mW/(m K)]	S_{Bet} [m^2/g]
Commercial silica aerogel granulate (Cabot P300)	76	17.9	702
One-pot aerogel	83	17.4	-
One-pot aerogel (sieved)	78	18.7	797

CONCLUSIONS

We demonstrated the successful scale-up of silica aerogel granulate production by means of a novel synthesis route [8] to the 75 liter scale. The resulting, superinsulating, aerogel granulate has identical properties to commercially available materials. The novel one-pot process does not require any solvent exchanges and this enables fast production times, lower infrastructure investment cost (CAPEX) and lower operation cost (OPEX). This method is a promising technique for the inexpensive large-scale manufacture of silica aerogel granulates.

REFERENCES

1. Wong, J. C. H., Kaymak, H., Brunner, S. & Koebel, M. M. Mechanical properties of monolithic silica aerogels made from polyethoxydisiloxanes. *Microporous Mesoporous Mater.* **183**, 23–29 (2014).

2. Koebel, M., Rigacci, A. & Achard, P. Aerogel-based thermal superinsulation: an overview. *J. Sol-Gel Sci. Technol.* **63**, 315–339 (2012).

3. Kistler, S. S. Coherent Expanded-Aerogels. *J. Phys. Chem.* **36**, 52–64 (1931).

4. Kistler, S. S. Coherent Expanded Aerogels and Jellies. *Nature* **127**, (1931).

5. Nicolaon, G. A. & Teichner, S. J. Preparation of silica aerogels from methyl orthosilicate in alcoholic medium, and their properties. *Bull Soc Chim Fr 1906–1911* (1968).

6. Schwertfeger, F., Frank, D. & Schmidt, M. Hydrophobic waterglass based aerogels without solvent exchange or supercritical drying. *J. Non. Cryst. Solids* **225**, 24–29 (1998).

7. Aegerter, M. A., Prassas, M. & Koebel, M. M. *Advances in Sol-Gel Derived Materials and Technologies*. (Springer publishing, 2011).

8. Koebel, M., Zhao, S., Brunner, S. & Simmen, C. Process for the production of an aerogel material. (2015) WO2015014813A1

9. Brunauer, S., Emmett, P. H. & Teller, E. Gases in Multimolecular Layers. *J. Am. Chem. Soc.* **60**, 309–319 (1938).

10. Neugebauer, A. *et al.* Thermal conductivity and characterization of compacted, granular silica aerogel. *Energy Build.* **79**, 47–57 (2014).

LASER ABLATION AND NANOIMPRINT LITHOGRAPHY FOR THE FABRICATION OF EMBEDDED LIGHT REDIRECTING MICROMIRRORS

A. Kostro[1], M. A. Gonzalez Lazo[2], Y. Leterrier[2], E. Siringil[3], P. Hoffmann[3], A. M. Schüler[1]

1: LESO-PB, EPFL, Station 18, Bâtiment LE, EPFL, 1015 Lausanne, Switzerland

2: LTC, Station 12, Bâtiment MX, EPFL, 1015 Lausanne, Switzerland;

3: EMPA, Advanced material processing, Feuerwerkerstrasse 39, 3602 Thun, Switzerland;

ABSTRACT

Light redirecting devices usually increase the daylight illuminance level far from the window but also affect the visual comfort to some extent. Some designs achieve high redirection rate but are not transparent, others offer a partial view through but with reduced performance. Miniaturizing the light redirecting mirrors and encapsulating them has the potential to increase both view and performance. The shape of such encapsulated micro mirrors was optimised in a Monte Carlo ray-tracing model. In simulations, the redirected proportion of light could be increased with minimal influence on the transparency of the device. Maximal transparency was conserved at near to normal incidence with a strong redirection of light beams providing both daylight and glare protection.

In this study, the fabrication process of micro mirrors embedded in a transparent medium is described. The later process consists of a succession of four steps: mould fabrication, replication in an ultraviolet (UV) curable resin, partial coating with a reflective material at an imposed deposition angle and embedding using the same UV curable resin. The mould was fabricated by laser ablation at EMPA and replicated into polydimethylsiloxane (PDMS) to enable correct unmoulding of the resin. This negative mould was used to replicate the original structure into a transparent low-shrinkage hyperbranched acrylate polymer (HBP). It was identified that the direction in which the UV curable resin is polymerised is of crucial importance. Embedded micro mirrors provide transparency at normal incidence and the redirected proportion of light impinging at 60° was measured to be greater than 80%.

Keywords: Microstructures, daylighting, Nanoimprint lithography, laser ablation

INTRODUCTION

The combination of light redirection and elevation angle dependent transmittance offers the possibility to combine daylighting, glare protection and seasonal thermal control. Indeed, light redirection extends the depth where daylight is available; glare from the direct sunlight is simultaneously reduced. And with a low transmittance only for elevation angles corresponding to summer sun, the thermal gains are reduced in summer while they remain important in winter. Through Monte Carlo ray tracing, an advanced microstructure with such properties was proposed [1]. In addition the view through at near to normal incidence with such a design fabricated on a micrometric scale should be preserved. The design comprises an embedded parabolic mirror and a second mirror on the back surface of the device, located at the focus point of the first parabola. The parabola is designed to focus light incoming with an elevation angle equal to that of the summer sun and the back mirror reflects light from this direction. The high aspect ratio of the embedded mirrors enables the redirection of a major part of light incident at elevations angles between 35° and 90°. Challenges and results on the

fabrication of the embedded mirrors are presented in this paper. The various questions regarding the backside mirror will not be assessed.

To embed parabolic mirrors, a four step process is proposed. Firstly, the shape of the desired mirror needs to be fabricated in a hard material later referred to as the mother mould. The mould has to reproduce the desired geometry accurately and present smooth surfaces of optical quality. Secondly, the shape is replicated to a transparent polymer, for this purpose an intermediate PDMS mould later referred to as the mother mould is used. For replication an acrylated HBP is hardened by photo-polymerisation using a UV nanoimpront lithography process (UVNIL). Thirdly the resulting structure is placed in vacuum in a physical vapour deposition chamber and coated with aluminium. To coat only one side of the structure, the sample is tilted. Finally the resulting structure is encapsulated in the same transparent resin to obtain two parallel surfaces and provide transparency. This process is illustrated in Figure 1. The main challenges are in the fabrication of a proper mould and in the encapsulation step.

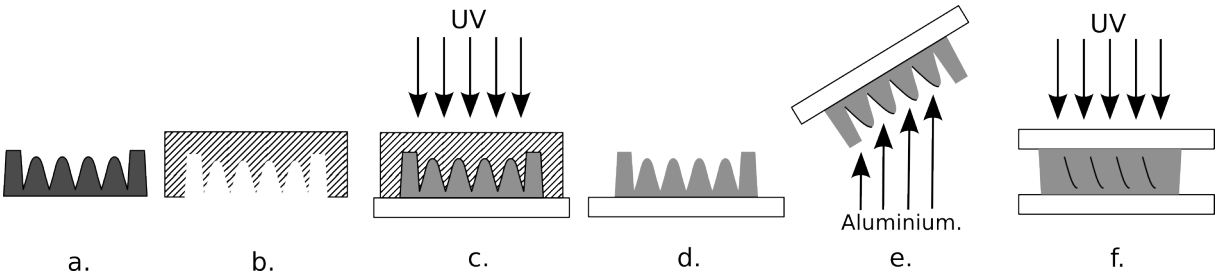

Figure 1: Fabrication process for embedded micromirrors: a-b. Father PDMS mould made from mother mould. c-d. Replication by UV nanoimprint lithography. e. Coating with aluminium at tilted angle of incidence, d. Embedding of micromirrors into the resin (UV polymerisation).

For the mould, the required dimensions (50-300 microns for period and respectively 112-700 microns depth) are well above the nano scale and at the lower limit of micro scale. Few techniques are suited to produce structures with high aspect ratios in this range. In addition, the produced surfaces need to be of optical quality. Several techniques were studied: mechanical tooling, electrical discharge machining (EDM), conventional lithography, grey scale lithography, interference lithography, 3D printing, stereo lithography and laser ablation. EDM was first used to fabricate a mould with a resolution below a micrometre but generated rough surfaces not suitable for optical devices. Laser ablation was retained as the alternative choice because the offered aspect ratio and surface quality comply with the requirements.

UVNIL is a well-established process for the replication of micron and sub-micron scale features into photopolymerizable resins. Different shapes, namely gratings or stellar like structures with dimensions between 30 *nm* and 100 *nm* have been successfully transferred on silicon wafers with good dimensional stability [2] and in HBP composites with high fidelity [6-9]. For window-like transparency it is important that the uncoated surface disappears completely when embedding the structured polymer. This implies that no interfaces remain and no void should be formed following the shrinkage of the resin.

METHOD

Laser ablated mould

Pulsed lasers are well established in industry where these are used as tools to machine materials. Lasers with femto- or picoseconds pulses or nanosecond pulses with deep UV radiation allow direct ablation of material with little heat-affected zones (HAZs). The use of

excimer lasers (at 193 *nm* or 248 *nm* for example) allows very high resolution especially in aromatic polymers. The laser is used to structure polymers directly; typical individual feature sizes are in the range of 2 to 200 microns. The first significant advantage is that the machined structures directly present optical quality. The second main advantage of this technique for application to glazing is the possibility to produce optical devices on large areas [3,4]. Well-engineered micro geometries can be machined over large areas up to 3 m^2.

PDMS mould

By reproducing the microstructure into an intermediate moulding material, a negative mould is created. This intermediate step makes it possible to choose a material well suited for moulding of the final material: such as a UV curable HBP introduced hereafter. PDMS (Dow Corning DC 184 in this work) is a silicone based organic polymer that is known to work well as a mould for most resins and has been widely used to replicate microstructures. An interesting feature of PDMS is its low, temperature dependent shrinkage. At about 55°*C* it is slightly above 0.5% and rises almost linearly to 3% at 140°*C* [5]. To fabricate the mother mould, a container for the PDMS in liquid state is required.

Resin replication

Numerous different types of UV-curable resins exist, amongst them two types were studied in this project: an epoxy resin with a cationic polymerisation mechanism and an acrylate with a free radical polymerisation mechanism. The epoxy was rapidly abandoned because of its yellow colouration and because high aspect ratios were harder to unmould. Amongst acrylate resins, HBP were found to be well suited for nano and micro-replication due to their low polymerisation shrinkage and low internal stress [6,7]. Acrylated HBPs were previously used to fabricate polymer micro- and nano-structures with high accuracy [8,9]. The HBP used in this study was a polyester acrylate oligomer (CN2302, Sartomer) with functionality of 16, a volumetric shrinkage 9% and a glass transition temperature in cured state equal to 165°*C* (by dynamic mechanical analysis). The photoinitiator was trimethylbenzoyl phosphine oxide (Esacure TPO, Lamberti) at a concentration of 6 *wt*%.

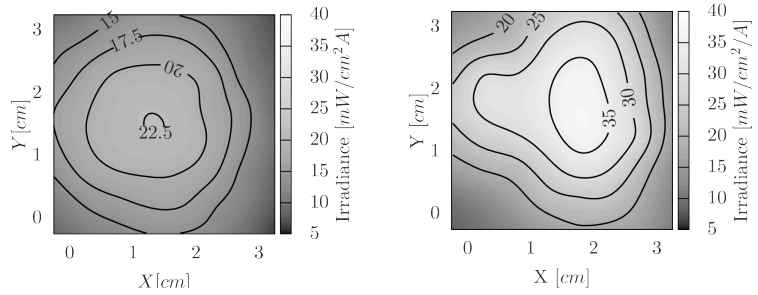

Figure 2: Distribution of UV radiation as generated by the LED UV source without (left hand side) and with diffuser.

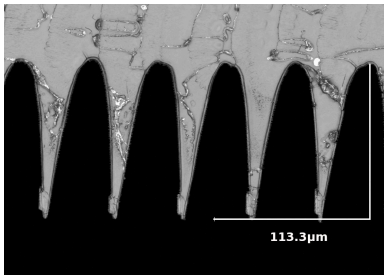

Figure 3: confocal microscopy image of mould profile.

A custom UV source was built using a timer, a controllable power source, three power UV light-emitting diodes (LEDs) with a peak centred at 375 *nm* and a cooling board from a computer graphical card. The LEDs are fabricated by Seoul Semiconductors (P8D2 275) and have an optical power output of approximately 250 *mW* each with a full width at half maximum (FWHM) of 11*nm*. The light from the LEDs was collimated using optical reflectors designed to provide a narrow, 6° wide cone of light. The resulting distribution of intensity was measured with a UV wattmeter in a plane at 12 *cm* distance, taking measurements every 0.5 *cm*. The intensity distribution for the area of interest is shown in Figure 2a. The distance

was increased to 15 *cm* and an etched glass produced by Fällander was added to increase the uniformity of the distribution as shown in Figure 2b.

RESULTS AND DISCUSSION

Mould obtained by laser ablation

First trials using the 248 *nm* excimer laser setup resulted in a sample of parabolic like structures engraved directly in polycarbonate (PC) with a period of 50 μm. The short pulse duration of about 20 *ns* limits the HAZ in polymers to some tens of nanometres. After a cleaning process the depth of the grooves is about 93 μm. A confocal microscopy image illustrates the profile of this sample (Figure 3), the structure is asymmetric and provides two different facets, one tilted at appropriately 4° and the other one at 12°. The produced samples with not optimized laser ablation parameters did not yet have the exact desired shape; to reach the desired geometry some ablation parameters in the mould fabrication have to be modified. This first structure was however used to produce promising light redirecting samples with embedded mirrors. The laser ablation was performed on an area of approximately 2 cm^2, this can be extended to larger areas on the same equipment. Direct laser writing combined with chemical etching of glass is a new technique that is being looked into for prototype fabrication. The latter technique is however limited to 10x10 *cm* samples.

PDMS mould

The structured PC sheet was placed at the bottom of a formwork and an alignment gauge was added to ensure the structures are perpendicular to the sample edge during replication. An extra gauge was added to the formwork in order to provide a constant and controlled thickness in the replicated structure. This reference also prevents contact (and hence deformation of the soft mould) between the mould peaks and the substrate during the UVNIL step. The formwork was fabricated out of aluminium using a milling cutter. The accuracy of the used cutter is in the order of 10 μm to 50 μm, making it possible to create gauge with dimensions of several tenth of a millimetre. 150 μm grooves were milled in the PC to provide a separation between the structures and the substrate. The gauge required to provide and control the gap during the embedding step could not be fabricated. Because of its limited thickness (0.5 *mm*), the structured PC part could not be maintained mechanically and was fixed with double sided tape in the bottom of a flat container.

Resin choice and limitations of the replication process

To achieve a satisfying optical performance, the used resin needed to be transparent and colourless. As already mentioned, the epoxide resin, which has a yellow tint, was eliminated for this reason. As illustrated in Figure 4, the acrylate HBP showed promising optical properties wit a spectrally flat transmittance of 80% in the visible range. However the attenuation of the UV radiation after half a millimetre of resin was found to be larger than 300 fold using a UV luxmeter. In such a range of thickness, the resin blocks UV light and polymerisation can no longer continue. Above this thickness, a haze can appear at some viewing angles when looking through the sample. Varying refractive indexes between polymerised and unpolymerised resin might cause the haze. It was found that by putting the PDMS stamp first in the path of a light beam, the flux of the source was not reduced significantly. This can be verified in the transmittance measurement shown in Figure 4 (90% transmittance). The polymerisation process however then starts on the structured side, which enables easier unmoulding and better finish of the replicated structure tips. Furthermore the interface between resin and glass polymerises last; it is likely that this reduces internal stresses that are responsible for delaminations in case the substrate is placed first. This

delamination of the structured resin from the substrate happens in particular if the UV dose is large and the polymerisation fast.

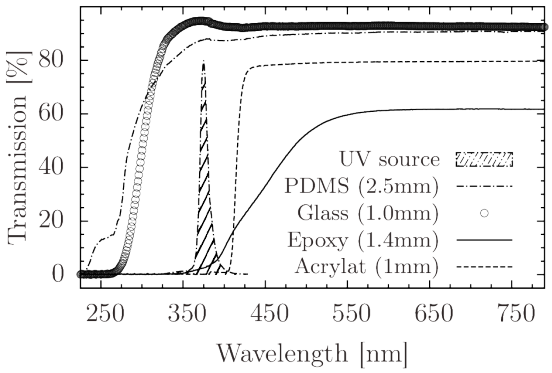

Figure 4: Spectral transmittance of PDMS, Glass, Epoxy resin and Acrylate Resin compared to the emission peak of the UV LED used for polymerisation.

Parameters of the embedding process

Regarding the embedding step, structures without coating were embedded first and two challenges were faced. Firstly, during embedding and probably due to resin shrinkage, voids appear at the very bottom of the structures. Secondly, even when no voids are present, the sample is not fully transparent but generates haze.

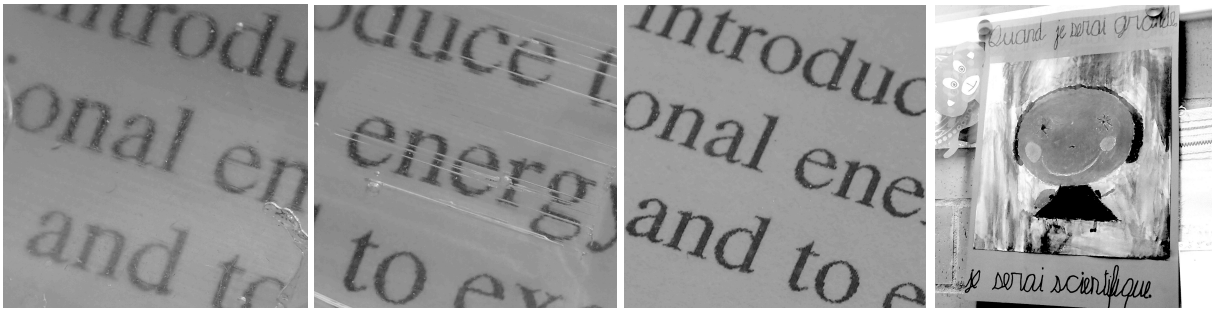

a) b) c) d)

Figure 5: . a-c) Assessment of transparency: un-coated microstructures should be invisible when embedded in a material with same refractive index. Results for various thicknesses and surface qualities: a) 880 µm, with rough surface, b) 540 µm, smooth surface. c) 180 µm, optical surface. d) View trough a sample with embedded mirrors.

The voids disappeared when slowing down the polymerisation. It is supposed that rapid polymerisation from one direction only favours curing on the side exposed to the UV source. Because the polymer shrinks during the curing process, lack of material and higher constraints are created on the opposite side towards the end of the curing process. It was also observed that bubbles could be formed overnight due to ageing processes in the resin during the first days. This also is possibly linked to the shrinkage of resin that was not fully polymerised.

The partial transparency can be explained if the interfaces do not disappear completely when a resin structure is filled with the same material. This creates certain diffusion and reduces overall transparency. A small index mismatch combined with the strong roughness of the interface enhances this effect. Reducing roughness should dramatically decrease this effect. Various other samples with no coating (3M prism, flat shape with rough surface) were also encapsulated in order to verify if the embedded surface becomes invisible. These experiments confirmed that the roughness of the embedded surface highly influences its invisible

integration. In particular, the significant roughness of a flat mould fabricated by EDM is still visible once embedded and creates a slight haze in transmission.

When embedding the smaller structures with surfaces of optical quality, as those produced by laser ablation at EMPA, both problems disappeared as illustrated in Figure 5. In this case the total resin thickness is only 180 μm; in comparison, the first samples had a total thickness of 880 μm. The polymerisation was carried out through the mould in the replication step and through the structured sample in the embedding step. When polymerising from the side where resin is added to embed the structure, bubbles appear. These findings confirm that during embedding it is advantageous to expose the side in contact with structures first and that total thickness and surface roughness are key parameters for a clean encapsulation. A sample coated with aluminium was also embedded and is shown in Figure 5.

CONCLUSION

A fabrication process was proposed for the encapsulation of micro mirrors. It has been tested and light redirecting samples with see-trough properties have been produced. The encapsulation problems have been solved and the thickness limitation was identified. At an incident elevation angle of 60°, the produced samples redirect 80% of light, most of it in a near to horizontal direction. At normal incidence, the samples remain highly transparent and the view through is not altered. This promising result opens up for new perspectives in the field of light redirecting devices. The up scaling of the process can possibly be realized in a roll-to-roll approach.

ACKNOWLEGMENTS

The authors would like to thank the Swiss federal office of energy (OFEN) and the Swiss competence centre for energy research (SCCER) for founding. The authors are grateful to Pierre Loesch for the mechanical tooling and to Eve Gasser for her drawings.

REFERENCES

1. Kostro, A. et al : Embedded microstructures for daylighting and seasonal thermal control, Optics and Photonics - Proceedings of SPIE, vol. 8485, 2012.
2. Vratzov, B. et al: Large scale ultraviolet-based nanoimprint lithography, Journal of Vacuum Science & Technology B: Microelectronics and Nanometer Structures, 21, 2003.
3. Boehlen, K.L. et al : Advanced laser micro-structuring of super-large-area optical films. Progress in Biomedical Optics and Imaging - Proceedings of SPIE, volume 5720, 2005.
4. Pedder, J. E. A et al : Pulsed Laser Ablation for Volume Micro-Optical Arrays on Large Area Substrates. Photonics West - Proceedings of SPIE, volume 6462, 2007.
5. Krogh, M. : My Little Guide to Soft Lithography, 2003.
6. Schmidt, L. E. et al: Time-intensity transformation and internal stress in UV-curable hyperbranched acrylates, Rheologica Acta, 46(5), pp 693–701, 2007.
7. Schmidt, L. E et al: Acrylated hyperbranched polymer photoresist for ultra-thick and low-stress high aspect ratio micropatterns. Micromechanics and Microengineering, 2008.
8. Geiser,V. et al: Nanoimprint Lithography with UV-Curable Hyperbranched Polymer Nanocomposites. Macromolecular Symposia, 296(1), pp 144–153, 2010.
9. González Lazo et al. : UV-nanoimprint lithography and large area roll-to-roll texturization with hyperbranched polymer nanocomposites for light-trapping applications. Solar Energy Materials and Solar Cells, 103, pp 147–156 , 2012.

POTENTIAL OF MAGNETRON SPUTTERED MAGNESIUM FLUORIDE CONTAINING THIN FILMS FOR THE MULTILAYER DESIGN OF COLOURED COATINGS FOR SOLAR COLLECTOR GLAZING

Stefan Mertin[1]; Paul Muralt[1]; Jean-Louis Scartezzini[2]

[1] *Ceramics Laboratory, EPFL - STI - IMX LC, Station 12, Bâtiment MXC, 1015 Lausanne, Switzerland*
[2] *Solar Energy and Building Physics Laboratory, EPFL - ENAC - IIC LESO-PB, Station 18, Bâtiment LE, 1015 Lausanne, Switzerland*

ABSTRACT

In this work, the potential of magnetron sputtered magnesium fluoride (MgF_2) and MgF_2 containing composite coatings for coloured solar collector glazing is investigated. Coloured thin-film interference coatings on the reverse side of the collector cover glass give solar collectors an aesthetic appearance, which facilitates their integration into the building's envelope. Hereby, integration means that the solar collector is no longer recognisable as technical device. Moreover, its appearance is the one of an architectural design element.

Four years ago we showed that it is possible to match the colours of solar glazing with those of commercial sun protection glasses by means of thin-film optical filters [1]. These filters are based on alternating high- and low-refractive index materials. Adding MgF_2 or Mg–F–Si–O as a second low-refractive-index material enables even more flexibility and freedom to design coatings with a specific reflection colour, especially for bright colours.

A novel concept of coloured filters involving MgF_2 has been developed. They exhibit – independent of their colour hue – a uniform high solar transmittance 85–85.7% combined with a bright reflection. First results are very promising and confirm the future potential of MgF_2 containing multilayers for coloured solar collectors.

Keywords: coloured solar collectors, colour matching, magnesium fluoride, solar transmittance, magnetron sputtering

INTRODUCTION

Solar thermal collectors are well established worldwide as a technology converting solar radiation into heat. Most of them are used for domestic hot water (DHW), or to heat swimming pools. The majority is installed on the rooftop and one rarely finds façade-mounted collectors [2]. Nevertheless, in European latitudes, mounting them on façades could be advantageous, because the energy output is almost constant from spring to autumn for south facing vertical solar collectors [2, 3]. Such a steady energy supply makes the sizing of solar heating systems and their integration as heat producers into building services easier [4]. The negative appearance of the usually black or dark blueish absorber, including welding traces, tubing and corrugated metal sheets, however, makes it rather difficult to integrate them from an aesthetic point of view into the building's façade [5, 6]. Matching the exposed part of solar thermal collectors with a façade colour or design element would grant architects complete freedom for their building integration [3]. An even more important aspect is that an aesthetically satisfying integration might even have a greater impact on the solar market consumers than price or performance improvements [2].

The colour matching of solar collector glazing with commercial windows was shown four years ago at CISBAT 2011 [1]. The energy performance of these coatings as well as the colour values were recently published [7]. Furthermore, new prototypes based on these designs were produced by an industrial partner. The coloured coatings are based on optical interference filters consisting of alternating high- and low-refractive-index thin films. The principle as well as several coating designs are described in various publications [7, 8, 9, 10].

In this work, the authors present a novel concept for coloured solar thermal collector glazing. The multilayer design is a modified narrowband filter based on alternating titanium dioxide (TiO_2) and silicon dioxide (SiO_2) layers, supplemented with a magnesium fluoride (MgF_2, $n = 1.38$) inter-layer. This novel 3-material 4-layer design opens the possibility to achieve an almost colour-invariant solar transmittance. This would facilitate the planning and configuration of solar DHW and/or space heating plants with coloured collectors, since the aesthetics of the collectors as well as their energy performance are no longer interrelated. Furthermore, this could also simplify the certification procedure of coloured collectors, as the coating performance remains identical for different colour hues.

METHOD

In general, the optical properties of thin-film filters can be computed by numerical simulations using the method of the complex matrix multiplication, where a characteristic matrix represents each layer. A detailed description of the method can be found e. g. in Macleod [11]. The assembly of a multilayer stack on a substrate can be described as

$$\begin{bmatrix} B \\ C \end{bmatrix} = \prod_{r=1}^{q} M_r \cdot \begin{bmatrix} 1 \\ \eta_{\mathrm{sub}}(\lambda) \end{bmatrix} \tag{1}$$

where Equation (1) is called matrix of the assembly. The optical admittance of the parallel components of the incident electromagnetic wave at the outermost surface is given by $Y(\lambda) = H(\lambda)/E(\lambda) = C/B$. M_r is the characteristic matrix of each layer, $\eta_{\mathrm{sub}}(\lambda)$ the optical admittance of the substrate and q the number of layers in the stack. Negligible absorptance is assumed, which is consistent with the quasi-nil-absorptance requirement and with the used dielectric coating materials. The reflectance is then given by

$$R(\lambda) = \left(\frac{\eta_0(\lambda) - Y(\lambda)}{\eta_0(\lambda) + Y(\lambda)} \right)^2 \tag{2}$$

and the transmittance by

$$T(\lambda) = \frac{4 \cdot \eta_0(\lambda) Y(\lambda)}{(\eta_0(\lambda) + Y(\lambda))^2} \tag{3}$$

where $\eta_0(\lambda) = 1$ for the incident medium air. For non-absorbing media the energy conservation equation is simply:

$$1 = R + T \tag{4}$$

Equation (4) is very general, and valid for spectral values as well as for integrated quantities, such as solar transmittance T_{sol} or visible reflectance R_{vis}. T_{sol} is defined as the ratio between incident and transmitted solar radiation, whereas R_{vis} is defined as the ratio between incident and reflected daylight (CIE D_{65}) weighted by the photopic luminous efficiency function $V(\lambda)$

of the human eye [12]. In order to be able to improve the energy performance of the coloured filters, all relevant quantities, such as T_{sol}, R_{vis}, colour coordinates, etc., need to be accounted for in the numerical simulations. A new thin-film simulation tool for optical solar coatings was written on the basis of Wolfram Mathematica^{TM} since commercial software packages did not fulfil the requirement of simulating T_{sol} and R_{vis} in combination with the spectral values.

By the nature of the architectural application of coloured solar collectors, the achievement of a precise coloured reflection is extremely important, especially when matching the coloured reflection to commercial products [7]. The spectral curves of the thin-film interference filters depend on both, the optical constants n and k of the coating materials, as well as the thickness of each layer. In practice, however, n and k are usually pre-defined by the established deposition processes [13, 14]. Therefore, it is the thickness of the layers, which is tuned to adjust the spectral properties of the filters following the so-called coating development cycle shown in Figure 1. First, the thickness of the layers is determined by optical measurements, such as spectrophotometry and spectroscopic ellipsometry, then the deposition parameters are adapted to refine all layer thicknesses before the coating is re-deposited. This procedure needs to be iteratively repeated, until the required coloured reflection combined with a sufficiently high T_{sol} value is achieved. Consequently, a coating design consisting of only a small number of layers to be tuned and adjusted during the iterative development cycle is an important key factor to develop and produces new colour hues.

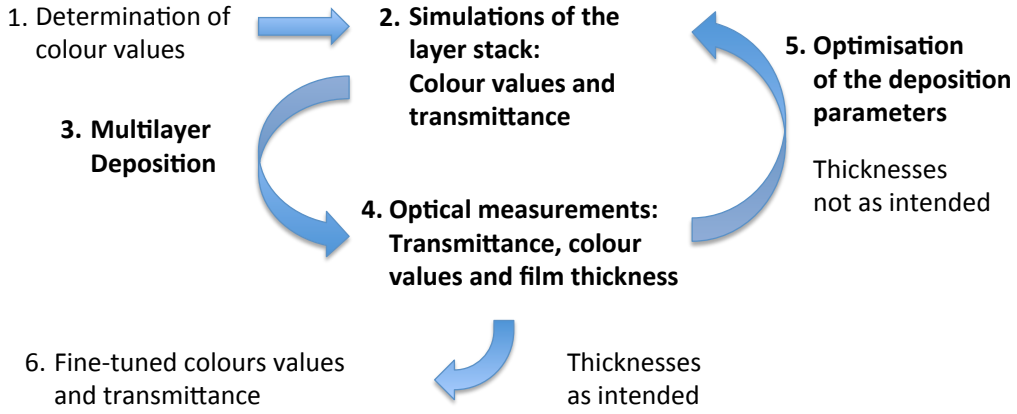

Figure 1: Coating development cycle for coloured solar collector coatings. Steps 2–5 need to be repeated until the required coloured reflection and solar transmittance are reached.

RESULTS AND DISCUSSION

Starting from a 3-layer coating design of alternating TiO_2 and SiO_2 layers, published in Ref. [7], a novel concept with a 4-layer 3-material multilayered system was developed. To tune the hue of the coloured reflection, a supplementary layer is added between the SiO_2 and the innermost TiO_2 layer with a refractive index lower than the one of the SiO_2 (see Figure 2a). Due to their very-low refractive indices and zero absorption in the solar spectral range, MgF_2 thin films and MgF_2 containing composite films are proposed for this additional layer. In the former coloured 3-layer coating design (glass$\|\frac{H}{x}LL\frac{H}{y}\|$air) all layers are modified related to the reference wavelength λ_{ref} to tune the reflection colour. The acronyms H and L represent the corresponding optical quarter-wave thickness of the high-index (TiO_2) and low-index (SiO_2) material, respectively, with x and y being any number larger than 1. In the novel 4-layer coating design, only the MgF_2 layer thickness must be modified to achieve a similar variation of the colour hue.

Increasing the layer thickness shifts the reflection peak towards longer wavelengths, while its intensity slightly decreases (see Figure 2b). The introduced MgF_2 layer is therefore also referred as colour-tuning layer and the corresponding multilayer design as colour-tuning-layer (CTL) design.

To be able to realise such novel coloured filters on solar glazing, suitable sputtering processes for MgF_2 coatings needed to be found, since magnetron sputtering is the dominant technology for large-area glass coating [15]. In the framework of a doctoral thesis [16], such novel deposition processes were developed: nanocrystalline MgF_2 films deposited by reactive magnetron sputtering and nano-composite Mg–F–Si–O films deposited by co-sputtering. The films exhibit excellent optical properties: e. g. a low refractive index ($n = 1.382$ [16, 17] and $n = 1.423$ [16], respectively, at 550 nm) and a negligible absorption.

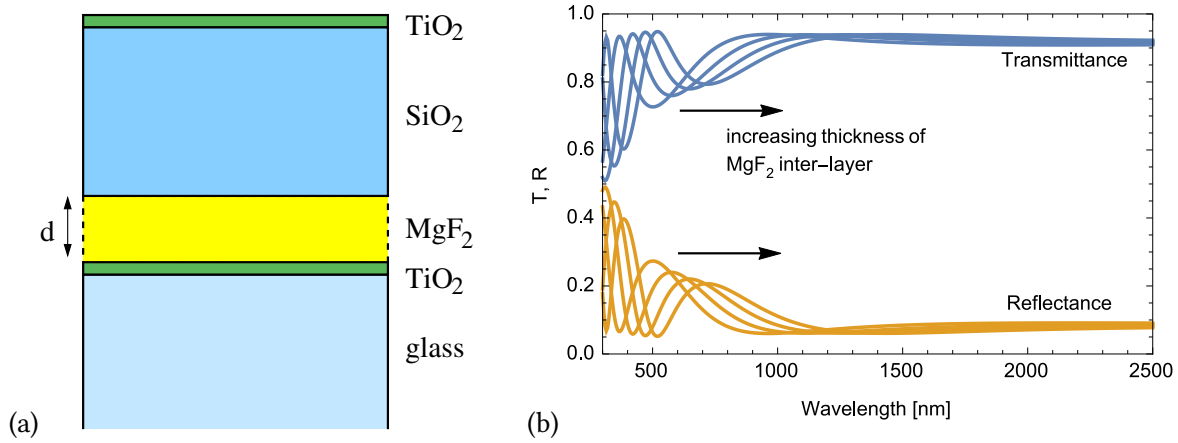

Figure 2: (a) Coloured CTL filter design with MgF_2 inter-layer. It can be written as $glass||\frac{H}{2.8}(MgF_2)LL\frac{H}{2.8}||air$. (b) Simulated transmittance and reflectance spectra of the coloured filter at $\lambda_{ref} = 400\,nm$. By increasing the layer thickness of the MgF_2 layer (28.8, 57.6, 86.3, and 115.1 nm), the reflectance peak shifts to longer wavelength, while its amplitude slightly decreases.

In Figure 3 the simulated T_{sol} and R_{vis} values are plotted for the novel CTL design in comparison with a standard 3-layer design. For TiO_2 and SiO_2, the optical data of sputtered films from Ref. [7] were used and for MgF_2 from Ref. [17]. Both designs exhibit a solar transmittance higher than 85% for blue to yellow colours, which remains within the T_{sol} acceptance limit of a few percent in comparison to the uncoated substrate ($T_{sol} = 91.8\%$) [8, 10]. For the standard design – while increasing λ_{ref} – T_{sol} decreases from 88% at blue-greenish to 83% at deep red coloured reflections.

One advantage of coloured coatings based on the proposed novel design is that for different hues, only the thickness of a single layer has to be re-adjusted during the development cycle, making on-demand colour tuning easier. A second feature of the design stands out among others: the quasi-constant value of T_{sol} remaining in the range 85–85.7% for all colours. According to the best knowledge of the authors, there is no other way to colour solar thermal collectors in combination with an invariant energy performance. In other words, with this novel design a whole palette of different coloured cover glasses could be provided, exposing the solar thermal absorbers behind to a quasi-identical solar radiation. Moreover, since same materials are involved in the coating and T_{sol} remains within the typical accuracy limit of spectrophotometry measurements (< 1%), with the proposed CTL design, a re-certification of the collector glazing for every new colour hue might become unnecessary.

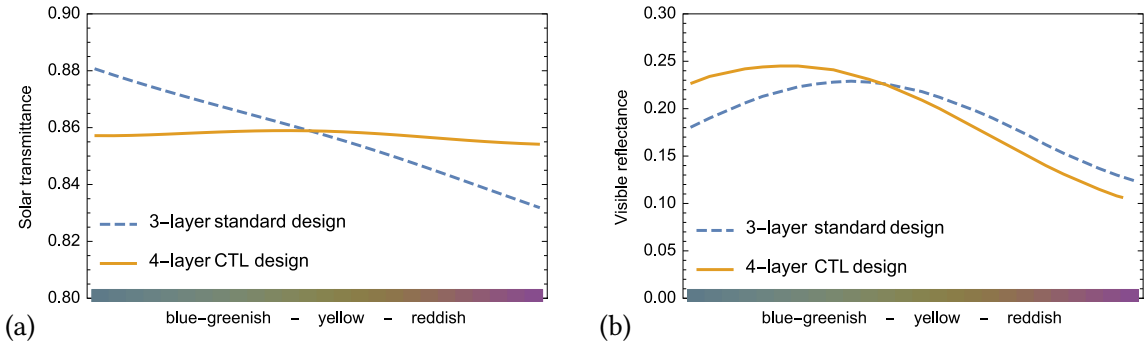

Figure 3: Simulated solar transmittance and visible reflectance of the standard and the CTL design. The reflection colour of both design types follow the same trajectory in the a^*b^*-plane, which is indicated on the x-axis in form of calculated colours in the CIELAB system.

When comparing the coloured reflections R_{vis}, both designs show similar colour brightness in the yellowish colour range. Between blue and green the R_{vis} function flattens for the CTL design and its brightness is a little higher; this is reversed for the orange and reddish hues. Since building façades shine often in bright greenish and blueish colours, which fits to the colours of sky and flora, the lack of visible reflection intensity for orange-reddish hues might be even advantageous. While saturated orange colour shades are of interest for roof installations, soft orange tones, such as terracotta might be it for façades.

CONCLUSION AND OUTLOOK

A novel approach for advanced coloured solar coatings was investigated by means of numerical thin-film simulations. The proposed 4-layer design is a derivative of the before discussed coloured filter by adding a supplementary inter-layer with a very-low refractive index such as MgF_2. It has the advantage that only the thickness of a single layer needs to be adjusted during the coating deposition in order to tune the coloured reflection, whereas when using the standard 3-layer design all three layers must be adjusted. Therefore, not only the coating-designing phase, but also the prototype-production phase on a vacuum coater could be shortened. The proposed novel approach is a step forward to on-demand production of coloured coatings for solar collectors. Moreover, this design has in addition the outstanding property of a reflection-colour-invariant solar transmittance of 85–85.7%. Aesthetics and functionality of solar thermal collectors can be accordingly separated, making the certification of the collector glazing easier and granting architects and solar system engineers with a full freedom in their colour choice for the solar thermal collectors, independently of the required energy performance or sizing of the building services.

ACKNOWLEDGEMENTS

The authors would like to thank Paul Gantenbein and Iris Mack for inspiring discussions as well as SwissINSO SA and the EPFL ENAC School for financial support.

REFERENCES

1. Mertin, S., Hody-Le Caër, V., Joly, M., Scartezzini, J.-L., and Schüler, A.: Coloured Coatings for Glazing of Active Solar Thermal Façades by Reactive Magnetron Sputtering. In *CISBAT*

2011, pages 31–36, 2011.

2. Weiss, W., editor: *Solar heating systems for houses: a design handbook for solar combisystems.* James & James (Science Publisher) Ltd, London, 2003.
3. Munari Probst, M. C. and Roecker, C.: *Architectural Integration and Design of Solar Thermal Systems.* EPFL Press, Lausanne, 2011.
4. Duffie, J. A. and Beckmann, W. A., editors: *Solar Engineering of Thermal Processes.* John Wiley & Sons, Hoboken, 4th edition, 2013.
5. Hestnes, A. G.: Building Integration of Solar Energy Systems. *Sol. Energy*, 67(4-6):181–187, 1999.
6. Krippner, R. and Herzog, T.: Architectural Aspects of Solar Techniques. Studies on the Integration of Solar Energy Systems into the Building Skin. In *Eurosun 2000. Visions New Millenn. 3th ISES-Europe Sol. Congr.*, Copenhagen, 2000. International Solar Energy Society.
7. Mertin, S., Hody-Le Caër, V., Joly, M., Mack, I., Oelhafen, P., Scartezzini, J. L., and Schüler, A.: Reactively sputtered coatings on architectural glazing for coloured active solar thermal façades. *Energy Build.*, 68(PART C):764–770, 2014.
8. Schüler, A., Roecker, C., Boudaden, J., Oelhafen, P., and Scartezzini, J.-L.: Potential of quarterwave interference stacks for colored thermal solar collectors. *Sol. Energy*, 79(2):122–130, Aug. 2005.
9. Schüler, A., Boudaden, J., Oelhafen, P., de Chambrier, E., Roecker, C., and Scartezzini, J.-L.: Thin film multilayer design types for colored glazed thermal solar collectors. *Sol. Energy Mater. Sol. Cells*, 89(2-3):219–231, Nov. 2005.
10. Roecker, C., Munari Probst, M. C., de Chambrier, E., Schüler, A., and Scartezzini, J.-L.: Façade Integration of Solar Thermal Collectors: A Breakthrough. In *Proc. ISES World Congr. 2007 (Vol. I – Vol. V)*, pages 337–341, 2009.
11. Macleod, H. A.: *Thin-Film Optical Filters.* Institute of Physics Publishing, Bristol and Philadelphia, London, 3. edition, 2001.
12. Glass in building - Determination of luminous and solar characteristics of glazing; German version of DIN EN 410:1998-12, 1998.
13. Bräuer, G.: Large area glass coating. *Surf. Coatings Technol.*, 112:358–365, 1999.
14. Szczyrbowski, J., Bräuer, G., Teschner, G., and Zmelty, A.: Large-scale antireflective coatings on glass produced by reactive magnetron sputtering. *Surf. Coatings Technol.*, 98:1460–1466, 1998.
15. Kaiser, N. and Pulker, H., editors: *Optical Interference Coatings.* Springer, Berlin, 2003.
16. Mertin, S. *Reactively Sputtered Nano-Structured Multilayer Coatings on Architectural Glazing for Active Solar Energy Façades.* PhD thesis, EPFL, 2015.
17. Mertin, S., Marot, L., Sandu, C. S., Steiner, R., Scartezzini, J.-L., and Muralt, P.: Nanocrystalline Low-Refractive Magnesium Fluoride Films Deposited by Reactive Magnetron Sputtering: Optical and Structural Properties. *Adv. Eng. Mater.*, (in press, DOI:10.1002/adem.201500129), 2015.

LOW COST SILICA AEROGEL PRODUCTION

Ana Stojanovic and Matthias Koebel

Empa, Building Energy Materials, Überlandstrasse 129, 8600 Dübendorf, Switzerland

ABSTRACT

Buildings form a major part of the energy demand in Switzerland. Silica aerogels as high performance insulation materials have the potential to reduce the energy demand for heating and cooling. Silica aerogel insulation materials, can achieve the same thermal insulation performance with only half of the thickness of conventional insulation materials. Translucent, superinsulating silica aerogels exhibit the lowest thermal conductivity of any solid known, typically of the order of 0.015 $W \cdot m^{-1} \cdot K^{-1}$ at ambient temperature, pressure, and relative humidity. The interest in silica aerogels as insulation materials is illustrated by the rapid growth of the aerogel market: in 2004, only about 25 million US$ of aerogel insulation materials were sold, but this had increased to about 500 million US$ by 2013. Still the major drawback for a large scale usage of silica aerogels as standard insulating material in the building sector is their production cost. As a result, most of the current aerogel production is used for industrial applications such as pipeline insulation, rather than building insulation.

Silicon alkoxides such as tetramethoxysilane (TMOS), and tetraethoxysilane (TEOS) are the most common precursors for the production of silica aerogel. Although the chemistry of silicon alkoxide gelation is straightforward from a chemical perspective, alkoxides have their drawbacks, for example their high production cost due to a multi-step synthesis procedure. Although less reactive, TEOS is often preferred over TMOS because its price is about four times lower and because it is less hazardous. Still the minimum material cost of the raw materials for silica aerogel production is 700-800 CHF/m^3 of aerogel.

Our group developed an alternative route for the silica aerogel production using low cost silica precursors and ambient pressure drying technique. This potentially lowers the material cost by a factor of two or more. With the development of more cost-efficient large-scale production technologies, silica aerogel materials have the potential to gain a significant share of the building insulation market by 2020, particularly for retrofit applications.

Keywords: insulation, silica aerogel, raw materials

INTRODUCTION

Energy saving and lowering CO_2 emissions are hot topics in many areas of science and economics worldwide. Still, it is a surprise to many people that HVAC (heating, ventilation and air conditioning) of buildings account for approximately 40 % of the global energy consumption. HVAC systems of buildings can be improved with minimal effort by installing a proper thermal insulation and thus reduce CO_2 emission cost-effectively.

The most economical approach to decrease thermal losses of buildings is to install thicker layers of conventional insulation materials. There is naturally an aesthetic disadvantage linked

to such façade construction: the insulated object occupies more space and the usable living space decreases. Silica aerogel insulation materials, can achieve the same thermal insulation performance with only half of the thickness of the conventional insulation materials (Figure 1). Thermal conductivity is a material property which defines the potential of a material as a thermal insulator. Transparent silica aerogels exhibit the lowest thermal conductivity of any solid known, typically of the order of 0.015 $W \cdot m^{-1} \cdot K^{-1}$ at ambient temperature, pressure, and relative humidity. This extremely low thermal conductivity is due to the combination of low density and small pores [1]. With such thermal conductivity value they belong to the group of so called "super-insulation" or ''high-performance insulation'' materials [2,3].

In the building industry, space saving is the most important reason for the use of superinsulation. Typical cases are interior insulation solutions for building retrofit as well as thin facade insulation for the renovation of old historically important buildings, side balcony and roof balcony constructions. For practical reasons in the construction industry the thermal conductivity is expressed through U-value. The U-value shows heat loss through a given thickness of a specific material, taking account the three major ways in which heat loss occurs – conduction, convection and radiation. In Figure 1 you can see comparison of U and cost values for the most standard insulating materials including silica aerogels.

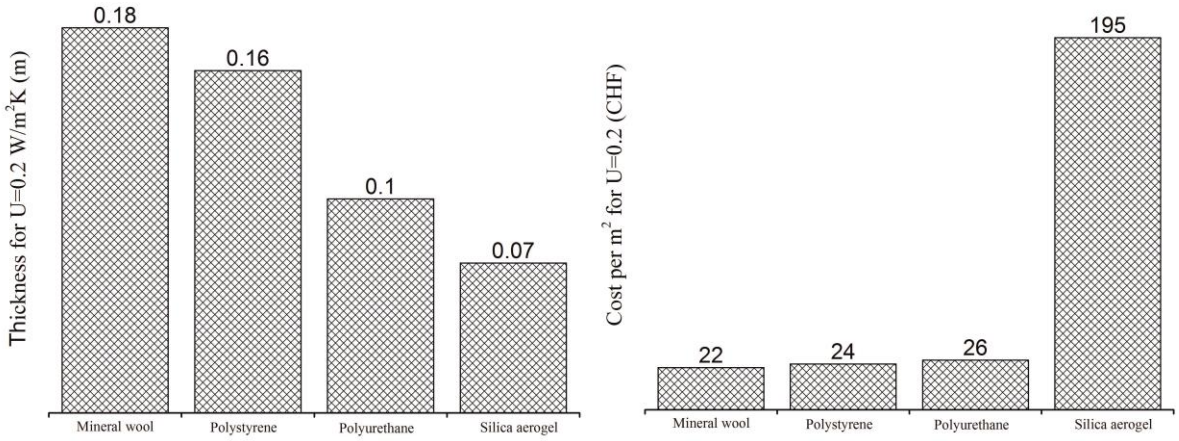

Figure 1. Comparison of thermal properties (U-value) and cost per m^2 of most common thermal insulation materials

Despite their clearly superior thermal properties, silica aerogels are still not used in the large extent in the construction industry due to very high production costs. The main reasons for the high production costs are expensive raw materials and complicated/expensive processing technology. Lately, a lot of work has been done in simplifying processing technology by using ambient drying instead of super critical drying, the details about could be found elsewhere [4,5]. Our group also worked on optimization of process of production of silica aerogels, the current state of art will be presented by Lukas Huber at CISBAT 15 [6].

Sodium silicate is relatively inexpensive and was the first material used for silica aerogel production, but the aerogel manufacturing process is expensive, time and solvent consuming because it requires multiple solvent exchange processes [7]. Silicon alkoxides such as tetramethoxysilane (TMOS) and tetraethoxysilane (TEOS) allow for easier processing and are

the most commonly used raw materials for the production of silica aerogels today. TEOS is often preferred over TMOS because its price is about four times lower and because it is less hazardous. Still, even TEOS based raw materials are expensive and they dominate the cost of the final product. Our group have been intensively working on strategies to find the cheaper raw materials and optimise the process with them. In Table 1 the prices of TEOS and possible other raw materials which can be used as precursors to silica aerogels are shown. From table it is clear that alternative raw materials such as silicon tetrachloride would cut the cost by at least half of the price.

Raw material	Cost (CHF/kg)	SiO_2/kg (kg)	Cost/kg SiO_2(CHF)
Metallurgical Si	2.2	2.14	1.03
Silicon tetrachloride	0.3	0.35	0.85
TEOS	1.6	0.29	5.51
Sodium silicate	0.4	0.28	0.70

Table 1: Prices and silica yield of raw materials which can be used as silica precursors

PREPARATION OF TEOS

In order to decrease the costs of raw materials we developed an alternative processing cycle for the production of silica aerogels (Figure 2). Instead of buying TEOS from a manufacturer, the idea is to start with metallurgical silicon, make silicon tetrachloride and from there make TEOS as a precursor to silica aerogel. The advantage of this process is that during TEOS synthesis from silicon tetrachloride, hydrochloric acid is produced as side product and this can be later easily decomposed to chlorine and hydrogen. The chlorine gas can then be used for a production of silicon tetrachloride from metallurgical silicon. Furthermore, most of the ethanol can be also recycled from final product and reused for a production of TEOS from silicon tetrachloride.

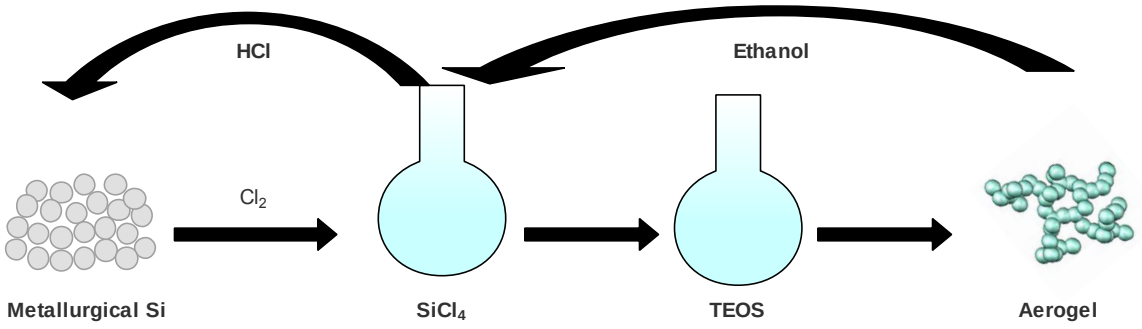

Figure 2: Schematically illustrated process of circular raw material/aerogel production

In order to start producing silica aerogels in such circular system, we first optimise the synthesis of TEOS from silicon tetrachloride. When anhydrous ethanol is treated with silicon tetrachloride the product is TEOS, as shown in chemical reaction below:

$$SiCl_4 + 4EtOH \rightarrow Si(OEt)_4 + 4HCl \quad (1)$$

If ethanol contains some water, as it typically does, pre-hydrolysed TEOS can be synthesized and the amount of water in the reaction determines hydrolysis degree of TEOS [8,9].

Anhydrous ethanol (99.9%) was added to silicon tetrachloride (99%, Sigma Aldrich) in pre-determined rates by syringe pump at 50°C. The reaction is performed in 3 necks round bottom flasks, and the tube for introducing ethanol was in the close proximity of magnetic stirrer to ensure immediate mixing with silicon tetrachloride. The final solution was left for two hours at 50°C and after that remaining HCl in the solution is removed by sparging the solution with compressed air for four hours: the bubbling time and stirring speed pH are optimized to reach the desired pH value. Small aliquots are taken for pH measurements. After achieving the desired pH (2-3), the solution is stored in fridge at 5°C.

The TEOS solutions prepared from silicon tetrachloride are stable for more than three months when they are sealed and stored in the fridge. The ^{1}H-^{29}Si HMBC NMR spectra of commercially available TEOS (Evonik Degusa, Germany) and TEOS synthesized in our group are shown in Figure 3. The sample prepared in our laboratory shows that the solution consists of ca. 70% of monomers (Q^0 at -80 ppm in the Si dimension, $Si(OEt)_4$) and 30% of dimers (Q^1 at -88 ppm in the Si dimension, $(EtO)_3Si\text{-}O\text{-}Si(OEt)_3$). The commercially available TEOS consist only of the monomer. The presence of the dimer indicates that the reaction conditions were not completely free of water.

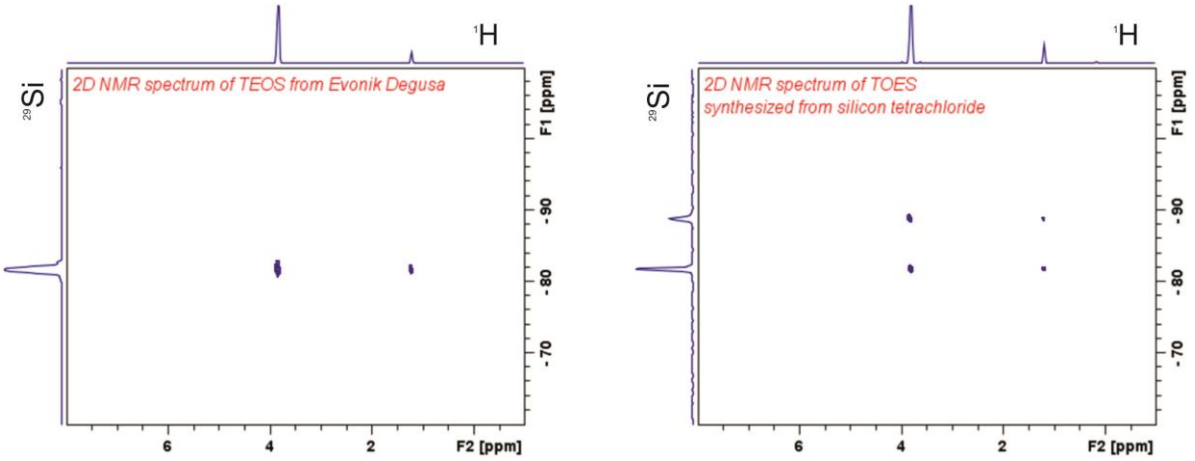

Figure 3: ^{1}H-^{29}Si HMBC NMR spectra of commercially available TEOS (left) and TEOS synthesized in our laboratory (right).

A mixture of monomers and dimers is not a disadvantage to further sol-gel process since dimers, trimers and higher molecular clusters are all formed during the condensation step in sol-gel process anyway. Freshly synthesized TEOS was used for the synthesis of aerogels according to the procedure described below.

AEROGELS SYNTHESIS

The TEOS solution prepared at EMPA was used to prepare polyethoxydisiloxane (PEDS), a pre-polymerized form of TEOS and common intermediate in aerogel production containing. The PEDS was prepared from water/TEOS in a molar ratio of 1.5 and a SiO_2 content of w/w 20%, according to the recipe found in literature [9]. Freshly prepared PEDS was mixed with ethanol, water and 5.5 M ammonia under constant stirring to form a gelation-initiated sol. This was then poured into polystyrene boxes and allowed to gel and age at 65°C for 24 hours. The aged gels were then transferred to glass beakers and and additional amount of ethanol, HMDSO and HCl was added to graft hydrophobic organic groups onto the silica surfaces and prevent shrinkage. The hydrophobization occurred at 65°C for an additional 24 hours. Finally, the aerogels were dried at 150°C for three hours.

The appearance (Figure 3b) and density of silica aerogels are the same regardless whether TEOS prepared at EMPA or commercial TEOS is used. The density of the synthesized silica aerogels measured by the powder displacement method (GeoPyc 1360, Micromeritics, US) is 0.15 g/cm^3. The mesoporous structure with pore size between 20 and 50 nm, which give rise to the low thermal conductivity of aerogels, can clearly be observed in the Scanning Electron Microscopy image (SEM) (Figure 4a).

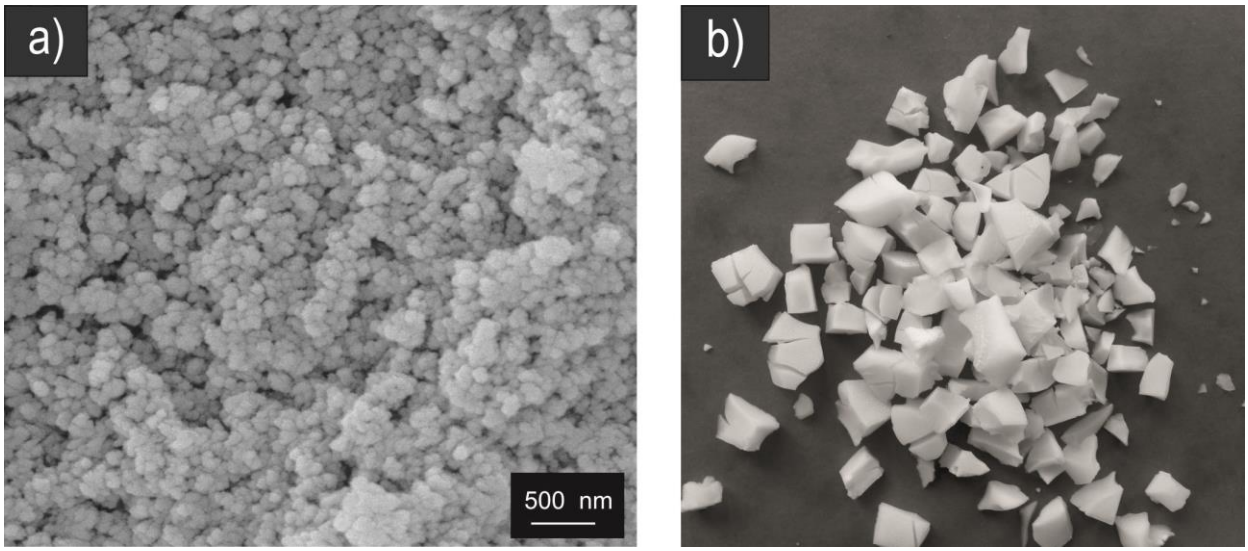

Figure 4: a) SEM image and b) photo of silica aerogels prepared from TEOS synthesized from silicon tetrachloride in our laboratory

CONCLUSIONS

Building insulation requires much larger volumes compared to industrial insulation (e.g. pipes). Thus, aerogels can only take a significant share of the building insulation market if we can capitalize on their thermal superinsulation properties at a lower price than is currently available [10]. Thus, traditional ways of preparing aerogels, which includes expensive raw materials and supercritical drying processes, are suppressing further commercialization and usage on the large scale and the development of new, cheaper raw materials is an absolute pre-requisite for the further expansion silica aerogel in the building insulation market. The

optimization of the synthesis of TEOS from silicon tetra chloride presented here is the first step in optimization of the entire production chain. A plant where most of the compounds will be re-cycled on site is the most ecologically and economically viable way for further scale up of silica aerogel production.

ACKNOWLEDGMENTS

We thank Daniel Rentsch for the NMR measurements. This work was supported by the Swiss Competence Center in Energy Research (SCCER-FEEB&D).

REFERENCES

[1] M. Koebel, A. Rigacci, P. Achard, *J. Sol-Gel Sci. Technol.* **2012**, *63*, 315.

[2] H. G. Emblem, *Mater. Chem. Phys.* **1983**, *8*, 265.

[3] D. A. P. Bulla, N. I. Morimoto, *Thin Solid Films* **1998**, *334*, 60.

[4] S. S. Prakash, C. J. Brinker, A. J. Hurd, S. M. Rao, *Nature* **1995**, *374*, 439.

[5] A. P. Rao, G. M. Pajonk, A. V. Rao, *J. Mater. Sci.* **2005**, *40*, 3481.

[6] M. Koebel, S. Zhao, S. Brunner, C. Simmen, Process for the Production of an Aerogel Material **2015**.

[7] S.S Kistler, *Nature* **1931**, 127,741

[8] W. A. Crocker, D. L. Hug, Method of preparing ethyl silicate **1983**.

[9] G. M. Pajonk, E. Elaloui, P. Achard, B. Chevalier, J.-L. Chevalier, M. Durant, *J. Non-Cryst. Solids* **1995**, *186*, 1.

[10] P. C. Thapliyal, K. Singh, *J. Mater.* **2014**, *2014*, e127049.

1.

IN SITU PHOTOELECTRON SPECTROSCOPY: A POWERFUL TOOL TO DEVELOP ELECTROCHROMIC MATERIALS

Olivia Bouvard[1]; Marina A. González Lazo[1]; Anna Krammer[1]; Andreas Schüler[1].

[1]*Solar Energy and Building Physics Laboratory (LESO-PB), Ecole Polytechnique Fédérale de Lausanne (EPFL), CH – 1015 Lausanne (Switzerland)*

ABSTRACT

In the building sector, a highly glazed envelope can lead to overheating in summer. In return, it increases daylighting and provides passive solar heating in winter. In order to make the best use of the solar resource, the use of a window with dynamic solar gain would be advantageous. Electrochromic coatings can darken on demand and thus modulate the solar gains. Some products are on the market but there are still several drawbacks with existing technologies such as the dynamic range, the switching speed, the color, the energy efficiency and the durability. Nanomaterials can improve the properties of such coatings.

In this work, thin film materials for electrochromic glazing are studied in detail using X-ray photoelectron spectroscopy. The thin films are deposited via reactive magnetron sputtering and transferred to the analysis equipment without breaking the vacuum. The surface of the samples is therefore characterised as deposited, ex situ contamination is avoided and the surface state is not modified because no additional argon sputtering is required. X-ray photoelectron spectroscopy (XPS) provides information on the electronic structure of the sample. The quantification of the chemical composition can be determined through integration of peak areas. Information on stoichiometry can thus be obtained precisely on the same day of sample preparation and provides feedback to improve deposition parameters rapidly.

In this study, an electrochromic material, tungsten oxide, is deposited by reactive magnetron sputtering and studied by XPS. Elemental compositions of the deposited films have been determined by in situ core-level photoelectron spectroscopy. The influence of deposition parameters, such as working pressure and O_2/Ar mass flow ratio, on the electronic, electrochromic and optical properties has been studied. It was shown that in situ analysis by X-ray photoelectron spectroscopy is a powerful tool to investigate and develop new nanomaterials for electrochromic windows.

Keywords: In situ X-ray photoelectron spectroscopy (XPS), electrochromism, tungsten oxide, nanomaterials, magnetron sputtering.

INTRODUCTION

Electrochromic windows are useful for regulating the solar gains. They allow some solar gains in winter and reduce undesired heat in summer. Commercial electrochromic windows are starting to enter the market. However, they still suffer several drawbacks in terms of switching time, durability or color rendering [1, 2].

Magnetron reactive co-sputtering is a widespread method to deposit coatings. Despite the fact it needs vacuum and therefore expensive equipment, it allow precise control of deposition parameters. This deposition technique is used for low emissivity coatings which are now of general use in new windows [3].

In order to develop new electrochromic materials with improved performances, one needs to obtain a feedback on the deposited material. The stoichiometry, for instance, is an important parameter. X-ray photoelectron electron spectroscopy (XPS) allows the determination of the elemental composition of a sample. The stoichiometry can be found by integration of the areas of the core level peaks corresponding to the elements present in the sample.

In this study, reactive magnetron sputtering was used to deposit electrochromic materials. The samples were then transferred to the XPS measurement chamber without taking the sample out of the vacuum. Likewise, in situ XPS analysis could be performed immediately. No sputtering was necessary as little contamination or adsorbed water could reach the sample. Therefore, the surface of the sample was measured as prepared.

Tungsten trioxide is one of the most widely studied electrochromic material. Tungsten trioxide can undergo a reversible transition from WO_3 to M_xWO_3 tungsten bronzes which display a dark blue color (M can be any atom of the first column of the periodic table: H, Li, Na…) as shown in equation 1 [4].

$$\underset{\text{transparent}}{WO_3} + xM^+ + xe^- \longleftrightarrow \underset{\text{dark blue}}{M_xWO_3} \quad (1)$$

An electrochromic device is generally composed of five layers. A transparent conductive oxide serves as electrode, an electrochromic oxide acts as the color changing layer, and an electrolyte either liquid, gel or solid, is permeable for the ions but electrically insulating. A counter electrochromic layer and another transparent conductive oxide complete the device.

Tungsten oxide coatings were deposited by reactive magnetron sputtering varying different parameters. The effect of the total working pressure on the oxygen content was investigated. Then, the oxygen/argon mass flow ratio was adjusted to obtain a tungsten trioxide.

METHOD

Thin-film deposition and in-situ characterization of electronic properties

Reactive sputtering with sputter-up configuration was used as depicted in Figure 1 a). The base pressure in the deposition chamber was $4 \cdot 10^{-8}$ mbar or better. A metallic target of Tungsten (99.95% purity from Kurt J. Lesker) was used. Argon gas was used for the plasma (Ar 99.999% purity) and oxygen as the reactive gas to deposit oxides (O_2 99.995% purity). Deposition parameters of the studied samples can be found in table 1. Medium Frequency (MF) bipolar pulsed power supply from MKS was used.

The coatings to be analysed by XPS were deposited on Si wafer substrates. Electrochemical and optical properties were determined on samples deposited on ITO-coated glass.

Deposition chamber and XPS measurement chamber were connected; Figure 1 b) is a photograph of the two chambers. The base pressure in the measurement chamber was $6 \cdot 10^{-9}$ mbar or better. XPS measurements were performed with an EA11 energy analyser from SPECS with a photon energy of 1253.6 eV (Mg K_α). The survey scans were measured at a pass energy of 50.4 eV at the energy analyser. The high-resolution scans of the elements were measured at a pass energy of 29.9 eV.

As a reference, the Au 4f7/2 core level signal from a gold bulk element (99.99% purity) was measured. The concentrations of elements were obtained by integrating over the core level signal after subtracting a Shirley background.

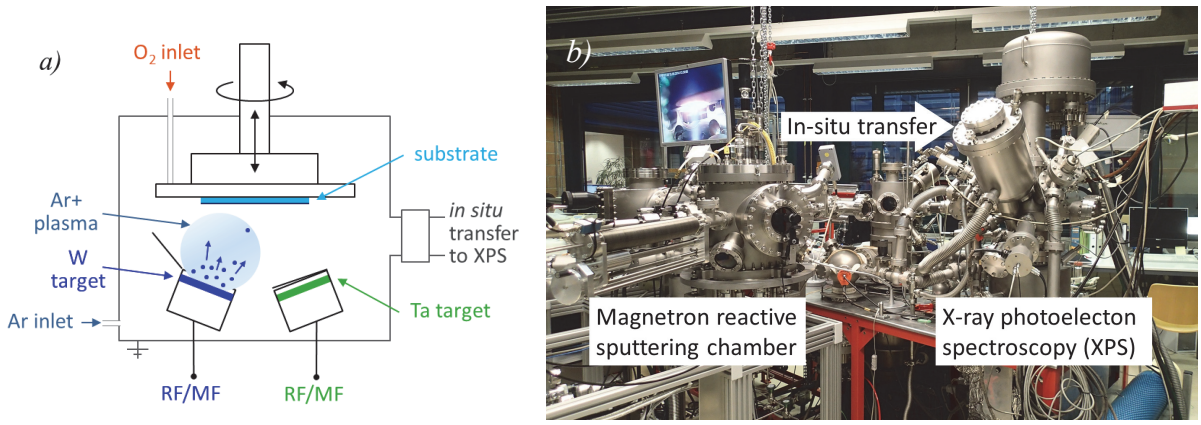

Figure 1: a) Diagram of the magnetron reactive sputtering chamber, b) Photograph of the deposition chamber, the transfer and the measurement chamber.

Optical and electrochemical characterizations

A Multispec 77400 spectrometer from ORIEL was used to determine the transmittance and reflectance of the sample in the visible wavelength range. Visible transmittance coefficients are calculated according to EN 410 standard using illuminant $D_{65}(\lambda)$ spectral power distribution and the photopic luminous efficiency function $V(\lambda)$. [5]

For electrochemical characterisation, tungsten trioxide was deposited on ITO coated glass (Delta Technologies, Ltd). Lithium perchlorate in polycarbonate (Li-PC) 1 M was used as the electrolyte. A graphite rod was used as a counter electrode. A constant voltage of 2.5 V was applied during charge, -2.5 V was applied for discharge.

RESULTS

The effects of deposition parameters on the properties of the films were studied. Particularly, the consequences of change in total pressure and oxygen:argon mass flow ratio (O_2/Ar) were investigated. Table 1 shows the deposition parameters used for the investigated tungsten oxide samples. Flow of argon and oxygen as well as the power applied on the target were maintained constant for sample A and B. Subsequently, a sample with higher O_2/Ar ratio was deposited (sample C).

	Sample A	**Sample B**	**Sample C**
Applied power	MF 150 W	MF 150 W	MF 150 W
Ratio O_2/Ar	0.48	0.48	0.61
Working pressure	$3{,}1.10^{-3}$ mbar (low working pressure)	$2{,}4.10^{-2}$ mbar (high working pressure)	$2{,}8.10^{-2}$ mbar (high working pressure)

Table 1: Deposition parameters

Right after deposition, the samples were transferred to the measurement chamber. Figure 2 displays the obtained XPS spectrum. Figure 2 a) represent the survey spectrum, it can be seen that only peaks from tungsten or oxygen can be observed. No carbon or traces of contaminants are detected, as expected for *in situ* XPS. Figure 2 b) shows the W 4f core-level spectra including the well-resolved doublet peaks belonging to W 4f 5/2 and W 4f 7/2 states

for sample B and C. However, the spectrum is more complex for sample A. Figure 2 c) shows the spectrum of O 1s core level peak.

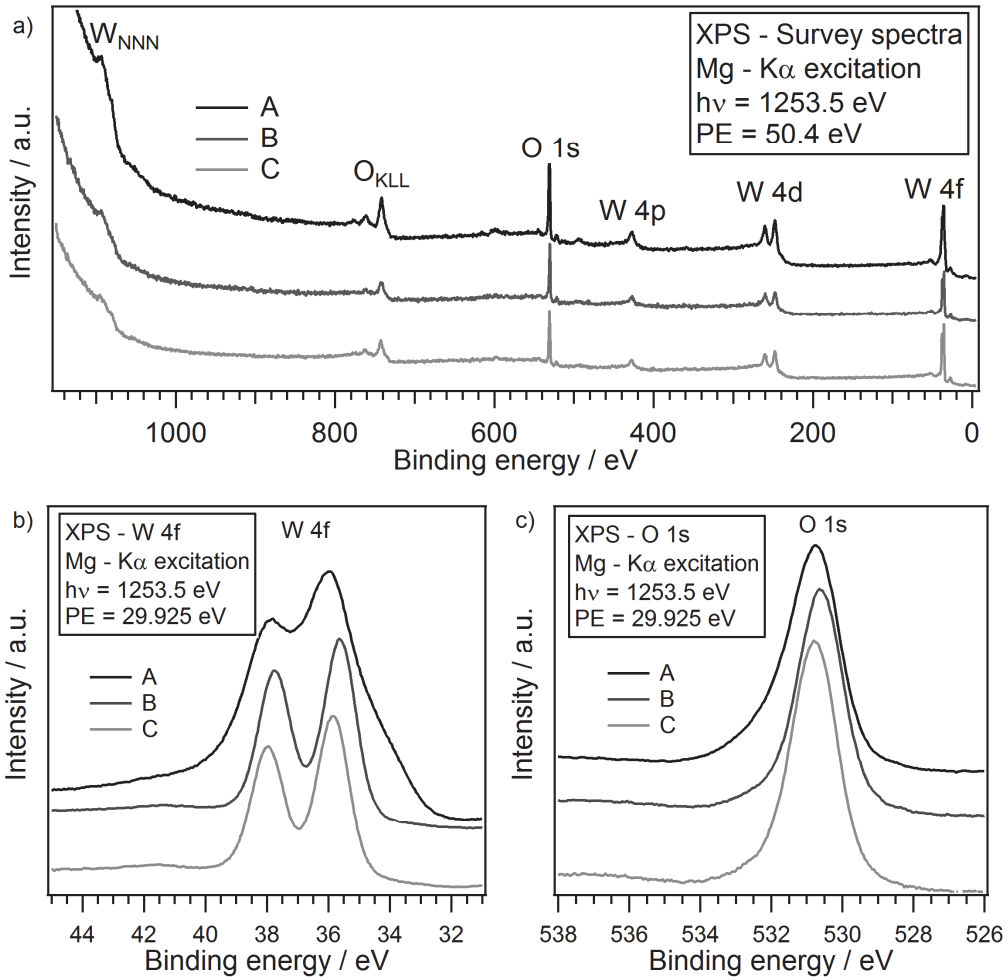

Figure 2: a) XPS survey spectrum of three samples of tungsten oxide. Sample A was made with a low working pressure (10^{-3} mbar range). Sample B and C were made with a high working pressure (10^{-2} mbar range). b) High resolution spectrum of the W 4f doublet peak. c) High resolution spectrum of the O 1s region.

Table 2 indicates the elemental composition of the samples determined by integration of peak area of W4f and O1s peaks. It can be observed that the oxygen amount is lower in the sample deposited at lower working pressure. Following the results obtained for samples A and B, the O_2/Ar ratio was increased to obtain a WO_3 thin film. According to XPS quantification, sample C has effectively a stoichiometry close to tungsten trioxide.

	O	**W**	**Corresponding formula**
Sample A	72.9	27.1	$WO_{2.69}$
Sample B	74.1	25.9	$WO_{2.86}$
Sample C	74.9	25.1	$WO_{2.98}$

Table 2: Quantification results obtained from integration of O 1s and W 4f core level peaks

In order to investigate the optical properties of these coatings, samples with same deposition parameters were deposited on ITO-coated glass. Sample A' was deposited, as sample A, at

low working pressure (WP) e.g. in the 10^{-3} mbar range. Sample B' was deposited as sample B at high WP (10^{-2} mbar range).

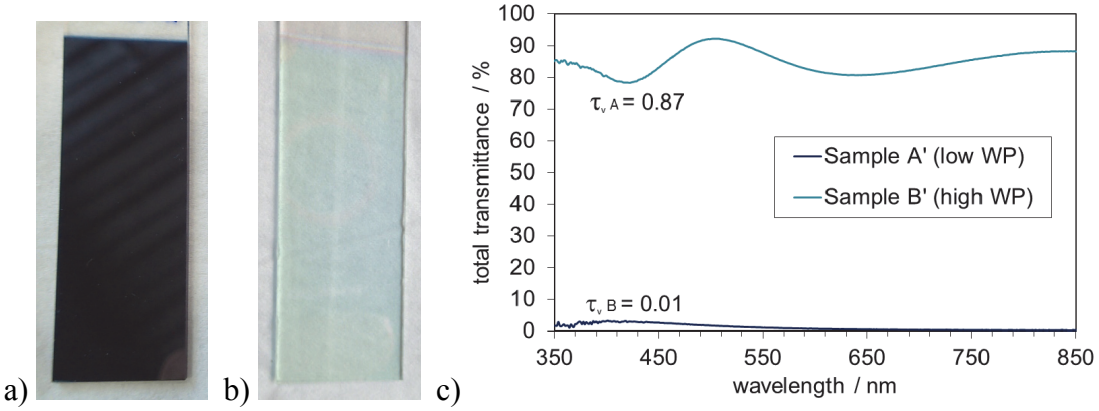

Figure 3: a) and b) Photograph of the samples A' and B' as deposited. c) Measured total transmittance of the two samples in the visible range. Visible transmittance τ_v determined according to EN410 is also indicated.

It can be observed that the sample deposited at low working pressure (sample A') at a very dark blue tint. Its visible transmittance is only 1 %. With the same mass flow of reactive gas, sample A' is transparent. Its visible transmittance reaches 87 %. As a comparison, the ITO-coated glass substrate alone has a visible transmittance of 88 %.

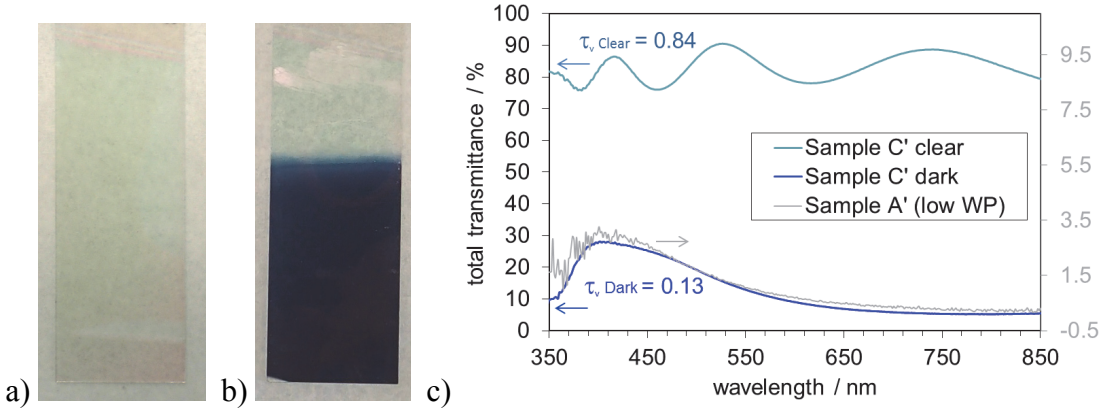

Figure 4: a) and b) Photograph of the sample C' in clear and dark states. c) Measured total transmittance and visible transmittance of the two states of sample C in the visible range. For comparison, sample A' with an adapted scale is also shown.

Sample C' was deposited, as sample C, with a higher O_2/Ar ratio and at a high working pressure. Figure 4 a) displays the clear as-deposited state. Figure 4 b) shows the dark state obtained after lithium intercalation in Li-PC with a voltage of 2.5 V. The visible transmittance in the clear state is similar to the one obtained for sample B'. The slight difference can be explained by a difference in thickness. A thicker sample was found to yield better results in terms of electrochromism. The visible transmittance in the dark state is reduced to 13 % and presents the distinctive blue color of tungsten trioxide.

DISCUSSION

Electrochromic oxides can be deposited by magnetron reactive sputtering from metallic tungsten and oxygen as a reactive gas. The different deposition parameters affect the stoichiometry and morphology of the film. The working pressure during deposition is known

to affect morphology of the film [1]; higher working pressures are commonly used in order to get a porous film. However, the working pressure also has an impact on the stoichiometry of the film for a given O_2/Ar mass flow ratio. At higher pressure, the mean free path of sputtered tungsten atoms is shorter. Therefore, the probability they get oxidised is higher. The XPS analysis allowed us to confirm the fact that the sample produced at lower working pressure (10^{-3} mbar range) contained less oxygen. These oxygen vacancies seem to affect the oxidation state of tungsten. As reported by Green at al., W4f 7/2 peak for tungsten shifts depending on the oxidation state [6]. The complex W4f spectra of the sample deposited at low working pressure (sample A) can therefore be explained by the presence of W^{4+}, W^{5+} and W^{6+}. A similar effect was demonstrated by Li et al [7]. By reducing the partial pressure of oxygen in the deposition chamber, dark samples were obtained.

Upon lithium intercalation, the clear tungsten trioxide becomes blue until reaching the dark blue final color depicted in this paper. The visible transmittance coefficient is higher for the electrochromic sample in the dark state (C') comparing to the sample with low oxygen content (A'). However, their visible transmittance spectrum is similar when normalised as shown in Figure 4 c). This observation suggests that lithium intercalation leads to a similar effect than low oxygen content in the film.

CONCLUSION

In this study, in-situ x-ray photoelectron spectroscopy was used for rapid determination of the elemental composition of the sample. Therefore, it allowed us to rapidly find the deposition parameters for electrochromic WO_3. The sample produced reached a modulation of the visible transmittance of 71 percentage point ($\Delta\tau_v$ = 71 pp). In addition, it enables us to identify the impact of working pressure on oxygen content. Furthermore, the observation of the W 4f core level peak gave us information on the oxidation state of tungsten. In the sample deposited at low working pressure, it could be found that tungsten is present at multiple oxidation states such as W^{4+}, W^{5+} and W^{6+} and that even in the absence of lithium or other intercalation cation, it affects the optical properties.

REFERENCES

1. C.G. Granqvist, Electrochromics for smart windows: Oxide-based thin films and devices, Thin Solid Films, 2014.
2. Jelle, B. P. *et al.* Fenestration of today and tomorrow: A state-of-the-art review and future research opportunities. *Solar Energy Materials and Solar Cells* **96,** 1–28, 2012.
3. Leftheriotis, G. & Yianoulis, P. in Comprehensive Renewable Energy 313–355. Elsevier, 2012.
4. Granqvist, C. G. Handbook of inorganic electrochromic materials. Elsevier, 2002.
5. NF EN 410, Glass in building, Determination of luminous and solar characteristics of glazing. 2011. AFNOR
6. Green, S. V., Granqvist, C. G. & Niklasson, G. A. Structure and optical properties of electrochromic tungsten-containing nickel oxide films. *Solar Energy Materials and Solar Cells* **126,** 248–259 (2014).
7. Li, C., Hsieh, J. H., Hung, M.-T. & Huang, B. Q. Electrochromic study on amorphous tungsten oxide films by sputtering. *Thin Solid Films* (2014). doi:10.1016/j.tsf.2014.12.022

HIGH PERFORMANCE THERMAL INSULATION - EXAMPLES FROM THE SWISS BUILT ENVIRONMENT

S. Brunner, J. Wernery, M. M. Koebel

Empa, Laboratory for Building Energy Materials and Components, Ueberlandstrasse 129, CH-8600 Duebendorf, Switzerland

ABSTRACT

Aerogel based solutions offer opportunities which combine aesthetics and cultural heritage criteria, often times in a unique way. In the field of energy efficient buildings, the search for improved envelope solutions has established Switzerland at the forefront of this type of applied research. Examples with granulate, aerogel sheets and aerogel render from 2002, 2008 and 2011 are presented [1, 2, 3]. For the development of the aerogel render [4], the speaker and his team received the Swiss environmental award for innovation in 2014. These are only a few selected examples of aerogel-based superinsulating solutions with many new ones being developed all over Europe. Experts and market analysts predict that aerogel materials will have a significant impact on the future built environment offering slim solutions, assuming that the high cost of production can be lowered to allow main markets penetration.

Vacuum Insulation Panels (VIPs) are a second class of high performance thermal insulation products with earlier market entry than aerogels, thus allowing us to look back on a full decade of experience with their applications and aging behaviour [5, 6, 7]. It was found that the aging behaviour of VIPs installed in 2004 is linear under the challenging conditions existing in flat roof terrace installations. This confirms that the prediction model [8] is applicable. Sufficient data exists to confirm that VIPs in Europe are of sufficient quality to be used in the building envelope..

In the context of a new project - the IEA EBC Annex 65 - the long term questions of aerogel and VIPs will be discussed on a top level. Having a team at Empa that synthesises a whole variety of aerogel is clearly helpful [10].

Keywords: Aerogel, Vacuum Insulation Panels (VIP), aging 10 years, aerogel granulate, aerogel sheets and render

INTRODUCTION

High performance thermal insulation as covered in this paper deals with aerogel and vacuum insulation panels. What aerogels are and how they are produced is the topic of two other contributions presented at CISBAT (oral presentations of Ana Stojanovic and of Lukas Huber).

Three pioneering projects with aerogel are revisited in this work in the context of a case study on applications motivated by the recently started IEA EBC project Annex 65 “Long Term Performance of Super-Insulating Materials in Building Components and Systems” [10]. Worldwide these three applications are the first of their kind and show the role of the Swiss market in building retrofit which is amongst the few trend-setting players which promote new solutions to reach energy efficiency under the stringent conditions of aesthetic and/or cultural heritage constraints.

AEROGEL GRANUALTE TRANSLUCENT APPLICATION

Perhaps surpisingly, the very first building for which aerogel was used in large quantities in the building envelope was a new construction. In 2003 the use of aerogel in a wide part of the building envelope started with the school building "Buchwiesen" in Zürich (Fig. 1). In this pioneering application aerogel was filled into cavities in fibre-reinforced façade elements. This was possible, as in that year, big enough quantities of aerogel got available at Cabot's pilot plant in Frankfurt. Previously, the concept was shown at the ZAE Bayern Building constructed in 1999 with demonstration and testing areas. For the construction as used at the "Buchwiesen" building the testing of thermal Performance and Solar gains were performed at Empa considering the constructive thermal bridging effects (U-values 0.48 W/m^2 K and G-values 0.25± 0.03).

Figure 1: Translucent facade seen from the inner side in 2004 and the outer weathered façade photographed a decade later in October 2014. The inset visualises the granules which fill up the cavity and insulate.

Nowadays, similar façade solutions are offered by many companies worldwide with aerogel between polycarbonate or glass panes where the view on the aerogel granules is part of the sold aesthetical solution. (The Swiss pioneer product Scobatherm, by the way, is now offered by Supramat Swiss GmbH, where still the same key person, Mr. Steger, is involved.). With these applications, the original vision of Aerogel used in the building envelope (e.g. [11]) made a prominent market entry.

SHEET SHAPED AEROGELS

While the building mentioned above was the first large scale application of aerogel granulate, aerogel sheets / blankets did not make their first appearance in the building sector but in the oil and gas industry and in applications such as spacecraft and military in the USA. Related to the pipe insulation in the oil and gas industry general technical pipe insulation emerged as a promising business sector for aerogels. As early as 2004, first samples of these products were received at Empa which helped bringing pioneering industry partners together.

In Switzerland, a first application was pipe insulation in a joint heating system for several older, existing buildings. With this high-performance insulation already validated in oil and gas applications, the same marketing and communication channels were adopted for building

systems. As a result contemporary insulations standards could be met with ease, which would not have been possible otherwise due to extreme space constraints.

A second application for aerogel sheets are existing buildings of particular cultural and aesthetical value with insufficient thermal insulation. Here, conventional insulation materials are often not a convincing or possible solution because of the necessary thickness or the potential for moisture problems. An old mill, shown in Fig. 2, was retrofitted with double-layered aerogel sheets in 2008, constituting the worldwide going-to-market for building envelopes. The improvement of the thermal envelope thus allows the usage of heat pumps or other low carbon-emission heat sources, which otherwise would be too energy inefficient in these kinds of buildings. For the IEA EBC project Annex 65 [10] dealing with the long time performance of superinsulation material, the mentioned building (Fig. 2) was reviewed by Valentina Zanotto, Amstein+Walthert AG. It still performs well after 7 years. On that building two layers of 1cm thick sheets were used as outside insulation in order to achieve high enough temperatures on the inside, in particular around the wooden ceiling beams, in order to prevent damage of the building structure or mould on the walls.

Figure 2: Aerogel sheets of 1 cm thicknesses like the old mill in Oberhallau near Schaffhausen, CH

With the year 2012 thicker aerogel solutions became available on the Swiss market in the form of aerogel render and plates. Both forms constitute the solutions used nowadays on Swiss facades while the sheet type in its high temperature variation is used in technical insulations. Also ducts for controlled air circulation are under the reference objects [12]. A list of the reference buildings where aerogel panels are used on the facade is [13]. 50% of these building are Swiss examples which can be found in more details at [14].

AEROGEL INSULATION RENDER

The third pioneer building with the aerogel high performance insulating aerogel render (“Dämmputz”) was completed in 2012. While granulate is a form of a material which can be poured directly into a cavity, sheets and plates have roughly constant thickness. The advantage of a granulate-based plaster is to equalize surface roughness at mm to cm scale which is typical for historical facades in one step allowing for an original curved or wavy topography which is so typical for classical historical facades.

Figure 3: Aerogel granules (left) as used in the aerogel plaster (centre images), and the 2012 retrofitted old mill at Sissach near Basel, CH (left)

Following the first buildings in 2012, about 70 buildings were retrofitted in that way in the subsequent two years, with now 19 reference objects online at one of the producing companies' website [15].

Looking at a second class of high performance thermal insulation, a decade of experience with aging behaviour of Vacuum Insulation Panels (VIPs) has been gained [5, 6, 7]. It was found that the aging behaviour of VIPs installed in 2004 is linear under the demanding conditions of a flat roof terrace installation. This confirms that the prediction model [8] is applicable. Consistent with an earlier presentation dating back to CISBAT2003, sufficient data exists to confirm that there are VIPs in Europe offered by leading companies of sufficient quality to be used in the building envelope.

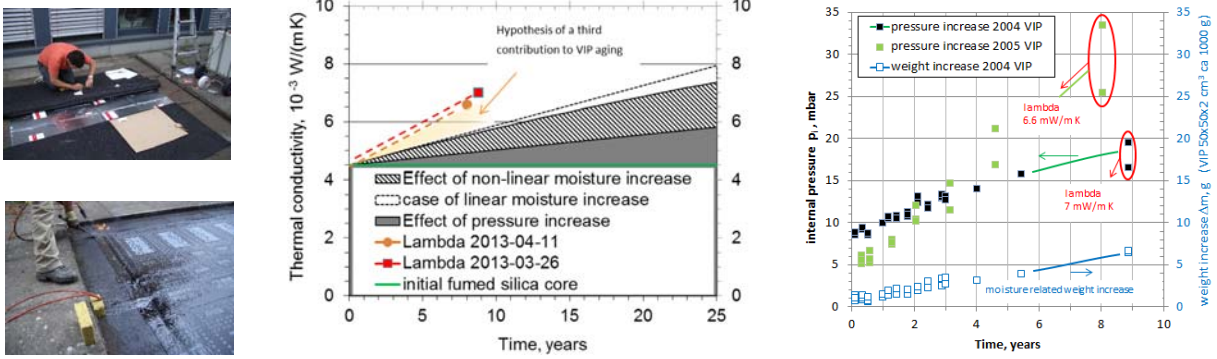

Figure 4: Vacuum Insulation Panels (VIPs) showed a thermal conductivity of 6.8 mW/(m K) after 8.8 years, constituting the best known performance in a real application. Building insulation is regarded as critical in [16] with more severe uncertainties than most other VIP applications: Photos from the installation in 2004 (left), a graph with the 2008 prediction plot [9] which is calculated for the measured temperature histogram at 80%rh moisture load (centre) and internal pressure increase curve showing the linear in both pressure and moisture increase (right) [5].

Among the different parts of the building envelope the application to build a terrace is ranked as the most severe one regarding water vapour permeation [16], and luckily, it is the best documented application worldwide [5,9] regarding the aging of VIPs.

In the context of a new project - the IEA EBC Annex 65 - the long term questions of aerogel and VIPs will be discussed on a top level. Having a team at Empa that synthesises a whole variety of aerogel is clearly helpful [10 and CISBAT contributions of Ana Stojanovic and of Lukas Huber].

REFERENCES

1. "Handbook of Aerogel " from 2011, chapter "Aerogels for Superinsulation: A Synoptic View". 2011, http://www.springer.com/materials/special+types/book/978-1-4419-7477-8
2. Koebel. M, Arnaud Rigacci, A., Achard R., Aerogel-based thermal superinsulation: an overview, Journal of Sol-Gel Science and Technology, 2012, 63, 3, 315-339 http://dx.doi.org/10.1007/s10971-012-2792-9
3. www.forumholzbau.com/pdf_05/nl11_turnhalle.pdf 2005
4. Stahl Th., Brunner S., Zimmermann M., Ghazi Wakili K., Thermo-hygric properties of a newly developed aerogel based insulation rendering for both exterior and interior applications, Energy and Buildings 44 (2012) 114–117 http://dx.doi.org/10.1016/j.enbuild.2011.09.041
5. Brunner, S., Ghazi Wakili K., Hints for an additional aging factor regarding the thermal performance of vacuum insulation panels with pyrogenic silica core, Vacuum , 2014:100:4–6, http://dx.doi.org/10.1016/j.vacuum.2013.07.033
6. Brunner S., Ghazi Wakili K., Stahl Th., Binder B., Vacuum insulation panels for building applications—Continuous challenges and developments, Energy and Buildings 85 (2014) 592–596, http://dx.doi.org/10.1016/j.enbuild.2014.09.016
7. Brunner S., IEA EBC Annex 65 Kick-off meeting, 2014-09-11/12 Grenoble, France
8. H. Simmler, S. Brunner, Vacuum insulation panels for building application Basic properties, aging mechanisms and service life, Energy and Buildings 37 (2005) 1122-1131 http://dx.doi.org/10.1016/j.enbuild.2005.06.015
9. S. Brunner, H. Simmler, In situ performance assessment of vacuum insulation panels in a flat roof construction, Vacuum 82 (2008) 700–707 http://dx.doi.org/10.1016/j.vacuum.2007.10.016
10. Wong J.C.H, Kaymak H., Brunner S., Koebel M., Mechanical properties of monolithic silica aerogels made from polyethoxydisiloxanes, Microporous and Mesoporous Materials , 183, 23-29, 2014 http://dx.doi.org/10.1016/j.micromeso.2013.08.029
11. Fricke J., Spektrum der Wissenschaft 1988, 7, 60 in German / English in Sci. Am. 1988, 256(5), 92.
12. http://agitec.ch/referenzobjekte/spezial-anwendungen , -> http://agitec.ch/fileadmin/images/img/Referenzobjekte/Deutsch/Lueftungsisolation_Coop_St._Annahof__Zuerich.pdf , downloaded 2015-05-10
13. http://www.wall-systems.com/produkte/referenzobjekte.html -> with selection of Warengruppe "WDVS Multitherm Aero"
14. http://agitec.ch/referenzobjekte/fassade
15. Yrieix B., Benoît M., Pons E., VIP service life assessment: Interactions between barrier laminates and core material, and significance of silica core ageing, Energy and Buildings, 85, 2014, 617–630 http://dx.doi.org/10.1016/j.enbuild.2014.07.035
16. www.fixit.ch/aerogel ->Referenzobjekte

DURABILITY OF ALUMINIUM BASED SOLAR SELECTIVE ABSORBERS UNDER CONDENSED WATER

M. Dudita[1,2], L. Omlin[1], F. Ruesch[1], P. Gantenbein[1], S. Brunold[1], A. Duta[2]

1: Institute for Solar Technologies SPF, HSR University of Applied Sciences, Oberseestrase 10, CH-8640 Rapperswil, Switzerland

2: Renewable Energy System and Recycling Centre, R&D Institute of the Transilvania University of Brasov, Eroilor 29 Street, 500036 Brasov, Romania

ABSTRACT

Sustainable building technology requires the use of solar collectors for heating and cooling purposes. The collectors' efficiency is mainly influenced by the solar absorber performance. Besides the optical properties of the absorber coating, i.e. high absorption of the incident solar radiation and low heat emission, the degradation due to environmental factors should be considered when designing solar absorbers. However, there is a lack of knowledge on the degradation mechanisms. The current standard methodology from ISO 22975-3, created within TASK 10 IEA Solar and Heating Programme only considers the optical degradation. This study focuses on the performance and durability of eight types of aluminium multi-layered absorbers. The combined effect of high humidity (95% RH), condensation and temperature (40°C and 60°C) was studied. The test samples were measured after different testing time intervals to assess the surface/interface (TEM), chemical (EDX) and optical modifications (UV-Vis-NIR and FTIR spectroscopy). The results revealed that the tested conditions are not strongly influencing the optical properties (solar absorptance and thermal emittance) in the case of the samples with anti-reflective layer and/or humidity protection barrier. All these types are qualified according to ISO 22975-3. However, strong colour modifications, layers alteration and chemical composition changes are recorded. The colour stability of the absorber should be a requirement, especially for architectural integration of solar collectors. Moreover, this study has shown that for modern aluminium based coatings, the predominant degradation process is not the formation of aluminium hydroxide, but the reduction of the antireflective layer thickness.

Keywords: accelerated test procedure, lifetime assessment, spectral selectivity, aluminium based solar selective absorbers, degradation mechanism

INTRODUCTION

The research priorities established by the new EU Framework Programme Horizon 2020 are related to foster clean and efficient energy, especially solar energy. Heat generation for domestic or industrial purposes requires almost 50 % of the total energy consumption in Europe. Using solar-thermal systems can help to decrease the fossil fuels consumption and the pollution, also significantly contributing to the EU's energy security strategy.

Considering the components of a solar collector (glazing, absorber, heat insulation, casing), the solar absorber is drastically influencing the collectors' efficiency. Efficient solar absorbers with high absorption (α_s) of the incident solar radiation and low heat emission (ε_t) are already reported in many papers and reviews which synthesize the state of the art [1, 2]. Nevertheless, the long term stability of the solar absorber materials should be assessed, as the manifold micro-climatic conditions can significantly deteriorate the material's performance. The minimum lifetime of a solar thermal system is estimated to be 20-25 years. Thus, the

materials should maintain the optical performance within this period [3]. Most of the papers report only the (initial) optimized optical values and the durability is rather neglected.

The main degradation processes are due to high temperature, high humidity and water condensation, and/or sulphur dioxide as an airborne pollutant [4].The method used for assessing the resistance to the factors mentioned is described in ISO 22975-3:2014 part 3 and it was developed about 20 years ago. The new and efficient solar absorbers are generally based on multilayers with complex degradation mechanisms. Moreover, aluminium and stainless steel absorbers are about to replace the formerly predominant copper in the worldwide market because of strongly increased copper prices. There is a lack of knowledge on the lifetime assessment of these solar selective absorbers and only a few reports on this topic exist [5, 6]. The stability to temperature of some aluminium based absorbers with and without anodized layer was evaluated by M. Kotilainen et al. [5]. The influence of a thin Al IR reflective layer on the absorber's durability was also investigated. In the case of humidity, there are even fewer reports [6], most of the research was done in the framework of Task X.

The paper presents the combined effect of high humidity (95% RH), condensation and temperature (40-60°C) for different selective coatings which are commercially available or under development. The test samples were measured after different testing time intervals to assess the surface/interface (TEM), chemical (EDX) and optical modifications (UV-Vis-NIR and FTIR spectroscopy).

.

EXPERIMENTAL DETAILS

Different modern solar selective absorbers obtained by physical vapour deposition were tested in high humidity and condensation at 40°C, or at 60°C and 95% RH humidity. The report codes denote the following types of absorbers: type 1: standard product, deposited on modified aluminium substrate, type 2: standard product, type 3: standard product, deposited on thin eloxal layer type 4: electrochemically anodized Al, optically dense Al layer, modified absorber layer, type 5: electrochemically anodized Al, optically dense sputtered Al layer, type 6: Al Constellium, no anodization, with chemical passivation layer, type 7: selective absorber with humidity protection layer, type 8: selective absorber without humidity protection layer.

The condensation tests were performed in a climatic chamber (Horstmann HS 220 K 45, volume 0.22 m^3) with a cooled sample holder designed according to the recommendation from ISO 22975-3:2014 part 3. The sample temperature was controlled using a thermostatic bath (Lauda RK8 KP). Three samples (5x5 cm) from each type were exposed to high humidity and condensation (HHC) and measured before and after different ageing times.

Optical measurements (Bruker IFS66) were performed to calculate the following parameters: *a) solar absorptance (α_s)* which represents the fraction of solar radiation energy absorbed by the absorber surface, *b) thermal emittance ($\varepsilon_{t,\ 100}$)* which represents the ratio between the energy radiated (per unit area) by the absorber surface at 100°C and the corresponding energy radiated by a perfect black body at the same temperature, and *c) performance criterion* function which shows the changes in performance of an absorber surface in terms of solar absorptance and thermal emittance (Eq. 1).

$$PC = -\Delta\alpha_s + 0.50\ \Delta\varepsilon_{t,100} \leq 0.05 \qquad \text{Eq. 1}$$

where: $\Delta\alpha_s$ is the change in the solar absorptance: $\Delta\alpha_s = \alpha_{s,t} - \alpha_{s,i}$, ($\alpha_{s,t}$ is the solar absorptance at the actual testing time and $\alpha_{s,i}$ is the initial solar absorptance), and $\Delta\varepsilon_{t,100}$ is the change in the thermal emittance: $\Delta\varepsilon_{t,100} = \varepsilon_t - \varepsilon_i$ (with ε_t - the thermal emittance at the testing time t and ε_i is initial thermal emittance. The average optical values are reported for each sample type.

Microstructural and elemental composition modifications after ageing were studied using a transmission electron microscope (TEM, FEI Talos F200X) equipped with an energy dispersive X-ray spectrometer.

RESULTS AND DISCUSSION

The samples were first visual inspected after each degradation time intervals and then the optical measurements were performed in order to calculate the solar absorptance, thermal emittance and PC values.

Strong colour degradation was observed for most of the samples exposed for longer testing times (1056h) at 60°C and 95%RH (Figure 1). For the samples tested at lower temperature (40°C), even after approx. 1500 h, the colour was unchanged. A pitting corrosion was however observed.

Although the aspect of the samples has changed in some cases dramatically, the absorbers' optical performance was still very good. The performance criterion values were generally very small, even after approx. 1500 h of testing (Table 1). Only the samples without humidity protection barrier have failed after first measurements when the value of the thermal emittance was similar with the one recorded for the uncoated aluminium substrate. Thus, the PC value was higher than 0.3, much higher than the maximum admitted value (0.05) which corresponds to a relative decrease of the annual solar fraction of a typical domestic hot water system by 5%. This type was not further included in the tests.

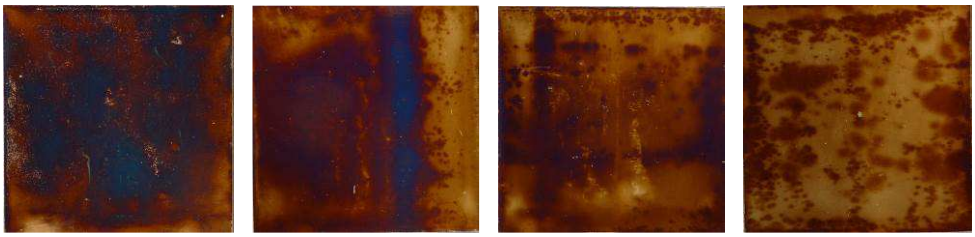

a. Sample T1 b. Sample T2 c. Sample T3 d. Sample T4

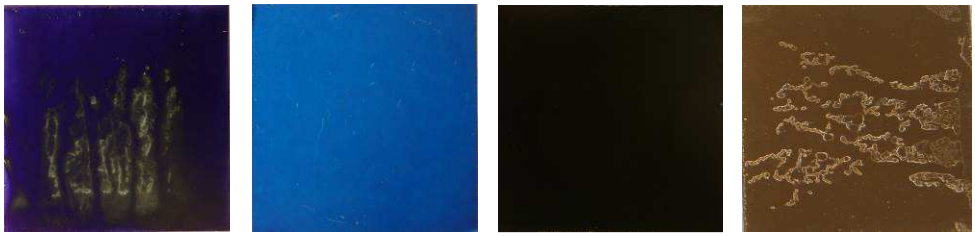

e. Sample T5 f. Sample T6 g. Sample T7 h. Sample T8

Figure 1: Samples after exposure to condensation and high humidity (60°C, 95%RH) after 1056 h (44 days) of testing (a. - g.), and after 384 hours of testing (h.), respectively.

For the tested aluminium based absorbers, longer testing periods are necessary in order to obtain a consistent change in the optical properties for the calculation of the activation energy based on the Arrhenius plot. After more than 1000 h of testing, no significant variation was obtained. In this case, testing at higher temperature to accelerate the degradation processes might be a solution. However, the hypothesis from Task X was that the degradation is different at higher temperatures due to the formation of more stable aluminium compounds.

Sample	PC values after different testing time intervals at 40°C				PC values after different testing time intervals at 60°C		
	270h	384h	1056h	1464h	384h	816h	1056h
T1	0.012	0.011	0.013	0.012	0.022	0.025	0.012
T2	0.004	0.002	-0.002	-0.003	0.001	0.006	0.007
T3	-0.001	-0.001	-0.003	-0.003	0.000	0.003	0.007
T4	0.008	0.005	0.002	0.000	-0.004	0.007	0.021
T5	-0.001	0.004	0.003	0.003	-0.004	-0.002	0.000
T6	0.000	0.004	0.001	-0.001	0.002	0.009	0.014
T7	0.006	0.006	0.007	0.006	0.004	0.008	0.004
T8	0.380		-	-	0.384	-	-

Table 1: Average PC values calculated after different degradation intervals for the samples tested in high humidity and condensation at 40°C and 60°C with 95%RH.

The possible degradation mechanisms/compounds were further investigated by performing HAADF-STEM (High Angle Annular Dark Field - Scanning Transmission Electron Microscopy) combined with energy-dispersive X-ray (EDX) measurements. The depth composition for the un-aged sample T4 and for the aged sample at 40°C (after 32h) is presented in Figure 3 and in Figure 5. The sample T4 has an anodized aluminium substrate (with the thickness of the anodized aluminium oxide about 140 nm, Figure 2). Two thin metallic layers are used as IR reflectors and diffusion barrier before depositing the Cr based absorbing coating. The antireflective coating is SiO_2 with a thickness of approx. 85 nm. The cross section of the un-aged sample was examined by HAADF-STEM (Figure 2) and it shows a sharp interface between the layers. However, after degradation, the layers and especially the interface between layers are modified (Figure 4) due to diffusion of elements, hydratization and other possible degradation mechanisms. Depth composition measurements were performed by EDX for each individual layer visible on the HAADF STEM image. What is interesting to notice from these depth profiles is that Al and Cr are present at the surface in the as received as well as in the aged sample, with Al slightly increasing in the aged sample. At the surface, different reactions depending on the pH of the environment might occur (Eq. 2-7), with the formation of different (soluble) aluminium compounds.

$$Al_2O_{3\,(s)} + 6H^+_{\,(aq)} \rightarrow 2Al^{3+}_{\,(aq)} + 3H_2O_{\,(l)} \qquad \text{Eq. 2}$$

$$Al_2O_{3\,(s)} + 2OH^-_{\,(aq)} \rightarrow 2AlO_2^-{}_{(aq)} + H_2O_{\,(l)} \qquad \text{Eq. 3}$$

$$AlO_2^-{}_{(aq)} + H_3O^+_{\,(aq)} \rightarrow Al(OH)_{3\,(s)} \qquad \text{Eq. 4}$$

$$Al(OH)_{3\,(s)} + 3H^+_{\,(aq)} \rightarrow Al^{3+}_{\,(aq)} + 3H_2O_{\,(l)} \qquad \text{Eq. 5}$$

$$Al(OH)_{3\,(s)} + OH^-_{\,(aq)} \rightarrow Al(OH)_4^-{}_{(aq)} \qquad \text{Eq. 6}$$

$$Al^{3+}_{(aq)} + 6H_2O_{(l)} \leftrightarrow [Al(H_2O)_6]^{3+}_{\,(aq)} \qquad \text{Eq. 7}$$

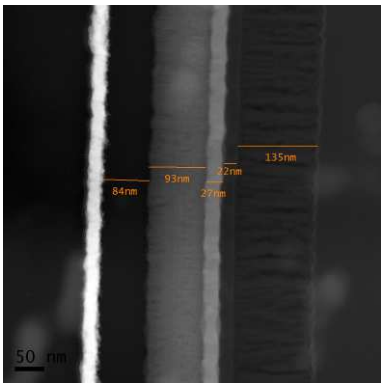

Figure 2: HAADF STEM image of the un-aged sample T4

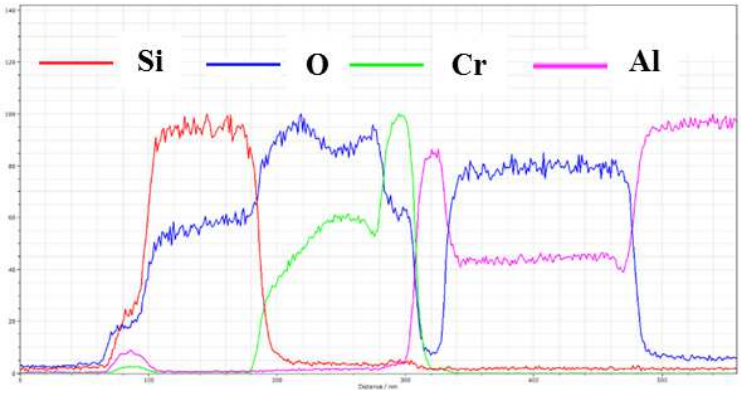

Figure 3: Depth composition for the un-aged sample T4

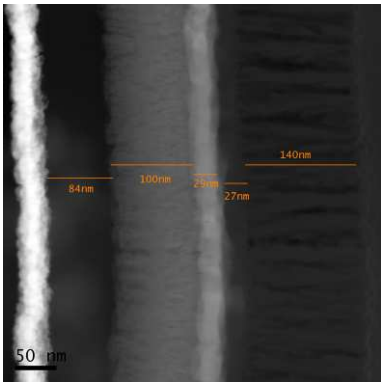

Figure 4: HAADF STEM image of the aged sample T4

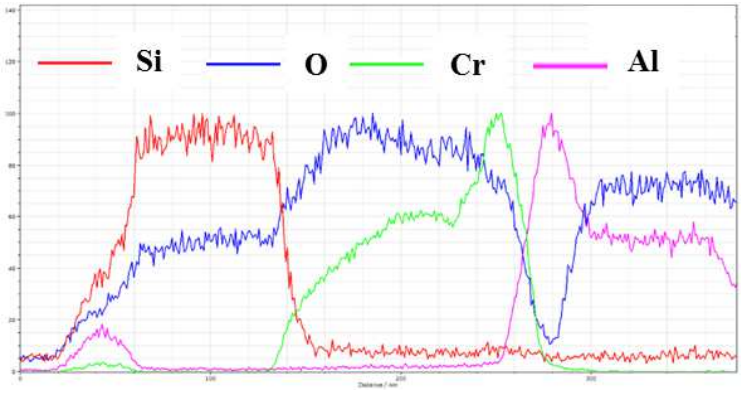

Figure 5: Depth composition for the aged sample T4

Besides diffusion, another mechanism was identified. The modification of the antireflective layer was observed in the UV-Vis-IR spectra. The characteristic band from 1085 cm^{-1} (approx. 9.2 µm) which correspond to the Si-O-Si stretching [7] is decreasing in intensity for all the aged samples (Figure 6). In some cases, for example for sample T4 after 1056 h of testing at 60°C is no longer visible (Figure 6). This is in accordance with the spectroscopic measurements performed in the UV-Vis wavelength range. The interference peaks are shifted towards lower wavelengths (Figure 7), indicating film (optical) thinning. Therefore, it is very likely that the SiO_2 film which gives the blue reflection is partially washed away or destroyed.

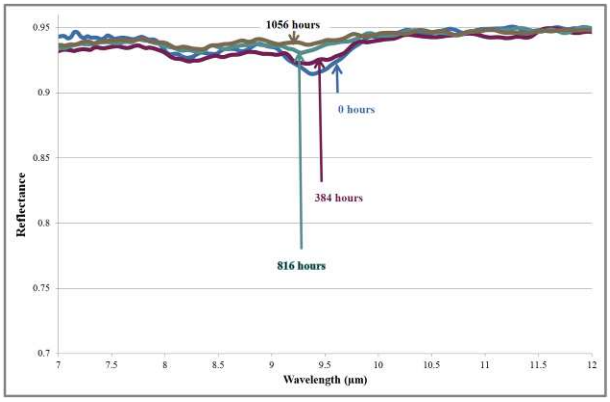

Figure 6: IR spectra (selection) for the un-aged and aged sample at 60°C and 95%RH (sample T4)

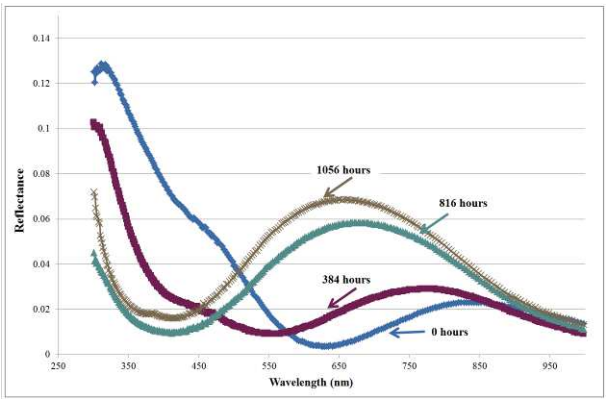

Figure 7: UV-Vis spectra of the un-aged and aged sample at 60°C and 95%RH (sample T4)

CONCLUSION

The combined effect of high humidity, condensation and temperature (40°C and 60°C) was studied for eight types of aluminium based solar selective absorbers. The results indicate that the testing conditions are not strongly influencing the optical properties of most of the samples. Only one absorber type which had no humidity barrier has failed the PC criteria after the first 270h. The other absorber types are qualified according to ISO 22975-3. However, other modifications were recorded, depending on the testing conditions: colour modifications, layers alteration and chemical composition changes. Different degradation/corrosion mechanisms in the tested conditions are proposed.

Although the absorbers were able to maintain their optical performance, the colour changed considerably for the samples tested at 60°C and 95%RH. This is due to the fact that the antireflective layer (SiO_2) which gives the blue reflection was partially destroyed and/or washed away. Especially for architectural integration of solar collectors, the colour stability of the absorber should be a requirement.

For the experiments carried out during the Task X, the main degradation mechanism for aluminium based coatings was the formation of hydroxide, which did not allow testing temperatures above 40°C. This study has shown that the predominant degradation mechanism for modern coatings is different and for this reason is not bound to testing temperatures below 40 °C. In this case, testing at higher temperatures to accelerate the degradation processes and to decrease the testing time might be a solution, but further studies are required.

REFERENCES

1. Amri, A. et all: Developments in the synthesis of flat plate solar selective absorber materials via sol–gel methods: A review. Renewable and Sustainable Energy Reviews, Vol 36, pp 316–328, 2014.
2. Selvakumar, N., Barshilia, H.C.: Review of physical vapor deposited (PVD) spectrally selective coatings for mid-and high-temperature solar thermal applications. Solar Energy Materials and Solar Cells, Vol 98, pp 1-23, 2012.
3. Carlsson, B. et all: Qualification test procedure for solar absorber surface durability. Solar Energy Materials and Solar Cells, Vol 61, pp 255-275, 2000.
4. Köhl, M. et all: Advanced procedure for the assessment of the lifetime of solar absorber coatings. Solar Energy Materials and Solar Cells, Vol 84, pp 275–289, 2004.
5. Kotilainen, M. et all: Temperature-induced ageing of solar absorbers on plain and anodized aluminium substrates. Solar Energy Materials and Solar Cells, Vol 134, pp 244-251, 2015.
6. Dudita, M. et all: Durability of solar selective absorbers under condensation test. 25 th. Symposium Solar Thermal Energy, Bad Staffelstein, Germany, 2015.
7. Shokri, B. et all: FTIR analysis of silicon dioxide thin film deposited by metal organic-based PECVD. 19th International Plasma Chemistry Society Conference, Germany, 2009.

ACKNOWLEDGEMENT

This work was supported by the Sciex - Scientific Exchange Programme NMS. The authors are grateful for the TEM measurements which were performed by the Scientific Center for Optical and Electron Microscopy (ScopeM) in collaboration with the Helmut Fischer Technology Ltd and for the photographs of the aged samples which were made by Felix Flueckiger (SPF).

POSSIBILITIES OF AEROGELS APPLICATION FOR ARCHITECTURAL HERITAGE CONSERVATION

Michal Ganobjak[1], Eva Kráľová[2]

[1] *PhD., researcher, Faculty of Architecture, Slovak University of Technology, Institute of History and Theory of Architecture and Monument Restoration, Námestie slobody 19, 812 45 Bratislava, Slovakia,* ganobjakm@gmail.com

[2] *Thesis supervisor, Assoc. prof., Faculty of Architecture, Slovak University of Technology, Institute of History and Theory of Architecture and Monument Restoration, Námestie slobody 19, 812 45 Bratislava, Slovakia,* kralova@fa.stuba.sk

ABSTRACT

Reconstruction of buildings has strategic importance for ensuring energy efficiency in the future. According to the current situation, it is estimated that in 2050 approximately 80% of energy consumption of buildings will be consumed by the current building stock [1]. A special category of building improvement is the reconstruction of historic buildings with structured or valuable facade surfaces or details, where insulation retrofit from the exterior side is undesirable for the loss of its cultural values. Although the architectural heritage buildings are not subject of the conditions for absolute achievement of energy efficiency, less energy consuming buildings increase the perspective of their future sustainability in all aspects. This assumption recognized that achieved effective conservation (preservation) of the existing cultural values is addition to the active use of older modernized buildings.

On the market there are new progressive materials containing aerogel, which announce an exceptional combination of properties, suitable for historic structures. The current scientific articles concentrate on research and development, however the articles do not follow the obtained results or caused effects of application on building structures. However, some insulation products based on aerogels are already offered on the construction market. The paper discusses the possibility of the use of new aerogel based materials for increasing energy efficiency while preserving the cultural values of the architectural heritage based on literature and market review.

International Charters and recommendations for the protection of cultural heritage define the principles and professional standards for the use of new materials: "*Where traditional techniques prove inadequate, the consolidation of a monument can be achieved by the use of any modern technique for conservation and construction, the efficacy of which has been shown by scientific data and proved by experience*." (Venice charter, Article 10.). In the absence of reliable information on the effects and impacts of aerogels on historic building materials, a series of experiments were conducted [2] to obtain their effects in key aspects of historic building preservation. An inventory of disposable materials based on aerogels from literature was prepared. Individual insulation materials have been classified according to the criteria for maintaining the authenticity and integrity which are the well-grounded attributes of preservation of cultural heritage values.

It seems that in the legislation or in the methodology there are no obstacles that limit the use of new materials in the restoration of monuments. As aerogels expand the variety of forms and intended use, they represent a potential material that can effectively contribute to improving of energy efficiency of historic buildings, but more targeted experiments and a long-term monitoring of impacts are required.

Keywords: aerogel, insulation materials, building retrofit, architectural heritage, historic building, building envelope

INTRODUCTION

The current standards reflecting the recent requirements for living and work space invoke the need to reduce the energy demands of the existing buildings which show significant energy losses.

Reconstruction of buildings by using additional insulation is a way to enhance the balance of the internal environment without dependence on supply. [2] The reconstruction of some types of structures is confronted with architectural limits related to materials or aesthetics. Materials that represent the architectural style by their color, texture or structure (stone, brick, exposed wooden structures, timber framing, etc.), or a work of art (paintings, frescoes, reliefs, decorative elements) are the direct bearer of cultural values [3]. It is therefore necessary, that the new added insulation and its attachment does not cover or degrade them. The new intervention to increase the insulation performance of the original building must fulfill several key requirements or criteria [4]. These must be respected on historically valuable objects and they should be applied also to other unregistered (unlisted) historic buildings that bear individual architectural features.

Figure 1: Rendering Fixit 222 with aerogel (EMPA) [5], Ultra-thin transparent insulation paint coating [6] (Industrial Nanotech) aerogel insulation blanket Spaceloft [7] (Aspen Aerogels)

The studied materials containing aerogel [3], which in the recent period are emerging on the construction market, appear to be potentially appropriate in the reconstruction of historic buildings to improve their energy performance. The real effect of these materials is however necessary to be examined and determined adequacy of use in terms of their impact on historic values of structures at their restoration. [4]

The current scientific articles indicate a much about research and development of these materials [7 - 24], but only few follow their interaction with building materials or issues related to practical application in building structures [25, 26, 27]. The presented paper shows an overview of applications of aerogel insulation materials and demonstrates the possibility of their use in reconstruction of historically valuable architecture by additional retrofit insulation, while pursuing key criteria that the new material should satisfy in interaction with the original material.

METHODS

The current content periodicals of international significance provide a wide range of scientific articles on topics related to aerogels [8, 12, 13], as well as on the topics of restoration of historic facades, and reduction of historic buildings´ energy demands [2, 27]. Articles which would present the intersection of these aspects, however, do not seem to exist. Following the observed lack of references on the use of aerogel insulation in exterior / interior locations of buildings, this article reviews commercial information provided by producers and fundamental research.

The current scientific and technical literature and commercial offer of aerogel was analyzed. The data obtained from the literature are summarized in tabular form, reflecting the impact of interferences. The

experience gained in the implementation of experiments [3] was developed into an applicable methodology for testing new materials.

A review of internationally accepted conceptual documents [4, 30, 31] on conditions of use of new materials in preservation of architectural heritage (= monument preservation) has been made. Documents set out the principles (conditions, criteria) of use of the new materials. In the case of retrofit insulation use in the refurbishment of historic buildings certain criteria must be followed.

RESULTS

Aerogel based applications are developed especially for the reconstruction of the existing buildings (Table 1) as the reconstruction constitutes a real opportunity for the future reduction of energy demands of the building. The developed materials with aerogel are intended mainly for the use in applications with limited space [1]. Historically valuable structures represent a specific group of refurbishment, where it is necessary to contend with the physical lack of space for additional thermal insulation and also with restrictions related to the requirements that the original character of the building is not changed and that the insulation will be compatible with the original material.

An assembled list of aerogel based products (Table 1) shows different materials are available in the reconstruction of buildings as for retrofit insulation. The base silica aerogel can be used in pure or composite form. As pure it is used in the form of granules of affordable different fractions, which are used as an addition to other composites. The solid - monolith pieces of the material in pure form for building construction are the subject of research [18]. The composites offered on the market are available in fibrous form or as mixtures. The available number of compositions can be used for refurbishment just as an added retrofitting insulation. (Table 1)

Table 1: Inventory of disposable materials with aerogel [2] for new construction (N) or refurbishment (R). 0 filling/ingredient material, 1 retrofit material without need of fixings/anchoring, 2 retrofit materials with fixings, 3 self-supporting construction materials

material		*class*	*form*	*use*		*type*
Silica aerogel SiO_2	basic material	compact form (monolith)	solid sheet, boards and blocks of different form	N/R	3	Constr. element
			films and sheets	N/R	3	
		grainy	grains, granules, pellets, powder	N/R	0	Ingredient material
				N/R	0	
	composite	with fibres (*crosslinked, filled, layered*)	insulation blanket, fabric	N/R	2	Retrofitting material
			solid panels, boards	R	2	
		mixtures	paints and coatings	R	1	
			plaster (interior/exterior)	R	1	
			poured construction materials	N	3	Constr. material
			building blocks, construction panels	N	3	

The available range of materials observed by inventory shows possible uses and applications for large-scale use and/or for details, the direct use for the perimeter masonry, or indirectly with the maintenance of structured expression by insulation improvement of other buildings components. There are also transparent forms and vacuum insulation panels (VIP) being researched currently [16]. Translucent panels are available and affordable. Transparent and translucent forms of products have the potential to reduce the energy requirements of the buildings of cultural heritage by improving the thermal performance of the original illumination openings: eg. tabular fillers of industrial windows, large-scale skylights of lofts, or large-scale diffuse glazed illuminating walls. Thermal insulation and other building materials follow the trend of improvements with the help of aerogel properties, which

are pursuing the objective to offer more efficient insulation at smaller thickness to construction market. The favorable combination of properties of available retrofit materials - strong thermal insulation properties at lower thickness, no wettability and water vapour permeability appear to be compatible and also potentially useful in restoring architectural heritage. These effects, however, need to be tested with respect to a number of the monument protection criteria. (Table 2)

International conventions and documents [4, 30, 31] permit the use of new materials in restoration of architectural heritage buildings in case they are compatible and have been tested, and their effects on the original material are not negative. Applied Materials shall meet the conditions for compatibility with the physical original, minimize invasive intervention in the authenticity and integrity of the original and should satisfy the condition of reversibility of intervention. [3]. Therefore the required criteria were summarized in the matrix, with grade of suitability. (Table 2)

Table 2: Methodological criteria for selection of a new retrofit material for case of monument refurbishment. Refurbishment of architectural heritage = thermal improvement of building and the preservation of cultural values

		Methodological criteria					
		Preservation / *Primary*				**Energy Efficiency / *Secondary***	
		Authenticity	**Integrity**	**Compatibility**	**Reversibility**	**Energy savings**	**Effectivity of intervention**
the suitability of intervention / description of the effects	**+**	• Added material preserves the original appearance and materiality	• The new material is added to the original • The integrity of the original remains intact	• Symbiotic or irrelevant interaction of materials after application	• It is possible to completely remove the new material to original authentic state, with no need of restoration of original material	• Added material brings significant energy savings • Significant reduction in energy consumption • > 30% of former consumption	• Interventions are simple and convenient for construction and maintenance • Without secondary effects
	±	• Partially added of replaced material preserves the original appearance	• The new material enters the original and partially undermines the integrity of the original	• Insignificant impact on properties resulting from interaction	• Removal of new material to original is possible with the need of small, manageable adjustments	• Added material brings small reduction in energy consumption • < 30% of former consumption	• Unknown and unaccountable efficiency factors • Secondary effects are unclear
	–	• Added material changes the appearance of the original material while maintaining the former properties	• The new material fully enters the volume of the original and disrupts its integrity	• One-off deterioration of visual/utilitarian properties after application	• The new material and its anchoring leaves readable traces after removal • Low possibility of new material removal	• The new added material insignificantly reduces energy consumption • Energy savings are not observed or clear	• New material brings obvious disad-vantages in construction and maintenance • Secondary impacts are negative
	!	• Added material completely changes the appearance and properties of the original material	• The new material extensively disrupts the volume and changes the properties of the original	• Significant or progressive deterioration after application of new material with aggressive and destructive effect	• The new material does not allow reversibility to the original condition • There is a loss/destruction of the original material after removal	• The new added material doesn´t heal persistent energy leaks, • Unbearable energy consumption, waste of energy or numerous heat bridges remains	• The intervention with new material is costly and technically complicated • Disadvantages in comparison with established procedures

The mentioned methodological criteria for selection of new materials for refurbishment should be used not only in buildings that are registered (listed) as cultural monuments but can be used also for other historical buildings that may contain a specific value of uniqueness. When selecting new materials for refurbishment, achievement of higher ratings (+ or close to this grade) by submitted criteria (Table 2) can objectively protect the values of old buildings, which are not registered as heritage.

The table of criteria (Table 2) shows the suitability of the material for its use in restoration of historic buildings. The potential use of new materials with aerogels is rated by four grades (from "+" to "!"), which can be objectively tested, observed or predicted. The first three grades ("+", "±" and "-") refer to the level/adequacy of intervention. The "+" when the used new material is seen as the best in all evaluated criteria. Material with this assessment is highly suitable for the use in the reconstruction of historical architecture. The "±" shows certain negative impacts on the monitored criteria. Application of the material should be reconsidered. The "-" grade indicates that the observed negative aspects are

significant. The material that achieves these values is inappropriate for the use in preservation. The fourth grade of extreme action marked with "!" is described as highly inappropriate in terms of monuments in all evaluated criteria. This grade indicates inappropriateness and restriction of use in refurbishment of monuments.

DISCUSSION

The review of available aerogel based materials (Table 1) shows the current offer of the materials and direction of their development as well as their applications due to their additional insulation properties and their suitability for renovation and refurbishment. For historical structures, it to test / verify application in terms of visual impact and ways of attachment (or conditions requiring additional anchoring system of materials) proves necessary. It is necessary to evaluate the impact of the application of any new retrofit products in terms of the monuments protection criteria. (Table 2) The way of physical performance of application in combination with material affordability also affects the selection of material for the use. It is necessary to observe the long-term effects on hygro-thermal performance of the building and explore the nanosafety of new aerogel based materials.

CONCLUSION

The need to reduce energy demands of the existing buildings is a hot topic. The permanent solution is achieved by additional insulation. The new aerogel-based materials bring new challenges in this respect. Highly efficient thermal insulation materials with a wide range of applications represent specific group of materials especially for historic buildings. Development of new materials with aerogels should respect the criteria for protection of monuments. Reliable verification of the complex impacts on the structure (ie, the thermal effect and impact on appearance) should precede the implementation of new materials into the process of restoration of historic buildings.

ACKNOWLEDGEMENTS

English language reviewed by PhDr. Danica Brečková

REFERENCES

1. International Energy Agency. Technology Roadmap : Energy Efficient Building Envelopes. [online]. Paris, 2013. [cit. 20.04.2014] Access: <http://www.iea.org/media/freepublications/technologyroadmaps/foldout/TechnologyRoadmapEnergyEfficientBuildingEnvelopes_FOLDOUT.pdf>, p. 30
2. Giebeler, Georg – FISCH, Rainer – KRAUSE, Harald et al.: Refurbishment manual. Munich: Edition Detail, 2009. ISBN 978-3-7643-9947-44. 280 p.
3. Ganobjak, Michal. Application of New Materials in Conversion of Selected Abandoned Power Plants. The Example of Aerogels Usage in Brick Facade Restoration. : Dissertation thesis. Bratislava : Faculty of Architecture STU, 2014. 138. p.
4. ICOMOS charter. International Charter for the Conservation and Restoration of Monuments and Sites (The Venice Charter) - 1964
5. FIXIT. Applikation Maschinelle Applikation Fixit 222 Aerogel Hochleistungsdämmputz. Dickschichtiger Auftrag nass in nass. [online]. Access: <http://www.fixit.ch/aerogel/?w=download>
6. Industrial Nanotech. Nansulate. [online]. Access: <http://www.nansulate.com/images/gallery/me-housing-2.jpg>
7. Beatens, Ruben – Jelle, Bjorn – Gustavsen, Arild. Aerogel insulation for building applications: A state-of-the-art review. In Energy and Buildings. p. 762 ISSN: 0378-7788, 2011, vol. 43,
8. Aegerter, Michel – Leventis, Nicholas – Koebel, M. Matthias. Aerogels Handbook : Advances in Sol-Gel Derived Materials and Technologies. USA, Springer science, 2011. ISBN 978-1-4419-7477- 8. 932 p.
9. Koebel, Matthias - Rigacci, Arnaud - Achard, Patrick. Aerogel-based thermal superinsulation: an overview. In. Journal of Sol-Gel Sci , 2012. vol 63. P. 315–339

10. Stahl Th. - Brunner, S. - Zimmermann, M. - Wakili, K. Ghazi. Thermo-hygric properties of a newly developed aerogel based insulation rendering for both exterior and interior applications. In. Energy and Buildings, p. 114–117. ISSN 0378-7788. Vol. 44 (2012)
11. Mohamad, Ibrahim. Aerogel-based coatings for energy-efficient building envelopes. In. Advanced Building Skins : Conference Proceedings of the 9th ENERGY FORUM. Munich, Economic Forum, 2014. ISBN 978-3-98120537-4. p. 753 – 774
12. Jelle, Bjorn Petter. Traditional, state-of-the-art and future thermal building insulation materials and solutions – Properties, requirements and possibilities. In Energy and Buildings. ISSN 0378-7788, 2011, vol. 43, s. 2554
13. Beatens, Ruben – Jelle, Bjorn – Gustavsen, Arild. Aerogel insulation for building applications: A state-of-the-art review. In Energy and Buildings. p. 762 ISSN: 0378-7788, 2011, vol. 43,
14. Hummer, E. - Rettelbach, Th. - Fricke, X. Lu, J. Opacified Silica Aerogel Powder Insulation. In Thermochimica Acta. ISSN: 0040-6031, 2993, no. 218, p. 269-276
15. Hunt, Arlon – Ayers, Michael. History of Silica Aerogels. [online]. [cit. 5.8.2014]. Access: <http://energy.lbl.gov/ecs/aerogels/ >
16. Jensen, K. I. – Schultz, J. M. – Kristiansen, F. H.: Development of windows based on highly insulating aerogel glazings. In Journal of Non-Crystalline Solids. ISSN: 0022-3093, 2004, no. 350, p. 351-357
17. SHI, Jianjun et al.. Heat insulation performance, mechanics and hydrophobic modification of cellulose–SiO2 composite aerogels In Carbohydrate Polymers. ISSN: 0144-8617,
18. Schmidt, M. – Schwertfeger, F. Applications for silica aerogel products. aerogels In Journal of Non-Crystalline Solids. ISSN: 0022-3093, 1998, no. 186, p. 364 – 368
19. Schultz, J. M. – Jensen, K. I. – Kristiansen, F. H.: Super insulating aerogel glazing. In Solar Energy Materials & Solar Cells. ISSN: 0927-0248. 2005, no. 89, p. 275-285.
20. Smith, Douglas – Maskara, Alok – Boes, Ulrich. Aerogel-based thermal insulation In Journal of Non-Crystalline Solids. ISSN: 0022-3093, 1998, no. 225, p. 254-259
21. Solomon, Nancy B. Architects Slowly Begin to Expand the Traditioal Palette of Materials :Case study: aerogel goes mainstream. In Architectural record. ISSN 0003-858X. p. 198-197. November 2003. Vol 191. No. 11
22. Wei, Gaosheng et al.. Radiative heat transfer study on silica aerogel and its composite insulation materials In Journal of Non-Crystalline Solids. ISSN: 0022-3093, 2013, no. 362, p. 231-236.
23. Zhao, Jun-Jie et al.. Radiative properties and heat transfer characteristics of fiber-loaded silica aerogel composites for thermal insulation. In International Journal of Heat and Mass Transfer. ISSN: 0017-9310, 2012, no. 55, p. 5196–5204.
24. Du Ai et al. A Special Material or a New State of Matter: A Review and Reconsideration of the Aerogel. In Material. ISSN 1996-1944, [open access] 2013, Vol. 6, p. 943
25. Interior insulation retrofit of a historical brick wall using vacuum insulation panels: Hygrothermal numerical simulations and laboratory investigations, Johansson et al, Building and Environment 79 (2014) 31-45
26. Ghazi Wakilia,∗, B. Bindera, M. Zimmermanna, Ch. Tanner . Efficiency verification of a combination of high performance andconventional insulation layers in retrofitting a 130-year old building. In Energy and Buildings. p. 237–242. ISSN 0378-7788. Vol. 82 (2014)
27. Smutný, Milan a kol. Energetická efektívnosť obnovy historických budov. Bratislava : Vydavateľstvo Eurostav, 2005. ISBN 80-969024-8-2. str. 89
28. Pascal Biwole1, Patrick Achard2. Thermal behavior of a passive solar wall with silica aerogel and phase change materials. In. Advanced Building Skins : Conference Proceedings of the 9th ENERGY FORUM. Munich, Economic Forum, 2014. ISBN 978-3-98120537-4. p. 197 – 208
29. Ganobjak, Michal. Aerogel based insulation for facade renovation of historical buildings. In. Advanced Building Skins : Conference Proceedings of the 9th ENERGY FORUM. Munich, Economic Forum, 2014. ISBN 978-3-98120537-4. p. 775 – 792
30. The Nara Document on Authenticity (1994). [online]. accessible: <http://www.icomos.org/en/charters-and-texts>
31. ICOMOS Charter – Principles for the Analysis, Conservation and Structural Restoration of Architectural Heritage. 2003, [online]. accessible: http://www.icomos.org/en/charters-and-texts

CHARACTERIZATION OF TRANSPARENT AND CONDUCTING DOPED TITANIUM DIOXIDE FOR ENERGY CONVERSION

Potlog Tamara[1], Duca Dumitru[1] , Dobromir Marius[2], Radu Apetrei[2] and Luca Dumitru[2]

1: Physics Department and Engineering, Moldova State University, MD 2009, Chisinau Moldova
2: Faculty of Physics, Alexandru Ioan Cuza University, 11 Carol I Blvd., Iasi 700506, Romania

ABSTRACT

Niobium-Doped Titanium Dioxide thin films were prepared by RF magnetron sputtering at room temperature. The TiO_2 thin films were deposited with thicknesses of about 400 nm, doped with different concentration of niobium and then annealed in H_2 environment at 460^{o}C. The influence of doping and post deposition annealing in H_2 environment on the structural and composition was studied by X-ray diffraction (XRD) and X-ray photoelectron spectroscopy (XPS). The structure and composition of the prepared films were found to be affected by the Nb dopant concentration and the post deposition annealing. This study found that doping TiO_2 with Nb implying improved conductivity compared to pure TiO_2 which exhibits insulating properties. TiO_2/*p*-CdTe photovoltaic devices with efficiency of about 2 % were fabricated.

Keywords: titanium dioxide, niobium doping, XRD, XPS, photovoltaic device

INTRODUCTION

Titanium dioxide is widely used in a range of applications such as sensing, photocatalyst, antimicrobial coatings, air purification, water treatment, dye-sensitized solar cells (DSSCs), etc. For the practical applications anatase and rutile structures are widely used and are easier synthesized in thin film form. Metal-doping was the dominant way at the initial stage of the study about doping effect on the photocatalytic properties of TiO_2. It was reported that the introduction of metal ions into the TiO_2 matrix could significantly influence photoactivity, charge carrier recombination rates, and interfacial electron-transfer rates.

METHOD

Fabrication of nanostructured Nb doped TiO_2 thin films

TiO_2 thin films were prepared on glass substrates by RF magnetron sputtering of Ti target of 99.99% purity. To obtain doped films, sintered pellets made of Nb_2O_5 powder (99.999% purity) were placed on the titanium target in the circular high-intensity sputter track region. The sputtering was performed under a mixture of 5 sccm (standard cubic centimeters per minute) of Ar (99.99%) and 1 sccm of O_2 (99.99%) atmosphere supplied as working and reactive gases, respectively, through an independent mass-flow controller. The sputtering chamber was evacuated down to 1×10^{-5} mbar by the turbo molecular pump and the working pressure was kept at about 5×10^{-3} mbar. The distance between the target and the substrate was kept constant at 6 cm. Before the deposition, the glass substrates were sequentially cleaned in an ultrasonic bath with acetone and ethanol. Finally, the substrates were rinsed with distilled

water and dried. After the deposition, undoped and Nb-doped TiO_2 films were annealed in hydrogen environment. This paper reports the effect of niobium doping on structural and composition of TiO_2 prepared by RF magnetron sputtering and also, discuss the influence of annealing in H_2 atmosphere at 460^oC for 30 min at a pressure of $2.0 \cdot 10^{-3}$ mbar.

Characterization of samples

The structure of the films was investigated by X-ray diffraction (XRD) using a Bruker-AXS D8 Advance diffractometer (CuK_a radiation, 40 mA, 40 kV). The surface morphology was investigated using an NT-MDT Solver Pro-M atomic force microscope operated in tapping mode. X-ray Photoelectron Spectroscopy measurements, using a Physical Electronics PHI 5000 VersaProbe instrument, were carried out to determine the surface elemental composition of the samples and the oxidation state of the elements. The photovoltaic characteristics of solar cells were evaluated from the current–voltage characteristics, under 100 mW/cm^2 illumination, by means of a Spectra Physics Oriel 300W Solar Simulator.

RESULTS AND DISCUSSION

Effect of Nb doping on the structure and composition of TiO_2 thin films

Figure 1 illustrates diffraction pattern of TiO_2 thin films with different atomic concentrations of Nb. The diffraction peaks of Nb doped TiO_2 thin films shift towards lower diffraction angles with increased dopant concentration. The shift of diffraction angles indicates increase in the lattice parameters with increasing Nb doping according to well know Bragg's Law equation. With further increasing of the Nb concentration X-ray diffraction patterns show that the films are amorphous.

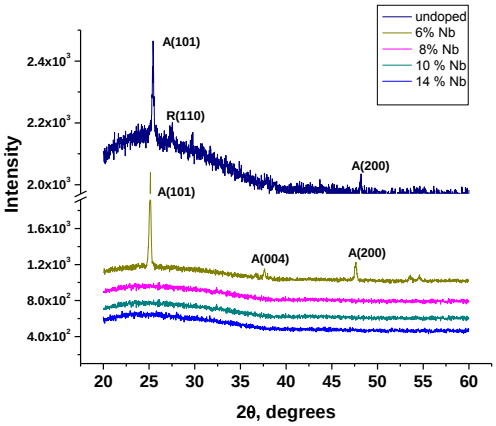

Fig. 1 XRD patterns of the undoped and Nb-doped TiO_2 thin films

Table 1 Structural parameters of TiO_2 thin films

	a, Å	c, Å
undoped	3. 7842	9.5185
6 at. % Nb	3.8214	9.5868

Table 1 indicates noticeable increase of the lattice parameters with increasing of Nb concentration. No characteristic peaks of Nb_2O_5 were observed in Nb-doped TiO_2 thin films.The survey XPS spectra of the Nb doped TiO_2 films in the whole binding energy region showed in the first atomic layers (10 nm) the characteristic peaks of C1s, O1s, Nb3d and Ti2p. Fig. 2 and Fig. 3 show the high-resolution Nb3d doublet and Ti2p doublet regions of TiO_2 films with different Nb dopant concentrations. As one can see Nb3d peak intensity increases with increasing concentration of Nb, while the Ti2p peak intensity decreases. Also, a slight shift to higher binding energy with increasing Nb content in XPS spectra of Nb3d

region is observed. Development of photovoltaic devices with higher efficiency requires nanostructured conductive materials. Therefore further we studied the effect of annealing in H_2 environment on the Nb-doped TiO_2 nanocrystalline structure.

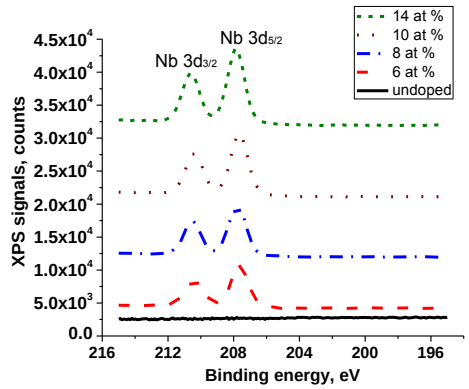

Fig. 2 XPS spectra of Nb3d region of TiO_2 with different Nb concentration

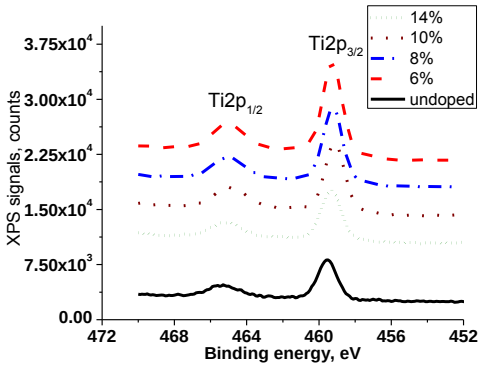

Fig. 3 XPS spectra of Ti2p region of TiO_2 with different Nb concentration

Effect of annealing in hydrogen atmosphere on the structure and composition

The diffraction pattern of the undoped, 6 at. % Nb-doped TiO_2 film and 6 at. % Nb-doped TiO_2 film annealed in H_2 environment at 460^{o}C , 30 min is shown in Fig. 4. The various diffraction peaks could be assigned to reflections corresponding to the anatase and rutile phases of TiO_2 for the undoped. The weight percentage of the anatase phase is 59.3%.

The 6 at.% Nb-doped TiO_2 films and 6 at. % Nb-doped TiO_2 films annealed in H_2 environment at 460^{o}C, 30 min TiO_2 films exhibit only the anatase phase. Also, the XRD data show that the crystallinity is improved when the films are doped. Annealing at 460 °C in H_2 atmosphere results in an increase in the intensity of the diffraction peak located at 2θ = 25.2° and it is found that the peak position of (101) anatase plane shifts to smaller diffraction angle value. We suppose that the primary hydrogen annealing mechanism is the chemisorptions of the dissociated hydrogen on the surface of the films. The half width of all the peaks of the Nb-doped and annealed TiO_2 thin films increases. The crystallite size was calculated by Scherer equation using anatase (101) phase. For comparison the crystallite size increases from 47 nm for not annealed Nb-doped TiO_2 film to 55 nm for Nb-doped annealed in H_2 atmosphere at 460 °C.

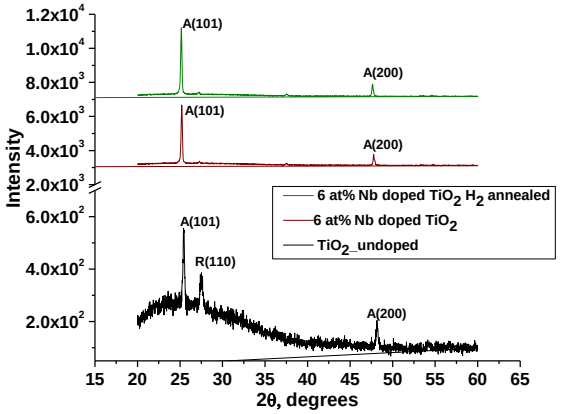

Fig. 4 XRD patterns of the TiO_2 thin films

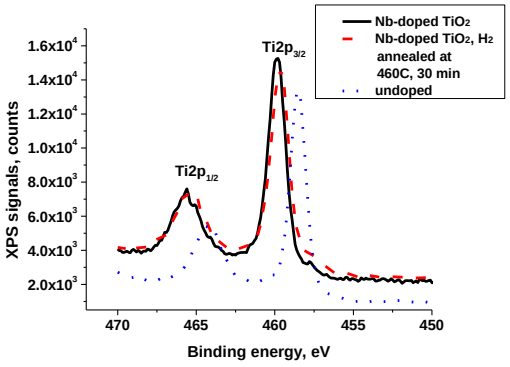

Fig. 5 XPS spectra of Ti2p region of TiO_2 thin films

Fig. 5 shows the high-resolution Ti2p doublet of the undoped TiO_2 films, 6 at.% Nb-doped and 6 at.% Nb-doped annealed in H_2 environment at 460°C, 30 min. For the undoped TiO_2 film the spectrum indicates binding energies at 458.5 ± 0.2 eV for Ti2p3/2 and 464.3 ± 0.2 eV for Ti2*p*1/2, respectively, which are very close to the values of the Ti^{4+} valence state of stoichiometric rutile TiO_2 [1, 2]. The Ti2p XPS spectra of 6 at.% Nb-doped TiO_2 films show values of binding energies of 459.7± 0.2 eV for $Ti2p_{3/2}$ and 464.9 ± 0.2 eV for $Ti2p_{1/2}$, respectively. For the film doped and annealed in H_2 atmosphere, a slight shift (~ 0.2 eV) towards higher BE values is seen for Ti $2p_{3/2}$ and (~ 0.6 eV) for Ti $2p_{1/2}$. The position of the Ti $2p_{3/2}$ peak (458.8 eV) is close to the value reported for Ti^{3+} states in the anatase phase (458.7 eV) [3]. We believe that the H_2 annealing changes the Ti^{3+}/Ti^{4+} ratio in the TiO_2 thin film. Both $Ti2p_{1/2}$ and $Ti2p_{3/2}$ binding energies showed a change in Ti^{3+} states and the Ti^{4+} ions, as a consequence of the H_2 treatment. A chemical shift of the BE is known to mean changes in the structure. Since the ionic radius of Nb^{5+} (0.70 Å) is larger than the ionic radius (0.68 Å) of the titanium, we can thus conclude that the Nb is easily built into a lattice, adding electrons. The theoretical calculations of Morgan [4] predict a small-polaronic Ti^{3+}gap state within an Nb-doped TiO_2 thin film. For Nb dopant at this concentration, the defect can be characterized as Nb^{5+} and Ti^{3+}/Ti^{4+} ratio. The XPS spectra of the Nb3d region of 6 at.% Nb doped TiO_2 and of 6 at.% Nb doped TiO_2 and annealed in H_2 environment at 460°C, 30 min are illustrated in Fig.6. The peaks correspond to that of Nb^{5+} oxidation state [5, 6]. The Nb3d binding energy for the 6 at.% Nb-doped TiO_2 film was determined to be 208.2 ± 0.2 eV for Nb $3d_{5/2}$ and 211.0 ± 0.2 eV for Nb $3d_{3/2}$, while for the annealed in hydrogen, the BE values are 207.9 ± 0.2 eV and 210.8 ± 0.2 eV, respectively. We suppose that observed slight shift is caused by the effect of annealing in H_2 atmosphere. To maintain the charge equilibrium, the extra-positive charge due to Nb^{5+} may be compensated by the creation of an equivalent amount of Ti^{3+} ions [7] or by the presence of vacancies in the cation sites [8]. Nb^{5+} species, substituting for Ti^{4+} in the crystalline lattice could be a reason for anatase stabilization.

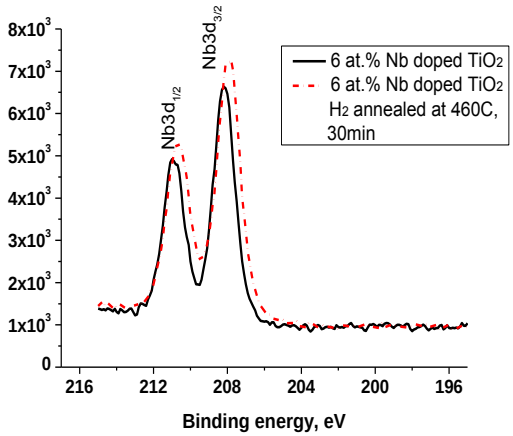

Fig.6 XPS spectra of Nb3d region of TiO_2 thin films

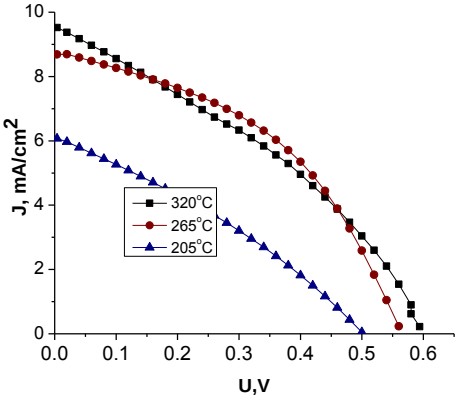

Fig.7 J-Vcharacteristics of the TiO_2/CdTe photovoltaic devices under 100 mW/cm^2 illumination, 300 K.

Characterization of the TiO_2/*p*-CdTe photovoltaic devices

The 6 at.% Nb-doped TiO_2 films annealed in H_2 environment at 460^{o}C has been applied in the fabrication of the photovoltaic devices. The load current-voltage characteristics of the TiO_2/*p*CdTe photovoltaic devices under illumination 100 mW/cm^2 are shown in Figure 7. The photovoltaic parameters depend on the shape of the J-U curve which is influenced by the substrate temperature of the CdTe thin films. An inspection of Table 2 where are presented the photovoltaic parameters shows that the efficiency of the devices is low because of the low values of the open circuit voltage and the fill factor. Poor efficiency of these devices could be attributed first to the higher sheet resistance of TiO_2 films and secondly to the relatively high concentration of mismatch dislocations at the TiO_2/CdTe heterojunction interface.

Table 2 Photovoltaic parameters of TiO_2/CdTe photovoltaic devices

T_s,^{o}C,	J_{sc}, mA/cm^2	U_{oc}, V	*FF*	η, %
225	6.1	0.51	0.27	0.85
298	9.12	0.43	0.42	1.63
320	9.5	0.59	0.36	1.98

CONCLUSION

Annealing in hydrogen atmosphere showed substantial improvement of structural properties of Nb-doped TiO_2 thin films. The Nb ions incorporate into the TiO_2 lattice. The XPS results indicate that the charge transfer from Nb metal ions to Ti leads to a change in the oxidation state of titanium. The H_2 annealing changes the Ti^{3+}/Ti^{4+} ratio in the TiO_2 thin film. The highest efficiency achieved at TiO_2/CdTe photovoltaic devices is about 2%.

REFERENCES

[1] H.S. Kim, S.H. Kang, Effect of hydrogen treatment on anatase TiO2 nanotube arrays for photoelectrochemical water splitting bull, Korean Chem. Soc. 34 (7) (2013) 2067-2072.

[2] H.J. Bae, S.H. Park, A. Nakamura, K. Koike, K. Fujii, H.J. Park, et al., The effect of rapid temperature annealing with N2 and H2 on photoelectrochemical properties of u-TiO2, J. Electrochem. Soc. 160 (11) (2013) H800-H802.

[3] M. Sacerdoti, M.C. Dalconi, M.C. Carotta et al., XAS investigation of tantalum and niobium in nanostructured TiO2 anatase, Journal of Solid State Chemistry 177 (6) (2004) 1781-1788.

[4] B.J. Morgan, D.O. Scanlon, G.W. Watson, Intrinsic n-type defect formation in TiO2: A comparison of rutile and anatase from GGA + U Calculations, Journal of Materials Chemistry 19 (2009) 5175-5178.

[5] M.Z. Atashbar, H.T. Sun, B. Gong, W. Wlodarski, R. Lamb, XPS study of Nb-doped oxygen sensing TiO2 thin films prepared by sol-gel method, Thin Solid Films 326 (1-2) (1998) 238-244.

[6] J.F. Moulder, W.F. Stickle, P.E. Sool, K.D. Bomben, Handbook of X-Ray Photoelectron Spectroscopy, Perkin-Elmer Corporation, Eden Prairie, Minn, USA, 1999.

[7] M. Valigi, D. Cordischi, G. Minelli, P. Natale, P. Porta, A structural, thermogravimetric, magnetic, electron spin resonance, and optical reflectance study of the NbOxTiO2 system, Journal of Solid State Chemistry 77 (2) (1988) 255-263.

[8] M. Sacerdoti, M.C. Dalconi, M.C. Carotta, B. Cavicchi, M. Ferroni, S. Colonna, M.L. Di Vona, XAS investigation of tantalum and niobium in nanostructured TiO2 anatase, J. Solid State Chem.177 (6) (2004) 1781-1788.

Sustainable Building Envelopes

SMART WINDOW - A WINDOW FOR DYNAMIC CONTROL OF BUILDING ENERGY PERFORMANCE

Kaitlin Allen and Yupeng Wu

Architecture and Built Environment, Faculty of Engineering, University of Nottingham, University Park, Nottingham, UK NG72RD

ABSTRACT

Thermochromic (TC) and Thermotropic (TT) glazing theoretically has the potential to significantly reduce the energy demand in buildings, by allowing transmission of visible light for daylighting but passively controlling solar gains; heat gains are minimised during the cooling season while allowing useful solar gains in the heating season.

In this study, a thermotropic layer made of hydroxypropylcellulose (HPC) and Sodium Chloride (NaCl) was synthesized and tested by the Evolution 201 UV-VIS spectrophotometer. The developed thermotropic layer has a transition temperature of 32-33˚C. Below the transition temperature visible transmission ranges between 65-95% while solar transmission ranges between 40-90%. Above the transition temperature visible transmission ranges between 5-35 % while solar transmission ranges between 10-50%.

In addition, simulations of a typical office with the developed TT and a TC installed were carried out using simulation software Energy Plus. The chosen TC window has a transition temperature of 20-21°C, constant visible transmission of 65% and solar transmission of 80% below the transition temperature and 15% above the transition temperature. From an annual energy prediction, exploring how the ambient environmental conditions affected the state of the TC, it was found that the incident solar radiation plays a large role in the tinting of the window, as heat gain within the film was predominately due to radiation, and was less reliant on convection. The performance of the TC was compared to a standard double glazing unit (DG); the use of the TC in comparison to the DG resulted in a 14.4 kWh/m2 –floor, 32%, reduction in HVAC energy annually but a 3.87 kWh/m2 –floor, 30% increase in lighting energy. Overall the TC saved 21% of combined energy annually; a significant reduction in energy use. The solar heat gain coefficient (SHGC) of the TC when tinted was 0.31 almost half that of the DG at 0.56; as the majority energy demand comes from cooling loads, this reduction in transmitted radiation, at peak temperatures greatly reduces this load. The results indicate that the TC technology would work best in areas with high levels of incident solar radiation and hot climates.

1. INTRODUCTION

Internationally the operation of buildings accounts for 30-40% of global energy consumption, leading to 30% of greenhouse gas emissions [1]. Windows themselves are extremely thermally weak components within the envelope and contribute to over 20% [2] of energy lost from buildings. It is imperative that new technology is developed to improve window thermal properties, while maintaining the visual and thermal comfort of the occupants.

Although technology that aims to stabilise the temperature of a highly glazed room has been improved many are still either steady state and inflexible, or dynamic control is given but at an energy cost. Therefore there is an opportunity to explore technologies being developed to provide passive, dynamic control of heat gain/loss through glazing, in order to reduce the

energy consumption. In this project, the energy performances of a typical office building with thermochromic and thermotropic smart window applied were investigated.

2. THERMOCHROMIC AND THERMOTROPIC WINDOWS

Traditional methods for improving windows provide many benefits and energy savings but they still suffer from problems such as glare, reduction in passive heating during winter, etc. Variable transmission glazing (VTG) are smart windows where the transmission properties vary to achieve the optimum luminous and thermal environments. One of the main types of VTG are chromogenic coatings, coming from the Greek, meaning colour creating. There are two methods of switching, passive devices which respond to changes in the environment and active devices which respond to a sensor input.

Thermochromics (TCs) are passive VGTs relying on temperature to dictate the switch between clear and coloured states. The TCs have certain temperature, $T_{t,}$ which is the threshold between states; under this temperature the window appears clear, with a monolithic structure that is semiconducting and non-absorbing in the IR spectrum. Above, the structure transforms into a metallic one, reflective in the IR spectrum. This means that during hot summer days incident solar radiation is rejected maintaining a cooler internal temperature while during cold winter days all incident radiation is allowed to enter.

Currently the T_t of TCs are too high (≈70°C) [3] for practical applications meaning further research into lowering this temperature needs to be done. The primary material in TCs is vanadium dioxide, VO_2, replacing some of this with other elements, such as tungsten, or doping, can lower the switching temperature to a more practical level.

Thermotropics (TTs) are similar to TCs; they are dependent on temperature to indicate switching however while TCs switch the optical properties, TTs switch the light scattering properties. This means that the view through the window becomes obscured becoming translucent instead of consistently transparent with changing tints.

The ideal transmission properties according to previous research [3] provide constant visible transmittance and reflectance at 60% and 17% respectively while the infrared transmittance changes from 80% to 15% with the reflectance changing from 12% to 77%. A transition temperature of 20 - 21°C is recommended [4].

At present, TC and TT windows do not meet these requirements with the largest solar transition given by 'RF sputtered CeO_2-VO_2 bilayers on SiO_2 substrates' changing from 37% to 20% [3]. Pure VO_2 crystals transition at 68°C with a brown/yellow film colour [4]. This transition temperature is far too high for practical applications in the built environment; via fluorine doping this transition can be brought down to a temperature of 25°C. Although practical the film colour remains brown/yellow, an extremely unappealing window colour for windows. The film colour can be changed to blue/green via gold nanoparticle doping, which also has a positive effect on the transition lowering the temperature to 15 -20°C. However doping using gold nanoparticles is an extremely expensive method and too costly for commercial availability. Considering this, the best option is therefore tungsten doping, providing a blue film colour with a transition temperature of 20 -25°C, at a reasonable price for commercial products [5].

3. BUILDING ENERGY PERFORMANCE SIMULATION

Building simulations have been carried out using Energy Plus software; a developed TT and a potential TC have been tested against a reference double glazed window to determine their viability and effect on energy saving.

A typical office room with dimensions 5m x 4m x 3m was used with a window of dimensions 2m x 1.5m (25% of the wall), placed centrally. The room is considered as part of a larger façade and building meaning that only the south wall of the room is exposed to external conditions while the other surfaces of the room are buffered by mechanically conditioned spaces and therefore experience no heat loss. The simulations have been run assuming the building is located in London, England; a marine west coast climate. This type of climate requires mainly heating in the winter and cooling in the summer. The annual average temperature is 10°C with a maximum temperature of 27°C and a minimum of -5°C. Daylight controls were used to ensure that 500lux of light was provided either naturally or via artificial lighting. The external wall has a U-Value of 0.15 w/m^{2}K, while the reference double glazing has a U-Value of 2.7 W/m^{2}K with T_{vis} = 88% and T_{IR} = 78%. A viable thermotropic layer has been developed, at the lab in the Energy Technologies Building, University of Nottingham, UK, using the cellulose derivatives hydroxypropylcellulose (HPC) and hydroxyethylcellulose (HEC) as well as sodium chloride (NaCl) which allows for the transition temperature to be controlled based on the amount added. The use of organic compounds reduces the cost as well as the hazard of toxicity. The optical performance of the developed TT was tested by the Evolution 201 UV-VIS spectrophotometer. A potential TC has been formulated from 'ideal' spectral performance [3].

Both the TC and TT have a U-Value of 1.8 W/m^{2}K with their transmission spectra shown in Figures 2 and 3, respectively. The transition points, T_t are 21°C and 32-33°C respectively.

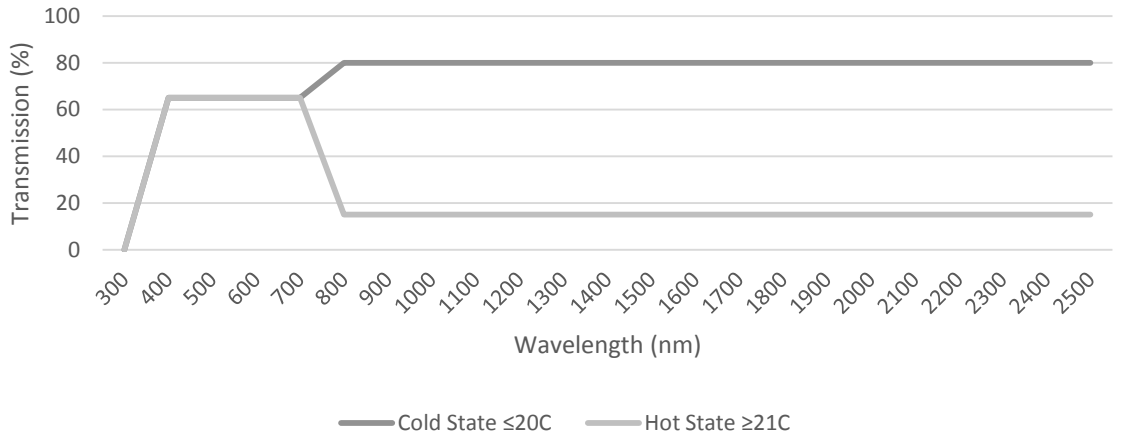

Figure 2 – Thermochormic Transmission Spectra

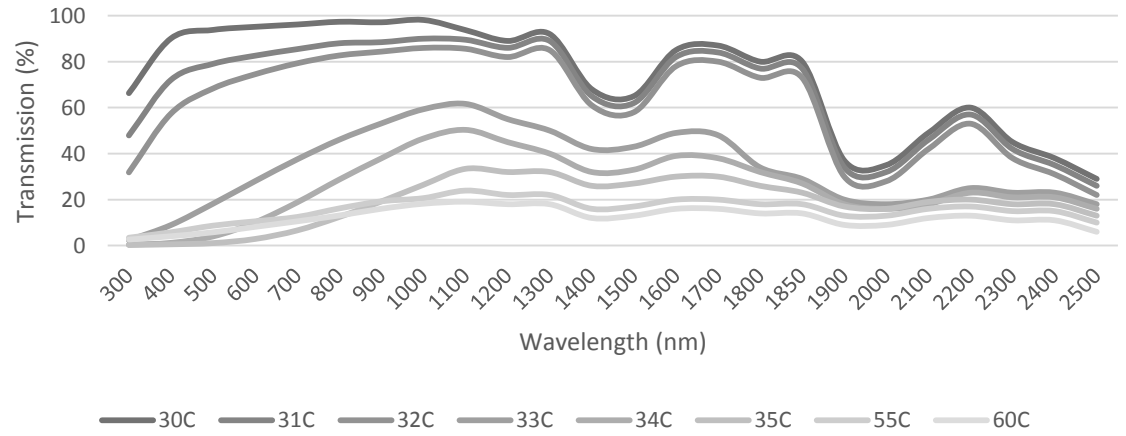

Figure 3 – Thermotropic Transmission Spectra

4. ANALYSIS

The ambient air temperature and incident solar radiation have a key role as they are what dictates room temperature but also the switching of states. There is a strong correlation of switching response to both outdoor air temperature and incident solar radiation [6]. Figure 5 shows hourly sets of data acquired through simulation for a consecutive 3 day period in winter and 3 day period in summer.

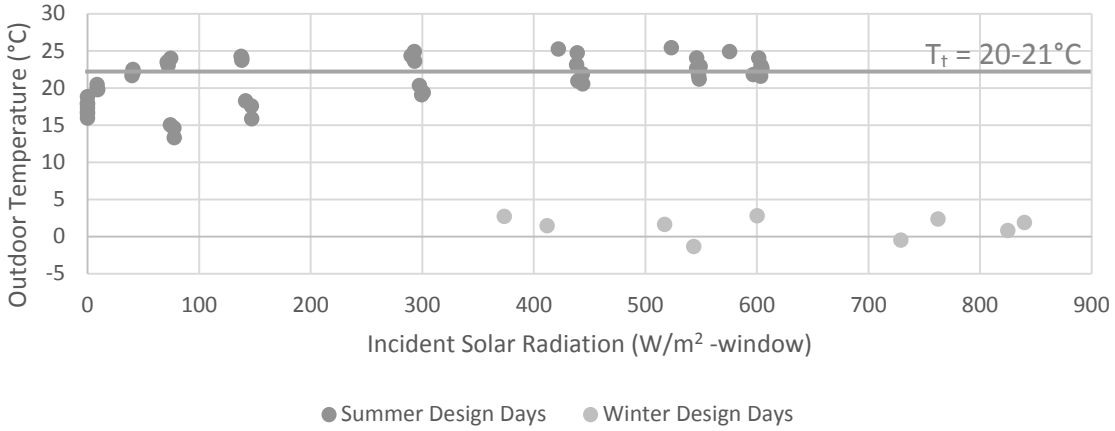

Figure 5 – Sets of outdoor drybulb temperatures and incident radiation resulting in tinting

The TC was tinted for 58 hrs of the 144 hr simulation, 40%; winter simulation tinted for 9 of 72 hrs, 13 %, while the summer simulation tinted for 49 of 72 hrs, 68%. The summer simulation shows that, for the majority of cases, tinting occurs when the outdoor temperature is near or above T_t; although tinting does occur at lower outdoor temperatures and 0 w/m^2 because of the heating effect from the HVAC system. The winter simulation shows that there are still occurrences of tinting when the outdoor temperature is much lower than the transition temperature due mainly to the high levels of incident solar radiation/ window heat gain as on a sunny winter's day as shown in Figure 6. The construction of the window with the TC layer closer to the interior also helps to maintain a higher temperature for longer, resulting in more tinting.

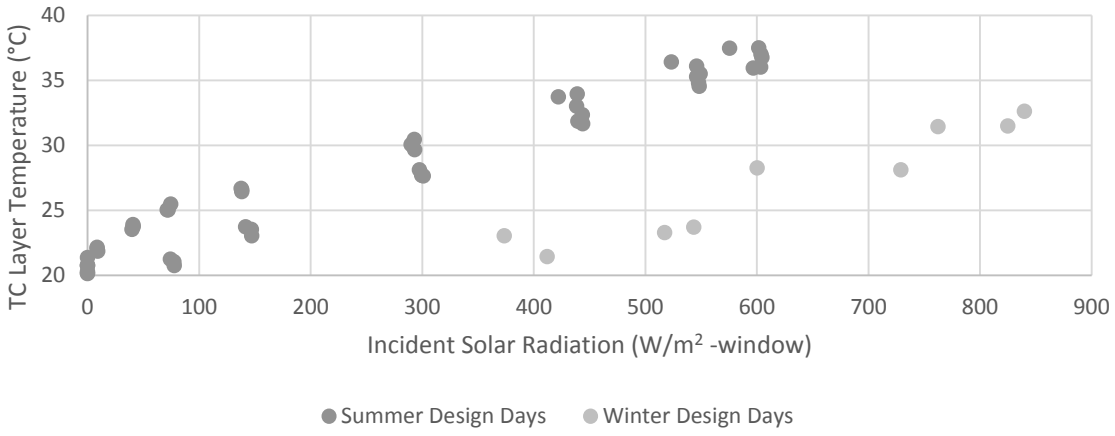

Figure 6 – Sets of thermochormic glazing temperatures and incident radiation resulting in tinting

Figure 7 shows the incident solar radiation with the concurrent window heat gains. The heat gain shown provides a balance between solar radiation, convective and long wave radiation

heat transfer processes. The dotted line 'SHGC' represents the average solar heat gain coefficient, for the 6 simulated days when tinted, which can be determined by dividing the window total heat gain by the incident solar radiation, giving a value of SHGC = 0.31. By comparing the winter and summer data sets, it can be seen that window heat gain is predominantly due to incident solar radiation and is much less reliant on convection. The winter design points provide higher levels of total heat gain, showing the importance of incident solar radiation and the low significance of the outdoor temperature

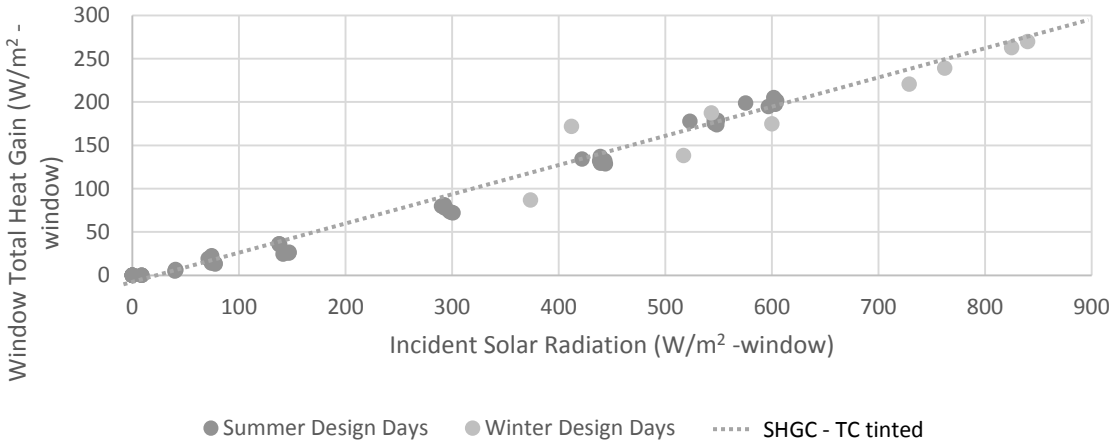

Figure 7 – Sets of window total heat gains and incident radiation resulting in tinting

Figure 8 shows the resulting power consumption of the reference DG and the TC and TT windows. Although the TC and TT sometimes act in a negative way, e.g. preventing passive heating on sunny winter days and decreasing natural illuminance, the overall combined effect of both windows is positive. The TC provides a saving of 10.53 kWh/m^2 –floor per year, 21% while the TT provides a saving of 1.41 kWh/m^2 –floor per year, 3%.

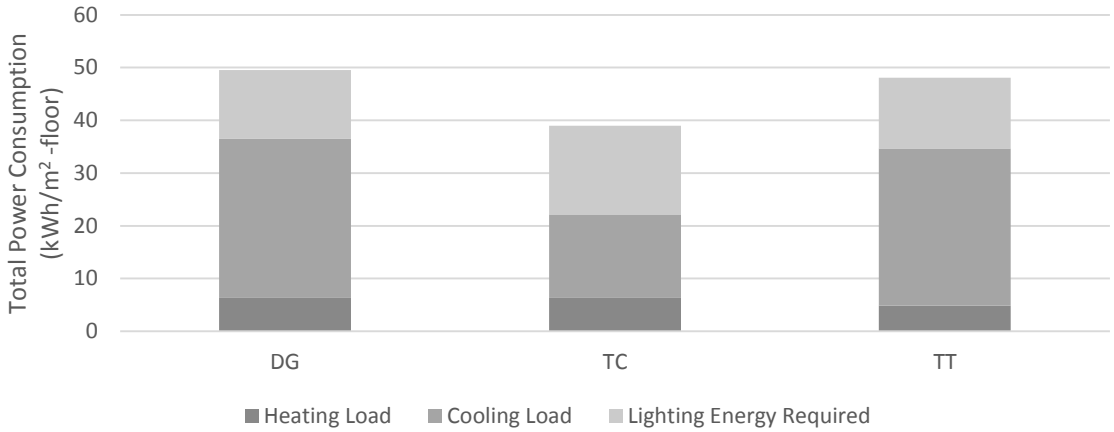

5. CONCLUSIONS

In this paper, a thermotropic layer made of HPC and NaCl was synthesized and tested at the University of Nottingham. The developed thermotropic layer has a transmission temperature of 32-33˚C. Below the Transition T_{vis} = 65-95%, T_{IR} = 40-90% above the transition T_{vis} = 5-35 %, T_{IR} = 10-50%.

In addition, simulations of a typical office with the developed TT and a TC installed were carried out using simulation software Energy Plus. The chosen TC window has a transition temperature of 20-21°C, T_{vis} = 65%, below transition T_{ir} = 80%, and above T_{ir} = 15%. From an annual energy prediction, exploring how the ambient environmental conditions affected the state of the TC, it was found that the incident solar radiation plays a large role in the tinting of the window, as heat gain within the film was predominately due to radiation and is less reliant on convection. The performance of the TC was compared to a standard double glazing unit; the use of the TC in comparison to the DG resulted in a 14.4 kWh/m^2 –floor, 32%, reduction in HVAC energy annually but a 3.87 kWh/m^2 –floor, 30% increase in lighting energy. Overall the TC saved 21% of combined energy annually; a significant reduction in energy use. The SHGC of the TC when tinted was 0.31 almost half that of the DG at 0.56, as the majority energy demand comes from cooling loads this reduction in transmitted radiation at peak temperatures greatly reduces this load. The results indicate that the TC technology would work best in areas with high levels of incident solar radiation and hot climates.

In addition simulation of typical hot days and cold days has also been carried out to evaluate fully the climatic impact on the window temperature and their capability to moderate solar heat gain. This can be seen through the results of the TT layer; the TT layer was only capable of tinting during the hottest days for very few hours, 5/72hr, 7% during the three day summer simulation, stunting the benefits of reducing the window heat gains, however this did allow for passive solar heating in the winter. The illuminance within the space was reduced, requiring extra lighting energy. However, when considering the whole system, the TT layer also provided a small energy saving of 1.41 kWh/m^2 –floor per year, 3%.

REFERENCES

[1] UK Green Building Council, "Key Statistics," 2012. [Online]. Available: http://www.ukgbc.org/content/key-statistics-0. [Accessed 17 November 2014].

[2] National Insulation Association, "Did You Know Facts," 2014. [Online]. Available: http://www.nia-uk.org/householder/index.php?page=did-you-know-facts. [Accessed 20 August 2014].

[3] M. Kamalisarvestani, R. Saidur, S. Mekhilef and F. Javadi, "Performance Materials and Coating Technologies of Thermochromic Thin Films on Smart Windows," *Renewable and Sustainable Energy Reviews,* vol. 26, pp. 353-364, 2013.

[4] L. Long and H. Ye, "How to be Samrt and Energy Efficient: A General Disscussion on Thermochromic Windows," *Scientific Reports,* no. 4, p. Article 6427, 2014.

[5] K. W. G. M. Resch, "Thermotropic Layers for Flat-Plate Collectors: A Review pf Various Concepts for Overheating Protection with Polymeric Materials," *Solar Energy Materials and Solar Cells* , vol. 93, no. 1, pp. 119-128, 2008.

[6] S. Hoffmann, E. S. Lee and C. Calvero, "Examination of the Technical Potential of Near-Infrared Switchin Thermochromic Windows for Commercial Building Applications," *Solar Energy Materials and Solar Cells,* vol. 123, pp. 65-80, 2014.

[7] R. Baetens, B. P. Jelle and A. Gustavsen, "Properties, Requirements and Possibilities of Smart Windows for Dynamic Daylight and Solar Energy Control in Buildings: A State-of-the-art Review," *Solar Energy Materials and Solar Cells,* vol. 94, no. 2, pp. 87-105, 2009.

[8] H. Ye, L. Long, H. Zhang and Y. Gao, "The Energy Saving Index and the Performance Evaluation of Thermochromic Windows in Passive Buildings," *Renewable Energy* , vol. 66, pp. 215-221, 2013.

[9] M. Saeli, C. Piccirillo, I. P. Parkin, R. Binions and I. Ridley, "Energy Modelling Studies of Thermochromic Glazing," *Energy and Buildings,* vol. 42, no. 10, pp. 1666-1673, 2010.

[10] M. E. A. Warwick, R. Binions and R. Ridley, "The Effect of Transition Gradient in Thermochromic Glazing Systems," *Energy and Buildings,* vol. 77, pp. 80-90, 2014.

[11] J. Schneider and A. Seeboth, "Natural Thermotropic Materials for Solar Switching Glazing," *Materialwissenschaft und Werkstofftechnik,* vol. 32, no. 3, pp. 231-237, 2001.

[12] H. Watanabe, "Intelligent Window using a Hydrogel Layer for Energy Efficiency," *Solar Energy and Solar Cells,* vol. 54, pp. 203-211, 1998.

[13] J. Schneider, A. Seeboth and A. Patzak, "Materials for Intelligent Sun Protecting Glazing," *Solar Energy and Solar Cells,* vol. 60, no. 3, pp. 263-277, 1999.

THERMAL AND VISUAL COMFORT ANALYSIS OF AN OFFICE WITH THERMOCHROMIC SMART WINDOWS APPLIED

R Liang; Y Wu; R Wilson

Department of architecture and built environment, University of Nottingham, Nottingham, NG7 2RD, UK

ABSTRACT

Although windows are important for providing daylight and solar heat gain control, they are also a direct cause of about 50% energy loss through convection, conduction and radiation through what is typically a heavily insulated envelope within which they sit. Hence improving the performance of windows is critical for saving energy consumption of buildings. Thermochromic (TC) smart windows, which change colour and optical properties in response to temperature variations, are one of the most promising technologies for regulating energy consumption in buildings. In this paper, an office room with two different types of TC smart windows were studied at three different climatic conditions (Harbin, Guangzhou and London) using building simulation software Energyplus. The selected two TC smart windows are W-doped VO_2 film and VO_2 nanoparticles coated double glazing with transition temperatures of 20°C and 40°C, respectively. The results show that there is an over 50% reduction in cooling loads of the office building with the W-doped VO_2 TC smart window installed, and approximately 15% of annual total energy saving, compared with the office with normal double glazing installed at the same climatic condition - mild and humid climate, however, due to TC windows having a relatively lower visible transmittance (e.g. For the VO_2 nanoparticles coated TC glazing, the visible transmittance is 63% below the transition temperature and 60% above the transition temperature), the total annual artificial lighting energy consumption is increased. In hot climates, W-doped VO_2 film TC window induces a nearly 9.7 % increase of cumulative thermal comfort hours. In terms of thermal comfort, it is concluded that TC smart windows are suitable to be applied in regions with very hot summer and warm winter. It is also found that TC windows reduce illuminance below a comfortable range, therefore, increase the use of indoor artificial light, however, it reduces the appearance of glare. A comprehensive understanding of TC windows performance at various climatic conditions will benefit their future application on practical buildings.

Keywords: Thermochromic materials, Simulation, Thermal comfort, Visual comfort, Energy consumption

INTRUDUCTION

The Building is one of the major energy consuming sectors – In the UK, buildings currently account for approximately 40% of its national energy consumption. While in terms of buildings, windows are significant for providing daylight and solar heat gains of the internal environment, they are also responsible for over 50% energy loss. [1] Hence improving the performance of windows is critical for saving energy consumption of buildings. Thermochromic (TC) smart windows, one of the most promising chromogenic technologies for moderating energy consumption in buildings, have been widely investigated. They are designed to regulate the amount of transmitted solar radiation in response to an applied stimulus – heat. When above the transition temperature (hot state), a thermochromic smart window transmits visible light, but reflects the majority of Near Infrared Radiation (NIR, ~43% of total incident solar radiation). This also leads to the colour change of the glazing (tinted). The reduction in solar radiation entering a building in hot seasons will reduce the air conditioning load. During cooler weather, with the glazing in its clear state below the

transition temperature (cold state), both visible and NIR parts of the solar spectrum are transmitted through the window, providing daylighting and passive heating for the building. Vanadium dioxide (VO_2) is most researched TC materials.[2] Most of the recent studies of the TC windows were focused on improving the performance of TC (suitable transition temperature, improving visible transmittance, etc.), using hypothetical or ideal TC windows for building simulation.[3,4] Few studies used the practical developed TC materials to optimise the building energy performance.[6,7] In this work, building energy simulations with practical developed TC windows at various climatic conditions were carried out. It has the potential to provide a guidance on using the TC windows in buildings.

METHOD

In this section, building simulation software – EnergyPlus was used to study the building energy performance of a typical office room at different climatic conditions, where various types of thermochomic smart windows and a standard double glazing window were applied.

Properties of Thermochormic Windows

Two typical types of VO_2 glazing are chosen for this study, and their optical properties are given in Table 1. Glazing A is a VO_2 nanoparticles coated double glazing, it has T_{vis} of ~60% on both cold and hot state, while glazing B is W-doped VO_2 film coated double glazing with T_{vis} of only 39%, which is much lower than the normal glazing and also glazing A. However, the transition temperature (T_t) of glazing B (20°C) is lower than that of glazing A (~40°C). And the transition temperature range from cold to hot state for TC glazing A and glazing B is 8°C. Glazing C is a standard double glazing unit used as reference. A common office room installed with these three types of windows respectively was studied in the following section. The U-value of each double glazing unit was defined as 2.7 W/m^{2}k.

Properties	The glass panel with VO_2 nanoparticles coated of glazing A		The glass panel with W-doped VO_2 film coated of glazing B		6mm single panel of glazing C
	Cold state	Hot state	Cold state	Hot state	
Transition temperature (T_t)	~ 40°C		20°C		
	Start at 36°C, complete at 44°C		Start at 16°C, complete at 24°C		
Solar transmittance (T_{sol})	0.69	0.57	0.44	0.39	0.78
Visible transmittance (T_{vis})	0.63	0.60	0.39	0.39	0.88
Solar reflectance	0.05	0.06	0.18	0.20	0.08
Solar absorptivity	0.26	0.37	0.38	0.42	0.14
Front & back side emissivity	0.84	0.84	0.84	0.84	0.84

Table 1. Properties of two typical VO_2-based TC glazing [3,4,8].

Simulation Set Up

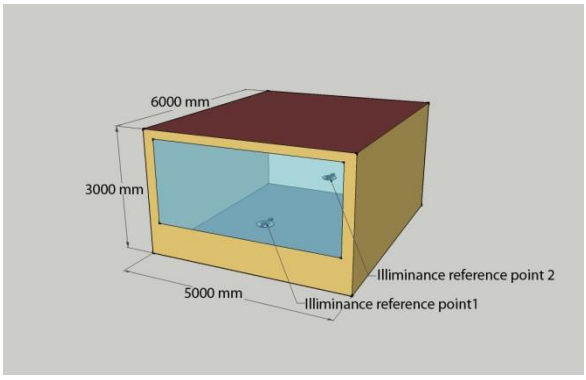

Fig. 1. Dimensions of the selected office room where three types of glazing were installed

Previous studies have indicated that EnergyPlus is promising software for building energy simulation and is also suitable to evaluate the performance of smart windows. Therefore, EnergyPlus was chosen in this work. One mid-floor common office room in a multi-story office building was selected and developed in EnergyPlus, where three types of glazing were

studied respectively. The internal dimensions of this office room are 6m×5m×3m, with a southern facing window and window-to-wall ratio of 60%. It is assumed that the adjacent rooms to this selected room were under the same environmental conditions, therefore, there is no heat transfer through the internal walls, ceiling and floor but only the southern external wall with U-value of 0.18. [5] According to the ASHRAE90.1-2010 energy efficiency code, the following parameters were used in the simulation: 1) Occupant density was defined as 18.6m^2/person, 2) loads of office equipments were 13W/m^2, and 3) lighting loads were 9W/m^2. Working Schedule for occupants, equipment and lighting was defined from 9:00am to 5:00pm on weekdays, and HVAC follows the same schedule. For the HVAC system, the setpoint temperature for heating is 21°C and 24°C for cooling. Continuous dimming mode of artificial lighting was also applied in the simulation to evaluate the energy saving potential of TC windows. With that, the lighting can be dimmed to meet the setpoint illuminance level of 500lux. Two illuminance reference points were set as detect sensors at distance of 1m and 5m from the window and with a height of 0.8m above the floor, respectively.

Three different climatic conditions shown in Table 2 representing cold (Harbin), mild (London) and hot (Guangzhou) weather were used for the building energy simulation. Heating and cooling degree hours for each climate are illustrated in Fig. 2. From Fig. 2 it can be seen that in London, heating is almost required throughout the year, but cooling is rarely needed in the summer months. In Harbin, substantial heating is required in winter (over 15000 degree hours in Jan, Feb and Mar respectively), and there are also over 1500 cooling degree hours in summer months. There is no heating requirement in Guangzhou, but the large cooling load is required.

Cities	London		Harbin		Guangzhou	
	summer	winter	summer	winter	summer	winter
Monthly Average temperature (°C)	17	4	22	-18	28	14
Solar radiation intensity (Avg hourly) W/m^2	433	220	442	540	360	262
Location	51.15°N, 0.18°W		45.72°N, 126.68°E		23.13°N, 113.32°E	
Features	Cool winter, warm summer		Cold winter, hot summer		Warm winter, hotsummer	

Table 2. Meteorological data of three representative climates

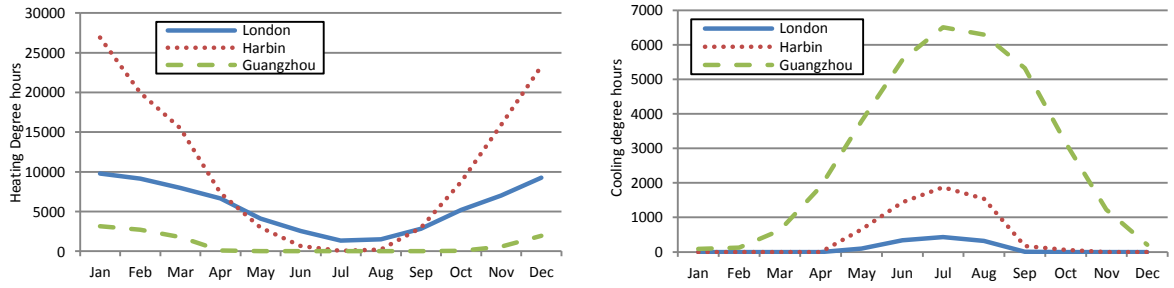

Fig. 2. Heating hours at 18 °C (left) and cooling hours at 20 °C (right) of three different climates

RESULTS AND DISCUSSION

Thermal Performance of TC Glazing Applied

In this selected typical office room, there will be a large solar heat gain through windows, due to the large window-to-wall ratio. The large window will contribute to the cooling load in summer, but might reduce the winter heating load, due to the passive heating. Indoor room temperature, heating and cooling loads are the most suitable parameters to reflect the influence of the TC window on building thermal performance. In addition, the indoor and outdoor temperature will also affect the window temperature, thus it might affect the tinted total hours of the TC window. Therefore, the simulation consists of two parts to discuss above window and building performance: HVAC off simulation mode and HVAC on simulation mode that maintains the indoor temperature between 21 and 24°C during occupied time.

Firstly, indoor thermal comfort was studied under HVAC off state. The window temperature and the transmitted solar radiation through a window of consecutive three summer days in London are shown in Fig. 3 and Fig. 4, respectively. From the Figures, it can be seen that there is a sharp decrease of the solar radiation through glazing A around 12:00 on each day, it is because that the temperature of glazing A is over the transition temperature (starting at 36°C) at that time. While there is a gradual decrease of it for glazing B, due to the lower transition temperature (starting at 14°C) of glazing B. TC windows A and B both reduce indoor room temperature during daytimes, compared with the standard double glazing C, due to the reduced solar heat gains through windows. Glazing A reduces the average room temperature by approximately 1°C, while it is reduced by approximately 3°C by glazing B. This means that both TC windows perform better than normal double glazing in summer, and TC glazing B is more effective to reduce solar heat gains. Over 40% and 50% of the transmitted solar heat gain is reduced by glazing A and glazing B, respectively, when compared with reference glazing C.

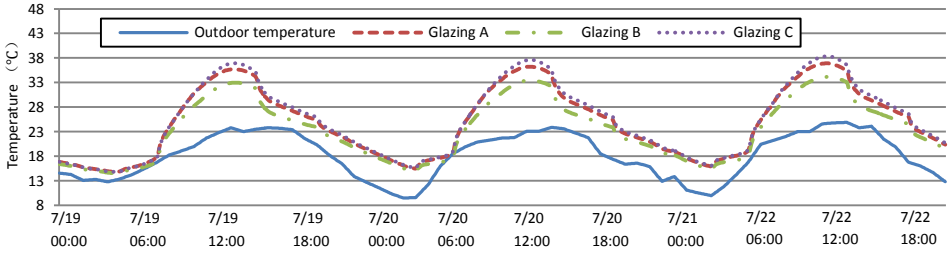

Fig. 3. Indoor temperature varies with different glazing installed.

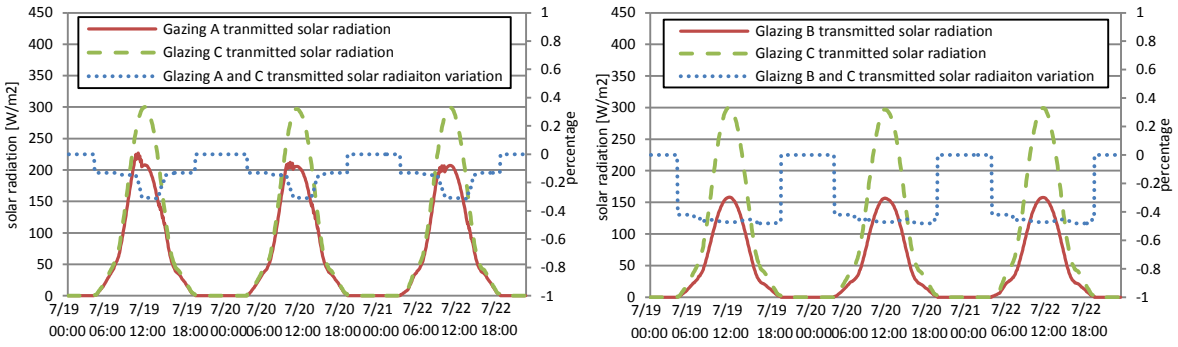

Fig. 4. Transmitted solar radiation of glazing A (left) and B (right) compared with glazing C in London summer days

The indoor annual total comfort hours and glazing tinted hours (hours when TC glazing in hot state) at different climatic conditions are shown in Fig. 5 In London, the office with glazing A has slightly more thermal comfort hours compared with glazing C. A reduction of approximately 10% in comfort hours is observed when glazing B is applied. This is because glazing B has a lower transition temperature, which has blocked a significant amount of solar heat gains during cooler seasons. In Harbin, there is no significant difference in comfort hours when these three types of glazing are installed. It might be because Harbin has a short summer, but a long cold winter. Although glazing A and glazing B both perform better than glazing C during summer, due to reduced transmitted solar radiation of their TC glass panels even at cold state, there is a decrease of comfort hours during winter. In Guangzhou, glazing A is outstanding for improving the comfort hours by 9.7% and glazing B also induces a significant increase of it. It means that, generally in terms of improving thermal comfort level, TC windows are more suitable for climates with hot summer and warm winter such as Guangzhou. It can be seen from the tinted hours points illustrated in Fig. 5, glazing B has more tinted hours than glazing A for each climate, which indicates that even in winter, glazing B can still be tinted and cause unnecessary reduction of solar heat gains through windows.

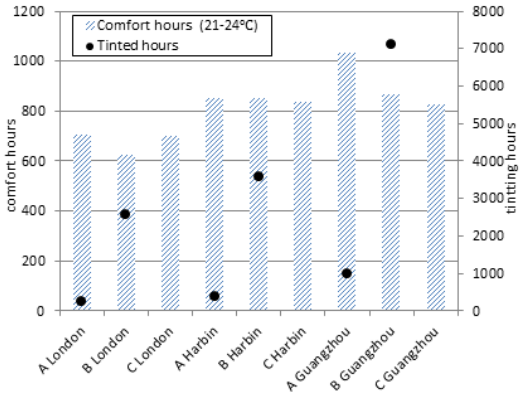

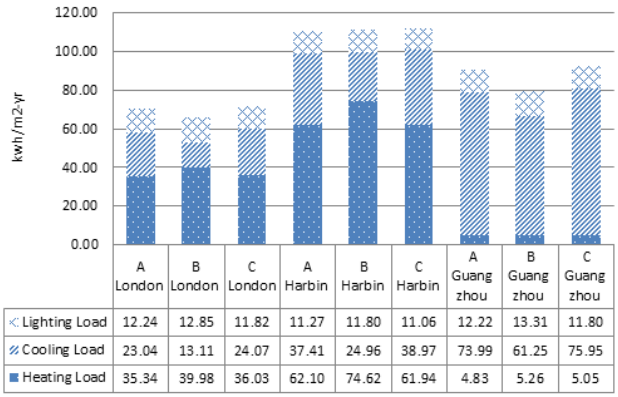

	A London	B London	C London	A Harbin	B Harbin	C Harbin	A Guang zhou	B Guang zhou	C Guang zhou
Lighting Load	12.24	12.85	11.82	11.27	11.80	11.06	12.22	13.31	11.80
Cooling Load	23.04	13.11	24.07	37.41	24.96	38.97	73.99	61.25	75.95
Heating Load	35.34	39.98	36.03	62.10	74.62	61.94	4.83	5.26	5.05

Fig. 5. (left) Comfort hours and tinted hours of glazing A, B and C in different climates
Fig. 6. (right) Comparison of heating, cooling and lighting load in three typical climate. HVAC schedule: weekday deadband is 21-24°C

With simulation under HVAC on mode, energy consumption for heating and cooling as well as lighting influenced by TC windows is shown in Fig. 6. Generally, TC glazing A and B both reduce building total energy consumption compared with normal glazing C to a different extent. Especially in London and Guangzhou, glazing B induces 10% and 15% of energy saving per year respectively. It can be seen that glazing B results in an obvious decrease of cooling load and increase of heating in all three climates. And glazing A has not shown an apparent benefit on energy saving compared with normal double glazing, because of the relatively high T_t that rarely achieved. In Harbin, the cooling load is reduced by TC glazing, however, this energy saving is counteracted with increase of heating load caused by lower solar heat gains, which results in almost no change of energy consumption in total. However, considering the practical situation, few cooling devices are used in London because summer is not so hot and few heating devices are used in Guangzhou due to its warm winter. Reducing cooling load in hot climate by TC windows is more significant. Additionally, lighting loads only increases slightly because of relatively low T_{vis} of TC glazing A and B by about 1 kWh/m^2 per year.

Visual Comfort of TC Glazing Applied

When simulations are under HVAC off mode, taking glazing A as an example, the illuminance levels of reference point1 (1m away from window) and point 2 (5m away from window) were studied under three consecutive summer days and are shown in Fig. 7. It can be seen that compared with normal glazing, TC glazing A results in a delay of achieving 500lux (visual comfort threshold value) of point 2 and a reduction of the peak illuminance value of point 1 by over 50%, which means that because of lower solar transmittance, TC glazing provides better daylighting and therefore would reduce energy consumption for shading potentially.

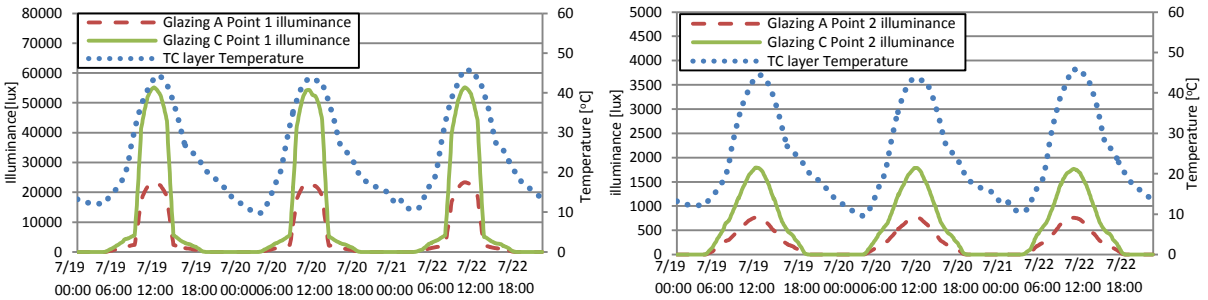

Fig. 7. Illuminance plot of point 1 (left) and point 2 (right) in three summer days

The Useful daylighting Index (UDI), a dynamic daylight performance indicator, was applied to estimate indoor visual comfort. By considering realistic climatic conditions and variables in the time, the UDI is based on work plane illuminance and is defined on hour basis absolute values of daylight illuminance. It aims to determine when daylight levels are suitable for the

occupants. When illumiance <100lux, it is too dark for occupants, however, when illumiance >2000lux, it is too bright. Both are able to cause visual discomfort. Occupants can tolerate UDI 100-500lux, and feel very comfortable with UDI 500-2000lux [9]

In Table 3, the percentages of daytime hours among one year when each UDI metric was achieved are presented. It is obvious that both of glazing A and glazing B improve the percentage of UDI reaching 100-500lux and 500-2000lux compared with normal glazing. In addition, they also reduce the percentage of UDI>2000lux. In London, up to 15% of UDI 500-2000 is increased by glazing B, and 8% by glazing A, which is the most effective increase. It means that TC windows are able to improve visual comfort and reduce the risk of discomfort daylighting glare.

UDI	London			Guangzhou			Harbin		
Illumiance [lux]	Glazing A	Glazing B	Glazing C	Glazing A	Glazing B	Glazing C	Glazing A	Glazing B	Glazing C
<100 (insufficient)	3%	6%	2%	5%	7%	3%	0.9%	2%	0.3%
100-500 (tolerable)	13%	17%	11%	13%	18%	12%	10%	11%	7%
500-2000 (comfort)	28%	35%	20%	30%	33%	24%	17%	26%	13%
>2000 (discomfort)	56%	42%	67%	52%	42%	61%	72%	61%	79%

Table 3. UDI of illuminance at reference point1 with glazing A, B and C installed in three climates, respectively.

CONCLUSION

The performance of a common mid-floor office room installed with practical TC glazing A (VO_2 nanoparticles), glazing B (W-doped VO_2 film) and reference glazing C was studied with the building simulation software EnergyPlus. From the results, the following conclusions can be obtained, 1) Both types of TC glazing can improve indoor thermal comfort by reducing solar heat gains through windows in the hot season and improve comfort hours up to 9.7% for VO_2 nanoparticles in Guangzhou, while low T_t might cause indoor heat gain reduction in the cooler seasons and therefore increase the building heating loads. 2) Although the cooling load in summer is reduced, the heating load in winter increases simultaneously. This indicates that both types of TC glazing would be suitable to be used in climates with hot summer and warm winter without the requirement of heating loads. 3) Both types of TC glazing can improve indoor visual comfort and reduce the risk of glare, and glazing B shows a better performance because of relatively lower T_t that is easy to be reached, although lighting loads increase slightly. The feedback this research gives on the application of two types of potential TC glazing installed in an office room may provide guidance for the utilization of TC windows in the future.

ACKNOWLEDGEMENTS

This work was supported by the Faculty of Engineering, University of Nottingham through a PhD studentship to Runqi Liang.

REFERENCES

1. Hong, Y., Xianchun, M., Bin X.:Theoretical discussions of perfect window, ideal near infrared solar spectrum regulating window and current thermochromic window. Energy and Buildings, 49, 164–172, 2012
2. P, H., et al.: Preparation and thermochromic property of VO_2/mica pigments, Materials Research Bulletin, 46 (6) 966–969. 2011
3. Ivan P. P. et al.: Atmospheric pressure chemical vapour deposition of thermochromic tungsten doped vanadium dioxide thin films for use in architectural glazing. Thin Solid Films, 517, 4565–4570, 2009.
4. Shuyi, L.: VO_2-based Thermochromic and Nanothermochromic Materials for Energy-Efficient Windows: Computational and Experimental Studies. Digital Comprehensive Summaries of Uppsala Dissertations from the Faculty of Science and Technology, 1095, 2013.
5. ANSI/ASHRAE/IES Standard 90.1-2010, Energy Standard for Buildings except Low-Rise Residential Buildings.
6. Hong, Y, Linshuang L. : Smart or not? A theoretical discussion on the smart regulation capacity of vanadium dioxide glazing. Solar Energy Materials & Solar Cells, 120, 669–674, 2014.
7. Manfredi, S. et al.: Energy modelling studies of thermochromic glazing, Energy and Buildings, 42, 1666–1673, 2010.
8. Yanfeng, G. et al.: Nanoceramic VO_2 thermochromic smart glass: A review on progress in solution processing. Nano Energy, 1, 221-246, 2012.
9. Michela, B. et al.: Energy saving through the sun: Analysis of visual comfort and energy consumption in office space. Energy Procedia 30, 693-703, 2012

THE DESIGN OF A DECENTRALIZED VENTILATION SYSTEM FOR AN OFFICE IN SINGAPORE: KEY FINDINGS FOR FUTURE RESEARCH

A. M. Rysanek[1], P. Murray[2], J. Pantelic[1], C. Miller[1], F. Meggers[3], M. Mast[2]; A. Schlueter[1]

[1]*Institute of Technology in Architecture, ETH Zurich, Schafmattstrasse 32, 8093 Zurich, Switzerland*
[2]*Singapore-ETH Centre Future Cities Laboratory, 1 CREATE Way, Singapore 138602*
[3]*Andlinger Center for Energy and Environment, Princeton University, B301 Engineering Quadrangle, Princeton, New Jersey, 08544*

ABSTRACT

In this paper, we present what was learned in the research & design process of a decentralized ventilation system with chilled ceilings for a commercial office in Singapore. We make two key observations from the knowledge gathered. First, we observe, in quantitative terms, that present-day radiant cooling panel products may not provide sufficient sensible cooling capacity for commercial offices in hot and humid climates. However, upon considering the use of passive chilled beams as an alternative chilled ceiling product, we do observe that a decentralized ventilation system comprising both recirculating and dedicated outdoor air fan coil units may reduce daily electricity requirements for air-conditioning in Singaporean office spaces by over 15%.

Keywords: decentralized ventilation, radiant cooling, chilled ceilings, commercial buildings, hot and humid climates

INTRODUCTION

In the pursuit of furthering empirical research on the comparison between centralized and decentralized air-conditioning and mechanical ventilation (ACMV) systems [1], a new research project is underway in Singapore in which a 550 m^2 office will be designed by researchers in collaboration with professional partners and fit-out with a prototype decentralized ACMV system similar to the system previously evaluated by Meggers et al. [2]. The system will couple decentralized ventilation units - configured to provide primarily latent cooling - with a high-temperature chilled ceiling system for sensible cooling. Learning from the design phase of this project has allowed for the establishment of some design principles on the adaptation of decentralized ACMV systems for, at least, persistently hot and humid climates. Some of these principles are to be explored in this paper under the context of the pilot implementation project, such as:

- evaluating the applicability of chilled ceiling technologies for hot and humid climates; and
- simulating the performance of various state-of-the-art decentralized ventilation systems and discussing some of their benefits and drawbacks.

1.1 The case study building area

The project implementation area fits within a larger, four-storey, 20,000 m^2 multi-purpose building under construction in Singapore at time of this writing. A provisional floor plan is shown in figure 1. The entire building, including the project area, has been designed to achieve Singapore's "GreenMark Platinum" accreditation status[1]. The main implication of this for the current analysis is that the indicated façades in figure 1 are targeted to yield a net heat gain coefficient[2] no more than 40 W/m^2 at any time of year. Not indicated in the figure is that the floor-to-ceiling height for the project implementation area is 4.0 m.

In predicting total sensible cooling loads for the project space, three interior zones are isolated and described further in figure 1: a private office located adjacent to a façade, a centrally-located open office area, and a boardroom that can also serve as an auxiliary office. Design conditions for internally- and externally-driven heat gain parameters are provided by the project's local engineering consulting team[3]. The design thermal comfort conditions of the office space is 24 °C and 50% relative humidity when occupied. This results in a targeted indoor dew-point temperature of 14.5 °C.

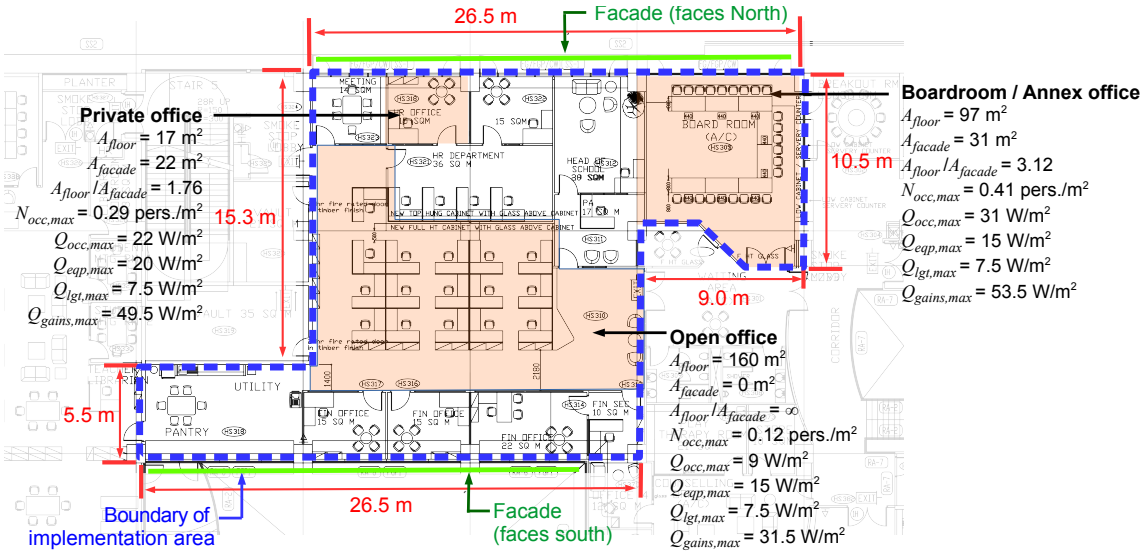

Figure 1: Provisional floor area of implementation area for pilot project in Singapore; a 550 m^2 area on a single floor within a four-storey 20,000 m^2 multipurpose building

2 ON THE APPLICABILITY OF CHILLED CEILING TECHNOLOGIES FOR SENSIBLE COOLING IN SINGAPORE

During the research and design phase of the pilot project, it was planned to identify a radiant cooling panel product that would satisfy the entire sensible cooling energy load of the project implementation area. Doing so would provide an opportunity to achieve significant improvements to chiller plant efficiency in the long-term. As the sensible cooling delivered by chilled ceilings could be achieved using chilled water at relatively high temperatures, it would become feasible to implement, in the future, a low-lift chiller with COP exceeding 9-10 [3].

[1]For more information, see `http://www.bca.gov.sg/greenmark/green_mark_buildings.html`

[2]including convective infiltration gains, solar radiative heat gains, and conduction gains

[3]peak occupant density and electrical appliance layout is predicted directly from the interior floor plan (75 W/person sensible heat gain assumed for human occupants), LED lighting assumed throughout with power density of 7.5 W/m^2

However, an interesting caveat was encountered when assessing the applicability of radiant panels to this project. Figure 2 has been produced to elaborate on this. It was generated upon a study of several commercial products available in the radiant cooling and passive chilled beam market[4]. The vertical axis of the figure provides the maximum permissible floor-to-façade area ratios for a given chilled ceiling technology and heat gain conditions, both internally- and externally-generated. When this figure was compared against the three building zones identified in figure 1, it was found that only the open office area would have been suitable for radiant panels. The private office and board room could only be sensibly cooled with passive chilled beams, comparatively larger devices in terms of equipment height.

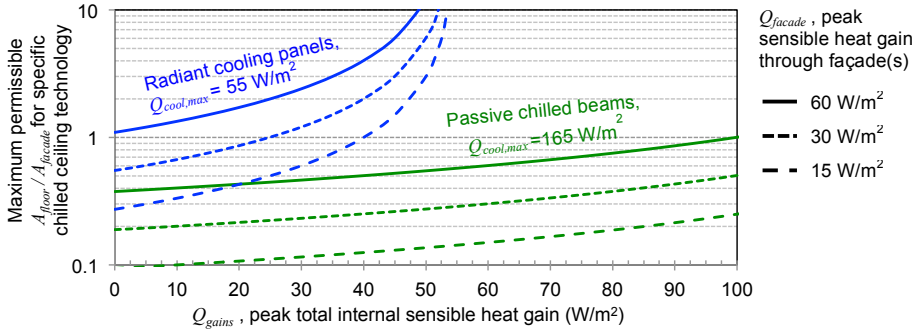

Figure 2: Maximum permissible "floor-to-façade" ratio for total sensible cooling demand to be met by chilled ceiling technology; assumes indoor air conditions of 24.5 °C, 55% relative humidity, and 17.5 °C water supply temperature for chilled ceiling system

What makes this finding interesting is that the design conditions facing the project space are not particularly unique for Singapore. In fact, deliberately optimistic, or low values for interior and exterior heat gains were targeted due to the overall design objectives of the project (i.e., to achieve Singapore GreenMark Platinum status). Thus, to make the project area applicable for radiant panels, it seems it would have been required to broadly reconfigure the interior layout of the project space and more-or-less combine all spaces into a single large open area. Alternatively, it could have been proposed to lower the design supply water temperature of the chilled ceiling panels, thereby increasing their cooling capacity. However, this would have required a reduction to indoor air humidity set-points, in order to avoid surface condensation, resulting in a penalty on energy consumption given Singapore's persistently humid climate. Thus, in lieu of these findings, it was decided to employ passive chilled beams of the type assessed in figure 2.

An expansion of this analysis is warranted, particularly on the general choice between radiant ceiling panels and passive chilled beams. For instance, it's notable that the former are applicable to both heating and cooling applications, whereas the latter are cooling-specific.

3 COUPLING OF CHILLED CEILING SYSTEM WITH DECENTRALIZED VENTILATION UNITS

Whilst the chilled ceiling system is intended to satisfy the majority of sensible cooling energy demand, a mechanical ventilation system is required to satisfy fresh air require-

[4]Products reviewed: ECOPHIT Activation Board (http://www.ecophit.com), REHAU Akustikkuhldecke mit Lochbild 6/18 R (http://www.rehau.com), and TROX PKV (http://www.trox.de)

ments and latent cooling loads. In keeping to the decentralized approach sought by this work, a system configuration was chosen in line with the illustration of the project area's boardroom shown in figure 3. For each interior zone in the project area, displacement ventilation would be provided from a mixture of airflow supplied by two decentralized ventilation units installed in the nearest façade sections. Form factor constraints on the integration of ventilation units in the façade played a significant role in the selection of candidate ventilation unit products - the cross-sectional dimensions of any ventilation unit could not exceed 600 mm x 600 mm.

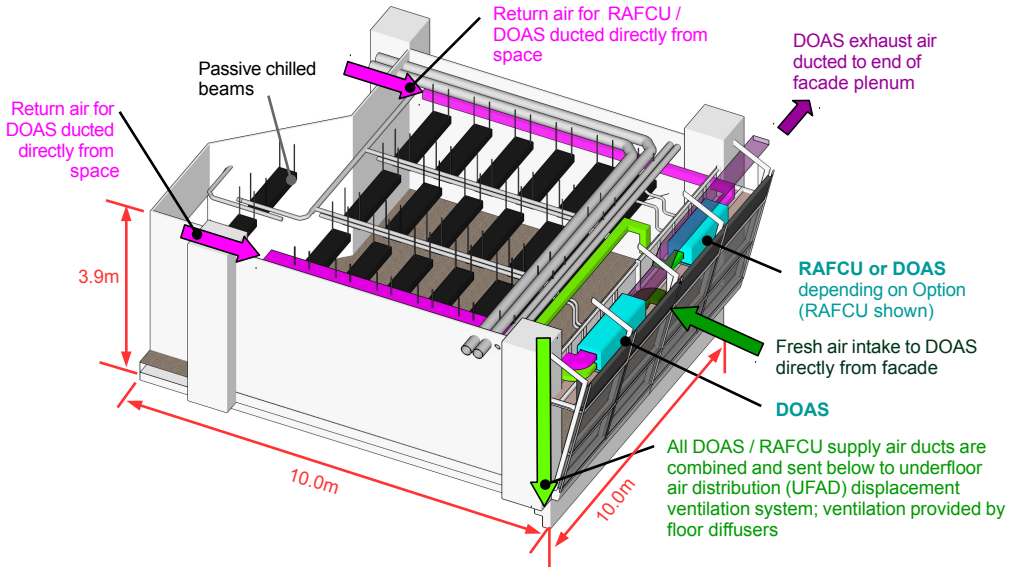

Figure 3: Overview of boardroom zone within project area with chosen decentralized ACMV configuration

Another constraint on the selection of ventilation units was the requirement for passive forms of reheat in order to satisfy minimum supply air temperature requirements for the displacement ventilation system. Active reheat, via heating cools, is prohibited in Singapore, yet supplying untreated off-coil supply air through floor diffusers could lead to thermally uncomfortable conditions for occupants. Hence, two candidate decentralized ventilation units were chosen for analysis: 1) a dedicated outdoor air system (DOAS) with integrated energy recovery wheels; 2) a fan coil unit with integrated heat pipe that could serve in either DOAS or 100% recirculated air (RAFCU) mode. From this, we identified four plausible system configurations: 1) a 100% outdoor system provided by two heat-pipe fan coil units operating in DOAS model, 2) the same approach but using wheel-based DOAS units, 3) a mixed system of heat pipe fan coil units where one unit serves as a DOAS and a second as an RAFCU, and 4) the same approach although replacing the heat pipe-based DOAS with a wheel-based DOAS. These options are respectively identified by systems A to D in figure 4. Steady-state system performance specifications of identified commercial products are also provided.

More information about the theoretical performance of the wheel-based DOAS units can be found in Mumma [4]. Of the configurations shown in figure 4, it should be noted that the gross fan power of the wheel-based DOAS units is much higher the fan coil units, even under the same rated air flow rates. This is attributed to the high pressure drop induced across the unit's recovery wheels as well as the narrow flow channels permitted for supply and return air streams due to the form factor of the unit.

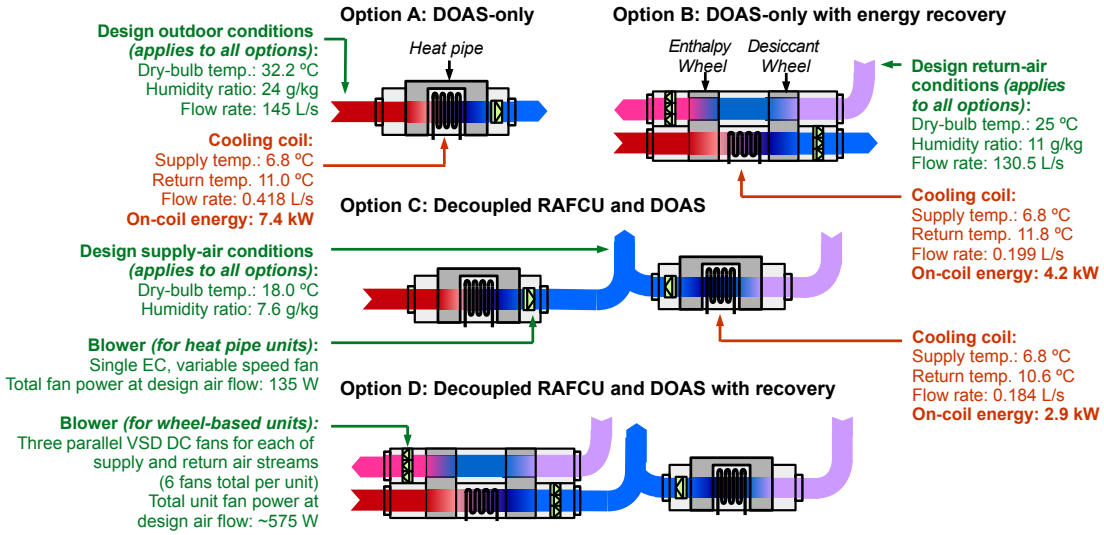

Figure 4: Possible configurations for decentralized ventilation systems coupled with chilled ceilings

Regarding the system's control logic, two approaches have been considered. For Options A and B, it's assumed a 2-stage control logic is employed. During normal operation cycles: 1) the DOAS is operated at whichever minimum flow rates (air and water) achieve both latent cooling and fresh air requirements; 2) the passive chilled beam network operates at whichever minimum chilled water flow rate and temperature required to satisfy sensible cooling requirements and avoid condensation. For Options C and D, a 3-stage priority control logic is employed. During normal operation cycles: 1) the DOAS system is operated at whichever minimum flowrate satisfies fresh air requirements, 2) the RAFCU operates at whichever minimum flowrate satisfies latent cooling loads not met by the DOAS, 3) the passive chilled beam network operates as above to satisfy remaining sensible cooling loads.

In Rysanek et al. [5], a TRNSYS simulation was developed for predictive performance evaluation of the ventilation system's thermodynamic components and control logic. That study evaluated a single control zone, the board room shown in figure 3, and compared the performance of Option D with a conventional centralized air handling system. In figure 5, we present results of an expanded TRNSYS simulation of Options A, B, and C undertaken for this study. It illustrates daily average electrical energy requirements for operation of the entire ACMV system, barring pumps for the low-temperature chiller plant. A constant, central chiller COP of 4 was used for all conversions of on-coil energy to electrical energy.

On review of the net simulation results in figure 5, it was decided to adopt Option D for the implementation project. We view its predicted performance to be attributed to the system ensuring outdoor air is introduced to conditioned spaces only when needed for indoor air quality, and recovers enthalpy from the exhausted air stream when doing so. We also observe that, in comparison to the central air handling system, the decentralized system provides improved controllability of indoor air, humidity, and dry-bulb temperatures, ensuring that neither property is over-satisfied. However, as with our analysis of chilled ceiling technologies, these are preliminary findings that warrant further analysis.

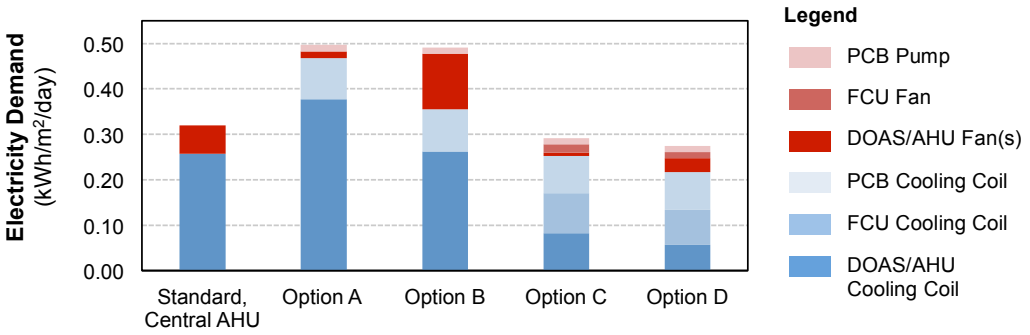

Figure 5: Estimated average daily electricity requirements for assessed decentralized ventilation options

4 CONCLUSIONS

In a brief study, we have examined a few technical aspects of the adaptation of chilled ceilings and decentralized ventilation units for hot and humid climates. The backdrop for this analysis has been the design process undertaken for the fit-out of a real-world office in Singapore with such a system. Many of the preliminary findings in this paper warrant further study, much of which will be conducted empirically in the pilot project area over the coming years. Nevertheless, in the conducted performance simulation, with results shown in figure 5, it was found that a decentralized ventilation system which couples small packaged outdoor-air fan coil units, recirculated-air fan coil units, and a chilled ceiling, could reduce total daily electricity consumption for air-conditioning use by at least 15% in a commercial office space in Singapore.

REFERENCES

1. Baldini, L. *Advanced Building Ventilation System Based on the Paradigms of Decentralization and Exergy Minimization Using a Highly Interlaced Network Structure for the Supply and a Sensorbased Local Control Approach for the Exhaust.* Doctoral Thesis, ETH Zrich, Zurich, Switzerland, 2009.

2. Meggers, F., Pantelic, J., Baldini, L., Kuen Kim, M., and Saber, E.: Evaluating and adapting low exergy systems with decentralized ventilation for tropical climates. *Energy & Buildings*, 67:559–567, 2013.

3. Armstrong, P. R., Jiang, W., Winiarski, D., Katipamula, S., Norford, L. K., and Willingham, R. A.: Efficient Low-Lift Cooling with Radiant Distribution, Thermal Storage, and Variable-Speed Chiller ControlsPart I: Component and Subsystem Models. *HVAC&R Research*, 15(2):366–400, Mar. 2009.

4. Mumma, S. A.: DOAS and Desiccants. *Engineered Systems*, pages 37–42, 2007.

5. Rysanek, A., Murray, P., Miller, C., Pantelic, J., Mast, M., and Schlueter, A.: Simulation analysis of a low-exergy decentralized air-conditioning system for hot and humid climates. In *14th International Conference of the International Building Performance Simulation Association (IBPSA)*, Hyderabad, India. IBPSA, in review.

THERMAL AND OPTICAL ANALYSIS OF A NOVEL GLAZING FAÇADE SYSTEM WITH PARALLEL SLATS TRANSPARENT INSULATION MATERIAL (PS-TIM)

Y Sun; Y Wu; R Wilson; Z Zhu.

Department of Architecture and Built Environment, The University of Nottingham, Nottingham, NG7 2RD, UK

ABSTRACT

With the increase of the awareness of sustainability in the built environment, it has never been stopped to continuously improve the performance of glazing façade systems leading to indoor comfortable and building energy conservation. An innovative façade system where parallel transparent plastic slats are sandwiched in between two glass panes to form a Transparent Insulation Material (PS-TIM) structure is proposed to effectively reduce the coupled convective and radiative heat transfer, therefore increasing the thermal resistance of the façade, meanwhile keep sufficient sunlight penetrating into rooms. A numerical investigation of the thermal and optical performance of this PS-TIM façade were conducted and presented in this paper. The detailed modelling of the thermal characteristics of the PS-TIMs was undertaken using a finite volume Computational Fluid Dynamic (CFD) package FLUENT while the optical simulation is realised by a commercial ray-tracing tool TracyPro. The thermal numerical model was validated with previously published experimental measurements. The CFD predictions show that: an aspect ratio of *A=0.35* can provide full suppression in convection; the PS-TIM structure can reach *35%-46%* reduction of thermal conductance compared with standard double glazing at the same size with no slat installed in the air cavity; In addition, the trade-off analysis between *U-value* and light transmittance at various solar incidence angles have also been investigated. The results provide a better understanding of the benefits of parallel plastic slats Transparent Insulation Material (PS-TIM) in energy saving and also leads to better designs of glazing façade systems.

Keywords: parallel plastic slats Transparent Insulation Material (PS-TIM), Computational Fluid Dynamic (CFD), building simulation, heat transfer, optical performance

1. INTRODUCTION

Since the 60s in the last century, glass has become the most popular façade material for buildings. With the increase of the awareness of sustainability, people paid more attention to improve the poor thermal insulation property of glazing façade. A Transparent Insulation Material (TIM) structure, which is sandwiched in a double-glazed unit, is proposed to reduce the heat transfer through the glazing unit more effectively and meanwhile keep sufficient sunlight penetrating into rooms. The parallel slats structure of TIM (perpendicular TIM) is the most suitable structure for window application and thus selected in this research. As shown in Figure 1 (a), the structure walls that are vertical to glazing panes divide the whole air gap into small cells. These walls provide additional viscous resistance to the onset of free convection and meanwhile interfere the thermal radiation transferred from one side to the other. Therefore, the employment of a well-designed perpendicular TIM structure can effectively reduce the heat transfer coefficient of a double-glazing unit. In the past decades, the thermal behaviours of perpendicular TIM have been researched numerically and experimentally, but most of the studies are focused on their application in solar collectors [1-3]. However, when TIMs are vertically applied for windows or glazing façades, their thermal and optical performances are entirely different but were rarely studied. To address the gap, the work

presented in this paper details the optical and thermal analysis of parallel plastic slats TIM (PS-TIM) structures that were sandwiched in between two glazing panes. A two-dimensional model was developed in the commercial CFD package FLUENT to comprehensively explore the convective, conductive and radiative heat transfer that occurs in the double glazing air cavity with and without parallel slats structure. The Nusselt number, which represents the ratio between the pure conduction resistances to a convection resistance, is used to indicate the intensity of convection. Finally, the *U-value* was calculated and ray-tracing technique was used to analyse the optical transmittance under different solar incidence angles.

2. METHODOLOGY

Schematic diagrams illustrating the geometry of a double-glazing unit with and without a PS-TIM structure are shown in Figure 1 (b) and (c), respectively. A double-glazing unit with an air gap of *15mm* width and *300mm* length was researched by adding 4 different geometries of PS-TIM structure (four different interval distances between the parallel slats). The interval distance, which is D_a, varies from *3mm*, *5mm* to *7.5mm* and *10mm*.

Two-dimensional finite volume models were developed in the commercial CFD package FLUENT. To simplify the CFD simulation process, the following assumptions were made: 1) the internal surfaces of the left and right glass panels were set as two isothermal walls with different temperatures to represent the temperature difference between indoor and outdoor environments, while the top and bottom ends were assumed to be adiabatic; 2) the enclosure was filled with air with $Pr = 0.71$, all thermophysical properties (e.g. ρ, C_p, k) of the fluid were assumed to be constant [4-6], except for the fluid density and viscosity, which varies with temperature. The flows in the vertical cavity or cells remain laminar, because the Grasholf Numbers never reach the related critical value [7].

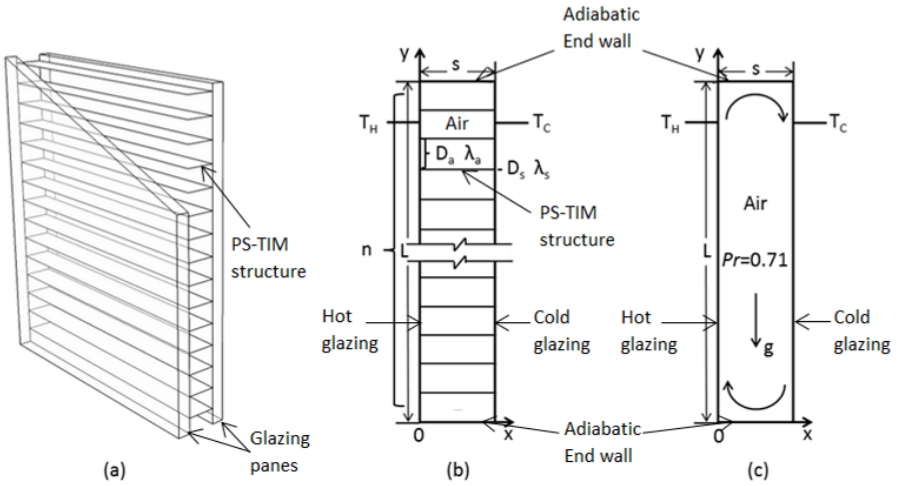

Figure 1: (a) PS-TIM structure in a double-glazing (b) 2D schematic diagram illustrating the geometry of the air gap with PS-TIM structure (c) 2D schematic diagram illustrating geometry of air gap without PS-TIM structure

In order to evaluate the effect of parallel slats structure on the convection, the radiative heat transfer between the two glazing panes was separated initially. It was only included when calculating the overall performance of the heat transfer through the air cavity and the *U-value*. The discrete ordinates (DO) radiation model was used to solve the radiative transfer equation.

Four temperature differences between the two glazing panes (*10K*, *20K*, *30K* and *40K*) were set as the boundary conditions, but the mean temperature of the two isothermal surfaces was kept at 10^oC. And in order to provide a more accurate consideration of the boundary layers,

the mesh size was defined as smaller near the boundaries (*0.025mm×0.025mm*), and then gradually increased toward the centre. Extensive mesh independent studies were undertaken. Iterative convergence was achieved when the normalized residuals were less than 10^{-3} for the continuity, and 10^{-7} for the energy and momentum equations.

The module validation was undertaken using the experimental date published by Lee and Korpela [8]. The simulated results well matched, as the percentages of difference of the Nusselt numbers in the same Grashof numbers were less than *4%*.

The estimated result of local convective heat flux and combined convective and radiative heat flux were calculated from the converged temperature field. The results of convective heat flux at the boundaries were used to express the local Nusselt number (*Nu*) as follows:

$$Nu = \frac{(\frac{\partial T}{\partial x})_w s}{\Delta T} = \frac{qs}{\lambda_a \Delta T} \quad (1)$$

where $(\frac{\partial T}{\partial x})_w$ is the air temperature gradient on the wall and q(W/m^2) is the average convective heat flux that transfers across the two surfaces. ΔT(K) is the temperature difference between the hot and cold surfaces.

3. RESULTS AND DISCUSSION

In this section, the simulation results concerning the convective, conductive and radiative heat transfer of the PS-TIM structure in the double-glazing air cavity are discussed. And the overall *U-value* and optical performance of the novel PS-TIM system are presented.

3.1 Aspect ratio for convective suppression

The PS-TIM structure is proposed to suppress the convective heat transfer in the air cavity of a double-glazing unit. However, it is useful to understand the free convection that occurs in a single air cavity at various dimensions firstly to improve our understanding of the underlying convective suppression. In this section, the aspect ratio of a double-glazing units (where $A = \frac{L}{s}$ is illustrated in Figure 1(c)) and the aspect ratio of a PS-TIM cell ($A = \frac{D_a}{s}$ is shown in in Figure 1(b)) to provide convective suppression are investigated.

Figure 2 shows the relationship between the variation of the Nusselt number and different aspect ratio at different Grashof numbers of a single air cavity. The right hand side of the graph represents the performance of air cavity in a conventional double-glazing unit with the aspect ratio increase from 1 to 100. While the left hand side represents the performance of a cell of the PS-TIM structure, whose aspect ratio changes from *0.1* to *1*. It can be seen that the Nusselt number reaches the peak value when the aspect ratio is equal to *1*. This means that a shape of square provides the smallest viscous resistance to the onset of free convection. In the range of *A=1* to *100*, with the increase of aspect ratio, the Nusselt number decreases, but there is no significant difference of the Nuseelt number when the aspect ration increase from 40 to 100. This indicates that the shape of the vertical space has an important influence on the free convection until it becomes sufficiently tall. In the range of *A=1* to *100*, a high Grashof number leads to a high Nusselt number. This means that a higher temperature difference increases the convection in the cavity; therefore the convective heat transfer cannot be fully suppressed. On the other hand, the left hand side of Figure 2 shows the aspect ratio is less than 1, which means the height of the cavity is smaller than its width to create a cell in the shape of horizontal rectangle. With the decrease of the aspect ratio from *1* to *0.1*, the Nusselt

number declines sharply until it reaches *Nu=1* when *A=0.35*. This indicates that it is capable of achieving full convection suppression in the PS-TIM cell other than in the vertical slot. This is because the increased viscous resistance is along the direction of the temperature gradient in the cell while it is perpendicular to the direction in the vertical slot. Thus, the convection in the cell can be fully suppressed once the resistance is sufficiently high no matter what the temperature difference between the two panes is.

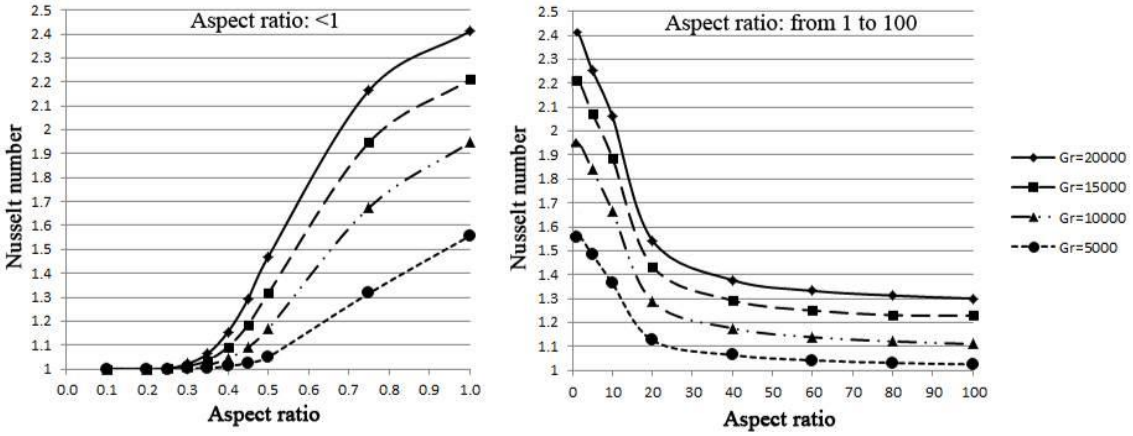

Figure 2：Relationship of the Nusselt number vs Aspect ratio for different Grashof number

3.2 The convection that occurs in the PS-TIM structures

From section 3.1, it can be seen that creating small horizontal rectangle cells leads full convection suppression within air cavity. The application of adding horizontal slats in the air cavity of a double-glazing unit to create a PS-TIM structure with small cells were further studied. Four different PS-TIM structures were analysed and also compared with no-slat cavity.

The relative average Nusselt numbers of an air cavity of a double-glazing unit with and without different geometries of PS-TIM structures (D_a*=3mm, 5mm, 7.5mm* and *10mm*) are shown in Figure 3 (left). The free convection within *3mm*- and *5mm*-cell structures is fully suppressed, when the Grashof number increases from *5000* to *20,000*, however, it increases with the increase of the Grashof number in *7.5mm*- and *10mm*-cell structures. The *3mm*-, *5mm*- and *7.5mm*-cell structures can effectively reduce the average Nusselt number and hence reduce convective heat transfer rate, when compared with the air cavity without slat at the same Grashof number. For the *7.5mm*-cell structure, though its Nusselt number increases with Grashof number, but it only reaches *1.2*. This indicates that the convective heat transfer is not significant [8]. The *10 mm*-cell structure provides less convection suppression as the average Nusselt numbers are similar to or larger than that of no-slat, this is because the viscous resistance of *10mm*-cell is less than the tall vertical air cavity of double glazing.

3.3 Thermal conductance of air gap with the PS-TIM structures

In this section, a "convective-conductive-radiative" model was used to investigate the thermal conductance (where $h = \frac{\lambda_a}{s} \cdot \frac{D_a n}{L} + \frac{\lambda_s}{s} \cdot \frac{D_s(n-1)}{L}$, see Figure 1 for symbols representation) of the air cavity with four different PS-TIM structures. The reduction in heat transfer effect is quantified by using the thermal conductance ratio $h_{PS\text{-}TIM}/h_{no\text{-}slat}$. It can be seen in Figure 3 (right), all of the four PS-TIM structures are able to provide a reduction in thermal conductance at different Gr numbers, even including the *10mm* one (which cannot provide convection suppression as mentioned in the previous section). This is because the added

interfering walls blocks the long-wave radiative heat transfer between two glazing panes caused by temperature difference. The smaller the cell's height, the smaller the thermal conductance is. The *3mm*-cell structure can reach *35%-46%* decrease of thermal conductance while a *10mm*-cell structure can reduce it by *16%-18%*. Meanwhile, for *3mm*-, *5mm*- and *7.5mm*-cell structures, with the increasing of temperature difference, the reduction rate grows. But 10mm-cell structure changes in an opposite trend. This is because 10mm-cell can only suppress the radiative heat transfer, but has a less convective thermal resistance than no-slat at higher temperature differences.

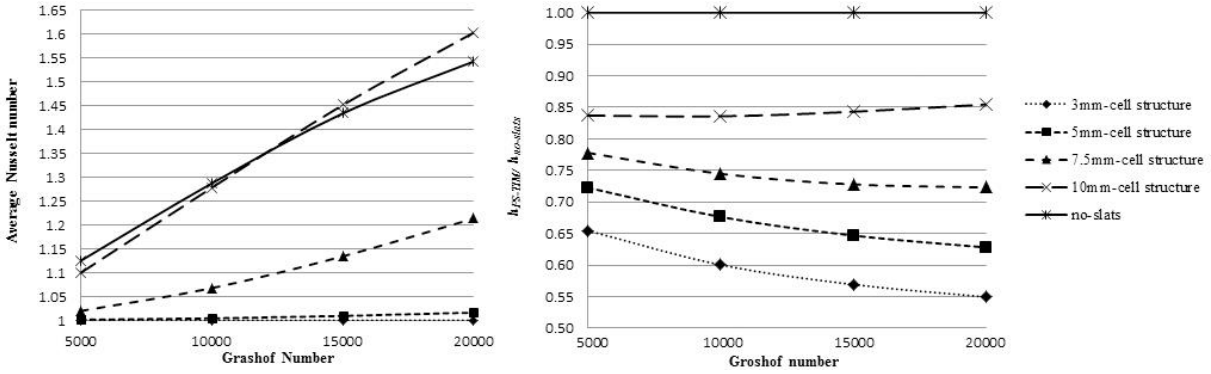

Figure 3. (left) Average Nusselt number vs Grashof numbers for different PS-TIM structure types, (right) Thermal conductance reduction of different PS-TIM structure types vs various temperature differences (D_s=0.1mm, λ_s= 0.15W/mK and ε=0.65)

3.4 An overall consideration of U-value and light transmittance of these four different types PS-TIM

The overall heat transfer between the air gaps under standard testing conditions EN 673 (i.e. temperature difference of *15K* between two panes, average panes temperature of *10°C*) was simulated by FLUENT and discussed in this section. The *U-values* of four PS-TIM structures are shown in Figure 4 (left). The ray-tracing simulation results of the transmittance of these four TIM systems at five different solar incidence angles (*15°, 30°, 45°, 60° and 75°*) are shown in Figure 4 (right).

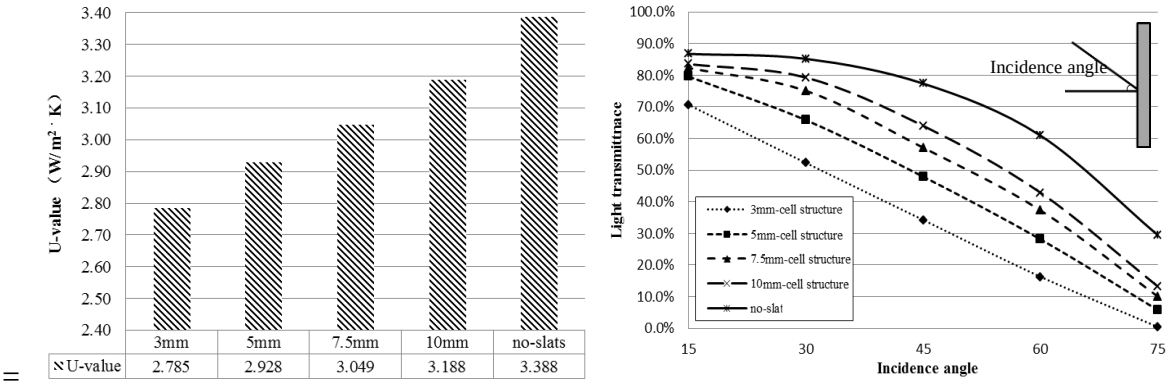

	3mm	5mm	7.5mm	10mm	no-slats
U-value	2.785	2.928	3.049	3.188	3.388

Figure 4. (left) U-value of different PS-TIM structure types; (right) Light transmittance at different incidence angles of different PS-TIM structure types

It can be seen in Figure 4, generally, adding TIM structure and reducing the slats interval distance from *10mm* to *3mm* leads to a gradually reduction of *U-value*, while this also results in a decrease of light transmittance. The *7.5mm* cells and *10mm* cells have a better light transmittance than the *3mm* and *5mm* ones. By compared with air gap without TIM structure,

they only have *5%-10%* loss of light transmittance for a low incidence altitude angle (*15°* and *30°*) and *20%* for high incidence altitude angle, and reduce the U-value by *10%* and *5%*, respectively. These systems will be able to provide sufficient daylight transmitted into room for both lighting and passive heating requirements in the wintertime (where the solar incidence angle is low). On the opposite, *5mm* and *3mm* cells have better thermal resistance, but the light transmittances drop *10%* and *20%* respectively compared with *7.5mm* cells.

Thus, for a mild climate with a small temperature difference between indoor and outdoor environment with large daylight requirement, *10mm* and *7.5mm* cells would be recommended. For climate with large temperature difference, but less daylight requirement, *3mm* and *5mm* cells may provide good insulation and a certain degree of shading.

4. CONCLUSION

A detailed research of the thermal and optical simulation of parallel slats TIM (PS-TIM) structure that has been sandwiched in two glazing panes has been conducted. The following conclusion can be obtained: 1) When the aspect ratio of a PS-TIM structure's cell is less than *0.35*, the free convection is fully suppressed despite the temperature difference between the two surface panes; 2) In practice, design a suitable interval distance of the parallel slats in the air cavity to maintain the Nusselt number less than *1.2* can provide good reduction of the convective heat transfer coefficient; 3) The results of a convection, conduction and radiation model show that a *3mm*-cell structure can reach *35%-46%* decrease of thermal conductance while a *10mm*-cell structure can reduce it by *16%-18%*; 4) An overall consideration of light transmittance and U-value has been analysed. This study will provide a general guidance for architects and engineers to apply parallel slats TIM on windows or glazing facades.

ACHNOWLEDGEMENTS

This work was supported by the Faculty of Engineering, University of Nottingham and the China Scholarship Council through a joint PhD studentship to Yanyi Sun.

REFERENCES

1. Kaushika, N.D. Padmapriya, P. Arulanantham, M. Sharma, P.K. : Transparent insulation characteristics of honeycomb and slat arrays. Energy, Vol 19 (10), pp. 1037-1041, 1994.
2. Kumar, P. Kaushika, N.D. : Convective effects in air layers bound by cellular honeycomb arrays. Journal of Scientific & Industrial Research, Vol 64, pp. 602-612, 2005.
3. Arulanantham, M. Kaushika, N. D. : Coupled radiative and conductive thermal transfers across transparent honeycomb insulation materials. Applied Thermal Engineering, Vol 16 (3), pp. 209-212, 1996.
4. Collins, M. Tasnim, S. Wright, J.: Numerical analysis of convective heat transfer in fenestration with between-the-glass louvered shades. Building and Environment, Vol 44 (10), pp. 2185-2192, 2009.
5. Avedissian, T. Naylor, D.: Free convective heat transfer in an enclosure with an internal louvered blind. International Journal of Heat and Mass Transfer, Vol 51(1–2), pp. 283-293, 2008.
6. De Giorgi, L. Bertola, V. Cafaro, E.: Thermal convection in double glazed windows with structured gap. Energy and Buildings, Vol 43 (8), pp. 2034-2038, 2011.
7. Dalal, R. Naylor, D. Roeleveld, D.: A CFD study of convection in a double glazed window with an enclosed pleated blind. Energy and Buildings, Vol 41 (11), pp. 1256-1262, 2009.
8. Lee, Y. Korpela, S. A.: Multicellular natural convection in a vertical slot. J. Fluid mech, Vol 126, pp. 91-121, 1983.

CONSEQUENCES OF GLOBAL WARMING ON THE ENERGY PERFORMANCE OF CFS WITH SEASONAL THERMAL CONTROL

Vanzo S.[1]; Kostro A.[2]; Gong J.[1]; Schüler A.[1]

1: Solar Energy and Building Physics Laboratory, École Polytechnique Fédérale de Lausanne: EPFL, LESO-PB, 1015 Lausanne, Switzerland.

ABSTRACT

Fenestrations systems play a very important role in the energy balance of a building, impacting both on thermal and visual comfort. Especially in southern regions of Europe, windows can lead to high solar gains and glare problems. Both can strongly influence energy consumption and indoor comfort. With global warming and the increase of average temperatures, overheating may particularly be a problem in a higher range of latitudes. The changes on thermal loads induced by global warming will vary depending on locations but also on the building envelope.

This study investigates the future thermal loads for heating and cooling, in order to evaluate the total energy consumption during the year. The aim is to evaluate the performance of a novel technology for glazing envelopes such as embedded microstructures, in a climate change scenario. The overall effect of the global warming on the energy demand depends on the meteorological parameters as well as on the type of building. Focusing on a well-insulated building, a microstructured glass is considered, in order to evaluate its performance at different latitudes. Meteorological data for the probabilistic future climate projections are provided by the Meteonorm database. Simulations have been performed choosing twenty-one European locations at different latitudes.

In general the analysis shows that the predicted energy consumption is growing for southern European locations, due to a relevant increase in the cooling demand. As the latitude rises, the majority of thermal loads are increasing, up to a latitude of around 53°N; from this latitude, annual loads are getting slightly lower. All over Europe, expected energy savings provided by the studied microstructured glass, in comparison with a sun protective glass, are in a range between 3% and 18%. Such Complex Fenestration Systems (CFS), compared with conventional windows, help to decrease cooling energy demand, which is expected to increase considerably in the upcoming years.

Keywords: embedded microstructures, climate change, cooling loads, relative energy savings

INTRODUCTION

Nowadays, climate change is one of the most critical phenomena. Excessive use of fossil fuels, combined with rapid urbanization and extreme soil exploitation, are the major causes of the greenhouse effect. An increase of the mean monthly temperatures has been detected in different geographical areas since the mid-twentieth century. The last decades have been marked by a global warming of the Earth with a temperature increase between 0,6°C and 0,9°C [1]. Consequently, mitigation strategies are needed in order to reduce of the global warming effect.

In the residential and commercial building sector in particular, the energy consumption could be significantly reduced by improvements in the building envelope, through reduction of heat transfers or use of energy efficient windows [2]. The fenestration system of the building has an important influence on the HVAC requirements because it is responsible for about 40% of

the heat losses in a typical building envelope [3]. Therefore, the reduction of the heating and cooling energy consumption can be realized through the installation of novel glazing technologies, such as embedded microstructures. This novel CFS is composed of a polymer film, laminated to a double glazing with low-e coating. Parabolic micro-mirrors are embedded in the polymer film and aligned with striped reflectors in such a fashion that a seasonal g-value is obtained [4]. Thermal gains are maximized in winter and reduced in summer. The proposed glazing envelope guarantees a good level of daylighting, a clear view toward outside and a significant amount of energy savings through the HVAC system [5].

This study aims at evaluating the thermal performance of the novel microstructured glass in a future scenario of global warming (in 2050), analysing the impact on the energy balance of the building at different latitudes.

METHOD AND INPUT DATA

A parametric analysis is carried out in order to estimate the influence of the microstructured glass on the required thermal loads in an office building, under future meteorological conditions induced by the climate change. Energy savings obtained by the use of embedded microstructures have been calculated and compared with a sun protective glass, both in the current climatic conditions and in the future scenario.

Chosen locations

Twenty-one locations were selected, distributed all over Europe, according to [5] in order to consider a sufficient wide range of latitudes. In Figure 1, a list of the twenty-one European locations is displayed, with the corresponding extreme latitudes (Athens and Bergen). The latitude of Lausanne is also indicated because the Swiss city is the reference location, for which the geometric configuration of the embedded micro-mirrors has been optimized, minimizing the annual thermal loads.

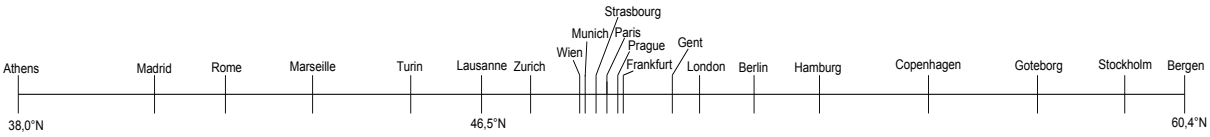

Figure 1: List of the twenty-one chosen European locations; the range of latitude is between 38°N (Athens) and 60,4°N (Bergen).

Weather data

Simulations have been performed for each location using a ray tracing program, based on the Monte Carlo method. This tool is based on the statistical evaluation of the path taken by sun rays through the glass, as explained in [4]. Meteorological variables are needed as input in the program, in order to climatically characterize the region. The sky distribution for diffuse radiation is considered according to the Perez model, taking into account hourly the direct and diffuse horizontal irradiance levels [6]. Meteorological data are provided by the Meteonorm database [7], both for the current climatic conditions and for the probabilistic future climate projections. Projections until 2050 were selected, following the A1B scenario developed by the Intergovernmental Panel on Climate Change (IPCC). The A1B scenario from the Special Report on Emissions Scenarios belongs to the A1 group, corresponding to a positive perspective. The A1 storyline describes a future world of very rapid economic growth, global population that peaks in mid-century and declines thereafter and the rapid introduction of new

and more efficient technologies. This scenario is distinguished in three groups that describe alternative directions of technological changes in the energy system: fossil intensive (A1FI), non-fossil energy sources (A1T) and a balance across all sources (A1B) [8].

Reference office room

A south-oriented office room has been defined, in order to perform all the simulations varying the latitude and the glazing envelope. The geometric characteristics of the reference office room comprise a floor area equal to 30 m^2 and a façade wall area that amounts to 10 m^2. The window to wall ratio is about 40%. Concerning the thermal properties, the external wall is well-insulated, with a U-value of 0,15 W/m^2K. Besides the microstructured glass, a conventional glazing, such a sun protective glass, is examined. For both glazing envelopes the U-value of the window is assumed equal to 1,3 W/m^2K.

RESULTS AND DISCUSSION

Figure 2 shows the obtained thermal loads with the microstructured glass in the current situation and in the future climatic scenario. Three ranges of latitudes can be distinguished: in southern locations the annual loads are increased, in the continental region the variation is not significant and in the north of Europe the thermal loads are decreased. In the lowest range of latitudes, between 38°N and 46,5°N, the expected future thermal loads range from 22,6 kWh/m^2 (Turin) to 37,0 kWh/m^2 (Athens). In the current climatic conditions, in this range of latitudes, the cumulated loads vary from 16,7 kWh/m^2 to 29,7 kWh/m^2, corresponding to the same cities. From Zurich (47,4°N) to Berlin (52,5°N), the annual loads are slightly higher in the future scenario, except in Prague, where they decrease by 1,7 kWh/m^2. At these latitudes, the highest increment of thermal loads is in Frankfurt, equal to 3,0 kWh/m^2. The northern European locations (from Hamburg to Bergen) are characterized by a decrease of the annual loads, more accentuated in Copenhagen, Goteborg and Bergen, where the difference is around 2,5 kWh/m^2.

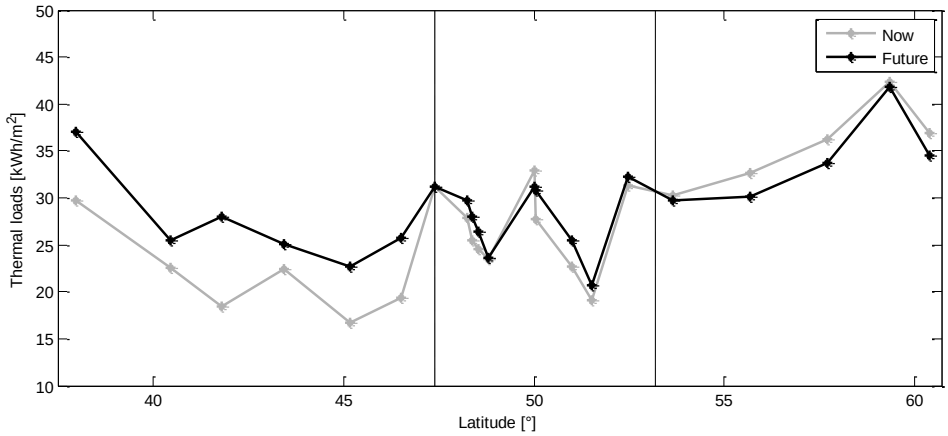

Figure 2: Annual thermal loads at different latitudes for the microstructured glass nowadays (grey line) and in the future (black line).

In general, the thermal loads are expected to significantly increase in lower latitudes (until around 46°N) and they slightly decrease in the north of Europe. This is explained by the larger increment of mean monthly temperatures for the low range of latitudes (until around 48°N). The temperature is expected to increase by between 1°C and 2,7°C in these locations. In the continental region, including locations like Frankfurt and Munich, the climate change is less significant.

In Figure 3, energy savings are shown, as compared with a sun protective glass.

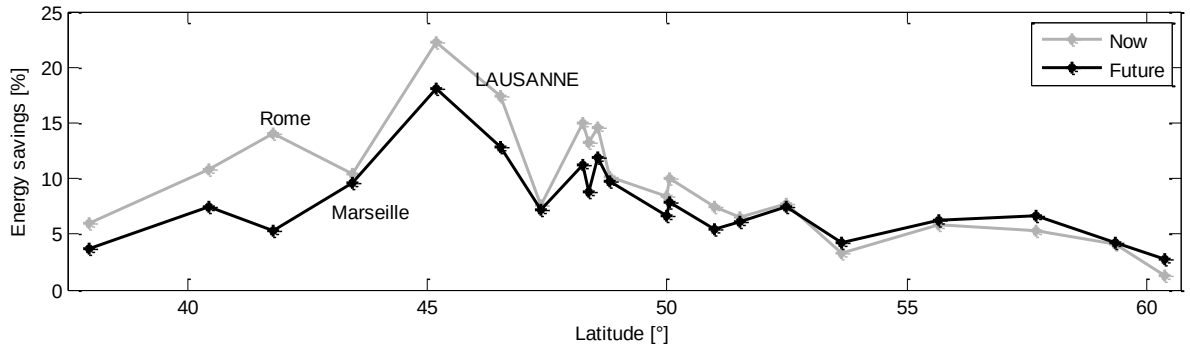

Figure 3: Relative energy savings at different latitudes for the microstructured glass, compared with the sun protective glass in the current and future scenario.

The curve representing the energy savings has the same shape in the future and present climatic scenario, with the exception of Rome, that will be described in more detail in the following paragraph. Until a latitude of 52,6°N, relative energy savings are decreasing in the future climatic conditions. Especially southern locations are characterized by a considerable reduction of the saved energy; in Athens they diminish from 6% to 3,6% (40% of reduction) and in Lausanne the decrease is about 26%. In the north of Europe, where the latitude is above 53°N, relative savings are increasing, except in Stockholm, where they remain almost the same, rising from 4,1% to 4,2%. In Hamburg the increment is of 23%, in Copenhagen around 8% and in Goteborg is 20%. In Bergen, finally, energy savings are expected to grow from 1,3% to 2,7%.

As can be noticed in Figure 4a, in Rome the direct irradiance is expected to significantly increase in the future decades.

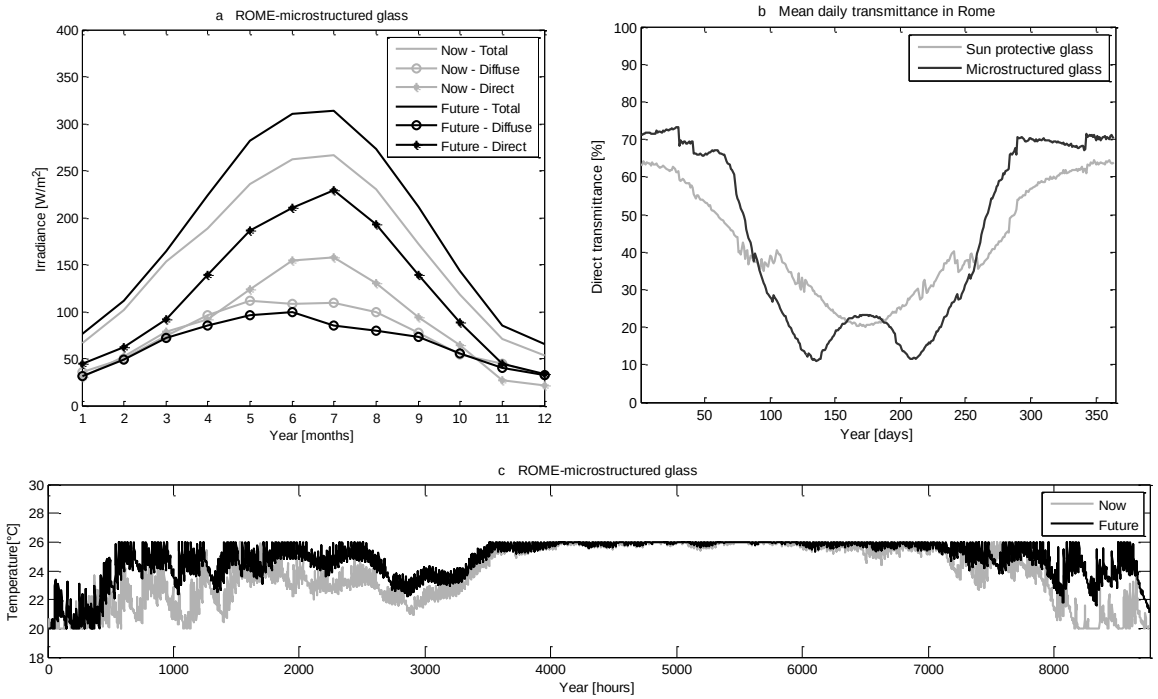

Figure 4: (a) Global horizontal, diffuse and direct irradiance in Rome (b) Daily direct transmittance in Rome with the sun protective glass and the microstructured glass and (c) Mean hourly temperatures in Rome for the microstructured glass in current and in future scenario.

During summertime, the increase is about 30%, causing considerable solar gains. In winter the direct horizontal radiation increases by between 14% and 40%, depending on the month. The diffuse irradiance is slightly decreasing during the hot season; consequently, the global irradiance is increased all over the year. The increased temperatures combined with the rise of the direct portion of the irradiance induce overheating. In Figure 4c, it can be noticed that, according to the IPCC projections, there is a first need of cooling from the end of January until April. In these months, the transmitted energy through the microstructured glass is around 70% (Figure 4b). When the direct transmittance is between 30% and 11% in spring, there is no need for cooling. Then the cooling is required again in the end of May until December. In Rome, heating requirements are drastically reduced in a future scenario (by about 81%), while the cooling loads are increasing by 43,6%. In a future scenario of global warming, the annual thermal loads in Rome are increased by 34%, going from 18,4 kWh/m^2 to 27,9 kWh/m^2.

Another particular case among southern locations is Marseille, where the saved energy is almost the same, passing from 10,4% to 9,6%. The reason is that future and present meteorological conditions in this location are comparable. Both in the current and in future years, high solar gains will be registered in the building early during the year, before the sun elevation angle reaches the blocking range of the embedded microstructures.

The variation of the energy savings all over Europe can be explained by the change in distribution of thermal loads between cooling and heating. The expected cooling and heating loads are shown in Figure 5a and 5b, respectively.

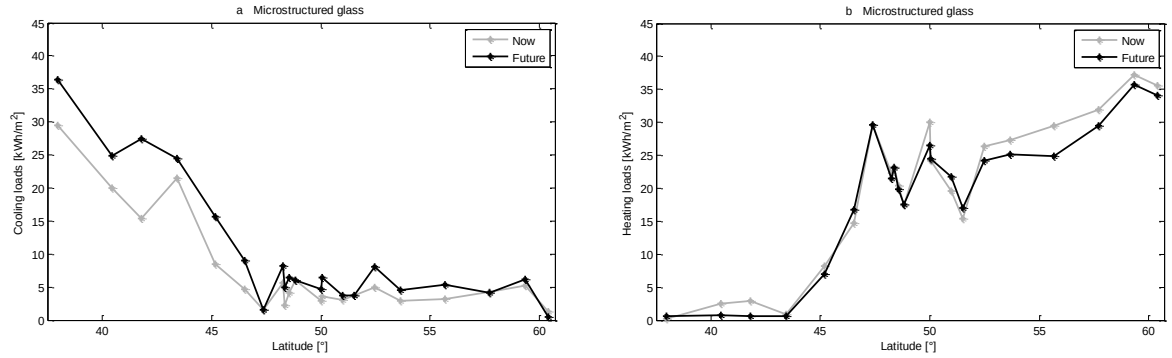

Figure 5: Current and future (a) cooling loads and (b) heating loads for the microstructured glass at different European latitudes.

In general, as can be seen in Figure 5a, the requirement for cooling is increasing for all the locations except Zurich, Paris, London and Goteborg, where it is roughly maintained. The highest increment of cooling loads is seen in southern European locations. In Athens, cooling loads currently amount to 29,7 kWh/m^2, while in the future they are reaching 36,4 kWh/m^2. The increase of cooling consumption is less accentuated at higher latitudes; there is a peak in Berlin, where the cooling is expected to vary from 5 kWh/m^2 to 8 kWh/m^2. Concerning the annual heating loads, Figure 5b shows the trend at different latitudes. In Madrid and Rome the heating loads undergo a significant decrease. In Madrid it is expected to diminish from 2,5 kWh/m^2 to 0,7 kWh/m^2 (of about 72%), while in Rome from 3 kWh/m^2 to 0,55 kWh/m^2 (down to 81%). For the locations situated in a middle range (between 43°N and 52°N), the heating consumption is not importantly changed according to the future climatic projections. At higher latitudes (above 52°N), where energy savings are expected to slightly increase, heating loads decrease by around 4%-16%. The reduction of heating energy consumption depends on the location and is negligible in continental Europe.

CONCLUSION

Several studies on climate change indicate that in 2050 the mean global temperature and the irradiance are expected to rise, more or less significantly, depending on the location. In the south of Europe this increment is larger, amounting to more than 2°C. In the north the increase of mean temperatures is less accentuated but still foreseen. The attention to energy consumption in buildings is becoming important as well as the promotion of a smarter energy management. In this paper, the impact of global warming on the thermal loads in a well-insulated building has been investigated. In particular, the thermal performance of a microstructured glass is evaluated in a climate change scenario, in comparison with a sun protective glazing. Focusing on the microstructured glass performance, it can be affirmed that climate change significantly alters the heating and cooling requirements. Despite the variation of climatic conditions, relevant energy savings are still achieved by the novel CFS technology. With the global warming effect, the energy consumption for heating tends to decrease; on the other hand, the need for cooling rises. The effect of climate change is more acute in southern European regions, where the need for cooling is more important. For this range of latitudes, also a proper design of the sun protective glass can potentially be a solution for the reduction of the cooling loads in a future scenario. Additionally, a further optimization of the geometric configuration of the micro-mirrors is possible in southern locations, in order to obtain a more significant reduction of the annual loads. In locations situated at latitudes higher than 53°N, the increment of temperature is larger in winter than in summer. Consequently, the cooling consumption is not importantly increasing in the north of Europe, while heating loads slightly diminish. The analysis shows that, all over Europe, energy savings expected with a microstructured glass compared to a sun protective glass are between 3% and 18%. The microstructured glass could be a potential solution in a future climate scenario, for the reduction of overheating in buildings, helping to decrease the cooling energy consumption, which is likely expected to grow more and more in the coming up years.

REFERENCES

1. Le Treut, H.: Les scénarios globaux de changement climatique et leur incertitudes. C. R. Geoscience, Vol 335, pp 525-533, Université Pierre et Marie Curie, Paris, 2003.
2. Watson R.T., Zinyowera M.C., Moss R.H. (eds.): Technologies, policies and measures for mitigating climate change. Intergovernmental panel on climate change, IPCC Technical Paper I, 1996.
3. Gustavsen A., Grynning S., Arasteh D., Jelle B.P., Goudey H.: Key elements of and material performance targets for highly insulating window frames. Energy and buildings, Vol 43, Issue 10, pp 2583-2594, Elsevier, October 2011.
4. Kostro A., Scartezzini J.L., Schüler A.: Mixed-dimensionality approach for advanced ray tracing of lamellar structures for daylighting and thermal control. Proc. of CISBAT Conference, Lausanne (Switzerland), 2013.
5. Vanzo S., Kostro A., Schüler A.: Location based study of the annual thermal loads with microstructured windows in European climates. Proc. Of IBPC Conference, Turin (Italy), 2015.
6. Perez R., Seals R., Michalsky J.: All-weather model for sky luminance distribution – preliminary configuration and validation. Solar Energy, Vol 50, No 3, pp 235-245, 1993.
7. Meteonorm Software version 7.1.2 2014, Meteotest, Berne (Switzerland).
8. Intergovernmental Panel on Climate Change (IPCC): IPCC Special Report – Emissions scenarios. Summary for Policymakers, Special Report of Working Group III, 2000.

ROOFTOP GREENHOUSES: LCA AND ENERGY SIMULATION

K. Benis[1]; R. Gomes[1]; R. Vicente[1]; P. Ferrão[1] ; J.E. Fernández[2]

1: IN+ Instituto Superior Técnico, Av. Rovisco Pais 1, 1049-001 Lisbon

2: MIT Department of Architecture, 77 Massachusetts Avenue, Cambridge, MA 02139-4307

ABSTRACT

Building-Integrated Agriculture (BIA) has the potential to offer a new dimension to our buildings, providing locally grown food that increase urban resilience. There are two main forms of BIA: Rooftop Greenhouses (RG) and Vertically Integrated Greenhouses (VIG). This paper focuses on RG, i.e. setting up hydroponic greenhouses on top of flat roofs. With 85% of Lisbon's building stock built before 1980, when there were no insulation requirements, there is a strong retrofitting potential using RGs. This should be considered together with the energy requirements of hydroponic environments, particularly for indoor temperature control.

This work combines Life Cycle Assessment (LCA) and energy simulation of a RG implemented on a residential building located in Lisbon. The analysis is aimed at quantifying the environmental impact, but also the energy requirements of the RG through its operation phase. The effect of the RG on the indoor temperature of the last floor apartments was analyzed. The first results show an improvement of the indoor temperature in the winter period and an undesirable increase in the indoor temperature during summer. These results highlight the need to evaluate different scenarios such as recovering part of the cooling loads used in the greenhouse and transferring them to the building, the application of insulation in the rooftop slab and the evaluation of night ventilation.

The aim of this study is to constitute a first step towards a quantitative basis for decision-making in the implementation of RGs in building retrofit interventions, by showing what alternatives would be most effective in delivering CO_2 emissions reductions, along with their respective costs and amounts of saved energy —thus offering an indication of which option is to be favored to guarantee sustainability and cost-effectiveness.

Keywords: Building-Integrated Agriculture, Rooftop Greenhouse, LCA, energy simulation, indoor temperature, controlled environment

INTRODUCTION

Building Integrated Agriculture (BIA) consists of the application of hydroponic greenhouse methods adapted for use on top of or in buildings [1]. This study analyzes the implementation of a RG for lettuce and leafy greens production on a low-rise multi-family dwelling located in Lisbon, with 18 apartments and 60 estimated inhabitants.

Lettuce production systems use Nutrient Film Technique (NFT), a system where re-circulated nutrient solution is pumped from a reservoir to slopping polyethylene or PVC channels, in which plant roots are placed in planting holes separated by a distance of 15 to 30 cm.

The RG occupies the whole area of the flat rooftop (i.e., 270m^2 with a production area of 225m^2) with 26 plant sites per m^2, which provide a yearly yield of 16,85 tons (threefold of the demand of the building's inhabitants). Sizing characteristics were adapted from information provided by local growers. The 21 identical existing buildings in the neighborhood offer the possibility of diversifying hydroponic cultures to cover local needs.

LIFE CYCLE ASSESSMENT

Goal and Scope

The goal of this LCA is to quantify the environmental impacts of rooftop greenhouse hydroponics production systems in a residential building in the city of Lisbon. The functional unit is 1 ton of greenhouse food produced (lettuce and leafy greens). The system boundary was defined as in Figure 1 (cradle-to-gate). The LCA was modeled on *SimaPro*, using the *EcoInvent 3.1* database. The model includes five main processes: (1) *greenhouse structure*; (2) *electricity*; (3) *water use*; (4) *growing process*; (5) *waste management*.

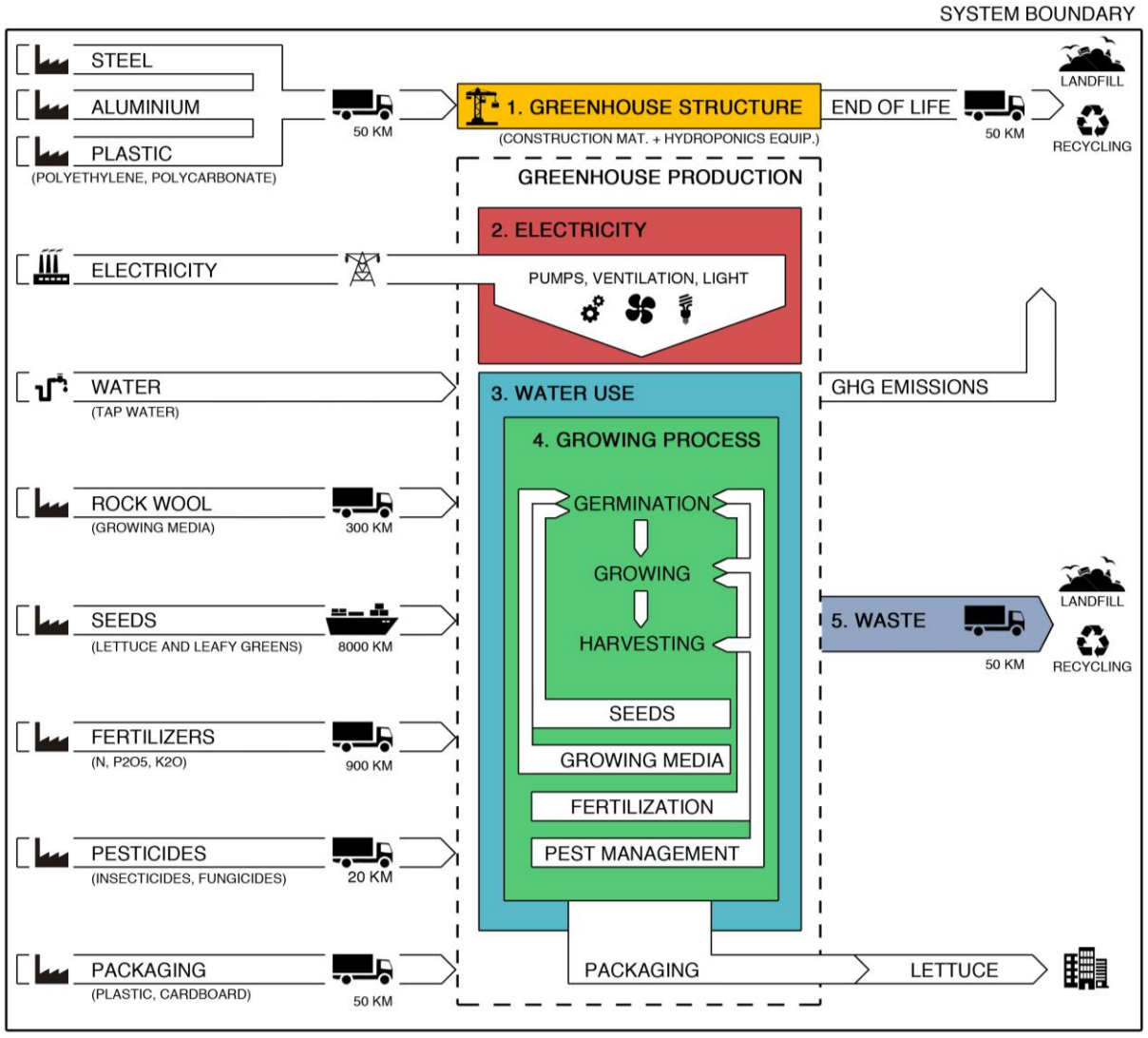

Figure 1: Life Cycle Inventory of greenhouse lettuce production system (hydroponics)

Life Cycle Inventory

The *greenhouse structure* is made from steel, aluminum and polycarbonate. Hydroponics growing channels are made of polyethylene. For this study, a leading Portuguese greenhouse manufacturer provided information concerning the characteristics and quantities of materials used in a "standard" greenhouse, which were adapted to this particular case. Local growers provided the specific dimensions and quantities of hydroponic equipment for growing lettuce.

The *electricity* process includes total electricity consumption (kWh) for the entire greenhouse activities (i.e., pumping systems, ventilation and lighting).

The *water use* process includes total water consumption (m^3). Whereas conventional agricultural production requires 120 liters of water per kg of lettuce, water use efficiencies in hydroponics are usually around 20 liters per kg of lettuce [2]. Based on data provided by local growers, the calculations for this case study led to a result of 19,23 liters of water per kg of lettuce.

In the *growing process*, the production of *seeds* was not considered because of lack of data. The *growing medium* process includes material and energy inputs for the manufacturing of substrate (i.e. rock wool), and its *packaging* (plastic and cardboard). The *fertilizers* process includes building infrastructure and electricity needed for the production of fertilizers. The *pesticides* process considers the production of pesticides including materials, energy use, and infrastructure.

Electricity consumption rates, *water use*, and quantities of *seeds*, *growing medium*, *fertilizers* and *pesticides* used per kg of production were also obtained from local growers. The Portuguese electricity mix was used in the model.

Different *waste scenarios* were modeled depending on the nature of the waste: (1) *greenhouse structure*, namely construction materials and hydroponics equipments (steel, aluminum and plastic); (2) *organic* (plant roots and waste); (3) *inorganic* (rock wool); (4) *plastic and cardboard packaging*. The RG construction materials, excluding plastic, were assumed to have a lifespan of 25 years. For the roof and walls composed of polycarbonate, the lifespan considered was 10 years. For hydroponic polyethylene equipment (i.e. channels and pipes), the lifespan considered was 4 years. Distances of transportation were considered, as well as GHG emissions from the waste treatment process. In LCA studies of greenhouse food production, the *cut-off method* [3] is the most commonly applied for the allocation of compost and recycling process: only loads directly caused by a product are allocated to it. Thus, composting of organic waste and recycling processes (for metals and plastics) were excluded.

All processes required transportation from production sites to the greenhouse, and were calculated using the formula: t x km. Distances traveled were based on the discussions with local hydroponic lettuce producers, regarding the locations of their suppliers.

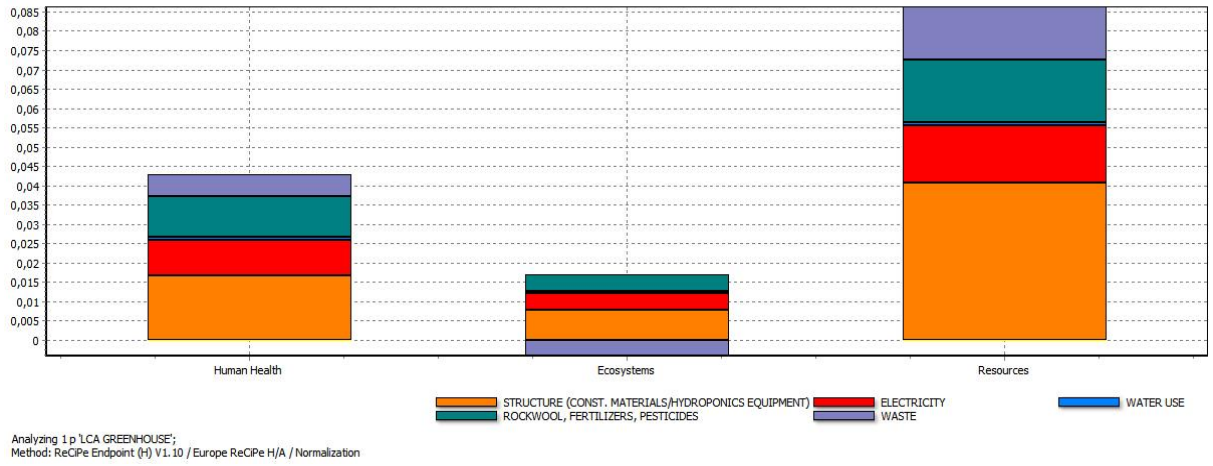

Figure 2: Life Cycle Inventory of greenhouse lettuce production system (hydroponics)

Life Cycle Impact Assessment

Environmental impacts of hydroponic production of lettuce and leafy greens in the RG are shown in Figure 2. The production process (i.e. *electricity*, *water use* and *growing process*) has

a significant share in most of the categories (*ReCiPe Endpoint (H)* Assessment Method, Europe). Among the *growing process* components, *pesticides* are the major contributors to the impacts. *Greenhouse structure* and *waste* have less environmental impacts, since most of the materials are to be recycled at their end of life.

BUILDING AND GREENHOUSE SIMULATION

The building energy modelling allows performing an initial assessment of the thermal needs of the building and of the greenhouse during the operating phase and the possibility to evaluate different solutions for its acclimatization.

Simulation inputs of the building

The energy simulation of the building was performed using the software *Energy Plus version 8* and the geometry was defined using *Google Sketchup*. It is important to note that this simulation needs to be calibrated with *in situ* measurements to better represent the energy performance of the existing building. Therefore, the results presented here are a first analysis of the building thermal needs.

For this simulation, the building zoning was done considering spaces with different uses (i.e., kitchen, rooms and living rooms). The building was constructed in 1960 and the constructive solutions defined in the simulation were a double brick wall with air space for the exterior walls and a precast concrete joist and brick panel for the slabs.

The windows defined in the simulation are constituted by a clear 6mm glass installed in an aluminum frame, with external plastic shutters. Internal gains of the building were defined, namely occupation, lighting and equipment, considering predicted and reasonable values for the building typology. The air infiltration values were defined accordingly to specific bibliography [4] but are expected to have more accurate results in the future with *in situ* measurements.

Simulation inputs for the greenhouse

One main purpose for considering a greenhouse structure in a building rooftop is to create a controlled environment in terms of temperature and humidity for optimum growing conditions within a predictable and repeatable time schedule when compared to growing outside in a non-controlled environment. Considering the greenhouse structure, construction materials and design, it can become too warm in the summer and cold in the winter which could affect the crop production. The best indoor conditions control systems should not only be effective in providing the desired environment, but also be designed to be unobtrusive within the greenhouse system. Evaporative cooling is a common way to reduce indoor temperatures for greenhouses in dry climates [9] and basically consists of a process that reduces air temperature by water evaporation into the airstream. As water evaporates, it absorbs energy from the surrounding environment (greenhouse) decreasing the temperature of the air flow. Fan and pad evaporative systems consist of exhaust fans at one end of the greenhouse and a pump circulating water through and over a porous pad installed at the opposite end [5, 6, 7, 8]. The cooling efficiency is dependent of the pad wall material (corrugated cellulose, aspen pads or aluminum and plastic fibers) and air flow velocity and can vary between 70 to 80% [6, 9]. Additionally, the outside air conditions, namely the relative humidity and temperature, affect the cooling potential of the pad wall system [8, 9].

Evaporative pad cooling system

The ventilation sizing for the evaporative pad system considered in this greenhouse was performed considering the air flow value of 2.4 m^3 min^{-1} per m^2 of floor area [8]. Considering the greenhouse geometry it was considered that the system has three fans, one for each zone

considered in the simulation of the greenhouse. The pad wall considered is constituted by corrugated cellulose since this is the most widely type used for evaporative pad walls [8]. The pad wall was considered to be in the north façade of each zone since this is the direction of the prevailing winds in Lisbon [11], increasing the efficiency of the pad system. For heating purposes it was considered an electric baseboard equipment to heat the greenhouse. The indoor temperature setpoint defined for the greenhouse was 24-28ºC.

Results

As it was expected considering the building typology and the constructive solutions, there are significant heating and cooling needs in all the apartments, as the number of annual hours with indoor temperatures above 26ºC in the summer period and below 18ºC in winter period is considerably high (considering no HVAC systems). The effect of the rooftop greenhouse in the building indoor temperature can be observed in the figure 3. As the temperature of the greenhouse was defined to be between 24 and 28ºC during all year it can be observed that the temperature of one room in the last floor increased with the implementation of the RG. This is a result from an increase of the heat gains from the greenhouse considering the low thermal resistance of the existing rooftop slab. Although this can be considered positive in the winter period, it represents a thermal comfort disadvantage in the summer period. One possibility to overcome this situation could be to improve the slab insulation or increase the night ventilation on the building.

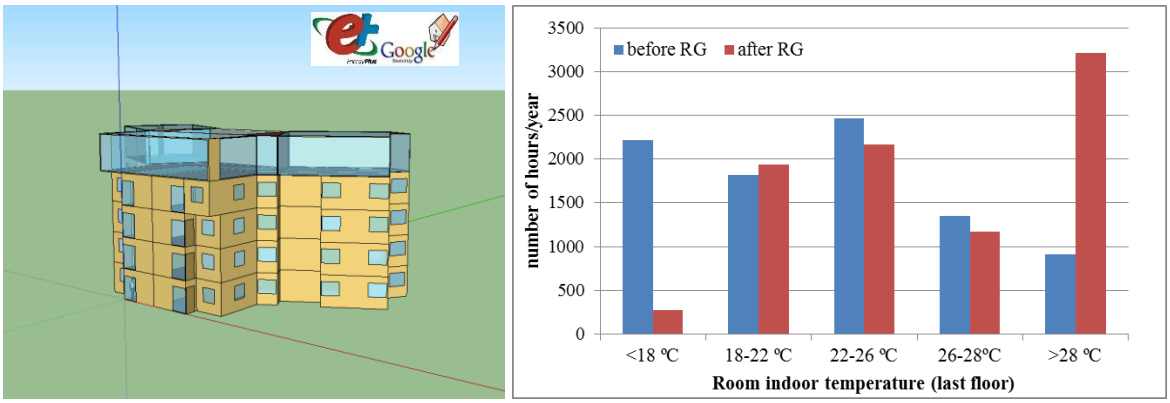

Figure 3: Building simulation model (southeast view) and annual indoor temperature in one room of the last floor before and after the rooftop greenhouse

Simulation limitations

Several limitations regarding the simulation of the building and of the greenhouse can be highlighted. The calibration of the model with *in situ* measurements in the existing building, energy audits, occupation patterns evaluation and other relevant parameters, will contribute to a more accurate building simulation and a better analysis of the operative phase of the building with and without the greenhouse. Regarding the greenhouse, it is relevant to highlight the possibility of the existence of a gradient of air temperature between the pad wall and the fans (not considered in the simulation). In fact it is expected that the temperature near the fans will be higher than on the opposite side of the greenhouse. Other relevant aspect to be analyzed is the effect of the wind on the pad evaporative system. The wind profile specific from the building location will contribute to this analysis.

ONGOING AND FUTURE WORK

In a next step, the energy modeling of the greenhouse will allow for the assessment of its heating and/or cooling energy consumptions, which will constitute an additional process of

this LCA model, increasing the environmental impact of the use phase of the RG. A sensitivity analysis looking at reducing the impacts of the major contributors to the environmental impacts will be performed. This assessment will rely on the analysis of different scenarios such as the evaluation of different greenhouse acclimatization solutions, building insulation application, and passive solutions in order to reduce LCA impact of the greenhouse together with existing building. For all the scenarios, the energy savings will be calculated but will also be considered the input material such as ducts, fans, heat recover units and other materials and construction works. Also, the possibility of implementing a photovoltaic system to provide energy to the greenhouse will be considered and analyzed from a LCA perspective.

Besides, the size of the greenhouse and consequently the crop production should be evaluated in order to define the most suitable solution regarding global environmental impact. The main goal is to achieve the best scenario that includes solutions for the building as well as for the greenhouse.

A Life Cycle Cost (LCC) analysis performed in parallel to the energy flows scenarios will lead to the constitution of a quantitative basis for decision-making, by showing what alternative would be most effective in delivering CO2 emissions reductions, along with their respective costs and amounts of saved energy —thus offering an indication of which option is to be favored to guarantee sustainability and cost-effectiveness.

REFERENCES

1. Puri, V., Caplow, T.: How to grow food in the 100% renewable city: Building-integrated agriculture. In P. Droege (ed.). 100% Renewable: Energy Autonomy in Action. Earthscan, London, UK, pp 229-241, 2009
2. Kratky, B.A.: Three non-circulating hydroponic methods for growing lettuce. Proceedings of the International Symposium on Soilless Culture and Hydroponics. Acta. Hort. 843:65-72, 2009
3. Ekvall, T., Tillman, A.M.: Open-Loop Recycling: Criteria for Allocation Procedures. International Journal of Life Cycle Assessment, 2 (3), pp 155-162, 1997
4. Villi, G., Peretti, C., Graci, S.: Building leakage analysis and infiltration modeling for an Italian multi-family building. Journal of Building Performance Simulation, 2012
5. Caplow, T., Nelkin, J.: Building-integrated greenhouse systems for low energy cooling. New York Sun Works, USA, 2007
6. Strobel, B.R., Stowell, R.R., Short, T.H.: Evaporative Cooling Pads: Use in Lowering Indoor Air Temperature, Food, Agricultural and Biological Engineering, http://ohioline.osu.edu/aex-fact/0127.html, consulted in May 2015
7. Bucklin, R.A., Leary, J.D., McConnell, D.B., Wilkerson, E. G.: Fan and Pad Greenhouse Evaporative Cooling Systems, University of Florida, Florida, 2010
8. The Center for Agriculture, Food and Environment. Fan and Pad Evaporative Cooling Systems. https://ag.umass.edu/fact-sheets/fan-pad-evaporative-cooling-systems, consulted in May 2015
9. Giacomelli, G.A.: Evaporative cooling system: pad and fan, Controlled Environment Agricultural Center, The University of Arizona, USA, 2003
10. Franco, A., Valera, D.L., Peña, A.: Energy Efficiency in Greenhouse Evaporative Cooling Techniques: Cooling Boxes versus Cellulose Pads, Energies 2014
11. Windfinder, http://pt.windfinder.com/windstatistics/lisboa, consulted in May 2015

EXPERIMENTAL INVESTIGATION OF A NEW SOLID WOOD PANEL FOR ROOM TEMPERATURE CONTROL – ANALYSIS OF THE COOLING PERFORMANCE

N. Bishara[1,2]; R. Plagge[2]

1: Faculty of Science and Technology, Free University of Bozen, Bozen, Italy

2: Institute of Building Climatology, Dresden University of Technology, Germany

ABSTRACT

Wood industry's current economic development shows an increase of selling multilayered solid wood panel products accompanied by a crescent functionalization of those panels. Within an industry driven project an additional functionalization in form of pipe elements for heating and cooling are to be applied to a multilayered solid wood construction. The development of this innovative radiant heating and cooling system requires extensive laboratory analysis. Investigations are focusing on thermal optimization as well as thermal and hygric long-term performance and durability. Previous studies devoted to optimize panel structure during a heating process, enabling efficient heat distribution within the panel as well as to the enclosing room. Whereas, current studies are concentrating on the cooling performance, which was analysed by means of specially manufactured prototypes of a solid wood panel. Laboratory measurements were carried out using a climatic test chamber as well as test benches, equipped with an infrared thermographic camera and several sensors for measuring temperature, relative air humidity, and heat flux density. Climate test chamber measurements are aiming at exploring material performance and stability of selected panel prototypes under defined boundary conditions. The performance of the overall panel system is investigated in specially built test benches, which allow statements to be made about the effectiveness of the radiant heating and cooling system with respect to a defined space. Within this paper measurement procedures of a laboratory panel investigation are described and first results are shown. Main criteria and boundary conditions of the measurement procedure are discussed. Measurement results are evaluated, particularly with regard to formation of condensation and moisture during a cooling load. Significant statements about functionality and cooling performance of the new developed wooden panel for room temperature control are made.

Keywords: solid wood panel, radiant heating and cooling, moisture management of wood, laboratory performance and damage analysis

INTRODUCTION

Radiant heating and cooling systems are an efficient solution for room temperature control. For heating purposes they are preferably installed in floor and wall constructions. With a cooling purpose they are applied to ceiling structures, but also to wall areas. Often, the systems are installed in new buildings or in complex rehabilitation measures. An innovative, sustainable and cost effective variant represents the development of a new radiant heating and cooling system based on a complex multilayered solid wood construction. This panel is suitable, due to the production as a visible wall element, especially for the renovation of existing buildings.

The panel to be developed consists of three wooden layers bonded with melamine-urea-formaldehyde resin and a multilayer composite pipe element which is installed in a middle layer. Figure 1 depicts the structure of an optimized panel chosen from a variation study carried

out by Bishara [1]. Its total thickness is 33.4 mm and pipe distance is 80 mm, occasionally 100 mm. For laboratory testing prototypes measuring 800 mm by 800 mm are manufactured whereby pipes with a diameter of 16 mm are arranged in spiral course.

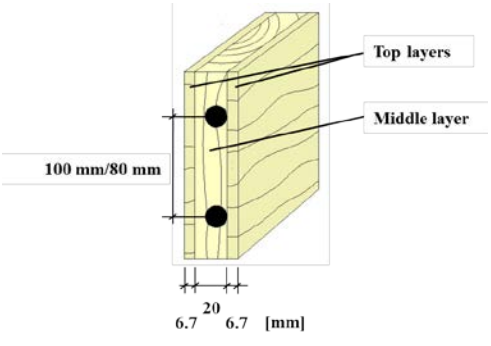

Figure 1: Structure of the wooden tempering system

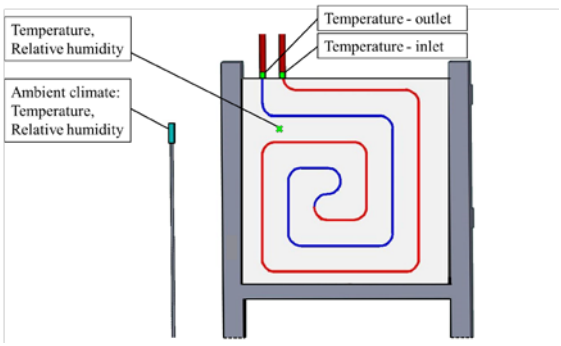

Figure 2: Climate test chamber experiment-measurement setup

Three different panel variants of a prototype were chosen for experimental investigation in laboratory. They differ in choice of material and pipe distance as can be seen in Table 1.

Panel type	Top layer material	Middle layer material	Pipe distance	Experimental investigation
1	Spruce	MDF	8 cm	Climate chamber experiment: long-term cooling
2	Spruce	Spruce	8 cm	Climate chamber experiment: complex cooling
3	Spruce	Spruce	10 cm	Test bench

Table 1: Panel variants for laboratory investigation

METHOD

Measurement setup of a climate test chamber experiment

1 - Long-term cooling

Panel type 1 was installed in a climate test chamber in order to achieve statements about the hygrothermal material strain during a cooling period. This panel variant comprises an MDF middle layer. A cooling period was defined with an ambient temperature of 28°C and an ambient relative air humidity (RH) of 65%. During a loading duration of 23 days, the solid wood panel was operating with a constant flow temperature of 16°C.

The measurement setup is represented in Figure 2. An insulation layer was installed in the panel`s rear area in order to restrict heat flow to one direction. Ambient climatic conditions were monitored with a negative temperature coefficient thermistor sensor (NTC) ensuring an accuracy of ± 0.1 K, and a capacitive sensor with an accuracy of ± 2 % RH. Temperature inlet and outlet were recorded with NTC sensors directly on the pipe`s surface. Additionally, the pipes were thermally isolated with polyethylene to avoid interaction with ambient climate. The hygrothermal behavior inside the panel was monitored with capacitive and NTC sensors.

2 - Complex cooling

A panel type 2 was investigated in a more complex cooling experiment. Boundary conditions for this cooling experiment are represented in Table 2, defined as a sequence of summer day and night conditions. The measuring run started with a day mode, followed by a night mode, and a repetition of both phases. During day mode, ambient temperature was set to 28°C, and flow temperature to 16°C. Night mode was defined as night shut down of the cooling function

and an ambient temperature of 20°C. Relative humidity was supposed to be 65% during the whole measuring circle.

Mode	Duration	Ambient climate		Temperature pipe element
		Temperature	Relative humidity	
Day mode	20 h	28°C	65%	16°C
Night mode	24 h	20°C	65%	-
Day mode	24 h	28°C	65%	16°C
Night mode	93 h	20°C	65%	-

Table 2: Boundary conditions of a complex cooling experiment

Measurement setup of the test bench experiment

Figure 3 depicts a test facility, comprising an air volume of 1 m³, for the installation of a panel in a wall area. A wall construction was built on one of the room`s side walls consisting of a brick layer (thickness 117 mm) and a layer of capillary-active insulation (thickness 100 mm). In the brick layer`s rear area, an additional tempering system was installed, generating defined surface temperatures. A panel type 3 to be monitored was installed in connection to the internal insulation layer.

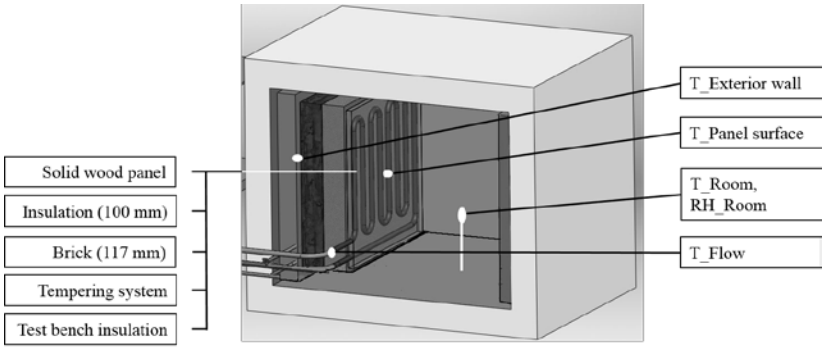

Figure 3: Test bench - experimental setup

At the beginning of the experiment, a defined temperature of 47°C was set to the brick layer`s outside, until room temperature reached 28°C. Once this temperature was reached, the wooden panel`s pipe system was provided with a flow temperature of 16°C and a cooling process started. The aim was to define that period of time which was needed for reaching a room temperature of 26°C. This value corresponds to the standard internal temperature for the application of cooling systems, according to European Standard EN 1264-3 [2].
Subsequently, the panel operation was driven by a temperature-controlled thermostat. At a temperature set point of 25.5°C the cooling operation switched off automatically, and at a set point of 26.5°C it switched on again. A comparison was made between duration of cooling period and cooling break.

Within the test bench, extensive measuring equipment was installed. Air temperature and relative humidity inside the test stand were measured with NTC and capacitive sensors. NTC sensors were also installed on inlet and outlet of the solid wood panel, directly on the pipe surface, to monitor flow and return temperatures. Temperature in a plane between additional tempering system and wall outside layer (T_Exterior wall) was recorded with an NTC sensor.
The test bench was sealed airtight and sheathed with a 100 mm thick insulation layer. During measurements, this test stand was positioned in a laboratory facility with controlled climatic conditions, which were also monitored with NTC and capacitive sensors.

RESULTS AND DISCUSSION

Climate test chamber experiment

Figure 4 provides measurement results of a long-term cooling period. Ambient temperature was measured at average 28.8°C. Relative humidity ranges slightly between 64% and 69%. Recorded temperature values inside the panel construction are declining very slightly from 24.3°C to 24.0°C. In contrast, related relative humidity values increase throughout the entire cooling period. Cause for this is the hygroscopic property of the wood material, which aspires to take a moisture balance with its environment. In this regard, water vapor diffusion occurs due to a vapor pressure gradient between ambient climate (higher vapor partial pressure) and wood material (lower vapor partial pressure). Due to a high resistance of a radial spruce wood direction to vapor diffusion (measured μ_{dry}-value of 475) this process takes correspondingly long-time. No state of equilibrium has been reached at the end of the cooling experiment.

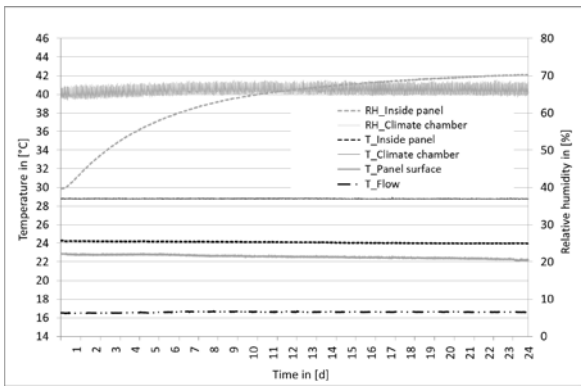

Figure 4: Measurement results of a long-term cooling period

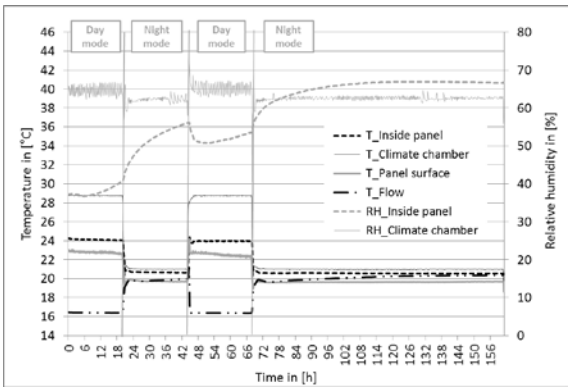

Figure 5: Measurement results of a complex cooling period

In general, a damage-free operation of the panel to an equilibrium moisture content of 95 % RH is assumed, due to capillary property of wooden materials. This threshold is not exceeded in the area around the sensor inside the panel construction.
However, most critical and thus decisive points exist directly above the pipe. At the interface between pipe and wood material, where temperature is lowest, pipe surface temperature is 16.1°C. Thus is resulting in a lower deviation of dew point temperature by 1.8 K (based on the measured humidity value inside the panel). Consequently, a safe system design under given boundary conditions is given only up to a measured relative humidity of 58 %, which is reached already after 5.2 days.
At a measured room climate of 28.8°C and 69% RH, dew point temperature at the panel`s surface is 22.5°C. This value is reached after 13 days of operation. Consequently, moisture damage occurs at the panel`s surface, however in a significantly lower extent as expected. Surface moist occurred only in the area of sensor cables as well as in the area of two larger branches. Additionally, moisture accumulation inside the MDF is assumed, due to a much lower sorption capacity of MDF compared with spruce [3]. However, the pipe course did not become visible on surface and also cracks could not be observed.

Figure 5 shows an excerpt of measurement results from a complex cooling experiment. With the change from day mode to night mode (cooling operation switches off), a temperature drop occurs in the air around the sensor. Thereby saturation of vapour pressure of the air decreases abruptly. Hence, a much lower maximum amount of water vapour particles can be absorbed. This leads to a rapid increase in measured relative humidity. The curve flattens over time during night mode, since temperature does not change further.

However, humidity continues to rise, due to the fact of a partial pressure gradient between wood element and environment. Conversely, saturation vapour pressure rises with heating of the wood material in leap from night mode to day mode. Thus, relative humidity decreases rapidly, as the heated air can now absorb much more vapour particles in relation to its equal volume retarded. After this rapid drop, air humidity increases again steadily.
Within a subsequent longer night phase, relative humidity around the sensor increases constantly, until it has reached a maximum value of 70%. At this point a wood moisture assessment in accordance to Kollmann [4] is performed. Kollmann offers a diagram which is used to derive the moisture content of spruce wood from ambient climatic conditions. Within the experiment, a maximum relative humidity (70 %) faces a temperature of 20.5°C which is resulting in a wood moisture content of 13%. This value is below fiber saturation point of coniferous wood, defined by Niemz [5] at about 30 % and higher.
According to EN 1264 [2], a cooling system design has also to take dew point temperature into account. Flow temperature is supposed to be 1 K above dew point temperature, at minimum. With the given extremal boundary conditions of 28.8°C and 67% RH during a cooling period, dew point temperature is 22.1°C. The present flow temperature (16°C) is thus 6.1 K below required minimum value. Since this dew point value is not exceeded at the panel surface during an entire cooling period of 24 hours (measured minimum value is 22.4°C), no wood damage occurred. There were neither cracks on the panel`s surface, nor became the pipe course visible on the surface.

Test bench experiment

In Figure 6 measured values of an initial cooling process, carried out in a test bench experiment, are shown. After a phase of preconditioning, in which the room was heated to a temperature of 28.2°C, the cooling function was switched on. Cooling down of the tempering fluid to a flow temperature of 16°C took 30 minutes. From that moment on it takes 3.5 hours until room temperature measures 26°C. Throughout the entire duration of the cooling mode relative humidity remains almost constant at 53%, after a slight decrease at the beginning.
Measured values of a further experiment course are shown in Figure 7. A set point for automatic thermostat turn off is measured at 25.4°C. It turns automatically on again at a measured room temperature of 26.5°C. An exact period duration of cooling phases and breaks is readable from these values: on every 2.5 hours of cooling follows a 7 hour break. The panel operation switches itself on, 2.5 times a day in average. This periodic cycle was performed over a period of 4 days.

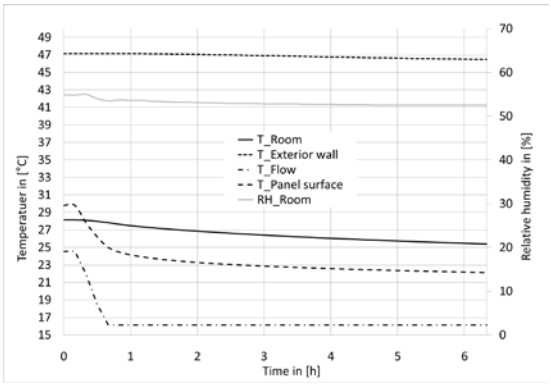

Figure 6: Measurement results of a test bench experiment – initial cooling

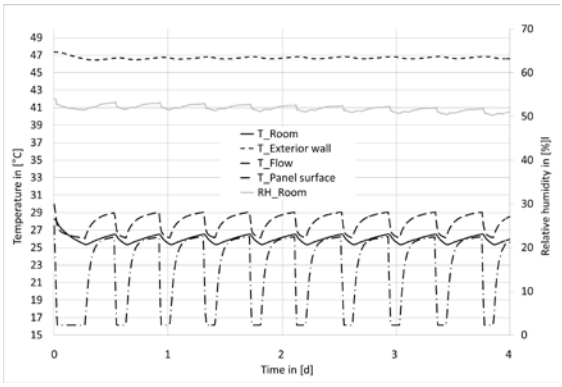

Figure 7: Measurement results of a test bench experiment – automatic switch on/off

Dew point analysis shows that with given boundary conditions of 28.2°C and 54% RH dew point temperature is 18.0°C. Thus, the system is operating 3 K below required flow

temperature minimum value, according to EN 1264 [2]. However, moisture damage could not be observed because moisture buffering capacity of a multi-layered solid wood panel within a certain hygroscopic range is even higher than the one of massive wood. An investigation, carried out by Popper [7], shows that equilibrium moisture content of a solid spruce wood panel is varying in dependence on the hygroscopic range. Below 65 % RH it is significantly higher than the one of spruce wood. Above this level, it is significantly below.

CONCLUSION

The cooling performance of an innovative multilayered solid wood panel with functional pipe element in the middle layer was laboratory examined.
An evaluation of climate chamber measurements shows that a panel structure could perform well even during intense climatic loads. Under prolonged hygric stress in combination with lower deviation of dew point temperature, moisture damage of a wooden panel with MDF middle layer could not be avoided. However, a solid spruce wood panel remained free of damage, even after 24 hours operation below dew point temperature.
An investigation of a panel`s cooling performance in connection to a defined space of 1 m^3 provides extensive measurement data. Measurement results show that cooling a room with a solid wood panel, although with temporary lower deviation of dew point temperature is possible. Even after a multi-day cooling cycle no damages due to moisture stress were evident. One crucial conclusion is: design criteria according to EN 1264 [2] should not be decisive, rather measured material limits of spruce wood should be considered. For defining these boundaries accurately, further laboratory studies are needed. Subsequently, an analysis of a damage free operation during a long-term test with real climate conditions and user behaviour is necessary.

ACKNOWLEDGEMENTS

This work is part of a research project conducted by the Institute of Building Climatology of Dresden University of Technology and the Institute of Wood Technology Dresden, and was supported by the German Federal Ministry for Economic Affairs and Energy via AiF/iVTH, IGF 17441 BR.

REFERENCES

1. Bishara N., Plagge R. Development of a Solid Wood Panel for Heating and Cooling of Floor, Wall and Ceiling Constructions. 10th NSB, pp 892-899, Lund, Sweden, 2014.

2. European Committee for Standardization. EN 1264-3. Water based surface embedded heating and cooling systems – Part 3: Dimensioning. 2009.

3. Niemz P., Sonderegger W. Untersuchungen zum Sorptionsverhalten von Holzwerkstoffen. *Bauphysik* 31(4): 244-249, 2009.

4. Kollmann F. Technologie des Holzes und der Holzwerkstoffe. Springer-Verlag, Berlin Heidelberg New York, 1982.

5. Niemz P. Physik des Holzes und der Holzwerkstoffe. DRW-Verlag Weinbrenner GmbH & Co, Leinfelden-Echterdingen, 1993.

6. Popper R., Niemz P., Eberle G. Untersuchungen zur Gleichgewichtsfeuchte und Quellung von Massivholzplatten. *Holz als Roh- und Werkstoff* 62: 209-217, 2004.

HOW SOLID IS OUR KNOWLEDGE OF SOLID WALLS? - COMPARING ENERGY SAVINGS THROUGH THREE DIFFERENT METHODS

Jonathan Chambers[1], Virginia Gori[1], Phillip Biddulph[1], Ian Hamilton[1], Tadj Oreszczyn[1], Cliff Elwell[1]

1: UCL Energy Institute, 14 Upper Woburn Place, London WC1H 0NN, UK

ABSTRACT

Recent UK-based studies have shown a performance gap between the energy performance of buildings calculated using tabulated thermophysical properties of solid walls and that estimated from in-situ measurements. Solid-walled buildings have been targeted by UK Government policies and incentive schemes to meet climate change mitigation targets and improve the efficiency of the building stock, as they are less efficient and more expensive to treat than cavity walls. Since it is common practice to estimate energy use and potential savings for buildings retrofit assuming standard values from the literature, the performance gap may have serious implications on the decision-making and the cost-effectiveness of energy-saving interventions.

The aim of this paper is to compare and contrast the results obtained from three different methods for estimating normalised dwelling energy demand:

a) the UK energy performance certificate (EPC) method, which uses the standard assessment procedure (SAP) with tabulated inputs (the business as usual case);

b) the SAP calculated using empirical air change rates from pressure tests and U-values estimated analysing monitored data with a Bayesian-based dynamic method developed by the authors;

c) a normalised annual consumption (NAC) method based on empirical energy consumption data from smart meter and weather data.

The analysis is performed on a sample of dwellings from the Energy Saving Trust "Solid Wall Field Trials" dataset. Results show that EPC estimates are systematically higher (between 7.5% and 22.0%) than SAP. Conversely, the NAC displayed a large range of relative differences (between -77% and +99%) compared to the EPC.

This raises questions about the relative merits and purpose of the EPC and SAP bottom up methods compared to the smart-meter data-driven NAC method. Further research is suggested using SAP 2009 to isolate the thermal component of energy demand and compare it directly with the NAC component.

Keywords: SAP, in-situ U-values, smart meters, heat losses, big data, Bayesian statistics

INTRODUCTION

The EU requires member states to develop an energy performance certificate (EPC) for residential properties to promote comparison of dwelling efficiency. EPCs are mandatory in the UK to either buy, rent or build a property [1]. The standard assessment procedure (SAP) underlies the EPC system in the UK. It defines a simplified model for estimating dwelling energy demand based on building design parameters, normalised for variance in occupancy and

operation [2]. The EPC applies SAP to existing dwellings by using standard tabulated inputs for parameters that are not readily determined in an existing building.

The thermal transmittance, also known as U-value, of external walls is a key parameter in the SAP calculation [3]. Typically assumed U-values of solid walls have recently come under scrutiny, as estimates from in-situ heat-flux measurements found significantly lower values compared to the standard [4]. In most cases the thermophysical performance of solid walls was considerably better than expected with potentially significant implications on EPC consumption estimates, EPC rating and cost-effectiveness of retrofitting interventions. Therefore, interest has risen in understanding the impact that using measured values rather than tabulated data would have on the final outcomes. In this paper SAP calculation was obtained using measurements of the air change rate and estimations of the U-value of walls derived from a novel Bayesian-based approach to analyse in-situ measurements of heat flux and temperatures [5].

Monitoring of dwelling energy demand through smart metering is now becoming widespread due to EU and UK policy [6, 7], making available an unprecedented wealth of data that can be used to extract new information or to validate predictive models. In this paper, monitored consumption was compared with building-design-based EPC consumption estimates. A method is proposed to calculate a normalised annual consumption (NAC) from smart meter data, based on earlier work in this area [8, 9]. Normalisation of the measured demand was needed to compare NAC with EPC and SAP as the latter two approaches are not intended to predict real consumption in an occupied dwelling in a given year. Instead, they calculate demand normalised for occupancy, occupant behaviour, and variations in climate from year to year [2]. The application of SAP to predict actual yearly consumption can be misleading, undermining its purpose as shown in [10].

DATASET

The dataset analysed is a sample of dwellings from the Energy Saving Trust "Solid Wall Insulation Field Trial" project, which aimed at performing deep energy efficiency retrofits on solid-walled buildings (brick and stone) across the UK [11, 12]. We used pre-retrofit data collected through site surveys, including SAP/EPC calculations, air tightness tests and heat flux and air temperature measurements on two close locations of a representative wall.

Due to limitations and issues in the dataset, a subset of dwellings was selected by imposing the following criteria:

- non-ambiguous address to associate climate data and gas calorific values;
- complete pre-retrofit SAP survey;
- both electricity and gas smart meter data covering the period;
- non corrupted consumption measurements. Dwellings with over 100 kW daily average demand (around 50 times the national average [13]) were discarded;
- heat flux and temperature measurements for the period;
- a difference between minimum and maximum temperatures of at least 8˚C (a requirement of the normalised consumption method);
- relative difference of the two estimated U-values less than 10% [11].

A total of 13 sites from the original 83 in the data provided were retained for this analysis. External temperature data [14] was associated with each dwelling based on its address. Gas energy use was calculated from the smart meter volumetric readings according to the National Grid method [15] using historical daily calorific values retrieved for each building location.

METHOD

A three-way comparison was performed between the yearly energy consumption per unit area calculated using: SAP, EPC, and NAC.

The SAP 2005 [2] revision was used as this was the version adopted in the original study [11]. The worksheets calculated energy consumption using ventilation rates and U-values derived from in-situ measurements. U-values were estimated according to the single thermal mass method developed by the authors and described in [5].

The UK EPC energy demand estimate is defined as SAP applied using standard tabulated values for those inputs where measured values are not available (facilitating its applicability to existing buildings).

The NAC value was derived from smart meter data using a variation of the PRISM method described in [8] and building on the work in [9]. In brief, this method uses a 3-parameter consumption model where the total power (P_{tot}) is estimated as:

$$\begin{cases} P_{\text{tot}} = \text{PGT}(T_{\text{ext}} - T_{\text{ref}}) + P_{\text{bl}} & T_{\text{ext}} < T_{\text{ref}} \\ P_{\text{tot}} = P_{\text{bl}} & T_{\text{ext}} \geqslant T_{\text{ref.}} \end{cases} \quad (1)$$

The power temperature gradient (PTG), the baseload power (P_{bl}), and the reference temperature (T_{ref}) are determined by fitting to daily average total consumption and external temperature (T_{ext}) for a given dwelling.

NAC is the sum of monthly demand calculated using SAP reference monthly average temperatures (analogously to PRISM which used US temperatures) [2, 8]. When calculating NAC, T_{ref} is replaced by the SAP external reference temperature to normalise for occupant choice of heating set-point, which in turn determines T_{ref}. PTG and P_{bl} are independent of T_{ref}, so this matches the SAP assumptions for occupant behaviour and makes NAC and SAP commensurable. Per unit area values were obtained using the floor area from the surveys.

RESULTS AND DISCUSSION

The yearly consumption per unit area calculated through each method is shown in Figure 1.

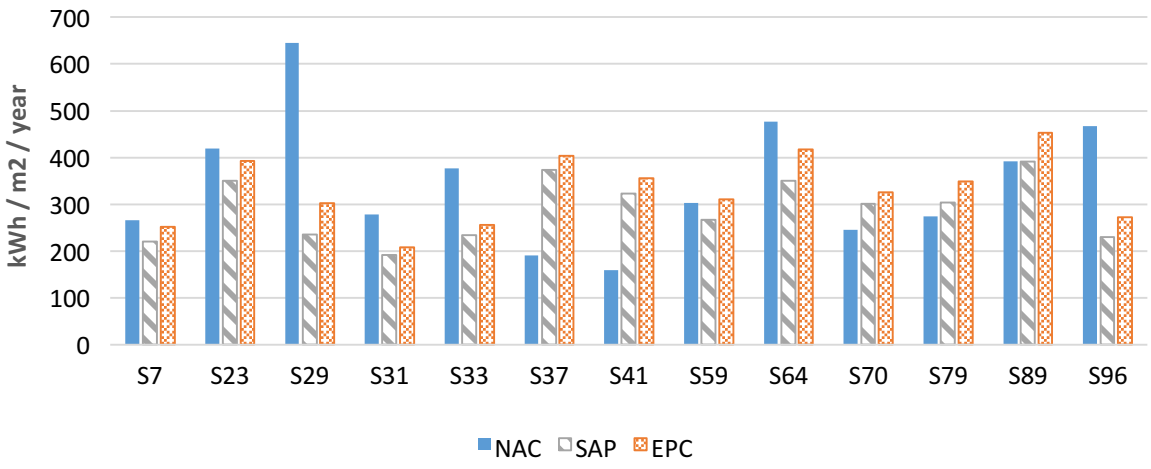

Figure 1: Yearly energy consumption per unit area for each dwelling obtained from the EPC (tabulated values), the SAP (air change rates and U-values from measurements) and the NAC (smart meter data) methods.

Using measured U-values and air change rates reduces the SAP estimate between -7.5% and -22.0% relative to the EPC estimate. The measured U-value, with an average of 1.4 W/m²K

(ranging between 0.7 and 1.8 W/m²K), is considerably lower than the standard value of 2.1 W/m²K for solid walls. The external heating reference temperature, derived in the SAP method from the dwelling thermal properties and gains, saw a corresponding average decrease of 0.4˚C (between -0.2˚C and -1.0˚C). As a result, energy consumption per square metre estimated by SAP decreased by 12.0% on average (between -7.5% and -22.0%) compared to the EPC (Figure 2).

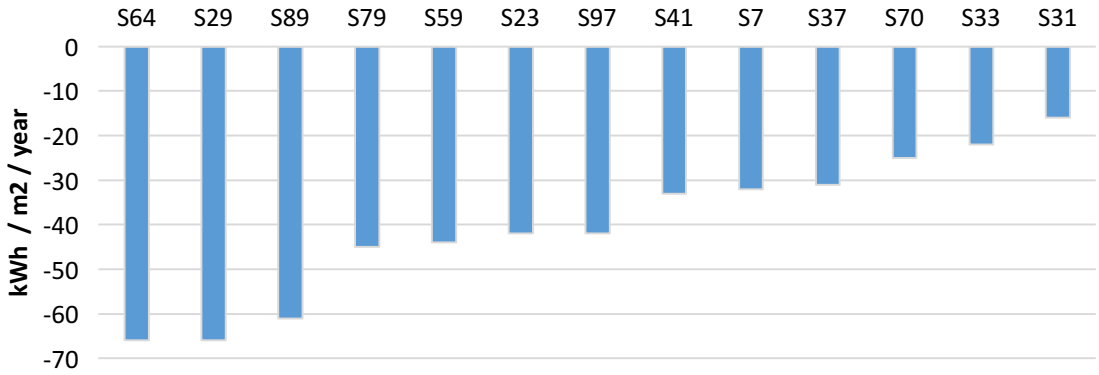

Figure 2: Difference in the yearly energy consumption per unit area of EPC and SAP.

Conversely, the NAC values from measured consumption were on average 14.1% higher than the EPC estimates. However, as is clear from Figure 3 (left), the range of differences is very large and does not follow any evident pattern. While a few sites remain within 10.0% of the EPC estimate, others diverge considerably with differences ranging from -77.0% to +99.0%.

The NAC is on average 0.4% higher than the SAP estimate. However this may be misleading as shown in Figure 3 (right). The divergence is even larger than with the EPC, with NAC ranging from -74.0% below to +155.0% above SAP. Using measured data in the SAP model surprisingly resulted in worse agreement. There are many potential causes for the difference between EPC and NAC estimates of energy use, including:

- NAC accounting for a baseload term which can differ from the EPC assumption;
- U-values of roofs and windows;
- hidden thermal bridges;
- efficiencies of heating systems which may differ from manufacturer quotes.

To identify sources of difference between SAP and NAC, a partial comparison using only the PTG thermal loss component could be performed. To obtain a PTG from SAP, monthly energy demand values are needed. The SAP 2009 revision [16] of the standard added monthly estimates, but it was not used here since the trial used SAP 2005. Future work could use SAP 2009 to perform this comparison.

The results could be further consolidated by recovering additional sites by repairing the input data. Dwellings with full heat-flux and ventilation rate measurements are rare, as current methods for the evaluation of U-values from in-situ measurements require long monitoring campaigns (up to two weeks) and are seasonally bounded to the wintertime [5]. Therefore, the immediate prospective dataset is limited to the 85 dwellings in the Solid Wall Field Trial. However, the U-value estimation method developed by Biddulph [5] could enable more buildings to be tested rapidly, as its dynamic Bayesian-based approach needs shorter time series and can in principle be used in all seasons. Smart meter data should also be extensively available in the near future. It would be particularly interesting to compare results for different wall types.

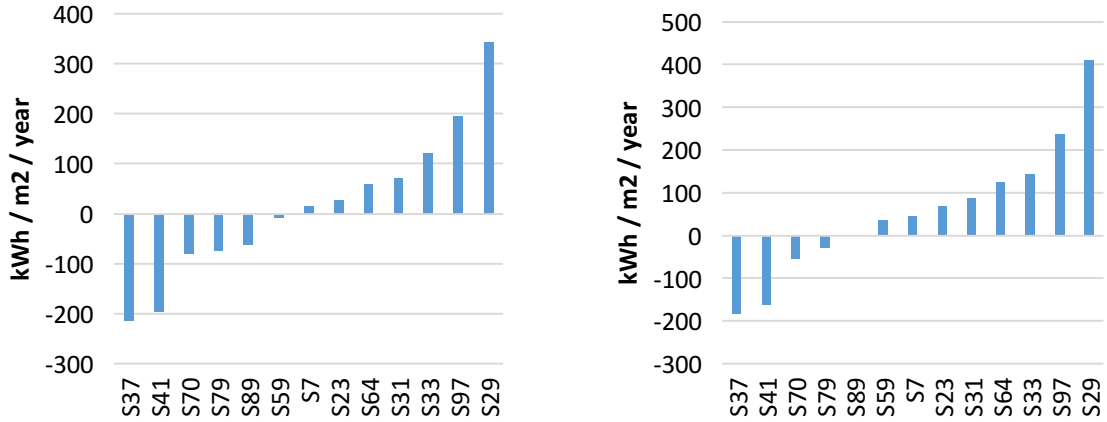

Figure 3: Difference between NAC and EPC (left) and SAP (right).

CONCLUSION

This study performed a three-way comparison between the EPC - which is the standard method for characterising dwelling energy demand, SAP - which uses the same model but with measured rather than tabulated air change rates and wall U-values, and NAC - which normalises measured energy consumption for reference temperature. Thirteen sites with good quality data were selected from the "Solid Wall Field Trials" dataset [11, 12]. It was found that EPC estimates of energy demand for solid-walled buildings were systematically higher (between +7.5% and +22.0%) compared to SAP. However, the NAC varied greatly compared to SAP and EPC, with values of yearly energy demand per square meter as low as -77% below the EPC rating and as high as +99% above it. Future work could consolidate this result by enlarging the sample and extending the analysis to other wall types. The use of SAP 2009 [16], which includes a power-temperature-gradient thermal loss term, could also enable the direct comparison SAP and NAC approaches eliminating potential sources of uncertainty.

This study raises questions about the relative representativeness and applicability of the three methods investigated. EPC does not address as-built performance or in-use behaviour as it is only based on models, visual inspections, building plans and standard tabulated thermophysical properties. Although SAP tries to overcome this limitation by introducing the possibility of using measured properties instead of tabulated ones, it uses spot measurements that may still not account for all aspects contributing to the overall thermal performance of a real dwelling, such as ventilation practices and occupants' thermal comfort. This highlights the challenge of using modelling tools to estimate real building performance.

Smart-meter data-driven methods like NAC may represent a solution to provide a whole-house as-built performance and reconcile models and measurements. However, these approaches may lead to highly variable results as they encapsulate a range of unknowns (e.g., occupants' behaviour, materials performance or build quality) that may be difficult to isolate and quantify. This poses the question whether different assessment tools should be considered to assess the design or the whole system performance to reflect the goals of the evaluation.

ACKNOWLEDGEMENTS

This research was made possible by support from: the EPSRC Centre for Doctoral Training in Energy Demand (LoLo), grant numbers EP/L01517X/1 and EP/H009612/1; DECC under the 'Analysis of Solid Wall Field Trial Data' project; EPSRC and EDF Energy R&D UK; EPSRC 'Research Councils UK (RCUK) Centre for Energy Epidemiology' under EP/ K011839/1.

REFERENCES

1. UK-Gov: Buying or selling your home - GOV.UK. Retrieved May 7, 2015, https://www.gov.uk/buy-sell-your-home/energy-performance-certificates .
2. BRE: SAP2005 - The Government's Standard Assessment Procedure for Energy Rating of Dwellings. 2005.
3. Hughes, M., Palmer, J., Cheng, V., Shipworth, D.: Global sensitivity analysis of England's housing energy model. Journal of Building Performance Simulation, 2014.
4. Li, F.G.N., Smith, A.Z.P., Biddulph, P., Hamilton, I.G., Lowe, R., Mavrogianni, A., Oikonomou, E., Raslan, R., Stamp, S., Stone, A., Summerfield, A.J., Veitch, D., Gori, V., Oreszczyn, T.: Solid-wall U-values: heat flux measurements compared with standard assumptions. Building Research & Information, 43(2), 1-15, 2015.
5. Biddulph, P., Gori, V., Elwell, C. A., Scott, C., Rye, C., Lowe, R., & Oreszczyn, T.: Inferring the thermal resistance and effective thermal mass of a wall using frequent temperature and heat flux measurements. Energy and Buildings, 78, 10-16, 2014.
6. European Comission: Over 70% European consumers to have a smart meter for electricity by 2020. 2014. Retrieved October 1, 2014, https://ec.europa.eu/jrc/en/news/over-70-percent-european-consumers-have-smart-meter-electricity-2020 .
7. DECC: Smart meters - Helping households to cut their energy bills - Policies - GOV.UK. 2014. Retrieved March 18, 2014, https://www.gov.uk/government/policies/helping-households-to-cut-their-energy-bills/supporting-pages/smart-meters .
8. Fels, M. F.: PRISM: An introduction. Energy and Buildings, 9(1-2), 5–18, 1986.
9. Summerfield, A. J., Oreszczyn, T., Hamilton, I. G., Shipworth, D., Huebner, G. M., Lowe, R. J., & Ruyssevelt, P.: Empirical variation in 24-h profiles of delivered power for a sample of UK dwellings: Implications for evaluating energy savings. Energy and Buildings, 88, 193-202, 2015.
10. Kelly, S., Crawford-Brown, D., & Pollitt, M. G.: Building performance evaluation and certification in the UK: Is SAP fit for purpose? Renewable and Sustainable Energy Reviews, 16(9), 6861–6878, 2012.
11. Birtchall, S., Pearson, C., Brown, R.: Solid Wall Insulation Field Trial - Baseline Performance of the Property Sample. Report 53588/x, BSRIA Limited, Bracknell (UK), 2011.
12. Stevens, G., & Bradford, J.: Do U-value insulation ? England's field trial of solid wall insulation. Eceee 2013 Summer Study, 1269–1280, 2013.
13. DECC: Domestic energy consumption in the UK between 1970 and 2012. In *Energy Consumption in the UK*, 2013.
14. Sharp, E., Dodds, P., Barrett, M., & Spataru, C.: Evaluating the accuracy of CFSR reanalysis hourly wind speed forecasts for the UK, using in situ measurements and geographical information. *Renewable Energy*, *77*, 2015.
15. NationalGrid: Calorific Value Information. Retrieved April 17, 2015, http://www2.nationalgrid.com/UK/Industry-information/Gas-transmission-operational-data/calorific-value-description/ .
16. BRE: SAP2009 - The Government's Standard Assessment Procedure for Energy Rating of Dwellings. 2009.

SENSITIVITY ANALYSIS OF THE LIFE CYCLE EMISSIONS FROM AN NZEB CONCEPT

A.A. Houlihan Wiberg[1]; L. Georges[2]; S.M. Fufa[3]; C.S. Good[1]; B. Risholt[3];

1: Zero Emissions Research Centre (ZEB), The Faculty of Architecture and Fine Art, Norwegian University of Science and Technology (NTNU), N-7491 Trondheim, Norway
2: Department of Energy and Process Engineering, Norwegian University of Science and Technology (NTNU), N-7491 Trondheim, Norway
2: SINTEF Building and Infrastructure, Høgskoleringen 7b, N-7465 Trondheim, Norway

ABSTRACT

The *net-zero emissions building* (nZEB) performance is investigated for building operation and embodied emissions in materials for Norway's cold climate. An nZEB concept for new residential buildings was developed in order to understand the balance and implications between operational and embodied emissions over the building's life. The main drivers for the CO_2 equivalent (CO_{2eq}) emissions were revealed for the building concept through a detailed emissions calculation.

Previous investigations showed that the criterion for zero emissions in operation is easily reached by the nZEB concept (independent of the CO_{2eq} factor considered). Nevertheless, embodied emissions from materials appeared significant compared to operational emissions. It was found that an overall emissions balance, including both operational and embodied energy, is difficult to reach and would be unobtainable in a scenario of low carbon electricity from the grid i.e. low CO_{2eq} factor for electricity.

In order to make these conclusions robust, a sensitivity analysis was performed on the dominant sources of CO_{2eq} emissions, as well as, on how it impacts the emission balance during the building lifetime. In the baseline work, *embodied emissions* were evaluated using the EcoInvent database in order to get a consistent life cycle assessment (LCA) method for all the building materials. The first step of this sensitivity analysis is therefore performed to compare embodied emissions when specific Norwegian *Environmental Product Declarations* (EPD) were used instead of generic data from EcoInvent thus making data more representative for the Norwegian context.

In addition, the photovoltaic (PV) system, which supplies renewable electricity to the building, also contributes significantly to the embodied emissions. The second step of the analysis evaluates different PV system design options in order to find the one with highest net emissions reduction. Finally, since the building concept was based on a highly-insulated building envelope, the dominant source of emissions during building operation turned out to be electric appliances. The third step of the analysis thus discusses the energy consumption of electric appliances and how it could be reduced through more efficient products, especially the so-called *hot-fed* machines (i.e. washing machines, tumble dryer and dishwasher).

Keywords: Generic and specific EPD data, embodied emissions materials, ZEB balance

INTRODUCTION

This sensitivity analysis represents further work based on the results of the original ZEB concept study published in 2013 [1], where the calculations of embodied emissions (EE) from the construction materials and components were based on generic material data from the Ecoinvent database. In the original ZEB report, the EE of the materials in the ZEB concept residential building were calculated to provide an overview of embodied emission using traditional materials in the envelope, ventilation & heating systems, as well as, those associated with the renewable energy system, such as the photovoltaic panels and solar thermal units. The objective was to identify the key materials and components l which contribute the most to EE. For instance, results show that the total EE from materials correspond to 7.2 $kgCO_{2eq}/m^2$ per year (59%) of the overall emissions, whilst the emissions from operation correspond to 5.0 $kgCO_{2eq}/m^2$ per year.

The main research question in this sensitivity analysis is to investigate if it is possible to achieve a ZEB OM ambition level if the EE for the construction materials used in the ZEB concept building is

calculated using Norwegian EPD data rather than generic Ecoinvent data. A secondary question is to analyse the effect of using different CO_{2eq} factors for the electricity used in operation and see how this factor affects the ZEB ambition level for the residential concept building and the payback of CO_{2eq} emissions over the building's lifetime. The impact of reduced loads from electrical appliances is also included in this study. Full details of this sensitivity analysis can be found in Houlihan Wiberg et al., 2015. [2]

METHOD

Goal and Scope

The goal of this work is to investigate not only the effect on EE of materials and the overall performance of ZEB concept residential building, of using specific Norwegian EPD data instead of generic Ecoinvent data. The method includes the calculation of the CO_{2eq} emissions from both materials and operation. A functional unit of 1 m^2 of heated floor area in the residential building over the 60 year estimated lifetime of the building is used. The results are presented for emissions on an annual basis, where the functional unit of 1 m^2 is divided by the building lifetime. The estimated service lifetime of the different materials and components is mainly based on the guidelines from different product category rules. The analysis is limited to cradle-to-gate for the material emissions (product stage: A1-A3) and replacement (B4) has been included.

Simulation Tools

The 3D architectural drawings and 3D BIM modeling have been done using Revit version 2012 Embodied emission. The material quantities have been imported from the Revit BIM-model, via Excel. The embodied emissions calculations have been done using the LCA Software tool SimaPro version 7.3.3 [3] which uses emissions data from the Ecoinvent v.2.2 database [4]. Simulation of annual heating and cooling demand, peak heating and cooling load, net energy budget, heat loss calculation, thermal comfort simulation and CO2-level simulation have been done in SIMIEN version 5.011 [5]. Thermal bridge calculations have been done in the numerical software tool Therm [6]. Performance calculations of the air source heat pump combined with solar thermal collectors have been done using PolySun [7]. Performance of the PV-systems has been calculated with simplified spreadsheet models (Excel), but is verified by the PV-tool PV-syst [8].

Concrete, insulation, plasterboard materials EPD data have been selected for this first step of the sensitivity study since these are responsible for the highest emissions, apart from PV. Even though the EE from PV contribute the most emissions, they are not included in this analysis since there are no available Norwegian EPDs for this product. Instead, the influence of different PV technologies and different module orientations on the embodied and avoided emissions is incorporated from the work presented by Good et el.(2014) at the Eurosun conference [9]. Wood was also selected in this sensitivity study to study the benefits of using locally resourced materials using Norwegian EPD data.

For both the generic data and EPD material data, tables containing detailed information on the process, place of production, density, grid electricity mix ($kgCO_{2eq}/kWh$) and EE ($kgCO_{2eq}/m^3$) together with references can be found in the full sensitivity report [2]. An example of the table used for the analysis can be shown with concrete which exists in the foundation and ground works, and apart from PV, was one of the materials driving the highest emissions in the original study of the residential concept building. The Norwegian EPD data for Betong Øst [10] produced in Norway based on 1 m^3 of product, according to precast concrete PCR [11], is used for the sensitivity analysis (Table 1).

Table 1. Concrete materials used for the sensitivity analysis.

Concrete	Process	Place of Production	Density (kg)	Electricity mix	Embodied emissions (kg CO_2eq/m^3)
ZEB original data	Concrete, normal, at plant/CH U ZEB	Switzerland	2380	CH U	261,2
Norwegian EPD	Ferdigbetong B25M60	Norway	2358	Nordpool	189, 9

It should be noted that when conducting EPDs for building materials, the choice of emission factor used for the electricity mix varies between different consultants and researchers. Some researchers and

consultants use the production/consumption electricity mix for Norway based on an average for the last three years while others use the Nordic electricity mix with a higher emission factor. Currently there is no consensus on which electricity mix should be used for Norwegian EPDs other than that the emission factor used for electricity in the production of the material should be stated on the EPD.

The emissions from the building needs to be balanced (offset) by renewable electricity production (e.g. PV), which is either used for self-consumption (reducing delivered electricity) or exported electricity to the grid. The design of the onsite electricity production and the total life cycle CO_{2eq} balance is calculated to see if the PV-production meets the (different) ZEB-definition levels. At a given location, the electricity yield of a PV system is highly dependent on the design of the installation. Four different design options were evaluated in order to find the most favourable in terms of EE versus electricity yield. The amount of emissions that are replaced by the electricity from the PV system also depends on the grid factor of the electricity it replaces. Four alternative design options suitable for flat roofs, each with three different PV technologies (mono-Si, poly-Si and CIS), were simulated in PVsyst [1]. The design alternatives were A) optimal orientation (south facing at 40° tilt), B) south facing at 15° tilt, C) south/north facing at 15° tilt, and D) east/west facing at 40° tilt. The total EE for the systems were calculated as well as the net emissions reduction, i.e. difference between *avoided* emissions from the renewable electricity and the *EE* of the modules.

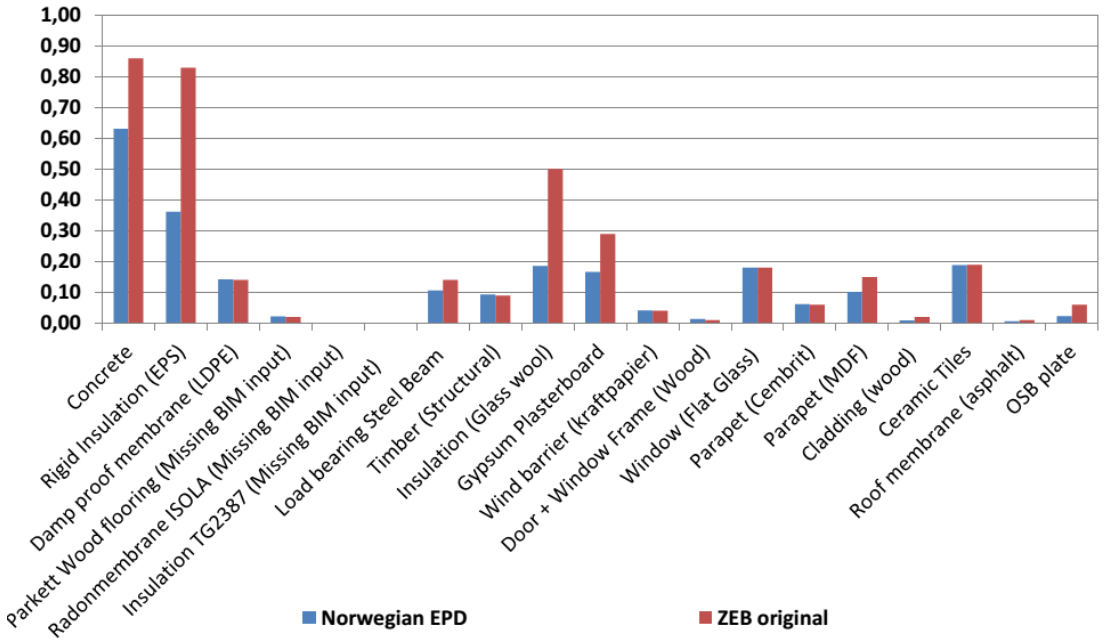

Figure 1. CO_{2eq} emission comparisons between ZEB original study and Norwegian EPD switch for main materials inputs.

RESULTS

The reduction in emissions resulting from the switch to specific Norwegian EPD data compared to those used in the original ZEB residential building using generic Ecoinvent data, is shown in Figure 1.

The overall results show that by identifying the materials responsible for the highest emissions such as concrete, mineral wool and EPS insulation, plasterboard (and wood even though this is not a high emitter) in all the building components, the total EE for these materials can be reduced from the baseline of 7,2 to 5,8 $kgCO_{2eq}/m^2/year$ when the Norwegian EPD data was substituted for the generic data. Although, this reduction is largely as a result of the Norwegian EPD using a much lower emission factor for the Nordel electricity mix and that the material efficiency, process technique used, heat energy and other factors can also play a crucial role.

PV System

The analysis of the three module types showed that CIS modules had the lowest amount of EE per generated kilowatt hour, i.e. the "greenest" electricity, but that the mono-Si modules had the highest

net emissions reduction due to their high efficiency. The PV system simulations showed that amount of net avoided emissions was largest for system C, with low-tilt modules facing north and south, even though the EE of this system was largest. System A performed better in terms of kilowatt hours per module, and the north facing modules in system C gave only 70% of the electricity compared to the modules in system A. The avoided emissions (negative) are larger with the EU grid factor (0.45 kg CO_{2eq}/kWh) is used, than when the ZEB grid factor (0.132 kg CO_{2eq}/kWh) whereas the EE (positive) are the same.

Emissions from operation of electric appliances and hot-fed machines

Finally, since the building concept is based on a highly-insulated building envelope, the dominant source of emissions during building operation turned out to be electric appliances. In the baseline work, the estimated yearly electricity consumption was taken as 2388 kWh/year. A literature survey [2] proved that this value is well representative for the average yearly electricity consumption of existing households in Norway. Therefore, this value does not account for best equipments with the highest efficiency, or neither accounts for user behaviors that promote energy saving. This average electricity consumption of 2388 kWh/year can thus be reduced but it is difficult to quantify this potential of reduction.

Among electric appliances, the dishwasher, the clothes dryer and the washing machine account for 765 kWh. Being a large contributor to the total electricity load, alternative strategies to reduce their consumption are here investigated. Basically, these equipments use electricity to directly warm up the water during a cycle. This way of converting electricity is known to be ineffective. On the contrary, *heat-fed* machines are equipped with a built-in heat exchanger that enables the centralized heating system of the building to provide for the heat to warm the water as well as the content of the machine (e.g. structure, the crockery). A recent experimental study [3-5] as shown that, using an inlet hot water at 80°C, 81% of the electricity for the washing machine can be substituted by hot water, 80% for the dishwasher and 87% for the clothes dryer. Unfortunately, this quantity drops drastically if an inlet temperature of 55°C is used: the substitution is then reduced to 55%, 50% and 78%, respectively. This temperature limit of 55°C does well correspond to the heat pump technology used in the ZEB residential concept. Assuming yearly average COP of 2.5 for produced water at 55°C, calculations show a reduction of ~300 kWh. It thus corresponds to a ~40% reduction compared to the initial 765 kWh. It clearly proves that this kind of improvement should be considered in a sound ZEB concept.

CO_{2eq} factors for grid electricity during operation

The baseline factor of 132gCO_{2eq}/kWh is based on a specific scenario termed UltraGreen. It assumes that the Nordic and European grids will be strongly interconnected and that a massive de-carbonization of the European electricity grid will take place in the next 40 years is in good agreement with the objective of the European Union. In practice, the 132 gCO_{2eq}/kWh is taken as the 60-year average of this evolution, explaining its relatively low value. Even though realistic, the performance of the ZEB concept with regards to alternative scenarios for the CO_{2eq} factor is investigated and is detailed in Georges et al. [17]. Only the main results will be reported here.

Modified Model

In the modified model, the generic data has been replaced with the EPDs resulting in the EE from materials being reduced from 7.2 to 5.8 kgCO_{2eq}/m²year. In addition, the electricity load can be reduced from the 14.9 to 11.6 kWh/m² per year essentially using more consolidated data for household appliances and hot-fed machines. This corresponds to an annual CO_{2eq} reduction of 0.24 kg/m^2.The balance of CO_{2eq} emissions is changed when both the emissions from materials and

operation are included together depending on the choice of the grid mix as shown Figure 3

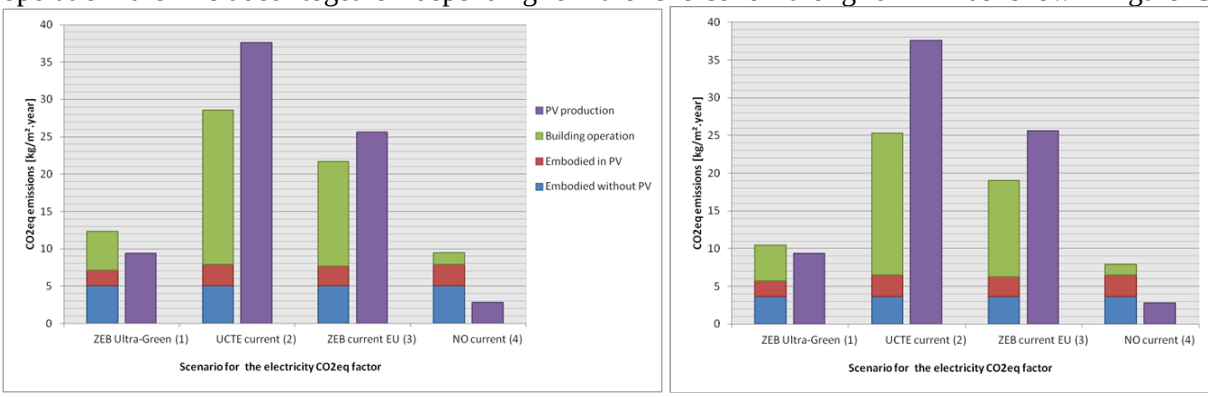

Figure 3. Annual CO_{2eq} emissions and offset from PV for the original (left) and modified (right) ZEB concept, for the different CO_{2eq} factors for the electricity [2].

The improvement in the modified model is clearly noticeable but does not alter conclusions. It proves that previous conclusions as regards the ZEB concept performance were robust. It is nevertheless important to note that ZEB-OM is almost reached when the ZEB Ultra-Green CO_{2eq} factor is used. The magnitude of EE and EO is also significantly improved. In the ZEB Ultra-Green scenario (i.e. low-carbon grid), EE in materials can be dominant and the largest improvement is due their reduction..

DISCUSSION AND CONCLUSION

The results from the switch to specific Norwegian EPD data show a significant reduction in total EE for materials from 7.2 to 5.8 $kgCO_{2eq}/m^2$ per year. The EE data are extracted from publicly available Norwegian EPDs that are performed according to EN 15804. However, it should be noted that these calculations reflect cradle to gate emissions (A1-A3) and replacement (B4) but do not reflect the even greater potential if calculated for cradle to grave emissions where the longer term benefits of wood as a carbon store can be seen. It should be made clear that emissions related to transport from cradle to factory gate (A2) are accounted for in our calculations but those emissions related to transport from gate to construction site (A4) have not been included. The true benefits of using specific data for those products produced in Norway would be seen if the system boundary is extended to include transport emissions.

It should also be noted that the results for the Norwegian EPD switch are based on the emission factor calculated using the CO_{2eq} factor for the Nordel mix compared to a much higher value used for RER or average European mix, which can result in a significant reduction in emissions as can be seen in the case of concrete where the much lower CO_{2eq} factor for the Nordel mix is used in the calculations. Even if the calculation of embodied emission has uncertainties, preliminary results indicate significant reduction of EE by replacing generic data with specific data from EPDs.

As regards the PV installation, the net emissions reduction was largest for the design alternative with north and south facing modules at low tilt angles (i.e. design "C"). However, the benefit of installing low-performing north facing modules in order to reach an emission balance can be questioned, since the performance of these modules was low. The highest net emissions reduction was found to result from the largest PV system with the highest efficiency modules (system C with mono-Si modules), even though this system also resulted in the highest amount of EE.

The CO_{2eq} factor considered for the electricity imported and exported to the grid has a large influence on the net ZEB balance. For instance, the ZEB-OM balance is not reached in the context of a low-carbon grid which corresponds either to the Norwegian grid connected to the future de-carbonisation European grid, or to the current situation with a Norwegian grid that has some transmission capacity to Nordic countries, but are only to a limited degree connected to the European grid. In this context, the EE can be higher than the emissions for the building operation during the 60 year lifetime. On the contrary, if the emission factor grid electricity is relatively high, a scenario corresponding to a Norwegian grid fully connected to a European grid without de-carbonization, the ZEB-OM balance is reached and the emissions for building operation dominate over EE.

Finally, this paper investigates the influence of using Norwegian emission data (from EPDs), using different CO_{2eq} factors (for electricity in the operational phase) and electricity load from household appliances (using data for household appliances and hot-fed machines) on the overall ZEB residential building performance. This sensitivity analysis showed that the previous conclusions about the performance of the ZEB residential concept were essential correct. The ZEB-OM is difficult to reach in the context of a low-carbon electricity grid, even though improvements proposed in the paper managed to get close to the strict balance of emissions.

When discussing the performance of ZEB, one should be very careful as this performance is not only limited to a balance of CO_{2eq} emissions. In fact, the overall ZEB performance is the combination of its energy efficiency, reduced EE and emissions for building operation, on-site renewable energy conversion, flexibility offered to the electricity grid (e.g. grid interaction), as well as, balance of CO_{2eq} emissions. By the way, in the context of a low-carbon grid, it is not because the ZEB-OM balance is not reached that the interest into the ZEB concept is essentially lost. For instance, ZEBs are considered necessarily to shift to this low-carbon grid due to their high energy efficiency, onsite renewables and the flexibility they can provide to the grid.

REFERENCES

1. HoulihanWiberg,A.,Georges,L.,Dokka,T.H.,Haase,M.,Time,B.,Lien,A.G.,Mellegård, S., Maltha, M. *A net zero emission concept analysis of a single-family house.* Energy and Buildings, 2014. **74**: p. 101-110.
2. HoulihanWiberg,A.A,Georges,L.,Mamo Fufa,S.,Good,C.,Risholt,B. *A zero emission concept analysis of a single family house: Part 2 sensitivity analysis*. The Research Centre on Zero Emission Buildings (ZEB), Editor. 2015, SINTEF
3. PRe´ Consultant. SimaPro Life Cycle Analysis, Simapro 7.3 (Version 7.3.). 2012, Amersfoort, the Netherlands.
4. Ecoinvent version 2.2. Swiss Center for Life Cycle Inventories. (2010)., Accessed from http://www.ecoinvent.ch/
5. ProgramByggerne. SIMIEN, SIMulation of Indoor climate and ENergy use (Version 5.0.14). 2012, Skollenborg. Retrieved from http://www.programbyggerne.no/SIMIEN
6. THERM software. No reference.
7. S. Vela, Polysun, 2012, 5.10.9, available from: http://www.velasolaris.com
8. PVsyst SA, *PV-syst 5.73, Photovoltaic System Software* A. Mermoud, Editor. 2011, University of Geneva.
9. Good, C., Kristjansdottír, T., Houlihan Wiberg, A.A., Georges, L., Hestnes, A.G. A comparative study of different PV installations for a Norwegian net ZERO emission building concept in Eurosun conference. 2014. Aix-les-Bains, France.
10. NPCR 020, *Product-category rules for Precast concrete products, NPCR 020*. 2012, The Norwegian EPD Foundation, Oslo, Norway.
11. NEPD 123N, *Ferdigbetong B25 M60 , Betong Øst, NEPD nr.: 123N*. 2013, The Norwegian EPD Foundation, Oslo, Norway.
12. 13. Sæle, H., Rosenberg, E., Feilberg, N., State-of-the-art projects for estimating the electricity end-use demand. 2010, SINTEF: Trondheim.
14. Persson, T., Dishwasher and washing machine heated by a hot water circulation loop. Applied Thermal Engineering, 2007. **27**: p. 102-128.
15. Persson, T. and R. Renström, Fjärrvärmedrivna vitvaror: erfarenheter från utveckling, installationer och kostnadsberäkningar. 2013, Svensk Fjärrvärme AB.
16. Persson, T. and M. Rönnelid, Increasing solar gains by using hot water to heat dishwashers and washing machines. Applied Thermal Engineering. **27**: p. 646-657.
17. Georges, L., Haase, M., Houlihan Wiberg, A.A., Kristjansdottir, T., Risholt, B. *A Life cycle emissions analysis of two nZEB concepts.* Building Research and Information, 2015. 43(1): p. 83-93

HOW CURRENT TRENDS IN THE DESIGN OF FACADES INFLUENCE THE FUNCTIONAL QUALITY OF INTERIOR SPACES

B. Paule[1], F. Flourentzos[1], M. Bauer[1], S. Pantet[1]

1: Estia SA, EPFL Innovation Park, Lausanne, Switzerland

ABSTRACT

During the last decade, all construction standards evolved rapidly and became increasingly demanding in terms of energy performance. The joint reduction of heating and cooling loads resulted in a rise of the relative importance of electricity consumption due to indoor lighting. As a result, the question of daylight is getting more and more important and has to be addressed carefuly in the design process.

In this context we can see the emergence of a dominant trend in the design of facades of non-residential buildings, which results in an alternating composition of glass and opaque vertical stripes. Beyond the aesthetic implications, we do not allow ourselves to judge, we can imagine that this type of system can be advantageous in terms of building rationality.

However, this paper shows that this design trend have some negative implications in terms of thermal behaviour without bringing any decisive advantage with respect to visual comfort and natural lighting. We evaluated the performance of three variants of this particular typology and compared them with a classical horizontal opening fitted with a 95 cm sill height. The results show that, when applied to the case of an individual office, this trend is far from optimal.

This study leads to clearly point out the main advantages and drawbacks of these typologies and we believe that the outcomes of this work could be useful to designers and contribute to promote efficient design solutions regarding both architectural quality and energy performance.

Keywords: Window, daylighting, overheating risks, heating loads, energy demand.

INTRODUCTION

In the early twentieth century, the window strip proposed by Le Corbusier was the subject of controversy in the architectural environment. Beyond academic considerations, the arguments to defend this new form of opening were the benefits associated with the use of daylight:

" It illuminates better: in fact, its shape allows him to gather all its light at the height useful which is that of the eyes of the inhabitant" [1].

Nearly a century later, curtain wall facades offer complete freedom in the façade composition between glazed and opaque parts. This freedom can be exploited to optimize all functions performed by the window, namely, daylighting, ventilation, contribution to solar gain and thermal insulation in winter and control of the overheating risks in summer.

Figure 1: View of the strip window of the « petite maison » in Corseaux (CH). Photography published by Le Corbusier in his Almanac of Modern Architecture, Paris, 1926, with the caption: «La fenêtre a 10,75 m de long. En hiver, le site "est là" comme si l'on était au jardin. Alors les jours ne sont plus tristes; de l'aube à la nuit, la nature déploie ses métamorphoses».

In our daily practice as a consulting firm in building physics, we see more and more projects whose facades are composed of vertical stripes, fitted with glazed parts from the floor to the ceiling (see Figure 2). Although this observation is not based on statistical data, we thought it was interesting to compare the overall performance of these types with the horizontal band mentioned above.

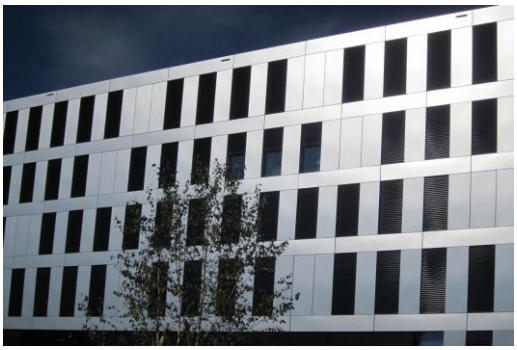

Figure 2: Office buildings in the Lausanne areas,
Left: D. Perrault architect, Right: CCHE architecture; photos Estia SA.

METHODOLOGY

We concentrate on an individual south oriented office room (depth = 5.50m, width = 3.50m, height = 2.70m) and we analysed the four typologies presented in Table 1 (WFR = total glazed area/floor area). The glazing characteristics are as follow: T_v = 0.80, g= 0.62, U_g = 1.1 W/m^2°K. The reflection coefficients are as follow: ρ_{floor}=0.3, ρ_{walls}=0.5, $\rho_{ceiling}$=0.7. The south facade is the only one in contact with outdoors (U_{value} of opaque part = 0.19 W/m^2°K). The occupancy scheme follows the Swiss regulation for office rooms: 7 am- 6 pm, 5 days per week, totaling 2871 hours of use per year. The required illumimance level is 500 lux on the work plane (height = 75 cm). The room is facing south.

	Type 1	Type 2	Type 3	Type 4
Axonometric	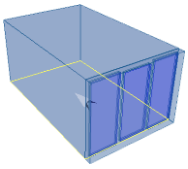	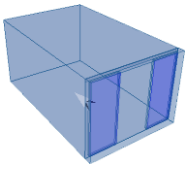	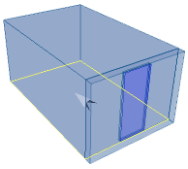	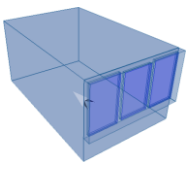
Window to floor ratio	39%	26%	12%	25%

Table 1: Schematic description of the four typologies that were analysed.

The following topics are addressed:

- Daylight contribution (Daylight factor, Diffuse Daylight autonomy)
- Heating loads
- Cooling loads
- Visual appraisal

The comparisons were made by means of numerical simulations with DIAL+ software [2]. The energy weighting factors follow the Minergie® recommendation [3], e.g. electricity : 2.0; fossil fuels (heating): 1.0, cooling : 0.5 (COP = 4).

RESULTS AND DISCUSSION

A) Daylighting

To compare the lighting performance of the different types, we calculated the diffuse daylight autonomy (DDA, [4]), on the basis of daylight factor values (DF). DDA represents the percentage of time during which the indoor illuminance exceeds a certain illuminance value (here 500 lux) only with the diffuse component of the sky. Table 1 summarizes the results of the lighting analysis of the 4 types. Obviously, Type 1 shows the best performance, Type 3 the lowest one, and Type 4 is very close to Type 1.

	Type 1	Type 2	Type 3	Type 4
Diffuse Daylighting Autonomy distribution (7am-6pm)			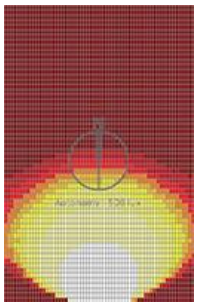	
Average DDA	56.7%	42.7	26.3%	53%
Average DF	6.0%	3.8%	2.1%	5.1%

Table 2: Daylighting contribution for the 4 types (simulations DIAL+Lighting).

B) Electric lighting

The electric lighting installation is composed of 4 downward luminaires Channel Office CLD 2x28W, with a total installed power of 246 W, e.g. 12.8 W/m^2. Switching of the luminaires is automated (ON if average illuminance < 500 lux & OFF if average illuminance > 500 lux). To estimate the energy consumption due to electric lighting, we applied the Swiss standard calculation procedure (SIA 380/4, [5]). Table 3 shows the results for each of the types.

	Type 1	Type 2	Type 3	Type 4
Full charge hours (7-18h) SIA	832 h	1185 h	2303 h	1205 h
Lighting demand SIA (7-18h)	10.7 kWh/m^2	15.3 kWh/m^2	29.7 kWh/m^2	15.5 kWh/m^2
Weighted energy SIA	21.4 kWh/m^2	30.6 kWh/m^2	59.4 kWh/m^2	31 kWh/m^2

Table 3: Energy consumption due to electric lighting according to SIA calculation.

We note that this calculation method clearly favors Type 1. Thus, the number of hours is reduced by about one third compared to type 4, while the difference in terms of autonomy is only 3.7% of the opening hours (56,7% vs 53%, see Table 2).

C) Heating / Cooling loads

To estimate the influence of each type on the heating loads, we performed dynamic thermal simulations with the thermal module of DIAL+[6,7,8,9]. In order to facilitate comparison, we decided to cool the room and to look at the specific cooling demand. Furthermore, in order to avoid bias related to users, we considered automated blinds.

The room characteristics follow the Swiss standard SIA 2024 for offices

- Room parameters: Floor: concrete slab + False floor; Outdoor Walls: Light wall, Insulation thickness: 20cm; Indoor walls: light walls; Ceiling: Concrete slab, no coating;
- Internal gains: Occupants: 5 W/m^2; Electric equipment: $7W/m^2$;
- Heating device: radiators, T_{min}: 21°C; P_{max}: 1,92 kW
- Cooling: Coil heater, T_{max} = 26.5°C, P_{max} = 3.85 kW (no openings)
- Ventilation: Air flow during room use: 49.5 m^3/h; Air flow when room not in use: $6m^3/h$
- Shading: Automated external venetian blinds,
  Blinds down when incident flow > $90W/m^2$ and Indoor Temp > 22°C

	Type 1	Type 2	Type 3	Type 4
Cooling demand	7.4 kWh/m^2	5.7 kWh/m^2	5.6 kWh/m^2	4.6 kWh/m^2
Weighted energy for Cooling	3.7 kWh/m^2	2.85 kWh/m^2	2.8 kWh/m^2	2.3 kWh/m^2
Heating demand	37.0 kWh/m^2	29.5 kWh/m^2	17.1 kWh/m^2	21.2 kWh/m^2
Weighted energy for Heating	37.0 kWh/m^2	29.5 kWh/m^2	17.1 kWh/m^2	21.2 kWh/m^2

Table 4: Energy consumption for heating and cooling according to SIA 380/4.

Type 1 is the one that shows the highest heating and cooling demands while Type 3 shows the lowest heating demand. Type 4 shows the lowest cooling demand which can be explained by the fact that, during summer, the glazing is better protected by the thickness of the facade. It is reasonable to think that the situation would have been worse with manual shading device, with a significant increase of the cooling demands due to a misuse of sunscreens [10].

D) Global energy consumption

The global energy consumption of the four types is calculated on the basis on the energy demand and, following the Swiss standard, is weighted by a factor 1 for gas or oil for heating, 2 for electricity and a ESEER value of 4 has been used to determine the electricity consumption required for cooling.

Figure 3 shows that Type 4 is the less energy intensive and that the three vertical stripes types show a lowest global efficacy. This figure also points out the fact that lighting has become a major area of consumption. We must emphasize here that the SIA calculation method for artificial lighting consumption does not take into account the actual geometry of the openings, which in this case, may favor Types 1 and 2 while penalizing the result of Type 4.

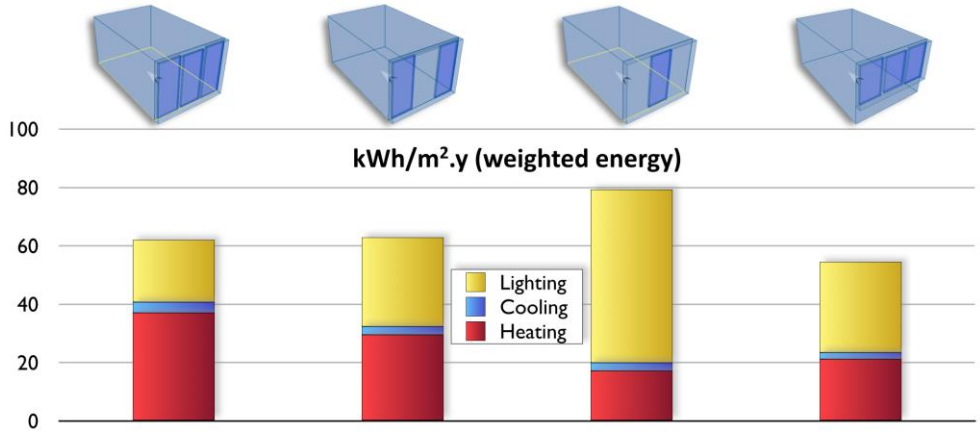

Figure 3: Comparison of the energy consumption of the 4 types according to SIA 380/4 and thermal dynamic simulations [5].

E) Visual appraisal

Figures 4 to 6 allow comparing the visual field of a "typical" user for each of the 3 vertical types with Type 4. The simulations conditions are as follow: Clear sky with sun, 21st of March 9 AM. The observer is looking towards the East and the sun is visible on the upper left corner of the window

The difference between type 1 and Type 4 is based solely on the cut-off of down vision due to the sill (fig.4). In type 2 (fig. 5), the outward view is almost completely cut off, but the sky portion that is still visible is very close to the computer screen and the potential for glare situations is still high. In Type 3 the view outside is partially maintained, but the daylight availability is significantly reduced (fig. 6). This comparison shows that type 4 represents a good compromise between the glass surface and the services offered to the user.

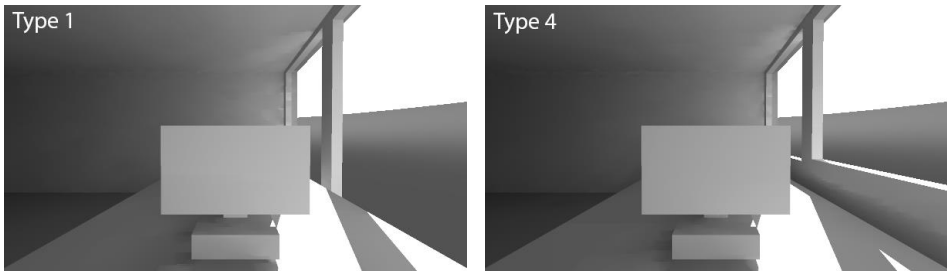

Figure 4: Type 1 / Type 4: Visual field of a typical user / clear sky with sun, march 21, 9 am. External view is completely free and glare is depending on movable shading device.

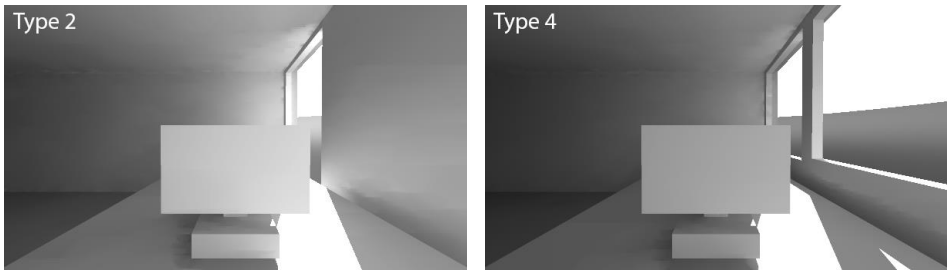

Figure 5: Type 2/ Visual field of a typical user / clear sky with sun, march 21, 9 am. External view is blocked but glare may still occur and depends on movable shading device.

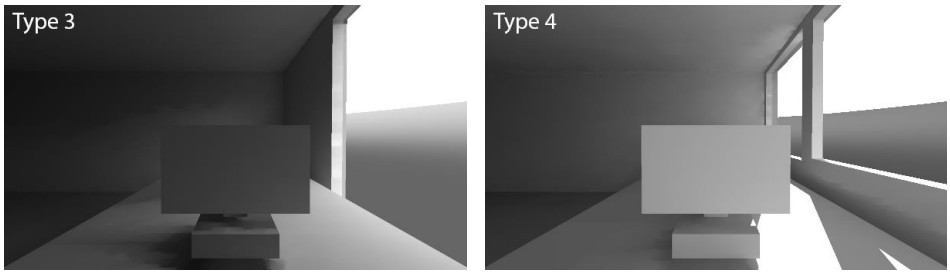

Figure 6: Type 3, / Visual field of a typical user / clear sky with sun, march 21, 9 am. External view is mainly maintained and glare is solved in this particular circumstance.

CONCLUSION

This study showed that the actual architectural trend, which consists in designing facades with vertical stripes of glazing from the floor to the ceiling, does not lead to improve the overall performance of the building. Compared with horizontal windows (type 4), each of the vertical type (1-3) we analyzed has a higher global energy demand (heating + cooling + lighting). Concerning Type 1 (fully glazed), it is reasonable to think that the situation would have been even worse with manual shading device, with a significant increase of the cooling demands. Type 2 (two vertical stripes) is less effective to let daylight penetrate deep into the room and reduces the outward visibility. Type 3 (one vertical stripe) does not allow activating the back part of the room with natural light and leads to a significant increase in lighting consumption.

This information is likely to call into question this architectural trend and should encourage architects to reconsider their approach to the design of buildings, especially if it comes to office buildings.

Finally, this study also confirms the fact that the weight of lighting in the overall building energy consumption becomes increasingly important. In the current context it is a major issue to change practices and regulations to be in line with the new targets regarding energy efficiency and sustainability.

REFERENCES

1. Baderre, G., « Seconde visite à Le Corbusier », Paris Journal 28 décembre 1923.
2. Paule, B. et al., DIAL+Suite: A complete but simple suite of tools to optimize the global performance of building openings; CISBAT'11, Lausanne, Switzerland, 2011.
3. The Minergie® standard for building, Bern, Oct. 2010.
4. Paule, B et al., "Diffuse Daylighting Autonomy: Towards new targets", Proceedings of the CISBAT'13 Conference, Lausanne, Switzerland, Sept. 2013.
5. SIA 380/4, L'énergie électrique dans le bâtiment, Norme Suisse 520/380/4, 2006.
6. EN 15255:2007, Energy performance of buildings. Sensible room cooling load calculation.
7. EN 15265:2007, Energy performance of buildings. Calculation of energy needs for space heating and cooling using dynamic methods.
8. ISO 13791:2012, Thermal performance of buildings. Calculation of internal temperatures of a room in summer without mechanical cooling.
9. SIA 2024, Conditions d'utilisation standard pour l'énergie et les installations du bâtiment, 2006.
10. Website: http://www.estia.ch/#!ofen-global-lighting/c8xx last visited: 04-22-2015.

LONG-TERM PERFORMANCE OF SUPER INSULATING MATERIALS IN BUILDING COMPONENTS & SYSTEMS – IEA-EBC ANNEX65

D. Quenard

CSTB-Centre Scientifique et Technique du Bâtiment; 24, Rue Joseph Fourier, 38400, Saint Martin d'Hères.

ABSTRACT

For households, heating and mobility are the two main loads of their energy burden. A large amount of the energy used for heating air and water is wasted through heat leaks of building envelopes and tank walls. For new building, it's possible to reach very low energy consumption thanks to a good design of building, a good airtightness, some solar gains in winter and efficient solar protections in summer but mainly and above all a good thermal insulation. In new building, the thickness of the insulating layer is ranking between 15 to 30 cm, with traditional insulating materials. This thickness in not acceptable for retrofitting and there is a growing interest in the so-called "super-insulating materials" (SIM), especially for internal thermal insulation. Except for a few types of cellular foams, all traditional insulating materials rely on still air embedded in cavities, pores or cells which prevent any convection. This is why the thermal conductivity of such materials reaches a minimum value, of about, 29 $mW.m^{-1}.K^{-1}$.

To go beyond this limit and achieve superinsulation, three main principles can be applied to reduce thermal conductivity:

- 1: Removing the gas : this technique is used for Vacuum Insulation Panels (VIP)
- 2: Entrapping the gas in tiny pores with a size lower than the mean free path of the entrapped gas in order to limit energy transfer between molecules: this technique is used for aerogel or other Advanced Porous Materials (APM).
- 3: Changing the gas : this technique is similar to the one use for double glazing filled with argon or krypton

Using one of these three options, the thermal conductivity of SIM is generally below 15 $m.W.m^{-1}.K^{-1}$ and can reach very low values (close to 5 $mW.m^{-1}.K^{-1}$). Only VIP and APM are now available on the market and integrated in building products but there is still a lack of information about long-term performances and installation techniques in order to foster the use of SIM in the building sector. The challenges of the IEA-EBC Annex 65 entitled "Long-Term Performance of SIM in Building Components & Systems" is to provide answer to these questions.

Keywords: building, energy, thermal insulation

INTRODUCTION

In the Building Sector, Space Heating (SH) and Domestic Hot Water (DHW) remain the most important energy users. Moreover, refrigeration & freezers (RF) account for around 25% of the whole household appliances. Finally, SH, DHW and RF represent about 80 % of the total energy consumption of household used to fulfil their needs for comfort, sanitary conditions and food storage and unfortunately most of this energy is wasted through heat losses and not used on purpose. Since the first oil crisis, the implementation of Building Regulations [1]

through a combination of higher efficiencies of equipment's and improved thermal performance of building envelope leads to a significant reduction in the per capita energy requirement for SH. Unfortunately, these efforts do not balance the increasing of energy consumption of appliances (especially small ones) and air-conditioning in a few countries.

The potential of energy saving has been estimated to be close to the energy consumption in the transport sector [2] and the current challenge is to make this potential a reality. The first target is to ensure that new buildings do not place additional strain upon energy resources. This goal should be reached by developing NZEB (Net Zero Energy Building) [3] and promoted in the new EPBD. But in most industrialized countries new buildings will only contribute between 10 % to 20 % additional energy consumption by 2050 whereas more than 80% will be influenced by the existing building stock and 75% of current buildings in OECD will still be standing in 2050. Accordingly, the big challenge is the renovation of existing buildings as these represent such a high proportion of energy consumption and they will be with us for many decades to come. According to the IEA BLUE map scenario, two-thirds of the energy savings come from the residential sector and the improvements in the building envelope coupled with energy savings in electrical end-uses dominate total CO_2 reductions. Furthermore, several studies [4,5] have shown that the most efficient way to curb the energy consumption in the building sector (new & existing) remain the reduction of the heat loss by improving the insulation of the building envelope (roof, floor, wall & windows).

A step beyond the current thermal performance of building envelope is essential to realize the world wide intended energy reduction in buildings. For example, in Europe, it appears [6] that the optimum U-values lie between 0.15 W/m².K to 0.3 W/m².K, with an average value close to 0.2 W/m².K. Using traditional insulating materials such as mineral wool or cellular foams, it means a thickness from 15 to 20 cm. For retrofitting and even for new buildings in cities, the thickness of internal or external insulation layers becomes a major issue of concern. For systems (DHW or RF) the reduction of thickness is essential. Therefore, there is a growing interest in the so-called super-insulating materials (SIM), such as VIP or APM.

The former Annex 39 HIPTI [7] have shown that VIP's products have reached a level of quality that customers can trust in for specific applications under well-defined conditions. However, there is still a need for test methods and evaluation procedures to characterize the suitability of SIM for wider applications in praxis. Actually, overall performance and durability of SIM must be investigated when the working life conditions are more severe (high/low temperature, high humidity, mechanical load …). Moreover, new types of SIM appear on the market and their durability and applicability needs to be answered on a scientific level.

OBJECTIVES AND SCOPE OF THE ANNEX

Objectives

An extensive renovation of existing buildings & the development of NZEB appear as the future tracks for 2050, in the building sector. To make both objectives a success, the thermal performance of the envelope is a top priority and SIM should greatly contribute to this challenge if reliable data (properties & durability) and secure implementation techniques are provided to the supply chain (designers, engineers, builders & workers on site).The sustainability of SIM (LCA-Life Cycle Assessment, LCC-Life Cycle Cost as well as EE - Embodied Energy) will be complementary aspect of the study.

Therefore, the current research proposal of Annex 65 has the following objectives:

- to make a state of the art of a decade of development of SIM by the industry and of applications in the building sector
- to develop experimental & numerical tools in order to provide reliable data (properties & durability) for manufacturers and designers.
- to write guidelines for secure installation
- to support standardization and assessment procedures
- to improve knowledge and confidence of the supply chain regarding SIM, thanks to sustainability analysis
- to foster a wider public acceptance of SIM in the future by communication

Scope of the Annex 65

The scope of the Annex65 will cover two types of SIM: the Vacuum Insulation Panel (VIP) and the Advanced-Porous Materials (APM), such as Porous Silica & Aerogel

Figure 1: Vacuum Insulation Panel (VIP) Courtesy: Porextherm

Figure 2: Aerogel Fibre Mat - Courtesy: Aspen Aerogel

Three scientific and technical issues will be addressed during this Annex:

- The performance & durability of SIM through the performance testing in laboratories, coupling with ageing procedures and the measurement on site.
- The installation techniques, indeed there is a high risk of degradation during handling and installation on site.
- The sustainability which is crucial for SIM as the raw materials used to produce them are very specific (TEOS, TMOS, aluminum …) and the manufacturing processes remains sophisticated (super-critical conditions, vacuum process …).

ORGANIZATION OF THE ANNEX

The Annex is organized in four subtasks.

Subtask 1: State of the Art on Materials & Components - Case Studies

The main objective of this task is to provide an up-to-date catalogue of commercially available materials & components. This catalogue will provide technical description of each product with technical data and information about the application domains and the implementation rules.

Furthermore, during the last decade, basic research and first demonstration projects [8] have shown that SIM can be applied in buildings. First European Technical Approvals [9,10]

(ETAs) have been issued for VIP and Aerogel for the use in buildings in the recent years. However, a large use of these components is still hindered by scepticism on the reliability in practice. In order to improve the confidence in these new components, this task will make a detailed analysis of these components offered by manufacturers. An overview on all the application areas such as external & internal wall insulation, roofs, floors, ceilings …will be investigated through a few case studies.

Subtask 2: Characterization of materials & components at the laboratory scale

As their structure and microstructure are completely different, SIM cannot be compared directly to traditional insulating materials, but worldwide acceptance of these materials will be improved, if the hygro-thermal and mechanical properties of SIM can be declared clearly and reproducible. In particular, nano-structured materials used to manufactured SIM are characterized by a high specific area (a few hundred of m^2/g) and narrow pores (smaller than 0.1 µm) which make them very sensitive to gas adsorption (H_2O, VOC …) and capillary condensation can occur in narrow and generate very high pressure. Both phenomena are responsible of drastic changes of the microstructure. Therefore, the methods of characterization must be adapted and even in some cases; new methods have to be developed to measure microstructural, hygro-thermal and mechanical properties of materials and barrier films.

In parallel, modelling methods to describe heat, moisture and air transfer through nano-structured materials and films will be developed (adsorption and desorption models, diffusion models, freezing-thawing …).

Of course, a few methods will be common to all SIM, for example the core materials of VIP can be an APM. But due to their completely different manufacturing process some specific methods have to be developed. For VIP, the durability depends strongly of the performances of the barrier film, such gas permeability (H_2O, N_2, O_2) which can be degraded by the manufacturing process (folding of the film and sealing) [11].

SIM can offer considerable advantages; however potential drawback effects should be known and considered in the planning process in order to optimise the development of these extraordinary properties and to prevent negative publicity which could be detrimental to this sector of emerging products. It's why ageing tests will be defined according to the conditions in use (temperature, moisture, pressure, mechanical load …).

One objective of artificial ageing is to understand potential degradation processes that could occur, such as densification of the porous materials due to water vapour adsorption for a long period [12]. The durability of the hydrophobic treatment will be also subject of discussion and investigation to prevent premature degradation.

At the component scale, additional characterizations are needed as in general panels or rolls are sold by manufacturers. In particular, thermal bridges will be carefully investigated, as the extraordinary thermal performance of SIM is sensitive for the influence of thermal bridges resulting for the film seam around VIP, as well as thermal bridges at the components and walls scales.

Subtask 3: Practical Applications – Retrofitting at the Building Scale – Field scale

The objective of this task will be to define the application areas of SIM and to describe the conditions of the intended use of the products. Indeed, it's clear that the requested performances of the SIM will strongly depend on the temperature & humidity and load

conditions. The local climate will play a great role as well as the application: terrace, roof, wall, floor, water tanks and refrigerator.

For on-site applications, requirements for storage, handling and installation will be also well defined as these three concerns appear to be pivotal for quality insurance.

Common and specific modelling methods will be also developed at the building scale in order to understand the impact of SIM on the performance of wall, roof and floors an even the whole envelope with regards mainly to thermal insulation, airtightness and risk of condensation as VIP can be considered as a vapour barrier and APM as a permeable layer.

Subtask 4: Sustainability – Risk & Benefit

The goal of this task is to assess the overall sustainability of SIMs through the evaluation of LCA and LCC, as well as EE of superinsulation materials over the entire life (production, use and end-of-life).

Life Cycle Inventories for the production step will be established relying on input from material and component producers. The in-use phase will be modelled in various climatic contexts and several building types, taking into account results from Task 2 and 3 alongside taking into account the fact that SIMs are expected to allow larger living or commercially usable areas in a building whilst achieving a lower or equivalent U-values. Current and potential future end-of-life treatment processes will be analysed and corresponding inventories established.

Inventories for all three phases will not only include material and energy flows but also economic flows, thus allowing evaluating the environmental profile of the materials, components and systems at the same time with costs over the whole life cycle. For example the impact of SIM on the living space saving should be considered in the LCC analysis.

DISCUSSION

As the core materials of VIP and APM are highly porous materials (porosity > 95%), two mains concerns need to be addressed in order to evaluate the long-term performance of SIM: the thermal conductivity of the gas entrapped in the porous media and the solid conductivity of the skeleton.

The thermal conductivity of air (λ_g) in a confined porous media which can be written as follows:

$$\lambda_g = \frac{\lambda_{g0}}{1 + C.\frac{T}{\delta \cdot P_g}} \quad (1)$$

C is a constant, λ_{g0} is the air conduction in normal condition and δ is the pore size.

The equation 1 emphasizes the great role of the term $\delta.P_g$ on the gas conduction λ_g.

On one hand, for long-term performance of VIP, it means that the low pressure of the entrapped gas mixture P_g must be kept for 20 to 50 years. Consequently, the gas-tightness (H_2O, O_2, N_2) of the film and the quality of the seams are the key drivers of the durability of VIP. Of course, if δ is small (lower than 0.1 µm), with a very low manufacturing pressure (about 0.001 bar) the expected life-span will be longer as the internal pressure can increase without any change of the thermal conductivity.

On the other hand, for VIP using micro-nano-porous core materials and APM, two ageing processes have been identified [13,14]:

- the water-vapour adsorption which can modified the connexion between silica grain,
- a densification effect resulting from microstructural change similar to Ostwald ripening when a hydrophilic nano-porous media is exposed to high humidity for a long time.

CONCLUSION

The SIM appear as very promising insulating materials, especially to tackle the renovation challenge but their long-term performance is still questionable, especially when exposed to high temperature and humidity. The IEA-EBC Annex 65 has gather the main actors of this sector (industrials, institutes …) and working together, they will brought answers by understanding basic phenomena, improving materials, measuring performances and providing guideline for secure application on site.

REFERENCES

1 : http://ec.europa.eu/enterprise/sectors/construction/studies/national-building-regulations_en.htm

2 : WBCSD – Energy Efficiency in Building – Transforming the Market : http://www.wbcsd.org/transformingthemarketeeb.aspx

3 : http://ec.europa.eu/energy/en/topics/energy-efficiency/buildings/nearly-zero-energy-buildings

4 : G. Verbeeck, H. Hens, Energy savings in retrofitted dwellings: economically viable? Energy & Building – 2004

5 : P.A Enkvist, T Naucler, J. Rosander, A cost curve for greenhouse gas reduction, The Mc Kinsey Quaterly, 2007

6 : http://www.eurima.org/uploads/ModuleXtender/Publications/13/EURIMA-Ecofys_VII_leaflet_0412071.pdf

7 : http://www.ecbcs.org/annexes/annex39.htm

8 : http://www.vip-bau.de/pdf/literatur/BMWi_0327321N_Schlussbericht%20VIP-PROVE.pdf

9 : http://www.porextherm.com/en/news-press/2013/329-european-technical-approval-eta-for-various-versions-of-vacupor-and-vacuspeed.html

10 : http://www.microthermgroup.com/low/EXEN/site/news-detail.aspx?vPK=508&vCat=&page=0

[11] : H. Simmler, S. Brunner, Vacuum insulation panels for building application : Basic properties, aging mechanisms and service life, Energy and Buildings 37 (2005) 1122–1131

[12] : B. Morel et al., Pyrogenic silica ageing under humid atmosphere, Powder Technology 190 (2009) 225–229.

[13] : Samuel Brunner, Karim Ghazi-Wakili, Hints for an additional aging factor regarding the thermal performance of vacuum insulation panels with pyrogenic silica core, Vacuum 100 (2014) 4-6.

[14] : B. Yrieix, B. Morel, E. Pons, VIP service life assessment: Interactions between barrier laminatesand core material, and significance of silica core ageing, Energy and Buildings 85 (2014) 617–630

TEENERGY EXPERIENCE: HOW TO REDUCE ENERGY DEMAND IN MEDITERRANEAN SCHOOLS

PhD. MSc. Eng. Giuseppina Alcamo[1]; Prof. Arch. Marco Sala[1]; PhD. MSc. Arch. Antonella Trombadore[1]

1: University of Florence, Department of Architecture, Palazzo Vegni, via San Niccolò 93, 50125 Firenze (Italy)

ABSTRACT

The European Union established appropriate regulations through the Energy Performance Building 2002/91/CE and EU Directive 2010/31 aiming to ensure efficient buildings using local and national policies in relation to local and specific climatic conditions. From 31st December 2018, we have to build *zero energy public buildings* and consequently we should have zero-energy school buildings. But do we know the average total amount of energy demand of schools in Europe? The research project TEENERGY Schools has been developed with the aim to find a common method to collect energy data consumptions, to analyze the building with its plants and promote energy efficiency solutions according to national legislations, finding the most suitable technical solution to reduce energy demand in existing schools and adopting appropriate strategies to implement indoor comfort. The paper focuses on the differences between the methodologies to assess the energy consumption of school buildings in the Mediterranean Area in order to reduce the energy demand. Criticism emerged due to the fact that each European country adopted the European Directive 2002 but with significant differences. Schools are comparable in energy consumption but to compare the energy savings due to retrofitting solutions a European common tool is necessary and a methodology for collecting data has to be defined, taking into account that comparison is possible if the same instruments are used. The research project gave the opportunity to reflect on potential energy savings due to retrofitting actions on existing school buildings and also on the most appropriate technologies for new building projects. Working with technological and plant solutions adapted to the climatic conditions, the result could be very effective.

Keywords: Sustainable Schools, Energy Audit, Energy Saving, Refurbishment Strategies

INTRODUCTION

Several schools in Europe have been built between 1945 and 1980: now they represent high-energy consumption buildings. In several countries, their annual energy consumption has not yet been collected; moreover, no common procedures to calculate building energy performance exist. Only in few European countries their annual heating energy consumption is registered and in comparison with local building consumption, they represent high-energy demand buildings i.e. 57 kWh/m^{2}year in Greece [1], 197 kWh/m^{2}year in Flanders [2], 119 kWh/m^{2}year in Northern Ireland [3].

The analysis of school buildings and the development of the Strategic Plan maintenance of schools is carried out within the European research project TEENERGY SCHOOLS [4], an experimental project to improve energy performance of school buildings, with the additional aim to decrease management costs. The project, financed by the MED Programme - transnational programme of European territorial cooperation - has successfully implemented a

Multi-Issue Platform as an interactive Network for the gathering of a common database and the dissemination of best practices related to energy efficient retrofitting and new secondary schools in the Mediterranean climate context.

The Project, developed by four countries of the Mediterranean (Greece, Italy, Spain, Cyprus), has pointed out the lack of energy saving benchmarks targeted to south Europe climatic conditions and the low energy efficiency of existing school buildings taking into account not only heating but also cooling energy demand.

An *Action Plan* and a *Common Strategy* are developed on the experimentation of: energy saving techniques, integration of innovative materials and renewable energy for reducing costs and consumption. Moreover, the project set a good practice benchmark based on data from an Energy Survey in the Mediterranean countries involved in the project providing representative values and comparing energy performance in secondary schools.
The energy consumption data of 72 school buildings are collected and an instrument to assess energy and economic retrofitting actions is developed.

METHOD

The methodological approach aims to order and to systematize the stages of a common process, identifying simple tools and technical instruments to optimize the management and to define common criteria for most efficient buildings.

The research is oriented to identify the best actions, in relation to costs-benefits analysis, in order to give to public administration a tool able to plan future energy retrofitting and economic actions.

The research is conducted on 72 existing buildings in Italy, Spain and Cyprus, divided into different climatic zones and periods of construction, identifying the morphological and construction features, and to orient and address the most appropriate strategy of retrofitting actions.

Climatic zones	Land, temperate climate
	Mountain, cold climate
	Costal marine area, hot climate
Age of construction	before 1945
	between 1945 and 1981
	after 1981

Table 1: school buildings are located in different climatic zones in Italy, Spain and Cyprus and the data collected in three different periods of construction.

The research is oriented to the development of a *Strategic Plan* and it is developed (for each case study) in four key actions:
- Preliminary analysis collecting energy consumption, infra-red thermographic analysis and energy audit;
- Energy simulation to quantify retrofitting strategies;
- Cost-benefits analysis of upgrading strategies;
- Drafting of a spreadsheet to estimate the cost of the retrofitting actions and place it into an appropriate time-schedule for the management issue.

Moreover, to evaluate and estimate the relation between the visual comfort and the level of daylighting for each building and for each *typical* classroom, the daylight factor is measured; in order to evaluate the possible energy saving achievable by an appropriate integration of natural and artificial light, simulations in Relux and Radiance are made.

RESULTS

Energy Audit. Teenergy project has defined a Common Energy Audit elaborating a standard Questionnaire that has been used to assess the buildings' usage condition, thermal-visual comfort of 72 schools in four countries. All the collected data have been implemented into a dedicated Project's ICT platform [5] in which results are uploaded in real time.

The audit has been finalized to collect the following data [6]:

- Annual energy consumption for space heating and cooling;
- Annual consumption for electricity;
- Area of the building;
- Year of construction of the building;
- Construction details;
- Number of students and staff;
- Installed power of the boiler and typology of the heating system;
- Length of heating and cooling season affecting the energy use.

Energy simulation. Energy simulations under stationary and dynamic regime are carried out on each building and for each strategy of retrofitting action. With these tools, we have mainly calculated:

- The thermal transmittance of the of the upgraded external envelope surfaces, opaque and transparent (U_{wall} e $U_{windows}$, W/m^2K)
- The requirement of primary energy for heating (kWh/m^3)
- The requirement of primary energy for hot water (kWh/m^3)
- The total primary energy requirement (kWh/m^3)
- The CO_2 Emission (kg/m^3 year)

The data collected during the audit and simulation stages are processed using the spreadsheet BENDS [7], developed by Turin Polytechnic for the European research DATAMINE [8]: it allows comparing energy data in schools.

The aim of the project was to compare data from different countries using harmonized data structure. Each project partner is able to use his own structure, which could later be translated into the DATAMINE [9] format, which, due to its common "language", allows for cross-country analyses.

The data structure includes the following quantities:

- Energy Certificate Data: basic data of the energy certificates;
- General data of the building: basic data of the type and size of the building, such as location, building utilization, conditioned floor area;
- Building envelope data: data describing the thermal performance of the building envelope, such as U-values and area of the opaque elements and window properties;
- System data: data describing the building energy supply systems, such as type of heat generation and distribution system, and air conditioning systems;
- Calculation energy demand: boundary conditions of asset rating and quantitative results;
- Basic parameters of operational rating: information on the conditions of operational rating;

- Summary of energy consumption and operational rating: summary of energy consumption and energy generation, in the first place for operational rating;
- Primary Energy, CO2 emissions and benchmarks: primary energy demand and CO2 emissions for both operational and asset rating.

Through the "DATAMINE Analysis Tool", realized in MS Excel Workbook, the exported data can be statistically analyzed. The Analysis Tool allows for comparison of parameters already present in the DATAMINE data fields, as well as of user-defined composed variables. Correlation of variables and overall statistics can be performed.

Building characteristics. The energy audit and the energy simulations need to focus on weakness of existing buildings to suggest strategies for upgrading energy performance of schools.

Italy					
Age of construction:	Wall W/m^2K	Windows W/m^2K	Roof W/m^2K	Ground floor W/m^2K	Annual energy demand kWh/m^3 year
Before 1945	1,02	4,83	2,0	1,56	56.62
Between 1945 and 1981	1,10	4,14	1,4	1,57	57,74
After 1981	0,37	4,51	1,63	1,68	47,51
Spain					
between 1945 and 1981	1,09	6,02	1,94	0,478	117,80
built after 1981	1,28	4,96	0,95	0,434	77,45
Cyprus					
before 1945	1,39	7,00	2,2	0,86	81,00
between 1945 and 1981	1,38	4,94	1,16	0,68	20,00
after 1981	1,37	4,30	0.70	0,68	18,95

Table 2: average values of 72 buildings analysed in Italy, Spain and Cyprus.

The analysis shows that the building envelope is the major cause of energy losses, because it is not well insulated, often not sufficiently massive; moreover, heating systems are not efficient: i.e radiators are located on the external walls, pipes are not insulated, the total efficiency is very low. Comparing these results with requirements of each national regulation, each country has school buildings with an annual energy demand about three times higher than the annual energy demand's limit value.

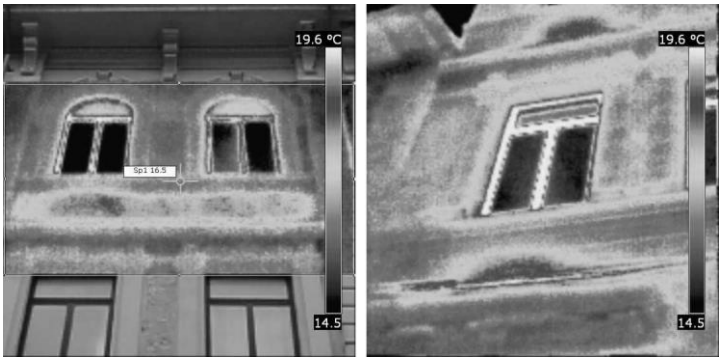

Fig. 1. IR picture of one pilot study case. The IR thermography has been used as instrument in the diagnosis phase to easily localize heat losses and consequently to investigate on retrofitting action for energy saving. This is an historical building used as secondary school in Italy. Radiators are located on the internal surface of external walls, under the windows.

DISCUSSION

The Teenergy research project merged the following problems:

a) in relation to the **energy monitoring phase**:

- Data on thermal performance of the building envelope (U-value of walls, roofs and windows) and heating system have to be measured with the same instruments;
- Difficulty to assess the IR thermo-graphic data, also using different calibrated cameras.

b) The **energy audit** was organized and conducted with a specific protocol, as a common analysis model; however, several problems incurred in data control and storage; i.e. the Bends Tool aimed to compare the data revealed that in many cases data were insufficiently collected to correctly compare the energy performance of buildings in different countries.

c) The **energy simulations**. Simulations are made to quantify the reduction of energy need due to retrofitting strategies:

- Difficulty to carry out energy simulations adopting the same methodology, as each country has adopted the EPBD and CEN standards in different ways
- Difficulty in choosing a software simulation that would allow to make a quick calculation of the building's energy demand.

Using the same simulation software, results are comparable and Guidelines on retrofitting action in schools are developed.

Simulation results show that:

- Window replacement, the cheapest retrofitting action, decreases by only 12% the building energy need with a long payback time, 15-20 years.
- Retrofitting action focused only on the thermal insulation of external walls cannot significantly upgrade the energy performance of the building.
- To ensure a valuable reduction in energy consumption -about 50%- and improve the energy performance of buildings, wall and roof insulation and windows upgrading is required at the same time.
- Upgrading of the heating system, replacing the original low efficient boiler, installing a radiant floor system with a thermostat control in each room, decreases the energy need of buildings by 25% with a cost of about € 100.000and a payback time of 35 years. However, changing the heating system without insulating the building envelope cannot be considered a

good retrofitting action, because the thermal bridges of the building envelope causing, anyway, high energy losses.
- Retrofitting of the building envelope and the heating system decreases the energy needs by 60% with a reduction of 50% of CO_2 emissions.
- Massive envelope and appropriate curtain or shading devises can reduce the overheating of 55% during the hottest seasons.

CONCLUSION

The research developed strategies applied on 12 pilot cases. The European experience shows that retrofitting action in schools in the Mediterranean area has to take strongly in account the local climatic conditions, hourly usage of the building, considering heating and cooling energy demand, avoiding overheating and use daylighting as better as possible. For new buildings, the common approach oriented to nearly zero energy buildings is possible integrating renewables, but we need common and simple tools and methodologies to assess the dynamic annual performance of the buildings, including internal gains and occupancies. We need to reduce the gap between monitored and calculated results and continue the research using the 12 pilot cases to measure the effective comfort level and energy consumption after retrofitting actions.

REFERENCES

[1] Santamouris, M., et al.: Using intelligent clustering techniques to classify the energy performance of school buildings, Energy and Buildings 39 (1) (2007) 45–51.

[2] Aernouts, K., Jespers K.: Bijlage bij de energiebalans Vlaanderen 2000: Onafhankelijke methode, Energiekengetallen van de tertiaire sector in Vlaanderen 2000, VITO, Editor, 2002.

[3] Jones, P.G., et al.: Energy benchmarks for public sector buildings in Northern Ireland, in: Proceedings of CIBSE National Conference, Dublin, 2000.

[4] Teenergy Schools. High energy efficiency schools in the Mediterranean Area, information available through: http://teenergy.commpla.com/

[5] www.teenergy.eu

[6] Gaitani, N., Lehmann, C., Santamouris, M., Mihalakakou, G., Patargias, P.: Using principal component and cluster analysis in the heating evaluation of the school building sector, in Applied Energy 87, Elsevier, pp. 2079 – 2086, 2009.

[7] Building Energy and Environmental Data Strucutre, http://bends.tebe-energy.eu/

[8] DATAMINE Website: www.meteo.noa.gr/datamine

[9] DATAMINE Project Team, DATAMINE, Collecting Data from Energy Certification to Monitor Performance Indicators for New and Existing Buildings. Final report. Institut Wohnen und Umwelt GmbH Annastr. 15 / D-64285 Darmstadt / GERMANY, www.iwu.de, January 2009

VERTICAL FARMS: INNOVATIVE TEACHING STRATEGY TOWARDS NEARLY ZERO ENERGY BUILDINGS

PhD. MSc. Eng. Giuseppina Alcamo[1]; PhD. MSc. Arch. Lucia Ceccherini Nelli[1]; Prof. Arch. Marco Sala[1]

1: University of Florence, Department of Architecture, Palazzo Vegni, via San Niccolò 93, 50125 Firenze (Italy)

ABSTRACT

The paper describes the experience made and results obtained during the experimental course *Laboratory of Architecture and Structure* at the University of Florence, in which the architecture process is explored including sustainable concepts versus Nearly Zero Energy Buildings, integrating renewable energies in high-rise buildings. The innovative approach was taken due to the fact that up to now, in most Architectural schools, projects are usually seen as a synergy of different competencies often not oriented toward efficient buildings. The synergy between different teachers and their specific knowledge has been very interesting in the development of a six-month course in which 75 students were involved. They produced a complex design in which technological aspects were investigated in an integrated approach as a language of design starting from the study of the climatic context. This should be one of the most diffused approach into architectural schools but normally requires different competencies and the effort has to be made first by a strong interaction through teachers. The course of 144 hours was divided in three sub-courses that in a synergic effort developed the following themes: structure, innovative technologies, design; the results are projects of a maximum height of 100 m, in which different functions – residential, commercial, administrative - are integrated and studied in connection with the public transport in Scandicci, near Florence. The educational approach and the synergies are all oriented versus a sustainable architecture of a Vertical Farm.

Keywords: Nearly zero energy buildings, vertical farm, education and sustainability

INTRODUCTION

Faculties of architecture are usually oriented to develop an architectural project with a prevalent and often monographic view. This approach does not give an integrated and structured basis to students: after university, they usually have to make a strong effort to see a project as a whole, converging different singular experiences made during their studies. The today required competencies in Europe are very extensive: a professional has to cover many aspects of the project and specialized teams are often dedicated to the improvement of such aspects, i.e. integration of renewable energies in buildings for more efficient solutions.

In this paper, the experience of the *Laboratory of Architecture and Structure* at the University of Florence represents a significant add-value for students as well as for teachers that have to find an appropriate manner to teach and to cover three main different aspects of a project like a professional team:

- Structural development and dimension
- Design of the project concept
- Development of technological aspects oriented to low energy buildings and sustainable habitat.

METHOD

The course is held at the fourth year of Architectural studies, followed by 75 students. Students are required to develop the project in small groups (two or three students). Lessons are held three times per week, 12 hours in three disciplines with a common theme to be developed. The course takes six months and students follow each lesson to better focalize on the objective of the course. In this first annual experience, teachers had to spend a major effort: they met students several hours outside their official lessons, giving their specific contribution under common revision sections for a better final elaboration of the project. The project to be developed is located in Scandicci, near Florence, in an area with the following dimensions: 100 x 100 square meters. In this area, the Municipality intends to realize a vertical farm of a maximum high of 100 meters. The tram that connects Florence center with Scandicci's Hospital marginally serves the area. The course mainly focused on reaching a complex approach to the design project; the design is conscious of several aspects such as the complexity of the structure of a high building, the climatic effect on huge buildings in which exposition can suggest different technological solutions or different final usages of particularly exposed portions of the building. The required integration of plants, not just as an additional theme of the project but as the main part of it, generated several interpretation of the design. The vertical farm with greenhouses, sometimes for the community, sometimes for external commercial products, has several and different interpretations: sometimes plants are on vertical facades also to mitigate the microclimatic condition, in other cases they are on flat terraces or in greenhouses. Different are also the formal, technological and structural solutions that sometimes change within the same project. For logistic mobility, it is required that the project integrates a tram-stop, on the line that connects Florence to Scandicci's Hospital.

RESULTS

The most interesting results reached by the experimental course are related to the following different aspects:

- The innovative interdisciplinary approach that requires a very good communication and interaction and integration of competencies through teachers of the course;
- A very strong effort made by students in the design of a complex building, in which residential and commercial and offices are designed under the optic of a sustainable building. The term "sustainable" is related to the most appropriate relation between people and: the Greenland, public sustainable mobility, energy efficient components for energy saving, integration of renewables, indoor comfort.

Some results are presented below.

Figure 1: Example of vertical farm project. External view of the building. Credits: Zabotina N.

Fig. 2. This project is based on the concept of a modular building, with an external dynamic surface and solar shading devises. The building can grow with the necessity of funcionalities. Several functions are included such as a restaurant, a supermarket, a library, a little space for music, flats and offices and commercial destinations are studied in a concept of a vertical city. Credits: D. Pedrini, L. Pilati

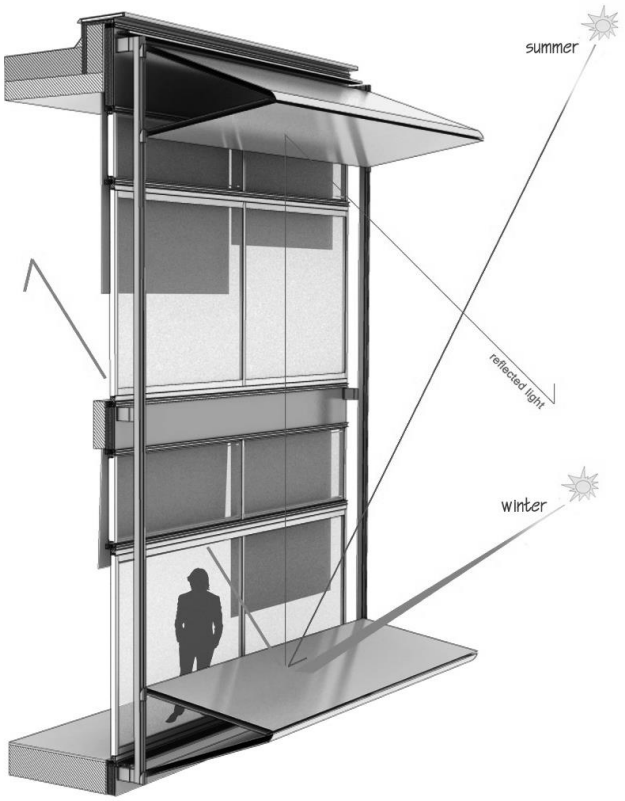

Fig. 3. All projects are simulated to better define solar shading devises or vertical green facades in the most appropriate orientation. Above, a detailed study of the solar shading device chosen in the project. Often, external shading devises are FV panels for the production of electric energy. Credits: D. Pedrini, L. Pilati

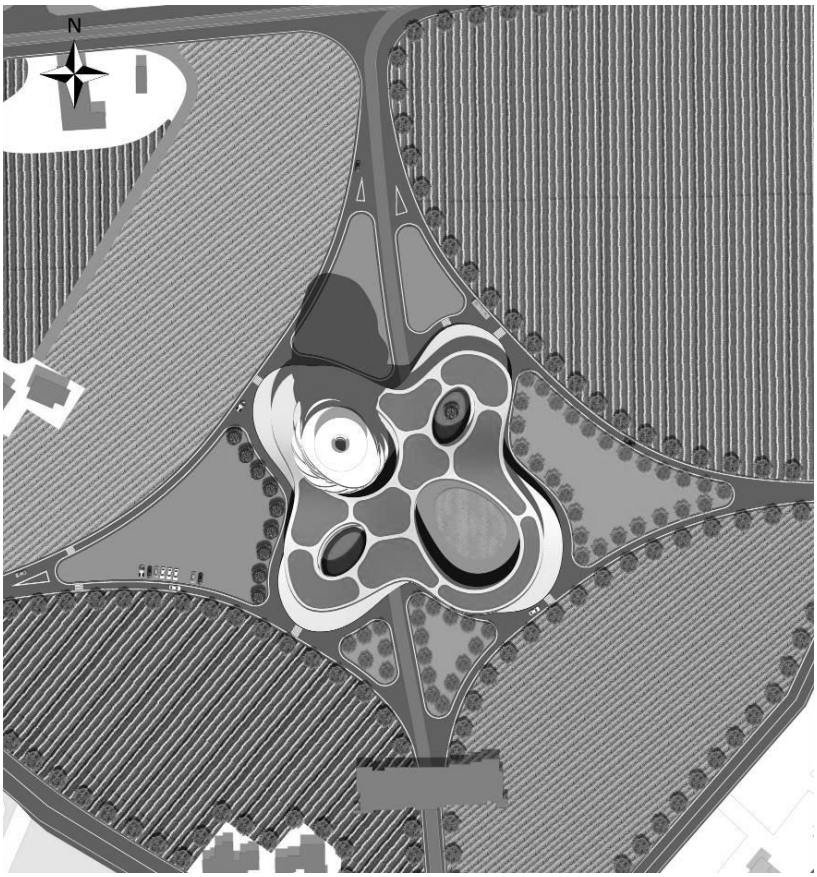

Figures 4, 5: Rendering of the Hill-Project and masterplan. The idea of the vertical farm is in this project developed with growing food on flat terrace at dedicated residential part of the building. As required, the tram has to stop nearest the new building. Credits: D. Locchi, W. B. Zhang

DISCUSSION

Each group has developed a project taking into account most of the requirement. The idea to design low energy buildings is often not fully developed due to the not adequate time given to the student for the development of the course; however renewables are normally integrated and building components adequately chosen with low U value and effective thermal mass on south, south east and south west orientation.

CONCLUSION

The theme proposed to students is very interesting but possibly too complex for a six-month course; nevertheless, the results were brilliant despite the fact that the final exams had to be postponed to allow more time to finish the projects. The experience calls for a more contained project from the dimensional point of view, giving the opportunity to all students to close the exam of the Laboratory in time.

REFERENCES

1. AA.VV: ALMANACCO DELL'ARCHITETTO, Proctor editore, Bologna 2013
2. AA.VV: Linee guida per l'edilizia sostenibile in Toscana , Regione Toscana 2010
3. AA. VV.: Ove Arup & partners, Arup, London, 1994
4. AA.VV: Sostenibilità nei paesi del Mediterraneo , ed. Alinea, Firenze 2001
5. Alagna, A.: Tecnologie per le forme dell'architettura contemporanea. I sistemi di chiusura: qualità ed efficienza energetica, Alinea, Firenze, 2007
6. Altomonte, S.: L'involucro architettonico come interfaccia dinamica. Strumenti e criteri per un' architettura sostenibile, Editrice Alinea, Firenze, 2004
7. Banham, R.: The Architecture of the Well – Tempered Environment, Architectural Press, Londra, 1969
8. Benedetti, C.: Costruire in legno, edifici a basso consumo energetico, Bolzen- Bolzano University Press 2010.
9. Bergamaschi P., Bertozzi P., Ghin A.: Il sistema stratificato a secco: Una tecnologia sostenibile per l'architettura della casa, Flaccovio Editore,Palermo,2010.
10. Ceccherini Nelli L.: Fotovoltaico in architettura, Alinea, Firenze, 2006
11. Ceccherini Nelli L.: Schermature Fotovoltaiche, Alinea, Firenze, 2007
12. Ceccherini Nelli L., D'Audino, E., Trombadore, A.: Schermature solari, Alinea, Firenze, 2007
13. Claudi De Saint Mihiel, A.: Superfici mutevoli. Tecnologie innovative per involucri trasparenti a prestazioni variabili, Clean, Napoli, 2007
14. Gallo, P., Sala, M. (a cura di): Progettazione sostenibile, ed. Alinea, Firenze 2005
15. Herzog, T., Krippner, R., Lang, W.,:Atlante delle facciate, UTET, Torino, 2005
16. Lavagna, M.: Tecniche e architettura, CittàStudi Edizioni, Novara 2013
17. IMPERADORI, M.: La progettazione con tecnologia stratificata a secco, Il Sole 24 Ore, 2006.
18. Lavagna M.: Sostenibilità e Risparmio energetico, soluzioni tecniche per involucri eco-efficienti, Clup, Milano, 2006

19. Meyhoferm, D.: Materiali per l'architettura contemporanea, legno, Motta Architettura,2009.
20. Natterer, J., Herzog, T., Voltz, M.: Atlante del Legno,a cura di R. Margaroli, Bologna, UTET, 1998.
21. Oesterle, L., Lutz, H.: Double-Skin facades: integrated planning, Prestel, Munich – London – New York, 2001
22. Schumacher, M., Schaeffer, O., Vogt, M.: Move: Architecture in Motion - Dynamic Components and Elements, Birkhauser, Hardback, 2010
23. Tenneggi R.: Bioarchitettura e costruzioni in legno, Edicom Edizioni,2006.
24. Tucci, F.: Involucro Ben Temperato, Alinea, Firenze, 2006
25. Zambelli, E., Vanoncini, P., Imperadori, M.: Costruzione stratificata a secco. Tecnologie edilizie innovative e metodi per la gestione del progetto, Maggioli Editore, 1998.

AN INNOVATIVE TRAINING MODEL FOR ECO-BUILDING TECHNOLOGIES IN RETROFITTING

Lucia Ceccherini Nelli, Marco Sala

DIDA Dept, Centro ABITA, University of Florence,Via S.Niccolò 93- 50125 - Firenze Italy
Tel +39 055 2755322 Email: lucia.ceccherininelli@unifi.it, marco.sala@unifi.it

ABSTRACT

The innovative training model for eco-building technologies in retrofitting projects (founded by EU Commission in the IEE programme in the REE_TROFIT project http://www.reetrofit.eu/content.php) aims to contribute to solve the shortage of local qualified and accredited retrofitting experts, as foreseen in the EPBD and its recast - and as indicated by various European countries in an assessment by the EC - for increasing the energy performance of the existing building stock. The retrofitting training model will use in-house know-how and experiences of participants in carrying out vocational courses on innovative eco-building technologies. The training model defines best practices for institutionalization and implementation of vocational courses on renewable energy solutions and energy efficiency in retrofitting, setting up and implementing a large-scale educational scheme and fostering exchange of knowledge and best practices among stakeholders. One of the major milestones of the project is to raise awareness in the regional, national and European policy makers for the full implementation of the EPBD and its recasts. Additionally, during its lifespan, it intends to define an exploitation strategy for assuring the sustainability of training beyond the project duration and increase the local retrofitting markets.

The training scheme is founded on an innovative educational model specifically targeted for building professionals; the adopted retrofitting training model offers the following attractive features:

- Flexibility: applicable in contexts with different regulatory frameworks, climate, landscape restrictions, qualification levels of learners, etc.
- Transferability: capable of responding to local training needs through methodologies and tools transferable at European level.
- Innovation: accessible, affordable and capable of overcoming the problems encountered by previous training program experimented in the partnering countries.
- Modularity: offers different training programs which are composed of independent, closed, domain-specific modules that may be activated according to the different training needs.
- Brevity: offers training courses with a short duration, which are decomposed in shorter training tracks in order to ease the attendance of the targeted professionals.
- Plurality: different training methods, tools and media might be used in the training process in order to take in regard the trainees needs and to guarantee effectiveness.

***Keywords**: Retrofitting buildings, training, courses, renewable energy.*

INTRODUCTION

One of the main goals of the REE_TROFIT project is to assure a massive replication of training beyond the project duration in the EU MS.
The Guide for the institutionalization of training courses is one of the results of the research project, published in the final report and adopted by the Consortium. It provides practical

knowledge, guidance and suggestions to have the REE_TROFIT training recognized by different stakeholders in Europe (focusing on the REE_TROFIT partnering countries), and outlines the way to gain mutual recognition of the acquired qualification. More detailed information can be found in the extended version of the Guidelines for the institutionalization of training courses developed by REE_TROFIT partners.

The Guide addresses the following levels of audience:
1) The consortium partners, in order to share experiences and best practices;
2) Chambers of Commerce and vocational Training organizations providing operational information on the best way to institutionalize the training program;
3) Other stakeholders that can assure the replication of training in other EU member states beyond the duration of project.
The institutionalization of training should bring to a certification designed and implemented in accordance with regional, national and European framework. Moreover, the obtained certification could bring some advantages for trained people depending on the regional or national regulation (grid of salaries, right of access to specific market etc.). Considering the different local contexts, the institutionalization of the training model has been achieved with different specific approaches and local strategies focusing on the endorsement of relevant stakeholders. As a result, due to the endorsement of several institutions, high level of participation to the REE_ TROFIT training courses was secured.
Results of this activity are reported in the table below.

Country	Institution involved	Outcome toward REE_TROFIT institutionalization
IT	National Italian Union of Chambers of Commerce	"Committee on Sustainable Building Industry" inside the National Union of Italian Chambers of Commerce adopted and promoted the REE_TROFIT model toward the Italian Chambers of Commerce.
DK	Regional Vocational Training Centre	EUC-North. The REE_TROFIT model was adopted by EUC-North which collaborated in the delivery and promotion of training activities, also beyond project duration.
HU	Hungarian Chambers of Commerce.	FAT (National Adult Training Accreditation Committee) accreditation requested for the REE_TROFIT training model in Hungary.
GR	TEIC (Technological Educational Institute of Crete), Region of Crete, Technical Chamber in Greece.	TEIC as Higher Educational Institutes, requested the certification for the REE_ TROFIT training to the Greek authorities.
BG	Bulgarian Chambers of Commerce, high school of civil engineers and architects in Sofia and University Chernorisetz Hrabar in Varna.	Bulgarian Chambers of Commerce, high school of civil engineers and architects in Sofia and University Chernorisetz Hrabar in Varna have adopted the REE_TROFIT training model.
FR	Recognized Grenelle Environment (RGE): quality mark issued to French companies about energy performance improvement work on buildings.	A procedure was define to obtain the quality mark RGE for the REE_TROFIT training.

METHODOLOGY

The certification standard should make qualified professionals identifiable on the labour market, thus bringing benefits to both professional and building companies; for this purpose it needs to be included in official, legitimate schemes. First, the organisation which is expected to assess and deliver the certification should be well known and recognized in the country and in the professional sector. In different countries, different certification schemes exist and this makes complex the choice of the suitable institution/organisation.

The following issues are important in order to identify the best way to address the institutionalisation of courses:
- type of occupation standard: complete job or part of an existing job;
- existence of a qualification organisation and/or qualification register;
- existence of certification in the professional sector.
Each framework has to be studied in each country in order to define the best certification system. The pathway to be covered will probably be different in different countries, but if all certifications are based on the same qualification standards (http://www.lucense.it/upload/file/REE_TROFIT_Final_Publishable_Report.pdf), the transparency of qualification acquired will be ensured, in accordance of European recommendation. Taking into consideration the intricate processes to identify the wide variety of qualifications, it is of utmost importance to implement a certification process that could be relevant in the different realities, for consistency and legitimacy purposes.
The new certification awarded may also be useful for professional qualification in local, regional or national regulations. The implementation of a tangible and coherent system serving the various actors' and users' needs then appears of utmost importance.
The general objective of the REE_TROFIT model is to elaborate an effective Vocational Educational Training (VET) model whose relevant characteristic is to provide short track training for already working people in the building market, able to assure the essence of sustainability in buildings is their capability to adapt to change over time.

Training quality

Quality assurance is a continuous and complex process, where feedback (made by trainers and tranees) plays a key role in reviewing the referenced criteria and indicators. The REE_TROFIT model suggests a framework for assuring quality taking into account four interrelated elements: planning, implementation, evaluation and assessment and review.

Figure 1: Scheme of certification and qualification standard

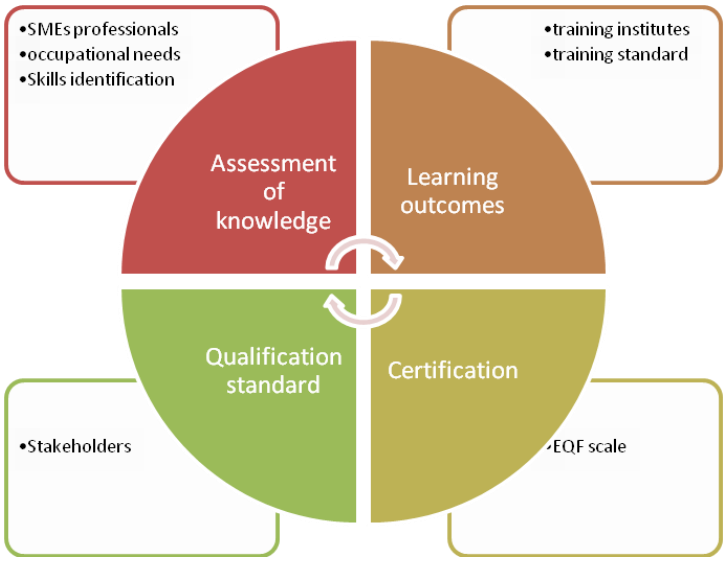

Evaluation and Assessment

The REE_TROFIT model recognises the importance of a continuous evaluation of the training programme and assessment of the training outcomes at different levels.

The REE_TROFIT model considers essential that the findings of the evaluation are provided to those concerned, including strengths, weaknesses, areas for improvement and recommendations for action. Also the relevant stakeholders (i.e. current and former trainees, staff, employers and trade union representatives) should be involved in discussions arising from evaluation results.

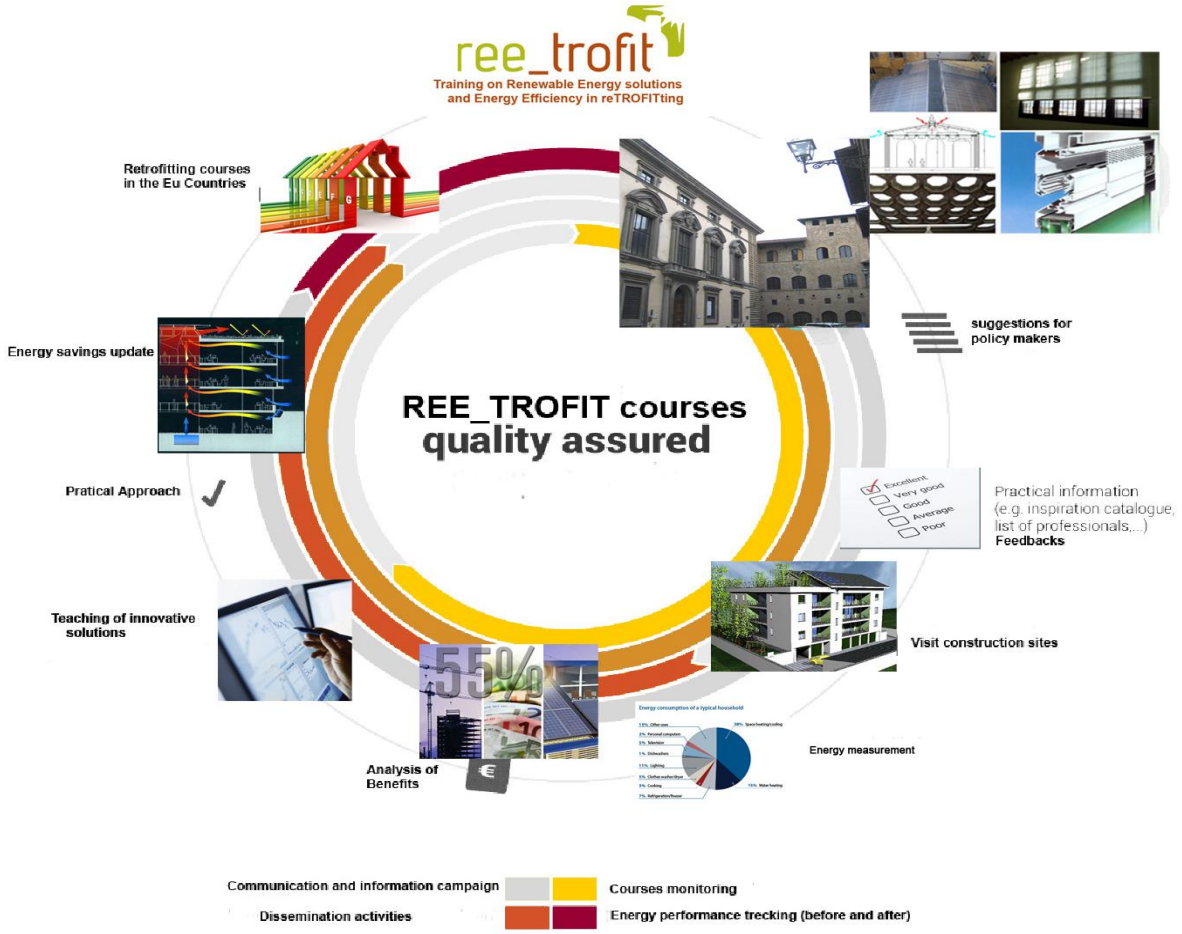

Figure 2: Scheme of the courses quality assured

Role and impact of trainees

REE_TROFIT courses include detailed information for cost-optimal energy saving retrofit, accompanied by financial analysis (i.e. payback times) and technical specifications, which haveproven crucial to evaluate energy benefit in retrofitting .
They provide energy experts and building professionals with energy advice tools that link to the EPBD methodology, and to grant or financial support (Regional and National, for instance Integration of renewable energies) schemes by imposing almost minimum levels for the overall energy performance of public or residential buildings after renovations. This methodology is important to firmly embed REE_TROFIT installers and builders as a key instrument in the start-up phase of any energy saving retrofit activity.
The existing cost differences between energy efficient and "standard" refurbishments have a great influence on the decision making process of the property owners. To encourage investment in ambitious energy saving retrofit, Public Institutions and policy makers are central. It is vital that policy makers' recommendations are accurate, based on robust data and analysis and are effectively communicated. But policy makers can decide that data and information can also play a dynamic role in the decision making process, beyond simply the information printed on the certificate. Further, the national or regional regulation issuing body can interact more with the supply chain, helping to create new systems that enable the select services such expert certified by Ree_trofit vocational courses and by Chambers of Commerce that participate to the Consortium.
More broadly, any programme's success in driving uptake for energy efficient and sustainable refurbishments is highly dependent on the quality of the advice and consultancy. This need for quality consultancy goes beyond the owners – for example to include landlords and tenant

representative bodies in rental situations. Such a "process management" role to ensure an integrated supply chain and seamless customer journey is something that is not formalised in most countries yet, but that we believe is necessary to maximise harvest of the energy efficiency potential of retrofits. It could however be performed by a number of different actors with the right level of training (site managers, assessors, project managers) and with the necessary independency and impartiality.

Training methods and Case Studies

Choice of the most useful training methods in relation to the training market context and the target group features. The standard course structure is a classroom phase, which lasts 16/24 hours divided into 3/4 hours modules.

The courses have a practical structure, based on:
• Case studies relating to building renovation, best if really existing, according to the logic of the guided project works. In fact, the trainer should analyze, together with the learners, a building renovation case, starting from analysis of the building features and context, and going on with the illustration of the existing solutions (technologies, systems, existing materials) in the different building sections and plants renovation, the identification of feasible solutions and finally the definition of the optimal option in the analyzed case.
• Brainstorming, discussion, problem solving: training should seek continuous involvement of participants through analysis and group discussions about explained topics. Of course, the number of attendees affect the active participation during the class work.
• Illustration of the existing solutions, through pictures, movies, viewing samples of products (workshop).
• Product exposition or training laboratory (optional): temporary or permanent showrooms of sustainable building products and systems (also organized with the products' manufacturers), as well as a training laboratory, allow for a "learning by doing" approach helping trainees to better understand and to have a pragmatic and realistic knowledge of the different topics.
• Study visits to building sites where eco-sustainable solutions are implemented: learning through sites and building visits is fundamental for vocational training considering that the trainees would have the possibility to directly experience real examples and realizations of the technologies and solutions discussed during the lessons.
• Solution of a practical problem. Practical problems and solutions are provided by the trainers and the trainees are guided through the process of finding the most viable solutions considering both the technical and economical viability.

The REE_TROFIT training courses provide tools and knowledge to evaluate different materials, components, technologies and building solutions, in order to choose the better approach to address high indoor comfort and high energy performance in building retrofitting. Moreover, the vocational courses allow the trainees to take contact and compare products and the materials of companies operating in different fields of the building sector allowing for the establishment of a potential working collaboration, besides the training activities. At the end of the vocational training course, participants are provided with a certificate of attendance and are registered on the on-line repository of the REE_TROFIT web portal in order to increase their visibility toward citizens, housing and consumer associations and customers in need of information regarding building companies and professionals able to implement a high energy efficient retrofitting solution.

RESULTS

During the project duration, the localized vocational courses have been implemented through 3 test trials (rolling cycles) in each of the 6 participating countries. The rolling cycle approach

allowed the training programs to be tested, improved upon and optimized for the following training batch. Courses were implemented in rolling cycles and partners organized, promoted and delivered vocational training courses over 3 iterative test batches in the 6 partner countries. Following the plan-do-check-act strategy, after each cycle, feedbacks from participants were collected and analyzed with a specific validation methodology, the training contents were enriched (e.g. new modules and multimedia) and the methodology improved through annual internal trainers' review workshops. Preparatory activities, organisation and delivery of three batches of training courses in each partnering country were successfully performed. The number of participants was higher than expected: 1483 professionals were trained (instead of the 450 foreseen participants), among which 453 electrical installers, 512 thermo-hydraulic installers, 518 construction professionals. 1293 trainees out of 1483 participants (87%) obtained a Certificate of Attendance. Moreover, the REE_ TROFIT training courses resulted in positive evaluation by trainees, in particular the overall evaluation about the training courses resulted on average 4,4 on 5.

CONCLUSION

The Ree_trofit project is demonstrating that by focusing on initiatives to link supply and demand for refurbishment with focus on energy saving, and particularly by promoting quality and building trust, vocational courses can successfully drive retrofit actions towards low energy buildings. However, assessing that impact of Ree_trofit certification action will, as things stand today, be difficult. Currently, levels of general retrofit activity are poorly monitored across Europe and there is virtually no monitoring of retrofit activity undertaken in response to Energy savings measures. There is in other words a huge potential for much better tracking and analysis to identify the remaining potential for action on energy efficiency and CO_2 emissions improvements in European homes. This is yet another important element that could support policy makers, market actors, local authorities, and householders themselves in planning low carbon improvement strategies.

Partners of the REE_TROFIT project: Italy: Lucense (Coordinator) Mr Stefan Guerra, Italy: Chamber of Commerce and Industry of Lucca Greece: Technological Educational Institute of Crete Hungary: Chamber of Commerce and Industry Bács-Kiskun County France: Chamber of Commerce and Industry of the Drôme Italy: Abita Interuniversity Research Centre Denmark: Engineering College of Aarhus Bulgaria: Bulgarian Chamber of Commerce and Industry Bulgaria: European Labour Institute

REFERENCES

1. Ceccherini Nelli. L, Gallo P.: Proceedings of Salford UK Conference 24-26 January 2012, An innovative project on Training on Renewable Energy solutions and energy Efficiency in retrofitting, Salford, 2012
2. Ceccherini Nelli. L: Proceedings of the 2nd World Sustainability Forum 1- 30 November 2012, European project for Training on Renewable Energy solutions and energy Efficiency in retrofitting (REE_TROFIT)
3. Ceccherini Nelli L. : Proceedings of the World Renewable Energy Congress 2014 - WREC2014- University of Kingston LONDON – UK, 3-8 August, 2014, Energy Efficiency in retrofitting an European project for Training on Renewable Energy solutions (REE_TROFIT).
4. Baeli M., Residential Retrofit: 20 Case Studies, Riba Publishing, London, 2013
5. https://ec.europa.eu/energy/intelligent/projects/en/projects/reetrofit
6. http://www.lucense.it/upload/file/REE_TROFIT_Final_Publishable_Report.pdf

THERMAL INERTIA OF HOLLOW WALL BLOCKS: ACTUAL BEHAVIOR AND MYTHS

M. Cianfrini[1]; M. Corcione[2]; R. de Lieto Vollaro[1]; E. Habib[2]; A. Quintino[2]

1:DIMI – Università degli Studi Roma Tre, via della Vasca Navale, 79 - 00146, Rome, Italy
2: DIAEE – Sapienza Università di Roma, via Eudossiana, 18 - 00184, Rome, Italy

ABSTRACT

In the context of growing requirements to save energy in buildings and high objectives for Net Zero Energy Buildings (NZEBs) in Europe, strong emphasis is placed on the thermal performance of building envelopes, and in particular on thermal inertia to save cooling energy.

High thermal inertia of outer walls leads to a mitigation of the daily heat wave, reducing cooling peak load and energy demand. Moreover, building envelopes with high heat capacity act as heat storages, increasing the effectiveness of natural ventilation for thermal comfort through a night-day energy shifting.

Even though there are some papers available in the open literature on dynamic heat transfer through hollow bricks, yet common calculation methods are applicable to homogeneous layers only. That is the case of ISO 13786 regulation "Thermal performance of building components - Dynamic thermal characteristics - Calculation methods", for example. On the other hand, hollow blocks are very commonly used in building envelopes. Thus, available methods are not suitable for prediction of dynamic thermal performances.

On the other hand, the widely common assumption that high mass means high thermal inertia leads to the use of higher mass blocks or bricks. Yet, numerical and experimental studies on thermal inertia of hollow envelope-components have not confirmed this general assumption, even though no systematic analysis has been found in the open literature.

In this framework, numerical simulations of the thermal performance of hollow bricks have been done with a specifically-developed finite-difference computational code. Three common basic shapes with different void fraction and thermal properties have been analyzed with a triangular pulse solicitation, in order to highlight the relevance of front mass and other parameters on the thermal inertia, measured through heat wave delay.

Results show that wall front mass is often misleading as thickness, number of cavities and clay thermal diffusivity are more important.

Keywords: building envelope, thermal inertia, hollow block, thermal pulse response

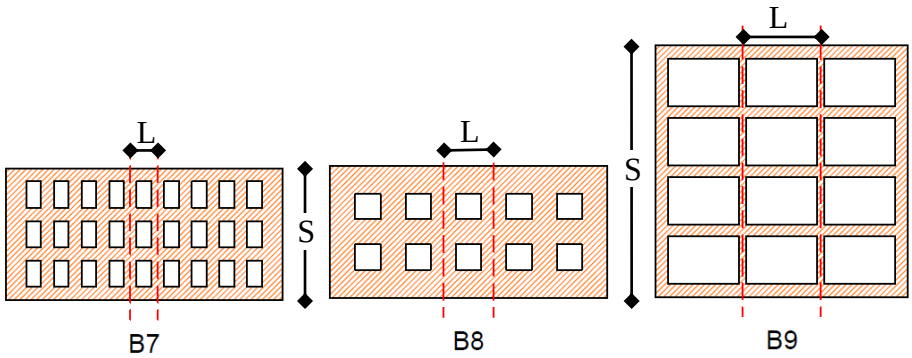

	S [mm]	L [mm]
B7	105	22
B8	105	40
B9	200	62

Figure 1: Sketch of the masonry units and integration domains.

INTRODUCTION

Dynamic heat transfer through building envelopes has been extensively studied, being of fundamental importance in building energy analysis. Different methods for the calculation of the heat gain through exterior roofs and walls are reported in [1] and [2]. However, as these methods apply uniquely to roofs and walls consisting of homogeneous layers, their employment is not suitable for common building envelopes. A limited number of studies are readily available in the open literature on the dynamic thermal features of non-homogeneous building components.

Lacarrière et al. [3] and Sala et al. [4] performed experimental studies with step and triangular pulse solicitation on hollow blocks arriving to different results. The first has found out that the effective specific heat per unit volume of the block was of the same order of that of the solid part of the masonry unit. The latter has found that the effective specific heat per unit volume resulted to be nearly one half of that of the clay which the solid part of the block consisted of. Regarding the numerical approach to the problem, some studies are available [5-7], with very different methods and envelope elements, thus their results are hardly comparable.

In this framework, the aim of the present study is to point out whether front mass is actually straight connected to thermal inertia. A two dimensional numerical study is performed under the assumption that the investigated brick is subjected to a triangular temperature pulse on one side. B7, B8 and B9 blocks among those reported in EN1745 [8] are chosen as much simplification of integration domain is possible. Reference masonry material is clay of three different densities as shown in Table 1.

	c_p (J/kg K)	ρ (kg/m³)	$c_p*\rho$ (kJ/m³ K)	k (W/m K)	α (m²/s)
LWC – Light Weight Clay	1000	1000	1000	0,27	$0,27 \times 10^{-6}$
MWC – Medium Weight Clay	1000	1700	1700	0,51	$0,30 \times 10^{-6}$
HWC – Heavy Weight Clay	1000	2400	2400	0,84	$0,35 \times 10^{-6}$

Table 1: Properties of masonry material [8].

MATHEMATICAL FORMULATION AND COMPUTATIONAL PROCEDURE

The reference masonry units are sketched in fig. 1. Real walls have mortar all around the block, giving fully 3-dimensional thermal field. As this study is meant to be a first approach to the phenomenon, a simpler field is studied, neglecting both the effect of mortar, of the lateral edges and of plaster or any other layer in the wall. The computational domains are the parts limited by dashed lines, including a line of cavities.

Thermal field equation is described by a Cartesian two-dimensional Fourier's equation for conducting fields.
In cavities, convection contribution to heat transfer is neglected as Rayleigh numbers are very low, even in vertical arrangement. So, radiation heat transfer is superimposed to conduction. At cavity boundary, heat flux conservation is given by:

$$k_a \left.\frac{\partial T}{\partial n}\right|_a + q_R = k_c \left.\frac{\partial T}{\partial n}\right|_c \quad (1)$$

where, k stands for thermal conductivity, T for temperature, n for direction perpendicular to boundary, either x or y, q_R for radiation heat transfer toward the cavity, and subscript a is for air and c is for clay. Radiation heat transfer is calculated through radiosity method with Hottel's crossed-string method for view factors.

Triangular pulse excitation is used to check dynamic heat transfer characteristics as it allows to simply identify heat transfer response in terms of time-lag, delay between pulse and response peak, and a damping degree, that is the ratio of stationary heat transfer at maximum temperature difference to actual peak heat transfer (equivalent to the reciprocal of decrement factor defined in [2]). A 1 K high, 2 hours wide pulse was chosen, with 20°C initial temperature. Along domain boundaries defined by the dashed lines, adiabatic condition is assumed, while the outer face that is not subject to the pulse is kept at constant temperature.

The governing equation, along with boundary and initial conditions stated above is solved through a control-volume formulation of the finite-difference method. A first-order backward scheme is used for time stepping. Radiation heat transfer is solved using the same faces of control volumes. The discretized equations lead to a linear system for conduction and for radiation in each cavity (as unknowns are radiation heat transfer). Iterative Jacobi algorithm [9] has been implemented to solve each system. At each time step, the conduction field is solved with previous radiation heat transfer that is then calculated in relation to the newly calculated cavity boundary temperatures, iteratively, up to when the new calculated radiation heat transfer is close to the previous one.

The average heat flux through constant temperature face (of length L) is calculated as:

$$q = \frac{1}{L}\int_0^L k_c \frac{\partial T}{\partial y} dx \tag{2}$$

The code was checked against reference simple analytic solutions, details can be found in [10]. Moreover, a self consistence test was conducted to get the optimal mesh-size, time step and variance limit for iterations. A 5 s time step and 10^{-4} variance limit has been found to be a good balance between calculation time and solution accuracy with mesh sizes between 21x103 and 44x210, depending on cavity number and geometry.

RESULTS

Numerical simulations have been performed for each kind of block, with the different types of clay. Cavities size in each block has been varied: for B7 type, with void fraction from 0% (full block) to 60% (standard blocks are 33%); for B8 type, with void fraction from 0% (full block) to 50% (standard blocks are 19%); for B9 type, with void fraction from 0% (full block) to standard one that is 69%. Cavities number and sides length ratio has been kept constant as well.

For each configuration, ratio of maximum heat flux under triangular pulse to heat flux under constant temperature difference was calculated as well as the delay between pulse peak and heat flux peak, as shown in fig. 2. Time-lag and decrement factor results are plotted against void fraction and front mass in figs. 3 to 5 for each block and clay type.

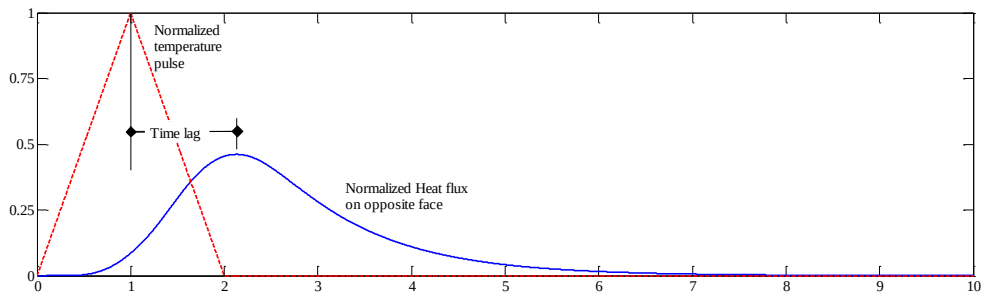

Figure 2: Temperature solicitation and heat flux response for B7 MWC block

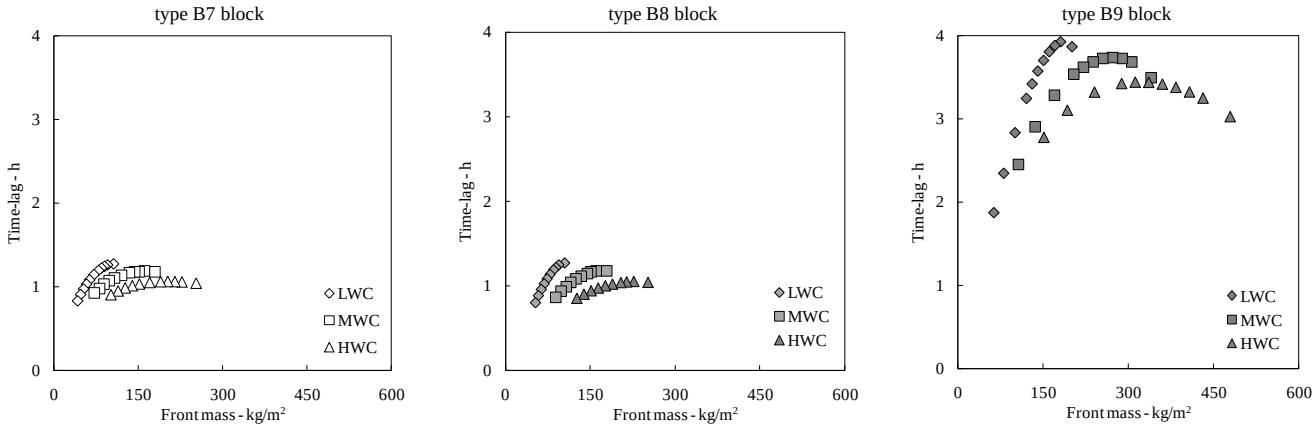

Figure 3: Time-lag vs. front mass

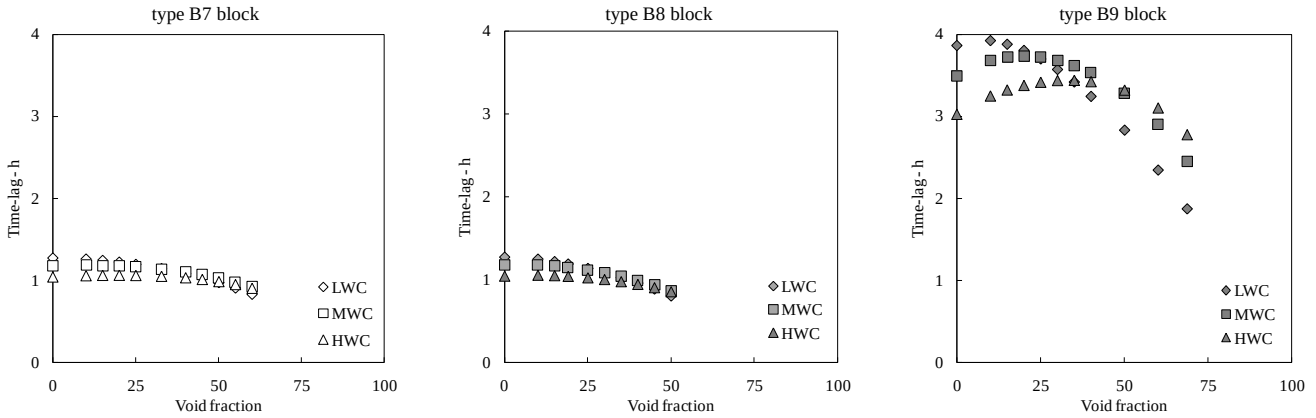

Figure 4: Time-lag vs. void fraction

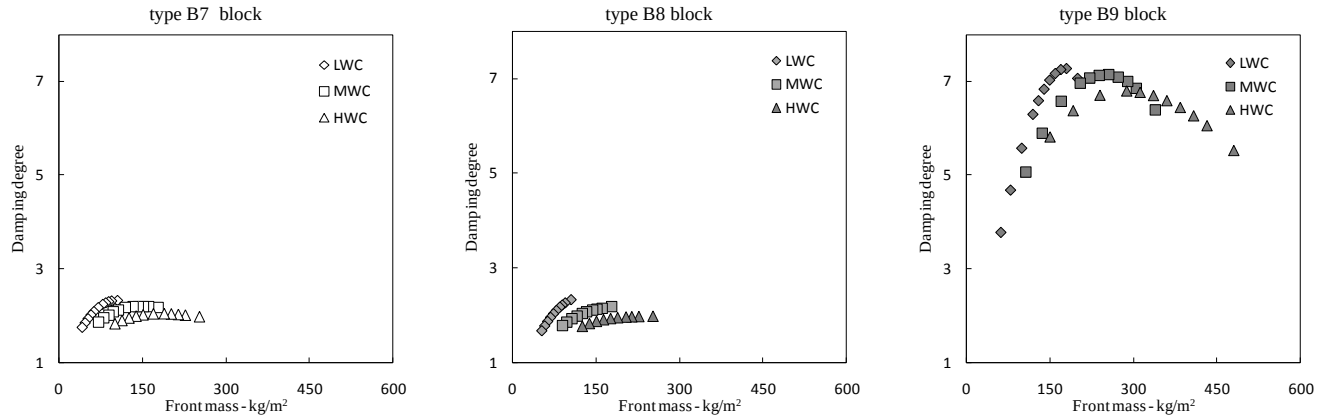

Figure 5: Damping degree vs. front mass

DISCUSSION

Results show that time-lag is far from being simply connected to front mass. Once the block type is given, lighter clays will give higher time-lags. Actually, lighter clays have lower thermal diffusivity and thus are less reactive to thermal solicitation. This is clearly shown by looking at time lag values of full blocks (the right-end of each sequence). Comparing these to thermal diffusivity and block thickness a direct proportion is found to the square of thickness divided by thermal diffusivity, as shown in fig. 6.

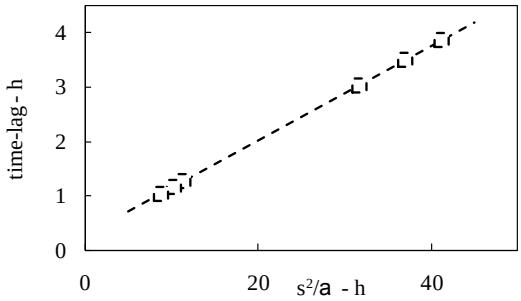

Figure 6: Full blocks, relation between time lag, thickness and thermal diffusivity

Moreover, at a given thickness and diffusivity of clay, higher front mass (due to smaller cavities) is linked to higher decrement factors only as long as void fraction is high. At low void fraction, time lag is insensitive to front mass for B7 and B8 block types. For B9 block type, at low void fractions, sensitivity of time lag to front mass is inverted, being lower for higher masses, especially for high thermal diffusivity clay. This could be due to a different effect of these small cavities: heat flux is not much reduced by cavities but, since it has to "go around" the cavities, the actual propagation length is increased, leading to a higher time-lag. This is more prominent in high diffusivity materials, in which the contribution to heat transfer of the instantaneous heat transfer by radiation across the cavity is less effective.

For light weight clay blocks, for each type, a straight dependence of time-lag to front mass is apparent, even though very different values are found for different blocks. The block types diverge for thickness and number of cavities. By normalizing time-lag with respect to these values, that is dividing time lag by block thickness and number of cavities, all the results appear to be quite aligned, as shown in fig. 7. This is not found for heavier clay blocks.

Moreover, comparing time-lag and damping degree, a linear correlation exists, as shown in fig. 8 and stated by eq. (3) with a standard deviation of 3.6%:

$$d = 1.9 \cdot \Delta\tau \tag{3}$$

where d is damping degree and $\Delta\tau$ is time lag (in hours).

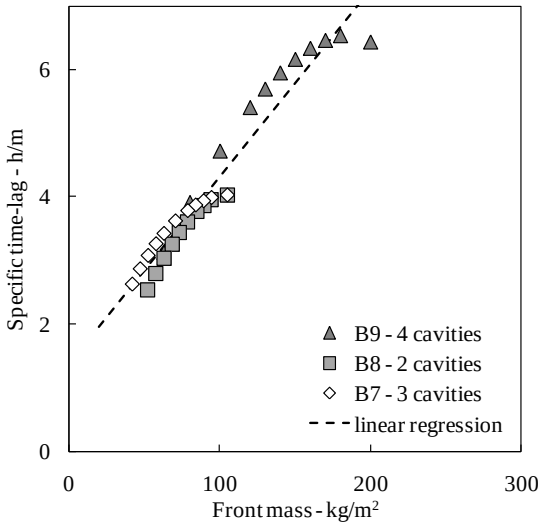

Figure 7: Specific time lag vs. front mass for light weight clay blocks, all types

CONCLUSION

Temperature pulse response of hollow blocks has been numerically studied for different block types, cavities size and clay. Even though there is some correlation between front mass and time-lag, cavities and block thickness play a major role. Thus, as a general rule, thicker blocks will give higher thermal inertia.

Nonetheless this is just a first approach to a wide field of research showing unexpected results. Much more work should be done in order to fully understand unsteady behaviour of hollow blocks. As there is a strict correlation between the newly defined damping degree and time-lag, analysis can be focused on the latter to figure out behaviour.

REFERENCES

1. ASHRAE Handbook – Fundamentals, ASHRAE, 2005
2. EN ISO 13786:1999 Thermal performances of building components – Dynamic thermal characteristics – Calculation methods
3. B. Lacarrière, A. Trombe, F. Monochoux: Experimental unsteady characterization of heat transfer in a multi-layer wall including air layers – Application to vertically perforated bricks, *Energy and Buildings* 38 (2006) 232-237
4. J.M. Sala, A. Urresti, K. Mrtìn, I. Flores, A. Apaolaza: Static and dynamic thermal characterisation of a hollow brick wall: Tests and numerical analysis, *Energy and Buildings* 40 (2008) 1513-1520
5. K.C.K. Vijaykumar, P.S.S. Srinivasan, S. Dhandapani: A performance of hollow clay tile (HCT) laid reinforced cement concrete (RCC) roof for tropical summer climate, *Energy and Buildings* 39 (2007) 886-892
6. Z.L. Zhang, B.J. Wachenfeldt: Numerical study on the heat storing capacity of concrete walls with air cavities, *Energy and Buildings* 41 (2009) 769-773
7. G.H. Dos Santos, N. Mendes: Heat, air and moisture transfer through hollow porous blocks, *Int. J. Heat Mass Trans.* 52 (2009) 2390-2398
8. EN 1745:2002 Masonry and masonry products – Methods for determining design thermal values
9. L. Gori: Calcolo numerico (*in Italian*), Edizioni Kappa, 1999
10. C. Cianfrini, M. Corcione, E. Habib: Dynamic Thermal Features of Insulated Concrete Bricks, Proc. of 7th HEFAT conference, pp. 1065-1071 Antalya, Turkey, 2010

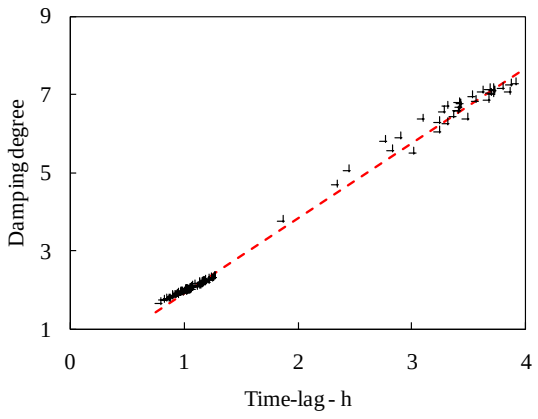

Figure 8: Damping degree vs. time-lag for all block types and void fractions

A STUDY ON OPTIMUM INSULATION THICKNESS IN WALLS AND ENERGY SAVINGS BASED ON DEGREE DAY APPROACH FOR THREE DIFFERENT DEMOSITES IN EUROPE

[1] Öykü DUMAN; [1] Aliihsan KOCA; [1] Ruşen Can ACET; [1] Mevlüt Gürsel ÇETİN; [1] Zafer GEMİCİ

1: Mir Technology Research and Development Co. Yildiz Technical University Technopark, Istanbul, 34522, Turkey

ABSTRACT

In the last decade, the energy industry has been facing major changes mostly because of concerns about sustainability. Countries worldwide, especially industrialized nations have been forced to improve the energy efficiency in several sectors with high energy consumption. The building industry is a major sector for energy consumption in the world.

Using thermal insulation in buildings helps to reduce the reliance on mechanical/electrical systems to operate buildings comfortably and therefore, conserves energy and the associated natural resources. An energy cost is an operating cost, and great energy savings can be achieved by using thermal insulation with little capital expenditure (only about 5% of the building construction cost). This does not only reduce operating cost but also reduces HVAC equipment initial cost due to reduced equipment size required. The use of thermal insulation not only saves energy operating cost, but also results in environmental benefits as reliance upon mechanical means with the associated emitted pollutants are reduced. The use of thermal insulation can reduce disturbing noise from neighboring spaces or from outside. This will enhance the acoustical comfort of insulated buildings, etc.

The optimum economic thickness is the value that provides the minimum total life-cycle cost. The thickness depends on the following parameters: the building type, function, shape, orientation, construction materials, climatic conditions, insulation material and cost, energy type and cost and the type and efficiency of the air-conditioning system.

This study, based on research conducted under the EU FP7 project, presents optimum insulation thickness calculation assessment for building envelop in three different demo-sites located in Europe. The study provides an economic and energy cost optimization, which has positive effects on reducing the energy demand and GHG emissions. Results show how the retrofitting actions can contribute to low energy and zero emission cities and urban areas, taking into account the technological availability for building retrofitting.

Keywords: energy saving, insulation, retrofitting, building

INTRODUCTION

Energy is essential for economic and social development and improved quality of life in all countries. Energy demand started with the Industrial Revolution. European energy need increased in parallel to growing technology and started to emphasis on the importance for the most needed concept day by day.

After the energy crisis occurred in 1970s, the importance of energy increased for the countries. The saving energy use studies started. The countries which have natural sources conducted studies to use their resources in the best way. Other countries tried to create various technics. Consequently renewable energy forms emerged.

The energy consumption of buildings has become a relevant international issue and different policy measures for energy saving are under discussion in many countries. In the EU, buildings account for about the 40% of the total energy consumption and they represent the largest sector in all end-users area, followed by transport with the 33% [1]; whereas in terms of CO_2 emission, buildings are responsible for about 36% of it. It is estimated that the residential sector alone represented about 25% (in 2011) of the final energy consumption in EU. [2]

Energy in households is consumed for different purposes, such as hot water, cooking and appliances, but the dominant energy end-use in Europe (responsible for around 70% of total consumption in households) is space heating. Among all the solutions proposed to the energy problems in buildings, experts agree that building insulation is the least-cost option for reducing energy consumption and CO_2 emissions. The determination of the optimum thickness of the building insulation materials has been a subject of interest for many years among the scientific community. The optimum insulation thickness depends on a large number of parameters. The scientific studies are primarily focused on analyzing the effect of the climatic parameters, the orientation, the thermal mass, the fuels and other parameters. [3]

The main goal of the insulation thickness studies is to optimize thermal insulation thickness based on degree-day heat loss analysis. The concept of optimum thermal insulation thickness considers both the initial cost of the insulation and the energy savings over the life cycle of the insulation material. The optimum insulation thickness corresponds to the value that provides minimum total life cycle cost. The analyses for optimum insulation thickness are commonly based on some parameters such as heating and cooling loads, the cost and the lifetime of the insulation materials, efficiencies of heating and cooling systems and the inflation rate. However, heating and cooling demands of buildings are mostly considered sufficient input parameters in order to perform an optimization work. In literature, generally the degree-day or degree-hour concept is used to predict the heating and cooling loads of buildings since the approach is quite simple.

METHODOLOGY

The concept of economic thermal insulation thickness considers the initial cost of the insulation system plus the ongoing value of energy savings over the expected service lifetime of the insulation.

The thickness is a function of the following: the building type, function, shape, orientation, construction materials, climatic conditions, insulation material and cost, energy type and cost, and the type and efficiency of air-conditioning system. [4]

In most studies, the optimum insulation thickness computations were performed based mainly on the heating and cooling loads and other parameters such as the costs of the insulation material and energy efficiencies of the heating and cooling systems, the lifetime and the current inflation and discount rates. For that reason, the annual heating and cooling energy requirements of a building were the main inputs required to analyze the optimum insulation thickness. Most studies estimate the heating and cooling energy requirements by the degree-time concept (degree-day, DD or degree-hour, DH), which is one of the simplest methods applied under static conditions. [5] On the other hand, only a limited number of analytical techniques were applied to analyze the transient behavior of multilayer building envelopes. [6]

$$HDD = \sum_{days}(T_b - T_0)^+ \quad (1)$$

$$CDD = \sum_{days}(T_0 - T_b)^+ \quad (2)$$

where Tb is the base temperature and To is the daily mean outdoor air temperature. The plus sign above the parentheses indicates that only positive values are to be counted. The heating and cooling degree-hours can be calculated in a similar manner with the hourly instead of the daily data.

The heat losses in buildings generally occur through external walls, windows, ceiling, floors and air infiltration. The heat loss from windows due to the infiltration is not taken into account since the insulation does not affect that heat loss. On the other hand, in these calculations only the heat loss from external walls is considered. Heat loss from per unit area of external wall is;

$$q = U * (T_b - T_o) \quad (3)$$

where U-value is the overall heat transfer coefficient.
The annual heat loss per unit area can be obtained from;

$$q_A = 86400 * DD * U \quad (4)$$

Annual energy requirement;

$$E_A = \frac{86400 * q_A * DD}{\eta} \quad (5)$$

After the evaluation the yearly heat demands to calculate cost accounting, the Present-Worth Factor (PWF) will be used.

If i < g;

$$r = \frac{(i-g)}{(1+g)} \quad (6)$$

If i > g;

$$r = \frac{(g-i)}{(1+i)} \quad (7)$$

$$PWF = \frac{(1+r)^N - 1}{r * (1+r)^N} \quad (8)$$

Total cost formula;

$$C_T = \frac{86400 * DD * PWF * C_f}{\left(R_{wt} + \frac{x}{k}\right) * H_U * \eta} + C_i * x_{opt} \quad (9)$$

$$x_{opt} = \left(\frac{86400 * DD * C_f * PWF * k}{H_U * C_i * \eta}\right)^{\frac{1}{2}} - k * R_{wt} \quad (10)$$

IMPLEMENTATION OF INSULATION THICKNESS OPTIMIZATION PROCEDURES IN THE DEMO SITES

In this section, calculations are made for three demo sites. Valladolid (Spain), Soma (Turkey) and Lund (Sweden) are considered.

Parameter		Valladolid	Soma	Lund
HDD	Heating degree day	3121 (20°C)	1783 (18°C)	3277 (17°C)
Fuel type		Biomass(Wood Chips)	Lignite	Biogas
η (%)	Fuel efficiency	0.80	0.65	0.8
Cf (€/kWh)	Fuel price	0.25	0.092	0.09
LHV (J/m^3)	Lower Heating Value	6.00E+06	2.30E+07	3.97E+07
Insulation material		EPS	EPS	Mineral wool
k (W/mK)	Conductivity	0.037	0.04	0.036
Ci (€/m^3)	Insulation material cost	40	70	60-90
ρ (kg/m^3)	Density	15-20	20	20-50
General information				
i (%)	Interest rate	0.3	0.8	0.3
g (%)	Inflation rate	4	0.749	1.1
N (year)	Lifetime of the system	20	20	20
Rwt (m^2K/W)	Total wall thermal resistance	0.7353	0.56179	2.5

Table 1 : Parameters used in each demo site

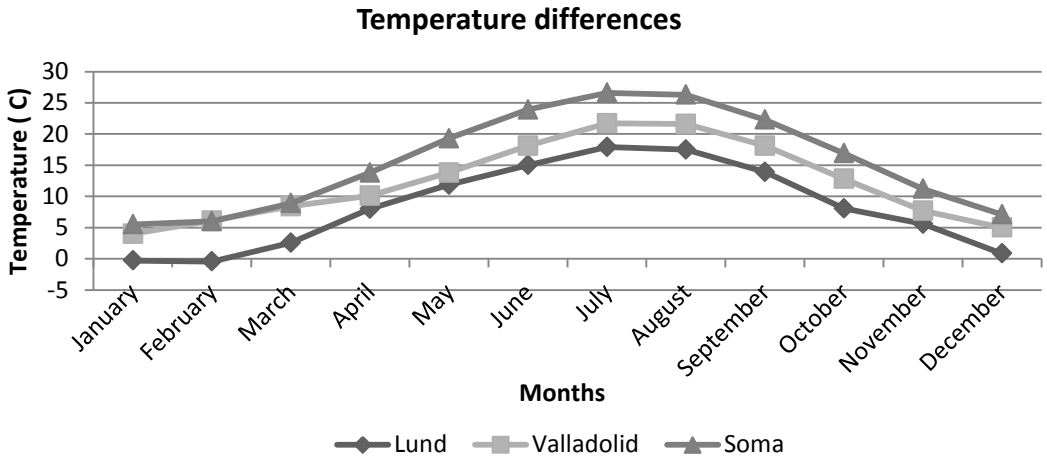

Figure 1 : Monthly average temperatures in Lund, Valladolid and Soma

The external wall's thermal characteristics information is given in the table below;

	Valladolid	Soma	Lund
External wall	1.36 W/m^2C	1.78 W/m^2C	0.35 W/m^2C

Table 2: Existing U values for external wall for each demo site

RESULTS

With regard to equations given above, the results are as follows;

Explanation		Valladolid	Soma	Lund
r	Interest rate adapted for inflation rate	2.8461	0.0291	0.6154
PWF	Present Worth Factor	0.3513	14.9937	1.6249
x opt (m)	Optimum insulation thickness	0.042	0.0679	0.06

Table 3: Optimum insulation thickness calculation results

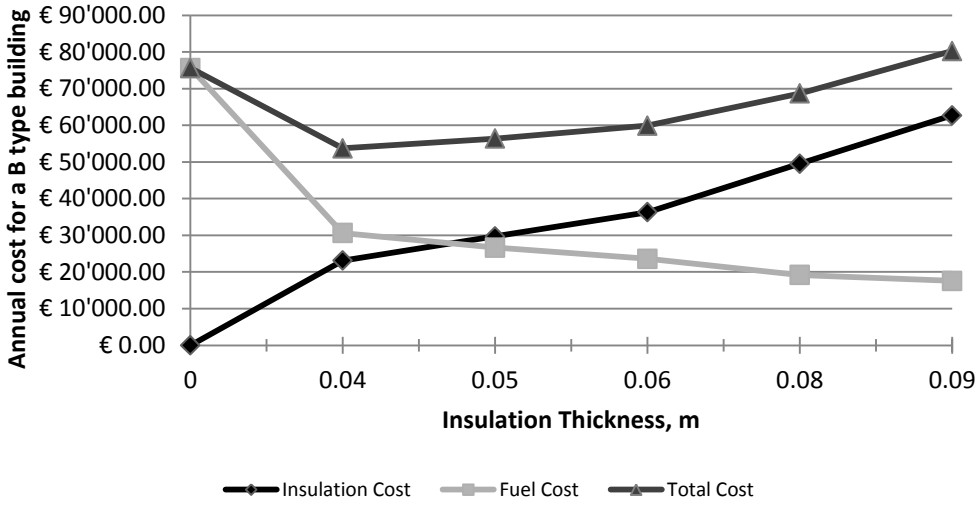

Figure 2: Annual costs versus insulation thickness in Valladolid demo site

For Valladolid, optimum thickness is 5cm according to calculations. Also in Valladolid, comparing to the existing conditions, 2 Mtce/year will be saved. For 20 year, the saved energy equals 40 Mtce.

For Lund, the used fuel is already more efficient and its lower heating value is really high. By the way, the U value for façade is too low. In Lund demo site, one of the external wall type already has 10 cm EPS. It has to be highlighted that besides EU FP7 project aims to focuse on reducing the energy demand, reducing GHG emissions and increasing the use of renewable energy sources by developing and implementing innovative technologies for building renovation are also important. Thereby, in Lund, insulation thickness affects other results as a reference model.

In Linero District, comparison with the existing condition, 17605 kWh-gas/year will be saved. For 20 year, it equals to 23.59 Mtoe for Lund.

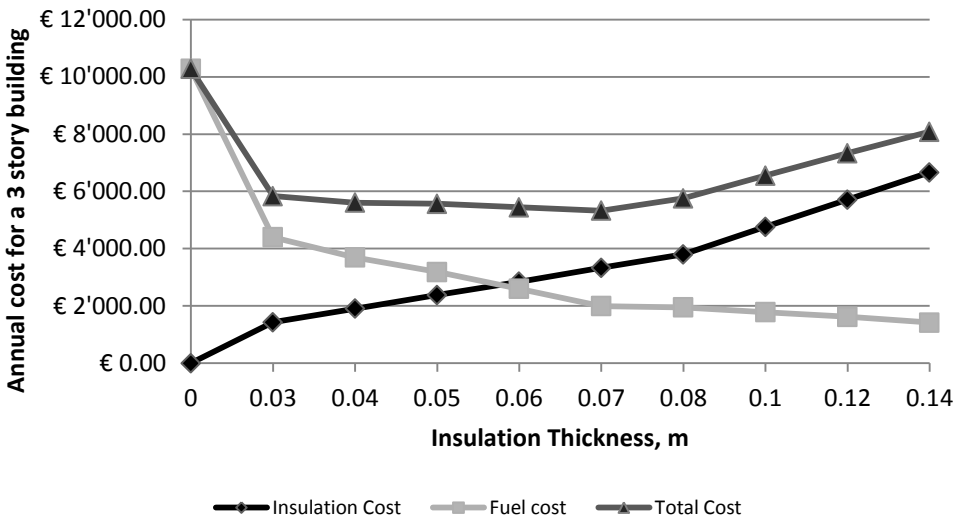

Figure 3: Heating and annual costs versus insulation thicknesses for 3 story building for Soma

For Soma, optimum insulation thickness is 7cm with regard to calculations. For 20 year, saved energy equals 133.09 Mtce for Soma demo site.

One of the aim for this study is that view and focusing on environmental aspects, the retrofitting uptake of low efficient building has impact in terms of CO_2 emissions reduction, and improvement of the indoor air quality. Under these circumstances, both substantially energy saved and CO_2 emissions are reduced for three demo sites.

In this study, optimal insulation thicknesses for different type of buildings are determined. Thanks to this calculations, energetic and economic cost optimization can be made, which has positive effects on reducing the energy demand and GHG emissions.

REFERENCES

1. Europe's buildings under the microscope, Buildings Performance Institute Europe (BPIE), 2011.
2. http://epp.eurostat.ec.europa.eu. [Online]
3. Barrau, J.: Impact of the optimization criteria on the determination of the insulation thickness, Energy and Buildings, 2014.
4. Mohammad S., Al-Homoud: Performance characteristics and practical applications of common building thermal insulation materials. Architectural Engineering Department, King Saud University, Saudi Arabia: Building and Environment, 2005.
5. Bolatturk, A.: Determination of optimum insulation thickness for building walls with respect to various fuels and climate zones in Turkey, Applied Thermal Engineering, 2006.
6. Zedan, MF, Mujahid, A.: An efficient solution for heat transfers in composite walls with periodic ambient temperature and solar radiation, Int. J. Ambient, 2008.

EXPERIMENTAL ANALYSIS OF AIR FLOW PROFILES IN A DOUBLE SKIN FAÇADE IN A MARITIME CLIMATE

Oliver Kinnane[1]; Daniel Murphy[2]; Michael Grimes[2].

1: Architecture at SPACE, Queens University Belfast, Northern Ireland.

2: Dept. Civil, Structural and Environmental Engineering, Trinity College Dublin, Ireland.

ABSTRACT

Glazed Double Skin Facades (DSF) offer the potential to improve the performance of all-glass building skins, common to commercial office buildings in which full facade glazing has almost become the standard. Single skin glazing results in increased heating and cooling costs over opaque walls, due to lower thermal resistance of glass, and the increased impact of solar gain through it. However, the performance benefit of DSF technology continues to be questioned and its operation poorly understood, particularly the nature of airflow through the cavity.

This paper deals specifically with the experimental analysis of the air flow characteristics in an automated double skin façade. The benefit of the DSF as a thermal buffer, and to limit overheating is evaluated through analysis of an extensive set of parameters including air and surface temperatures at each level in the DSF, airflow readings in the cavity and at the inlet and outlet, solar and wind data, and analytically derived pressure differentials. The temperature and air-flow are monitored in the cavity of a DSF using wireless sensors and hot wire anemometers respectively. Automated louvre operation and building set-points are monitored via the BMS.

Thermal stratification and air flow variation during changing weather conditions are shown to effect the performance of the DSF considerably and hence the energy performance of the building. The relative pressure effects due to buoyancy and wind are analysed and quantified.

This research aims to developed and validate models of DSFs in the maritime climate, using multi-season data from experimental monitoring. This extensive experimental study provides data for training and validation of models.

Keywords: double skin façade, air flow, energy efficiency, building skins

INTRODUCTION

Since the middle of the twentieth century glass has become the most common material choice for commercial building envelopes, particularly for office buildings. While glass cladding systems have become both affordable and constructionally efficient, their environmental performance continues to present problems. In comparison to insulated, but opaque skins, glass gives rise to high levels of heat loss and increased risk of overheating in buildings. Glazed Double Skin Facades (DSF) offer the potential to improve the performance of all glass building skins. However, a poorly designed DSF can further increase the risk of overheating in buildings [1].

The DSF generally consists of two glazed skins with an air cavity, of varying width (~0.15m-1.5m), between them. Using two separated layers of glass over multiple stories of the building

façade allows for air to rise up the cavity through buoyancy. Ventilating the cavity at top and bottom allows for the removal of heated air through the cavity rather than heating the internal building air - particularly worthwhile during summer season. Similar to single skin facades the risk of overheating is a consistent disadvantage of DSF. Other disadvantages include increased construction costs and a reduction in rentable office space.

Even though DSF technology and construction is now well resolved and commonplace, the performance benefit of DSFs continues to be questioned [2]. Their impact is reported in the literature to vary between possible energy savings of over 50% [3], and possible increases in building energy load [4]. Because DSFs are designed to suit the conditions and needs of a specific site, consistency of performance is varied. Also climatic conditions, orientation, construction and geometry are varied and hence comparison difficult and identification of a defining set of indices and thresholds complicated.

Although there has been extensive literature published on the performance of DSFs over the last decade there remains a paucity of experimental studies focused on analysis of real, installed DSFs. The literature has instead focused on CFD modelling based studies. Prolonged monitoring studies of DSF performance, and analysis of operational data during changing climate conditions are necessary to progress the understanding of complex DSF operation during different climatic conditions.

Temperature and airflows in the cavity are a result of many simultaneous thermal, optical, and free/forced convective turbulent fluid flow processes [5]. Solar radiant energy entering through the glass is absorbed by interior objects and surfaces, which then retransmit the energy as thermal radiation mainly in the far infra-red band (above 5 μm). Louvers and shades within the cavity are proposed to impact the air flow in the cavity due to the emittance of thermal radiation from their surfaces. To simply the problem key indices for evaluation of the thermal performance of DSFs are required and Pappas and Zhai (2008) outline a set including; i) airflow rate through cavity openings, ii) average cavity air temperature, iii) peak cavity air temperature and (iv) convective heat transfer through interior glazing.

The first of these, the airflow rate through openings into the cavity, is documented by only a few authors [6]. They generally report low airflow speeds. The standard equation for airflow through openings is generally represented as a function of the applied pressure difference across the opening and its length, cross sectional area and internal geometry.

$$q_v = C(\Delta p)^n \tag{1}$$

where, q_v is the volumetric flow rate through the opening (m^3/s) C is the flow coefficient ($m^3/s/Pa^n$) and n is the flow exponent [7]. The flow coefficient C may be replaced by the product of I_c and k_l, where I_c is the total length of opening (m) and k_l is the flow coefficient per unit length of opening ($L/s.m.Pa^n$). Similarly airflow through openings is also represented in terms of temperature; $q_v = C\Delta T^n$ where, Pappas and Zhai (2008) describe C and n as coefficients that describe the cavity size and geometry of the DSF [6].

The use of average air cavity temperatures to approximate the temperature in the DSF cavity in modelling studies misrepresents the real operation of DSF. Thermal stratification has been well established in previous research [8]. Although not often reported experimentally this seems to be a common occurrence in DSF cavities. Hot air stratifying in the upper stories has a differential and detrimental impact on comfort conditions and operating conditions in the adjoining building spaces. They provide correlations for cavity airflow rate, air temperature stratification, and interior convection coefficient.

Peak temperatures are often 10-15°C higher than average temperature over a 3 story range and can reach values of >35-40°C in the top levels of the cavity, with outdoor air temperatures of 15°C [8].

The convective heat transfer through the interior glazing is only of concern in the case of a DSF ventilated to the interior. This study is focused on a sealed cavity.

METHOD

Case Study DSF

The interior façade is the thermal barrier, with lower thermal, and solar, transmittance. The external glazing is single pane glazing with higher solar transmittance.

The airflow through the cavity is naturally, rather than mechanically driven, due to buoyancy and effects of wind pressure. However, the louvers at top and bottom of the façade are mechanically activated in response to excessive wind speeds (>7m/s) and high cavity temperatures (>24°C). The DSF is automated and works in closed (T_{cav} <24°C) and open (T_{cav} >24°C) modes during the winter period. Temperatures reach peak values of >35-40°C in the middle of the cavity. Airflow in the cavity is generally low (<1m/s) with peak variations during periods of high solar radiation.

Monitoring Study of DSF

A monitoring study was undertaken over a 4-month winter period. Data was gathered at weekly to fortnightly intervals. Temperatures at all levels were extensively monitored with multiple wireless temperature sensors. Two anemometers are used to monitor airflow at different locations in the DSF during different 2-weekly periods – the maximum extend of life of the remote battery, with additional power from attached PV panel.

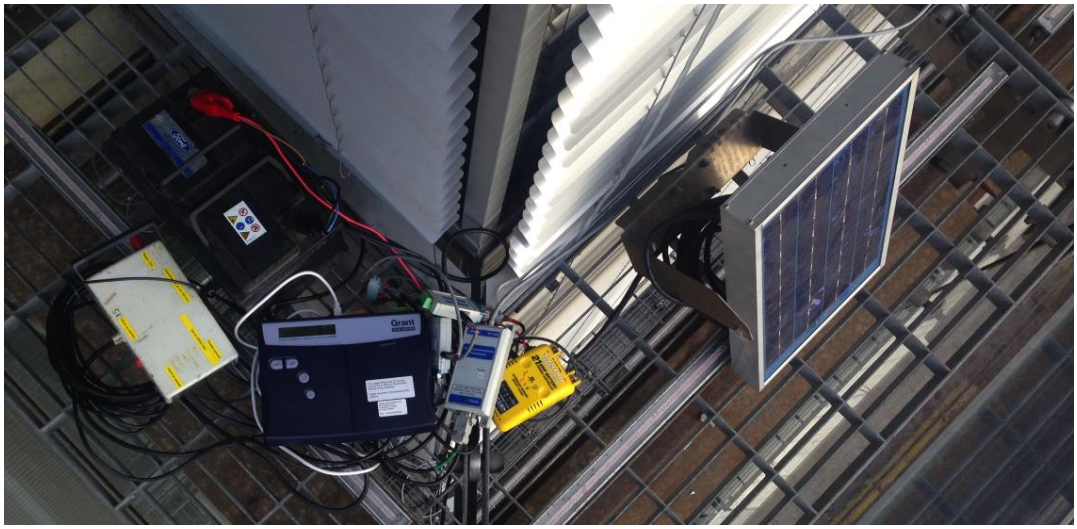

Figure 1: Equipment installed in the DSF to power anemometers to monitor air flow in DSF.

RESULTS

The following are the key results from the monitoring study of airflow within the DSF during the winter season of 2014/15. Shown are airflows at different levels in the façade and differential airflows during days of high and low levels of direct solar radiation. Airflow at mid and upper levels of the DSF cavity are shown in Figure 2. Days of high solar radiation exhibit higher air velocities than days of low solar radiation.

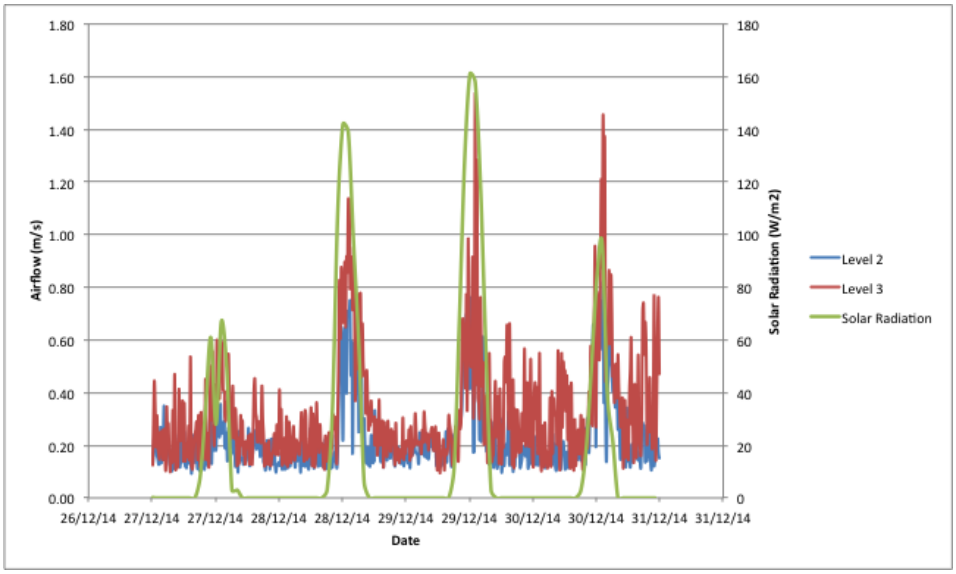

Figure 2: Airflow in mid (Level 2) and top (Level 3) levels of the 3-story DSF during a 4 day period.

The air velocity through the cavity due to buoyancy is low through the monitoring period, with values of < 0.6 m/s common.

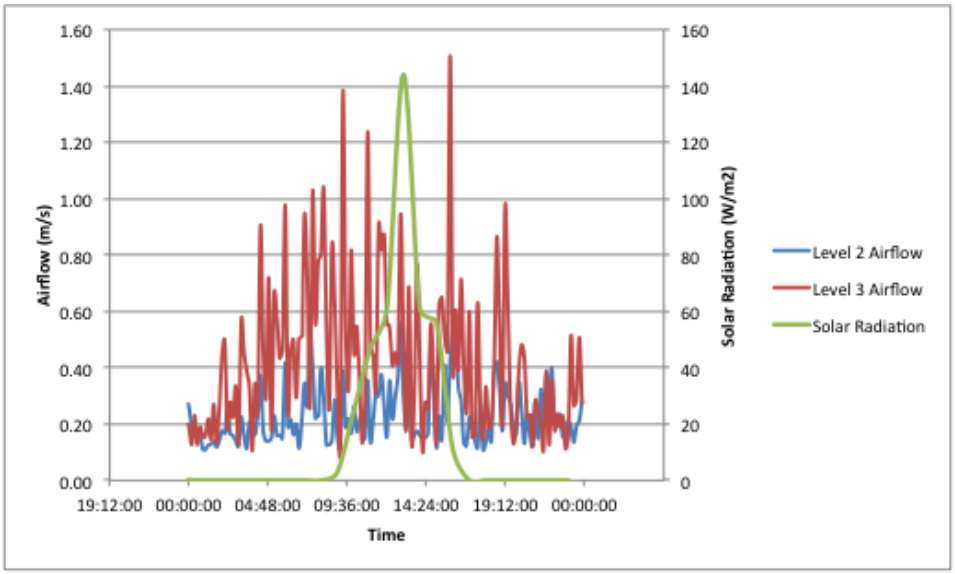

Figure 3: Airflow in mid (Level 2) and upper (Level 3) levels of the DSF on a day of average solar radiation.

Direct and diffuse airflow

The relative impact of diffuse and direct solar radiation, on the airflow characteristics in the DSF cavity, is plotted in Figure 4. During periods of strong direct solar radiation airflow in the mid and top cavity regions are seen to increase from 0.15 m/s to 0.4 m/s and 0.2 m/s to 0.54 m/s respectively.

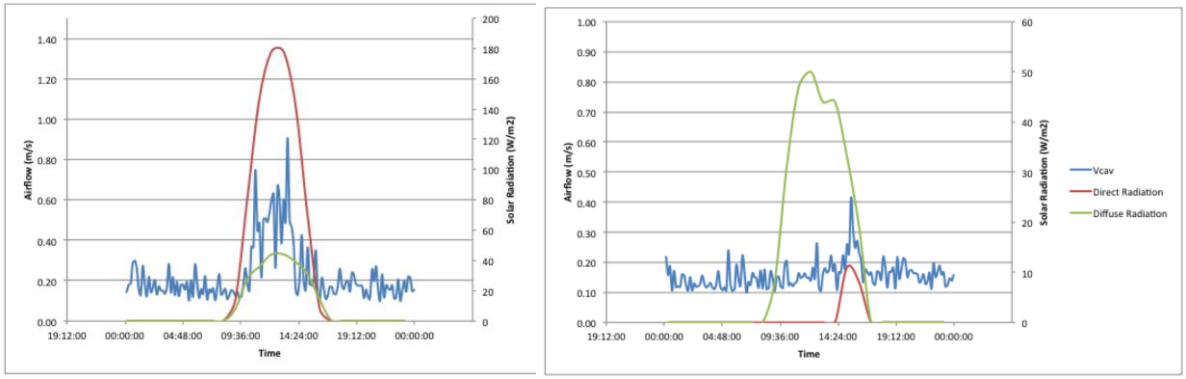

Figure 4: Evidence of the impact of direct and diffuse solar radiation on airflow.

Significant increases in airflow above the consistent night-time flow are observed when direct solar radiation predominates (Figure 4 (right)). On the day shown when diffuse radiation predominates (Figure 4 (left)) peaks in airflow are seen to correlate with late afternoon peaks in solar radiation.

DISCUSSION

Buoyancy drives airflow in the cavity and hence dominates DSF operation in the winter period monitored. Some airflow ingress is constant through designed gaps in louvers, but air velocity increases in the cavity are observed when solar radiation heating of the exterior glazed layer and hence, cavity air temperature.

Airflow velocity in the cavity is generally low (<1m/s) in agreement with those values reported in experimental and modelling studies [6]. During cloudy conditions, with predominantly diffuse solar radiation velocities of <0.2 m/s are commonplace. Airflow increases rapidly in response to direct solar radiation.

The airflow increase results from wind driven air being drawn into the cavity by the negative pressures set up due to the hot air rising in the cavity. Similarly at the outlet, the air is drawn out as a negative pressure zone is created on the backside of the façade. Given the orientation of the façade, slightly offset from the perpendicular to the prevailing wind direction, the impact of the wind needs also be considered.

Wind induced effects could be seen to augment operation at the inlet and outlet. Although the louvers remain ‘closed’ throughout the winter period monitored, gaps exist between the louvers and air can gust through these gaps. Hence prevailing southwesterly wind impacting the facade enhances the drive of air into the cavity, through the gaps in the louvers and out at the outlets. The cavity temperature remains below 24°C during the majority of the monitoring period hence the louvers do not activate for durations that would be viewed to affect the DSF operation significantly.

Given its Northern European geographical location Ireland has extensive cloud cover for long durations of the year. Hence its ratio of direct to diffuse solar radiation is much lower than many continental European cities.

This study is limited to winter season monitoring. Extended monitoring is required to develop an understanding of the contrasting airflows during summer months, when ambient temperatures and solar radiation can be expected to be significantly higher.

CONCLUSION

Based on the results of this study DSFs are observed as beneficial to building performance in Irish winter conditions. Although air movement is observed, flow velocities are generally low and warmed air is thereby retained in the cavity, at higher temperatures relative to the outdoor, to enable the DSF act as a buffer from lower temperatures outside.

Increased levels of airflow are observed in proximity to the inlet and outlet vents, although they remain predominantly 'closed' for the winter season. Airflow is highly responsive to direct solar radiation. A significant increase in airflow is observed in sunny, clear sky conditions even when the louvers remain 'closed'.

Inefficient operation of new and retrofit non-domestic buildings remains all too common in this age of climate change concern [9]. The DSF can provide a solution to glass buildings.

ACKNOWLEDGEMENT

The authors would like to express sincere thanks to Arup Dublin for supporting this project.

REFERENCES

[1] E. Gratia and A. De Herde, "Optimal operation of a south double-skin facade," *Energy Build.*, vol. 36, no. 1, pp. 41–60, Jan. 2004.

[2] T. Pasquay, "Natural ventilation in high-rise buildings with double facades, saving or waste of energy," *Energy Build.*, no. 4, pp. 381–389, 2004.

[3] W. N. Hien, W. Liping, A. N. Chandra, A. R. Pandey, and W. Xiaolin, "Effects of double glazed facade on energy consumption, thermal comfort and condensation for a typical office building in Singapore," *Energy Build.*, vol. 37, no. 6, pp. 563–572, Jun. 2005.

[4] Gertis, K., "Sind neue Fassadenentwicklungen bauphysikalisch sinnvoll? Teil 1: Transparente Wärmedämmung," *Bauphysik*, vol. 21, no. Nr.1, pp. 1–9, 1999.

[5] M. Coussirat, A. Guardo, E. Jou, E. Egusquiza, E. Cuerva, and P. Alavedra, "Performance and influence of numerical sub-models on the CFD simulation of free and forced convection in double-glazed ventilated façades," *Energy Build.*, vol. 40, no. 10, pp. 1781–1789, 2008.

[6] Z. Z. Alexandra Pappas, "Numerical investigation on thermal performance and correlations of double skin façade with buoyancy-driven airflow," *Energy Build.*, no. 4, pp. 466–475, 2008.

[7] CIBSE, "Concise Handbook," London, 2008.

[8] O. Kinnane and T. Prendergast, "Assessment of double skin facade passive thermal buffer effect.," presented at the Passive Low Energy Architecture Conference, Ahmedabad, India, 2014.

[9] O. Kinnane, M. Dyer, and T. Grey, "Energy and environmental forensic analysis of public buildings," *Proc. ICE - Eng. Sustain.*, vol. 167, no. 4, pp. 143–156, Aug. 2014.

OVERHEATING IN SCOTLAND: LESSONS FROM 26 MONITORED LOW ENERGY HOMES

C. Morgan[1]; J.A. Foster[1]; T. Sharpe[1]; A. Poston[1]

1: Mackintosh Environmental Architecture Research Unit (MEARU), Glasgow School of Art, 167 Renfrew Street, Glasgow, G3 6RQ

ABSTRACT

There is growing awareness in the UK that overheating is a significant problem and one that is likely to intensify with climate change, increasing urbanisation, an ageing population and the move towards 'low energy' buildings. Recent research suggested that while overheating may be an issue in the South of England, particularly in urban areas, it was not likely to be an issue for Scotland and the North of the UK in the medium term. This notion is reflected in the lack of awareness of the issue in Scotland. Monitoring of 26 new-build low energy and Passivhaus homes across Scotland over a two year period indicates overheating is prevalent in living areas and in particular in bedrooms where it is acknowledged that respite from high temperatures is important. This paper describes the quantitative and qualitative results, assesses relevant factors, comments on predictive tools used and seeks a robust series of measures to avoid overheating in future low energy homes in Scotland.

Keywords: Overheating, *Thermal Comfort, Occupancy, Behaviour, Comfort, Health*

INTRODUCTION

There are some concerns related to overheating which are purely energy based, such as excess internal gains from equipment, excess heat from slow response heating systems and the increased use of air conditioning, but the majority of concerns surrounding overheating relate to the health risks it poses. Overheating, or 'excess heat' in dwellings is one of the defined hazards in the UK Government's Housing Health and Safety Rating System (HHSRS) where it is noted high temperatures can increase cardiovascular strain and trauma and when temperatures exceed 25°C there is an increase in strokes and mortality [1].

While overheating may remain no more than an inconvenience for some, the risks become very serious for certain vulnerable groups, including infants, the elderly, the obese, socially isolated, chronic disease sufferers and those living in urban areas [2]. Mild heat-related health effects include dehydration, prickly heat, heat cramps, heat oedema (swelling), fainting and heat rash [2]. Concentration and productivity reduce as a result, while dehydration itself can be serious. More severe health effects include mental health consequences and heat exhaustion which can lead to heat stroke if not managed. Heat stroke can be fatal and is considered to be under-reported due to its similarity with strokes and heart attacks [2, 3]. Health risks are increased by higher night-time temperatures in bedrooms, due to the inability to recover from heat stress during the day [4].

There is growing awareness in the UK that overheating in dwellings is a significant problem [5, 6, 7] and one that is likely to intensify with a warming climate, increasing urbanisation, an ageing population, the move towards 'low energy' buildings [2, 8, 9] and variations in occupant behaviour [9, 10]. Research conducted to date has used computer simulation to assess likelihood of overheating which indicates a low risk of overheating in Scotland, compared with London [11].

EVIDENCE OF OVERHEATING IN SCOTLAND

Post occupancy evaluation (POE) was undertaken for two years in living rooms and bedrooms of 26 dwellings located in six separate developments in Scotland. The POE project was funded by Technology Strategy Board (TSB) now Innovate UK where an element of the study included remote monitoring of indoor air temperature (°C), relative humidity (%RH), carbon dioxide (CO_2) concentrations and window opening occurrences for each dwelling. Data loggers recorded these parameters every five minutes throughout the two year monitoring period. Surveys were undertaken as part of the project and these included a development wide survey on comfort. This paper uses data from occupied Scottish dwellings, constructed since 2009, to highlight overheating in Scotland and draws upon lessons learnt through the data collection period.

Dwelling Ref	**Living Room**			**Bedroom 1**			**Bedroom 2**		
	Orientation	**> 28°C (%)**	**PH > 25°C (%)**	**Orientation**	**> 26°C (%)**	**PH > 25°C (%)**	**Orientation**	**> 26°C (%)**	**PH > 25°C (%)**
BA1	SE	0	-	SE	4	-	-	-	-
BB1	SW	0	-	NE	1	-	-	-	-
BC1	NW	3	-	NE	6	-	-	-	-
DA1	S	1	23	S	50	65	N	46	64
DA2	S	1	18	S	18	27	-	-	-
DB1	S	0	13	S	7	18	-	-	-
DB2	S	2	23	S	15	25	N	24	34
GA1	SW	0	-	SW	7	-	-	-	-
GA2	SW	11	-	SW	69	-	-	-	-
GA3	NW	3	-	SE	22	-	-	-	-
GB1	NE	0	-	SW	0	-	-	-	-
GB2	NE	4	-	SW	8	-	-	-	-
GB3	N	0	-	S	3	-	-	-	-
IA1	W	10	-	W	3	-	E	14	-
IA2	W	0	-	W	9	-	E	3	-
IB1	W	0	-	W	17	-	E	47	-
IB2	W	0	-	W	1	-	E	2	-
IC1	S(W)	1	-	N	1	-	-	-	-
IC2	S(W)	2	-	N	0	-	-	-	-
ID1	W	2	-	S	0	-	-	-	-
ID2	W	1	-	N	4	-	-	-	-
LA5	E	2	-	W	15	-	-	-	-
LA6	E	1	-	W	10	-	-	-	-
TA1	E	0	-	E	0	-	W	0	-
TA2	E	0	-	E	0	-	W	1	-
TB1	E	0	4	E	0	0	W	1	2

Table 1: Percentage of hours exceeding CIBSE and Passivhaus thermal comfort thresholds for one year. > 28°C indicates percentage of year internal temperature exceeds 28°C with 1% considered acceptable. Similar for > 26°C. > 25°C indicates percentage of year internal temperature exceeds 25°C with 10% considered acceptable used for Passivhaus dwellings.

Analysis of the recorded data revealed overheating to be prevalent in the dwellings. Overheating was assessed using former CIBSE thermal comfort criteria where a room is considered to have overheated when temperatures exceed 26°C in bedrooms and 28°C in living rooms for more than 1% of annual occupied hours. This permitted comparison with 'as designed' assessments. The five Passivhaus dwellings were assessed against this criterion as well as the Passivhaus overheating criteria where internal space temperature should not exceed 25°C for more than 10% of the year. Findings from three of the developments are discussed in more detail.

Case Study 1 - Dumfriesshire

The Dormont Estate is situated in South-West Scotland at a latitude of around 55°N, broadly level with Newcastle. Four 3-bed and four 2-bed 2-storey, semi-detached houses were completed in 2011 and certified to the Passivhaus standard using lightweight Structural Insulated Panels panels with MVHR ventilation (complete with posst-heaters), wood stoves and solar thermal panels.

In addition to physical monitoring a range of occupant surveys and feedback exercises were undertaken. The principal and most widespread concern for occupants was that of overheating with comments such as "*Too hot in summer*" and "*Gets too warm upstairs especially difficult at night*".

The risk of overheating was not assessed as part of Building Warrant but the PHPP (Passivhaus Planning Package) assessment established there would be 0.2% overheating, i.e. 0.75% (18 hours) of one day across a year when the temperature in the house overall would rise above 25°C. Examination of the monitored temperatures indicates these temperatures were exceeded for a far greater percentage of the time than this (Table 1).

Figure 1 below shows the recorded data for a two week monitoring period in July 2013 in which the temperatures in all four main (south facing) bedrooms rarely dipped below 25°C and only then in one house and for short periods. For the remainder of the two week period, in all houses, temperatures in the bedrooms rose as high as 33°C but averaged around 27°C.

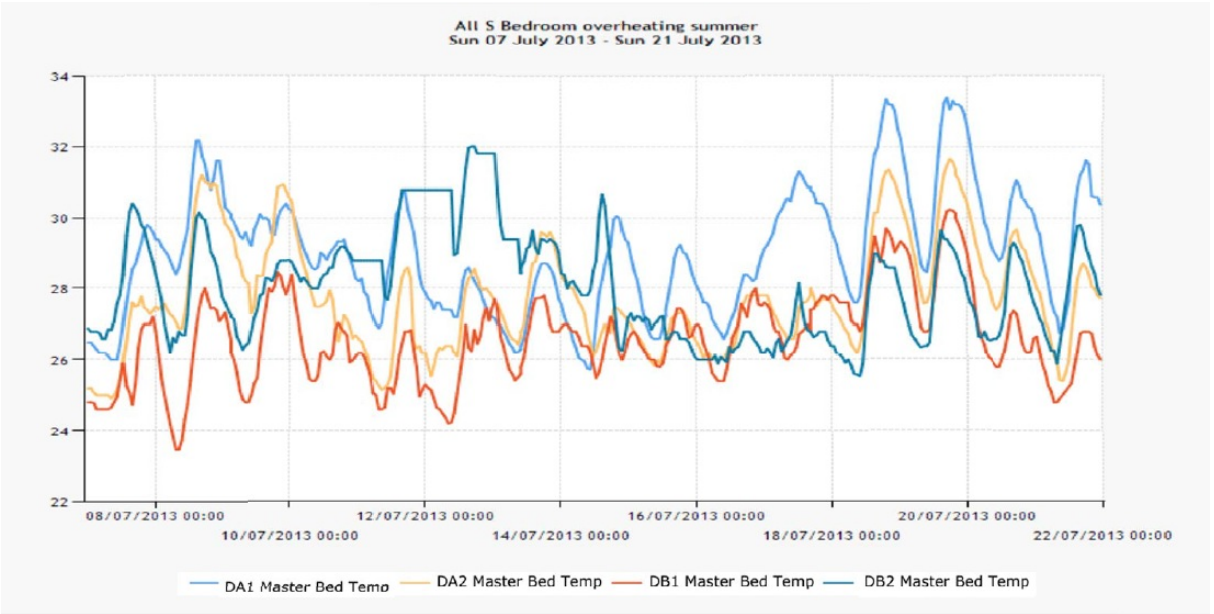

Figure 1: South facing bedroom temperatures in four monitored dwellings 7th – 21st July 2013.

The temperature profiles were similar but less pronounced in living rooms but overheating as defined by CIBSE allows for greater tolerance in living areas. A number of factors identified were attributable to occupants only, such as keeping bedroom doors closed, or being away during the day and unable to take measures necessary to contain the indoor temperatures. A number of the reasons for the overheating can be traced to design and construction decisions but differences between (identical) properties can be traced to occupant behaviour. The highest levels of overheating were found in the dwelling inhabited by a young, single mother with a toddler who of all occupants in the programme was, initially at least, the least interested and engaged in the monitoring process.

Case Study 2 – Central Glasgow

This development provides a total of 117 dwellings located in central Glasgow. Intensive monitoring was undertaken in three one-bedroom flats within a sheltered complex for the elderly and three two-bedroom flats for mainstream occupants. Each dwelling is naturally ventilated with intermittent mechanical extracts located in kitchens and bathrooms, trickle ventilators in the window heads or walls provide make up air. Basements in each block contain an energy centre providing communal central heating and domestic hot water to each dwelling with underfloor heating in the sheltered flats and conventional radiators in the mainstream flats.

The monitoring indicated high percentage of annual hours over the CIBSE comfort threshold temperatures (Table 1) in the bedrooms of the sheltered flats (GA1, GA2 and GA3) and two living rooms (GA2 and GA3). GA1 and GA2 are mostly occupied 24/7 where annual temperatures were found to exceed 26°C for 7% (GA1) and 69% (GA2) of the year. Overheating occurred mostly during the summer in GA1 and occurred extensively during all seasons in GA2, particularly spring and summer. While some of the high temperatures could be associated with solar gain due to the orientation, the research team observed high temperatures in GA2 on their visits to the property. In addition to this the occupant is unable to adapt the internal environment due to mobility issues and reliance is placed on home helpers to alter heating controls, open/close windows and remove clothing.

In the mainstream properties overheating was observed through a mixture of solar gain, internal gains and the preference for warm internal temperatures. However, the occupant of GB3 expressed dissatisfaction with the large south facing bedroom windows and the need to keep curtains closed in bedrooms to provide shade, bedrooms being sited over the communal boiler plant room and security concerns due to the dwellings ground floor position.

Case Study 3 – Inverness, Highland Scotland

In this development 52 dwellings were designed as part of Scotland's 2010 Housing Expo to showcase innovative sustainable housing. The timing of the construction of the development coincided with the recent recession and the contractors undertook a value engineering exercise on the architect designed homes so the dwellings could be constructed. Four pairs of naturally ventilated, timber frame homes (eight in total) were intensively monitored. Four of the dwellings were for social rental (2-storey houses IA1, IA2, IB1 and IB2) and four occupied by owner occupiers (1 and 2-bedroom flats IC1, IC2, ID1 and ID2). Surveys of the 52 dwellings indicated most of the households thought the homes were more comfortable and cheaper to run than former homes, with less heat input in winter due to the passive solar design. However, 62% of the surveyed households found their homes were too hot during the summer, indicating solar gain to be an issue due to west facing glazing and lack of operable windows to promote cross or stack ventilation.

Table 1 indicates 87% of bedrooms and one living room (IA1) in the 2-storey houses to have exhibited overheating. Dwellings IA1 and IA2 are within a terrace orientated east/west, with IA1 at the south end of the terrace. The study found the east facing bedroom to have overheated for 14% of the year, the peak space temperatures in this room were 27°C (winter), 29.6°C (spring), 30.8°C (summer) and 31.8°C (autumn). In the neighbouring dwelling of identical design and layout, IA2, the west facing bedroom was found to have had a higher percentage of time over 26°C with maximum temperatures of 30.4°C. Window opening in this room rarely happened due to an obstruction from a child's cot placed beneath the operable window. The east and west facing bedrooms in IB1 tended to exhibit overheating all year, with a higher proportion of overheating attributed to summer time. The data confirmed temperatures in the east facing bedroom were above 26°C for 47% of the year. This household routinely sets their thermostat to 25°C.

In the flatted dwellings of ID1 and ID2 there were concerns of overheating in the living rooms due to poor construction of the adjoining west facing solar sunspace, ID1 reached temperatures over 28°C for 2%. North facing bedroom in ID2 reached temperatures over 26°C for 4% of the year. Investigations revealed heat gains from the fridge/freezer in the kitchen were warming the separating wall and heating the bedroom, welcome in winter but not during summer.

DISCUSSION

Whilst it is evident low energy buildings in Scotland are overheating it appears that the causes are not clearly appreciated by those procuring, designing and building, even the few measures aimed at reducing overheating are often 'value engineered' out before completion. Nor are causes the same between dwellings. In some instances one dwelling from an identical pair is exhibiting serious overheating which can be linked to occupant behaviour and preference for warmer internal temperatures. In the case of the sheltered homes vulnerability of elderly residents is highlighted due to inability of some immobile occupants to adapt their thermal environment, exposing them to high temperatures both day and night. Internal gains from equipment such as fridge/freezers and televisions are contributing towards overheating in dwellings even when using 'A' rated white goods. Proximity to adjacent plant, uninsulated tanks and pipework and reluctance to open windows due to security fears are all possible contributors. In some cases solar gain can be shown to be an issue, particularly for south-west and west facing rooms but in other homes, North-facing rooms are overheating as much as others. None of the properties monitored had any form of external shading and many had insufficient ventilation arrangements. Four of the five Passivhaus dwellings are overheating considerably more than the design criteria which correlates with Sameni et als [12] findings.

CONCLUSIONS

In all projects discussed, the predictive tools used have failed to identify the overheating risks adequately. Beyond deficiencies in the tools themselves, this can be partly attributed to the varying nature of occupant comfort thresholds and behaviour.

Where models are created in which the same constructions are 'located' in different latitudes, it is to be expected that the risk and extent of overheating will be greater in warmer parts of the UK and in future projections of our warming climate. However, the evidence gathered by MEARU suggests that where low energy buildings have been built in Scotland, a combination of effective heat retention and recovery, occupant behaviour and poor design or installation essentially override the northerly location to create conditions of overheating sufficient to cause concern in the short term.

It could be suggested that after many years of lagging behind some of our European neighbours in designing effective, energy efficient homes for cold weather, the UK has caught up, but in so doing is not yet experienced in the implications of living within energy efficient buildings. Thus high levels of insulation and airtightness as well as insufficient thermal mass have all been blamed for causing overheating although it is often not appreciated that these very measures serve to keep heat out as well as in.

No one measure leads to overheating, it is the failure to understand the full implications of energy efficient designs and occupant behaviour with respect to the potential for overheating which leads to problems. For this reason it is important to address the general lack of awareness about overheating in Scotland and engage with occupants to help them avoid the problem, while ensuring the buildings they live in effectively keep them warm in winter and cool in summer.

REFERENCES

1. Office of the Deputy Prime Minister (ODPM). Housing Heath and Safety Rating System (HHSRS): Operating Guidance. London, ODPM, 2006.
2. NHBC Foundation (2012) Overheating in new homes: A review of the evidence.
3. Department of Health. Heat wave plan for England, 2011. www. dh.gov.uk/prod_consum_dh/groups/dh_digitalassets/documents/digitalasset/dh_127235.pdf.
4. Kovats, S., and Hajat, S. Heat stress and public health: A critical review. Annual Review of Public Health, 2008, 29 (9)1–9.15.
5. DCLG: Investigation into Overheating in Homes. Literature Review. AECOM July 2012.
6. DCLG: Investigation into Overheating in Homes: Analysis of gaps and Recommendations. AECOM March 2013.
7. Building Services Engineering Research and Technology Special Issue: Overheating and Indoor Air Quality Vol 36 (2) (Editorial) 2015.
8. Orme, M., Palmer, J. & Irving, S. (2003) Control of overheating in well-insulated housing. CIBSE/ASHRAE conference in Building Sustainability, Value and Profit. Edinburgh, 13th June 2003, FaberMaunsell Ltd. Available at: http://www.cibse.org/pdfs/7borne.pdf.
9. Porritt, S., Shao, L., Cropper, P.C. & Goodier, C.I. (2011) Assessment of interventions to reduce dwelling overheating during heat waves considering annual energy use and cost. CIBSE Technical Symposium, Leicester, 6th – 7th September 2011. Available at: https://dspace.lboro.ac.uk/
10. Sharpe, T. & Shearer, D. (2013) Learning from our experiments: monitored environmental performance of low energy buildings. Mackintosh Environmental Research Unit, Glasgow School of Art.
11. Arup/Bill Dunster Architects (2005) UK Housing and Climate Change – Heavyweight vs. lightweight construction, ARUP Research + Development, Bill Dunster Architects, UK
12. Sameni, S., Gaterell, M., Montazami, A., Ahmed, A. Overheating investigation in UK social housing flats built to the Passivhaus standard, Building and Environment (2015), doi: 10.1016/j.buildenv.2015.03.030.

IS 3D PRINTED HOUSE SUSTAINABLE?

Oberti I.; Plantamura F.

Politecnico di Milano, Dept. Architecture, Built Environment and Construction Engineering (ABC), Via Bonardi 9, 20133, Milan. ilaria.oberti@polimi.it, francesca.plantamura@polimi.it

ABSTRACT

"3D printing technology has the potential to revolutionize the way we make almost everything", so President Barack Obama recently said (Remarks by the President in the State of the Union Address, The White House, Office of the Press Secretary, 2013): the impression is that three dimensional (3D) printing is taking the world by storm in different areas.

If for objects of small dimensions, the technology is well-established, great developments are expected in the construction industry. As a matter of fact, since the beginning of 2000, with the first attempts for a large-scale 3D printing construction system, the innovators are working around automated additive manufacturing in order to print whole buildings as well as large-scale subcomponents. To date, different processes trial has started, from the printing of elements to the layer by layer construction of entire structures in a non-stop work session, starting from the foundation level and ending on the top of the roof. Even the materials trial has started: bio based plastic, mix of grinded-down rocks or sand held together with a liquid binding agent, fiber-reinforced concrete, etc.

The objective stated by different manufacturers and researchers involved is the sustainability of the built environment, in terms of economic, environmental and social benefits. But, is this innovation really sustainable? What about the environmental sustainability of these new construction processes?

The purpose of this study is to try to give an answer to this matter, through three research phases: 1. gathering and analysis of the current information on the 3D printing technology applied to construction; 2. identification and analysis of the main systems and case studies, including those with a longer experience in terms of research and experimentation (e.g., Contour Crafting and D-Shape) and the younger ones that are rapidly gaining visibility (e.g., Canal House and the Chinese system WinSun); 3. their evaluation in terms of environmental benefits and critical environmental issues.

The results obtained from each work phases, in particular the case studies analysis, leads us to think that the potential of 3D printing technology is substantial for the construction industry. If it continues to be developed, certainly it may revolutionize the construction process. However, implementing the technology will not be without its challenges.

Keywords: 3D printing, additive manufacturing, construction, sustainability.

INTRODUCTION

Additive Manufacturing (AM), commonly known as 3D printing, is defined as «a process of joining materials to make objects from 3D model data, usually layer upon layer, as opposed to subtractive manufacturing methodologies.» [1]. It derives from the field of rapid prototyping, developed during the late 1980s and 90s. The 3D printing process begins by digitally modelling a blueprint of the object that is to be printed in a design program; this one then "slices" the object into layers and sequentially sends this information to the 3D printer that constructs the object by making repeated passes, each time depositing a thin layer of material onto material previously deposited. The 3D printing fabrication has been largely adopted,

with applications in several sectors (e.g., automotive, aerospace, medical), up to current commercial availability of desktop-sized devices at affordable prices. If for small objects the technology is well-established, great developments are expected in the construction industry too, not only for the creation of scale models of buildings.

The use of additive manufacturing in construction (AMC) was suggested by Pegna in the late 1990s [2]. He investigated a new system of layered fabrication of small masonry structures, involved depositing a layer of reactive material (Portland cement) over a layer of matrix material (silica), activated by water vapor. The first attempts to apply this new technology date back to early 2000, with the experiments for a large-scale combined extrusion and trowel 'automated construction' system called Contour Crafting [3]. Since then, the innovators have been working around automated additive manufacturing and different processes trials started: from the printing of small components to be assembled to form architectural elements (e.g., Emerging Objects [4]), to the molding of hollow honeycomb elements subsequently filled and then assembled of the Amsterdam Canal House [5] and to the possibility of a layer by layer construction of entire structures in a non-stop work session, as with the D-Shape system [6]. Even the materials trial has started: bio based plastic, mix of grinded-down rocks or sand held together with a liquid binding agent, fiber-reinforced concrete, etc.

The objective, stated by different manufacturers and researchers involved, is the sustainability of the built environment, in terms of economic, environmental and social benefits, such as the aims stated in "Houses of the future" of Khoshnevisk [7]. But, is this innovation really sustainable? How will these houses be about environmental sustainability?

The aim of this paper is the attempt to give an answer to this question, through the identification of the main, experimental case studies and the analysis in terms of environmental benefits and potential problems.

METHOD

The research was developed in three phases:

1. Gathering of information on 3D printing in construction

3D printing technology applied to construction was analysed, gathering information from sources at different levels: scientific articles, information from manufacturers, informative articles. The keywords used for searching are both words that indicate the type of process (e.g., additive manufacturing or 3D print + automated construction; construction scale + additive fabrication / manufacturing) and trade names of systems (e.g., D-Shape).

2. Identification and technical analysis of main systems

A selection was made among the identified systems, narrowing the field of investigation on the following criteria:

- systems that are all actively undergoing development, rather than systems which, although their high scientific value, have been relegated essentially to the research area (i.e. Pegna);
- systems involve the use of large machines that can print from big elements up to entire buildings, instead of machines for printing small elements such as tiles or bricks;
- systems with technical information on the process and materials, needed for the purpose of an assessment of environmental quality.

The selected systems were analysed and for each some summarized sheets were elaborated. Only the information obtained from the manufacturers and scientific articles were included in these technical sheets; the information obtained from informative articles were overlooked.

3. Assessment of environmental sustainability

An environmental sustainability evaluation was carried out for the selected systems, with remarks on the possible positive or critical issues related to the spread of AMC. Currently, data are not available for a quantitative assessment of the environmental impact of AMC, nor with regard to different aspects (emissions, energy, etc), nor for the different life cycle stages of the manufactured products.

The assessment focused on some key aspects that the producers themselves highlight as higher environmental performance compared to the traditional construction process. In particular, some aspects, related to the cycle of the materials used for printing, were assessed: from the resources to the possibility of disassembly/recycling at end of building life, without neglecting indoor environment quality aspects.

RESULTS

1. Information and sources

The state of art analysis shows a literature that consists mainly in informative articles, freely accessible from online journals. From these sources, it is possible to find information about all the different systems, even the most recent ones, such as the current experimentations in Amsterdam with the Kamer Maker system for 3D Canal House [8] or those of the Chinese firm WIN SUN [9]. The amount of information discloses the relevance of the theme and the growing interest of designers and building contractors.

A large part of the available information is disclosed on the websites of the analyzed systems. However, due to the highly experimental nature of these systems, manufacturers spread mainly general information, without going into technical details of the process and materials, even when directly questioned.

The peer reviewed scientific articles are still few, and they are mainly related to the older systems and to those most connected to research institutions, such as Contour Crafting, developed at the University of Southern California [10], Loughborough University's Freeform Construction project (UK) [11], D-Shape by Enrico Dini [12].

2. Technical analysis of selected systems

Analyzing the results of the first phase, four systems are highlighted, on which the research work is focused: Contour Crafting (CC), D-Shape (DS), Kamer Maker (KM) e Win Sun (WS).

Each of these systems involves the use of large machines that can print from large elements up to entire buildings. In addition, even if they are in experimentation from different times, all of them are leading to concrete field trials.

The selected systems have some differences in both process technology both materials used for printing. For each of these systems, a data sheet was elaborated with the main technical information on materials and processes and with the environmental performance highlighted by the producers (see example in Table 1).

SYSTEM: D-SHAPE	
Process	**Environmental note**
The system operates by straining a binder on a sand layer. An aluminium structure holds the printer head. D-Shape can print any feature that can be enveloped into a cube 6x6 meters side. The process takes place in a non-stop work session, starting from the foundation level and ending on the top of the roof. The printing rises up in sections of 5-10 mm. During the printing of each section, a 'structural ink' is deposited by the printer's nozzles on the sand. Upon contact the solidification process starts and a new layer is added. The solidification process takes 24 hours to complete. Surplus sand that has not been embedded within the structure acts as a buttressing support while the solidification process takes place. This surplus sand can be reused on future buildings. (Source: http://www.d-shape.com)	*Transport*: The aluminum structure is very light and it can be easily transported, assembled and dismantled in a few hours by two workers. *Local material*: The possibility to use local sand, as zero-mile base material, makes D-shape like a technology attentive to the sustainability of the construction. *Air emissions*: The used binder is an inorganic bi-component, eco-friendly; chemically, the final artificial marble is 100% environmentally friendly. *Safety*: no human intervention means substantially reduced risk of accidents. (Source: http://www.dinitech.it)
Materials	
The D-shape binding chemistry exploits two inorganic reactants: the first one is a metallic oxide in powder form that is dispersed among the granular material and the powder component comprises at least one among Magnesium Oxide, Silicon Oxide, Iron Oxide, Calcium Oxide and Aluminium Oxide. The granular material is preferably selected from the group comprised of dolomite, calcareous or siliceous sands to which Magnesium Oxide is added, in a ratio set between 15% and 30% by weight. The second reactant is Magnesium Chloride ($MgCl_2$) and its various hydrates $MgCl_2(H_2O)_x$. These salts are typical ionic halides, being highly soluble in water. The hydrated Magnesium Chloride can be extracted from brine or sea water. (Cesaretti et al, 2014).	

Table 1: D-Shape technical sheet

Comparing the printing processes of the four selected systems, two typologies were identified:

- The first (KM, CC, WS) involves the direct spillage of the print material from one or more nozzles. The print material is quick-setting. The extruded elements, if with closed section, can be filled by pouring or injection of filler material such as concrete (CC, KM).
- The second (DS) involves two print steps. During the first step, a uniform horizontal layer of granular material (sand) is deposited by the machine. During the second step, a binding liquid is sprayed on those parts of the layer which has to be bound; surplus sand that has not been embedded within the structure acts as a buttressing support while the solidification process takes place. At the end of the process, this surplus has to be removed and can be reused on future buildings.

About the printing materials, there is a strong impulse to the experimentation of different possibilities (thermoplastic materials, ceramics, cement), even within the same system:

- currently, the most used materials are agglomerates of inert materials (e.g., sand) and binding agent, with some differences between the different systems. For example, the CC system is testing concrete mix with glass or carbon fiber as reinforcement, without affecting the surface quality of printed items (since this is controlled by trowels combined to nuzzle). The DS system uses inert granular material (sand) and inorganic binders: it operates by straining a binder on a layer of granular material; the granular material is preliminarily mixed with pulverized metal oxide which reacts later with the hydrated magnesium chloride of the binding liquid. The WS systems used an agglomerate created from recycled construction waste (i.e. sand, concrete, glass fiber), industrial waste and tailings. All of these systems envisage the possibility of treating the agglomerate with additives to accelerate the hardening and thus decrease the construction time.
- The KM prints with thermoplastics. Currently, it used Macromelt, a bioplastic made of 80% of vegetable oil. Hollow elements are printed; once solidified, they can be filled with concrete.

With regard to the place of printing, at the time the WS system allows printing building components in the factory, then assembled on the construction site, instead the other systems already allow the option of printing on site.

3. Performance and critical environmental issues

The selected systems analysis highlighted the environmental aspects for which AMC would be more performing than the conventional building processes. This increased environmental sustainability is indicated by the system manufacturers.

Among the most emphasized aspects, there are those related to the printing materials, such as:

- optimization of the raw materials, with the possibility of using local materials, reused or recycled, or rapid renewable (e.g., the KM experiments with bioplastics);
- reduction/elimination of construction waste, a specific characteristic of AM technology;
- reduction of air pollutants emission, both during construction and use phase;
- easy re-use of materials and components at the end of the building life (e.g., KM defines its artifacts as «easy to be disconnected in case the house needs to be relocated» [5]).

However, some of these features are not verifiable, in particular those relating to the emissions of pollutants in the air and the materials and components re-use. Being in an area still highly experimental, the reported performances are not always supported by comprehensive technical information. This happens because the features are evolving, and the producers need to maintain confidentiality of research aspects. For example, the WS system claims to use materials mainly from recycled construction waste and treat the mixture with additives in order to speed the curing of the printing layer. However, no data are provided on the technical characteristics and on the percentage of the printing mix and the used additives. This makes it difficult to evaluate some of the environmental performances declared by the manufacturer, such as «good work environment, workers less exposed to hazardous materials and noise» or «no harm to human body, no environmental pollution» [13].

In addition to the positive aspects, the systems analysis has also highlighted some critical aspects related to the AMC. These include:

- addition of additives (not known, but presumably of chemical origin), to speed up the hardening of the mixtures, could significantly modify the indoor air quality. These additives are crucial in maintaining rapid construction time for the AMC systems,

characterized by the successive deposition of layers of material with low heights, and where a new layer can be deposited when the previous one has sufficiently solidified;
- risk of emission of ultrafine particles in the air during the printing, with possible impacts on the worker health, due to the nature of the materials and the conditions in which printing is done;
- criticality, at end of life, in the disposal of thermoplastic materials, due to the percentage of polymeric materials likely present in the mixtures.

CONCLUSION

The results obtained from each of the three work phases, in particular the case studies analysis, lead us to think that the potential of 3D printing technology is substantial for the construction industry. If it continues to be developed, certainly it may revolutionize the construction process.

However, to declare the 3D construction processes as sustainable, it is necessary to have more certified information than that spread today by the producers. Some positive aspects are easy to identify as special features of the 3D construction process, such as faster and accurate construction, reduced labour costs, decreased construction waste, reduced safety risks for workers. Much further research has to be done on still unclear points such as the complete composition of the printing materials, which may have negative effects on indoor air quality in the construction and use phases and on management of demolition waste at end of life.

REFERENCES

1. ASTM: F2792 REV A - Standard Terminology for Additive Manufacturing Technologies. 2012.
2. Pegna, J. : Exploraty investigation of solid freeform construction. Automation in Construction, 5, pp 427-437, 1997.
3. Khoshnevis, B. : Automated construction by contour crafting related robotics and information technologies. Automation in Construction, 13(1), pp 5-19, 2004.
4. http://www.emergingobjects.com/
5. http://3dprintcanalhouse.com/
6. http://www.d-shape.com/index.htm
7. Khoshnevis, B. (2004). Houses of the Future. Construction by Contour Crafting Building Houses for Everyone. *Urban Initiative policy Brief.* USC-University of Southern California.
8. Sacchetti, V. (2013). Printable futures. *Domus*, 968/April 2013.
9. Balinski, B. (2014). Chinese company 3D prints 10 houses in a day from recycled material. Architecture & Design; 22 April, 2014.
10. Zhang, J., & Khoshnevis, B. (2013). Optimal machine operation planning for construction by Contour Crafting. Automation in Construction, 29(0), 50-67.
11. Buswell, R. A., Gibb, A. G., Soar, R., & Thorpe, A. (2007). Freeform construction: Mega-scale rapid manufacturing for construction. Automation in Construction, 16(2), 224-231.
12. Cesaretti, G., Dini, E., De Kestelier, X., Colla, V., & Pambaguian, L. (2014). Building components for an outpost on the lunar soil by means of a novel 3D printing technology. Acta Astronautica, 93(0), 430-450.
13. http://www.yhbm.com/

INTEGRATION OF SOLAR-CLIMATIC VISION AND STRUCTURAL DESIGN IN ARCHITECTURE OF TALL BUILDINGS

Aryan Shahabian[1]

1: PhD Candidate in the Institute of Architecture, University of Applied Arts Vienna, Oskar-Kokoschka-Platz 2, 1010 Vienna, Austria

ABSTRACT

This article introduces the methodology and the results of an integrated design approach to optimize both structural system and building energy performance through architectural design process. The book titled *Intelligent Design using Solar-Climatic Vision* [1], introduced a number of practical and effective design approaches towards the creation of energy-efficient building façades as well as comfortable urban environments. Applying solar-climatic vision, especially during the procedure of optimizing tall structural systems, can develop sustainable frameworks that maximize thermal comfort while minimizing waste of resources (e.g. embodied energy of building materials).

The integrated design approach consists of three main areas: architectural, solar-climatic, structural and the interconnections between each two of the three. The final solution, thus, will be the multipurpose one meeting all the needs from all three areas. Both top-down and bottom-up approaches are used in the process and the final solution is mapped in two poles of integration; first, in overall concepts and large scale and second, in parts and details. Therefore, architects and the leading team members of such design projects require inter-/multi-disciplinary knowledge, the ability of whole-system thinking and developing versatile tools.

In two case studies, *SOLARCHVISION* (building simulation tool) in combination with *Karamba* (structural interactive, parametric finite element program) are applied to optimize solutions for specific climates in the Middle East and the United States. With minor alterations in techniques, similar method with similar principles can be used in other climates as well. Diverse suggestible solutions include: Shading/reflecting devices that perform the role of the main structure framework too; the entire building structure deviates from the direction of gravity (verticality) to optimally shade itself as well as the surrounding. Analysing the results of the current research in practice shows impressive reduction of heating and cooling energy demand and primary energy by designing optimized passive structures of high-rise buildings.

Keywords: integrated design, solar-climatic, structural design, tall buildings, sustainability

INTRODUCTION

Why to focus on high-rise buildings?

High-rise buildings are typically wasteful in energy when they are built, maintained and eventually destroyed. They also carry exponentially heavier structural elements as a result of wind and earthquake loads as well as the weight of upper floors on the lower ones. However, high-rise buildings can potentially be more energy-sustainable than others; for instance, their higher density and smaller footprints cause reduction in commute, urban sprawl, traffic and air pollution [2, 3]. Having vast skin surface enables them to take advantage of environment and natural light too. Most importantly and less noticed, tall buildings are gifted by their height; a layer of main massive structural elements is close to the façade. There is an unexploited

potential for finding functionally consolidated elements responding to both structural loads and climate control factors.

Solar-climatic vision and ecological design

"There is much misperception about what is ecological design. We must not be misled and seduced by technology. There is a popular perception that if we assemble in one single building enough eco-gadgetry such as solar collectors, photo-voltaics, biological recycling systems, building automation systems and double-skin façades, we will instantaneously have an ecological architecture [4]." Robust design methodology combining network of parameters and approaches is close to passive design. Many old buildings used passive approaches that employs systems doing more than one thing (e.g. structural walls that also accumulate heat through thermal mass), since they were built in eras that oil was expensive or simply not available and transportation was hard. Modernism is essentially unsustainable as it evolved in the era of cheap fossil fuels. To achieve a new resilient architecture we need a big reconsideration about basic approaches, manufacturing, primary structural types [5, 6].

The book called *Intelligent Design using Solar-Climatic Vision* examines the critical role and influences of the sun on climate and built environment in varied scales and from different perspectives. 'To look from the sun' at objects and combination of solar beam radiation analysis with temperature patterns and other meteorological data (e.g. winds and clouds), enables the *SOLARCHVISION* building simulation tools to produce diagrams evaluating desirable/undesirable conditions in architecture as well as in urban scales. The research covers positive and negative effects of the sun in globally various climate zones including main cities from Australia to Europe and from Asia and Middle East to Canada and the US [1].

METHOD

The integrated architecture system evolves from three design areas: architectural, solar-climatic, and structural. Each two of the three sub-systems should collaborate to generate the final integrated solution. The system defines two poles of integration; one in large scale, overall conceptual stage of design and the other in small scale, in detailed design stage (Figure 1).

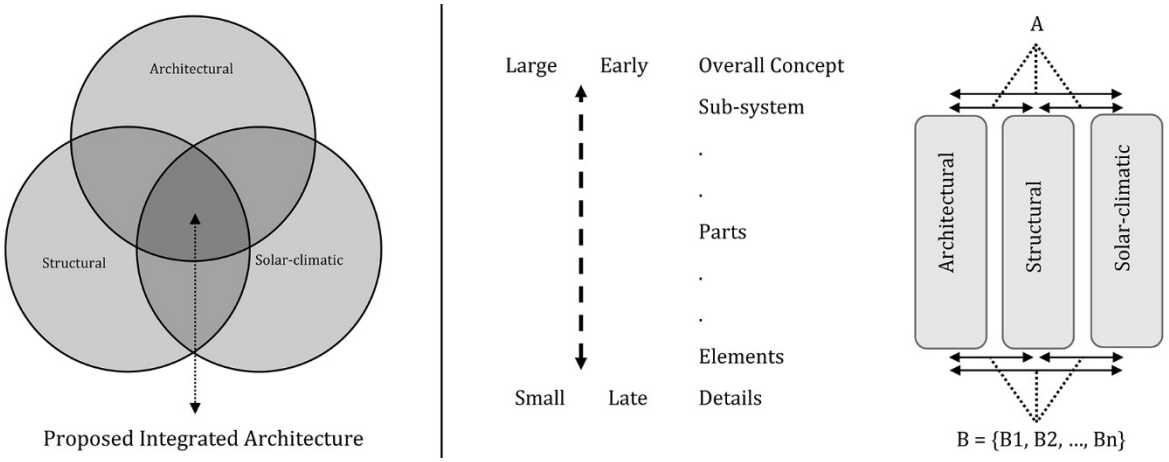

Figure 1: Integration takes place between two poles. Pole A represents conceptual early design stage and pole B consists of multiple combined solutions for various elements and details.

The criteria to evaluate the design products are: levels of visual integration (i.e. how things look unified), spatial integration (i.e. how things fit together), and functional integration (i.e. how things share roles) as well as sustainable interaction with the environment [7]. The method in action is a cycle which includes prototyping, evaluation of prototypes and reflections to produce design principles and techniques.

Case study 1. Cylindrical high-rise structure in Las Vegas

The reinforced concrete structure includes 40 floors slabs, a cylindrical central core, radial beams connecting the core to the outer ring beams and an exterior tube (Figure 2). The latter has the potential to adjust the sunlight. Therefore all the other parts have been optimized so that the only main question would be the design of the exterior tube.

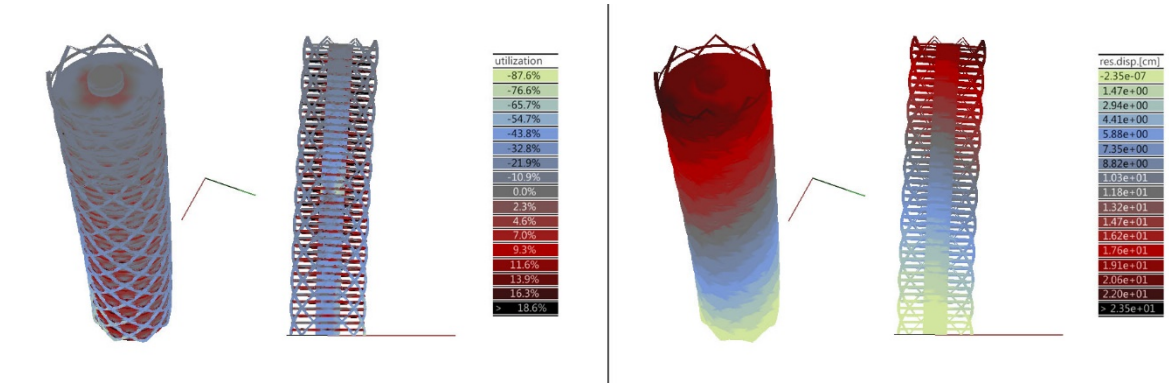

Figure 2: Karamba model view of the optimized structure (Alt.3) with gravity and wind loads.

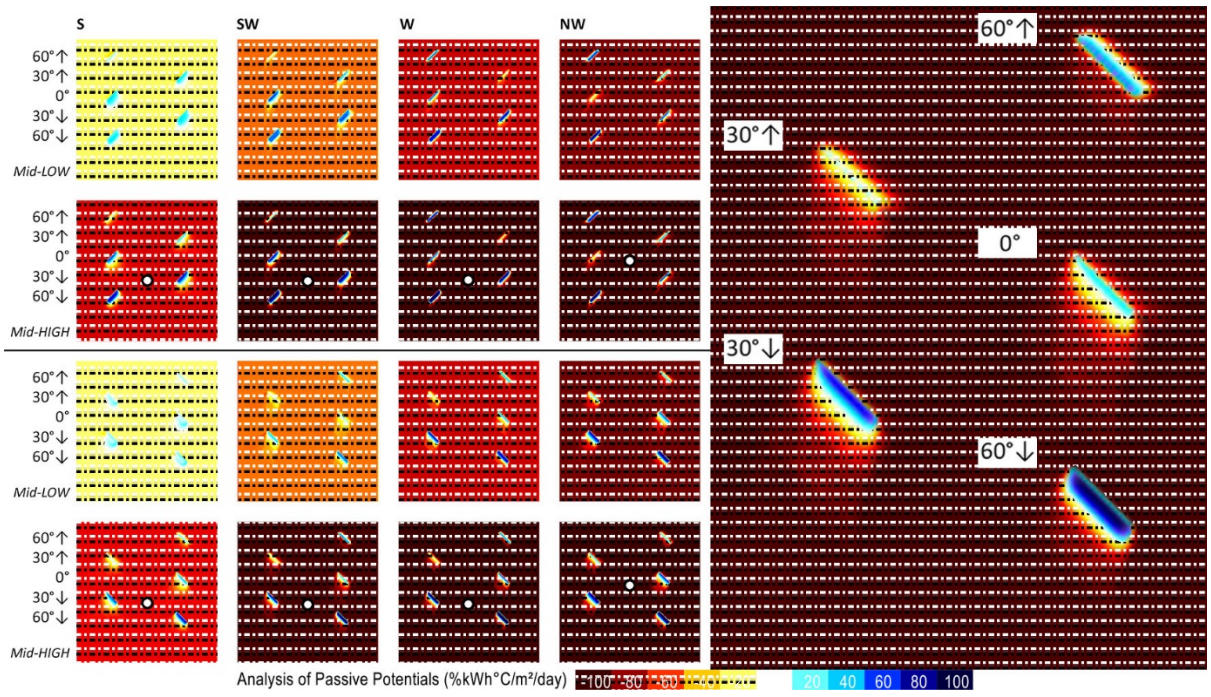

Figure 3: Diagrid orientations (up: ↗, dn:↖). S to NW. Right: SW Close-up view (30 °↓ picked)

Six different options are designed (Table 1) and in order to make them comparable, a maximum displacement value of 24 cm is set as fixed for all of the six structural systems. Gravity as well as the wind and possible storm loads in Las Vegas are applied in all models. The first one with radial framed tube positioned behind the glass façade. The second one is also 3 meters deep framed tube but with vertical elements exposed to the daylight. The rest alternatives are diagrid[1] structures with different cross-section properties; the third and the fourth have horizontal cross-sections with 1.5 and 3 meters depth.

An evaluation on various cross-section orientations of the diagrid elements is done to maximize annual solar-climatic performance (Figure 3). For this purpose, 5 different section angles from

[1] Diagrid elements vertical angles are set to about 47° to optimize the structural performance [8].

upwards to downwards in 8 main planar directions (N, NE, E, SE, S, SW, W, NW) are tested on two main direction of diagrid elements (↗ and ↖).

	Alternative 1	Alternative 2	Alternative 3	Alternative 4	Alternative 5	Alternative 6
view from southeast	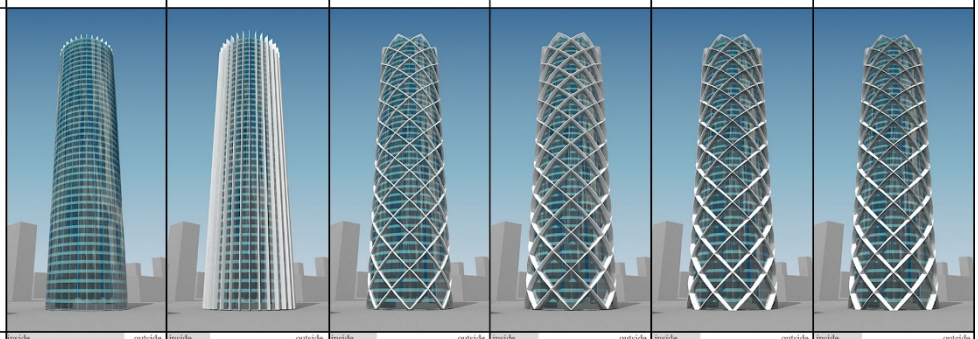					
tube elements cross-sections	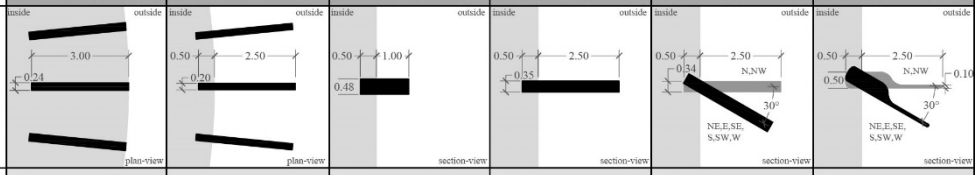					
solar-climatic performance analysis visual outputs for Mid-High temperature weather scenario Analysis of Passive Potentials (%kWh°C/m²/day) 20 40 60 80 100 east	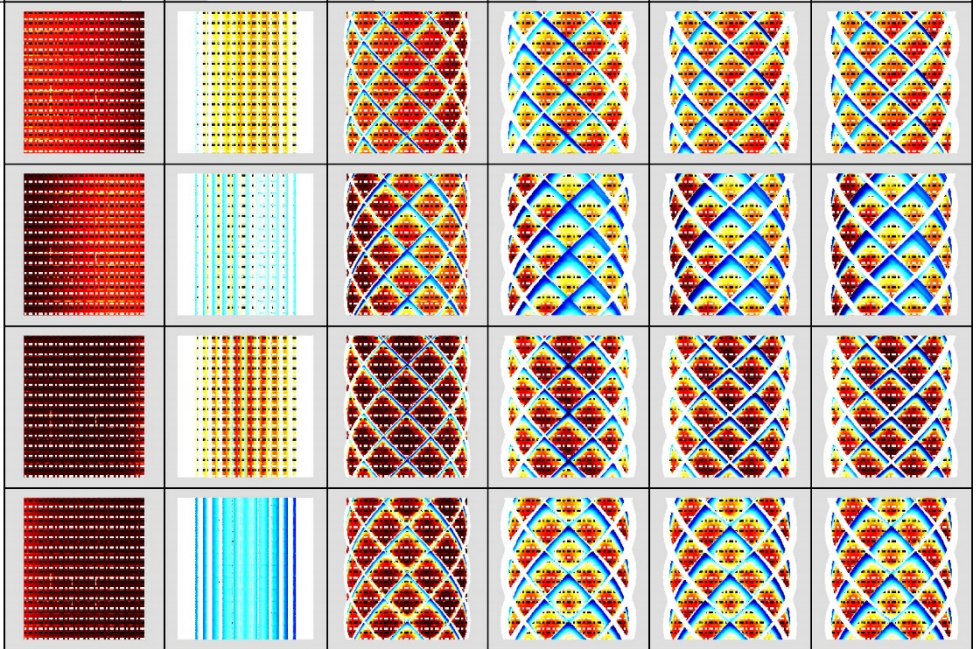					
south						
west						
north						
structure mass (kg)	4.0009 e+7	3.8519 e+7	3.7382 e+7	4.0322 e+7	3.9623 e+7	3.85630 e+7
energy efficiency index	-138.4	-79.1	-99.2	-71.6	-67.7	-67
relative structural efficiency	10.6%	61.3%	100%	0%	23.8%	59.8%
relative energy efficiency	0%	83%	54.9%	93.5%	99%	100%

Table 1: Solar-climatic and structural analysis of the six developed alternatives.

Results of case study 1

The 80 cross-section cases test results (Figure 3) show that in Las Vegas climate, the appropriate orientation for diagrid structural elements is about 30° downwards in all directions except the north and the northwest; whereas a horizontal device can perform better. These choices are selected due to the fact that the structural grid pattern is not dense and it is preferred that each element can affect a relatively vast area of the building skin. Thus for more dense patterns of louvers -to be added in next design stages- a slight change in orientation can be applied. The cross-section orientations of the fifth and the sixth alternatives are optimized due to solar-

climatic test results. As for the latter, cross-sections are also optimized from rectangular to a new shape in structural analysis.

Comparing structural properties of the alternative options illustrates that diagrid tube is the lightest structure (Alt. 3) (see Table 1). Combining diagrid system with optimized solar-climatic cross-section orientations (Alt. 5), results in a relatively light structure with maximum energy efficiency (Alt. 6). At this stage of design, none of the structural systems can provide complete thermal comfort conditions, so parts of the façade should be enhanced by secondary shading elements in smaller scales. For the environmentally-optimized alternatives (e.g. in the last proposed model), a smaller area of the façade requires extra shading devices in the next design stages. Therefore, such optimized structural systems ultimately result in lighter and less expensive buildings while providing comfort conditions.

Case study 2. Sustainable high-rise building skin in Tehran

The aim of the case study (Figure 4) is to design a sustainable cladding for a high-rise building in Tehran (Latitude 36N). The structure of the building is already designed and half built, so there is no chance to change its overall structural design. A layer of louvers can be attached to the main structure. The building façades mostly face west and east which by default overheat the structure in Tehran climate. The orientation of shadings should be optimized to provide desirable thermal comfort without adding too much weight to the main structure. Optimum orientation angles and proportions of shading devices in Tehran climate are indexed in the book ‘Intelligent Design using Solar-Climatic Vision’: in the western and eastern parts of the façade, the louvers cross-section should be slightly downwards and in the southern parts should be upwards while in the northern part there is no need to have horizontal louvers on the façade. The final solution is based on a network of louvers around the structure that their cross-section orientations gradually change on the round corners of the building.

Results of case study 2

Comparing the energy-efficiency calculation results of the proposed building skin with ordinary glass curtain-walls, shows a significant reduction in the demand for heating and cooling energy and primary energy use by applying solar-climatic principles in the design process. The calculations cover both direct and diffuse solar radiations in different hours and months.

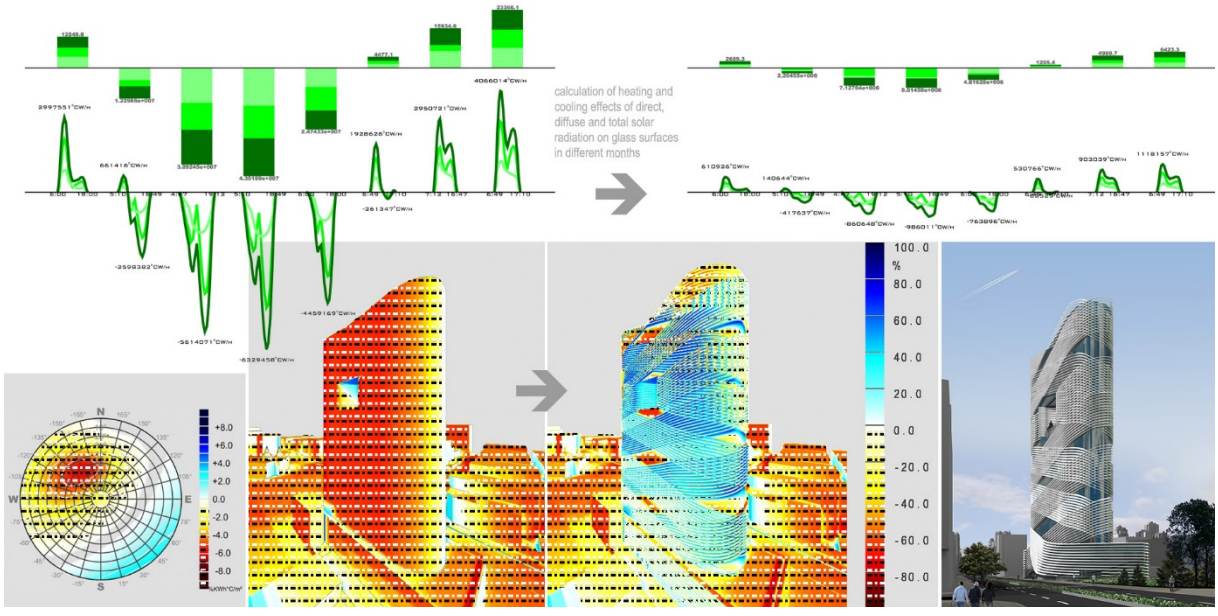

Figure 4: Reduction of heating and cooling energy demands by controlling solar radiation.

DISCUSSION & CONCLUSION

The design method and approach used in the case studies can be applied in an infinite spectrum of scales. For example, one can optimize orientations and proportions of building's overall structural system, through the method described in this article. Regarding location climate conditions, vertical 90 degree extrusion can be optimized to new direction, and it can introduce new typology of self-overshadowing tall structures. The interaction between structures and urban pattern situations can also be optimized by implementing similar strategy and new computational tools.

A further step in the research, should aim to define a measurement index in common between structural-efficiency and energy-efficiency. This will help in precise decision makings (e.g. where there are two good options, each having an advantage over the other).

Based on sustainable interaction with the environment, this essay attempts to introduce a systematic method of integrated design. While aiming to upgrade comfort, conserving energy and minimizing waste of materials, the methodological approach can result in a new visual, aesthetical and semantical alternative in architecture discourse. Solar-climatic vision and structural design are capable of being integrated into sustainable high-rise buildings architecture. This integration needs whole-system-thinking, close teamwork of professionals of the correlated fields and multidisciplinary approaches. The result of this integration would not only be more sustainable tall structures with minimum waste of building materials and embodied energy, but also passive desirable environments which bring health and comfort to the inhabitants of buildings and cities. In the holistic view, solar-climatic vision can be effective in preventing the growth of urban heat islands and global warming.

ACKNOWLEDGEMENT

The author acknowledges the assistance from *Mr. Mojtaba Samimi* of *R.M.M. Solarch Studio* for his help in learning more about applications of weather data details in planning.

REFERENCES

1. Samimi, M. and Nasrollahi, F. (2014). *Intelligent Design using Solar-Climatic Vision; Energy and Comfort Improvement in Architecture and Urban Planning using SOLARCHVISION*. Technische Universität Berlin
2. Yeang, K. (1999). *The Green Skyscraper: The Basis for Designing Sustainable Intensive Buildings*. Munich: Prestel Verlag
3. Ali, M. M. and Armstrong, P. J. (2007). "Strategies for integrated design of sustainable tall buildings". University of Illinois
4. Yeang, K. (2008). "Ecoskyscrapers and Ecomimesis: New Tall Building Typologies". CTBUH 8th World Congress, Dubai
5. Mehaffy, M. and Salingaros, N. A. (2013) "Toward Resilient Architectures 2: Why Green Often Isn't" in Metropolis Mag 4/4/2013
6. Buchanan, P. (2012). "THE BIG RETHINK Part 2: Farewell to modernism − and modernity too". In The Architectural Review 30/1/2012
7. Bachman, L. R. (2003). *Integrated Buildings: The Systems Basis of Architecture*. John Wiley & Sons
8. Moon, K. S. (2012). "Sustainable Structural Design of Contemporary Tall Buildings", CTBUH Shanghai World Conference

DEVELOMENT AND EVALUATION OF ENVIRONMENTALLY FRIENDLY FAÇADE ELEMENTS FOR DEEP RETROFITTING OF BUILDINGS

Jan Tywoniak[1,2], Antonín Lupíšek[1,2], Michal Bureš[1,2], Martin Volf[1,2], Julie Hodková[1,2], Petr Hejtmánek[1,2], Jiří Nováček[1,2]

1: University Centre for Energy Efficient Buildings, Czech Technical University in Prague, Třinecká 1024, 273 43 Buštěhrad, Czech Republic

2: Faculty of Civil Engineering, Czech Technical University in Prague, 166 29 Prague, Czech Republic

ABSTRACT

The paper describes development and evaluation of a building envelope panel system based on advanced natural materials (thermally modified wood, laminated veneer lumber, wood fibre and cork thermal insulation). Properties of the product were proven by modelling, calculations and experiments inline with current standards on curtain walls systems and in addition life cycle assessment (LCA) has been performed. Heat and moisture simulations proved that the design does not suffer from thermal bridges and has U-values at levels suitable for passive housing; air tightness testing proved high quality of design. LCA calculations compared the system to an aluminium-based alternative and show significant potential for savings in embodied energy and carbon footprint by using the developed system.

Keywords: curtain wall, modular façade systems, panels, natural materials, deep retrofitting

INTRODUCTION

Efficiency of energy production and consumption became a key subject of European legislation and regulation of the recent years [1]. Proposed targets of 20% reduction in primary energy consumption in EU until 2020 focus on the sectors with the highest saving potential for the lowest investment – transportation and construction industry. In the construction industry of Central Europe the focus is shifting from new buildings to retrofitting. According to the study *Europe's buildings under the microscope* [2], 25 % of the European building stock is represented by non-residential buildings and 48 % of existing buildings was built between 1961 and 1990. Research and development presented in this paper is focused on non-residential buildings featuring light panel curtain walls built in the former Czechoslovakia between 1961 and 1990. Authors estimate that each tenth non-residential building built in the time period has the target type of envelope, so the results are generally applicable to approximately 1,2 % of building stock in the Czech Republic.

METHOD

Review of typical Central European buildings with light curtain wall envelope

The buildings of interest were those with a load bearing superstructure (typically made of reinforced concrete or steel) with light curtain walls. These structures were usually used for typologies like schools, kindergartens, office buildings, medical centres, firemen and police stations, railway facilities, hotels, and restaurants (see Figure 1).

Figure 1: Typical representatives of the target typology – buildings with envelope made of light panels. Left: Main train station in Munich, Germany. Right: Elementary school in Pilsen, Czech Republic. Façade segment with smaller windows already replaced.

These buildings are now after 30 to 55 years due for renovation. The typical issues related to light building envelopes are: faded colors, obsolete look and loss of attractiveness for potential tenants; insufficient level of thermal insulation; malfunction of window hinges and locks rendering some windows out of order, failures of fixing and seal elements, water leakages, consequent insufficient air tightness and related winter discomfort and high operation cost. These buildings also lack shading devices resulting in summer overheating and some of the elements may contain asbestos boards (health risks).

In addition to the issues assigned to the envelopes, these buildings also suffer in building services and related low level of user comfort: obsolete heating systems with poor control; outdated electric installations and water piping; malfunctioning or often non-existent HVAC systems; ad-hoc-made data infrastructures.

Many of these buildings have been successfully renovated in the past 15 years, but a significant portion of the building stock still waits for renovation. Basically there are two most typical retrofitting scenarios, in both cases the obsolete envelope is completely removed. In the first (low-cost) scenario, mullion walls made of light autoclaved aerated concrete bricks with external thermal insulation system (ETICS) and plastic windows are used. In the second scenario the envelope is replaced by some modern curtain wall system, typically made of steel or aluminum. The research challenge was to make it from more environmentally friendly materials with lower embodied energy, whilst matching or surpassing the other typical technical features.

Design methodology

The research objective was to find a technical solution, which would serve the same purpose as traditional metallic building light envelope systems, whilst having lower environmental impact and comparable or better thermal properties, over 50% of the mass consisting of renewable materials, maximally utilizing local materials (produced in the country), dismantling and recyclability of the envelope system being as simple as possible.

The development has been made by a multidisciplinary team comprising structural engineer, building engineer, building physicist, experts on fire resistance, acoustics, air tightness, manufacturing of prefabricated timber elements and structures, and life cycle assessment. The design strategies were inline with the methodology developed in IEA EBC Annex 57, Subtask 4 [3, 4]. The optimized product was developed by utilization of the design strategies: components' service life optimization, substitution for bio-based materials, use of innovative materials with lower environmental impacts, design for deconstruction and use of recyclable materials. The design process has been iterative, step-by-step developing samples and continuously testing their properties.

RESULTS

Description of developed light envelope system based on natural materials

The research resulted in utilization of several advanced bio-based materials. Thermally modified wood with improved durability against decay well suited to applications involving demanding weather conditions (λ_d = 0,12 W/m^2·K), has been used for exterior elements. Cork thermal insulation (λ_d = 0,064 W/m^2·K), has been utilized for detailing in the window structure. The main structural elements of the façade panels were made of laminated veneer lumber (λ_d = 0,18 W/m^2·K), engineered wood product that uses multiple layers of thin wood assembled with adhesives. Wood fibers (λ_d = 0,038 W/m^2·K) were used as thermal insulation.

The resulting product is panel-based envelope system dubbed Envilop consisting of panels, which can have width between 1.2 and 1.8 meters; height can vary from 2.5 to 4.2 meters. There were designed two basic panels – transparent (Figure 2) and opaque. Standard thickness of the opaque parts of panels is 240 mm with mean thermal transmittance values ranging from 0.24 to 0.16 W/(m^2.K), depending on the type of the thermal insulation material used (basic panel comes with wood fibres). The panels' anchoring to the superstructure is designed in a way that all the modules are independent of each other and the design allows the panels to be installed quickly and it is also possible to deal with the entire load the envelope has to bear. For external surface can be used any type of light double-skin ventilated facade cladding or even standard ETICS. Default options come with glass, wood, and fibre-cement boards. Transparent panels are fitted with wooden windows Slavona Progression certified as class A by Passivhaus Institut; thermal transmittance of used triple glazing ranges from 0.70 to 0.54 W/(m^2.K). Technical solution of the casement allows the window to be fitted without the frame visible from the exterior. For limitation of summer sola heat gains, the panels are equipped with motor-controlled venetian blinds in an imbedded lintel box, separated from the structure by a vacuum insulation panel to limit thermal bridges. There were developed also design alternatives utilizing active renewable energy components (photovoltaic panels, solar heat collectors, or hybrid PV-T panels) and units for de-centralized mechanical ventilation with heat recovery. Default options for the interior side finishing are gypsum boards or standard additional wall with a cavity for electrical wiring, data cabling or heating system elements.

Figure 2: Typical composition of transparent panels.

Analyses and laboratory testing of real performance

Comparative life cycle assessment

The main motivation for the development of the new generation of light building envelope system was to achieve improved environmental performance in comparison with traditional metal-based light envelope systems. The optimization and evaluation of environmental performance was based on a simplified LCA, which compared two panels – typical aluminium panel (produced by SKANSKA LOP company) and the new wooden panel. Both products have the same U-values, thus the operational energy consumption and environmental performance of building operation are considered as equal and the main difference lays in embodied energy and embodied environmental loads. Details of the LCA are described in [5].

During the development was important to find the main critical points in the environmental performance of the envelope system. Therefore the contribution of different materials to the overall impacts was studied. All key environmental indicators of the wood-based variant were lower than in case of the aluminium-based variant (non-renewable primary energy input 41%; global warming potential 3%; ozone depletion potential 98%; acidification potential 30%; eutrophication potential 84%; and photochemical ozone creation potential 34%). The objective of creating a structure, which is friendlier to the environment than the conventional aluminium-based solution has been reached.

Hygro-thermal analyses

Set of 2-D dynamic simulations of both opaque and transparent panels and their crucial details have been performed. Special attention was given to the details with the highest potential for creation of systematic thermal bridges – horizontal and vertical joints of panels, box for rolled up blinds and installation of glazing units into window frames.

Durability testing

Envilop panels are subject to long-term testing. Four prototypes of full-scale modules were manufactured and installed in a façade opening of 3 x 3 m in size (Figure 3, left). The installed modules are of two different compositions using: wood-fibre and vacuum insulation; and wood-fibre and aerogel insulation. Two modules placed above each other have the same composition, both bottom opaque panels have the same wooden cladding and the upper panels with glazing are equipped with photovoltaic panels and electric-run shading system. The installed samples face the natural outdoor environment on their exterior side and a simulated interior environment of conventional buildings on their interior side. The behaviour of the samples is monitored using temperature sensors, relative humidity sensors and weight of moisture sensors embedded in panels and in modules' connections. The test started in November 2014 and is designed to run for at least 12 months to acquire the year-round data.

After thorough laboratory testing and further fine-tuning of details, the final elements will be installed on a testing steel frame in front of south façade of the University Centre for Energy Efficient Buildings in total area of 48 m^2 (see scheme on Figure 3, right). The main purpose of the installation is to show to potential producers and customers the system as a whole in various dimensions, levels of equipments (venetian blinds, horizontal shading devices,) and exterior finishes.

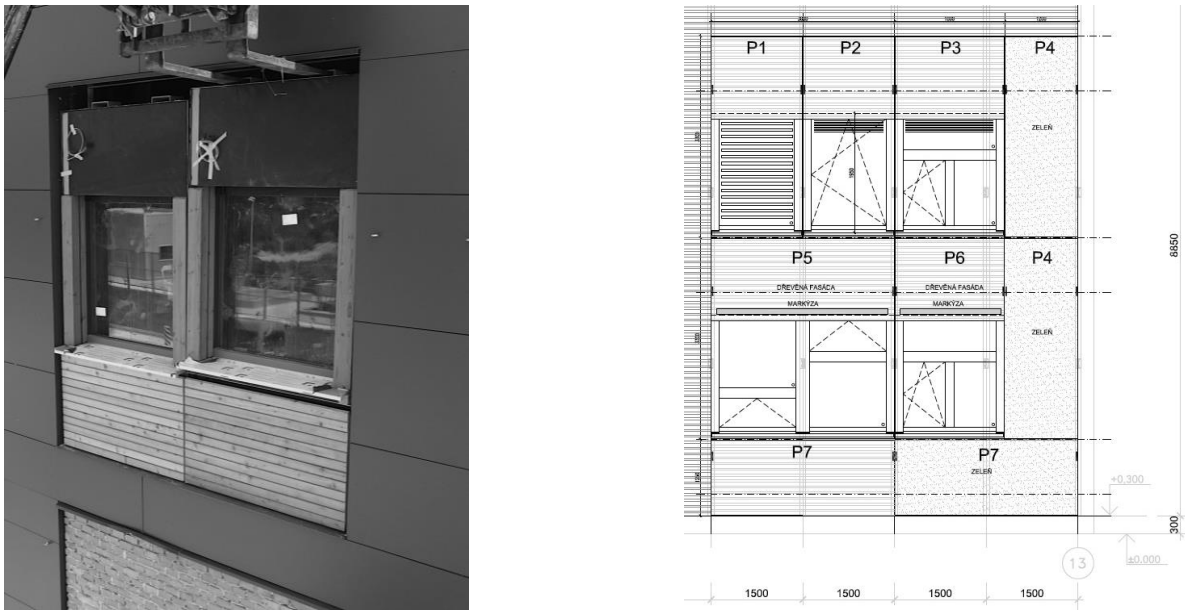

Figure 3: Long-term durability testing of the light bio-based envelope system. Left: Installation of four panels equipped with temperature sensors, relative humidity sensors and weight of moisture sensors embedded in panels and in modules' connections (measurement since November 2014). Right: Experimental setting of panels with various surface finishing (total area 48 m^2, installation June 2015).

Laboratory testing of acoustics and fire resistance

The Envilop panels have undergone accredited tests in a professional acoustic chamber according to standards ČSN EN ISO 10140-1, 2 and 4 and ČSN EN ISO 717-1. The measured weighted airborne sound insulation R_W (C; C_{tr}) of the opaque panels was 41 (-2; -6) dB and 38 (-2; -5) of the transparent panels (with triple-glazed wooden windows). Special fire resistant variant of the panel was designed by replacing interior and exterior wooden oriented strain boards by fire resistant boars; fire expansion tapes were installed into joints' sealing. The measured fire resistances were 60 and 90 minutes EI(I>O) 60 DP3 and EI(I<O) 90 DP3 according to ČSN EN 1364-3:2014 (Figure 4).

Figure 4: Testing of fire resistance EI(I<O) of EnvilopFIRE – laboratory setting, view into fire chamber after 90 minutes of experiment, and thermal monitoring of surface temperatures.

CONCLUSIONS AND FUTURE WORK

The project has proved that bio-based envelopes for buildings represent a viable alternative to the traditional metallic systems. The future development will continue with focus to reach higher flexibility in shape and sizing, to improve external design and to integrate additional features. The research results are further developed within H2020 project MORE-CONNECT (Development and advanced prefabrication of innovative, multifunctional building envelope elements for MOdular REtrofitting and smart CONNECTions) which aims at development of prefabricated modular solutions for a quick massive renovation of existing buildings to nearly zero energy standard.

ACKNOWLEDGEMENTS

The design strategies for reduction on EE and EC were formulated within IEA EBC Annex 57 Evaluation of Embodied Energy & Carbon Dioxide Emissions for Building Construction, Subtask 4. The presented research has been supported by the European Union, OP RDI project No. CZ.1.05/2.1.00/03.0091 – University Centre for Energy Efficient Buildings; OP RDI project No. CZ.1.05/3.1.00/13.0283 – Intelligent Buildings; and Technology Agency of the Czech Republic through project No. TE02000077 Smart Regions – Buildings and Settlements Information Modelling, Technology and Infrastructure for Sustainable Development and project No. TA03010501 Optimized Subtle Frame for Energy Efficient Buildings. Research results are further utilized in the on-going H2020 project No. 633477 MORE-CONNECT. All support is gratefully acknowledged.

REFERENCES

1. Decision No 406/2009/EC of the European Parliament and of the Council of 23 April 2009 on the effort of Member States to reduce their greenhouse gas emissions to meet the Community's greenhouse gas emission reduction commitments up to 2020
2. Buildings Performance Institute Europe (BPIE): Europe's buildings under the microscope: A country-by-country review of the energy performance of buildings. 2011, ISBN: 9789491143014.
3. IEA EBC Annex 57 Evaluation of Embodied Energy & Carbon Dioxide Emissions for Building Construction: IEA EBC Annex 57 – Objectives, available from http://www.annex57.org/?page_id=79 [online]; accessed 9.3.2015.
4. Lupíšek A. et al.: Design strategies for low embodied carbon and low embodied energy buildings: principles and examples. Submitted to 7th International Conference on Sustainability in Energy and Buildings, Lisbon, Portugal, 1-3 July 2015.
5. Lupíšek A. et al.: Development and testing of environmentally friendly envelope for energy efficient buildings in the Czech Republic. Submitted to 6th International Building Physics Conference, IBPC 2015, Torino, Italy, 14-17 June 2015.

BIO-REINFORCED LIGHTWEIGHT REVERSIBLE PANEL CONSTRUCTION FOR LOW-RISE BUILDING

Lynnette Widder[1]; Dr. Joy Ko[2]

1: Columbia University, Sustainability Management 2929 Broadway New York NY 10027
2: Rhode Island School of Design Division of Architecture and Design 2 College St. Providence RI 02903

ABSTRACT

Light-weighting that results from the substitution of fibre-reinforced flowed composites has long been part of aerospace and nautical engineering. (Heuss et al, 2012) Building construction can benefit from this approach as a way to reduce material intensity and embodied energy, and to gain performance efficiency and formal possibilities. The opportunity to apply current research in bio-based flowed matrices and fibre reinforcing is particularly high in building construction because of the relative predictability, stability and scale of the loads to which it is subjected. Another potential benefit we identify is increased reusability of construction materials.

A thin shell construction can advantageously unify the functions of moisture, air, shear and lateral loading resistance, which are assumed by no fewer than three different layers in conventional construction. By eliminating the need for lamination among layers, thin shell construction increases the opportunities to harvest and reuse materials. Whereas moisture and air resistance is inherent to the material, such other properties as stability are best achieved by geometric manipulations. For example, by moving material out of the axis of inertia, thin shell panels can be given appropriate stiffness where resistance is needed while preserving local flexibility to facilitate installation, repair or de-installation. Our work focused on the use of local geometric manipulation to create panel joinery and calibrate panel flex.

Our work identified a series of joint and panel typologies and applied an empirical methodology relying upon the generation of physical models. Using hand-making in concert with PLA/3-D printing technology, we undertook to optimize panel-to-panel connections and to develop panel types uniquely suited to the implementation of the joints we identified. Our outcomes hold promise for a next series of design iterations and testing at large scale.

Keywords: light-weighting, bio-based materials, joinery, planar geometry

INTRODUCTION

Our research concerns the potential application of fibre reinforced, engineered composite materials for built environment applications. Favoured for use in transportation design, including aerospace, automotive and ship building, ‘composites’ have proved invaluable to light-weighting, an approach in which traditional metal alloys are replaced with equally high performing carbon or graphite-reinforced epoxy composites. Reduced weight greatly reduces the amount of energy needed to propel these vessels at the high speeds desired. The trade-off, however, is that these materials are typically extremely high in embodied energy, especially from fibre production. (Kara and Manmek, 2009) This downside has in turn spurred increasing research in the use of natural vegetable fibres such as hennequin, flax, pineapple and hemp for reinforcing. (Westman et al, 2010; Van Vuure, 2008) The resulting vegetable-reinforced materials, often captured in bio-based epoxy flows, offer much greater environmental benefit but because their performance is less easily engineered, they are less appropriate to transportation applications. We foresee in this class of materials an invaluable

opportunity to introduce lightweighting into an architectural context. Our on-going work (Ko, Widder, 2013) has focused on the design of panels realized in bio-reinforced, bio-based epoxy flowed, that fulfil many of the complex demands placed on an exterior wall – waterproofing, structural stability, air-tightness – while also being inherently de-mountable and reusable. Panel to panel joinery can be integral to the panel shape, taking advantage of extruded or pulltruded composite production techniques and variable stranded reinforcing to give greater strength at the points required.

Our current research has developed a typology of joints categorized by the way in which they relate the two meeting panels: interlock, overlap, involution, friction and clip. Each type was mapped against eight salient properties, resulting in visual tools to immediately identify affinities and trade-offs among these types. The joints were then associated with a design for self-stabilizing panels. The most promising joint/panel types and characteristics were then systematically transferred into a 3-D modelling environment (Rhino and AutoCAD) and prototyped as a 3-D printed form. Through analogy to US standard wood frame, low-rise construction, a series of performance criteria were derived for panel to panel and panel to foundation junctures. The resulting artefacts explore a variety of geometric configurations for each juncture. Value was given to the reversibility of each connection. Material failure due to stress or fatigue at model scale was taken as an indication of where reinforcing mesh could be engineered once full-scale prototyping in bio-based composite material can commence.

METHOD

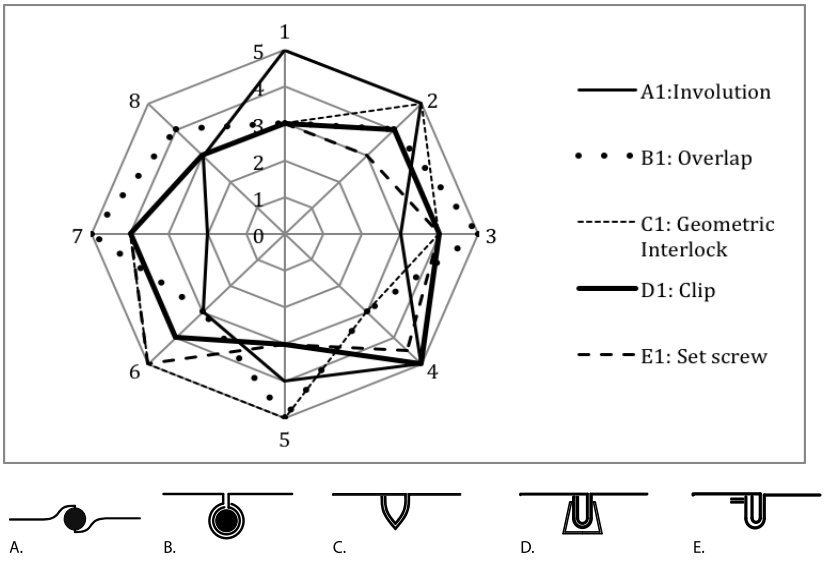

Fig. 1: Typologies A-D with a 'Spider' graph comparing the performance of the five different basic typologies; criteria 1) Flexibility 2) Strength of Shape 3) Depth of Shape 4) Tension 5) Friction 6) Pressure 7) Resistance to Horizontal Forces 8) Resistance to Vertical Forces (See Fig. 2 also)

Our project adapted the use of performance criteria to capture properties of materials and manufacturing processes, already a validated method (Ashby, 2010). We undertook an initial typological characterization of promising joinery methods: involution, overlap/interlock, snap-in configuration and two different friction connections, one using a set screw for punctual pressure and the other using a linear clip along the joint's full length. Each type was evaluated relative to significant criteria that affect in-situ structural performance as well as those that affect construction through ease of use and potential for reversibility. These

properties include flexibility, reliance upon geometry, tension, friction, pressure and resistance to horizontal or vertical forces. By normalizing values for each criterion on a unitless, common scale of 0-5, we generated visualizations that allow quick comparison in performance of joint typologies across a range of materials and fabricational methods.

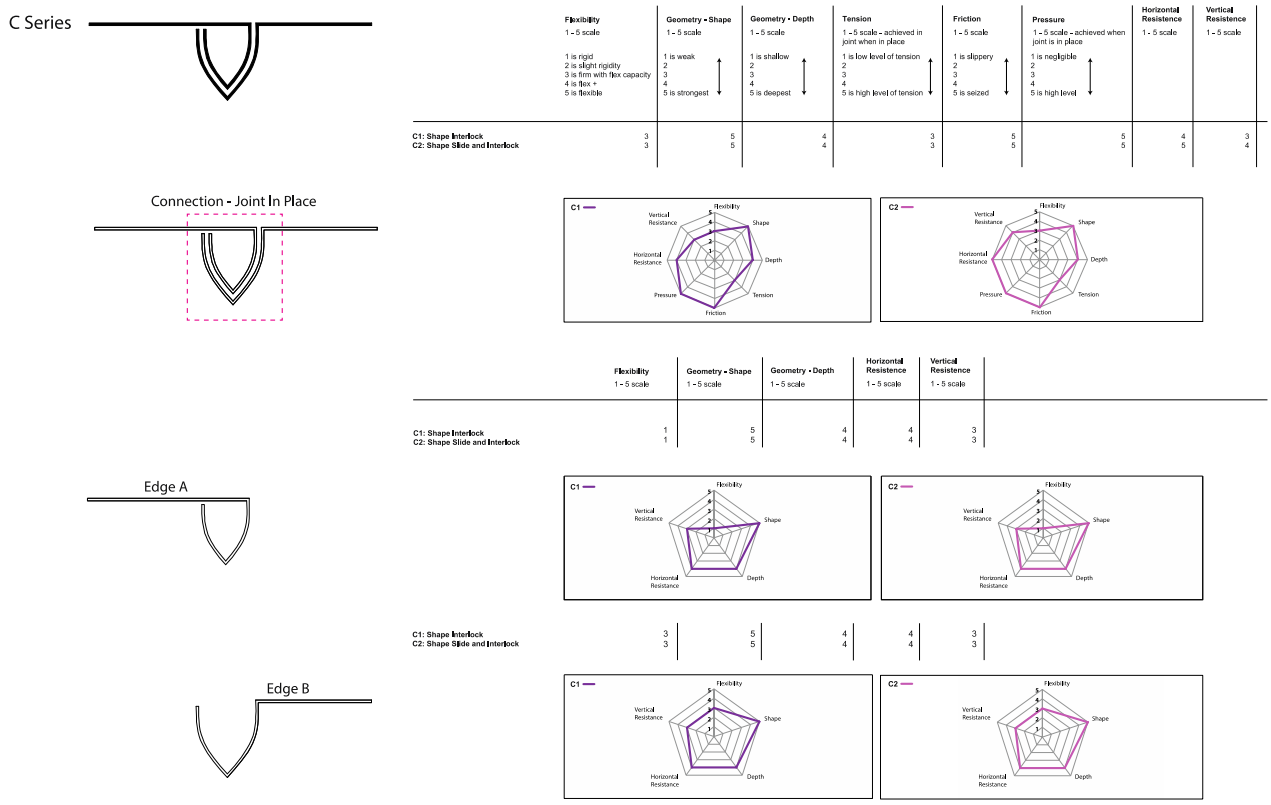

Fig. 2: Type C 'Geometric Interlock', a sample typological analysis. Each radius on the spider graphs represents a quality that is valuable for any joints' capacity to be set in place, and to withstand forces once completed. Those characteristics considered here as methods to create joinery are: the capacity for flex; geometric configuration; and a tensile, compressive or frictional connection between parts. The spider graph also indicates on a scale of 1 to 5 the resulting joint's capacity to resist horizontal/lateral or vertical/gravitational force.

In a multidisciplinary team drawing from diverse areas of architecture, sustainability management, design computation and rapid manufacture, this type of data capture and analysis has become a critical part of our collaborative workflow. Especially in the initial stages of design and prototyping, this analysis allows for a common awareness of relevant parameters affecting performance as well as potential trade-offs resulting from making adjustments. In the subsequent stage of prototype formulation and development, we employed an iterative design process, in which each idea progressed with the application of both hand-drawn and rapid prototyping techniques. Any failings and potentials then informed our subsequent design iterations.

PROTOTYPE FORMULATION AND DEVELOPMENT

To stay within the scope of our current fabrication capacity, we began by pursuing type B 'overlap' and C 'geometric interlock. Beginning with simple clip forms and evolving the joint form so that it could stand when set on a flat surface, we focused the design and fabrication on two basic joint classes. One was based on a triangular interlocking joint and the other on a

cylindrical overlap joint. The base geometries of circle and triangle exploit these figures' inherent geometric stability to lend the overall construction bearing capacity in analogy to wood framing. Various joint iterations were in turn tested for reversibility and adequate resistance to lateral stresses when in place. The joints were first printed as flat pieces to test their interlock mechanisms; later iterations depicted the full height of an 8ft wall panel at scale. For the purpose of testing the joints, the panels were simplified and modelled only as flat planes.

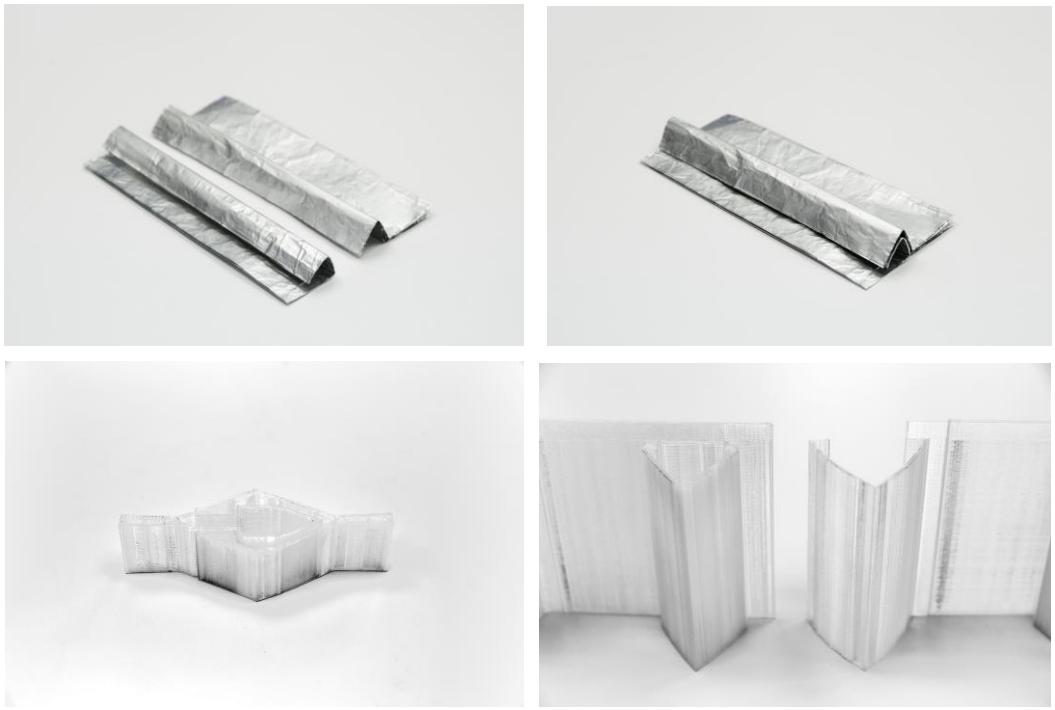

Fig. 3: Iterative models of triangle/ogee-shaped male-female joint in metal and PLA

After studying these two joints, we moved to the design of their associated panels. Here, we sought stability at the panel's centre and adequate flexibility at its ends to ensure the ability to implement and reverse the joint to the next panel. The PLA 3-D printed flat panels showed significant warping, which we took to be indicative at scale of the likely panel performance in any synthetic material. For this reason, panel stabilization became our focus as the project continued. Initially, we used struts positioned in an X configuration for stabilization. Although these struts offset warping and instability, they interfered with the snap-in joint and the required flexibility at the panel's end. We recognized that the struts functioned in two ways: by moving material to the points of instability at the panel's centre; and by creating geometry, which tied the sides together. These two strategies were used as the basis for further iterations of panel designs, one associated with the triangular joint and the other with the cylindrical overlap joint.

JOINT/PANEL ITERATIONS

The triangular/ogee-shaped male/female snap-in joint, integrated directly along the panel's edge, provides excellent vertical stability with little material intensity. A closed, hollow triangle at the 'male' end was slightly offset from the surface of the panel, creating a depression into which the female element would clip. The 'female' portion comprised two legs of an ogee, which fit on top of the 'male' element, as well as an additional edge to complete the clip. It is not difficult to imagine how these linear elements might clip into place on the construction site using a simple tool to slide along the length of the 'female' element, moving it out of plane and into the grove along the 'male' element behind it.

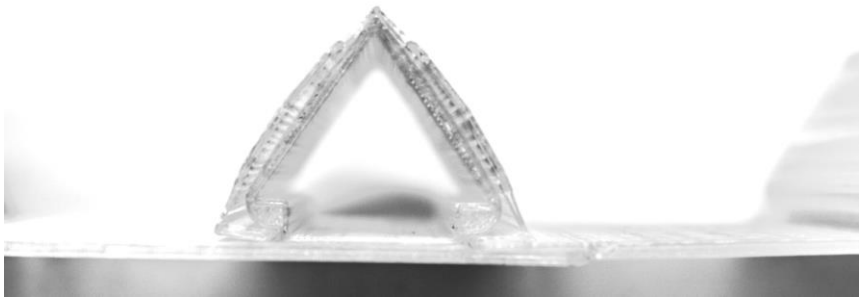

Fig. 4 Triangular/Ogee joint

Construction systems require much more than panel-to-panel connections. We therefore explored several variants to account for the way panels could attach to a sill plate or foundation while retaining reversibility. Another challenge was maintaining clearances that facilitate the placement and snap-in of panels while creating an overhanging edge on the panel, which can waterproof the gap between sill plate, foundation and wall. We devised three distinct iterations of a fuller wall construction system:

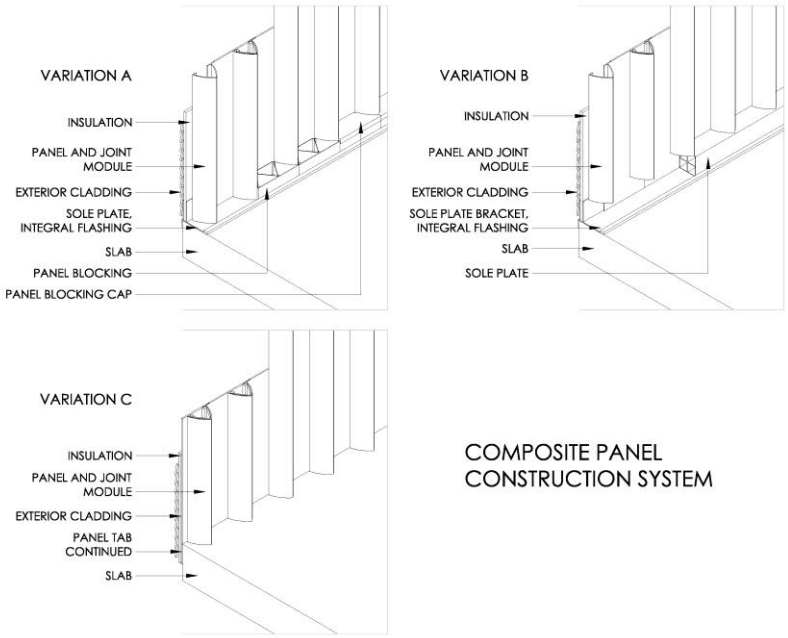

Fig. 4: Three variations on panel/sill plate connection and exterior finish

We tested each iteration, especially the customized sill plate and the friction connection designed to hold the wall stable. Models indicated the challenges of overturning and the limitations of a friction-only connection. Some potential remedies at building scale include using fasteners in holes that are provided in the panels during the fabrication process or weak adhesives that can temporarily hold elements in place while construction is completed.

Refocusing our efforts on the panel, we pursued strategies for the triangular joint panel type, which considered the displacement of material from the neutral axis as its means of stabilization. Three-dimensional corrugation-like deflections along the surface of the panel were fine-tuned through multiple model iterations to balance adequate rigidity in place with flex at the panel's ends. Within the limitations of the PLA material, we were able to achieve appropriate stability at the panel centre while maintaining flex at the edges using an egg crate corrugation pattern displaced symmetrically about the neutral axis.

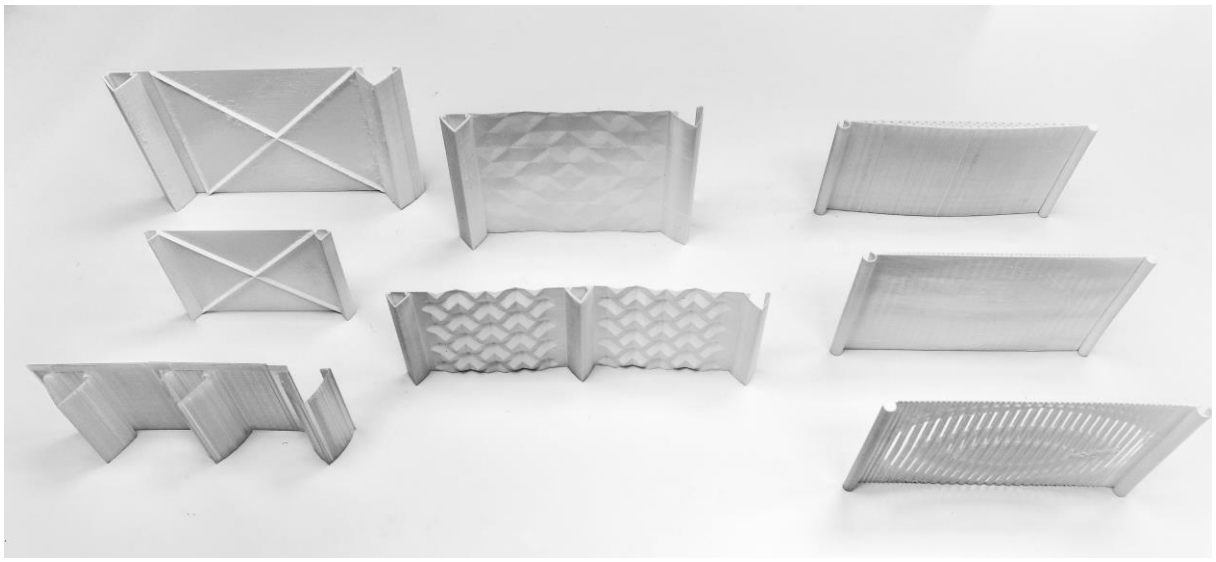

Fig. 5: Panel iterations with struts, egg crate corrugation and honeycomb

The cylindrical joint with overlapping 3/4 round concave component had an interesting capacity to hinge, and to form interior corners. Its disadvantages in comparison to the triangular configuration were its greater material intensity, required to give stability to the much smaller cross-sectional area at the joint; and the difficulty of increasing the size of the joint's cross-section. While the depth and geometry of the triangular piece can be almost endlessly varied in comparison to the equilateral triangle we chose, the circle can only be manipulated based on diameter.

In developing a strategy through which to stabilize this panel, we chose to explore a different approach, which we believed to be more formally compatible with the round joint geometry. We adapted interior honeycomb geometry, typically used in lightweight panel construction to form a diaphragm between the two exterior sheathing members. After several iterations, we discovered that thickening the panel towards its geometric centre – as if the panel had been intersected by a sphere – and retaining only the exterior sheathing provided an appropriate balance between flexibility at the ends and stability elsewhere.

CONCLUSION

The outcomes argue persuasively for the potentials of lightweight, panelized construction that unifies the three primary functions of a wall in one. The families of joints and panels in their 3-D printed forms at 1:20 scale demonstrate how effective simple geometric manipulations can be, even when prototyped in an unreinforced, isotropic material. Next steps include a fuller engineering stress analysis and the prototyping at full scale of joinery systems in vegetable fibre reinforced bio-based composite material.

REFERENCES

1. Heuss, R et al, 'Lightweight, heavy impact' McKinsey & Co., 2012
2. Manmek, S and Kara, S. 'Composites : Calculating Their Embodied Energy'
3. Westman, M.P. et al, 'Natural Fiber Composites: A Review' Pacific Northwest National Lab and US Department of Energy, 2010
4. Van Vuure, A., 'Natural Fibre Composites; Recent Developments' Sirris and Katholieke Universiteit Leuven, 2008
5. Ashby, M., Material Selection in Mechanical Design. Elsevier, Oxford, 2010

METHODOLOGICAL ISSUES IN EVALUATING INTEGRAL SUSTAINABLE RENOVATIONS

L. Wijnants[1]; K. Allacker[1]; D. Trigaux[1]; G. Vankerckhoven[1], F. De Troyer[1]

1: KU Leuven - Faculty of Engineering Science - Department of Architecture - Division of Architectural Engineering, Kasteelpark Arenberg 1 bus 2431, 3001 Leuven, Belgium

ABSTRACT

Ongoing research in Europe related to sustainable renovation mainly focuses on improving the energy performance of buildings. These studies have a limited scope regarding sustainability as operational energy is often the only focus. A screening of current practices in Flanders moreover shows that renovations are often limited to small interventions, whereby a long term vision is missing. We are convinced that a more integral approach is necessary to strive for sustainable renovation. This research aims at supporting the construction sector in the challenge for an increased renovation rate with more in depth transformations of the existing housing stock in Flanders. The objective is moreover to stimulate a transition from energy-focused renovations towards integral sustainable renovations from a life cycle perspective. In this context, the research aims among others at developing a number of affordable and innovative 'open-renovation-systems', with the focus on interventions such as splitting, combining, wrapping and extending residential buildings. To compare and analyze these renovation systems, a method to evaluate the environmental and financial impact of the renovation interventions over their whole life cycle is being developed. This evaluation method is based on the LCA (life cycle assessment) and LCC (life cycle costing) methodology. This paper focuses on two methodological issues in evaluating the environmental impact of renovation interventions: the allocation of the environmental impact of existing structures and materials to the life cycle before and after renovation, and the role of the estimation of the building lifespan (before and after renovation) in decision taking. The results of the analyzed case study show that the chosen allocation approach does not influence the overall conclusions regarding renovation or demolition followed by new construction. However, the case study reveals that the estimation of the second building lifespan can affect the results in a significant manner.

Keywords: Life Cycle Assessment (LCA), sustainable renovation, allocation, building lifespan

INTRODUCTION

The construction sector faces an important challenge in order to achieve the European objectives concerning sustainability and energy consumption. These objectives require a 20% reduction of the greenhouse gas emissions from 1990 levels by 2020 [1]. As buildings account for a major share in greenhouse gas emissions (i.e. more than 35% in the EU [2]), improving the energy efficiency of buildings is an important priority although the greenhouse gas emissions during the production of materials should not be ignored. Therefore, important priorities are energy-efficient newly built houses and thorough renovations of the existing housing stock. As the amount of newly built houses is limited compared to the existing buildings (i.e. little more than 1% of the building stock per annum in the EU [2]), renovation plays a major role in achieving these objectives. Ongoing research in Europe related to sustainable renovation mainly focuses on improving the energy performance of buildings and transforming existing buildings into nearly zero energy buildings ([3] - [6]). These studies have a limited scope regarding sustainability as operational energy is the only focus. Some

studies enlarge the scope by including embedded energy and by following an energy-based life cycle approach [7]. Some researchers (e.g. Thiers and Peuportier [8]) even evaluate a wide range of environmental impacts, but still limit their scope to energy improvement measures. However, once the energy demand is reduced, the choice of materials and resulting maintenance, repair and replacement scenarios become relatively more important.

A screening of current practices in Flanders confirms that renovations are often limited to small interventions to improve the energy performance. In Flanders, we are mainly dealing with a privative housing ownership whereby renovations are ad hoc solutions for ad hoc questions. These interventions are often expensive and time consuming because of their specificity. Examples in other contexts show that a different approach is possible. In the Netherlands, for example, prefabricated industrial building systems are more and more used, resulting in faster and cheaper renovations. In addition, current renovations of residential buildings in Flanders often miss a long term vision. Flexibility and adaptability are important keywords because of the household changing needs over time, such as family expansion and contraction and evolving comfort requirements. To deal with these changing needs and to avoid spatially underused buildings, interventions as splitting, combining and extending buildings will often be used in the future. Therefore, there is a need for affordable and adaptable building systems with a low environmental impact. The aim of this paper is to analyze some methodological issues in evaluating renovation measures in the overall aim to strive for sustainable solutions. More specifically two issues are analyzed in detail: (1) the allocation of the existing structures and materials over the two building life cycles (i.e. before and after renovation), and (2) the role of the estimation of the building lifespan (before and after renovation) in decision taking.

METHOD

The European standards EN15804 [9] and EN15978 [10] recommend the use of a life cycle assessment (LCA) for the evaluation of construction materials and buildings. The life cycle of a building consists of several phases, mainly classified as the production, construction, use and end-of-life (EOL). At any moment during the life cycle of a building, it can be decided to (1) consolidate, (2) renovate or (3) demolish the building and build a new one. An important issue related to the preferred choice between the three options from an environmental point of view, is how to account for the environmental impact of the existing building. Two main approaches can be distinguished when analysing the renovation of a building: (1) excluding the environmental impact of the existing building from the comparison and (2) using annual depreciation and hence allocating part of the environmental impact of the first phase to the second building life cycle. The two approaches might influence the preferred option and hence a carefully selected methodology is important. In this context, an analysis of both approaches has been made based on a literature study and a case study in the Belgian context. Since the current dwelling stock in Belgium consists of 32% terraced buildings, of which 65 % is built before 1945 [11], this dwelling type is selected for the case study. The calculations are based on a small not insulated working-class terraced house of 99m² as defined by Allacker [12]. The results are briefly summarised in the subsequent section.

RESULTS

Results literature study

The “exclude the past” approach, consisting in allocating the impact of the existing building entirely to the first life cycle (i.e. before renovation), is used by several researchers. Quantis [13] applied this approach to identify under which conditions rehabilitation and retrofit of a

building is preferred over demolition and new construction from an environmental perspective. Their arguments for this approach are the following: (1) the choice to rehabilitate a building has no impact on the production of existing materials which is the result of past decisions (2) there is a lack of information concerning the type, quantity and original impacts of the remaining materials, which could have been produced when the industrial systems were radically different [13]. When using this approach, one should also decide how to allocate the impact of the parts that are demolished. Several approaches are again possible: allocating the impact to the first life cycle or allocating it to the renovated house (at the start of the second life cycle), or allocating it partially to both. Hansen et al. [14] for example stated that the impact related to the removal and waste of the existing building elements can mostly be allocated to the previous service life. Their argument is that the removed building elements often had such a long service life that it is justified to allocate them to the previous service life. However, for the elements that are still useful and with a long expected remaining service life, they argued to allocate part of the impacts to the previous phase.

"W/E-adviseurs" [15] used the depreciation approach for the allocation of the impact of the existing building. In this study the research question focused on the preference between the improvement of an existing office or demolition and new construction. "W/E-adviseurs" [15] preferred this methodology because the first approach does not consider the building age, which means that there is no difference between a building of 10 or 100 years, although the demolition of a building after 10 years can be seen as destruction of environmental capital. The main idea of this approach is to determine which building parts are not yet at the end of their predicted life cycle. The environmental impact of these elements (i.e. due to production and EOL) is partially allocated to the second life cycle according to the ratio of remaining life span to the predicted life span. The new life cycle of the building consists of three types of impact: (1) the partial impact of the components that not yet reached the originally predicted service life at the moment of their replacement, (2) the impact of maintenance and replacement of the parts that remain in use and (3) the life cycle impact of the new components and materials.

In the depreciation approach, the estimation of the life span of the original building is crucial as it determines the ratio of the environmental impact allocated to the second life cycle. When the goal of the research is to compare the impact of 'lifespan extension due to renovation' with 'demolition and new construction', this life span estimation is an important issue. The uncertainty on the lifespan is however high, and hence many studies include sensitivity analyses. In [15] appears that for the considered offices the assumptions concerning the life span of a building have a significant influence on the results. Certainly for demolition followed by new construction, the expected lifespan is important when both the new construction and the residual load of the existing building have to be allocated to a short period, which may lead to different conclusions.

The first study [13] concluded that, if the renovated building has the same energy performance as newly-built houses, the renovation scenario remains environmentally favourable even after a century. When the newly-built house is more energy efficient than the renovated building, the newly-built house can be preferred although this can take decades. The outcome of this study is that preferences depend on the remaining building life span. It can be more environmentally preferable to renovate a building without major energy improvements when the remaining life span is relatively short. Several previous LCA studies pointed out that the operational energy use has a major share in the total environmental impact of a building over its whole life span. The estimation of the operational energy use is hence an important aspect when comparing renovation and demolition followed by new construction but is not further addressed in this paper.

Results of case study

Four scenarios are analysed and compared in the terraced house case study: (1) consolidation (i.e. further use of the existing building without any upgrading), (2) energetic renovation, (3) thorough renovation and (4) demolition followed by new construction. A description of the scenarios is given in Table 1. The analysis was also done for a timber frame construction, but the results are similar with the fourth scenario and are therefore not discussed in this paper.

SCENARIO	Energetic renovation	Thorough renovation	Demolition and new construction
INTERVENTIONS	New condensing gas boiler		
	• Outer wall: exterior insulation of 10 cm EPS inclusive exterior plaster • Roof: 17,5 cm rockwool between collar beams and twills • Windows: double glazed and PVC profiles	• Demolition of non-structural parts (only foundation, outer walls, floors and common walls are reused) • New inner walls in timber frame • Composition of the building skin is the same as in the scenario with an energetic renovation	• Foundation and common walls are reused • The floor plan and the composition of the inner walls are the same as in the scenario with a thorough renovation • Insulation: *Outer wall*: 22 cm rockwool *Floor on grade*: 15 cm PUR *Roof*: 17,5 cm rockwool between collar beams and twills *Windows*: double glazed and PVC profiles

Table 1: Description of the analysed scenarios

The environmental impact calculation is based on the MMG LCA method, developed by OVAM [16]. Figure 1 shows the yearly environmental cost of the four scenarios, based on the depreciation approach. The assumption is made that the predicted building lifespan for the first phase was 90 years and that the intervention takes place 20 years before the foreseen end of life, i.e. at a building age of 70 years. The same analysis is made for a predicted lifespan for the first phase between 60 and 200 years. The life span of the new phase is a parameter from 15 years to 120, in steps of 15 year.

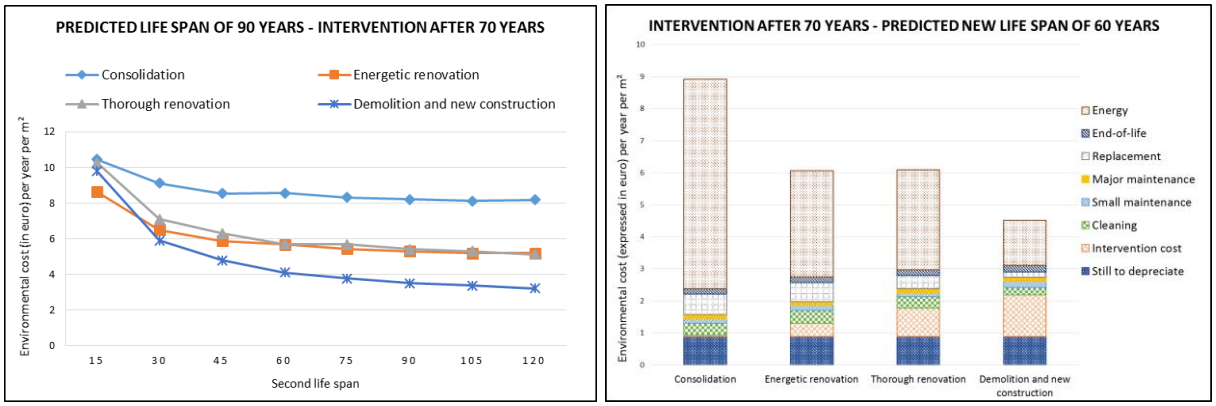

Figure 1: Environmental cost of the four scenarios per year per m² floor, in function of the duration of the second building lifespan, considering a first predicted lifespan of 90 years and an intervention after 70 years (left) and environmental cost of the four scenarios per year per m²floor, divided per life cycle phase, considering a first predicted lifespan of 90 years, an intervention after 70 years and a second lifespan of 60 years (right).

The results reveal that for this case study the environmental load for the second phase is only marginally influenced by the originally predicted lifespan of the existing building. The results per life cycle phase for a first predicted lifespan of 90 years are shown in Figure 1. The energy consumption is responsible for a major share of the environmental cost. The environmental cost of the existing components that has to be allocated in this case is just a small share of the yearly cost. The EOL cost of the parts that are removed is included in the intervention cost.

The "exclude the past" approach was also used to analyse the case study. For this approach, it is assumed that the EOL of the demolished parts is allocated to the new building life cycle, as

in the depreciation approach. In Figure 2, the results are compared with the one from the depreciation approach for a thorough renovation (left) and demolition and new construction (right). The results reveal that the choice of the allocation approach has, in this case, no influence on the conclusions. Concerning the depreciation method, the estimation of the second building lifespan can affect the results significantly, certainly if the remaining life span of the building is relatively short. Furthermore, when the second lifespan is shorter than, in this case, 22 years, the yearly environmental costs are lower for renovation than demolition and newly-built, due to the higher investment cost for newly-built that has to be amortized over a short period. The same analysis is made for an energetic renovation with a similar energy efficiency to newly-built construction, which shows that renovation remains environmental preferable when the second lifespan is shorter than approximately, in this case, 70 years. However, even with this improved energy efficiency the choice of allocation approach has no influence on the conclusions.

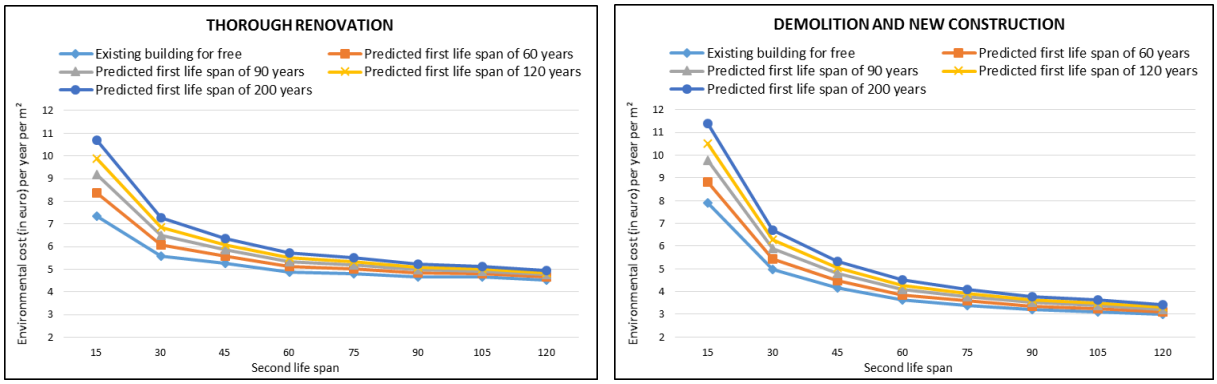

Figure 2: Environmental cost per year per m² of the thorough renovation (left) and demolition and new construction (right) for an intervention after 70 year, using both allocation approaches. For the depreciation approach, several predicted life spans for the first life cycle are compared.

Finally we also considered the possibility of even not taking the EOL of the existing building into account. As the impact of the EOL is small compared to the total impact of the life cycle phases (i.e. approximately 2% for renovation and 3.5% for newly-built when considering a second life span of 60 years), allocating it or not to the existing structure does not change the overall results.

CONCLUSION AND FURTHER RESEARCH

In this paper two main approaches for allocating the environmental impact of the existing building are compared via a case study: (1) allocating the environmental impact of the existing building entirely to the first life cycle, whether or not taking the EOL during the intervention into account and (2) allocation based on annual linear depreciation. The results of the case study show that the choice of allocation approach does not influence the overall conclusions regarding renovation or new construction. However, the estimation of the second building lifespan and differences in energy efficiency can affect the results significantly. Simulating the effect of originally estimated life spans, different ages of intervention and different ratios of energy cost versus investment cost is required in future.

ACKNOWLEDGEMENTS

This paper is part of a doctoral research funded by the Agency for Innovation by Science and Technology (IWT).

REFERENCES

1. European Commission (2014): Een energie–efficiënt Europa. Retrieved on August 21th 2014 from http://ec.europa.eu/news/energy/110622_nl.htm.
2. Eurima (2011): Energy efficiency in buildings. Retrieved on April 22th 2015 from http://www.eurima.org/energy-efficiency-in-buildings.
3. Silva, P. C.P., Almeida, M., Bragança, L. and Mesquita, V.: Development of Prefabricated Retrofit Module towards Nearly Zero Energy Buildings. Energy and Buildings, Vol 56, pp 115–125, 2013.
4. Ma, Z., Cooper, P., Daly, D., and Ledo, L.: Existing Building Retrofits: Methodology and State-of-the-Art. Energy and Buildings, Vol 55, pp 889–902, 2012.
5. Asadi, E., Gameiro da Silva, M., Henggeler Antunes, C., and Dias, L.: Multi-Objective Optimization for Building Retrofit Strategies: A Model and an Application. Energy and Buildings, Vol 44, pp 81–87, 2012.
6. Brown, N. W.O., Malmqvist, T., Bai, W. and Molinari M.: Sustainability Assessment of Renovation Packages for Increased Energy Efficiency for Multi-Family Buildings in Sweden. Building and Environment, Vol 61, pp 140–148, 2013.
7. Famuyibo, A.A., Duffy, A., and Strachan P.: Achieving a Holistic View of the Life Cycle Performance of Existing Dwellings. Building and Environment, Vol 70, pp 90–101, 2013.
8. Thiers, S. and Peuportier B.: Energy and Environmental Assessment of Two High Energy Performance Residential Buildings. Building and Environment, Vol 51, pp 276–284, 2012.
9. CEN (2012+A1:2013) CEN TC350 - EN 15804+A1 - Sustainability of construction works - Environmental product declarations - Core rules for the product category of construction products.
10. CEN (2011) CEN TC350 - EN 15978 - Sustainability of construction works - Assessment of environmental performance of buildings - Calculation method.
11. Belgian Federal Government (2013): Het gebouwenpark. Retrieved on May 4th 2015 from http://statbel.fgov.be/nl/statistieken/cijfers/economie/bouw_industrie/gebouwenpark/.
12. Allacker, K.: Sustainable Building: The development of an evaluation method. PhD dissertation, Heverlee, 2010, 464 pages.
13. Quantis US: Quantifying the Value of Building Reuse - A Life Cycle Assessment of Rehabilitation and New Construction. Boston, 2012, www.preservationnation.org, 158 pages.
14. Hansen, K., Holleris Petersen, E.: Environmental assessment of renovation projects. Proceedings of Sustainable Building 2002, Oslo, 2002.
15. W/E adviseurs: Kiezen voor nieuwbouw of het verbeteren van het huidige kantoor – Eindrapport. Agentschap-NL, Utrecht, 2010, http://www.rvo.nl/sites/default/files/bijlagen/Eindrapport%20Kiezen%20voor%20nieuwbouw%20of%20het%20verbeteren%20van%20het%20huidige%20kantoor_0.pdf, 85 pages.
16. Allacker, K., Debacker, W., Delem, L., De Nocker, L., De Troyer, F., Janssen, A., Peeters, K., Servaes, R., Spirinckx, C., and Van Dessel, J. : Environmental profile of building elements. OVAM, Mechelen, 2013, www.ovam.be/materiaalprestatie-gebouwen.

Daylighting and Electric Lighting

COMPARISON OF MEASURED AND COMPUTED BSDF OF A DAYLIGHT REDIRECTING COMPONENT

L. O. Grobe[1,2]; A. Noback[1]; S. Wittkopf[1]; Z. T. Kazanasmaz[2]

[1]*Lucerne University of Applied Sciences and Arts, Technikumstrasse 21, CH-6048 Horw*
[2]*Izmir Institute of Technology, Department of Architecture, Urla, TR-35430 Izmir*

ABSTRACT

The Bidirectional Scatter Distribution Function (BSDF) of a selected Daylight Redirecting Component (DRC) is computed by a virtual goniophotometer using the enhanced photon map extension in Radiance, and compared to measured BSDF data.

The DRC comprises a stack of tilted aluminum louvers with configurable inclination angle. The profile of the louvers is designed to control transmission depending on sun altitude, and to redirect light up towards the ceiling.

The measured BSDF of the DRC is obtained from a scanning goniophotometer. For a sparse set of three source directions, the distribution is recorded at $\simeq$ 250,000 receiver directions. The asymmetric angular resolution allows detailed observation of characteristic features in the distribution, which are assumed to persist over a range of source directions. For each pair of source and receiver directions in the measurement, the computed BSDF is generated from a model of the DRC, replicating the measurement with a virtual goniophotometer. The simulation relies only on the enhanced photon map extension for Radiance. The BSDF from measurement and simulation are compared qualitatively and quantitatively to discuss the degree of accordance. The presence of characteristic features and their topology is evaluated by comparing polar surface plots of the distributions and profiles of the scatter plane. The direct-hemispherical transmission is compared for each measurement and simulation. The RMSE of each computed distribution against the corresponding measurements is calculated to quantify the directionally resolved deviation.

A high degree of qualitative accordance between the computed and the measured BSDF is achieved. Prominent features in the BSDF are represented by the model. A deviation of -6% to $+15\%$ is observed in a quantitative comparison of direct-hemispherical transmission by integration of computed and measured BSDF. The RMSE indicates higher deviations for lower source altitudes, where a direct transmission peak in the distribution is underestimated by the model. The method is proposed as a means to validate the capability of the enhanced photon map to predict transmission through DRC.

Keywords: daylight simulation, modeling, validation, daylight redirection, BSDF

INTRODUCTION

Daylight Redirecting Components (DRC) reduce solar gains and energy demands for electrical lighting in buildings, and improve visual comfort for occupants. Planners aim at finding the minimum required transmission providing sufficient and evenly distributed illuminance during occupancy hours. Daylight simulation supports this optimization by providing illuminance and luminance data for assessments based on metrics such as Spatial Daylight Autonomy and Daylight Glare Probability.

Light transport through DRC [1] is a challenge to backward ray-tracing algorithms such as implemented in Radiance [2]. To avoid the limitations of the stochastic indirect-diffuse algorithm, the transmission through DRC can be pre-computed by dedicated software [3]. The geometry of the DRC is then replaced by the corresponding average Bidirectional Scatter Distribution Function (BSDF) [4, 5] as a uniform property. In the direct calculation, the actual geometry can be maintained to preserve phenomena such as shadow patterns or the visibility of geometric detail.

While the abstraction of DRC by their BSDF has been demonstrated as a suitable method for the calculation of illuminance and derived metrics [6], detail in the patterns of highlights and shadows caused by non-uniform transmission is lost. Such phenomena influence the visual appearance of adjacent surfaces and may affect visual comfort and glare probability. The reuse of pre-computed BSDF as libraries can reduce the time-consuming computation of BSDF. However, when relying on pre-computed BSDF, the parameters determining the BSDF are not accessible during the simulation, hindering e.g. the application of optimization algorithms that need to vary such parameters based on the simulation outcomes. To consider e.g. the adaptivity of a louver system by changing tilt angles, for any possible configuration a pre-computed BSDF would have to be provided.

An enhanced implementation of a forward-tracing photon-mapping algorithm in Radiance addresses these limitations [7]. Combined with advanced techniques such as progressive photon-mapping, it has been demonstrated to be capable to maintain even subtle patterns of reflection, including concentration and redirection [8].

METHOD

This work proposes that a model of a sample is valid, if the BSDF calculated from it matches the measured BSDF of the sample. For this to be true, the model must accurately represent the geometry and surface properties of the sample. The measurement conditions, such as the illuminator and the resolution, must be replicated in the simulation. If both conditions are met, the computed BSDF can be compared to the measurement.

The BSDF of a DRC sample (figure 2), consisting of 39 fixed slats, is measured using a scanning goniophotometer [9]. As the redirection properties of the DRC depend on the louver assembly, the glazing is not included. To cover a representative area by the measurement, the illuminator is configured to a sampling aperture [5] of diameter $d_i \simeq 65mm$ on the sample with a collimated beam. The sampling aperture covers 6-7 slats of the DRC. A short-pass filter blocks wavelengths in the near infrared and limits the measurement to visible light. During the measurement, the receiver records irradiance at regular time intervals in a continuous scanning movement around the center of the sample, at a distance of $d_s = 1020mm$. First, the receiver scans the unobstructed beam and records the irradiance received, $E_{s,n}$. The power in the unobstructed beam, equal to the incident power on the sample, P_i, is calculated from n measurements of $E_{s,n}$ and their corresponding solid angles $\Omega_{s,n}$:

$$P_i = \sum_n E_{s,n}\Omega_{s,n} \tag{1}$$

After the measurement of the beam, the distributions of $E_{s,n}$ after transmission through the sample are scanned at high resolution for three source directions $\theta_i = 35°, 40°, 45°$ (with invariant $\phi_i = 0°$). The scan path is refined in areas where high variance of the signal is observed, leading to an adaptive resolution of the measurement. By dividing each

of the n measurements by P_i, the Differential Scattering Function DSF and the BSDF can then be calculated for each combination of (θ_i, ϕ_i) and (θ_s, ϕ_s):

$$BSDF_n = \frac{DSF_n}{\cos\theta_{s,n}} = \frac{E_{s,n}}{P_i \cdot \cos\theta_{s,n}} \tag{2}$$

The division by $\cos\theta_s$ as defined in the BSDF formulation leads to anomalies at source directions $\theta_s \simeq 90.0°$. As can be seen in equation 2, describing the transmission characteristics by the DSF is equivalent to the BSDF [5]. For better comprehensiveness, the DSF formulation is used in the comparison and in the discussion of results.

Based on the slats' profiles, inclination angles and distances (figure 2), a geometric model of the sample is prepared. The reflection properties of the slats' surfaces are modeled using the metal and plastic materials in Radiance. A virtual goniophotometer is set up to compute the BSDF of the model. The illuminator comprises a distant source with an opening angle of $\alpha = 0.5°$, illuminating a sample aperture of $d_i = 70mm$ diameter resembling the collimated beam of the measurement. A spherical receiver surface to store photon hit points surrounds the sample and represents possible positions of the receiver. The setup of this virtual goniophotometer and the orientation of the sample coordinate system is shown in figure 1.

Each simulation consists of a photon-distribution and a photon-gathering pass. In the first pass, photons are distributed from the light source and stored in photon maps after hitting the sample or the receiver sphere. In the second pass, the indirect irradiance on the receiver surface is estimated from the (local) photon density (rtrace -ab -1) on the receiver surface. For each receiver position recorded in the measurement, the irradiance $E_{s,n}$ is computed.

First, the distribution of the unobstructed beam is scanned in analogy to the procedure of the physical goniophotometer. The integral of the resulting set of measurements is calculated as a measure of the power received by the sample P_i as in the measurement.

With the simulation model of the sample placed in the center of the receiver sphere, the source is rotated to the source directions [5] ($\theta_i = 35°, \theta_i = 40°, \theta_i = 35°$, later on referred to as source altitude, in the scatter plane $\phi = 0°$). The irradiance distribution on the receiver surface is computed for the entire transmission hemisphere ($\theta_s = 90°$ to $\theta_s = 180°$, $\phi_s = 0°$ to $\phi_s = 360°$). The DSF for any receiver location is then defined by equation equation 2.

Polar plots of the measured and computed DSF, centered at $\theta = 180°, \phi = 0°$ with the radius corresponding to the altitude angle θ, are provided. To enhance visibility of details, a logarithmic scale is applied to the z-axis. The occurrence, location and shape of features such as peaks, ridges and other structures that are observed in the computed DSF shall match those in the measurement.

For a quantitative comparison, the integral of the computed DSF for each source direction, the transmission τ, is compared to the measured transmission. Root Mean Square Error RMSE and Coefficient of Variance CV are calculated for each source direction:

$$RMSE = \sqrt{\left\langle |DSF_{n,comp} - DSF_{n,meas}|^2 \right\rangle}, \qquad CV = \frac{RMSE \cdot 2}{|DSF_{n,comp}| + |DSF_{n,meas}|} \tag{3}$$

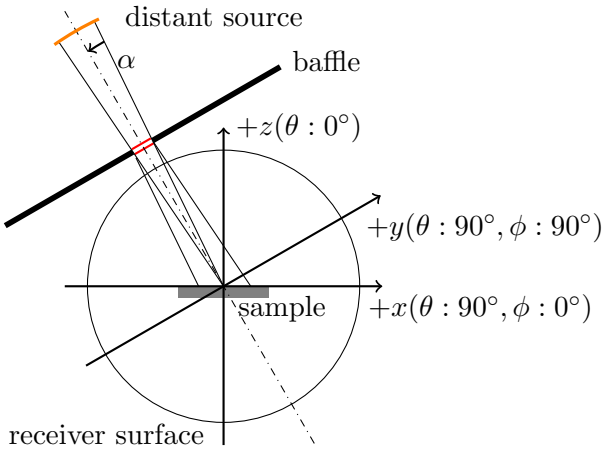

Figure 1: Sample coordinate system and setup of the virtual goniophotometer used in the computation of the BSDF.

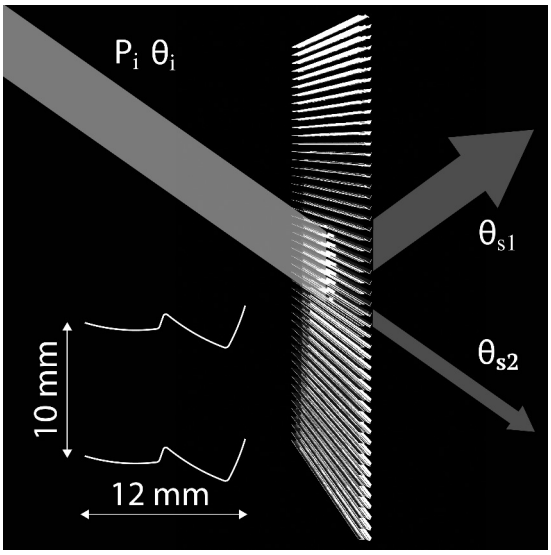

Figure 2: Main transmission directions through the DRC (Luxtherm, patent Köster), profile of the slats.

RESULTS

The computed and measured DSF show the same topology of peaks and ridges (figures 3, 4). For both presented source directions, a ridge, ranging from $\theta = 130°$ to $\theta = 180°$, indicates upwards redirection by the reflector. The ridge is labeled as $\theta_{s,1}$ on the plots and corresponds to the range of upwards-scatter in figure 2. Both, the computed and the measured DSF, show a diffuse background with a characteristic trench due to the linear structure of the system. The computed transmission appears to be less smooth, spikes can be observed especially in the ridges.

At a source altitude of $\theta = 35°$ (figures 3, 4), a direct transmission peak (labeled $\theta_{s,2}$, as in figure 2) is visible at $\theta = -145°$ in the computed and measured distributions. Compared to the upwards-directed ridge $\theta_{s,1}$, the direct transmission peak is higher in the measured, lower in the computed distribution.

Direct transmission is blocked at a source altitude of $\theta = 45°$. A second, weaker ridge arises in a range from $\theta = -90°$ to $\theta = 180°$, indicating light transmitted downwards by reflection in the system. Redirection towards the ceiling ($\theta_{s,2}$) is maintained.

Directional-hemispherical transmittance [4] was calculated from the DSF for three source directions using equation 1 and is shown in table 1. A deviation in a range from -6% to +15% is observed. At a source altitude of $\theta = 35°$, with direct transmission occurring, the computed integral is lower than the measured one. Both RMSE and CV indicate a better fit for higher source altitudes, as can be seen in table 2.

	$\theta_{in} = 35°$	$\theta_{in} = 40°$	$\theta_{in} = 45°$
τ_m	0.398	0.434	0.479
τ_c	0.376	0.493	0.549

Table 1: Measured and computed direct-hemispherical transmission τ_m, τ_c.

	$\theta_{in} = 35°$	$\theta_{in} = 40°$	$\theta_{in} = 45°$
RMSE	0.1164	0.0283	0.0166
CV	0.6624	0.0615	0.0323

Table 2: Root Mean Square Error RMSE and Coefficient of Variance CV.

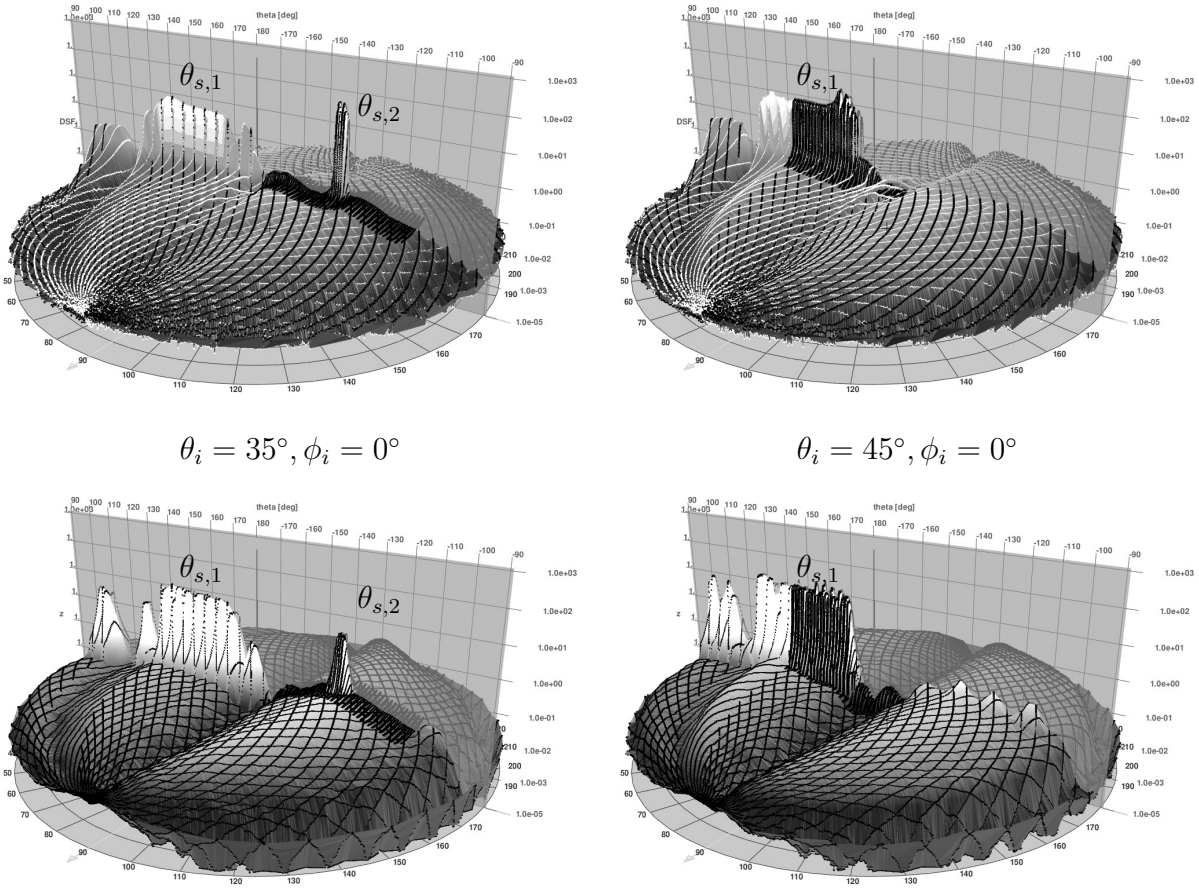

Figure 3: Measured (top) and computed (bottom) DSF for two source altitudes. The dark lines indicate the path of the receiver in the measurement and the simulation.

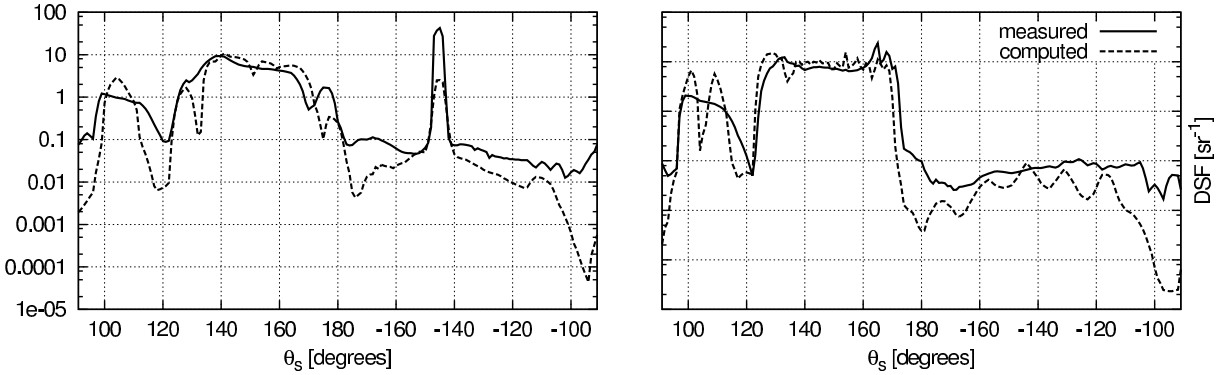

Figure 4: Profiles of the measured and computed DSF in the scatter plane ($\phi = 0°$) for two source altitudes $\theta_i = 35°$ (left) and $\theta_i = 45°$ (right).

DISCUSSION

The comparison of computed and measured DSF has shown that, in principle, the enhanced photon map extension for Radiance is capable to model transmission through DRC and to represent the characteristic features in the distribution.

A better understanding of the observed deviations requires further investigation of the simulation algorithm and its parametrization, the measurement and the particular sample. Artifacts such as spikes in the DSF are expected for a faceted surface model, and can be controlled by its geometric resolution. The deviations in the computed and measured direct-hemispherical transmission, related to the underestimated direct transmission, require further investigation. Particular conditions of measurement and sample must be considered as well as the inherent bias [7] of the simulation algorithm. The selected DRC, with its angular selectivity and cut-off angles, is a particular challenge, as slight deviations between model and physical sample can cause drastic changes in the transmission. The measured BSDF as a reference is of limited reliability, as imperfections of the sample and the instrument signature have a high impact on both qualitative and quantitative results.

ACKNOWLEDGMENTS

This research was supported by the Swiss National Science Foundation as part of the project Simulation- based assessment of daylight redirecting components for energy savings in office buildings (#147053). This contribution benefits from the doctoral degree support scheme of Lucerne University of Applied Sciences and Arts in collaboration with Izmir Institute of Technology. At the same time I would like to show my appreciation to my colleagues Marek Krehel for providing me with the measured BSDF data and Roland Schregle, author of the enhanced photon map extension for Radiance, for his support.

REFERENCES

1. Köster, H.: Automatic heat control with mirror optics. In *Proceedings of the 3rd Workshop on Transparent Insolation*, 1989.
2. Larson, G. W., Shakespeare, R., Ehrlich, C., Mardaljevic, J., Phillips, E., and Apian-Bennewitz, P.: *Rendering with Radiance: the art and science of lighting visualization*. Morgan Kaufmann San Francisco, CA, 1998.
3. Kohler, C.: Simulation of complex glazing products; from optical data measurements to model based predictive controls. 2014.
4. Nicodemus, F. E., Richmond, J. C., Hsia, J. J., Ginsberg, I. W., and Limperis, T.: *Geometrical considerations and nomenclature for reflectance*, volume 160. US Department of Commerce, National Bureau of Standards Washington, DC, USA, 1977.
5. ASTM: Standard practice for goniometric optical scatter measurements. In *ASTM E 2387-05*. ASTM International, 2005.
6. McNeil, A., Jonsson, C., Appelfeld, D., Ward, G., and Lee, E.: A validation of a ray-tracing tool used to generate bi-directional scattering distribution functions for complex fenestration systems. *Solar Energy*, 98:404 – 414, 2013.
7. Schregle, R. Development and integration of the Radiance Photon Map Extension. Technical report, Lucerne University of Applied Sciences and Arts, 2015.
8. Schregle, R., Grobe, L., and Wittkopf, S.: Progressive photon mapping for daylight redirecting components. *Solar Energy*, 114:327–336, 2015.
9. Apian-Bennewitz, P.: New scanning gonio-photometer for extended BRTF measurements. In *SPIE Optical Engineering+ Applications*. SPIE, 2010.

CHARACTERISATION AND MODELLING OF ADVANCED DAYLIGHT REDIRECTION SYSTEMS WITH DIFFERENT GONIOPHOTOMETERS

Marek Krehel[1], Jérôme Kämpf[2], Stephen Wittkopf[1]

[1] *Lucerne University of Applied Sciences and Arts, Technikumstrasse 21. CH-6048 Horw*
[2] *Ecole Polytechnique Fédérale de Lausanne (EPFL), Station 18, CH-1015 Lausanne*

Abstract

In this work we present a characterisation of Daylight Redirecting Components (DRCs) by comparing a scanning with an image based Goniophotometer (GPs). Both GPs can be employed in order to measure Bidirectional Scattering Distribution Function (BSDF). The measurements of the BSDF can be transformed into BSDF data driven model. The latter one can be in turn used to perform light scattering simulations. The aim of this work is to validate the correlation between the measurements from both systems. Three different DRCs (Laser Cut Panel (LCP), Daylight Redirecting Film (RF) and Daylight Redirecting Prisms (DRP)) with dimensions 15 x 30 cm^2, 34 x 34 cm^2 and 30 x 30 cm^2 respectively were measured. The results for each sample for one light incident direction (θ (altitude)=24° and ϕ (azimuth)=60°) from both GPs were analysed and visualised in the software *Mountain V3.0.1*. DRCs LCP and RF correlate to each other relatively well. The only discrepancy is their slightly wider scattered light distribution. However the DRP sample correlates to smaller extent, the scattered peaks are not only much wider but slightly differently positioned. The wider light distribution can be explained by different instrument signature (light beam diameter and resolution of the measurements). In addition to the visual assessment the total light transmission and Full Width at Half Maximum were compared. Similarly to the visual evaluation DRCs RF and LCP samples showed more coherent results (79.8% vs 88.4% for RF and 89.8% vs 78.0% for LCP) whereas transmission values for DRP vary significantly more (76.9% vs 44.0%). The difference in RF sample can be explained by the instrument signature, however DRP sample requires further investigation in the future work.

Keywords: BSDF, Goniophotometry, Daylight Redirecting Components.

INTRODUCTION

DRCs attract more and more attention nowadays thanks to their possibility to bring high quality illumination to offices (lack of flicker, friendly colour temperature and uniformity) The others benefits brought by DRCs is low daylight glare probability, wellbeing and increased productivity both delivered by having the spectrum of natural daylight in the offices [1]. All of the above mentioned profits make the DRCs attractive candidates to replace the regular glazing systems in office buildings. However, a few factors like for instance position (latitude, longitude), shape and orientation of the buildings might require usage of different types or special adjustments of DRCs [3]. Therefore the planners often abandon the idea of incorporating the DRCs while planning. Thus, in order to foster the usage of the DRCs functional model for fast and accurate simulation have to be developed. A few approaches have been studied in order to conduct proper simulations of DRCs. For instance analytical models with estimated parameters or models fitted to measurements. However more complex behaviours are not addressed by analytical models, for instance with retro-reflection or multiple peaks. In such a case most accurate simulations can be performed by Bidirectional Scattering Distribution Function (BSDF) data driven models. BSDF is defined

as a fraction of light intensity scattered in a given direction divided by incident light intensity[2]. Nevertheless, a generation of these models require a large number of accurate measurements of the light scattering by the DRCs. The light scattering properties can be measured by means of goniophotometers. The results provided by two goniophotometery laboratories were chosen for the comparison, one placed in Luzern University of Applied Sciences and Arts in the Competence Centre Envelopes and Solar Energy (HSLU CCEASE) and one in Ecole Polytechnique Fédérale de Lausanne in the Solar Energy and Building Physics Laboratory (EPFL LESO-PB). Although both systems can characterise DRCs, to our best knowledge, a comparison between their measurements has never been done. Such a comparison is crucial for coherent modelling and simulation of DRCs.

MATERIALS AND METHODS

Selection of DRCs

A set of three DRCs (LCP, RF and DRP) was decided to be characterised by the GPs[3]. LCP sample was produced from a 7 mm thick plate of polymethylmethacrylate (PMMA) in which an array of cavities was produced by a laser cutter. These cavities were redirecting the light due to the internal reflecting interfaces. The light redirection in RF sample is based on micro structured prisms. This prismatic foil with thickness of 300 µm was mounted on window glass in order to prevent bending. Last sample - DRP was manufactured form PMMA material and its light redirection relies on light refraction by micro lenses on sun-façade side and micro prisms on inwards side.

Goniophotometers setups

The HSLU set-up comprises a dark room housing the scanning goniophotometer (GP-S) and separate control room. The GP-S setup with the description of the main parts is presented in Figure 1 [4]. The measurements are conducted as follows: Collimated light from the optical bench illuminates a vertically mounted sample. A detector spherically rotates around the sample and reports light levels reflected off and transmitted through the sample for every angle. Thus, the full spatial range of reflection and transmission scattering values can be measured. The post for sample mount is equipped with motor which allows automatic rotation of the sample, therefore incident angle can be varied automatically.

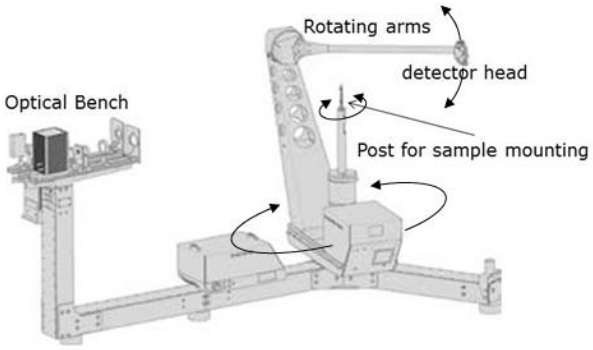

Figure 1: Sketch of the goniophotometer installed in the laboratory at HSLU with description of its main components [5].

The GP-S measures angularly resolved scattering values which results in BSDF values [5]. The resolution of measurement is independent on direction. Additionally, it features high resolution measurement in areas of interest by means of automatic peak scanning or manual configuration of fine scanning. The example of resolution of measurements is presented in the Figure 2 where each of the grey lines in the polar plot corresponds to the acquired data. Furthermore, refined peak scanning was performed in position θ=25° ϕ=210°.

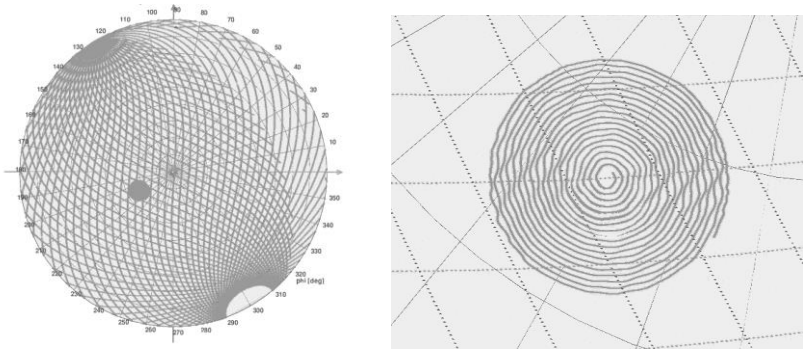

Figure 2: Dynamic resolution of GP-S. Left: whole hemisphere showing the measurement paints along the measurement path, right magnified local high resolution scanning.

The silicon detector working in the multistage amplification mode with V-lambda filter was used as a detector. Halogen lamp with hot mirror 700 nm was employed as a light source. Light was collimated by means of optical setup resulting in beam diameter of 6 cm.

The image based goniophotometer (GP-I) available at the LESO-PB uses advanced digital imaging techniques (CCD video camera) and is based on light incident directions following the 145 sky subdivisions of Tregenza. In Figure 3 schematic of transmitted light detection is presented.

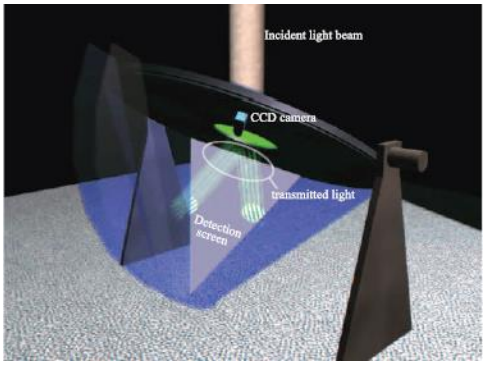

Figure 3: GP Detection of the transmitted light flux in the GP-I setup [6].

The output resolution of the outgoing light directions is fixed every 5° in azimuth and elevation, leading to a subdivision of the hemisphere in 1297 patches. The resolution of the measurements is presented in Figure 4, where one point of data acquisition can be seen in every 5° in azimuth and elevation.

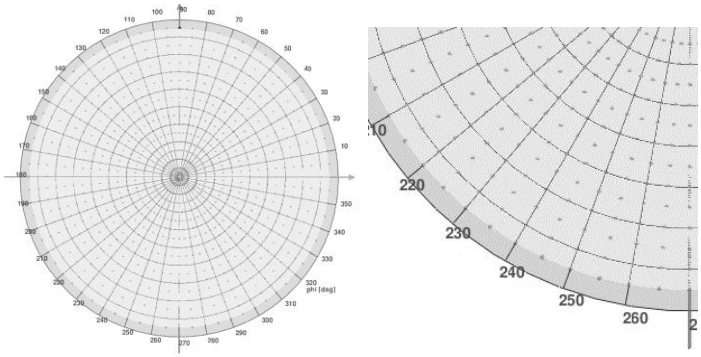

Figure 4: Fixed resolution of GP-I. Left: whole hemisphere, showing the measurement points in every 5° patch. Right: magnified part of the hemispherical projection.

The projector with a collimated light beam was used as a light source and was placed 10 m away from the samples. Hence, resulting in a strongly collimated light [3]. In Table 1 a main features of GP-I and GP-S are compared.

Features	GP-S	GP-I
Maximum sample size	90 x 100 cm^2	40 x 40 cm^2
Light beam diameter	Variable 1 – 7 cm	10 cm
Resolution	>100'000 points/hemisphere	1297 points/hemisphere
Resulting hemisphere	Transmission and reflection in one measurement	Transmission and reflection in separate measurement
Time of measurement for one incident direction	Approx. 10 min	Few seconds

Table 1 Comparison of the main features of both GP-S and GP-I [6].

Data post processing

Mountain software was applied for data visualisation and post processing. Post processing of the data includes: integration of transmission values and transformation from Differential Scattering Function (DSF) to BSDF. The standard import data format consists of ASCI text file with columns corresponding to θ, φ, and BSDF values. The angles θ and φ are according to standard spherical coordinate system. Post processed data are exported in the same format. Data from both GPs were analysed and exported by *Mountain*.

RESULTS

Scatter visualization

Each of the samples was measured for transmission with the following incident direction: θ=24° and ϕ=60°. In Figure 5 all the measured data are presented.

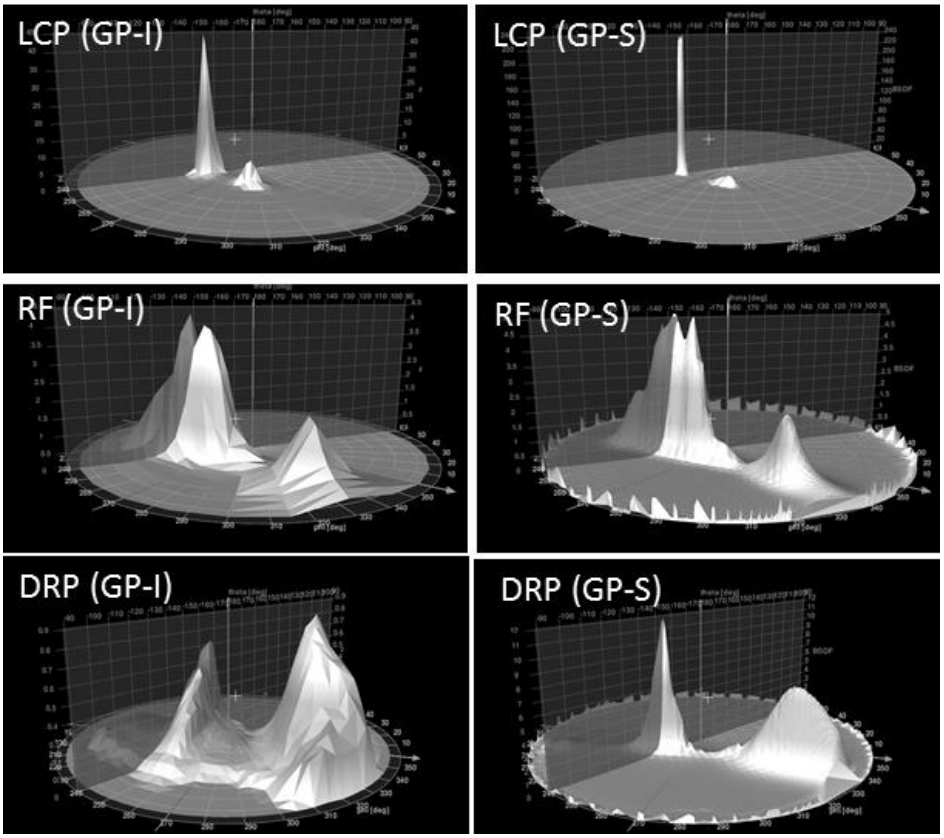

Figure 5: Light transmission characteristics through DRCs.

Transmission and FWHM values

In Table 2, a summary of FWHM values are listed. In the second and third column data post processed by *Mountain* are presented. Fourth column shows raw data from GP-I.

Sample acronym	GP-I		GP-S		GP-I raw
	Int. trans. [%]	FWHM [°]	Int. trans. [%]	FWHM [°]	Int. trans. [%]
LCP	77.9	4	89.8	3	78.0
RF	83.4	10	79.8	8.5	88.4
DRP	65.8	-*	76.9	-*	44.0

Table 2: Summary of light transmission and FWHM values from both system as post processed Mountain (expect last column with raw values from GP-I).
**-FWHM could not be reliably compered due to significant differences in the light scattering characteristics.*

DISCUSSION

LCP (most specular redirecting sample) appears quite similar across both GP. The visualization shows that both peaks are well refined and are placed in the same positions (θ=157° ϕ= 240° and θ=155° ϕ=240°). The only difference that can be noticed is slightly more scattered light distribution. However their FWHM are still at similar levels (4° vs 3°). Sample RF shows similar behaviour. Scattered light is distributed in a wider manner and the peaks are not as well defined. The FWHM values for both systems are comparable (10° vs 8.5°). Besides the above described discrepancies, it can be observed that the characteristics of the light scattering properties are maintained in the measurements from both systems. A source of the discrepancies found in measurements in samples LCP and RF can be explained by the instrument signature [7]. As described in the former chapter the light beam employed in goniophotometer at GP-I laboratory is larger in diameter, thus the resolution of the measurements is decreased. Furthermore, the resolution of acquired data is lower in GP-I laboratory which introduces additional differences. Both of those factors significantly lower the acquired resolution resulting in more spread light scattering properties. The measurements of the last sample, DRP, exhibit the largest dissimilarities. The main peaks can be still noticed, however, their spread is much wider. Main underling reason of these discrepancies is the same as for sample LCP and RF. However, the DRP sample is the most diffusive one, thus the deviations are the biggest. Additionally, the DRP exhibits different behaviour depending on where it was illuminated. Thus, these larger differences can be explained by different light beam diameter.

As for the transmission values, significant (close to 10 % for LCP and RF and more than 30% for DRP) differences can be observed in values calculated by software *Mountain* and the raw values from GP-I. In order to validate whether these discrepancies appeared due to the different calculation methods the raw BSDF from GP-I were evaluated by the same software. These values are presented in the second and third column and it can be noticed that the transmission values through the LCP are similar from both laboratories (77.9% for GP-I vs 89.8% for GP-S). This could be expected as the light scattering characteristics were very similar for both GPs. Values for sample RF also exhibit high correlation (83.4% for GP-I vs 79.8% for GP-S). Analogously, to the measurements of the LCP the light scattering characteristics remains in lower coherence. Transmission values of sample DRP did not show any similarity (up to 50 % relative differences), it can be explained by relatively big difference in measured scattering properties and requires further investigation.

CONCLUSION

A comparison of the analysis from two goniophotometers of three daylight redirecting components (LCP, RF and DRP) was achieved in this document for one light incident direction (θ=24°and ϕ=60°). Their light transmission distribution functions (BTDF) were compared together with their integrated transmission values to assess the differences between the goniophotometers. It was found that qualitatively they are similar, featuring the same topology but quantitatively they differ. The light scattering characteristics remains the same for more specular redirecting samples: the Laser Cut Panel shows the highest coherence followed by the RF sample. The more diffusing sample inhibited less similarity: the DRP acting as an example of sample without coherence between measurements. The reasons for the observed discrepancies for the diffusing sample must be further investigated and will be part of future work, together with using the monitored data in daylight simulations.

ACKNOWLEDGEMENTS

This research was supported by the Swiss National Science Foundation as part of the project "Simulation-based assessment of daylight redirecting component for energy savings in office buildings" (#147053) and Swiss Competence Center for Energy Research (SCCER) – Future and Energy Efficient Buildings and Districts (FEEB&D), Project no. KTI.2014.0119. At the same time I would like show my appreciation to my colleges: Lars O. Grobe, Roland Schregle and Andreas Noback who helped me with the data post processing.

REFERENCES

[1] L. Mohanty, X. Yang, and S. K. Wittkopf, "Optical scatter measurement and analysis of innovative daylight scattering materials," *Sol. Energy*, vol. 86, no. 1, pp. 505–519, 2012.

[2] F. O. Bartell, E. L. Dereniak, and W. L. Wolfe, "The Theory And Measurement Of Bidirectional Reflectance Distribution Function (Brdf) And Bidirectional Transmittance Distribution Function (BTDF)," *Proc. SPIE 0257, Radiat. Scatt. Opt. Syst.*, 1981.

[3] C. Basurto, "On advanced daylighting simulations and integrated performance assessment of complex fenestration systems for sunny climates," EPFL, PhD thesis No. 6425, 2014.

[4] P. Apian-Bennewitz, "New scanning gonio-photometer for extended BRTF measurements," *Proc. SPIE*, vol. 7792, pp. 77920O–1–20, 2010.

[5] L. O. Grobe and S. K. Wittkopf, "Optical characterization of materials and structures for daylighting and PV applications," 2010.

[6] M. Andersen, C. Roecker, and J. L. Scartezzini, "Design of a time-efficient video-goniophotometer combining bidirectional functions assessment for transmission and reflection," *Sol. Energy Mater. Sol. Cells*, vol. 88, no. 1, pp. 97–118, 2005.

[7] J. C. Stover, *Optical scattering: measurement and analysis*, vol. 2. SPIE optical engineering press Bellingham, WA, 1995.

EVALDRC: A TOOL FOR ANNUAL CHARACTERISATION OF DAYLIGHT REDIRECTING COMPONENTS WITH PHOTON MAPPING

R. Schregle, C. Bauer, L. O. Grobe; S. Wittkopf

Lucerne University of Applied Sciences and Arts, Technikumstrasse 21, CH-6048 Horw

ABSTRACT

Annual simulation is a significant indicator of a daylight redirecting component's performance, since it accounts for seasonal variations in daylight availability as well as the system's response under such conditions.

This study details the simulation of a representative redirecting component using a 3D forward raytracing technique to assess its annual daylighting performance. We streamline and largely automate this workflow with the EvalDRC tool, a Python script which implements a simulation frontend based on the Radiance photon map, coupled to a postprocessing and evaluation backend.

The redirecting component selected for our case study combines retroreflection with redirection and is designed for optimal daylight availability over the entire year without the need for adjustment. The lamella profile can be mounted in a forward and reversed configuration to combine retroreflection with redirection in the lower resp. upper portions of the fenestration.

We evaluate our simulations visually and numerically as high dynamic range (HDR) renderings and a spatial daylight autonomy (sDA) metric based on climate based sky distributions for Geneva, Switzerland. Our case study satisfies the sDA requirement that 55% of the workplane receives an illuminance exceeding 300 lux during 50% or more of the occupancy hours for a whole year. In addition, we propose the msDA, a detailed monthly breakdown of the sDA, for which the criteria are specifically met in the months March–September, while a minimum of 32% is predicted for December.

Our results demonstrate the effectiveness of photon mapping for this application, and that the simulation accurately predicts the redirecting component's expected seasonal behaviour for multiple solar angles and sky configurations. This applies in particular to complex redirecting systems which cannot be reliably simulated with a backward raytracer at reasonable computational cost.

Keywords: raytracing, photon mapping, redirection, spatial daylight autonomy

INTRODUCTION

The accurate simulation of daylit interiors is essential in assessing a building's performance in the context of energy saving potential through daylight autonomy. Raytracing techniques have proven to be expedient in this application as they accurately model the propagation of light within a typical office environment.

Forward raytracing from the light sources is particularly effective at modelling redirecting components for sun shading and glare reduction, which can dramatically affect daylight

availability. To this end, a photon mapping implementation has recently been integrated into the RADIANCE lighting simulation system [1].

Analyses are typically performed for an entire year (or half-year, due to symmetry) to account for temporal variations in solar irradiance and sky distribution, and can be reduced to a scalar metric such as the spatial daylight autonomy (sDA) [2].

The ability to quantify the contribution of each light source (i.e. solar altitude or sky patch) to the interior irradiance is essential to annual daylight simulation. RADIANCE's *rcontrib* tool computes and tabulates these contributions in a single raytracing pass for all sources [3], thus establishing an elegant and efficient workflow. This functionality is now also supported by the RADIANCE photon map via *contribution photons* to efficiently quantify the behaviour of specular redirecting components under seasonal variations.

METHOD

Contribution Photon Map

Photon mapping implements a Monte Carlo simulation of light "particle" transport and its interaction with the simulated geometry. Light source contributions are deposited on the geometry via the photons, which are emitted from the sources (combined annual sun positions and Tregenza sky patches) and then probabilistically scattered or absorbed by surfaces based on their material characteristics (see figure 1). This efficiently accounts for the specular reflections (caustics) fundamental to a redirecting component's behaviour.

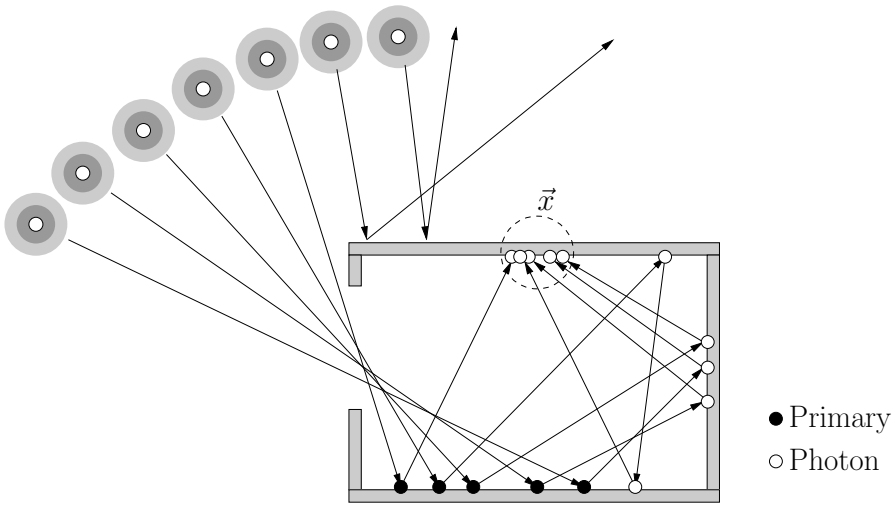

Figure 1: Photons along a path emitted from a light source reference their corresponding primary hitpoint, which in turn refers to its emitting light source. The contribution from each source to the irradiance at point $\vec{x}$ is then evaluated by a modified density estimate for a number of nearby photons around $\vec{x}$.

Each photon is characterised by its position $\vec{x}_p$ (hitpoint during forward raytracing), flux ϕ_p (energy in watts), and an index to its primary hitpoint (not stored as a photon) which identifies the emitting light source l_p. Note that a primary is multiply referenced by all photons it spawns along its path.

The contributions of each light source to the irradiance at a point $\vec{x}$ are then evaluated

by a modified photon density estimate [4]. We first locate the N nearest photons around $\vec{x}$, then collect the flux ϕ_p of each photon into a "bin" corresponding to its emitting light source l. This accumulated flux is then divided by the area defined by the search radius r containing the found photons, to obtain the irradiance E_l contributed by source l:

$$E_l(\vec{x}) \approx \sum_{i=1}^{N} K(\|\vec{x}, \vec{x}_{p,i}\|) \frac{\phi_{p,i}}{\pi r^2} \qquad \forall i : l_{p,i} = l,\ \|\vec{x}, \vec{x}_{p,i}\| \leq r, \tag{1}$$

where K is a normalised weighting function based on the photon's distance to $\vec{x}$.

Spatial Daylight Autonomy

The EvalDRC tool implements the spatial daylight autonomy (sDA) metric, which quantifies the daylight availability in both spatial and temporal dimensions [2]. The sDA specifies the percentage of a workplane area receiving sufficient daylight over the course of one year, assuming occupancy hours from 8 am to 6 pm. In addition, we also evaluate the daylight autonomy on a monthly basis for our case study, which we refer to as the msDA.

In typical illuminance calculations on a sensor point grid, a point is considered to be sufficiently illuminated if it receives 300 lux during at least 50% of the given time period. sDA values >55% represent a *nominal*, values >75% a *preferred* daylight sufficiency.

Annual Simulation Workflow with EvalDRC

Annual daylight simulations are traditionally performed with a daylight coefficient method [5]. A coefficient can be a rendering of the scene, illuminated by only one sky patch with normalised radiance, or an irradiance value for a sensor point. Coefficient accumulation, weighted by sky patch radiances, then produces the final result. Descriptions of these simulations with RADIANCE can be found in [6] and [7]. The sky patch radiances can be determined from actual weather data using the Perez sky model.

The direct sunlight contribution can be integrated by distributing the solar radiance among several neighbouring sky patches, but this is not appropriate for the simulation of redirecting systems which exhibit highly localised peaks, thus being very sensitive to the incoming light direction. Further subdividing the 146 Tregenza sky patches by small powers of 2 (usually 2^2 or 2^4) does not effectively eliminate this accuracy loss. McNeil [8] therefore proposed an extension which introduces a separate, also matrix based, calculation with a new solar vector derived from an extremely fine sky patch subdivision.

In contrast, the EVALDRC frontend uses the Tregenza model only for the hemispherical sky radiance distribution. Direct sunlight is simulated via separate 0.5° RADIANCE source primitives (see figure 2). The tool handles the addition of cumulative sun primitives automatically dependent on the chosen time and location settings.

A simulation with EVALDRC consists of the following steps:

1. *Sky configuration:* Setting up cumulative sun primitives and determining sky patch and solar radiance distributions for the chosen location and time interval settings
2. *Calculation:* Generating the photon maps and determining the separate sky patch and sun contribution coefficients
3. *Accumulation:* Superposition of the coefficients scaled by the corresponding sky patch and solar radiances to produce final results (sensor point irradiance values or

Figure 2: Sky model used in common annual RADIANCE *simulations using subdivided Tregenza patches (left); the solar radiance is distributed over the three nearest patches. The* EVALDRC *sky model (right) uses the pure Tregenza patches for the sky hemisphere, and an additional accurate 0.5° angle source primitive for the sun.*

HDR renderings) for each timestamp

4. *Reduction:* Applying daylight metrics to the results to derive characteristic parameters describing the daylight perfomance of the simulated scene

The new frontend follows a modular concept, making it suitable for a wide variety of tasks, e.g. automated annual runs or the analysis of individually chosen time periods. Coefficients may be repeatedly evaluated with different sky and solar radiance distributions without additional photon tracing. Several sky models are offered, either based on generic CIE formula or weather-data driven Perez skies. Both HDR renderings and workplane irradiance values including graphical representations can be generated.

The drawback of the method is a higher calculation effort and a somewhat reduced flexibility for repeated coefficient evaluation. Due to the use of exact sun primitives, the generated coefficients are fixed to the chosen time and interval settings.

Case Study

Our case study is performed in a standard 6×6m room located in Basel, Switzerland. The redirecting component is mounted in a single south-facing window which spans the entire width of the room. All room surfaces have a reflectance of 30%.

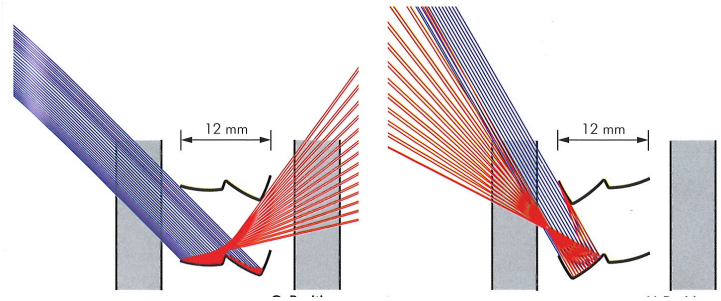

Figure 3: RETROLuxTherm retroreflecting blinds, patented by Helmut Köster. The upper portion of the fenestration redirects light towards the ceiling (left), while the lower portion retroreflects (right). Note the lamella is simply reversed. Reprinted with permission from [9].

The redirecting component for our case study is shown in figure 3. Lamellae are mounted within a double glazing in a forward and reversed configuration to effect retroreflection in the lower fenestration (1-1.75m height) and redirection in the upper fenestration (1.75-2.75m height) via an integrated lightshelf [9].

RESULTS

Figure 4 shows an excerpt from a series of 26 HDR renderings of a half-annual simulation of our case study scripted with EvalDRC using 100M photons. The sky radiance corresponds to a CIE clear sky model for consistency. Forward raytracing and accumulation of contributions for 26×600×400 pixels took 40 resp. 260 minutes on 10 cores.

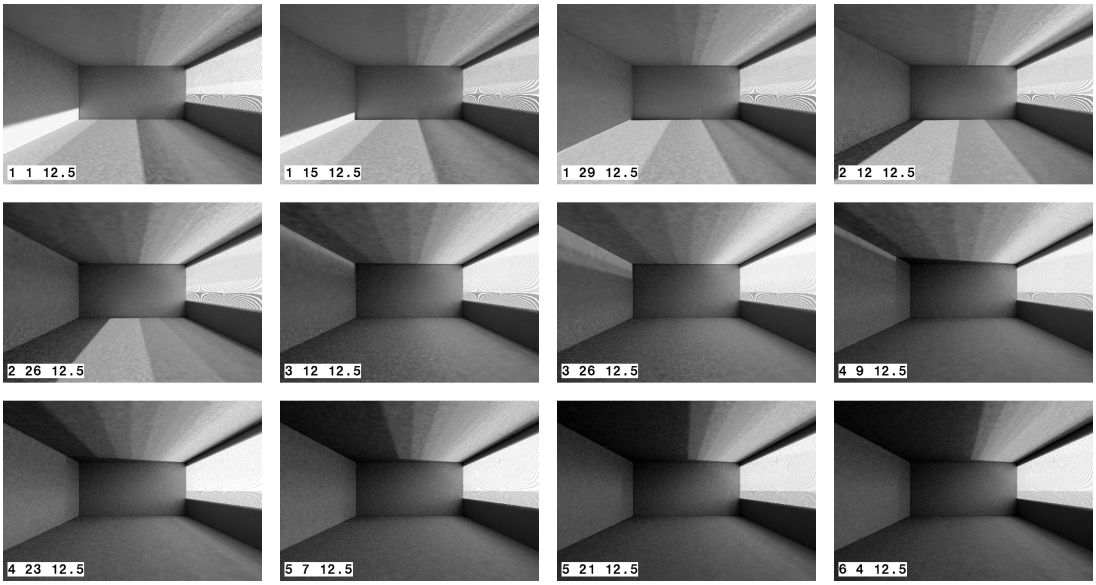

Figure 4: Renderings of our case study for a half year (January to June) at biweekly intervals for midday (12:30pm). Timestamps are in month-day-hour notation.

The redirecting component's behaviour as a function of solar angle is readily apparent. Redirection towards the ceiling can be observed at all times, thus maintaining a high degree of daylight penetration. Transmission, on the other hand, occurs at low solar angles until March, before transitioning into retroreflection at high solar angles.

Table 1 lists the sDA as predicted by EvalDRC with a Perez sky model based on weather data for Geneva, CH, together with the monthly values. The latter yield a more detailed analysis to identify problematic intervals which are subsumed under the annual value. Note that by definition, the annual sDA is not the average of the monthly values.

	Month												**Year**
	1	2	3	4	5	6	7	8	9	10	11	12	
(m)sDA [%]	61	85	100	100	100	100	100	100	100	98	69	32	100

Table 1: Monthly and annual spatial daylight autonomy for our case study.

Our case study predicts that the system performs well throughout the year in providing sufficient daylight on the workplane. Even during winter, the msDA is still above the minimum recommendation of 55% (except for December, for which unseasonably low solar radiation was recorded). Glare evaluation was deliberately excluded, as it demands a more detailed analysis also in terms of applicability of the corresponding annual sunlight exposure (ASE) metric [2] and its various parameters.

CONCLUSION

We have presented a method to efficiently simulate and evaluate the annual performance of redirecting components using our photon mapping implementation embedded in the EvalDRC scripting environment. The combination of visual and numeric analysis in the form of renderings, irradiance graphs, and our proposed monthly sDA metric provides an efficient and powerful planning tool to aid in optimising a redirecting system's annual daylighting performance.

We will continue developing EvalDRC to include the annual sunlight exposure (ASE) as an additional metric. Once in routine use, we shall extend the tool's application spectrum to compare various DRCs for their performance in different locations and urban settings.

ACKNOWLEDGEMENTS

This research was supported by the Swiss National Science Foundation as part of the project "Simulation-based assessment of daylight redirecting components for energy savings in office buildings" (SNSF #147053). We also thank our colleague, Andreas Noback, for beta testing of EvalDRC and for modelling the case study geometry.

REFERENCES

1. Schregle, R. Development and integration of the radiance photon map extension. Technical report, Lucerne University of Applied Sciences and Arts, Feb. 2015.
2. Heschong, L., van den Wymelenberg, K., Andersen, M., Digert, N., Fernandes, L., Keller, A., Loveland, J., McKay, H., Mistrick, R., Mosher, B., Reinhart, C., Rogers, Z., and Tanteri, M. Approved Method: IES Spatial Daylight Autonomy (sDA) and Annual Sunlight Exposure (ASE). IES standard LM-83-12. ISBN: 978-0-87995-272-3.
3. Ward, G. J., Mistrick, R. G., Lee, E. S., McNeil, A., and Jonsson, J. C. Simulating the daylight performance of complex fenestration systems using bidirectional scattering distribution functions within radiance. Technical Report LBNL-4414E, Lawrence Berkeley National Laboratory, Jan. 2011.
4. Silverman, B. W.: *Density Estimation for Statistics and Data Analysis*. Chapman & Hall, London, 1986.
5. Bourgeois, D., Reinhart, C., and Ward, G.: Standard daylight coefficient method for dynamic daylighting. *Building Reserach & Information*, 36:68 – 82, 2008.
6. Jacobs, A. Understanding rcontrib, 2010.
7. McNeil, A. The three-phase method for simulating complex fenestration, 2010.
8. McNeil, A. The five-phase method for simulating complex fenestration, 2013.
9. Köster, H.: *Daylight Modulation*. WITAG-Verlag, 2015. ISBN: 978-3-00-048400-1.

USING A PATTERN SEARCH ALGORITHM TO IMPROVE THE OPERATION OF A DAYLIGHT HARVESTING SYSTEM

A. Tsangrassoulis[1], L. Doulos[2], F. Topalis[2]

1. Dept. of Architecture, University of Thessaly, Pedion Areos, 383 34 Volos, Greece
2. Lighting Lab, National Technical University of Athens, Heroon Politechniou 9, 157 80 Zografou, Greece

ABSTRACT

Daylight exploitation represents the cornerstone of any strategy aiming at reducing energy consumption in office buildings. On the level of design , this can be achieved by adjusting the properties and dimension of the façade openings together with a possible increase in the daylight zone, while on the equipment level, mainly by adopting daylight harvesting systems . The structure of these consists of a photosensor (which is usually placed on the ceiling) and a controller regulating the operation of the luminaires based on a control strategy (usually closed loop). Its main objective is to maintain the lighting levels on the working at the design value. The position of the sensor on the ceiling presents a problem. The ratio of the ceiling sensor illuminance to the one at a corresponding point on the working surface is not constant during daytime, and this may result in an erratic operation. Increasing the distance of the photosenor from the opening (in side-lit spaces) and/or reducing its field of view (FOV) the control strategy approximates the ideal operation but energy savings are reduced.

Usually, manufacturers provide some recommendations regarding the distance of the photosensor from the opening in an effort to avoid the opening being in the sensor's FOV (closed loop control algorithm). However, in many cases, the exact positions of the furniture are not known during the design phase and thus the sensor is placed at the center of the controlled zone in an effort to increase the area with total illuminance larger than the design one (i.e 500 lux). Does this position represent the best option? Such a question can be answered through a parametric analysis for a number of variables, using simulation, a tedious and time-consuming process. In the present work an optimization methodology is examined , combining Genopt and Radiance using very basic information for the sensor, investigating if it can ensure a better solution than what is suggested by common practice. Inputs are the photosensors' FOV, their orientation and their position. The methodology is trying to minimize an objective function which depends on a) the lighting energy achieved and b) the percentage of the working surface with total illuminance more than the design one, for 90% of the working hours (spatial Lighting Adequacy). Results show that the optimization procedure concerning photosensor placing is time consuming without results differing greatly from those achieved through common practice.

Key words: Daylight, Dimming, Lighting

INTRODUCTION

Lighting energy consumption represents a significant percentage of a building's energy balance [1, 2] and daylight exploitation is an essential strategy for increasing energy savings in office buildings. Among various existing daylight dimming systems, a closed-loop one using the integral reset algorithm [3] is quite simple in its use and in a number of systems a single photosensor can be directly connected to a number of proper ballasts, making the solution cost effective. Since achieving the design illuminance in the space with maximum

energy savings is antagonistic, the proper position of the photosensor has to be estimated. Usually the sensor is placed at the center of the controlled zone. Integral reset is quite a common algorithm adopted by many manufacturers. The signal produced by the photosensor which is located on the ceiling is kept constant and equal to the signal during the night-time calibration procedure. The operational equations of this algorithm are the following [4] :

$$S_T(t)= S_{Edesign} \quad (1)$$

Where $S_T(t)$ is the time dependent signal produced by the photosensor while $S_{Edesign}$ is the signal produced during night-time calibration. During day-time operation the photosenor signal is the sum of daylight $S_D(t)$ and electric $S_E(t)$ light components . Thus

$$S_T(t)= S_D(t)+S_E(t)= S_D(t)+\delta*S_{Edesign} \quad (2)$$

Where δ is the fractional output of the lighting system. $\delta=1$ represents full light output and δ_{min} the minimum one. Combining the above equations, the fractional output can be calculated as follows:

$$\delta=1-(S_D(t)/S_{Edesign}) \quad (3)$$

For this study a linear relationship between fractional input power f_P and fractional light output δ was used. When the minimum lighting output is achieved (δ_{min}), there is a minimum power input f_{Pmin}. Both values depend on the type of the ballast. The relation between power f_P and δ is described by the following equations :

$$\text{If } \delta<\delta_{min} \text{ then } f_P=f_{Pmin} \quad \text{else} \quad \text{If } \delta_{min}<=\delta \text{ then } f_P=(\delta+(1-\delta)*f_{Pmin}-\delta_{min})/(1-\delta_{min}) \quad (4)$$

For the present calculation, a value of 0.1 was selected for f_{Pmin} while a value of 0.05 for δ_{min}.

The lighting levels on the working surface, when daylight is present, is given by the relationship

$$I_T(t)= I_D(t)+ I_{Edesign} * (1- S_D(t)/S_{Edesign}) \quad (5)$$

Where I_T is the total illuminance, I_D is the illuminance due to daylight and $I_{Edesign}$ the design illuminance. Sensor position and FOV affect $S_D(t)$ and $S_{Edesign}$ and hence lighting (δ) and power (f_P) fraction. The aim of the paper is to present an optimization framework capable of estimating a near optimum position for a given sensor using as criteria the maximization of energy savings together with the working surface area with $I_T(t)>= I_{Edesign}$.

OPTIMIZATION SCHEME

The use of global optimization methods, though not suitable for every case, can explore large regions of possible solutions when trying to find the best values for a set of variables which will minimize an objective function. There is a large number of optimization methods (pattern search, genetic algorithms etc), but when these are used in building design problems [5] there are some requirements that have to be met, such as the existence of the non-analytic expression of the objective function together with time consuming simulations. In the present paper, the optimization problem was solved using a hybrid approach, with Particle Swarm Optimization for global search and Hooke-Jeeves for its proved convergence properties. This approach can handle local minima problems more efficiently, since Hooke-Jeeves is strongly depended on the smoothness of the objective function.

While many studies [6-9] have been realized when examining techniques and systems in an effort to increase lighting energy savings, there is a small number of studies dealing with the photosensor, which are focused on the optimization of these systems' performance [10]. The aim of this paper is to examine if an optimization method can be used during the early design of the building's systems in order to optimize the position of a photosensor for an integral reset dimming system. A theoretical model of the system is used but the same methodology can be utilized for real systems as well. The simulated photosensor has an ideal cosine spatial sensitivity and is located at a centre of a small black sphere with an opening. The size of the opening determines the sensor's field of view while the direction can be altered by adjusting rotation around two axes as presented in the following graph.

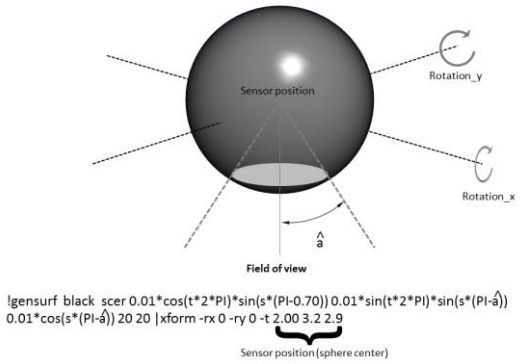

Figure 1. Schematic representation of the examined photosensor.

It is evident that the sensor's FOV is geometrically modified by adjusting the solid angle formed by the hole. Implementation of the optimization procedure was straightforward using Genopt [11]**.** Genopt is designed to minimize the value of an objective function by using user-selected parameters. This function was defined as follows:

$$OF=2\text{-}ESP - sLA \quad (6)$$

Where ESP is the energy savings percentage while the parameter sLA (spatial Lighting Adequacy) is similar to spatial Daylight Autonomy representing the percentage of the working surface where the lighting levels (from daylight and artificial lighting) is larger than the designed value (i.e 500 lux) by at least 90% for the period of the analysis. The parameters used are the coordinates of the sensor on the ceiling together with its axis rotation and field of view. Operation schedule is between 8:00-18:00 totaling 3650 hours annually, for Athens, Greece climatic file. In side lit spaces, any increase in the distance between sensor and opening reduces ESP and increases sLA.

A batch file was created and used as the simulation program. Its output is a delimited file with ESP and sLA values which is used by GENOPT to evaluate the objective function. The batch file contains commands: a) for reading the input file (sensor position, rotation, FOV) b) for creating sensor radiance files c) for running a simulation with artificial lighting to calibrate the sensor, d) for running the three phase method [12] e) for elaborating the simulation results and for writing the results in the output file. Calibration is performed by calculating the average illuminance over a grid on the working surface, together with the sensor illuminance. Depending on the design illuminance selected (500 lux in our case), sensor illuminance ($S_{Edesign}$) is adjusted accordingly.

The room that was used for the simulations is a typical space in an office building with dimensions of 4 x 5.5 x 2.8 m with one external façade**.** The electric lighting system consisted of four ceiling recessed fluorescent lamp (T26 2x36W) luminaires in a uniform layout. The

installed power was 12.9 W/m^2 while the average maintenance lighting levels on the working surface (0.8 m height) were 579 lux with 0.7 uniformity (minimum to average value). Since the lighting system is inside the perimeter zone as this is defined by EN 15193-2007 [13], it can be controlled with one sensor. Wall, ceiling and floor reflectances are 0.55, 0.8 and 0.3 accordingly while glazing transmittance is 0.73. External shading for the south oriented façade (overhang with dimensions 0.8 m x 4 m). Initially, hourly sensor illuminances from the batch simulation file were compared with results from DAYSIM [14] using the same geometry in an effort to tune radiance parameters. The following graph presents sensor illuminance (FOV 2x30^0) for south orientation at the center (x=2m, y=2.5 m) of the ceiling.

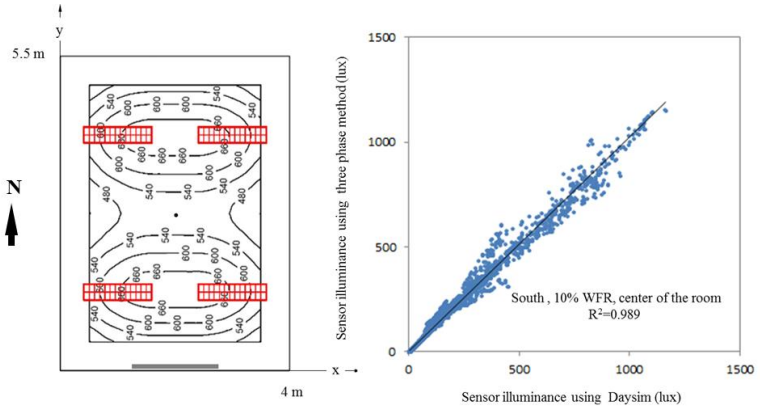

Figure 2. Comparison between sensor illuminance using three phase method against Daysim.

RESULTS

A problem that may affect optimization results is due to the stochastic nature of radiance calculation. Relaxing Radiance parameters, in an effort to speed up simulation, may result in an increase in the variability of calculated lighting energy saving values making the optimization algorithm's convergence harder. Another issue is that set point sensor illuminance as this is estimated during night time calibration can be easily achieved by daylight only, increasing calculated lighting energy savings. It seems that by moving the sensor position away from the opening there is a relatively small decrease in ESP parameter (maximum difference 7% for the narrowest FOV 2x20^0 and south orientation while the difference increases to 21% for north orientation).

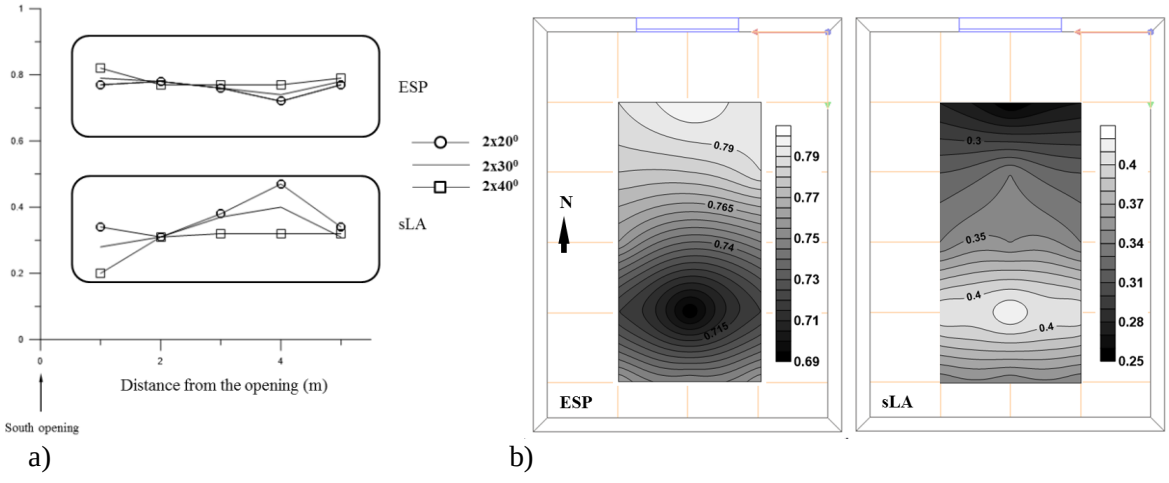

Figure 3: ESP and sLA as a function of the distance from the opening. a) Section, south oriented room 10% WFR. b) bottom view, north oriented room , 10% WFR.

On the other hand, sLA increased with the sensor's distance from the opening and this change is more pronounced for the south oriented room with narrow FOV ($2x20^0$), reaching 34%. Nevertheless, the estimated energy saving percentage is quite increased for both south and north orientation, a characteristic strongly associated with an integral reset algorithm. The objective function (OF) shows limited variance over sensor position since ESP and sLA are antagonistic. The optimization method was used for the south oriented room using a sensor with FOV $2x30^0$ pointing downwards.

A solution was found after 203 simulations indicating that the sensor's optimal position is 4 m away from the window achieving 75% lighting energy savings and 40% spatial lighting adequacy. When the sensor's aiming is considered as a simulation parameter, OF is minimized when the sensor is located 3.5 m and 10^0 tilt along east-west axis, away from the opening. The tilt angle is using a north oriented room (10% WFR) , the optimal solution (ESP=0.78, sLA=0.34) was achieved when the sensor's position is located 2 m away from the opening with 15^0 tilt. Along east –west axis the optimization process took approximately 45 mins in an Intel core i7-3520M processor.

CONCLUSIONS

Optimization methods can be used during the design phase so as to identify and estimate the parameters involved with the dimming system's performance. The definition of the objective function is quite crucial and some expert judgment is needed to simplify the optimization problem and reduce the size of the solution search space. The following main observations could be made:

1) The simulation program has to ensure the smoothness of the objective function. Since Radiance three phase method was used, proper selection of its parameters is crucial as they affect accuracy, processing time and convergence.

2) The optimization process was time consuming using approximately 200 discreet simulations. Judging from the results achieved, the solution that is suggested by common practice (sensor placement in the center of the controlled zone) differs in terms of energy savings by less than 3% from the optimal one (south oriented room). The optimal sensor position varied between 2 m (north oriented room) and 3.5 m (south oriented room) with 10^0 and 15^0 sensor tilt respectively and $2x30^0$ FOV.

3) Spatial lighting adequacy (sLA) can be used to characterize dimming systems' performance and complements energy savings.

This research has been co-financed by the European Union (European Social Fund – ESF) and Greek national funds through the Operational Program "Education and Lifelong Learning" of the National Strategic Reference Framework (NSRF) - Research Funding Program: **THALES**. Investing in knowledge society through the European Social Fund.

REFERENCES

[1] Li D.H.W, Mak A.H.L., Chan W.W.H., Cheng C.C.K. “Predicting energy saving and life-cycle cost analysis for lighting and daylighting schemes”. Int. J. of Green Energy 2009, 4, 359-370.

[2] Danny H.W. Li, K.L. Cheung, S.L. Wong, Tony N.T. Lam. “An analysis of energy-efficient light fittings and lighting controls”. Applied Energy 2010, 87 2, 558–567.

[3] F. Rubinstein et al., "Improving the Performance of Photo Electrically Controlled Lighting Systems," J Illum Eng Soc, 1989, pp. 70-94

[4] A. Bierman et al., "Characterizing Daylight Photosensor System Performance To Help Overcome Market Barriers," J Illum Eng Soc, 2000, pp. 101-115

[5] Machairas V, Tsangrassoulis A., Axarli K., Algorithms for optimization of building design: A review, Renewable and Sustainable Energy Reviews, 31, 2014, 101–112.

[6] Doulos, L., Tsangrassoulis, A., Topalis, F.V. “The role of spectral response of photosensors in daylight responsive systems”. Energy and Buildings 2008, 40, 588–599.

[7] Mistrick R., Thongtipaya J. “Analysis of daylight photocell placement and view in a small office”. J Illum Eng Soc 1997, 26, 2, 150-160.

[8] Mistrick R., Sarkar A. “A study of daylight-responsive photosensor control in five daylighted classrooms”, Leukos 2005, 3, 1, 51-74.

[9] Ranasinghe S, Mistrick R. “A study of photosensor configuration and performance in a daylighted classroom space”. J Illum Eng Soc 2003, 32, 2, 3–20.

[10] Doulos L., Tsangrassoulis A., Topalis F.V., Multi-criteria decision analysis to select the optimum position and proper field of view of a photosensor, Energy Conversion and Management 86 (2014) 1069–1077

[11] Wetter M. GenOpt, generic optimization program version 3.1. Building technologies program, simulation research group, Lawrence Berkeley National Laboratory, 2008.

[12] Andrew McNeil, Eleanor Lee, “A validation of the Radiance three phase simulation method for modeling annual daylight performance of optically complex fenestration systems, Journal of Building Performance Simulation, Vol. 6, Issue 1, 2013.

[13] EN 15193:2007, Energy performance of buildings. Energy requirements for lighting,2007.

[14] http://daysim.ning.com/

COMPARATIVE ANALYSIS OF A PASSIVE AND ACTIVE DAYLIGHT REDIRECTING BLIND IN SUPPORT OF EARLY STAGE DESIGN

Samson Yip[1]; Yuxiang Chen[1]; Andreas Athienitis[1]

1: Concordia University; 1455 de Maisonneuve West; EV6.159; Montreal, QC; H3G 1M8; Canada

ABSTRACT

A simulation case study is performed for a high-performance multi-storey open-plan double-perimeter zone office building in Golden, USA (40°N, 105°W) to compare the relative daylighting illuminance performance of passive and active daylight redirecting blinds. Key design parameters such as location/climate, glazing properties, building depth, façade orientation, window to wall ratio, and window head height are tested in different configurations to examine their effects on the daylighting illuminance in the office space. The spatial daylight autonomy metric $sDA_{300/50}$, defined as the percentage of the illumination analysis points in a space for which the daylight autonomy threshold of 300 lx is attained for more than 50 % of all hours between 08:00 and 18:00, is used to evaluate the annual daylight illuminance sufficiency over the floor area. Since the emphasis in this study is on providing early design stage support, a simplified radiosity model (calibrated with data collected on site) is used which yields an accuracy that is within the range of the uncertainties normally encountered in this early stage of the design process. The results show that for most of the combinations tested, the active blind performs as well as or better than the passive blind.

Keywords: daylight redirecting blinds, spatial daylight autonomy, early stage design, open-plan office space, perimeter zone

INTRODUCTION

Enhanced daylighting use is a promising energy efficiency solution that may significantly contribute to reducing lighting energy use in buildings enhance indoor environmental quality in workplaces. Electric lighting accounts for 12.3 %[1] of total electricity use in offices in Canada. The use of daylighting with controls like automated blinds and electric light switching and dimming contributes to reducing energy consumption [1-3] and can even play a role in reducing HVAC system sizes and peak building power load [4]. Daylighting can also have positive effects on building occupants such as increased productivity, mental functioning and attention, health, mood, and motivation [5-8].

One particular class of daylighting device, daylight redirecting blinds, is designed specifically to increase daylighting levels in buildings in addition to preventing unwanted solar gain and glare. As with all daylighting design, these blinds need to be evaluated on an annual basis in a specific climate to obtain an accurate assessment of their performance. However, because these blinds rely on many parameters such as complex geometry and may require automated controls to achieve their high illuminance performance, their angle-dependent optical characteristics cannot be represented or simulated accurately using the simple tools that are normally used at the beginning of the building design process when rapid assessments of design options are needed. Instead they currently require time- and resource-intensive,

1 http://oee.nrcan.gc.ca/corporate/statistics/neud/dpa/showTable.cfm?type=CP&sector=com&juris=ca&rn=20&page=0

simulation methods – such as the Radiance three-phase / five-phase method with support for bidirectional scattering distribution functions (BSDFs) [9]. These methods require many inputs (some of which are not yet known) and are often not interoperable with typical architectural design software, making them difficult to integrate into existing building design workflows at such an early stage of design [10]. Instead, architects place a high importance on rules of thumb, simple calculations, and simple, easy to learn and use simulation software that supports them in decision-making [11, 12].

Therefore design guidance for these daylight redirecting blinds is proposed in support of design decisions at the beginning of the building design process. As a project progresses from the initial design decisions supported by the proposed design guidance, and as an increasing number of design variables become fixed, more sophisticated tools can be introduced into the design process that parallel the increasing level of detail known of the building design.

METHODOLOGY

Since the emphasis in this study is on providing support to the early design stages of a building project, a simplified radiosity daylighting simulation model is used which yields an accuracy that is within the range of the uncertainties normally encountered in this early stage of the design process. The simulation model is developed to compute annual climate-based daylighting illuminance levels and validated using a case study. The simulation case study was performed for a high-performance multi-storey open-plan double-perimeter zone office building in Golden, USA (40°N, 105°W) to compare the relative daylighting illuminance performance of two types of daylight redirecting blinds. The first blind is passive/static (the LightLouver from LightLouver LLC) and the second is an active/motorized Venetian (the Vision Control from Unicel Architectural) (Figure 1). The blinds are installed in the equator-facing daylighting window, which is positioned above the line of sight of standing occupants. The radiosity model is calibrated using hourly illuminance data obtained onsite and sky irradiance data obtained from the onsite weather station. Sky irradiance data from EnergyPlus Weather files (EPW) is used for the annual simulations. This is used with the Perez model [13, 14] to calculate the illuminance values for the hourly time steps used in the simulations.

The active blind is controlled to maximize daylight transmittance. For each hourly time step, at insolation values of 100 W/m^2 or less (for cloudy skies) at the exterior window surface, the blinds are opened to the slat angle with the highest visible transmittance. At higher insolation values, the transmittance at slat angles from -85° (closed), in increments of 15°, up to the direct sun cut-off angle (maximum open slat angle for which direct sun is blocked) are determined and the blinds are set at the slat angle with the highest transmittance.

Figure 1 Left: LightLouver (Photo: Dennis Schroeder, NREL); right: Vision Control (Photo: Qian Peng)

The daylighting performance is evaluated using the spatial daylight autonomy (sDA) metric [15], which is defined as the percentage of the illumination analysis points in a space for which the daylight autonomy threshold of 300 lx is attained for more than 50 % of all hours

between 08:00 and 18:00 (symbolized as $sDA_{300/50}$.). Two levels of daylight sufficiency are defined in the metric: a "nominally" daylit space attains an $sDA_{300/50}$ of 55 %; and a "preferred" daylit space attains an $sDA_{300/50}$ of 75 %.

The simulation model consists of a typical one-storey cross-section and includes the glazed North and South facades. The North façade view and daylighting windows are surfaces 11 and 12, respectively, in Figure 2. The South façade ones are surfaces 10, and 9, respectively. Key design parameters that relate to building site (climate, and building orientation), building geometry (window to wall ratio, window head height, and building depth), and fenestration (visible light transmittance of windows and blinds) are tested as described in Table 1, and Table 2 to examine their effects on daylighting illuminance in the office space. The results are generalized into simple correlations between these building design parameters and daylight illuminance sufficiency in the space. These correlations form the basis of the design guidance to be used in the early days of the building design process in lieu of simulations.

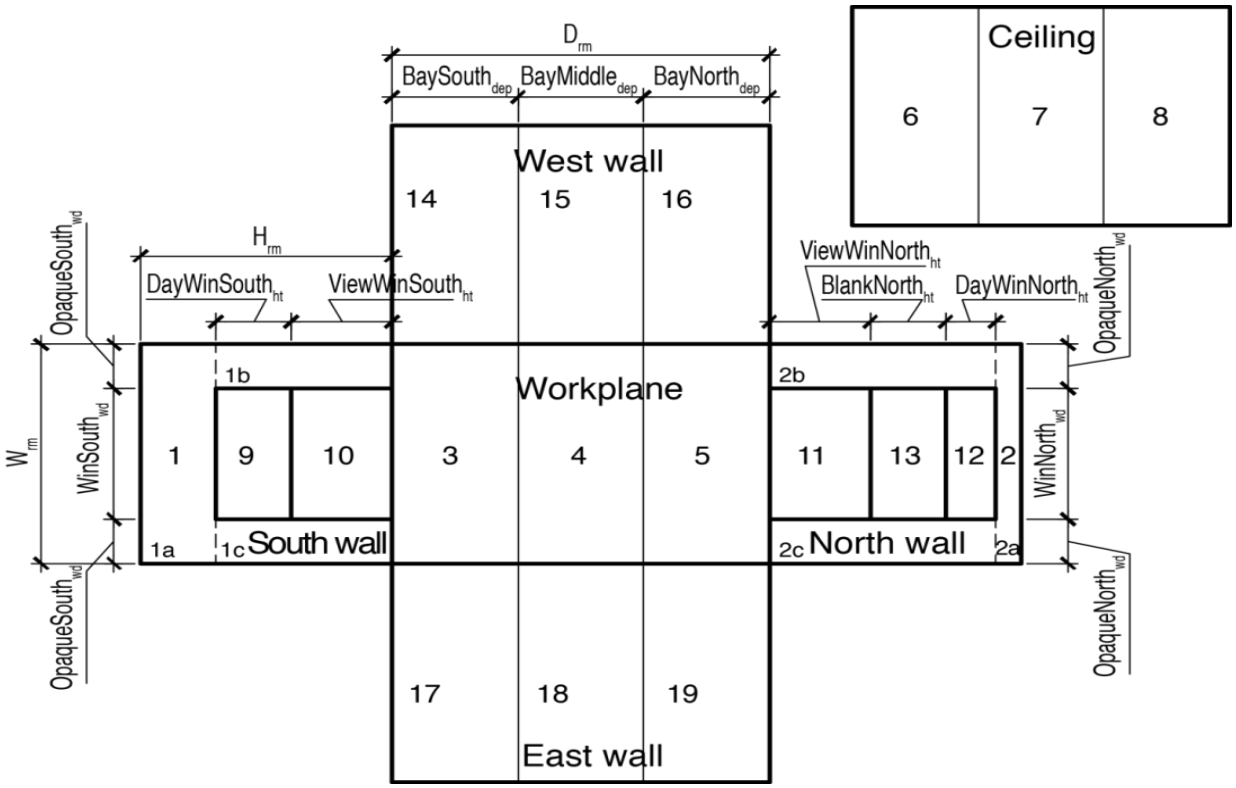

Figure 2: Representative cross-section unfolded, its surfaces labelled, and dimensioned

Parameter	**Values tested**
Building orientation (ψ)	-45°, -30°, -15°, 0, 15°, 30°, 45°
Daylight redirecting blind	LightLouver; Vision Control
Window Visible Light Transmittance	59 % (view window) and 70 % (daylighting window); 68 % (view window) and 76 % (daylighting window)
Building depth (D_{rm})	11 m, 12 m, 13 m, 14 m, 15 m, 16 m, 17 m, 18 m

Table 1: Summary of simulation parameters

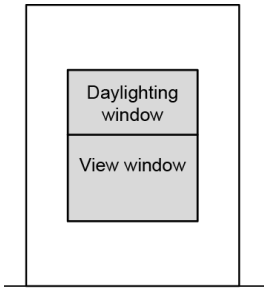

South interior elevation Base bldg

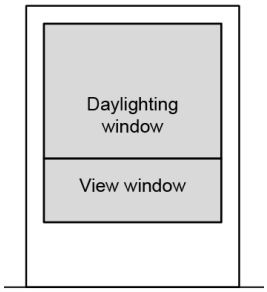

South interior elevation Config. A

Fenestration parameters (Refer to Figure 2)	**Base bldg**	**A**
D_{rm} (m)	18.000	18.000
W_{rm} (m)	3.000	3.000
H_{rm} (m)	3.048	3.048
$WinSouth_{wd}$ (m)	1.829	2.500
$DayWinSouth_{ht}$ (m)	0.914	1.900
$ViewWinSouth_{ht}$ (m)	1.219	0.900
$WinNorth_{wd}$ (m)	1.829	1.829
$DayWinNorth_{ht}$ (m)	0.762	0.762
$ViewWinNorth_{ht}$ (m)	1.219	1.219
$BlankNorth_{ht}$ (m)	0.914	0.914
Window to wall ratio, South façade, WWR_s	0.328	0.589
Window to wall ratio, North façade, WWR_n	0.305	0.305
Window to wall ratio, South daylight window, WWR_{ds}	0.141	0.400
Window to wall ratio, South view window, WWR_{vs}	0.188	0.189
* Window head height, South façade WHH_s (m)	3.048	3.714
* Window head height, North façade WHH_n (m)	3.810	3.810
* since the room cavity below the workplane is not modelled, the height of the workplane must be added to the window heights to obtain the room's WHH; (total room height is 3.963 m)		

Table 2: Schematic elevations (left) and table (right) of fenestration (window to wall ratio and window head height) configurations studied

RESULTS

For all façade orientations and configurations tested, the Vision Control blind daylighting performance is better than or equal to that of the LightLouver – by up to 18 % (Table 3).

In configuration A, the daylighting window is made larger and the window head height is made higher than in the base building. This results in increased all blind / window visible light transmittance (VLT) / orientation combinations attaining $sDA_{300/50}$ values above 55 % making them "nominally daylit" spaces – compared to a best case $sDA_{300/50}$ of 46 % for the base building for Vision Control blind/high VLT windows/$\psi = 15°$ (Table 3).

Furthermore, using the same configuration A, but a different time period of evaluation (August 01 and 02; and February 12 and 13) and timestep (15 min), Chen, Yip and Athienitis [16, 17] show that when thermal performance is taken into account, increasing WWR_{ds} from 14 % to 40 % contributes to a decrease in winter space heating for the Vision Control blind using the high SHGC and high VLT windows (from 9.7 kWh/m facade width to 7.1 kWh/m facade width) while it is practically constant for the LightLouver (from 10.5 kWh/m facade width to 10.1 kWh/m facade width). For space cooling performance, the same increase in WWR_{ds} increases the space cooling load slightly for the Vision Control blind using the low SHGC and low VLT windows (from -1.8 kWh/m facade width to -2.0 kWh/m facade width) and increases it further for the LightLouver (from -1.9 kWh/m facade width to -2.6 kWh/m facade width). Thus, when increasing WWR_{ds} to 40 %, both blinds' daylighting

performance increases equally, but the Vision Control blind has better thermal performance than the LightLouver.

Golden		ψ orientation (°)													
Building depth 18 m		-45		-30		-15		0		15		30		45	
Config. / blind		low VLT	high VLT	low VLT	high VLT	low VLT	high VLT	low VLT	high VLT	low VLT	high VLT	low VLT	high VLT	low VLT	high VLT
base bldg.	LL	28	35	33	41	39	44	39	44	33	44	33	41	28	35
	VC	33	35	39	41	44	44	39	44	39	46	33	41	30	35
A	LL	56	63	61	63	61	63	61	63	61	63	56	63	56	57
	VC	56	63	61	63	61	63	61	63	61	63	61	63	56	57

Table 3: Configuration comparison; $sDA_{300/50}$ [%] (LL is LightLouver; VC is Vision Control)

The maximum building depth for which the entire floor area is nominally daylit is determined for the base building and configuration A, representing a conservative and optimal case. The different orientations reach the nominally acceptable level of daylight sufficiency at different building depths depending on façade configuration and the blind used. This range is reflected in the results in (Table 4).

Golden (low VLT)	**Base building**	**Configuration A**
LightLouver	12.2 m – 14.0 m	18.7 m – 19.3 m
Vision Control	12.8 m – 14.5 m	18.7 m – 19.3 m

Table 4: Base bldg. and configuration A: maximum building depth at which daylighting illuminance is nominally acceptable (taking into account all tested ψ angles)

CONCLUSION

Two different daylight redirecting blinds were investigated in a comparative case study for daylighting performance taking into account design parameters that are important at the beginning of the design process. A simplified radiosity daylighting model was used that is capable of making predictions within the range of accuracy normally encountered in early stage design. A range of orientations, window visible light transmittance values, daylight redirecting blinds, and fenestration configurations was studied using this approach.

Active daylight redirecting blinds performed as well as or better than passive daylight redirecting blinds for the configurations tested. However, other criteria like visual glare and solar heat gain based on climate and orientation may affect blind selection. For example, a relatively simple, low-maintenance passive blind installed on the indoor side of a window may be acceptable for mild, temperate climates but may cause excessive overheating in climates with high cooling load.

The maximum depth of a double-perimeter open-plan space that is nominally daylit varies with orientation, window to wall ratio, window head height, visible transmittance, and daylight redirecting blind. These findings may be used as design guidance at the beginning of the design process when quick sketches and hand calculations are still common for design exploration before the building design has taken shape and the design team commits to developing specific design options and introducing simulation tools into the process.

REFERENCES

1. Bourgeois, D., C. Reinhart, and I. Macdonald, *Adding advanced behavioural models in whole building energy simulation: A study on the total energy impact of manual and automated lighting control.* Energy and Buildings, 2006. **38**(7): p. 814-823.
2. Athienitis, A.K. and A. Tzempelikos, *A methodology for simulation of daylight room illuminance distribution and light dimming for a room with a controlled shading device.* Solar Energy, 2002. **72**(4): p. 271-281.
3. Li, D.H.W. and J.C. Lam, *Evaluation of lighting performance in office buildings with daylighting controls.* Energy and Buildings, 2001. **33**(8): p. 793-803.
4. Li, D.H.W., J.C. Lam, and S.L. Wong, *Daylighting and its effects on peak load determination.* Energy, 2005. **30**(10): p. 1817-1831.
5. Ulrich, R.S., *View through a window may influence recovery from surgery.* Science, 1984. **224**(4647): p. 417-419.
6. Leslie, R.P., *Capturing the daylight dividend in buildings: Why and how?* Building and Environment, 2003. **38**(2): p. 381-385.
7. Edwards, L. and P. Torcellini, *A Literature Review of the Effects of Natural Light on Building Occupants*, 2002, NREL: Golden, Colorado.
8. Heschong, L., *Daylighting and human performance.* ASHRAE Journal, 2002. **44**(6): p. 65-67.
9. McNeil, A. and E.S. Lee, *A validation of the Radiance three-phase simulation method for modelling annual daylight performance of optically complex fenestration systems.* Journal of Building Performance Simulation, 2013. **6**(1): p. 24-37.
10. Horvat, M. and J. Kanters, *Needs of architects regarding digital tools for solar building design*, 2012, IEA: Toronto, Canada; Lund, Sweden.
11. Attia, S., et al., *Selection criteria for building performance simulation tools: Contrasting architects' and engineers' needs.* Journal of Building Performance Simulation, 2012. **5**(3): p. 155-169.
12. Galasiu, A.D. and C.F. Reinhart, *Current daylighting design practice: A survey.* Building Research and Information, 2008. **36**(2): p. 159-174.
13. Perez, R., et al., *Modeling daylight availability and irradiance components from direct and global irradiance.* Solar Energy, 1990. **44**(5): p. 271-289.
14. Perez, R., R. Seals, and J. Michalsky, *All-weather model for sky luminance distribution-Preliminary configuration and validation.* Solar Energy, 1993. **50**(3): p. 235-245.
15. IESNA, I., *LM-83-12 IES Spatial Daylight Autonomy (sDA) and Annual Sunlight Exposure (ASE)*, 2012, IESNA Lighting Measurement: New York, NY, USA.
16. Chen, Y., S. Yip, and A. Athienitis, *Effects of Fixed and Motorized Window Louvers on the Daylighting and Thermal Performance of Open-Plan Office Buildings*, in *3rd International High Performance Buildings Conference* 2014: West Lafayette, Indiana.
17. Chen, Y., S. Yip, and A. Athienitis, *A Case Study on the Daylighting and Thermal Effects of Fixed and Motorized Light Louvers*, in *eSim 2014* 2014: Ottawa, On.

VALIDATION AND PRELIMINARY EXPERIMENTS OF EMBEDDED DISCOMFORT GLARE ASSESSMENT THROUGH A NOVEL HDR VISION SENSOR

Ali Motamed; Laurent Deschamps; Jean-Louis Scartezzini

Solar Energy and Building Physics Laboratory (LESO-PB), Ecole Polytechnique Fédérale de Lausanne (EPFL), CH-1015 Lausanne, Switzerland

ABSTRACT

In spite of an abundant research on visual comfort models and integrated day- and electric lighting systems, the lighting engineering and research community is restricted to the use of ceiling-mounted luminance sensors, which do not faithfully reproduce the visual comfort sensations of building users in day-to-day practice. Moreover, the discomfort glare indices suggested in the past are evaluated through the luminance mapping of visual scenes generated by the way of a laborious High Dynamic Range (HDR) imaging process: this approach cannot be integrated into building automation. On the other hand, mitigation of the electricity demand for lighting by applying 'easy' photometric metrics, such as the luminance monitored from the ceiling, leads mostly to non-optimal situations regarding visual comfort and performance. In order to overcome these issues, a novel embedded HDR vision sensor fitted with a fisheye lens and capable of performing real-time, accurate and reliable luminance mapping together with an assessment of discomfort glare indices, is suggested. This novel device was successfully validated against the Evalglare software and its robustness on an embedded platform for long-term visual comfort assessments was demonstrated. Preliminary experiments were carried-out with two calibrated HDR vision sensors in order to deepen our knowledge regarding visual comfort in an office room of the LESO solar experimental building located on the EPFL campus in Lausanne (Switzerland). These experimental results are beneficial for the design phase of a sun shading and electric lighting control system that will be shortly evaluated on-site within the same occupied office room.

Keywords: Integrated day and electric lighting, high dynamic range vision sensor, discomfort glare indices, Evalglare software, embedded glare assessment, sensitivity analysis.

INTRODUCTION

In modern societies, around 90% of people spend most of their time in buildings. Indoor comfort, such as thermal and visual comfort, plays accordingly a significant role and has a large impact on the inhabitants' health, morale, working efficiency and satisfaction. Moreover, buildings account for more than one-third of total primary energy demand in the Western World and for more than 30% of the CO_2emissions [1]. Thus, there is an urgent demand for introducing practical solutions for mitigating the energy demand while maintaining the users' comfort in the built environment.

Visual comfort and lighting energy demand are fields that are not addressed properly by practitioners in spite of profound progress made by research during the past 30 years. Several metrics for quantifying the discomfort glare sensation, such as the Daylight Glare Index (DGI), the CIE Glare Index (CGI) and the Daylight Glare Probability (DGP), were developed through extensive field monitoring. However, despite of that, 'easy to use' variables, such the vertical and/or horizontal workplane illuminances remain the principal criteria for assessing the performance of daylighting and electric lighting systems. One of the impeding factors for implementation of the very valuable theoretical developments is the absence of an accurate and reliable monitoring device capable of performing luminance mappings of visual scenes,

similar to the human eye. Traditionally, this process is achieved by merging several Low Dynamic Range images captured with different exposure intervals in an attempt to reach a High Dynamic Range (HDR) imaging, capable to handle the sunlight with a deep and dark shadow in the same picture.

Recently, a few field studies were performed to address this issue by means of the traditional approach. Bellia et al. [2] used a classic HDR camera only for evaluation of glare indices (e.g. DGI). In 2010, Van Den Wymelenberg et al. [3] carried out a controlled study involving 18 participants in a daylit single-occupancy office to examine the applicability of 150 visual discomfort predictors. The study showed that the most effective predictor was the average luminance of the glare sources. In 2014 Konis [4] conducted a study in the core zone of a side-lit office building located in San Francisco, California. Subjective measurements of visual comfort were collected using a repeated-monitoring study involving fourteen participants over two weeks under clear sky conditions. The results showed that the discomfort indicators based on luminance contrasts and window luminance were more effective than glare metrics or more basic measurements such as the vertical or horizontal illuminance.

This paper presents the methodology used for the implementation, integration and validation of a novel HDR vision sensor for monitoring of visual comfort indices within office rooms.

METHODOLOGY

The specifications of the vision sensor are presented herein. On the other hand the robustness of the performance and the measurements capability of the device are explained. The validation procedure of the data monitoring by means of the renowned software *Evalglare* [5] is elaborated. Once the reliability of the measurements by the vision sensor was established, a sensitivity analysis of the photometric metrics with respect to its position and orientation was carried-out. In the next step, the main photometric variables were measured from different viewpoints using both HDR vision sensors. This 'on-site' monitoring allows a comparison of visual comfort assessments carriedout for an optimal location of the HDR vision sensor (user's point of view when sitting at his/her desk) with a more convenient one from a practical perspective (HDR sensor mounted on the VDT screen).

(a)  (b) 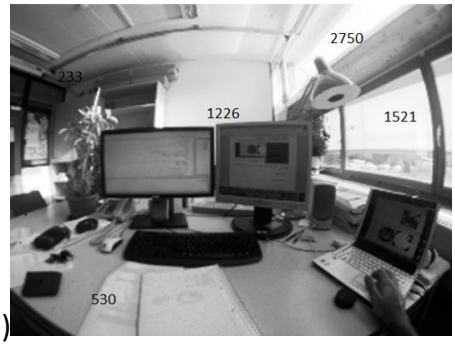

Figure 1: (a) *IcyCAM HDR vision sensor equipped with fisheye lens;* (b) *the captured luminance map*

HDR VISION SENSOR

Thanks to a fruitful collaboration between EPFL/LESO-PB and the Centre Suisse d'Electronique et de Microtechnique (CSEM), a novel embedded HDRI sensor (Figure 1 (a)) was developed and calibrated [6]; the photometric device allows real-time capturing and analysing of luminance maps of visual scenes with considerable accuracy and speed. It offers a 132dB intra-scene dynamic range encoded logarithmically with 149 steps per decade. Each HDR image therefore provides a complete record of the magnitude and spatial variation of the luminance in the field-of-view. Besides, its powerful system-on-chip (SoC) platform (32-bit DSP processor, 500MHz [7]) allows performing concurrent image processing for calculating

discomfort glare indices. Finally, this "artificial retina" was photometrically, spectrally and geometrically calibrated and equipped with fish-eye lens.

EMBEDDED DISCOMFORT GLARE ASSESSMENT

To date, the Evalglare software, a Radiance based tool for glare risks evaluation developed by Wienold [8], constitutes a reference for glare indices assessments. An embedded programme inspired by Evalglare was developed in order to perform a glare indices calculation on the HDR vision sensor. The essential features of the embedded program are: i) its computational efficiency (each cycle takes ~12 second); ii) an accurate image processing in spite of limited embedded RAM memory and iii) a telemetry transmission feature of whole records of a visual comfort analysis over LAN to a remote machine (MATLAB based interface).

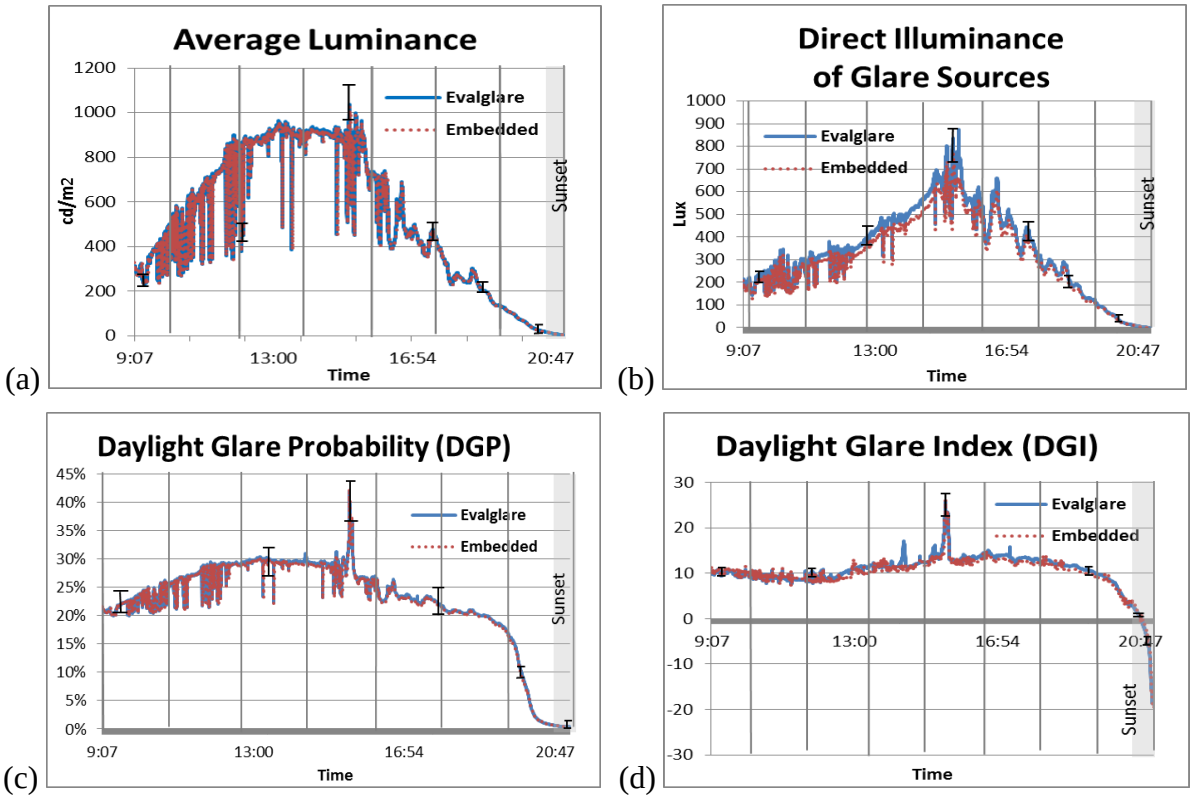

Figure 2: Validation of the HDR vision sensor embedded glare indices calculation versus the Evaglare software [5].

The software was validated through comparison of 5400 measurements captured under clear sky during approximately 18 hours from 9:20AM to 6:10AM on March 16 & 17, 2015; the sensor location is illustrated in Figure 5(b) (reference sensor). As shown in *Figure 2*, a reasonable matching was observed between the photometric variables (average luminance and direct illuminance of the glare sources) and glare indices (DGP and DGI) monitored with the sensor and those calculated with Evalglare. The relative discrepancy for the average luminance, the direct illuminance of glare sources, the DGP and DGI shows RMS values of 0.9%, 8.9%, 2.5%, 6.7% respectively. According to [9], the accuracy (average error) of the HDR vision sensor for daylight conditions with respect to a luminance meter (Minolta LS 110) was estimated around 20%.

PROOF OF ROBUSTNESS

In order to verify the robustness of the functioning of the HDR vision sensor, it was positioned in the location indicated in Figure 4(b) for more than 33 hours; the sun shadings were completely open and the office occupied for regular office tasks during that period. The electric lighting was turned on from 6:45 PM to 8:55 PM on the first day. The day was

partially cloudy and the second day sunny. During the latter, the sun disk was visible by the sensor: very large vertical pupilar illuminances for some moments of the day were accordingly observed. These illuminance values were properly reflected in the DGP (and to some extend in the CGI) while the other indices return values comparable to those monitored for overcast sky conditions. This observation is due to the strong linear relation of the DGP with the vertical pupilar illuminance.

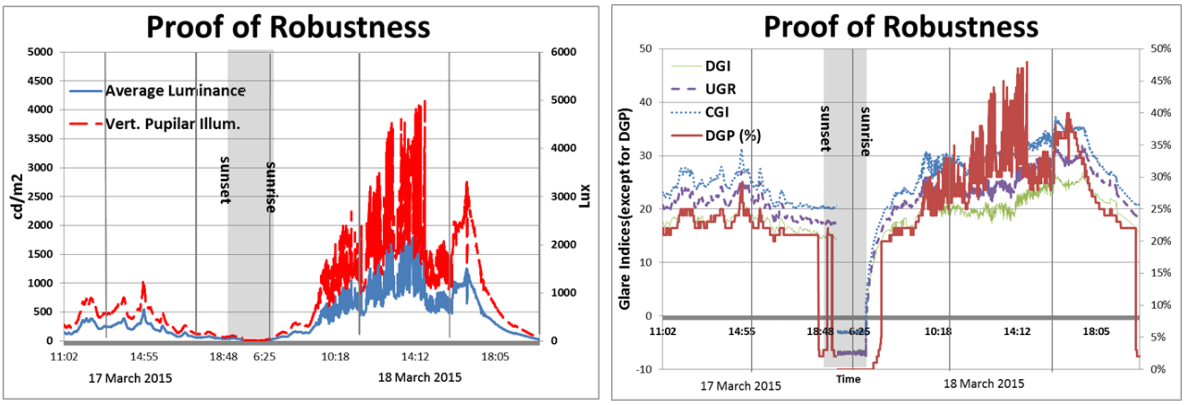

(a) (b)

Figure 3: Proof of functionality robustness of the HDR vision sensor during approx. 33 hours; (a) principal photometric variables: vertical pupilar illuminance (lx) and average luminance (cd/m2); (b) glare indices DGI, UGR, CGI and DGP

PRELIMINARY OBSERVATION

The purpose of these preliminary 'on-site' experiments was to assess the discomfort glare sensations of an office worker by the way of the HDR vision sensor mounted on his/her VDT screen. This study provides with a sound monitoring of the person's visual comfort in order to set up a fuzzy logic controller managing both the daylight and electric light fluxes in an office room. The experiments were carried out in a south-facing office room located in the LESO experimental building on the EPFL campus in Lausanne, Switzerland. Two calibrated HDR vision sensors were used for that purpose, the corresponding 'on-site' monitored photometric variables being coherent in terms of accuracy and reliability with well-known glare calculation software.

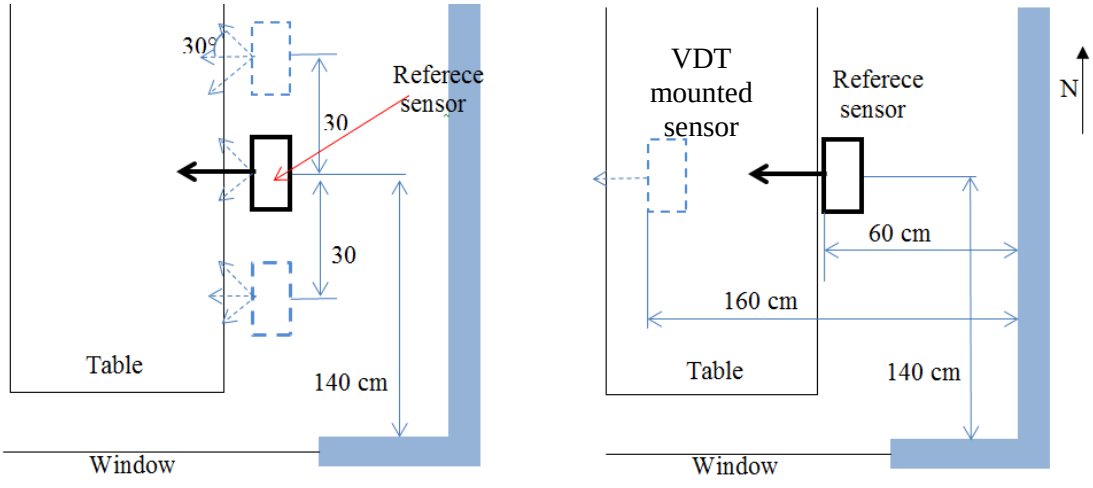

(a) (b)

Figure 4: Top view of the preliminary experimental setups; a) Sensitivity analysis; b) Comparison of visual comfort assessments from two different viewpoints. The solid box and array represent the reference HDR vision sensor.

A sensitivity analysis as well as a comparison of the visual comfort perceived at the desk by the office worker and the one monitored on the VDT screen (Figure 4), were carried out. The 'on-site' monitoring was carried out first by placing the HDR vision sensor in a way that it points toward the default user Field of View (FoV) and by applying translational and angular variations to the second device. Each experiment was performed for at least 15 minutes, including 60 snapshots. The second experimental setup was organised as shown in Figure 4(b) and performed for 12 hours (9:00AM till 9:00PM, 3040 measurements) under a clear sky.

RESULTS

The results show that DGP is less sensitive to a position variation than the average luminance and the vertical pupilar illuminance. On the other hand, the DGP is less sensitive to translational variations with respect to a rotational one. Moreover, the relative variations of the DGP reach a maximal value of *32%* in comparison the reference value. Thus, the DGP of experienced value for a typical user sitting at his desk moving ±30*cm* and ±30° from a reference position/orientation may vary of about ±*32%* around the DGP measured from the reference position/orientation.

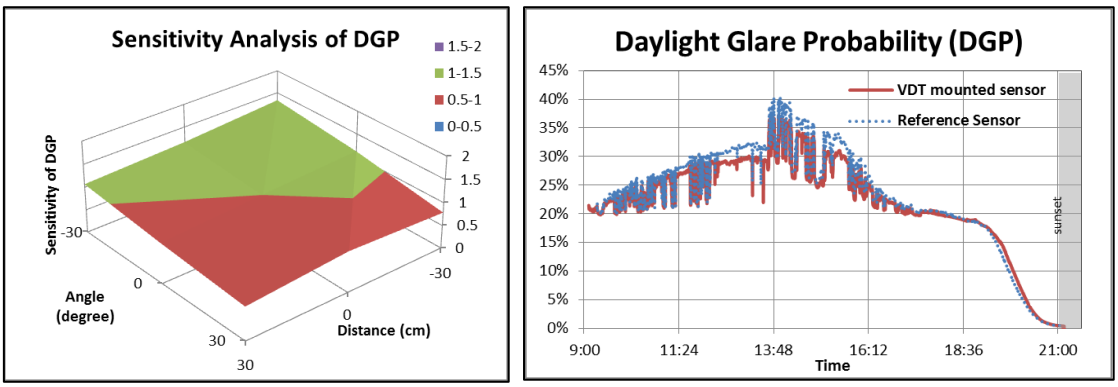

(a) (b)

Figure 5: (a) Sensitivity analysis of DGP with respect to translational and angular displacement; (b) Comparison of DGP measured from two points of view according to the experimental setup of Figure 4(b).

The comparison of the DGP measured from the reference viewpoint (eyes height of an office worker) and the one measured from the VDT screen (dotted line on Figure 5,b) shows that the evaluated glare indices follow a very similar trend; those measured at the VDT screen remains lower to the reference values. The RMS of the relative discrepancy between the two DGP readings sets is close to 11%; the latter is equal to 3.2% for the discrepancy of the absolute DGP values).

DISCUSSION AND CONCLUSION

It goes without saying that the closer the sensor is to the lateral window, higher the recorded photometric variables are. The DGP formula follows a linear function (with $R^2 = 0.98$); it is expected accordingly that the observer experiences visual discomfort sensations in the range of 30% around the values measured from reference point. On the other hand, the sensor placed on the VDT screen sensed in an acceptable way the same photometric variables measured from reference viewpoint (observer eyes). The difference between these two readings is moreover lower if glaring sources are absent of the observer FoV (before 11:00AM and after 4:00PM) as shown on Figure 5(b)).

A novel HDR vision sensor was set into practice for an "on-the-fly" discomfort glare assessment within an office room. A glare index calculation algorithm was set up and embedded on the device for this purpose. The sensor is able to achieve visual comfort

monitoring accurate enough to be compared to Evalglare software calculations on a PC. The device is accordingly ready for integration in a smart building control system for the optimisation of visual comfort in an office room and minimizing the lighting energy demand.

ACKNOWLEDGMENTS

The authors would like to thank Ms. Sigolène Bechetoille Pangaud (CSEM) for her important contribution to this work. This work was fully supported by Swiss Competence Centre for Energy Research (SCCER), in the framework of the Future Energy Efficient Building & Districts (FEED&B) project.

REFERENCES

[1] P. H. Shaikh, N. B. M. Nor, P. Nallagownden, I. Elamvazuthi, and T. Ibrahim, "A review on optimized control systems for building energy and comfort management of smart sustainable buildings," *Renew. Sustain. Energy Rev.*, vol. 34, pp. 409–429, Jun. 2014.

[2] L. Bellia, A. Cesarano, G. F. Iuliano, G. Spada, and N. Federico, "HDR Luminance Mapping Analysis System for Visual Comfort Evaluation," no. May, pp. 5–7, 2009.

[3] K. Van Den Wymelenberg, M. Inanici, and P. Johnson, "The Effect of Luminance Distribution Patterns on Occupant Preference in a Daylit Office Environment," *J. Illum. Eng. Soc. North Am.*, vol. 7, no. 2, pp. 37–41, 2010.

[4] K. Konis, "Predicting visual comfort in side-lit open-plan core zones: Results of a field study pairing high dynamic range images with subjective responses," *Energy Build.*, vol. 77, pp. 67–79, Jul. 2014.

[5] J. Wienold and J. Christoffersen, "Evaluation methods and development of a new glare prediction model for daylight environments with the use of CCD cameras," *Energy Build.*, vol. 38, no. 7, pp. 743–757, Jul. 2006.

[6] A. Borisuit, M. Münch, L. Deschamps, J. Kämpf, and J.-L. Scartezzini, "A new device for dynamic luminance mapping and glare risk assessment in buildings," *Proc. SPIE*, vol. 8485, p. 84850M–84850M–9, 2012.

[7] P. Rüedi, P. Heim, S. Gyger, and F. Kaess, "An SoC Combining a 132dB QVGA Pixel Array and a 32b DSP / MCU Processor for Vision Applications," in *IEEE International Solid-State Circuits Conference*, 2009, pp. 46–48.

[8] J. Wienold, "EvalGlare- A Radiance Based Tool for glare evaluation," 2012.

[9] A. Borisuit, J.-L. Scartezzini, and A. Thanachareonkit, "Visual discomfort and glare rating assessment of integrated daylighting and electric lighting systems using HDR imaging techniques," *Archit. Sci. Rev.*, vol. 53, no. 4, pp. 359–373, Nov. 2010.

SHADING DEVICE CONTROL: EFFECTIVE IMPACT ON DAYLIGHT CONTRIBUTION

B. Paule[1]; J. Boutillier[1], S. Pantet[1]

1: Estia SA, EPFL Innovation Park, Lausanne, Switzerland

ABSTRACT

This paper presents the results of a project funded by the Swiss Federal Office for Energy that focused on the effective use of movable shading devices in offices, and on the impact on the indoor daylighting availability.

The first part of the project consisted in the observation of the use of sunscreens when the command is not automated (office buildings, operating webcams from 01-02-2013 to 31-01-2014 over 125 openings, e.g. more than 500,000 individual blind positions analysed). The key finding is that sunscreens are adjusted infrequently (less than 2 movements blinds / week) regardless of the orientation or season. The consequence of this misuse is that the contribution of natural light is far from being optimised.

The second part of the project focused on the simulation of the actual contribution of daylight in each of the observed rooms (Simulations DIAL + / Radiance). This allowed us to compare the results with those that would have been achieved with automated blinds. The results of these simulations were then used to estimate the electricity consumption for lighting. This study shows that the energy savings associated with automated blinds can reach several kWh/m^2 per room and per year. Comparison with SIA 380/4 calculations points out that the actual version of the Swiss Standard underestimates the potential related to blinds automation and also tends to overestimate the effects of artificial lighting automated control.

The main conclusion of this study is that the implementation of automatic blinds can significantly increase the number of hours during which artificial lighting is not required while preserving the visual comfort and freedom of choice for users. The other conclusion is that the Swiss Standard should encourage the use of daylight by imposing specific targets on this topic.

Keywords: Movable blinds, Manual-use, Web-cams, Daylighting, Automation.

INTRODUCTION

Solar shading constitutes a major element in the energy performance of a building, both for the thermal balance and for lighting. The users are not always aware of this and move the shading for all kinds of reasons, except energy saving. This study quantifies how users handle manually operated shading devices and shows how this behaviour can affect electricity use for lighting when compared to automated operation of the shading devices.

This study is an observation of the solar shading devices (external venetian blinds) of three (3) office buildings in the EPFL Innovation Park area near Lausanne, Switzerland. The objective was to characterise the use of the blinds when these are not automated and its consequences on the level of natural light in the buildings. The purpose was also to make recommendations for a review of Swiss Standard 380/4 regarding lighting. The complete reports of this study is available on our website [1].

Figure 1: Photo of the west façade of building PSE-C on February 5, 2013, overcast sky

Figure 1 shows that there is no correlation between the position of the blinds (down or up) and the weather conditions. This building has 58 groups of blinds; only 11 windows show blinds in the 'up' position (red), while the sky is overcast and there is no risk of glare. The blinds are almost completely down on 7 windows (blue), preventing the harvesting of natural light. Behind 15 windows, the electric lights are on while the blinds are partially or completely down (yellow), in the middle of the afternoon of a day in February. In other offices, the lights are not switched on even when the blinds are down.

METHODOLOGY

The blinds were tracked over a period of one year and are situated on four levels, from the second to the fifth floor. The three buildings are occupied by start-ups of the EPFL (Swiss Federal Institute for Technology, Lausanne). Each building was observed with a webcam. The position of the blinds was recorded and saved every hour by full HD webcams, Model D-Link DCS2210. The images were subjected to visual analysis to determine at each time the position of the blinds.

Every hour, the covered area of the windows was recorded, in steps of 25%. The tilting angle of the blinds' slats was classified in one of the three following categories: vertical (closed), 45° tilted and horizontal). The testing period ran from February 1, 2013 till January 31, 2014. A blind going 'up' or 'down' is recorded as a 'movement'. A change of slat angle in a given blind position also represents a 'movement'. However, when the slat angle is changed during an 'up' or 'down' action, this is not considered a separate 'movement'.

RESULTS AND DISCUSSION

Movements recorded

Table 1 shows the total number of movements during the 365-day period of observation. The grey areas indicate the number of movements per window (total number of movements divided by the number of windows per façade). As the recording took place every hour, it is possible that some movements may not have been detected. However, it is highly improbable that a user will change the position of a blind twice in one hour, with the blind in exactly the same position the second time. We may therefore consider that the results are relevant.

Orientation (nb of window per facade)	East facade (28)		South facade(40)		West facade (58)	
	Movement per year	Movements per window	Movement per year	Movements per window	Movement per year	Movements per window
Movements "Up"	990	36.7	115	27.9	1189	20.5
Movements "Down"	1062	39.3	1126	30.7	1421	24.5
Slat angle change	365	13.5	697	17.4	3505	60.4
Total nb. of movements	2417	89.5	3038	76	6115	105.4
Average nb. of movements per week	48.5	1.72	58.4	1.46	117.6	2.03
Weighted average per week	1.74					

Table 1: Summary of blind movements during office hours on three façades – grey areas indicate movements per window.

Percentage of window covered

Apart from observing the 'up' and 'down' movements of the blinds, we have also looked at the degree of coverage of the glazed surface (Table 2). On the south façade, an average of 74% of the surface was covered by the blinds. On the west orientation, the percentage was 56%, while the east façade had the lowest percentage (35%) resulting in a weighted average of 57% for all the façades together, leaving 43% of the glazed surface uncovered. To the extent that we know that the top of the windows is also the most effective to bring light to the back of the room, we can predict that the manual management of blinds leads to a very poor use of natural light. It should be emphasized that the analysis period was characterized by a negative sunshine record between January and May [2], which may partly explain the difference between winter and summer for façade East.

Facade	Winter	Summer	Year
East (motorized)	22%	48%	35%
South (manual)	69%	78%	74%
West Manual	58%	55%	56%
Weighted average	53%	60%	57%

Table 2: Percentage of window covered as a function of the façade orientation and the season

Contribution to natural daylight in the offices

To evaluate how much natural daylight is brought into the offices, we conducted simulations, hour by hour during the complete test year, to calculate the daylight availability in each of the rooms, taking into account the blind position and the climatic conditions (from MétéoSuisse station in Pully). The simulations were made with an advanced release of the DIAL+Lighting software [3], based on the calculation engine RADIANCE [4], and targeted 5 points at 0.75m from the floor. To keep the simulation time within limits, the geometry of the slats has been simplified (flat slats with a diffuse reflectance coefficient of 0.30). The results may therefore be somewhat underestimated but the comparison between scenarios remains valid.

For a given room, the way the blinds are used is unpredictable and therefore the effective gain in natural light varies considerably. Figure 2 shows the annual diffuse daylight autonomy values [5] (percentage of time during which the indoor illuminance due to the diffuse component exceeds 500 lux) for west oriented rooms. The range is between 2% and 81% for

point 1, close to the window, between 2% and 34% in the centre of the room (point 3) and between 0% and 7% in point 5, furthest from the window.

The great differences between users, indicates that some of them are very 'tolerant', often leaving the blinds in the 'up' position, others are more 'protective', closing the blinds most of the time.

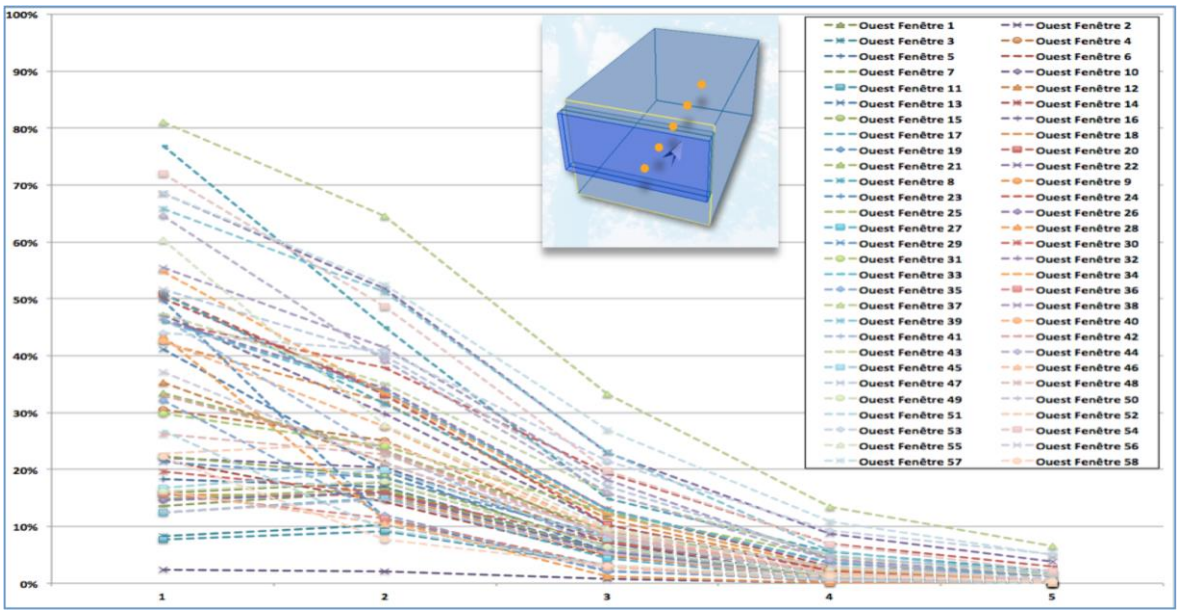

Figure 2: Percentage of the time (7AM- 6PM), during which daylight contribution ≥ 500 lux on the 5 reference points, for each of the 58 west oriented rooms. Each line corresponds to a room. Point 1 (left), is located close to the window and point 5 (right) at the back of the room.

Scenario for automating the blinds

The second part of the study deals with the comparison of the results if the blinds had been fully automated. It should be emphasised that the study did not focus on the thermal aspects but only on the lighting issues. With the DIAL+Lighting software [3], a second run of simulations was done, for every façade, hour by hour during one year, with an "Continuous" automation systems. In this scenario the blinds are lowered each time the incident solar radiation reaches 200 W/m² during the hourly measurements. In summertime, the blinds are lowered to cover 75% of the window area, in wintertime 100%. The slat angle varies with the position of the sun, from 0° to 20° to 25° and 45°. When the sun is absent, the blinds are raised to benefit from diffuse lighting, but a buffer time of one hour is set so that the users are not interrupted by too many movements.

The daylight level of 500 Lux is then calculated and compared between, on the one hand, the 'manual' situation, where the users operate (or not) the blinds, and on the other hand the automated situation. For each orientation, the maximum, minimum and median 'manual' results are graphically represented and compared. *Figure 3* shows an example of results for west oriented façade. The full report [1] shows all the detailed results of the calculations and measurements in the five points of each room in each of the three façades.

- In the first two measuring points, closest to the window, the results obtained with automated blinds are as good as, or better than, the one obtained by the most "tolerant" users (Maxi). In the centre of the rooms, the autonomy drops slightly but remains better than the 'median' manual result. In the back of the room (point 5) the results are similar to the median values.
- Compared with a median user, the blind automation reduces by 20% the number of hours that the lights are switched on, for an illumination level of 500 Lux.

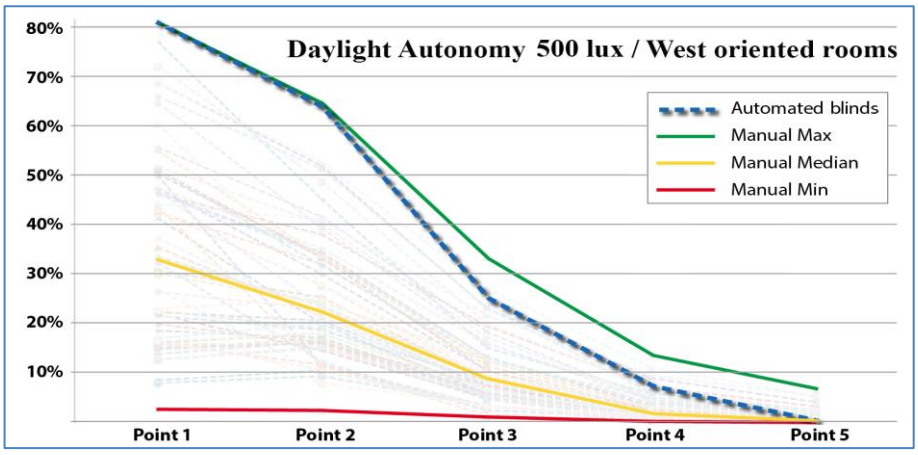

Figure 3: Daylight autonomy profiles for West oriented rooms (500 Lux required).
- Green line = Maximum observed (blinds almost always opened throughout the year).
- Orange line = Median values (50% of the users are above, 50% below).
- Red line = Minimum observed (blinds almost always closed throughout the year).
- Dark Blue dashed line = Daylight autonomy achieved with "Continuous" automated blinds.

Daylight Autonomy for 150 lux required

During this study we observed that, when electric lighting is not automated, users tend to turn on the lamps when the interior light level is usually less than 150 lux at the centre of the room. On the other hand, we know that very often, users also tend to forget to switch-off the lights, even if the daylight contribution exceeds 500 lux. To evaluate this "realistic" scenario, we have simulated the case when:

- Lights are turned ON when indoors illuminance ≤ 150 lux (centre of the room).
- Lights are switched-OFF when users leave the room (at 1 PM and 6 PM).

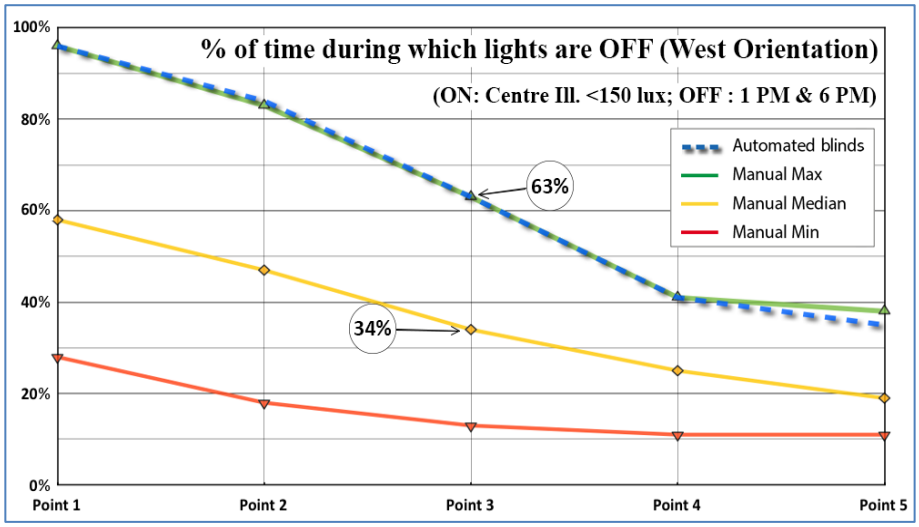

Figure 4: Percentage of time (7AM-6PM) during which lights are off. The conditions are as follow: - Lights turned-on if indoors illuminance ≤ 150 lux (centre of the room).
- Light turned-off at 1 PM & 6 PM.

Figure 4 shows that in this scenario, the percentage of time during which the lights are turned OFF is the same for "Automated blinds" and "Manual Maxi". It means that the time during which lights are turned ON is reduced to the minimum. Comparison with "Manual Median"

shows that the time without electric lighting is almost divided by two (63% vs. 34%). This gives an idea of the high potential for lighting energy savings linked to the implementation of automated blinds in office buildings.

CONCLUSION

The observation during 12 consecutive months has resulted in a considerable collection of data. These data have so far been analysed and used for information on the lighting of the rooms and have allowed several conclusions on the real-life use of non-automated solar shading blinds.

The main conclusion is that people are very poor users of their shading devices. With less than two movements per window and per week on average, the daylight contribution to the indoor lighting is far from optimum. Furthermore, the average position of the blinds leads to a significant obstruction. With an average of 57% of the window surface covered by the blinds, the use of electric lighting is almost mandatory for the back part of the room.

Thus the implementation of automation system to control the blinds position is of high interest. This study has shown that such systems can achieve performance comparable to those observed in the case of very "tolerant" users. In Switzerland, where the implementation of Venetian blinds is widespread, the issue of automation is particularly important and this information should be disseminated among designers and building owners.

The question is: how to combine the best shading device with the best use of it. In our daily practice, we are often faced with this problem. Most of the time we propose to our clients to implement automated control systems based on 2 or 3 reset movements per day. With such systems, whose parameters have to be carefully tailored to the different localizations and orientations, it is possible to largely improve the operation of shading devices without causing rejection reaction by users. In this case, the position of the blinds should also consider the thermal aspects (optimization of winter solar gains and reduction of overheating risks in summer).

We sincerely believe that this approach leads to greatly optimize the behavior of buildings and thus contribute to the necessary reduction in energy consumption and associated CO_2 emissions.

REFERENCES

1. http://www.estia.ch/#!ofen-global-lighting/c8xx: last visited: 04-29-2015
2. http://www.meteosuisse.admin.ch/home/recherche.html?query=2013, last visited 06-08-2015
3. Paule, B. et al: DIAL+Suite: A complete but simple suite of tools to optimize the global performance of building openings: CISBAT'11 Conference, Lausanne, Switzerland, 2011.
4. http://radsite.lbl.gov/radiance/refer/ray.html: last visited 04-29-2015
5. Paule, B et al., "Diffuse Daylighting Autonomy: Towards new targets", Proceedings of the CISBAT'13 Conference, Lausanne, Switzerland, Sept. 2013.
6. Wienold J., Christoffersen J.: Evaluation methods and development of a new glare prediction model for daylight environments with the use of CCD cameras. Energy and Buildings, 38(7): 743-757, 2006.
7. Paule, B. Boutillier, J. & Pantet, S. (2014): Global lighting performance, Annual report 2013-2014. Project 81 0083: Swiss Federal Office for Energy, Lausanne, 2014.

DAYLIGHTING AND SHADING OF THE ENERGY EFFICIENY CENTER – MONITORING RESULTS AND USER ACCEPTANCE

M. Reim[1]; W. Körner[1]; H. Weinläder[1]

1: ZAE Bayern, Bavarian Center for Applied Energy Research, Am Galgenberg 87, 97074 Würzburg, Germany, www.zae-bayern.de 1

ABSTRACT

The Energy Efficiency Center (EEC) is a combined office (1st floor) and laboratory (ground floor) building with a function room attached to the north side. The overall aim of the project is to create a reference building which implements innovative techniques and serves demonstrational purposes. The roof of the main building consists of membranes; parts of the ceiling of the 1st floor are transparent or translucent.

The operation of the lighting and sun protection systems as well as the associated control systems was tested for summer, intermediate and winter conditions. The interaction of the users with the control system was investigated by monitoring the manual user interventions during winter conditions. Furthermore a questionnaire was compiled to investigate the user acceptance of the control of the sun protection system and the artificial lighting, especially the lighting level and glare protection in the rooms.

Keywords: membrane; daylighting; artificial lighting; aerogel glazing; user acceptance

INTRODUCTION

The Energy Efficiency Center (EEC) is a combined office (1st floor) and laboratory (ground floor) located in Würzburg, Germany and finished in June 2013. The roof of the main building consists of translucent PTFE-glass-membranes and partially of transparent ETFE films. The translucent part of the roof consists of a PTFE-glass-membrane Type Sheerfill II with Everclean-Coating [1]. The transparent part consists of an ETFE-Film with a thickness of 250 µm printed with a hexagonal pattern with a pattern size of 9 mm and a print coverage ratio of 89%. The visual transmittances of the ETFE film and glass-PTFE membrane are 57% and 11%, respectively. The membrane acts as a climate interlayer above the thermal insulation level, the ceiling of the 1st floor. Parts of the ceiling of the 1st floor are transparent or translucent. The ceiling of the corridor consists of triple glazing. Part of the ceiling of the corridor and stairways is glazed with an aerogel glazing [2]. The ceilings of most of the office rooms contain a translucent double-skin-sheet filled with Lumira-aerogel [3] with a width of about 1 m located in the back of the room.

Figure 1 show the main building viewed from south-east. The main axis of the building runs east-west. Most of the office rooms are located on the south side on the 1st floor. In the north side there are staircases and lift, the library and two conference rooms as well as some office rooms. The basement mainly contains laboratories. To the north an additional single-story part contains a function room and a technical center.

The sun protection system on the south façade consists of outside blinds with spectrally selective lamellae. The solar reflectance of the lamellae in the visible spectral range is significantly higher than the reflectance in the solar spectral range [4]. The result is a total solar energy transmittance which is lower than that of non-selective lamellae with the same visual transmittance. The cut-off-angle is the angle to which the lamellae have to be closed in order to prevent direct radiation to pass through the sun protection system depending on the solar height. On the east and west façade triple glazing with integrated lamellae was used for

architectural reasons. On the north façade no sun protection system is used. In order to limit the solar energy input through the north façade a glazing with lower total solar energy transmittance was used there. Additionally, all rooms are equipped with an inside glare protection system, a roller blind with a low-emissivity coating on the inner surface to improve thermal comfort of the inhabitants. The luminaries are switched and dimmed automatically based on combined occupancy and illuminance sensors in each room. Depending on the heating or cooling demand of the room, the solar energy input through the facade can be varied by using either the outside (low solar energy input) or inside (high solar energy input) shading device. The operation of the lighting and sun protection system was tested for summer conditions, meaning high altitude of the sun and a control strategy for the sun protection system with the goal to minimize solar energy input through the façade [5]. Similar tests for intermediate and winter conditions were presented in Graz this spring [6]. When the correct operation of the control system was verified the interaction of the users with the control system was investigated by surveying the user interventions with the building control system during winter conditions. Other surveys for summer and intermediate conditions will follow.

Figure 1: Energy Efficiency Center viewed from south-east. Clearly visible is the textile roof with translucent PTFE-glass membranes and partially transparent ETFE films.

The goal of the lighting and shading concept is to minimize the energy consumption of the artificial lighting system by maximizing the daylight input into the rooms while at the same time reducing the heating/cooling loads by maximizing/minimizing the solar energy input into the rooms as applicable.

METHOD

Control of lighting and sun protection system

Each room is equipped with a ceiling-mounted combined occupancy and illuminance sensor. The occupancy sensor selects a low-power mode for the room when nobody is present. This includes switching off the light and operating the external sun protection system depending on whether there is heating or cooling demand for the room.

When occupied, a default illuminance level of 500 lx ([7] for office rooms) at the work places is maintained using dimmable artificial lighting if necessary. The position of the shading system depends on the outside illuminance on the respective façade:

- It is closed at an outside illuminance higher than 45 klx. The lamellae angle is set depending on the position of the sun and the heating or cooling demand of the room. When heating demand is present the lamellae are closed a few degrees more than the cut-off-angle, which ensures that no direct irradiation passes the sun protection system. When cooling is needed the lamellae angle is set 10° higher than the cut-off-angle or a minimum of about 20°, further reducing the solar energy input to the room.
- It is opened when the outside illuminance is lower than 20 klx for some time.
- When the outside illuminance is higher than 30 klx the sun protection system is closed with a lamellae angle of 0°. The same state is reached when the system is closed and the outside illuminance is lower than 30 klx.

The automatic settings for lighting and outside sun protection system can be overruled by the user; the system is reset to automatic mode after 30 minutes without occupancy. The roller blinds used as inside glare protection are controlled manually.

Monitoring

Two office rooms at the south and north façade were equipped with some additional illuminance sensors at the desktop and below the translucent part of the ceiling. The illuminance sensors at the work places were used to calibrate the ceiling-mounted sensors used for lighting control.

Measurements were performed in two comparable south oriented rooms with additional illuminance sensors – behind and above the monitors at the work places, one in the middle (Height 110 cm) and one in the back (Height 130 cm) of the room. One room is with working Aerogel ceiling, the other room is with shaded Aerogel ceiling.

RESULTS

Monitoring results

Figure 3 shows the illuminance below the translucent part of the ceiling in the south and north offices depending on the global solar irradiance for a period in summer 2014 and winter 2014/2015.

In summer this illuminance is approximately proportional to the global irradiance and peaks at about 2000 lx for the south room. The corresponding illuminance for the north room is significantly higher and peaks at above 8000 lx. This is caused by direct irradiation through the ETFE films above the corridor, which hits the translucent panels at the north side. As the visual transmittance of the ETFE films is significantly higher than the transmittance of the glass-PTFE-membrane this yields higher light input through the translucent panels for the north rooms compared to the south rooms. When comparing the illuminance Ev below the translucent part of the ceiling for overcast sky (direct solar irradiance near zero) the values for the north- and south-oriented rooms are identical.

Due to the lower elevation of the sun in winter, no direct radiation hits the translucent panels on the north side. Therefore, the illuminance below the translucent parts of the ceiling is nearly identical for the north- and south-oriented office rooms.

Measurements of the illuminance E_v and global irradiance G for south-facing rooms with open and shaded Aerogel ceiling showed that the Aerogel ceiling contributes on sunny days in winter with about 200 lx up to 400 lx to the room illumination, especially in the back of the rooms. Even at overcast skies in winter ($G < 200$ W/m^2) and closed sun protection system the illuminance through the Aerogel ceiling is about 100 lx in the back of the room. These results

show that the translucent aerogel ceiling has a significant effect on the room illumination, especially when regarding the illumination in the room depth. Even on overcast days, the aerogel ceiling contributes significantly to the room illumination thus reducing the electrical energy consumption for the luminaires.

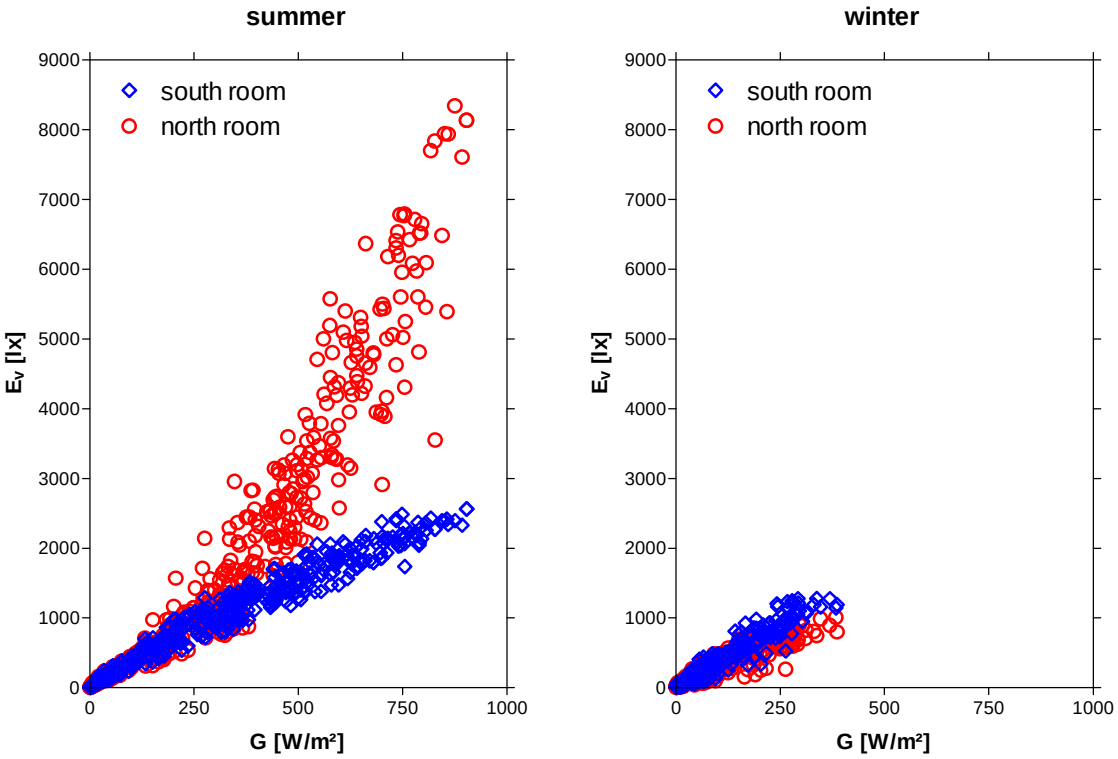

Figure 3: Illuminance E_v below the translucent part of the ceiling as a function of the global irradiance G on the horizontal for summer 2014 (left) and winter 2014/2015 (right).

Survey results

37 users participated in the first survey (24 male, 13 female). 6 users occupy a north-oriented room; they omitted the questions regarding the control of the outside sun protection system. 29 users work in rooms equipped with an outside sun protection system, 17 of them are male and 12 are female. The work places of 18 users are near the façade, 11 users are seated in the back of the room.

Tables 1 to 3 show the results of the first survey for winter conditions. The analysis showed almost no difference in gender related temperature perception regarding hot temperatures. However, there was a significant difference regarding cold temperature perception where 76% of the females sometimes or often feel cold compared to only 26% of the males. A difference was also found in luminance perception regarding daylight, where males seem to prefer darker environments – only 39% of the males sometimes or often feel too dark compared to 69% of the females. Regarding the luminance perception by artificial lighting, males as well as females find it often too bright – 26% and 46%, respectively. One additional result of this first survey was that there was no dependence between the interactions of the users with the control system regarding the time of day.

In general, the results show that the building control seems to work quite well. Usually, the users find the conditions acceptable – the category “often” is used by less than 10% of the people. Exemptions are the temperatures which are often too low for the females and the artificial lighting which is often too bright for males and females. The number of interactions

with the control shows, that there is still room for improvement: about 50% of the people manually intervene more than three times a day. There is no difference between males and females in interacting with the building control, whereas the position of the desktop in the room seems to influence the number of interactions significantly. Users near the façade intervene more often than users in the back of the room - despite the building control being located in the back of the room.

Table 1: Difference in temperature perception of male and female.

	Too hot		**Too cold**	
Temperature	**male (24)**	**female (13)**	**male (24)**	**female (13)**
Never...	54%	62%	71%	23%
Sometimes...	38%	31%	29%	38%
Often…	8%	8%	0%	38%

Table 2: Difference in daylight and in artificial lighting perception of male and female.

	Too bright		**Too dark**	
Daylight	**male (24)**	**female (13)**	**male (24)**	**female (13)**
Never…	58%	69%	58%	31%
Sometimes…	29%	31%	33%	54%
Often…	13%	0%	8%	15%
Artificial lighting	**male (24)**	**female (13)**	**male (24)**	**female (13)**
Never…	67%	46%	79%	69%
Sometimes…	8%	8%	17%	23%
Often…	25%	46%	4%	8%

Table 3: Nr. of interactions per day with the building control depending on gender and position in the room.

Interactions per day	**male (17)**	**female (12)**	**window (18)**	**back of the room (11)**
0 - 3	59%	50%	44%	64%
4 – 6	24%	33%	33%	27%
7 – 9	18%	17%	22%	9%
9 – 12	0%	0%	0%	0%

DISCUSSION AND CONCLUSION

After the analysis of the survey and discussion with the users we changed some points in the control strategy.

- The starting time for the room heating on Mondays after the weekend setback was changed from 6 am to 4 am to increase the room temperatures in the morning, especially in the corner offices.
- The maximal closing angle of the sun protection system of 50° was too big. Most of the users felt uncomfortable with the nearly fully closed shading system and artificial lighting switched on, so we set the maximum closing angle to 45°.
- At temperatures above 8°C, heating demand for the room and illuminance at the south façade above 45 klx the sun protection system was fully closed so far. In the rooms with room-high glazing we changed the control so that the sun protection system stops at 60% of the height of the façade for the case of heating demand in the room This

improves the user acceptance, allows better visual contact to the outside and additionally increases the solar gains during the heating period.

Up to now the control of artificial lighting is either automatic (500 lx at workstation offices) or by manual dimming. Another possibility is manual control of the set point of the lighting control system. This would allow the users to change the illuminance level in the room without disabling the control of the artificial lighting. It is not clear up to now if this is possible using the hardware installed in the rooms.

After one year of measurements and operational experience, we started a survey of the users to improve the control system. After the first survey this winter we optimized the control strategy and adapted the questionnaire. Now we will start an interactive, monthly repeating survey over one year to receive an impression of the user acceptance and potential for optimization including all seasonal conditions.

ACKNOWLEDGEMENTS

The Energy Efficiency Center is funded by the German Federal Ministry for Economic Affairs and Energy because of a decision of the German Bundestag, the Federal state of Bavaria and the Bürgerstiftung Würzburg und Umgebung.

We thank our sponsors and partners for their support:

Assmann Büromöbel GmbH & Co. KG, BSH Bosch und Siemens Hausgeräte GmbH, Cabot Aerogel, Doerken GmbH & Co. KG, DuPont de Nemours, EEV GmbH, Ehrenfels Isoliertüren GmbH, Energy Glas GmbH, Hightex, Knauf Gips KG, Lindner AG, Maincor AG, Okalux GmbH, Porextherm Dämmstoffe GmbH, Roto Frank Bauelemente GmbH, Rubitherm Technologies GmbH, Saint Gobain PPL Cologne GmbH, SGL Carbon SE, Siemens Schweiz AG, Siemens AG Building Technologies Division, Siteco Beleuchtungstechnik GmbH, Team Weber GmbH, Uhlmann & Zacher GmbH, uponor GmbH, va-q-tec AG, Versaidag-Indutex GmbH, Walter Stickling GmbH, Waldner Holding GmbH & Co. KG, Warema Renkhoff SE.

REFERENCES

1. Saint-Gobain, 2014. Data sheet “SHEERFILL® II EverClean® Architectural Membrane”, http://www.sheerfill.com/uploadedFiles/SGsheerfill/Documents/Sheerfill-II-EverClean-Architectural-DIN.pdf, downloaded Aug. 14, 2014.
2. OKALUX, 2013. OKAGEL light-diffusing high-performance insulating glass, http://www.okalux.de/fileadmin/Downloads/Downloads_englisch/Infotexte/i_okagel_e.pdf, downloaded Aug. 14, 2014.
3. Cabot, 2013. Data Sheet - Lumira aerogel particles, http://www.cabot-corp.com/wcm/download/en-us/ae/Translucent_1000_2000_DS_2013_v6_final lo res.pdf, downloaded Aug. 14, 2014.
4. Warema-Renkhoff SE, 2008. “Raffstoren mit selektiver Beschichtung” (in german), Dok.-Nr. 114300.02.2008, Art.-Nr. 869248..
5. Reim et al. 2014, Daylighting and shading of the Energy Efficiency Center, Eurosun 2014, Aix-les-Bains, 2014.
6. Reim et al. 2015, Innovative daylighting and shading concept – the Energy Efficiency Center, Advanced Building Skins, Graz, 2015.
7. EN 12464-1, 2011. Light and lighting - Lighting of work places - Part 1: Indoor work places; German version EN 12464-1:2011

MODEL-BASED SHADING AND LIGHTING CONTROLS CONSIDERING VISUAL COMFORT AND ENERGY USE

Jie Xiong[1], Ying-Chieh Chan[1], Athanasios Tzempelikos[1]

1: School of Civil Engineering, Purdue University, 550 Stadium Mall Dr., West Lafayette, IN 47907 USA

ABSTRACT

Dynamic facades with high performance glazing and automated shading have the potential to balance daylighting, comfort and energy use, when integrated with lighting and thermal control systems. This paper presents the development and implementation of a model-based control algorithm for automated shading and lighting operation, aiming at minimizing energy use while reducing the risk of glare. A detailed validated lighting-glare model is used to compute real-time interior lighting conditions, lighting energy use and DGP, based on the readings of two sensors on every building facade. The model-based operation ensures optimal shade position and light dimming levels that minimize energy use while satisfying glare constraints at each time step. The developed algorithm is demonstrated in a full-scale office space, controlling shades and electric lighting in real-time, using simple sensor readings as inputs. Finally, a comparison between control strategies and control intervals is discussed.

Keywords: Model-based control, facades, shading, glare, daylighting

1 INTRODUCTION

Façade design and control, integrated with lighting and thermal controls, should provide natural light while minimizing energy use and maintaining human comfort. To evaluate the impact of advanced control strategies, accurate and efficient models of dynamic façade and lighting systems are needed [1], and proper comfort indices. Fisher et al. [2] utilized an accurate illumination model for electric lighting control, trained by measurement from light sensors located at every seat. Shen et al. [3] studied independent and integrated open and closed loop strategies for shading and lighting. Kim and Park [4] used EnergyPlus as a model-based predictor for optimal slat angles within a 24 hr time horizon, with high computational effort. Thorough work on blind controllers with multi-objective optimization processes [5-6] provide promising solutions. Very few studies directly associated glare indices with shading controls. Wienold [7] used the simplified DGP to evaluate the efficiency of shading controls towards glare. Yun et al. [8] used DGP to evaluate blind control strategies towards glare and energy and stated that E_v is a good criterion for shading control. However, it is implied that no direct light conditions were met. Obtaining real-time DGP data is quite challenging. As the DGPs approximation uses only vertical illuminance, the potential of a model-based control based on DGPs needs to be investigated [9].

Real-time detailed simulation requires extensive sensor networks for acquiring necessary information with changing weather and sky conditions. In addition, improper or separate controls for façade and lighting systems could be ineffective and costly. Therefore a low-cost but reliable model with less exogenous inputs should be established. In this way, model-based control algorithms could be effective in management of façade, interior lighting and comfort [10]. This paper presents the development and implementation of shading and lighting model-based control algorithms based on different criteria, for the case of spaces with interior roller shades. The control was able to minimize lighting energy use while maintaining good visual comfort. Advanced control options that consider variable control intervals are also discussed.

2 METHODOLOGY

2.1 Model-Based control logic

Fig. 1 presents the flowchart of the developed model-based control (MBC) methodology. Input data (measured by sensors for real-time control or TMY3 for an annual analysis) are used together with space geometry to calculate interior illuminance and luminance distributions based on a validated hybrid ray-tracing and radiosity daylight model [11]. The model combines the accuracy of forward ray tracing for direct light with computational efficiency of radiosity for diffuse light entering the space. In the case or roller shades, the angular direct-direct and direct-diffuse transmittance is calculated using a validated semi-empirical model [12]. Other models can be used for different types of complex fenestration systems. The model outputs include work plane illuminance, vertical (on eye) illuminance, and DGP for a pre-selected calculation grid (occupant positions and view directions). These are calculated at each time step for 11 pre-defined shading positions (every 10%), from fully open to fully closed shades. Having discrete positions significantly improves computational efficiency. The sets of simulation results are then sent to a control decision maker. The decision maker selects the "highest" shading position (among the 11) that satisfies the following criteria, to maximize daylight provision and reduce lighting energy use at each time step. Three control criteria are compared in this study as shown in Fig. 1:

1. DGP-based control. The highest shading position for which DGP≤0.35 is selected. Daylight Glare Probability is calculated based on the original equation [13].
2. Vertical illuminance-based control. Recent studies [9] showed that DGPs, the simplified version of DGP, which depends only on vertical illuminance on the eye (E_v), is appropriate to use for all cases except when direct light falls on the eye.

$$DGPs = 6.22 \times 10^{-5} E_v + 0.184 \quad (1)$$

   DGPs equal to 0.35 corresponds to E_v= 2670 lx. Adding a small safety factor, the highest shading position for which E_v≤2500 lux is selected. Note that shades with noticeable openness transmit direct light–for these cases, the use of DGPs is not recommended [9].
3. Effective illuminance-based control. The highest shading position for which work plane illuminance E_{wp}≤2000 lx is selected, without any direct sunlight reaching the work plane. Instead of real-time simulation for this control, a threshold of effective transmitted illuminance through the window and the shade, E_{eff}, can be selected, corresponding to E_{wp}=2000 lx for the position closest to the windows (including the presence of shading). The advantage is that only one sensor on the window is required. The threshold is based on pre-calculated simulated results and will vary with orientation, and room geometry.
   If all shading positions fail to pass the comfort criteria, the shades would be left closed. After that, the controller extracts the simulated work plane illuminance (on the calculation grid) corresponding to the selected shading position and dims electric lights based on a work plane illuminance set point (500 lx). Light dimming can be implemented locally (per fixture or row of fixtures) or, for smaller rooms, based on the averaged E_{wp}. Lighting energy use is calculated from corresponding light dimming levels.

3 CONTROL IMPLEMENTATION IN A FULL-SCALE OFFICE

3.1 Experimental facility

Two identical, side-by-side test offices (Fig. 2), part of the Architectural Engineering Laboratories at Purdue University were used to implement the developed model-based control strategies. The offices (5m x 5.2m by 3.4m high) are equipped with reconfigurable façade,

shading and lighting systems for investigating the impact of façade design and control options on indoor environmental conditions and energy use. The south facing façade has 60% WWR. Both rooms are equipped with a high performance glazing unit (normal visible transmittance = 65%), and motorized roller shades (beam-total transmittance = 5%, measured with an integrated sphere). In each room, there are four light fixtures (two rows parallel to windows) with 54-W, T5 HO lamps. LICOR calibrated photometers were used to measure light levels, both exterior (horizontal and vertical illuminance) and interior (transmitted through window, horizontal work plane illuminance at several points, and vertical illuminance at the eye height level at 2.20 m from the window). Direct and diffuse incident solar radiation on the façade was measured with a SPN1 solar pyranometer, mounted on the exterior south wall. Some of these measurements are used as inputs in the model-based control. A calibrated Canon 550D dSLR camera, equipped with a Sigma 4.5mm fisheye lens was used for luminance mapping and glare measurements, located at a distance of 2.20m from the glass and in the center of the room. The calibration data was implemented in Labsoft v14.3.6, which was used for HDR creation, image processing and DGP calculation following the logic of Evalglare [14]. The control platform is a combination of Matlab and LabVIEW. Data acquisition and control output are handled by LabVIEW, while and model runs in Matlab using a built-in MathScript function in LabVIEW. Control commands for shades and lights are sent to respective devices using Ethernet connections.

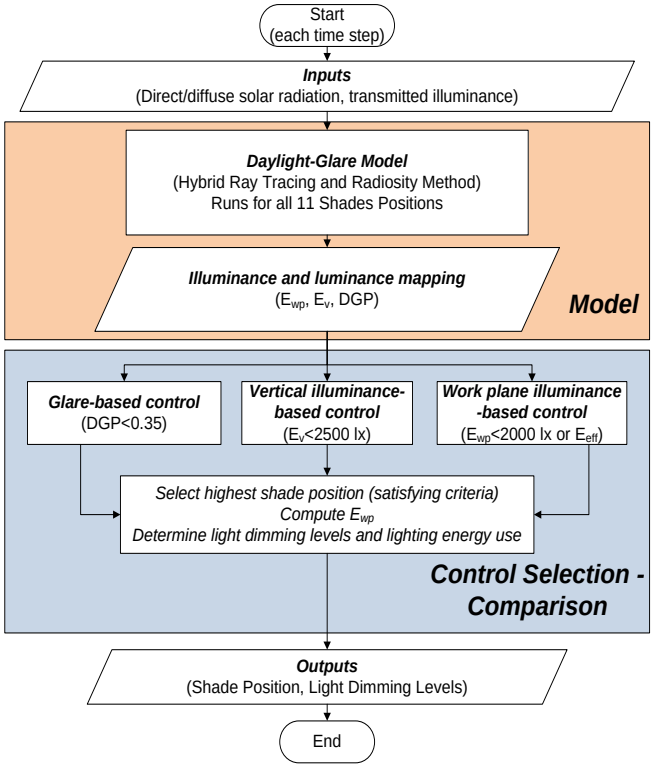

Figure 1. Model-based Control Flowchart

Figure 2. Exterior and interior views of the test offices and HDR camera

3.2 Implementation of model-based control strategies

The three control strategies were tested in the offices during February-April 2015, under a variety of sky conditions. Real-time measurements were used as inputs to the model, which runs every minute. A 5x5 work plane calculation grid was used. The threshold of E_{eff} for these offices is 6000 lux (work plane starts at 0.5m from the window). Electric lights were dimmed as a group, using 500 lx as a set point for averaged work plane illuminance. This was achieved by mapping dimming levels and E_{wp}, which will differ depending on the space and lighting system configuration and lighting control scheme. Representative results for three successive days –one cloudy, one mixed and one sunny- are shown in Fig. 3. The control system responds fast to changing outside conditions. Overall, the three control strategies were successfully implemented, achieving their objectives, while sufficient daylight is provided and electric light levels remain very low. The DGP and E_v-based controls result in similar illuminance and DGP conditions –measured DGP levels are maintained below 0.35 while E_{wp} remains high. The E_v-based control seems to be a stricter criterion than DGP, since resulting work plane illuminances (Fig. 3f) are lower. The E_{eff} control results lower shading fractions, higher DGP values (up to 0.4) and higher E_v values (up to 3500 lx), therefore it might result in instances with glare. However, the resulting E_{wp} values are higher with the DGP-based control.

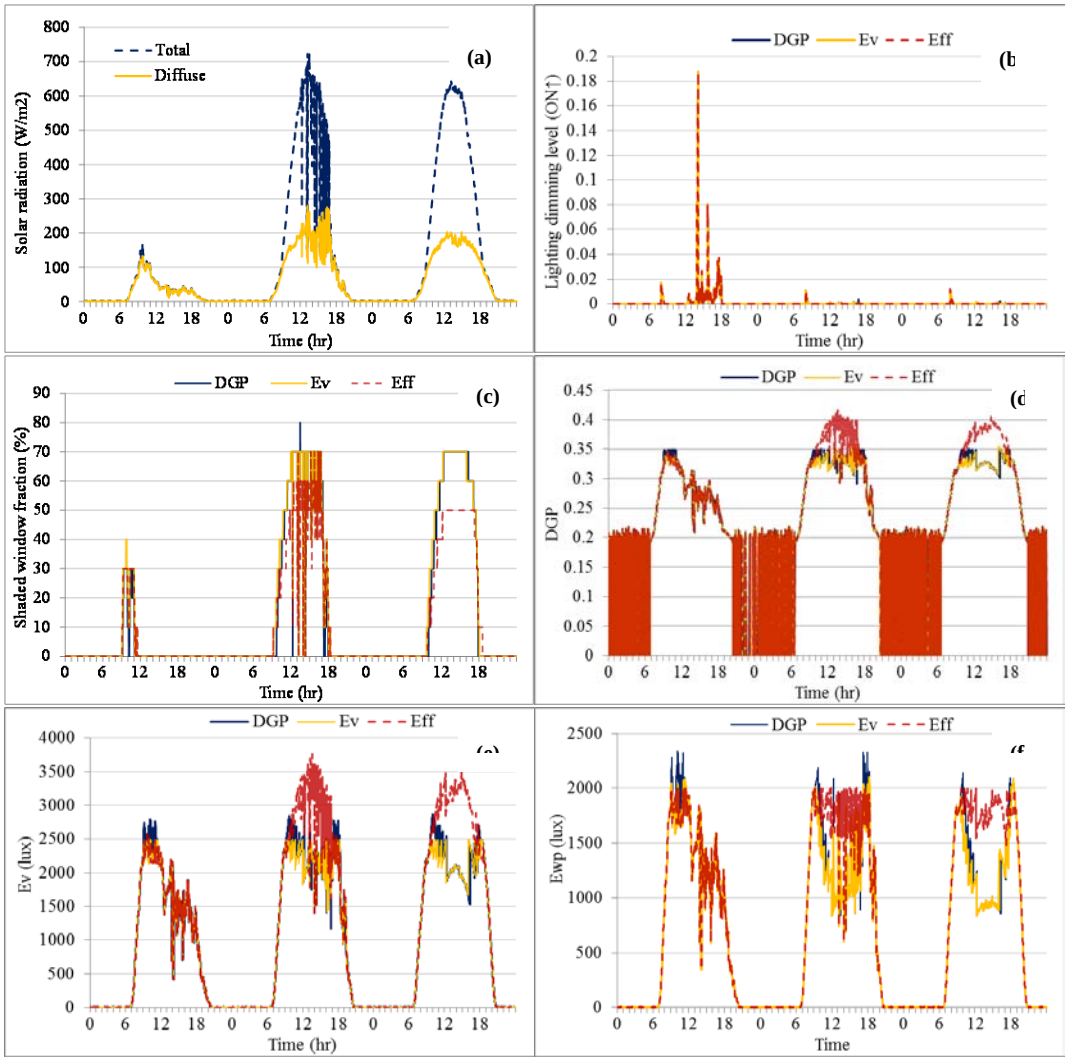

Figure 3. Experimental results using the three MBC strategies: (a) incident solar radiation on the façade (b) measured light dimming levels (c) recorded shading positions (d) camera-measured DGP (e) measured E_v and (f) measured E_{wp}.

3.3 Development of variable control interval strategies

To prevent frequent shading and electric lighting operation this, a different logic was developed (Fig. 4) using longer and variable control intervals, protecting from glare during mixed sky conditions (passing clouds), while otherwise reducing shading movement. Measurements are still recorded every minute but control actions are separately decided. In each time step, the shade position (MSP) predicted by the model-based control is compared with the current shade position (CSP). If MSP < CSP, which means shades need to lower for glare protection, control action is taken within a minute to move the shades to CSP, and the timer is reset to 0. If MSP > CSP and shades have not moved during the last 15 min, shades are set to the lowest MSP position recorded in the past interval; otherwise they remain in their current position and the timer moves to the next step. The new logic was implemented in the offices, to evaluate its effectiveness and compare with the 1-min control operation. Results for a day with turbulent sky conditions are shown in Fig. 5 for the DGP-based control option. The shades move less frequently while visual comfort is well maintained (DGP<0.35) even under fast-changing conditions. Lighting energy use is slightly affected, while E_{wp} is reduced.

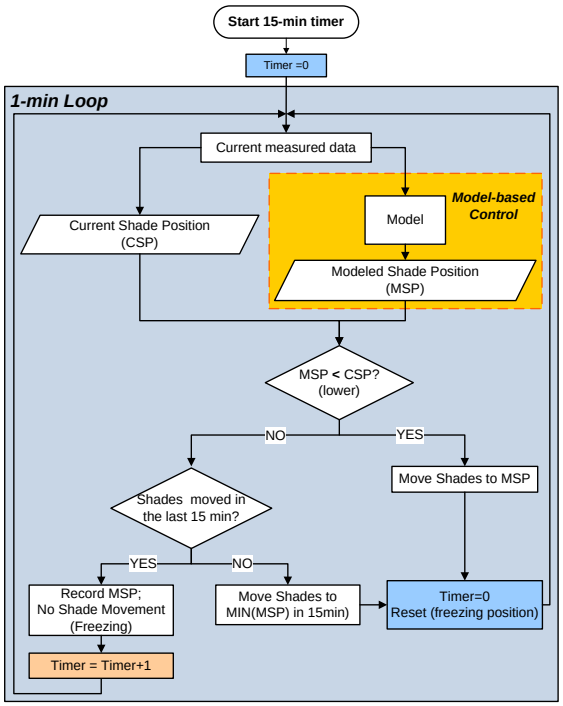

Figure 4. Variable Shading Control Interval Logic

4 CONCLUSION

This study presents advanced model-based shading and lighting control algorithms, aiming at minimizing lighting energy use while maintaining visual comfort using a small number of sensors. Three control criteria, based on DGP, vertical and horizontal illuminance were compared. The control strategies were successfully implemented in test offices with satisfactory results. DGP values remain below 0.35 for most cases while work plane illuminance levels were adequate. Lighting energy use was significantly reduced with all controls. The model-based control is able to capture rapidly changing sky conditions and take appropriate action. An advanced control interval logic was also successfully implemented, resulting in less frequent shade movement. The developed model and controls can decrease sensor network complexity while retaining reliability. Future work includes applying the developed controls in occupied offices, to evaluate human satisfaction and interactions; as well as thermal environment considerations for delivering integrated control solutions.

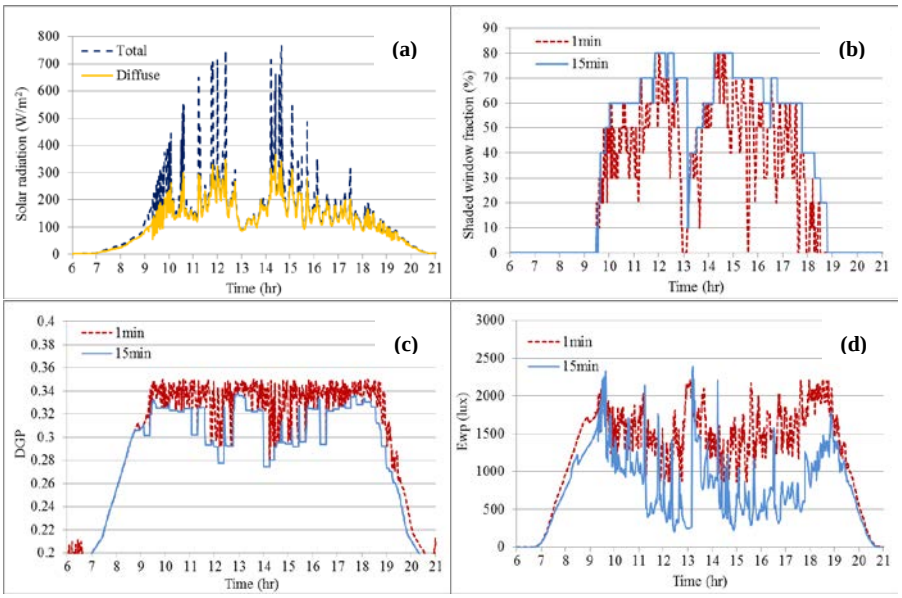

Figure 5. DGP-based results with 1-min vs variable control interval: (a) incident solar radiation (b) recorded shading position (c) camera-measured DGP (d) measured E_{wp}.

REFERENCES

1. Lindelof D. A fast daylight model suitable for embedded controllers. Sol. Energy 83, 57-68, 2009.
2. Fisher M., Wu K., Agathoklis P. Intelligent Illumination Model-Based Lighting Control. Proc. Of 32nd International Conference on Distributed Computing Systems Workshops, Macau, 2012.
3. Shen H., Hu J., Patel M. Energy and visual comfort analysis of lighting and daylight control strategies. Building and Environment 78, 155-170, 2014.
4. Kim D.W., Park C.S. Comparative control strategies of exterior and interior blind systems. *Lighting Research and Technology*, 44, 291-308, 2012.
5. Daum, D., Morel, N. Identifying important state variables for a blind controller. *Building and Environment*, 45, 887-900, 2010.
6. Guillemin, A., Molteni, S. An energy-efficient controller for shading devices self-adapting to the user wishes. *Building and Environment*, 37, 1091-1097, 2002.
7. Wienold J. Dynamic simulation of blind control strategies for visual comfort and energy balance analysis. Proceedings of IBPSA 2007 Conference, Beijing, China, pp. 1197-1204, 2007.
8. Yun G.Y., Yoon K.C., Kim K.S. The influence of shading control strategies on the visual comfort and energy demand of office buildings. Energy and Buildings 84, 70-85, 2014.
9. Konstantzos I., Tzempelikos A., Chan Y-C. Experimental and simulation analysis of daylight glare probability in offices with dynamic window shades. Building and Env., 87, 244-254, 2015.
10. Mahdavi A. Predictive Simulation-Based Lighting and Shading Systems Control in Buildings. Building Simulation, 1(1), 25-25, 2008.
11. Chan Y-C., Tzempelikos A. A hybrid ray-tracing and radiosity method for calculating radiation transport and illuminance distr. in spaces with blinds. Solar Energy, 86(11), 3109-3124, 2012.
12. Kotey N.A., Wright J., Collins M.R., Determining off-normal solar optical properties of roller blinds. ASHRAE Transactions 117 (1), 2009.
13. Wienold, J., Christoffersen, J. Evaluation methods and development of a new glare prediction model for daylight environments with CCD cameras. *Energy and Buildings*, 38, 743-757, 2006.
14. Wienold J., 2012. EvalGlare Version 1.0. Fraunhofer Institute for Solar Energy Systems, Freiburg.

PERFORMANCE ASSESSMENT AND ENERGY SAVING MEASURES FOR OUTDOOR LIGHTING IN AN INDUSTRIAL DISTRICT APPLICATION

G. Ciampi; A. Rosato; M. Scorpio; S. Sibilio

Second University of Naples, Department of Architecture and Industrial Design "Luigi Vanvitelli", via San Lorenzo, 81031, Aversa (CE), Italy

ABSTRACT

This paper presents a methodology to assess the performance of an outdoor lighting system in an industrial district through an on-site audit and the subsequent definition of specific Performances Indices. The methodology aims to focus on outdoor area illumination in order to assess the current status of the lighting system and subsequently propose how to optimize the energy efficiency, costs as well as reduce greenhouse gas emissions (GHG).

The results relating to 11 outdoor areas of industrial districts were analysed and presented, focusing on the exterior lighting and comparing their performances. In this perspective, the external lighting system of an industrial district can be regarded as a potential "demonstrator" upon which a numerical/experimental methodology will be developed so as to evaluate the performance of a lighting system from the point of view of its energetic and environmental impact. Finally, appropriate energy efficiency measures are proposed.

Keywords: energy saving, LED, industrial district, exterior lighting

INTRODUCTION

Energy savings can be regarded as "the first renewable source and the fastest, most effective and cost-efficient way to reduce greenhouse gas emissions" [1]. In Europe, it has been recognized that at least 20% of wasted energy is due to the low/poor efficiency of appliances and equipment, with the target of reducing these losses within 2020 having been set [2]. Among the indicators widely reported in current literature, it is worth noting how two-thirds of light sources installed in the European Union are based on a now-obsolete technology (developed prior to 1970) characterized by a low efficiency. Reduction of energy consumption of outdoor area lighting also contributes to the reduction of harmful emissions into the atmosphere as envisaged by the Kyoto Protocol [3].An action plan to improve the energy efficiency of outdoor area lighting characterized by vehicular traffic and internal circulation for goods and services delivery has to involve both technical and economic considerations and has to be compliant with standard and rules to ensure road safety; moreover it requires the optimization and reduction of maintenance and operating costs as well as the control of "dispersed" luminous flux to reduce the light pollution [4,5].

A methodology for the assessment and retrofitting of an outdoor lighting system in an industrial district is presented in this paper. First, the basic survey carried out to describe the present status of outdoor lighting and its main photometric performance by a measurement of both illuminances and luminance levels on road surface is discussed. Then, the procedure for the suitable assessment in terms of lighting performance and energy consumption (also considering present rules and standards) is reported, with the adoption of some key indicators finally leading to retrofitting proposals for the enhancement of energy efficiency, along with a reduction in cost and greenhouse gases emissions.

METHOD

The need to develop a "methodology" and then set up a suitable operating tool can be recognized from the finding that, at a regulatory level, there are no guidelines for analyzing the lighting system performances of the outdoor areas in industrial districts as well as for verifying the efficiency level. On the contrary, within the context of the public lighting of towns and cities, tools and methods for developing suitable guidelines have been already released [6-11] with the aim of identifying and defining key parameters and criteria to be followed for the design and installation of an efficient outdoor lighting system. Thus, the illumination of the outdoor areas of an industrial district can be considered a potential "demonstrator" upon which to develop a numerical/experimental methodology to evaluate the performance of a lighting system from the point of view of energy consumption as well as identify appropriate energy efficiency measures. The proposed procedure is based on two steps [11]:

1) **Audit**: collection and archiving of all data regarding the technical, economic, energetic characteristics as well as all the required measures to evaluate the status and photometric performance of the outdoor lighting system;
2) **Definition of Performance Indices**: definition of the energy, economic and environmental performance assessment of the lighting system using suitable parameters that might be related to statistical data and benchmark values available in current technical literature.

In the assessment of an external lighting installation, the first requirement is to provide for a detailed identification (mapping) of the power panels and luminaires as well as any general information about the site and measurement conditions, road surface characteristics, driving and visual conditions. In this paper, 11 outdoor areas of industrial districts were analysed; their lighting systems differ for the type and the nominal power of the light sources as well as the type and the arrangement of fixtures. The basic on-site measurements taken during this phase are reported in Figure 1. For each road of the 11 industrial areas, pictures of the night-time situation (1a) have been collected as well as measurements on the road surfaces (1b and 1c). Horizontal illuminance values were acquired by a Chroma Meter CL-200 (Konica Minolta with a measuring range from 0.1 lx to 100 klx and accuracy of ±2%), while the luminance values were acquired with a luminance meter Konica Minolta LS110 (acceptance angle of 1/3° and accuracy of ±2%).

The second phase of the methodology consisted of an operating procedure to define appropriate technical indices, from energetic (electrical power supplied and annual electrical energy required), economic (annual operating costs) and environmental (annual equivalent CO_2 tons emitted) points of view as well as identify critical bottlenecks of outdoor lighting systems and thus support measures for energy efficiency. The indices can also be used for the evaluation/comparison of performances between different zones of the outdoor lighting system of an industrial park or different park settlements. The indices used for a general performances description of a lighting system must cover several fields and should be presented as a "dimensionless" value when referring to both the number of fixtures (nf) as well as to the unit of road length (km). The Performance Indices considered in this study are described and listed in Table 1. The CO_2 emission was evaluate from the electric energy consumption using a conversion factor equal to 0.523 $kgCO_2/kWh$ [12], while the operating costs were evaluated considering an unit cost of electricity equal to 0.23 €/kWh. The Performance Indices allow to identify the zones with low efficiency, with it being beneficial

to suggest some renewal or retrofit operations that could be applied in order to improve the performance of the outdoor lighting system. On the basis of the road parameters and lighting situations found during the survey, all the roads were considered as secondary roads (C classification) with a speed limit of 50 km/h, therefore matching the reference lighting class ME4b.

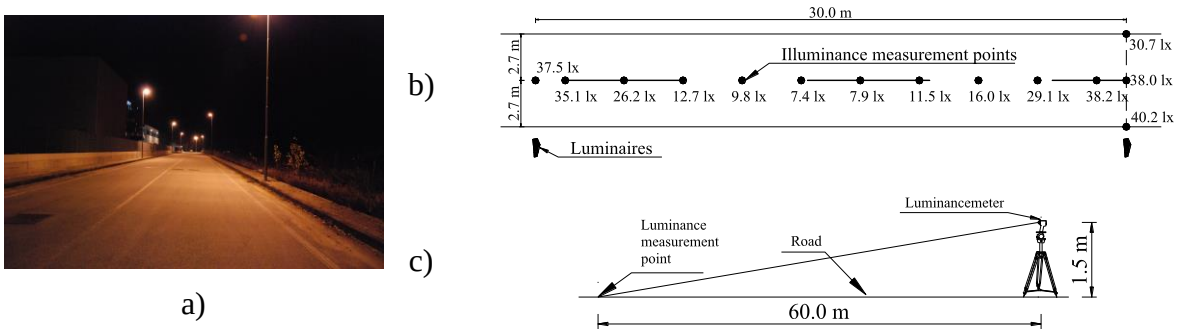

Figure 1: Assessments carried out during the audit, (a) picture of the road during the night, (b) illuminance measurement points and (c) arrangement for road luminance measurements.

Performance Indices proposed	Description	Units		
Economic impact	Total annual operating cost for electric energy per total road length/number of fixtures	k€/km	€/nf	
Power/Energy supplied	Total electric power or energy supplied per total road length/number of fixtures	kW/km	MWh/km	MWh/nf
Number and distribution of fixture	Total number of fixtures per total road length	nf/km		
Environmental impact	Total annual CO_2 emissions per total road length/number of fixtures	tCO_2/nf	tCO_2/km	

Table 1: Proposed indices.

Taking into account the information obtained during the audit and the limits defined by the current standard [13-16] and the Italian law [17], two different energy efficiency interventions were considered:

- **Scenario #1: optimization with respect to the reference lighting class**. When the measurement and simulation confirm the respect of the lighting requirements, the efficiency of the lighting system can be improved by considering different lighting classes (related to the real traffic flow) during the hours of darkness taking into account that it is possible to reduce the energy consumption by dimming the emitted luminous flux. Traffic flow, related lighting class and luminous flux dimming strategy considered for the different operating period are reported in Figure 2;
- **Scenario #2: optimization in terms of Best Available Technology (BAT)**. This strategy is based on the use of the best available technology in terms of energy savings, thus adopting high efficiency light sources integrated with photovoltaic modules (PV), while respecting the requirements of identified lighting class.

RESULTS AND DISCUSSION

In Figure 3, the values of the Performance Indices referring to the unit of road length (km) calculated for the Industrial Districts under investigation are reported. The figure shows that:

- the average values on the 11 industrial areas of power and energy supplied indices are 9.72 kW/km and about 38.2 MWh/km; the maximum values were observed for settlement #8 (21.9 kW/km and 86.3 MWh/km), while the minimum values for settlement #7 (4.43 kW/km and 17.1 MWh/km);
- the average value on the 11 industrial areas of number and distribution of the fixture index is 37.9 nf/km (ie. a fixture every 26.3 meters); the maximum value was observed for settlement #8 (75.6 nf/km), while the minimum value for settlement #7 (25.2 nf/km);
- the average value on the 11 industrial areas of the economic index is 8.8 k€/km; the maximum value was observed for settlement #8 (19.8 k€/km), while the minimum value for settlement #7 (3.93 k€/km);
- the average value on the 11 industrial areas of the environmental impact index is about 20.0 tCO_2/km; the maximum value was observed for settlement #8 (45.1 tCO_2/km), while the minimum value for settlement #7 (8.94 tCO_2/km).

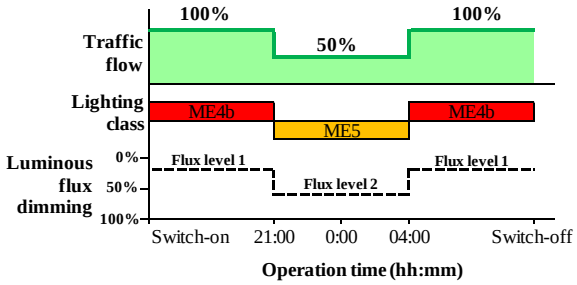

Figure 2: Traffic flow, lighting class considered and flux dimming.

Figure 4 shows the values of the Performance Indices referring to the number of fixtures (nf) for the Districts investigated. Figure 4 highlights an average value of 1.0 MWh/nf for the energy supplied index, 0.23 k€/nf for the economic index and 0.52 tCO_2/nf for the environmental impact index.

Figure 5 shows the results, in terms of both the energy saved and the CO_2 emission avoided, considering the two efficiency actions applied. On the basis of the on-site measurement performed during the audit, the lighting requirements were respected only by the lighting system of the Industrial Districts #1 and #3 therefore, Scenario #1 was analysed only for these two districts. For district #1, the flux was dimmed to 89 % for level 1 and 67 % for level 2, whereas for district #2, the flux was dimmed to 51 % for level 2 only. Scenario #2 allows for a complete self-sufficiency, eliminating the electric energy purchased from the grid and then the related environmental impact considering that the use of a lighting system with integrated PV modules covers all the energy requirements. As reported in Figure 5, the luminous flux control would enable energy savings and a CO_2 emissions reduction of about 25%. The solution, even if relevant for energy saving and environment protection, is, however, expensive in terms of installation costs. This is due to the high price of every single new pole as well as the fact that the luminous flux emitted by the fixture integrated with a photovoltaic module [18] was lower than the existing one and that the number of new poles required was greater than the existing one, which is on the average of about 3.4 times.

CONCLUSIONS

This paper describes a methodology for the analysis and subsequent proposal for renewal operations of an outdoor lighting system within an industrial district. In order to evaluate the effectiveness of the proposed methodology, it was applied to 11 industrial districts. Finally,

the benefit achievable through two energy efficiency scenarios were evaluated for each industrial district, in terms of energy saving and CO_2 emission reduction. The methodology started with a detailed audit based on an in-situ survey and measurement and proceeded with the calculation of some Indices required for assessing the economic, environmental and energy system performances. The audit phase showed that the lighting requirements were respected only by the lighting system of the Industrial Districts #1 and #3. For these districts, the application of Scenario #1 allowed to achieve significant energy savings on the average of 25%. The solution proposed in Scenario #2, if on one hand allowed for complete self-sufficiency, eliminating energy consumption and environmental impacts related to the use of lighting system, on the other presented very high installation costs.

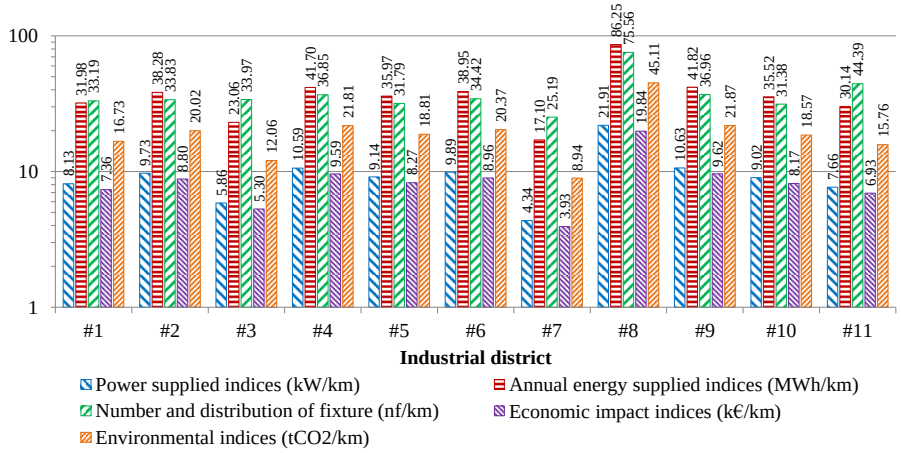

Figure 3: Performance indices referring to the unit of road length (km).

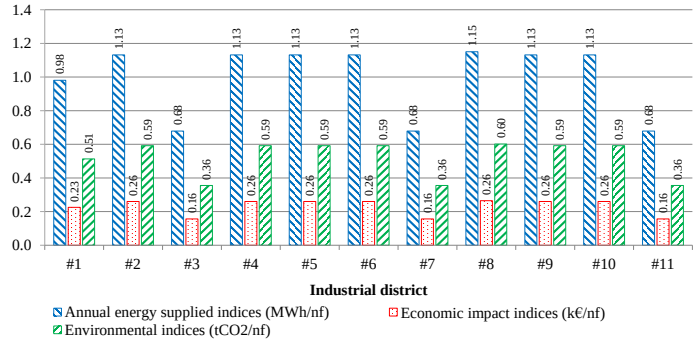

Figure 4: Performance indices referring to the number of fixtures (nf).

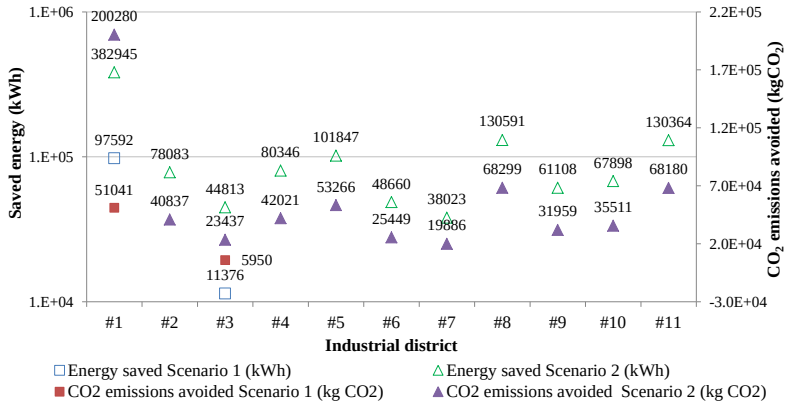

Figure 5: Yearly energy savings and CO_2 emissions avoided for the two different scenarios and different districts.

REFERENCES

1. European Commission, Green Paper on Energy Efficiency: Doing More with Less, 2005.
2. Communication from the Commission to the European Parliament, the Council, the European Economic and Social Committee and the Committee of the Regions, Energy Efficiency Plan 2011, COM 2011; 109, Brussels, 2011.
3. EEA, Greenhouse gas emission trends and projections in Europe 2012 - Tracking progress towards Kyoto and 2020 targets. A report by the European Environment Agency (EEA), Luxembourg: Publications Office of the European Union, doi:10.2800/56770, ISBN 978-92-9213-331-3, ISSN 1725-9177. Report No 6/2012, 2012.
4. Falchi, F., Cinzano P., Elvidge C.D., Keith D.M., Haim A.. "Limiting the impact of light pollution on human health, environment and stellar visibility." Journal of environmental management, Vol. 92, pp. 2714-2722, 2011.
5. Italian Standard UNI 10819 – Light and lighting - Outdoor lighting installations - requirements for the limitation of the upward scattered luminous flux, 1999.
6. Radulovic, D., Skok, S., Kirincic, V.. "Energy efficiency public lighting management in the cities." Energy, Vol. 36, pp. 1908-1915, 2011
7. Edler, J., Georghiou, L.. "Public procurement and innovation—Resurrecting the demand side." Research policy, Vol. 36, pp. 949-963, 2007.
8. Report for the European Commission DG Environment, Green Public Procurement - Street Lighting and Traffic Lights - Technical Background Report, 2011.
9. EuP Lot 9 Study: Public Street Lighting, VITO, GPP criteria for Street Lighting and Traffic signals, 2007
10. Enigma (Enlightenment & Innovation ensured through Pre-Commercial Procurement in CIties) - http://www.enigma-project.eu/en/, 2014.
11. ENEA Lumiere Project. http://www.progettolumiere.enea.it, 2014.
12. http://www.isprambiente.gov.it/contentfiles/00009400/9486-rapporto-135-2011.pdf/view.
13. UNI 11248:2012. Road lighting: Selection of lighting classes.
14. UNI EN 13201-2. Road lighting Part 2: Performance requirements.
15. UNI EN 13201-3. Road lighting Part 3: Calculation of performance.
16. UNI EN 13201-4. Road lighting Part 4: Methods of measuring lighting performance.
17. Regional Legislation n. 12/02. Norme per il contenimento dell'inquinamento luminoso e del consumo energetico da illuminazione esterna pubblica e privata a tutela dell'ambiente, per la tutela dell'attività svolta dagli osservatori astronomici professionali e non professionali e per la corretta valorizzazione dei centri storici.
18. Western CO. mod. SSL36B-W_160. http://www.western.it/lampioni-fotovoltaici-stradali-con-lampada-led-2/.

APPLICATION OF AN ANIDOLIC SYSTEM TO IMPROVE DAYLIGHTING IN EDUCATIONAL BUILDINGS

García Chávez J. R.[1]; García Ruiz A. K.[2]

1: Universidad Autónoma Metropolitana-Azcapotzalco. División de Ciencias y Artes para el Diseño, Departamento de Medio Ambiente, Laboratorio de Investigaciones en Arquitectura Bioclimática, Área de Arquitectura Bioclimática, Posgrado en Diseño. Arquitectura Bioclimática
San Pablo 180. Colonia Reynosa Tamaulipas. C.P. 02200, México, D.F. Tel. 52 55 5318-9110, e-mail: joserobertogsol@gmail.com

2: Universidad Autónoma Metropolitana-Azcapotzalco, División de Ciencias y Artes para el Diseño, Posgrado en Diseño. Arquitectura Bioclimática
San Pablo 180. Colonia Reynosa Tamaulipas., C.P. 02200, México, D.F. Tel. 52 55 5318-9110, e-mail: ark.zuir@gmail.com

ABSTRACT

The suitable interaction of daylight is an essential issue to reduce the energy consumption in buildings and to improve luminous comfort conditions of occupants. The aim of this work focused on investigating the potential of anidolic systems to enhance the daylighting conditions in an educational building whilst providing comfort for the students. Previous research has demonstrated the effectiveness of these systems [1, 2, 3, 4, and 5]. The case study building is a computer classroom of an elementary school located in the Mexico City Metropolitan Area (MCMA). During the first stage of this work, evaluation of the lighting conditions of the investigated space was carried out. Results indicated that natural light in the space was low and inadequate in most working stations. The physical and optical properties of the envelope components of the space were replicated in a 1:15 scaled physical model. The calibration process of the lighting conditions in the model showed similar conditions as in the actual building and then validated the procedure. Five different anidolic alternatives were implemented, investigated and evaluated in a scale physical model, located on the north facade of the case study space. These alternatives, assessed experimentally, showed a significant improvement of working plane illuminances and daylight factors, monitored under clear and overcast sky conditions relative to the reference model with a conventional facade. As a result, a significant improvement of the daylight autonomy can be expected and was confirmed with the implementation of computer simulation models. The most promising results were shown by an innovative system consisted of an anidolic arrangement integrated with a refractive panel system, that increased the lighting conditions in the space whilst improving visual comfort and overall performance. It is expected that the results of this work can be applied in other similar buildings aimed at providing suitable lighting conditions whilst reducing the energy consumption and the emission of greenhouse gases to the atmosphere, and to eventually promote sustainability in buildings.

Keywords: Anidolic system, innovative daylighting system, educational buildings, sustainability

INTRODUCTION

Natural light has played an important role in architecture since the first constructions of the human habitat. Nowadays, it is uncontroversial that light is a fundamental premise in architecture and that it must be considered to accomplish luminous and visual comfort for the building´s occupants as well as energy savings.In most buildings, with its climatic variations,

natural light can be the ideal, clean, free and efficient solution for energy savings and for the provision of luminous comfort conditions for the buildings occupants. The use of daylighting can also improve the health conditions of occupants in their work environments, particularly through physiological responses such as the regulation of the circadian rhythm and synthesis of vitamin D, and limit some detrimental effects of artificial light. Besides, the use of natural light in buildings implies the use a renewable energy source, which is a sustainable approach that reduces the emission of the greenhouse gases to the atmosphere.Therefore, natural light is an essential issue to be considered in any building from the conceptual design to the final documentation and construction stages. This research deals with the utilization of natural light by means of the implementation of anidolic systems applied in an educational building.

These systems incorporate the non-imaging optical principles used in a parabolic geometry to capture sunlight or daylight from the sun and the sky, concentrate the light into a focal point, and then redirect it into the building interior, and unlike the typical sidelighting systems that can perform fine under clear sky and sunny conditions, the anidolic systems perform well under overcast skies. This is due to its high concentration factor of its parabolic geometry that can use even the diffuse component of solar radiation and under direct solar radiation, without the use of any sun tracking mechanism [6]. Furthermore, anidolic systems, as static devices, minimize light losses and can accommodate a large spectrum of solar angles, which makes them suitable for most locations, during daily and seasonal changes and for a wide variety of building openings orientations. These type of systems were investigated and evaluated in this work.

RESEARCH OBJECTIVES

The objective of this work focused on investigating the potential of anidolic systems to improve the daylighting conditions in an educational building whilst providing visual comfort for the students. The case study building is a computer classroom of an elementary school located in the Mexico City Metropolitan Area (MCMA) (Figures 1 and 2).

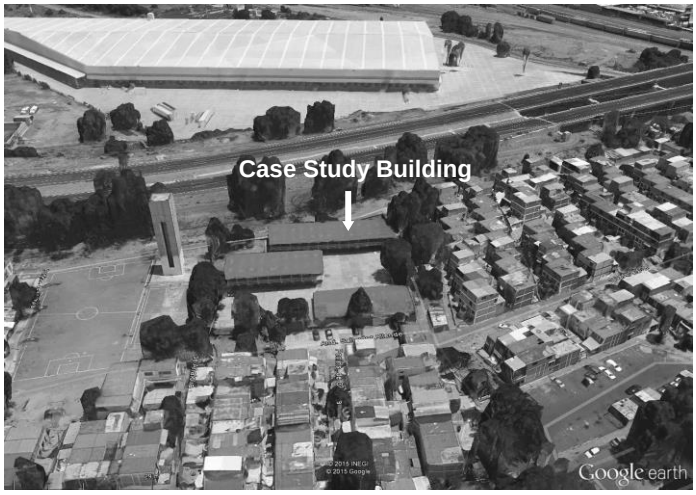

Figure 1: Aerial View of Case Study Building

During the preliminary evaluation of the lighting conditions, it was found that these were inadequate and did not comply with the recommended illuminance levels of the buildings standards [7]. The most critical space was found to be the computer room (Figure 3). The daylighting strategies proposed and investigated in this research were implemented in this space. The orientation of its main façade windows is south-southwest direction.

Figure 2: Main Façade of Case Study Building

Figure 3: Internal View of the Computer Room

METHODOLOGY

During the first stage of this work, the illuminance levels and daylight factors of the computer room were measured, and results indicated that the values were below the recommended building standards and to fulfil them, electric lighting has to be on throughout the school day [7]. The use of three dimensional physical scale models was selected for the evaluation of the daylighting strategies proposed. The model used in this research is at 1:15 scale.

Scale models are useful tools for daylighting analysis since light, travelling at its particular speed, does not require any scaling corrections, as the wavelengths of visible light are too short (from 380 to 780 nanometres), relative to the size of physical models, thus light behaviour is the same in a scale model as in the full size building.

Figure 4: Internal View of the Model with an Anidolic SystemImplemented During Exterior Analysis in Real Sky Conditions

The photometric and geometry properties: Optical reflectance and transmittance values of the internal envelope components of the real building, such as walls, ceiling, furniture and floor, and glazing, respectively were considered in the experimental procedure (Figure 4). The illuminance measurements were taken according to the local regulation methodology for this procedure (NOM-025-STPS-2008) in 25 points at desk level (0.75 mt).

Calibration of the model was conducted, measuring its illuminance levels and compare them with those of the computer room to guarantee that its optical properties were identical as those of the real building. Illuminance levels and Daylight Factors were measured in the 25 points of the space for assessing its quantitative performance, and photographs, from viewports, were recorded for qualitative analysis. The experimental evaluation was conducted under clear skies with real sky conditions, as the best possible scenario, and under an artificial sky using the CIE Standard Overcast Sky approach, as the worst possible daylight scenario (Figure 5).

Figure 5: Internal View of the Scale Physical Model with an Anidolic System in the artificial sky

The basic geometry of the anidolic systems evaluated is shown in Figure 6.

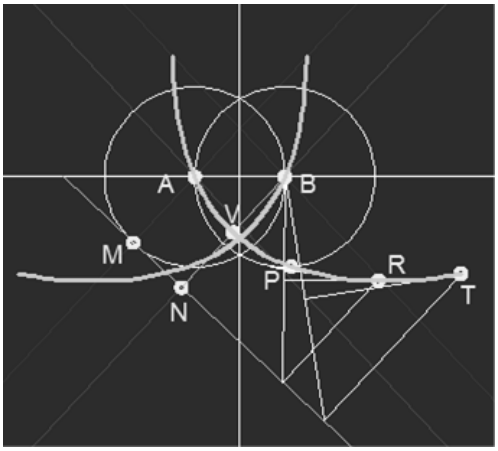

Figure 6: Basic Geometry of the Anidolic Systems Investigated

The anidolic systems have the distinctive capability to gather and redirect daylight from the exterior of a building into its interior with minimal light losses and significantly increase the

levels of natural light in a room, reaching deeper than other systems. The five anidolic systems selected for investigation were located on the north facade.

RESULTS

The experimental results were compared and complemented with the use of two computer simulation programs: Radiance, useful for daylighting and electric lighting analysis which is a physically accurate and comprehensive lighting and visualization analysis tool that calculates daylight factors, illuminances, luminances and daylight autonomy (Figure 7); and Daysim, which is a validated Radiance-based daylighting analysis software that models the annual amount of daylight in and around buildings and allows users to model a wide variety of dynamic and non-conventional façade systems such as light shelves, switchable glazing, including also complex electric lighting systems and controls (occupancy sensors, photocell controlled dimming, manual switches, etc.)

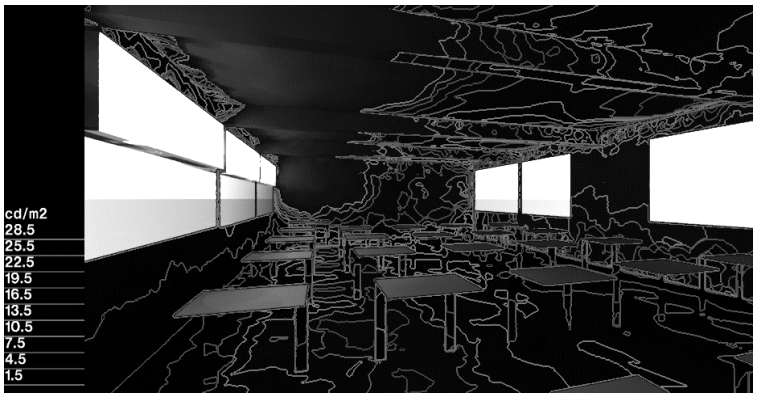

Figure 7: Luminance Values from Radiance. Summer Solstice at 12 hr

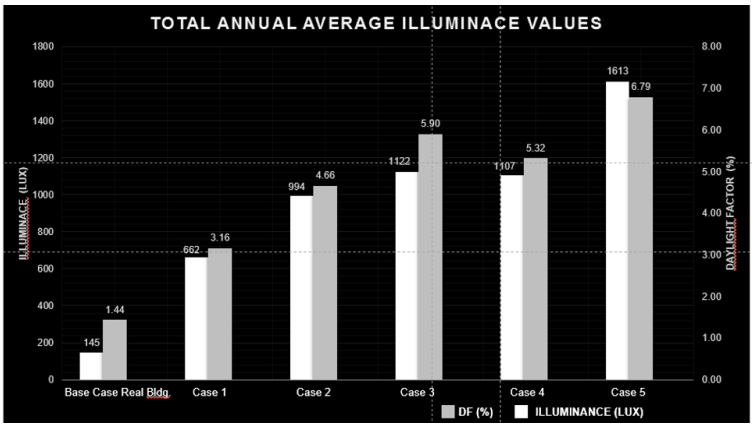

Figure 8: Annual Average Illuminance Values of all Anidolic Systems Investigated

ANALYSIS AND INTERPRETATION OF THE RESULTS

As shown in Figure 8, the anidolic prototype case 5 was the most promising alternative as provided an annual average of 1613 lux and 6.79 Daylight Factor (DF), relative to the base case without any system that registered 145 lux and 1.44 DF, respectively. The lowest values were obtained by Case 1. Cases 2, 3, and 4 were relatively similar, showing 994 lux, 4.66 DF; 1122 lux, 5.9 DF; and 1107 lux, 5.32 DF, respectively. Results indicated also that the use of a highly reflected film used in cases 2 to 5, provided better illuminance levels and DF´s. It was also observed that the use of a refractive layer implemented in cases 3, 4 and 5, increased the

values recorded and reduced significantly the light losses, and that of case 5 was the most promising and exceeded the recommended values of the local building standards.

CONCLUSIONS

The results of this work clearly indicate that the use of natural light can have great benefits both in new and existing buildings, which can also have a positive economic and environmental impact; furthermore, the occupants can have direct benefits in their health conditions and productivity. The implementation of anidolic systems in particular has a great potential to improve natural light into the spaces both in quantitative and qualitative terms for the overall performance and visual comfort of the occupants so that their daily activities can be carried out properly and thus they should be considered as a suitable alternative. To sum up, it was demonstrated the potential of anidolic systems provided they are carefully designed and, that variables such as the latitude of the location and the geometrical characteristics of the building, among others, are taken into account. It is expected that the systems examined in this work can be applied in similar buildings aimed at providing economic and global environmental benefits, which in turn can improve the productivity, efficiency and health of the occupants, and eventually, develop a more appropriate quality of living for the present and future generations, promoting at the same time a sustainable living approach.

REFERENCES

1. Aizlewood, M. E. Innovative daylighting systems: An experimental evaluation. *Lighting Research and Technology*, 25(4), pp. 141-152. 1993.
2. Andersen, M., Improving Daylighting in Existing Buildings: Characterizing the Effect of Anidolic Systems. Cambridge, Massachusetts. 2007.
3. García Chávez, J. R., Díaz, A. The Potential of an Innovative Sunlight System to Improve Luminous Comfort in Buildings. Application of a Specular Sunlight Device in Real Buildings. PLEA2012 - 28th Conference, Opportunities, Limits & Needs Towards an environmentally responsible architecture Lima, Perú 7-9 November 2012.
4. Welford, W. W. R., 1989. High Collection Nonimaging Optics. s.l.:Academic Press. 1989.
5. Jeong Tai Kima, Gon Kim. Overview and New Developments in Optical Daylighting Systems for Building a Healthy Indoor Environment. Building and Environment. Volume 45, Issue 2, February 2010, Pages 256–269. 2010.
6. Scartezzini, J.L., Courret, G. Anidolic Daylighting Systems. Solar Energy. Volume 73, Issue 2,August 2002, Pages 123–135. 2002.
7. CIE (Commission Internationale de l'Eclairage): http://www.cie.co. 2014.

DESIGN RECOMMENDATIONS FOR PERIMETER OFFICE SPACES BASED ON VISUAL PERFORMANCE CRITERIA

I. Konstantzos[1]; A. Tzempelikos[1]

1: Lyles School of Civil Engineering, Purdue University, 550 Stadium Mall Dr., West Lafayette, Indiana 47907 USA

ABSTRACT

Optimal positioning of workstations in perimeter offices is a key factor affecting visual comfort and satisfaction, depending on façade design and control. Visual comfort is related to different factors, such as daylight glare and light adequacy. In addition, connection to the outdoors, delivered through window views, is related to the amount of view as well as view clarity. This study presents a new approach to evaluate office workplaces in terms of overall visual environment. Visual comfort, daylight provision and outside view are used as the three basic criteria. A new index, the Effective Outside View (*EOV*), is introduced to characterize the connection to the outdoors considering the amount and clarity of outside view. In addition, the Visual Comfort Autonomy (*VCA*) is defined as the portion of time when visual comfort criteria, based on vertical illuminance on the eye, are satisfied. The spatial variation of these indices and continuous daylight autonomy are used to evaluate perimeter offices with glass facades and window shades. Detailed simulations, based on a validated daylighting-glare model, are used to evaluate visual conditions for different occupant positions and main view directions. A case study is presented for an open plan office with different façade orientations. Selected glazing and shading properties are used as an example to present results on appropriate seating configurations in order to reduce the risk of glare and maximize daylight use, while maintaining effective outside view. This study, along with future occupant surveys, will help define clear regulations and guidelines for comfortable daylit indoor environments.

Keywords: daylight, glare, window views, visual performance

INTRODUCTION

Open plan offices are a developing trend in commercial buildings. Not only they result to unified operations, encouraging team work and better cooperation, but they also lead to more efficient space utilization, a critical element in urban commercial districts. However, they are also associated with design challenges: since personalized comfort in larger spaces is quite challenging, visual and thermal comfort issues arise and generalized comfort regulations are helpful. In terms of visual comfort, the situation becomes more complex, as it is position-dependent, and in several cases, securing comfortable conditions for one group of occupants leads to unacceptable ones for another. There is a fair amount of literature covering the topic of open plan offices with respect to visual comfort and glare. Jakubiec and Reinhart [1] performed a survey in student facilities of Harvard to conclude that discomfort can be assessed in three different forms: glare, reflections and poor contrast. Hirning et al. [2] investigated open plan offices to obtain correlations with existing glare indices, while Konis [3] investigated the occupants' preferences in side-lit open plan offices. The viewing direction of occupants plays a significant role: rotated views can reduce or eliminate discomfort glare [4], while wall-facing directions lead to less uncomfortable conditions over the year [5]. Another visual aspect however, the connection to the outdoors, in terms of amount and clarity of view is not adequately studied, especially for open plan offices. Konis [3] found that occupants in perimeter zones left a portion of the window unshaded for most of the time to maintain adequate outdoor

view, despite the occurrence of visual discomfort. Other studies [6-7] pointed the qualitative relationship between sensation of glare and outside view, while Hellinga and Hester [8] presented a computational method to assess view and view quality.

This study proposes a methodology for comparing different spaces configurations with respect to visual comfort, lighting energy use and connection to the outdoors, all of which constitute a total Visual Performance Index. Towards that objective, two new terms, the annual visual comfort autonomy (*VCA*) and the effective outside view (*EOV*) are introduced.

METHOD

A set of metrics for assessing visual comfort, lighting energy savings potential and connection to the outdoors

As design decisions require annual performance data, an annual index is introduced, the Visual Comfort autonomy (*VCA*), defined as the portion of working hours when a person in a specific position is under comfortable conditions. While currently visual comfort is well predicted using the Daylight Glare Probability or DGP [9], Konstantzos et al. [10] stated that DGP may overestimate discomfort for occurrences with the sun directly visible through a shading fabric, especially for fabrics of low openness. That is due to the dramatic increase of the contrast term due to the extreme magnitude of the solar corona's luminance. While this high value is accurate by definition, DGP was not developed under such conditions and moreover, the way the human eye receives light through dense fabrics is not adequately studied. These facts, combined with common experience that fabrics of small (< 2%) openness do not result in significant discomfort, suggest that other criteria could be used to assess discomfort for these cases. Within that scope, Chan et al. [11] suggested a double discomfort criterion including (i) the 0.35 limit for DGPs [12] to account for total vertical illuminance on the eye and (ii) a 1000 lux limit for direct light on the eye, as a modification of IES Standard LM-83-12 [13]. As this study is focused on closed shades, these discomfort criteria are preferred. Therefore, the Visual Comfort Autonomy (*VCA*) is defined as the percentage of annual working hours when the restrictions of the above double criteria are met.

Foe daylight provision and lighting energy use reduction, the annual index of continuous Daylight Autonomy [14] is used. This metric is more suitable for obtaining light energy use for offices with light dimming control systems. A threshold of 300 lux on the work plane is used, complying with IES recommendations [13].

For the connection to the outdoors, a combined quantification of the amount and the clarity of view is proposed. As the quality of view is a highly subjective variable, dependent on the exterior scenery, the clarity of outside view is used instead, as a more objective and measurable concept. For that purpose, the View Clarity Index (*VCI*) is utilized, a metric recently developed [15] to characterize view clarity through windows with shading fabrics (Eq. 1), which depends on the basic optical properties of fabrics.

$$VCI = 1.43 \cdot (OF)^{0.48} + 0.64 \cdot \left(\frac{OF}{T_v}\right)^{1.1} - 0.22 \quad (1)$$

where *OF* is the openness factor and T_v is the normal total visible transmittance of the fabric as provided by manufacturers.

The amount of view is evaluated with the projected solid angle of the visible part of the window (for each position and view direction), normalized with the overall solid angle of the human visual field, Ω_{FOV} (circular cone with a half-angle of 78°), in order to provide a sense of measure against an "ideal" visual field, entirely connected to the exterior. In this process, the window is discretized into rectangular fragments to approximate the total solid angle of the window as the

sum of the respective solid angles of the fragments. This makes calculations straightforward and faster, compared to applying transformations and integrations otherwise required due to the spherical definition of solid angle [16]. The model checks whether each fragment is within the field of view for each viewing direction, and excludes the rest of the window from the view calculations. *VCI* is then merged with the projected solid angle of the visible part of the window in a new metric, the Effective Outside View (*EOV*), considering both the amount and the clarity of outdoor view for any seating position, view direction and shading fabric (Eq. 2).

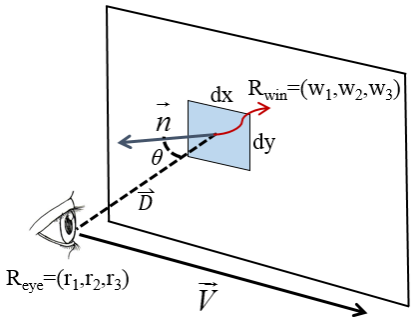

Figure 1: Geometry for calculation of differential solid angles and projected solid angle of each window segment in the direction of the observer.

$$EOV = \frac{\sum \Omega_{i\in(FOV)}^{proj} \cdot VCI}{\Omega_{FOV}} = \sum_{i\in(FOV)} \frac{\frac{A_i \cdot cos\vartheta_i \cdot VCI}{\left|\overrightarrow{D_i}\right|^2}}{2\pi \cdot (1 - cos78^0)} \quad (2)$$

where A_i is the area of each visible window fragment i, θ_i is the angle between the normal to the window and the line connecting the eye and the fragment, and D_i is the distance between the eye and the fragment as shown in Fig. 1. The spatial variation of the three metrics (*VCA*, *cDA* and *EOV*) is used to calculate respective annual Visual Performance Indices as described next.

Simulation Methodology and overall Visual Performance Indices

A validated hybrid ray tracing and radiosity model [17] was used for the daylighting simulation. The model uses: TMY3 or measured weather data and anisotropic sky models to calculate the incident illuminances on the façade; data from WINDOW software [18] to calculate the angular properties of the glazing system; and implements the semi-empirical model by Kotey et al. [19] for calculating the angular optical properties of roller shades. Then, a ray-tracing module computes direct illuminance on interior surfaces, while a radiosity module handles diffuse inter-reflections. The model outputs include a detailed luminance and illuminance mapping for all interior surfaces and for a specified grid of occupant seating locations (*n* total), as well as DGP values when desired. The direct and total vertical illuminance are calculated over the year for each of the *n* occupant positions. The continuous Daylight Autonomy (*cDA*) in this study considers a set point of 300 lux on the work plane (0.8 m from the floor) and is calculated from virtual sensors on the same grid.

The spatial variation of the three metrics (*VCA*, *cDA* and *EOV*) is finally used to calculate respective annual Visual Performance Indices for comfort, energy use and outdoor view (*VPIc*, *VPIe* and *VPIv*) as follows. Visual comfort is the main priority, therefore *VPIc* (Eq. 4) is first defined as the portion of comfort-autonomous area (number of seating locations satisfying the VCA criteria for 95% of the working hours). For that area only, *VPIe* and *VPIv* are calculated from *cDA* and *EOV* respectively, averaged over the remaining seating location grid, to obtain average VPI "scores" for each directional seating layout (Eqs. 5-6).

$$VPI_c = \frac{\sum_{i=1}^{n} i}{n} \Big| \, i \in (VCA > 95\%) \quad (4)$$

$$VPI_e = \frac{\sum_{i=1}^{n} cDA_i}{n} \Big| \, i \cap [n \in (VCA > 95\%)] \quad (5)$$

$$VPI_v = \frac{\sum_{i=1}^{n} EOV_i}{n} \Big| \, i \cap [n \in (VCA > 95\%)] \quad (6)$$

For each directional layout, the output is a triplet of *VPI* factors, which can be compared with results for alternate layouts on a relative basis, for an overall visual environment evaluation of any space with a given geometry, orientation, glazing and shading properties. The process is described in Fig. 2.

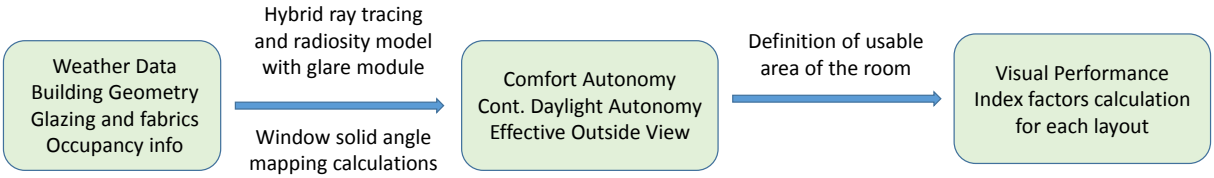

Figure 2: Flowchart of simulation methodology and VPI factors

RESULTS

For this case study, a 10 m x10 m x 4 m high open-plan office space is considered, with a 70% of the façade covered by double clear windows. A dark-colored shade is used with high *OF*=11.2% and T_v=12%, which has a high *VCI* (87%) and provides good connection to the outside even with closed shades. The simulation was performed for West Lafayette, Indiana, for different façade orientations and for two directional workstation layouts (facing the left side wall and facing the windows).

The results are presented in Figures 3-4. Orientation plays a significant role: for south-facing façades (Fig. 3), due to more sunlight exposure and low winter sun, a significant portion of the space (37%) does not satisfy the visual comfort autonomy criteria (VCA>95%) for window-facing positions. For the rest of the (acceptable) space, VPIe = 39% and VPIv = 8.2%, as all positions near the window (which contribute to higher effective view) are outside the "comfort-autonomous" zone. However, for left side wall-facing positions, the entire space is within acceptable comfort limits (VPIc=100%), therefore VPIe increases to 54% and VPIv slightly decreases to 7.3% due to not facing the window. For north-facing facades (Fig. 4), where the sun is not visible and the brightness conditions are lower, the entire space is "comfort-autonomous" for both viewing directions and therefore cDA is the same. However, the average EOV is by 12.7% higher for window-facing layouts, which makes this configuration better. The results for all other orientations can be seen in Table 1.

CONCLUSION

This paper presents a new methodology for evaluating the overall visual performance in offices based on visual comfort, lighting energy use and outdoor view criteria. The method can be used either during the design phase, to compare different envelope configurations, or for existing buildings, to make decisions about the directional layout of workstations. In this case study, wall facing layouts are the best option for south, east or west-facing facades, as they lead to higher space usability, lower lighting energy use and higher connection to the outdoors. This study part of ongoing research, aiming to provide more conclusive regulations for perimeter offices in terms of comfort, energy and connection to the outdoors. The presence of furniture and interior partitions was ignored; in reality, these surfaces will block a portion of daylight and will alter illuminance distributions and window views. Also, the issue of sunlight (through

closed shades) incident on computer screens was not considered; but the exact direction of the screen is up to the occupants. In any case, fabrics with limited openness and visible transmittance should be used to better protect from glare. Finally, there is a dependence of view clarity on viewing distance [15] that should be addressed in future studies.

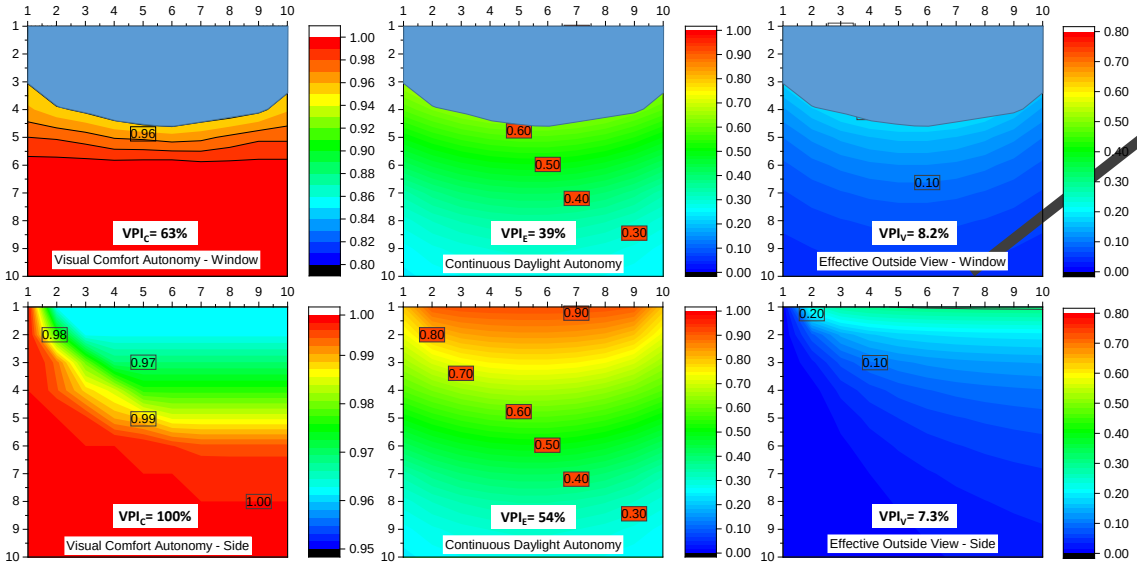

Figure 3: VPI factors for south facades –facing the window (top) and the left wall (bottom).

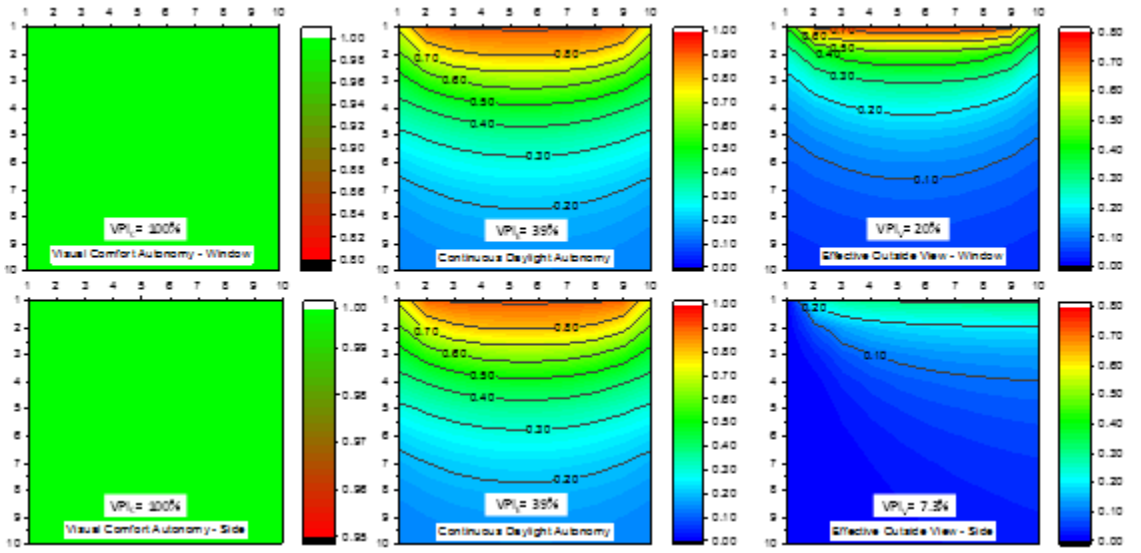

Figure 4: VPI factors for north facades –facing the window (top) and the left wall (bottom).

	VPIc (%)		VPIe (%)		VPIv (%)	
View direction	Window	Wall	Window	Wall	Window	Wall
South	63	100	39	54	8.2	7.3
North	100	100	39	39	20	7.3
West	41	100	33	52	6.2	7.3
East	68	100	35	48	9.4	7.3

Table 1: VPI factors for different orientations and view directions

REFERENCES

1. Jakubiec J.A., Reinhart C.F.: Predicting visual comfort conditions in a large daylit space based on long-term occupant evaluations –a field study. Proc. of IBPSA13, France, 2013.
2. Hirning M., Isoardi G., Cowling I.: Discomfort glare in open plan green buildings. Energy and Buildings 70, pp. 427-440, 2014.
3. Konis K.: Evaluating daylighting effectiveness and occupant visual comfort in a side-lit open-plan office building in San Francisco, California. Building and Environment 59, pp. 662-677, 2013.
4. Jakubiec J.A., Reinhart C.F.: The adaptive zone – a concept for assessing discomfort glare throughout daylit spaces. Lighting Research and Technology 44(2), pp. 149-170, 2012.
5. Chan Y.-C., Konstantzos I., Tzempelikos A.: Annual daylight glare evaluation for typical perimeter offices: simulation models versus full-scale experiments including shading controls. Proc. of ASHRAE Annual Conference, Seattle, Washington, 2014.
6. Aries M.B., Veitch J.A., Newsham G.R. Windows, view, and office characteristics predict physical and psychological discomfort. Journal of Environmental Psychology 30 (4), pp. 533-541, 2010.
7. Tuaycharoen N., Tregenza P. View and discomfort glare from windows. Lighting Research and Technology 39 (2), 185-200, 2007.
8. Hellinga H., Hordijk T.: The D&V analysis method: A method for the analysis of daylight access and view quality. Building and Environment 79, pp. 101-114, 2014.
9. Wienold J., Christoffersen J.: Evaluation methods and development of a new glare prediction model for daylight environments with the use of CCD cameras. Energy and Buildings 38(7), pp. 743-757, 2006.
10. Konstantzos I., Tzempelikos A., Chan Y-C.: Experimental and simulation analysis of daylight glare probability in offices with dynamic window shades. Building and Environment 87, pp. 244-254, 2015.
11. Chan Y.-C., Tzempelikos A., Konstantzos I.: A systematic method for selecting roller shade properties for glare protection. Energy and Buildings 92, pp. 81-94, 2015.
12. Wienold J.: Dynamic simulation of blind control strategies for visual comfort and energy balance analysis. Proc. of IBPSA 2007 Conference, Beijing, pp. 1197-1204, 2007.
13. IESNA: IES Standard LM-83-12. Approved method: IES Spatial Daylight Autonomy (sDA) and Annual Sunlight Exposure (ASE), New York, 2012.
14. Rogers, Z. Daylighting Meric Development Using Daylight Autonomy Calculations in the Sensor Placement Optimization Tool. Boulder: Architectural Energy Corporation, 2006.
15. Konstantzos I., Chan Y-C., Seibold J., Tzempelikos A., Proctor R.W., Protzman B.: View Clarity Index: a new metric to evaluate clarity of view through window shades. Building and Environment, in press, 2015.
16. Mathar, R. J.: Solid angle of a rectangular plate. Max-Planck Institute of Astronomy, Königstuhl, 17, 69117, 2012.
17. Chan Y.-C., Tzempelikos A.: A hybrid ray-tracing and radiosity method for calculating radiation transport and illuminance distribution in spaces with venetian blinds. Solar Energy 86(11), pp. 3109-3124, 2012.
18. LBNL, 2013. WINDOW 7 simulation manual. Lawrence Berkeley National Laboratory. http://windows.lbl.gov/software/window/7/
19. Kotey N.A., Wright J., Collins M.R.: Determining off-normal solar optical properties of roller blinds. ASHRAE Transactions 117 (1), 10 pages, 2009.

LIGHTING RETROFIT IN CURRENT PRACTICE: RESULTS FROM A SURVEY OF IEA TASK 50

B. Paule[1]; J. Kämpf[2,3]; M.-C. Dubois[4]

1: Estia SA, EPFL Innovation Park, Lausanne, Switzerland

2: Solar Energy and Building Physics Laboratory, EPFL, Lausanne, Switzerland

3: kaemco LLC, La Riaz 6, Corcelles-Concise, Switzerland

4: Lund University, Energy and Building Design, Sweden

ABSTRACT

Surveys and socio-professional studies carried out at national and international levels contribute to a better understanding of the lighting retrofit process. Within the framework of the International Energy Agency Task 50 - Advanced lighting solutions for retrofitting buildings- and its subtask C1 focusing on the analysis of workflows and needs, an online survey on lighting retrofit was initiated in December 2014. After 9 months, more than 1000 answers were collected. The survey provides clear insights about the workflow of building professionals and leads to a better understanding of their needs in terms of computer method and tools.

One of the main outcomes of the survey is that retrofitting strategies used in practice essentially focus on electric lighting actions such as of luminaire replacement and the use of controls. Generally, daylighting strategies are not rated as the highest priority. The results also indicate that practitioners mainly rely on their own experience and rarely involve external consultants in the lighting retrofit process. Furthermore, the survey results suggest that practitioners are interested in user-friendly tools allowing quick evaluations of their project, with a good compromise between cost and accuracy, and producing reports that can be directly presented to their client.

The survey also emphasized that the main barriers in using simulation tools are essentially their complexity and the amount of time it takes to perform a study. Practitioners are keen to use tools at preliminary design stage and would like to be able to estimate the cost and other key figures (energy consumption and lighting levels). The paper concludes with recommendations for the building software developers to address the needs of practitioners in a more suitable way.

Keywords: Survey, Lighting, Daylighting, Retrofitting, Methods, Tools

INTRODUCTION

Lighting accounts for approximately 19%, i.e. 2900 TWH, of the global electric energy consumption. Projections [1] by the IEA show that if governments only rely on current policies, global electricity use for lighting will grow to around 4250 TWh by 2030, an increase of more than 40%. Research and developments in the field of energy efficient lighting techniques encompassing daylighting, electric lighting and lighting controls combined with activities bringing these techniques to the market can significantly contribute to reduce worldwide electricity consumptions and CO_2 emissions. These activities will therefore be in line with several different governmental energy efficiency and sustainability targets.

With a small volume of new building constructions in the developed countries (~3%/year), the energy saving potential through lighting and daylighting (façade) mainly lies in the retrofitting of the existing building stock. Furthermore, in emerging economies already several quite young buildings need to be retrofitted. As lighting retrofit activities mainly depend on electricity prices, which show big deviations worldwide according to the energy mix, different levels of product complexity and prices need to be considered for different markets. These local specifics therefore are addressed in an overarching international project: the IEA SHC Task 50 "Advanced Lighting Solutions for Retrofitting Buildings".

Within this Task, Subtask C focuses on computer design tools and analysis methods with the general aim to improve the understanding of retrofit processes. Within the framework of the project area C1 focusing on the analysis of workflow and needs, a survey was conducted on national level to understand the workflows, wishes and needs with respect to computer method and tools of the stakeholders involved in a lighting retrofit process.

This paper presents the methodology developed to create and distribute the survey, the results obtained and an analysis of the outcomes. The paper concludes with recommendations for building software developers to address the needs of building professionals in a more suitable way.

METHODOLOGY

The international survey was created based on a previous one developed as part of a recent IEA Task 41 called "Solar Energy and Architecture". The survey of Task 41 pursued similar goals as the current one i.e. the survey addressed methods and tools used by building professionals but the area of focus was active and passive solar energy use. Many questions from this previous survey were simply adapted to the topic of lighting and daylighting retrofit.

The IEA Task 50 experts jointly developed the survey and published the online questionnaire [2] where the specific themes were: the importance of lighting within thermal retrofitting, the main retrofit strategies, the actual approaches for lighting design, the available information and, finally, the method and tools used within the retrofit process.

The survey was translated in eleven languages: Danish, Dutch, English, Finnish, French, German, Italian, Japanese, Portuguese (Brazil), Slovak and Spanish. Its online form was created using SurveyMonkey [3] with one full questionnaire per language. A front page for the language selection was hosted at EPFL in Switzerland [4]. Task participants of each country achieved the dissemination of the questionnaire during a period of nine months between January and September 2014.

RESULTS AND DISCUSSION

After three quarters of a year, more than 1000 answers from building professionals were collected. Out of 1187 answers, French speaking people were the most numerous (425 answers, the Belgian and Swiss accounted for the vast majority of responses while the French provided less than 20% of French respondents). German speaking people (224 answers) mainly originated from Germany but also from Switzerland and Austria. English speaking respondents (294 answers) originated from various countries with very few respondents from UK and USA (countries not represented in this IEA-50 Task). Most dutch speaking respondents (82 answers) were from Belgium. The rest of the answers came from various countries and covered about 13% (n=162) of the answers.

Amongst the 17 questions related to the lighting retrofit process and the seven questions related to the background information, this paper focuses on only six themes in addition to providing some key information about the respondents.

Importance of lighting within thermal retrofitting

One of the first outcomes of the survey is that within the retrofitting process, lighting (electric lighting and daylighting) is considered as "Important" by the vast majority of the respondents (respectively 58% and 66%). This is positive since the lighting energy share in the energy bill of buildings becomes more and more important with thermally efficient buildings. This result is in line with the results obtained in IEA Task 41, where respondents judged in a vast majority that solar energy was "very important".

As shown in Figure 1, for about half of the respondents, the lighting retrofit is almost always considered when heating and cooling retrofit measures are taken. However, incentives should be initiated to change the behaviour of about 30% of the respondents that never or almost never consider the lighting retrofit measures when thermally retrofitting a building. Indeed, the main driver of the retrofitting measures is often linked to thermal regulations, which usually do not take lighting into account. As an example in Switzerland, the Minergie-P regulation for passive buildings can be achieved without any glazed surfaces impairing the daylight availability and imposing only electric lighting. Another example is the Swedish energy code, which does not include the tenants' electricity use (plugs loads and lighting) and therefore fails to provide an incentive for lighting retrofit.

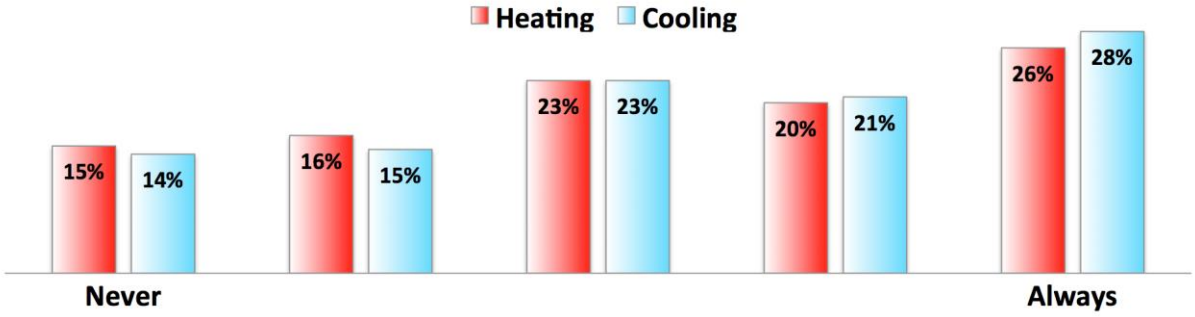

Figure 1: Rating of the integration of lighting purposes within thermal retrofitting

Main retrofit strategies

The three main retrofit strategies considered by the respondents are addressing only electric lighting technologies: going towards more efficient lighting technologies, using occupancy sensors to follow the occupation schedule and using task-ambient lighting design. The reduction of the maintained illuminance levels is not used in practice (e.g. from 500 to 400 lux), unlike the reduction of the temperature set-point in thermal retrofit measures. Furthermore, the spectral quality of the light source (colour rendering, blue component, etc.) is actually not frequently considered in the retrofitting practice.

Actual approaches for lighting design

In the preliminary design phase of the retrofitting projects considering daylight (Figure 2) and electric lighting, the results indicate that respondents mainly rely on their own experience by using rules of thumb and design guidelines. This is totally in line with previous results obtained as part of IEA Task 41 regarding active and passive solar energy. Computer simulations are indeed less considered at this stage, which may reflect the fact that common computer tools are too detailed and not adapted to the preliminary design stage.

Most of the respondents handle the design and decision process themselves, and often involve a lighting manufacturer. The results also show that multi-disciplinary workshops are almost

never used in the handling of the design and decision process. It is however to be noted that interactions with the owner remain important throughout the whole design process.

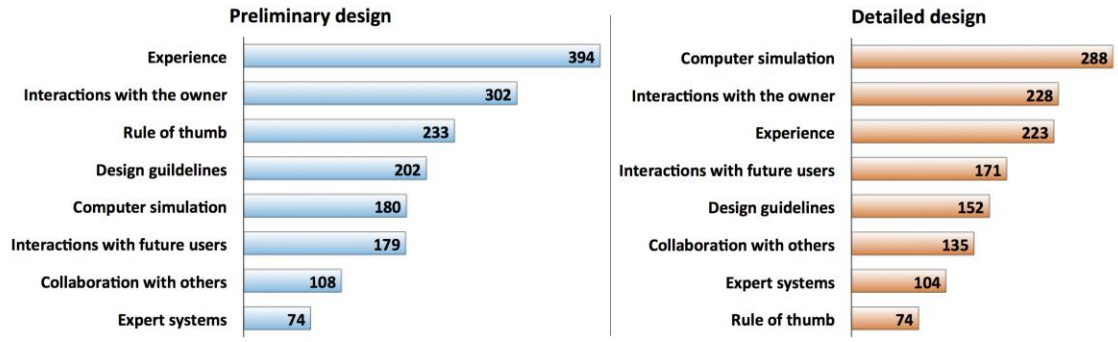

Figure 2: Ranking of the tools and methods used for daylighting design

Available information

From the survey, most of the building or infrastructure information is generally available in printed form, which is consistent with the fact that old buildings are generally refurbished. The poor availability of electronic documents is identified as a barrier to the use of computer simulation tools in the retrofitting process. Especially in the pre-design phase, the absence of BIM generates a large investment in time for the building professionals. Furthermore, the lighting electricity consumption is rarely known, unlike the total electricity consumption, which also comprises the other appliances. Installed power and luminaires' characteristics are often available; one should note that they can anyhow easily be determined by observation.

Methods and tools used within the retrofit process

The total number of respondents that use a specific tool for electric lighting (149) and daylighting (136) is higher than the number of respondents who declare that they use a combined lighting tool (224). This result is quite surprising since most of the leading simulation tools available on the market address the both subjects. Furthermore, one can notice in Figure 3 that a significant number of people do not use any tool. Finally, combined energy tools are not yet established in current practice.

Regarding respondents involved in the lighting retrofit process (501), a great number declare that their skills are acceptable (122) or advanced (138) and about a third describe their skills as poor or very poor, a result which is also in line with previous results of IEA Task 41. The tools and methods available are further divided into four categories: facility management, CAAD / CAD, visualisation and simulation. The answers of the respondents are analysed further down according to these categories.

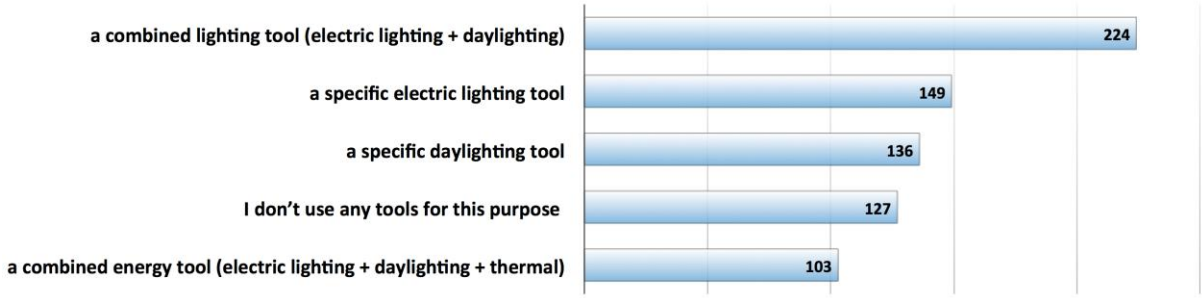

Figure 3: Type of tools used by the respondents for lighting analysis

In Facility management, most of the respondents do not use any tool in the lighting retrofit process; some have built in Excel sheets. In CAAD / CAD, Autocad is a dominant tool on the market, followed by Archicad, Revit and SketchUp. Many respondents of the questionnaire

use a combination of two or more tools in their practice and their global satisfaction is high to very high (at 66%). In Visualisation, Dialux, Sketchup and Relux are the three most used tools in the lighting retrofit process. The global satisfaction is similar to that of the CAAD / CAD category i.e. high to very high for 56% of the respondents. It is noteworthy that 17% of the respondents are very dissatisfied with the Visualisation tools.

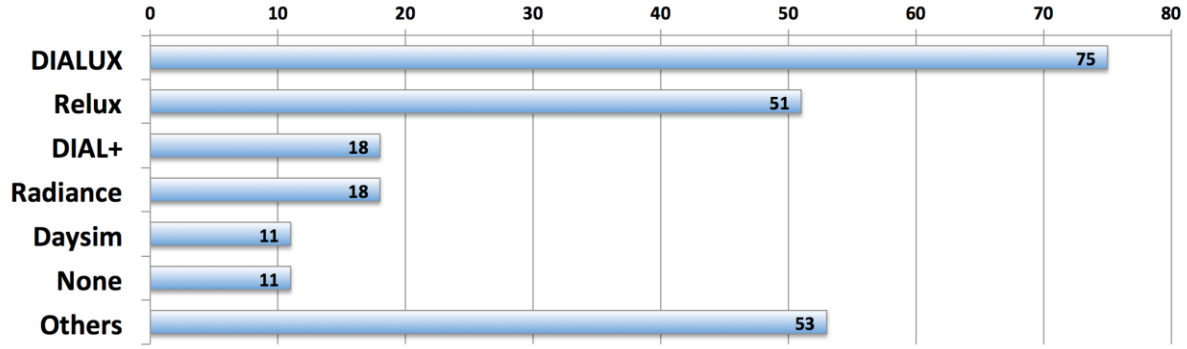

Figure 4: List of tools used to handle simulation in the retrofit process.

In Simulation (Figure 4), Dialux and Relux are the most used software by the respondents followed by DIAL+ and Radiance. The "Others" category includes the following tools: Design Builder (7), Sketchup (6), Ecotect (6), Energyplus (5), Lesosai (5), Diva (4), Velux Visualizer (4), IDA-ICE (3), DIVA for Rhino (3), Trnsys (2), 3DS-max (2), REVIT (1), SomfyDisk (1), Vasari (1), BSim (1), Lightworks (1), Photoshop (1). The global satisfaction for 57% of the respondents is high to very high, with a fifth (20%) very dissatisfied.

Figure 5 shows the list of factors that most influence the user's choice of software. The major issue leading to the choice is to have a user-friendly interface (253) that allows quick and efficient analysis (234). This result in again in line with results obtained in IEA Task 41. The cost of the software (217) is also a major concern, together with the accuracy of results (200) and the quality of the output produced to integrate in reports or presentations (178). Regulations are not often considered in the survey (100), showing that these may not provide real incentives.

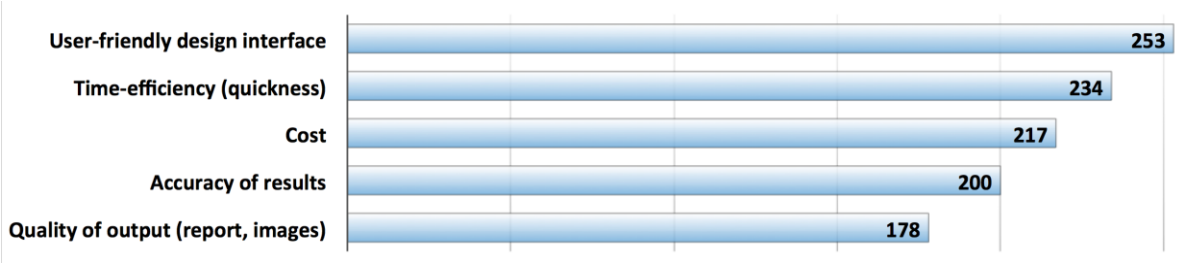

Figure 5: List of 5 factors that most influence the choice of software.

Some barriers were identified when applying lighting tools within the retrofit process: many of the respondents reported that tools are too time-consuming in their usage (154) and too complex (131). This is consistent with the fact that tools are considered as "not adequately supporting the conceptual design stage" by many respondents (87). The incompatibility with other software used by the company (70) and the fact that existing tools are not integrated in "normal workflow" (67) are mentioned by a significant number of respondents.
There is a consensus (145 answers) about the need for improved tools for preliminary sizing of lighting systems, for calculating payback times and investments in lighting and daylighting (144) and for providing key data about lighting levels and energy consumption (142).

General information on the respondents

For new buildings, the major part of the building categories that correspond to the current practice of the respondents were: Office buildings (233), Education and research buildings (188) and Commercial buildings (154). For retrofitting buildings, they were: Office buildings (238), Education and research buildings (210), Cultural buildings (144) and Commercial buildings (143).

Surprisingly, companies with more than 50 employees are the most represented (113) in the survey. In such firms, it is plausible that some people are specialized on lighting. On the other side Small and Medium Enterprises are also well represented (108), in which generalists who must be able to handle a wide array of skills are mainly found. Architects and physicists represent the vast majority of respondents. In comparison, lighting designers are very few but they also represent a rare species in the building sector. The majority of respondents have more than 10 years of experience and are only active on a national level, which probably reflects the fact that, historically, the building sector has a strong local presence.

CONCLUSION

An international survey distributed in 49 countries and translated in eleven languages collected more than 1000 answers from diverse professional groups relating to the lighting retrofitting of buildings. Current practice of the respondents, mainly architects and physicists, mainly entail the retrofit of office, educational and commercial buildings. Amongst these professionals, a majority considers the lighting retrofit process when thermally retrofitting the building, even though thermal regulations do not impose it. The retrofitting measures generally focus on electric lighting with more efficient lighting technologies, lighting controls and task ambient lighting. Rules of thumb and guidelines are mainly used at the pre-design phase, and computer simulation tools used at the detailed phase. The absence of BIM at the early stage of the retrofit process is a barrier to the use of computer tools, since only printed plans are available for the (generally) older building stock.

The methods and tools used by the practitioners involve specific daylight and electric lighting simulation tools, often combined but rarely including thermal calculations. The choice of software is mainly driven by user friendliness of the interface, the speed of the simulation process (data entry and computing time), its cost and the accuracy of the results. The main barriers in using digital tools are identified such as: too time consuming and too complex. Finally, the survey results suggest that the strongest need for improvement of the actual computer tools is connected to the pre-design phase for sizing lighting systems, for calculating payback times and investments and for providing key data about lighting levels and energy consumption. In general, many results of this survey are completely in line with the results of IEA Task 41 survey in the area of active and passive solar energy technologies.

REFERENCES

1. IEA-41: LIGHT'SLABOUR'S LOST, Policies for Energy-efficient Lighting, 2006.
2. M.-C. Dubois (Université Laval) M. Horvat (Ryerson University): International survey about digital tools used by architects for solar design, Subtask B2, 2010.
3. Dubois M-C, Horvat M, Kanters J (2011). Design tools and methods used by architects for solar design: results of an international survey in 14 countries. *CISBAT Conf.*, Lausanne (Switz.), Sept. 14-16. Book of abstracts p. 178.
4. Website: https://www.surveymonkey.com/, last visited: 04-14-2015.
5. Website: http://leso2.epfl.ch/task50/, last visited: 04-14-2015.

LIGHTING TARGETS IN SWISS REGULATION AND LABELS: WHAT WOULD IT TAKE TO CHANGE?

B. Paule[1], M. Giorgi[1]

1: Estia SA, EPFL Innovation Park, Lausanne, Switzerland

ABSTRACT

Switzerland has long been regarded as a pioneer in the field of lighting, especially for daylighting. It may be recalled for example that in the 80's, the Swiss Association for Lighting was the first to propose the concept of daylighting autonomy. Furthermore, one cannot ignore the deep involvement of EPFL in the development of daylighting methods and tools since the early 90's.

However, the use of natural lighting is hardly fostered by the current Swiss building regulation and that the trend for lighting is mainly concentrate on the use of high performance luminaires and advanced lighting control. Moreover, the present regulation can even lead to paradoxical situations such as, for example, a windowless room is more likely to fit with the standard than if it is equipped with large openings.

Daylight is renewable energy, and to achieve the objectives of a sustainable society, it is imperative to use its maximal potential. This is particularly relevant if one considers that the part of lighting in the building energy consumption is increasingly important.

This paper points out these limits of the Swiss standard through the study of five particular examples. It concludes with some proposals for improvements and suggests taking advantage of the latest developments in design & simulation tools which are now available on the market.

Keywords: Daylighting, Swiss standard.

INTRODUCTION

The Swiss regulation for lighting is primarily governed by the SIA-380/4 standard [1] and the technical specifications described in SIA-2024 [2]. These documents are part of the Swiss policy to reduce electricity consumption in the building. The principle of this standard is to use approximation rules in order to give an estimation of the lighting electricity consumption. The most influential parameters are aggregated to produce weighting factors. Current records date from 2006 and a new version of the documents is currently in preparation. The time is right for commenting on the flaws of the current regulations so that the new version could be improved. This paper particularly highlights four major areas of improvement:

For each point, we examine typical examples illustrating the potential for improvement. The proposed arguments are based either on in-situ observations, or on simulations performed using the DIAL+*Lighting* software [3]. In each case, we make some proposal for improving the new version of the standard.

ELECTRIC LIGHTING

In general, the current standard is largely focused on the performance of the electric lighting systems. It sure encourages developers to use efficient sources and high-efficiency luminaires, which is certainly appropriate. In addition, the standard also recommends implementing automated systems to manage the luminaires' switching. Among them, the Auto-ON-OFF system is particularly valuated in that standard as it grants them a potential 40% reduction in electricity consumption. This system is supposed to help the user to reduce the operating time of electric lighting by comparing the available illuminance (I_a) to the recommended illuminance value (I_r).

- If $I_a < I_r$: lights are switched ON
- if $I_a > I_r$: lights are switched OFF

A recent study conducted by the authors [4] tends to show that in office buildings, when daylight declines, users will light up the lamps when the illuminance level on their workstation is far below 500 lux. Figure 1 shows that half of the observed offices were not using electric lighting with an average daylight contribution lower than 156 lux. Such an observation leads us to believe that automatic triggering of lamps certainly supports the reduction of electricity consumption, but the automatic ignition most likely results in an increase of this consumption.

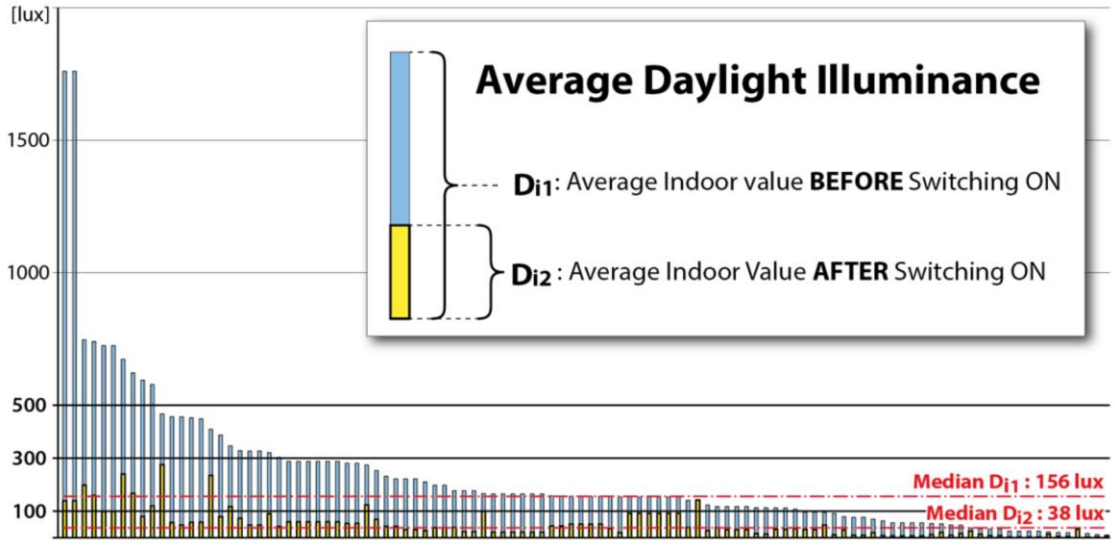

Figure 1: Average daylight illuminance before (blue) and after (yellow) that the occupants decided to switch-on the light [4].

We therefore recommend that in its new version, the standard discourages the Auto-ON systems for electric lighting .

DAYLIGHTING

Glazed area

Until now, there has never been any specific quantitative requirement for natural lighting in the Swiss regulation. This does not mean that this aspect is not treated, but the way to approach it is to calculate the lighting electricity consumption by taking into account a few isolated settings. As many other energy topics, lighting evaluation follows the structure of the Swiss building regulation, namely, according to its physical characteristics and its allocation, a *limit* value and a *target* value (*limit*: not to be exceeded; *target*: can be achieved if good

practices applied) are assigned to each room. Table 1 below shows that the current settings of the standard clearly favour a very poor glazed room (left) that can even reaches the Minergie label, while a strictly identical room with a large window cannot. The problem here lies in the fact that the limit and target values are shifted depending on the glass surface. The more the room is glazed, the more the standard is demanding. This runs counter the spirit of the law that should favour the reduction of the energy consumption through the implementation of significant glazed areas.

Axonometric	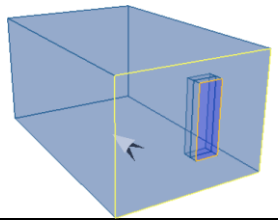	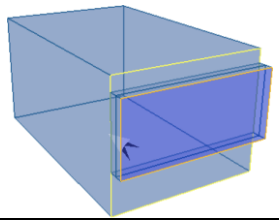
DF Distribution	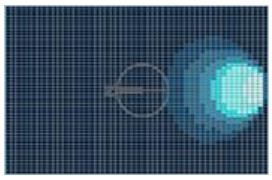	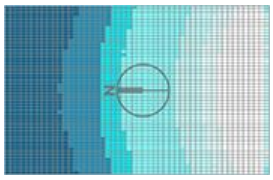
Window to Floor Ratio	4%	27%
Average DF Value	0.6%	5.0%
Limit Value SIA 380/4	49.3 kWh/m^2.y	9.8 kWh/m^2.y
Target Value SIA 380/4	28.4 kWh/m^2.y	32.6 kWh/m^2.y
Limit Minergie	33.6 kWh/m^2.y	15.5 kWh/m^2.y
Project Value	31.2 kWh/m^2.y	17.6 kWh/m^2.y
Minergie Achieved	YES	NO

Table 1: Comparison of the lighting performance of two identical rooms respectively equipped with a very small (left) or a large opening (right) (DIA+Lighting simulations).

We therefore recommend that the new version of the standard takes into account the actual contribution of daylight. A shift in thinking is necessary: determining clear objectives linked to the room use, instead of movable targets, so that the designer is encouraged to optimize the effective room performance. In the event of these changes would not be applied, it would be in the public interest that the Minergie label, which is the reference in Switzerland, free itself from the law and imposes specific daylighting targets.

Reflection coefficients

As an extension of the foregoing, it is important to note that, concerning the reflection coefficients of the indoor surfaces, the current standard only considers the three combinations mentioned in Table 2 below.

Lightness sets	$\rho_{Ceiling}$	ρ_{Walls}	ρ_{Floor}	Weighting coef.
“Light”	0.8	0.5	0.3	1.0
“Normal”	0.7	0.5	0.2	1.1
“Dark”	0.3	0.3	0.1	1.5

Table 2: Description of the three sets of reflection coefficients described in the norm and the corresponding weighting factors

The weighting coefficients are used to modulate the forecasted annual lighting electricity consumption. For example, if the room is "dark", the electricity consumption will be multiplied by 1.5. The two first sets are very close to each other while the last one is very pessimistic. In day-to-day practice there is a high probability that the room parameters are outside this range and that, to simplify, people tend to select the "Normal" set.

On this particular point, we recommend that the new standard leaves these sets and ask for independent values for each reflection coefficient. Furthermore, lighting simulations should be required in order to take into consideration the effective impact of these parameters.

Façade vs. Roof windows

Another weak point of the existing situation lies in the distinction between façade and roof apertures. Once the glazed area of a given room is described, the standard asks to select between façade or roof openings, and this choice will affect all the windows. There is no possibility to have a mix of façade and roof windows, and there is no specific distinction between horizontal, tilted and vertical roof openings. According to the standard, the selection of roof openings ends to a 25% reduction of the lighting electricity consumption. Experience teaches us that the performance gap between roof and facade openings is significantly higher, as it is shown in the example presented below (see Table 3).

Here again, we believe that this approach should be changed to be more representative of the various possible design solutions.

Axonometric	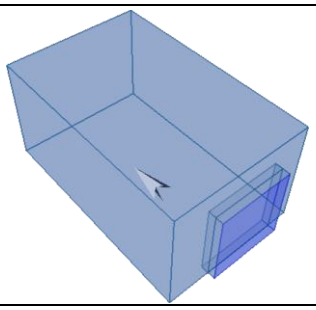	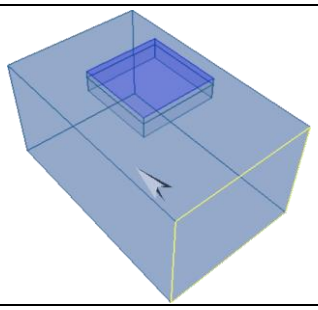
DF Distribution	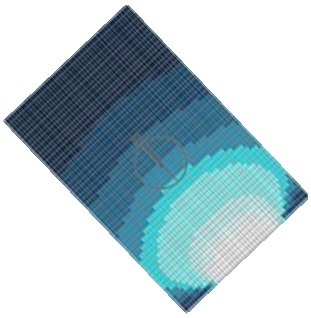	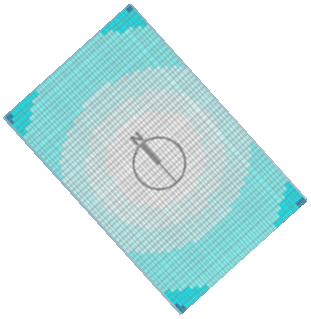
Average DF	2.3%	6.3%
Lighting Electricity consumption according to SIA	41.4 kWh/m^2	33.6 kWh/m^2

Table 3: Comparison of the lighting performance of two identical rooms respectively equipped with a facade (left) or a roof aperture (right) (DIAL+Lighting simulations)

Shading devices

As shown in Table 4 below, the Swiss standard only proposes three options to describe the shading devices. This classification makes a mix between different parameters and it is quite difficult to find out where to stand. For example where should we locate "*white automated fabric blinds*" in this table?

Category	Type	g coef.	Lightness	Weighting coef.
Degree 1	Automated blinds	$g \leq 0.4$	Very light: $\rho_{slats} > 0.60$	1.0
Degree 2	Manual venetian blinds	$0.4 \leq g \leq 0.6$	Light: $0.4 > \rho_{slats} > 0.60$	1.1
Degree 3	Fabric blinds	$g \geq 0.6$	Dark: $\rho_{slats} < 0.40$	1.4

Table 4: Description of the three blinds categories that are considered in SIA-380/4, and their corresponding weighting coefficients.

Certainly the impact of blinds on lighting is very difficult to consider to the extent it highly depends on the user and / or automatism and thus requires performing complex simulations. Nevertheless, the new standard should at least, clearly distinguish the different influencing parameters, as suggested in Figure 2, in order to be able to better characterize the possible solutions.

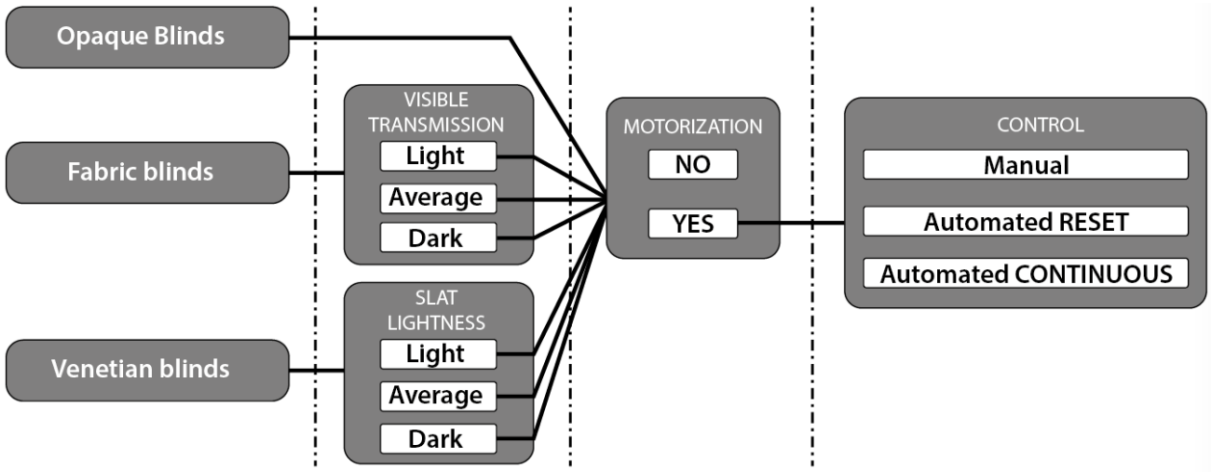

Figure 2: Schematic description of the minimum parameters that should be taken into account for the blinds description.

CONCLUSION

As shown in this paper, the Swiss standard lies on simplified algorithms aiming at processing a whole set of critical parameters. The main focus is on the estimation of the lighting electricity consumption, which is calculated by the mean of weighting coefficients. Examples presented here show that this approach can lead to a very rough approach of the lighting performance and sometimes even encourage poor design solutions.

Experience shows that energy consumption is strongly related to user behavior and the differences between forecasts and reality are often very important. We believe the time has come to radically change this approach. Today numerous tools are available on the market that allow performing detailed analysis on both electric lighting and daylighting. The new

version of the standard should be built on these tools in order to require a specific analysis of the lighting potential of each project.

Regarding electric lighting, this potential should be examined through the performance of the equipment, the installed power, and the control system. This should be supplemented by simulations showing the illuminance levels provided by the installation, in order to check that the dimensioning is correct.

Regarding daylighting, the potential should be checked through numerical simulations allowing to have quantitative and geometrical information on the daylight availability. Considering recent advances in simulation, we have the choice between several metrics.

The simplest one, is daylight factor (DF). Although this concept conceals serious limitations (no influence of orientation nor localisation), it nevertheless enables to make a fast approach of the daylighting performance of a given room and is appropriated in the early design stage.

Another option is to switch directly to daylight autonomy (DA)[5] or spatial daylight autonomy (sDA)[5]. Considering that these metrics imply hourly simulations and that, for each time step, an information about the position of the solar protection is required, the uncertainty of the results is still important. We thus believe the effort is probably disproportionate.

Another possibility would be to use climatic data in order to convert DF values into Diffuse Daylight Autonomy (DDA)[6]. Besides the fact that this method allows to take into account the location and the orientation of the project, it also has the advantage of being very fast and thus remains compatible with the design phase.

We recognize that achieving simulations requires a significant additional effort and that it may be difficult to integrate this demand into the regulation. However, it would be helpful if the Minergie label fully assumes this theme. This requires to develop its initial approach,which mainly consists in designating the right position between the limit and target values defined by the standard.

REFERENCES

1. SIA 380/4: L'énergie électrique dans le bâtiment, Norme Suisse 520/380/4, 2006.
2. SIA 2024: Conditions d'utilisation standard pour l'énergie et les installations du bâtiment, 2006.
3. Paule, B. et al. (2011): DIAL+Suite: A complete but simple suite of tools to optimize the global performance of building openings; CISBAT'11, Lausanne, Switzerland, 2011.
4. http://www.estia.ch/#!ofen-global-lighting/c8xx, Latest visit 04-29-2015.
5. Reinhart, C.F.; Mardaljevic, J.; Rogers, Z. Dynamic daylight performance metrics for sustainable building design. Leukos 2006, 3, 1-25.
6. Paule, B & Al, Diffuse Daylighting Autonomy: Towards new targets, Proceedings of the CISBAT'13 Conference, Lausanne, Switzerland, Sept. 2013.

FIELD STUDIES OF HUMAN LIGHT EXPOSURE DURING EVERYDAY ACTIVITIES – METHODOLOGICAL ASPECTS AND INITIAL RESULTS

P. Sonneborn, K. Voss

University of Wuppertal, Department D – Architecture, Building Physics and Technical Building Services, Haspeler Street 27, 42285 Wuppertal, Germany

ABSTRACT

Daylight significantly affects our health and our general well-being. At the same time, a daylight deficiency can be observed in modern society. We spend much of our time in buildings and vehicles, a trend which is reinforced by current re-urbanisation processes. Light exposure studies based on photometric sensors allow connections to be made between light exposure, human spatial environments and lifestyles. Although earlier light exposure studies based on interviews and personal log books are known [1], surveys that are supported by reliable measured data have only become possible recently due to modern technological advances. The rapid development of so-called "wearables" makes it feasible to use various sensors to obtain information on user behaviour and external influences (illuminance, temperature, etc.) on the user. Preliminary experimental tests with students at the University of Wuppertal have provided an initial basis to assess sensor-supported light exposure studies. The potential and deficits of various loggers and their position on the wearer's body were investigated and field tests were carried out by students equipped with simple data loggers. The primary objective was to optimise the methodology as a result of the experience gained, with the goal of developing a procedure to quantify the light exposure of different groups of test persons during their everyday activities.

Classification schemes in the form of individual light signatures and frequency distributions of the illuminance values measured during the test periods provide initial qualitative information on the test persons' exposure to light. However, the investigations to date also identify obstacles to analysing the measured results. For example, the predetermined measurement parameters, the spectral sensitivity of the photometer or the position of the logger on the wearer's body all influence the measured results and the conclusions which can be drawn from them.

Keywords: light exposure, measurement technology, field studies

INTRODUCTION

The effects of daylight on human health and well-being are of concern to physicians, chronobiologists, psychologists, architects and light designers. Recent studies have demonstrated the positive effect of daylight on the circadian rhythm, the synthesis of vitamin D3 and general vitality and well-being, for example [2]. Natural short-wave radiation has different effects on the human body, depending on its spectral range. "Visible light" (380 – 780 nm) affects melatonin suppression via the eyes, whereas UV-B radiation (290 – 315 nm) influences the formation of vitamin D3 through the skin [3]. Thus, sunlight is the most important source for vitamin D3 synthesis in the body, but at the same time, excessive exposure to sunlight is the main cause of skin cancer (UV-B) [4]. Behaviour related to daylight exposure is thus becoming increasingly relevant to preventive health and medical research. Among other effects, it has been determined that daylight as a resource is becoming

scarcer in modern society. On average, people in modern societies spend about 80 – 90 % of their time in buildings and vehicles [1, 5] and follow a daily routine which is increasingly disparate from the natural day-night rhythm [6]. Artificial lighting, increasingly densely populated urban spaces and changes in work-related and leisure behaviour have effects on individual exposure to daylight. Urbanisation and its effects on society and life in towns and cities have been observed since the industrialisation of the 19th century [7]. As a reaction to cramped urban living conditions, social residential reforms such as the "Garden City" models of the 20th century demanded a spatial balance between the various functions within a city, as well as between town and country [8]. The aim was to achieve socially equable and healthy urban living by town planning that led to a well-balanced distribution of building density. Today, the trend toward re-urbanisation [9] and the resulting rezoning toward higher-density building mean that the quality of urban life can be expected to change anew. The effect of densification processes and an urban lifestyle on light exposure is of interest, as are the possible consequences for health and well-being.

Quantitative exposure studies allow conclusions to be drawn on human interaction with daylight in urban and suburban habitats. Preliminary studies by students have investigated the measurement technology potential of selected simple, wearable data logger systems. The studies focused on critically assessing how field tests applying mobile data loggers could be used to gain reliable information on daylight exposure of groups of test persons over longer periods of time.

METHODOLOGY

As a first step, the requirements on the data loggers were defined. Selected loggers from different price categories were compared by identifying positive features and drawbacks. Over a period of two days, one test person checked possible effects on measurement results and user comfort due to the sensor position on the wearer's body. Student field tests, divided into two test periods (summer, autumn) of three weeks each, as well as further investigations with children, provided initial, measurement-based estimates of the light exposure of the test persons. In addition to determining the feasibility of such field tests, the primary focus was on developing the evaluation methodology and interpreting the initial measured results.

Comparison of Photometric Loggers

The rapid expansion of wearable technology has led to increased development of mobile data loggers with different integrated sensors. Thus, various parameters of the human working and living environment can be measured to investigate biological rhythms, sleep-wake cycles, activity levels and well-being, among other aspects.

To quantify light exposure, photometric sensors are used which measure the illuminance (lux), and in some cases, also the spectral irradiance (mW m^{-2} nm^{-1}) and/or the UV irradiance. Measurement of the UV radiation allows not only analysis relating to vitamin D3 synthesis but also differentiation between indoor and outdoor spaces, as conventional window glass is opaque to UV radiation. In order to draw conclusions on the availability of light in different outdoor spaces, the location of the test persons has to be determined. In this case, the logger also needs an additional Bluetooth connection to allow synchronised GPS tracking via a mobile phone or smart watch.

In a preliminary investigation, three selected loggers were assessed with regard to qualitative differences. This included comparisons of their technical construction and handling, as well as data capacity and data processing. The sensor position and attachment options of the loggers were assessed with respect to possible wearing positions. Comparative measurements with the

various data loggers and a reference luxmeter, outdoors and indoors (immediately behind a window), provided information on the measurement accuracy and range. The loggers were placed next to each other on a horizontal surface and the measurement intervals of one minute were synchronised. A number of measurement series were carried out under different daylight conditions, allowing conclusions to be drawn on the measurement accuracy of the sensors at different illuminance levels.

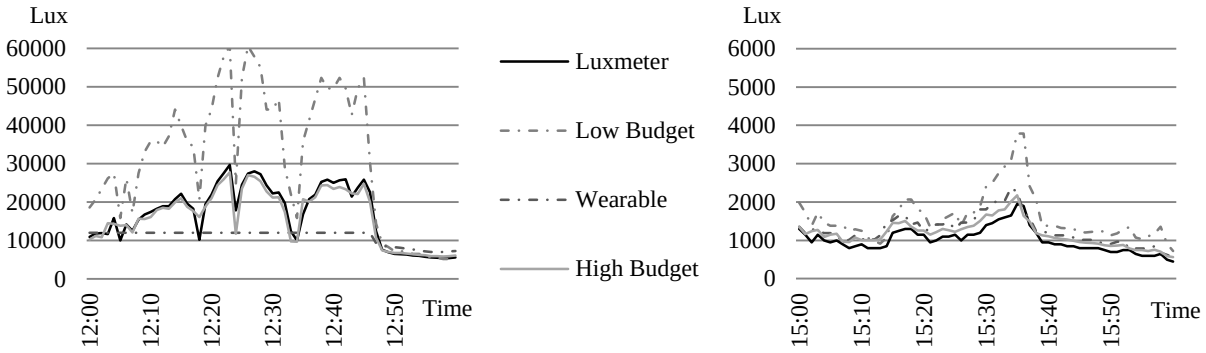

Figure 1: (left) Comparison of the measured outdoor illuminance (1-minute intervals) determined by three selected photometers and a professional luxmeter.

Figure 2: (right) Comparison of the measured illuminance for daylight indoors behind an uncoated double glazing.

Figures 1 and 2 present examples of illuminance time series measured outdoors and indoors. The measurements indicate the problems caused by the wide range of illuminance values with regard to measurement resolution and accuracy. An appropriate sensor and suitable AD converter must be selected, as otherwise either the dynamic range is too small or the resolution is too coarse. For instance, the "wearable" logger features better measurement accuracy in the low illuminance range, but it reaches saturation already at 12 000 lux. As a result, outdoor measurements cannot differentiate between cloudy and sunny conditions. The "low-budget" logger has a wider measurement range, at the cost of resolution. The values measured by this logger deviate significantly from those of the luxmeter for higher illuminance values. Only the "high-budget" logger provided comparably good values in both the high and the low illuminance ranges. All loggers measured more accurately in the low illuminance range.

Wearing Position for Logger

To draw conclusions about the effect of daylight exposure on the circadian rhythm, the sensor must be positioned close to the wearer's eye. To determine the relationship between daylight exposure and vitamin D3 synthesis, measurements near exposed skin are needed. Specifically, this implies measurements on the head and also on the upper body and arms. In addition, one test person was equipped with loggers on his forehead, spectacles, chest, right and left upper arms, to check the effect of the data logger wearing position on handling, user comfort and measurement results. The loggers were worn continuously during daily activities and tested for their practicability. They were taken off and kept in the same room as the test person while that person slept or washed. The predefined measurement period of two days provided information on various requirements specific to the weather and the user. Meteorological data for comparison were recorded with five identical sensors mounted outdoors. The measurement results were subsequently analysed and interpreted, taking previous values for the test person into account.

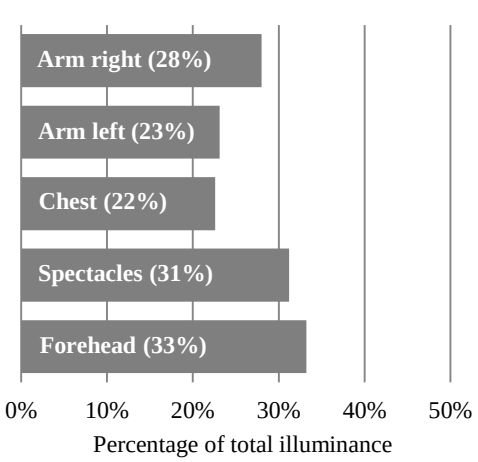

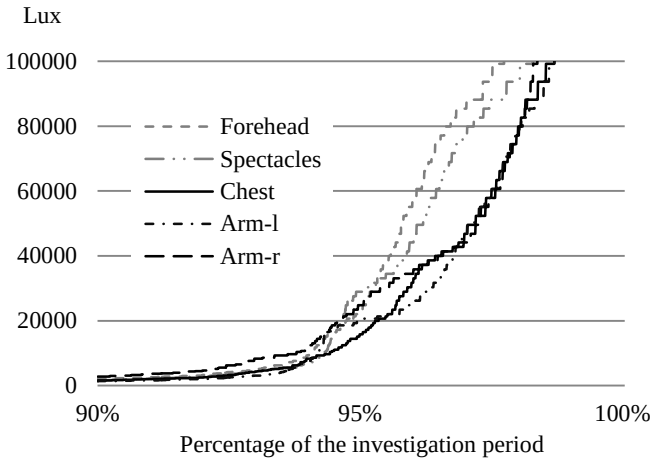

Figure 3: (left) Percentage of total illuminance measured by sensors worn on the body with respect to the reference outdoor values (average of four vertically mounted senses facing the four compass directions) in a period of two days.

Figure 4: (right) Frequency distribution of the illuminance values recorded by loggers worn at different positions.

The position and orientation of the sensors affect the measured results. Figure 3 shows the percentage of total illuminance measured by sensors worn on the body with respect to the reference outdoor values. The sensors mounted on the forehead and spectacles measured similar values. However, there are differences between the head zone and the chest, and between the right and left upper arms. The illuminance frequency distribution in Figure 4 illustrates that during this test period, the sensors on the forehead and spectacles measured a larger proportion of higher illuminance values than those attached to the upper arms. The exposed position of the sensors near the head had a direct effect on the measured results.

Field Tests with Students

An essential part of the preliminary investigations drew on measurement-based field tests with students of the University of Wuppertal, Germany. Two test periods in summer and autumn, each lasting three weeks, were intended to provide information on the students' exposure to light, taking the seasonal variation in available daylight into account. The three-week test period each time meant that a broad spectrum of living and working situations for the students was sampled (meteorological conditions, examination phase, holidays…)

The experimental design prescribed that each of the students wore a "low-budget" logger on his/her upper right arm (sensor mounted vertically and facing away from the right side of the body). In the context of these preliminary studies, the focus was on practicability and initial evaluation rather than on spectral response and measurement accuracy of the sensor. The relatively inexpensive, "low-budget" data logger featured a sufficiently wide measurement range and could be attached simply to the upper right arm with a Velcro® strap. During the field studies, illuminance and temperature data were recorded by the logger in 5-minute intervals. Meteorological reference data were supplied by the same type of logger, which was mounted on the university roof with the sensor oriented horizontally. As in the previous measurements comparing different wearing positions, the loggers were removed and kept in the same room as the test person while that person slept or washed. As a source of complementary information, the students kept individual log books of their activities.

The measured data were analysed on the basis of classification schemes in the form of individual light exposure signatures and frequency distributions (Figure 5). These provide information on user behaviour and characteristic features of light exposure, and guarantee good comparability of the various exposure profiles. Figure 6 illustrates how the temporal distribution underlying the exposure profiles can be presented and analysed in detail with the help of a carpet plot. Regular patterns and deviations in the daily schedule of the test persons become evident. By combining this information with that in the activity log books, the effects of the circadian rhythm and living and working habits on light exposure can be investigated. Increasing or decreasing illuminance values (near 0 lux) in the morning and evening hours allow conclusions to be drawn on the sleep-wake rhythm. In addition, it is interesting to note the recognisable effects of weekends on leisure activity and the correspondingly higher light exposure then.

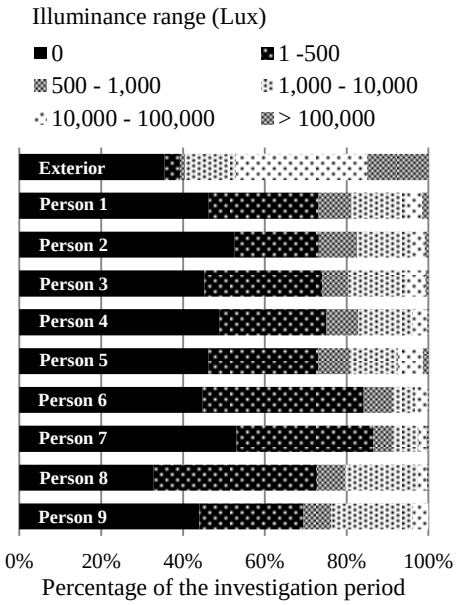

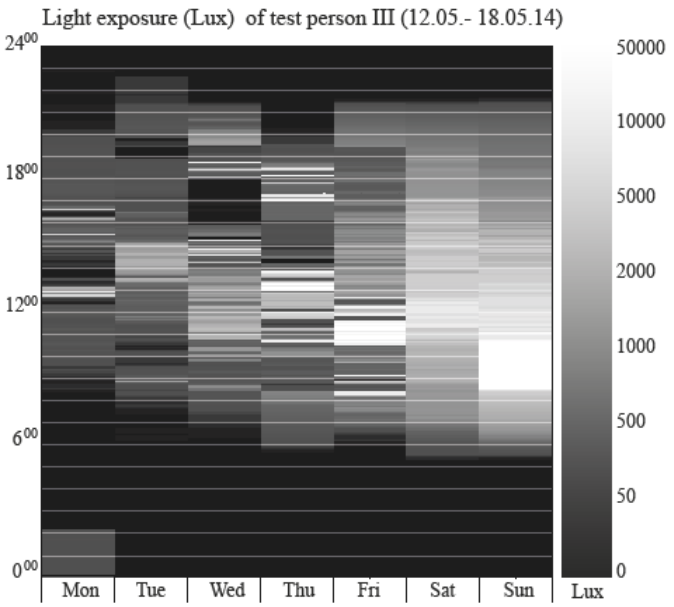

Figure 5: (left) Comparison of the light exposure signatures of nine students based on measured illuminance values, classified according to illuminance ranges.

Figure 6: (right) Carpet plot depicting the temporal distribution of the light exposure measured for one student during the period from 12.05.2014 to 18.05.2014.

CONCLUSIONS

The investigations revealed the potential and deficits of measurement-based light exposure studies. The choice of sensor determines the quality and the potential evaluation context of the measured results. Consequently, before field tests are started, it is important to determine the context in which information on light exposure is needed (melatonin, vitamin D3, skin cancer, well-being). Relatively inexpensive loggers already allow initial analyses to be made of the test persons' exposure to light. Going further, more expensive systems allow the incident light to be analysed spectrally and can provide information on UV-B radiation (differentiation between indoors and outdoors, vitamin D3) or blue-saturated light (melatonin, attentiveness). Further, the sensor position affects the measured results. Conclusions about the interaction between daylight exposure, melatonin and vitamin D3 production become more reliable if measurements are made near the head. However, a logger cannot be attached to the head without an additional mounting structure, which can be uncomfortable for the user. Pressure due to spectacles or head coverings can affect the user's well-being negatively. The

loggers vary in their suitability for mounting on spectacles, depending on the position of the sensor in the logger casing design, and the resulting effect on the wearer's field of view. Attaching a logger to the chest or upper arm with a Velcro® strap or safety pins is comparatively simple, but the measured results are more prone to error. These result from the loggers being covered by or removed together with clothing items (e.g. jackets, sweaters). The field tests with students demonstrated the practicability of using the loggers over longer periods of time. The measurement period is limited by the data capacity of the loggers, taking the selected measurement interval into account. Bluetooth-supported loggers which can save the data in an external cloud, such that they become accessible via Internet, offer an advantage here. The project team can then already react to unanticipated behaviour by the test persons during the test period. Overall, close cooperation between the test persons and the experiment supervisors is necessary to reduce the risk of unusable measurement results. The development of suitable analytical methods allows information on light exposure to be extracted, ranging from identification of typical features up to detailed, time-dependent analysis of exposure profiles with the help of carpet plots, activity log books and location detection by GPS.

REFERENCES

1. Klepeis, N.E. et al.: The National Human Activity Pattern Survey (NHAPS) - A resource for assessing the exposure to environmental pollutants. Journal of Exposure Analyses and Environmental Epidemiology, Vol.11, Issue 3, pp. 231-252, May / Jun. 2001
2. Fisch, J.: Licht und Gesundheit – Das Leben mit optischer Strahlung. Technical University of Ilmenau, 2000
3. Jüstel, T.: Licht und Gesundheit – Der Einfluss des Lichts auf Körper und Psyche. Science Festival Schlauraum, Münster, 11. Jun. 2013
4. National Health Service: Consensus Vitamin D position statement. http://www.nhs.uk/livewell/summerhealth/documents/concensus_statement%20_vitd_dec_2010.pdf, 2010
5. Schweizer, Chr. et al.: Indoor times - microenvironment – activity patterns in seven regions of Europe. Journal of Exposure Science and Experimental Epidemiology, Vol. 17, Issue 2, pp. 170-181, Mar. 2007
6. Fördergemeinschaft Gutes Licht: licht.wissen 19 – Wirkung des Lichts auf den Menschen. pp. 10-13, Frankfurt on the Main, 2014
7. Krückemeyer, T.: Gartenstadt als Reformmodell – Siedlungskonzeption zwischen Utopie und Wirklichkeit. Issue 1, Carl Böschen Publishers, Siegen, 1997
8. Fürst, F. et al.: Berichte aus dem Institut für Raumplanung. Leitbilder der räumlichen Stadtentwicklung im 20. Jahrhundert – Wege der Nachhaltigkeit? Vol. 41, pp. 17-23, University of Dortmund, 1999
9. Brake, K.: Reurbanisierung – Interdependenzen zum Strukturwandel. In: Brake, K., Herfert, G.: Reurbanisierung: Materialität und Diskurs in Deutschland. Issue 1, pp. 22-33, Springer VS Publishers, Wiesbaden, 2012

THE EFFECT OF ARCHITECTURAL DETAILS ON DAYLIGHT DISTRIBUTION INSIDE A ROOM

Mansoureh Tahbaz[1]; Shahrbanoo Djalilian[2], Fatemeh Mousavi[3]; Marzieh Kazemzadeh[4];

1: Associate Professor, School of Architecture, Shahid Beheshti Univeresity, Tehran, Iran.

2: Architect and independent researcher, Tehran, Iran.

3: Architect Lecturer, Azad University of Tehran West,Tehran, Iran.

4: PhD. Architect and lecturer, Azad University, Kerman, Iran.

ABSTRACT

In Iranian historical architecture one of the most important design criteria is daylight accessibility and quality. To evaluate daylighting conditions in a historical house in Kashan city in Iran, one of its main rooms was examined according to field and simulation studies in the year 2012 and 2014. To evaluate the effects of architectural design details on daylighting conditions of the room, some elements such as balcony, ceiling shape and height, window size and frame, glass size and colour, where changed or eliminated by simulation. The amount and distribution of daylight inside the room was simulated in the morning, noon and afternoon of two sunny days in summer and winter on a horizontal mesh at 80 cm height. The important UDI (useful daylight illumination) levels on different parts of the room were calculated on this height in all months of the year. On a column diagram, the results of this calculation show the percentage of daylight accessibility in a year.

The illumination amount and its distribution inside the room show great differences in different architectural detail conditions. The results show that the original condition of the room has a delightful daylighting in comparison to changed configurations. Also it has the best UDI daylight distribution in all seasons and hours. The other result is that with the same sky view and room dimension, changing detail design such as ceiling shape, window height and size, glass details, and so on, has great effect on illumination distribution and light level in different seasons inside the room. Therefore, in some cases, it is possible to modify the daylight condition of a room just by deliberate detail changes in architectural design.

Keywords: daylight distribution, ceiling shape, window mesh, colour glass, Orosi window

INTRODUCTION

In Iranian historical architecture one of the most important design criteria is daylight accessibility and quality [1]. To find out daylight conditions in a historical house, Kashan city was chosen as one of the most historical cities in Iran, with a hot arid climate and sunny skies most time of the year. In this city, Ameriha House of Zandieh and Qajar period is a great house with five yards and 85 rooms [2] with different daylighting strategies. To examine architectural and detail design effects on daylighting condition, one of the main rooms of this house was chosen for field and simulation studies in the year2012 [3] and 2014 [4].

METHOD

Data Collection

To gather the illumination data of the room, a field study was done in the morning, noon and afternoon of two sunny days in summer and winter, on a horizontal mesh at 80 cm height [5], by a digital illuminance meter TES 13339R. A reference illuminance data logger was located on the roof to gather sky illumination data. These data were used in the radiance software to simulate the illumination in the room for a sample year. The reflectance of the room surfaces were measured by a Lutron RGB1002 colour analyzer. The exact size and details of the room, ceiling and windows were measured by a 3D digital meter (Fig. 1). To find out the effects of detail architectural design on the daylight conditions of the room, some elements such as balcony, ceiling shape and height, window size and frame, glass size and colour, where changed or eliminated by simulation.

Illuminance meter TES 13339R

Colour analyzer Lutron RGB1002

Digital 3D meter Leica DISTO™ D3a

Figure 1: Field data collection instruments and location of the illuminance meters

The Case Study Room

The case room is a summer place located toward north/east (12 degrees from north) overlooking a large central yard with a wide sky view. The area of the room is 57.5 m^2 with a dome ceiling of 8.4 m height and a few decorative mirror works on its surface. The room has a three sash Orosi window [1] toward yard, with a crescent colour glass above it surrounded by three small colour glass circles. The room has extra indirect side lights from door/windows of the adjacent rooms. A balcony of 4.9 m deep and 9.3 m height is located in front of the room [3] (Fig. 2). The illumination information was gathered in 11-12 July 2011 & 10-12 Jan 2012.

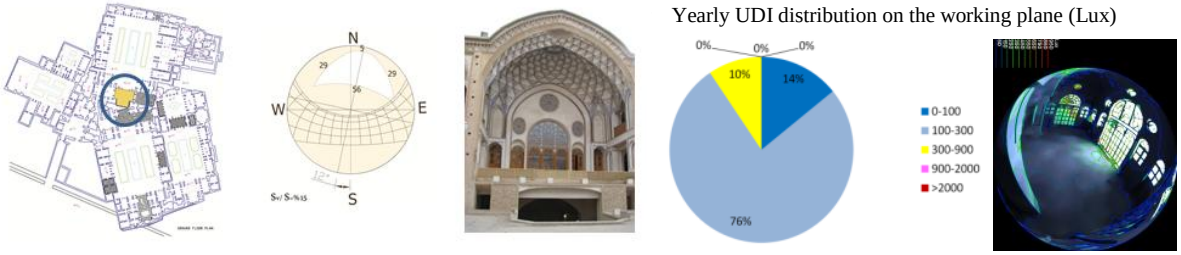

Figure 2: Architectural design condition of the study room on the yearly UDI distribution

RESULTS

To find out the effect of architectural and detail design changes on the daylighting condition, some changes were made in the room design and then the illumination results were simulated by the radiance software [4]. The changes were made in four groups: 1) eliminating the balcony, crescent of the main and side windows, 2) changing the roof shape and height, 3) changing the details of window mesh and glass colour, 4) changing the room to a modern ordinary room with flat low ceiling and transverse windows. The results are shown in Table 1.

The first and second column shows the made changes in the room. The middle columns show the illumination distribution on the plan of the room in a sample day in summer and winter in the morning (9am), noon (12 pm) and afternoon (15pm) on a horizontal mesh of 80 cm height. The field data gathering method is obtained through lighting standards [5, 6, 7, 8 and 9]. The last columns show diagram of UDI (useful daylight illumination) levels distribution in a whole year for illumination less than 100 Lux (fell short), 100-300 Lux (supplementary), 300-900-2000 Lux (autonomous) and more than 2000 Lux (exceeded) [10, 11].

DISCUSSION

The simulated results of Table 1 show:

1- In the original condition of the room, the horizontal observed surface has 14% illumination less than 100 lux, 76% between 100-300 lux and 10% more than 300 lux. It shows a balanced distribution of daylight in all times of the year.

2- Eliminating the balcony can increase the illumination inside the room in all seasons and hours. (36% 100-300 lux, 59% 300-900 lux and 5% more than 900 Lux). Although the illumination is increased, the low amount of uniformity may cause discomfort glare. The colour glass of the crescent window will adjust the light level.

3- Eliminating the crescent colour glass and the colour glass circles above the sash Orosi window, causes the lack of illumination especially in morning and afternoon. (39% less than 100 lux, 55% 100-300 lux and 6% more than 300 Lux). The illumination at the depth of the room is very low. It shows that the height of the crescent colour window in the middle of the wall window is designed according to the depth of the room in Shahneshin (VIP sitting place at the end of the room). The crescent parts at the top of the side windows help to illuminate the sides of the room.

4- Eliminating the side windows has no important effect on the amount of illumination inside the room. They only help to illuminate the side light and uniform better daylight distribution.

5- Using no colour glass in all windows will increase the illumination inside the room without a good uniformity. Eliminating all the mesh frames of the Orosi window and the crescent above it and using simple no-colour glass, the increasing of illumination in all seasons and hours is conspicuous. (9% 100-300 lux, 85% 300-900 lux, 6% more than 900 lux). The illumination near the window is greater than in other parts of the room and the uniformity is not appropriate. The room will become much more illuminated in summer than in winter.

6- Decreasing the ceiling height to 4 meters and replacing it with a flat ceiling, has a considerable effect on reducing the illumination. (26% less than 100 Lux, 66% 100-300-900 Lux and 8% more than 900 Lux). In this case the differences of illumination from window to the depth of the room may cause discomfort glare.

7- Changing the room to an ordinary modern room with a low flat ceiling and transverse windows, causes non uniform distribution of daylight with 71% 100-300 Lux and 25% 300-900 Lux illumination in a year. Eliminating the balcony in this case may help for more illumination inside the room (26% 100-300 Lux and 72% 300-900 Lux) but in summer morning the sun patch may cause glare and the uniformity of daylight is not appropriate.

Room changes			Illumination distribution on the working plane of the room			Yearly UDI levels on the working plane area of the room	
			morning	noon	afternoon	9am-12pm-15pm	yearly
1- Original condition		21 Jan	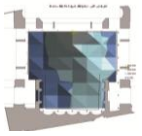	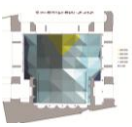	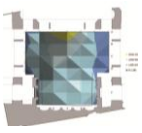		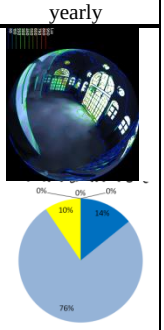
		21 June	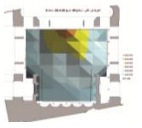	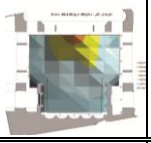	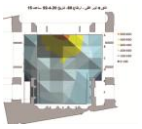		
2- Balcony eliminating	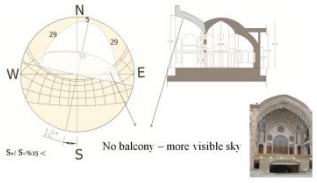	21 Jan	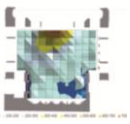	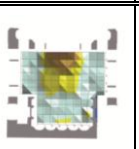	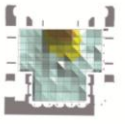	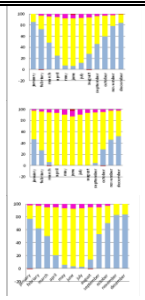	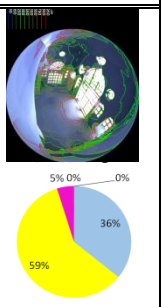
		21 June	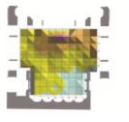	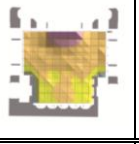	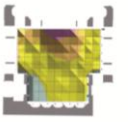		
3- Crescent windows eliminating	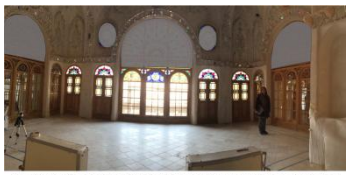 No crescent colour glass and no colour glass circles above the sash Orosi and side windows	21 Jan	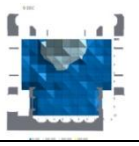	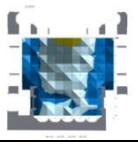	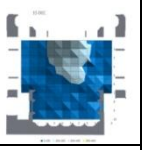		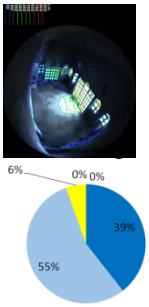
		21 June	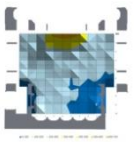	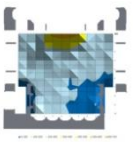	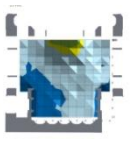		
4- Side windows eliminating	 No side window	21 Jan	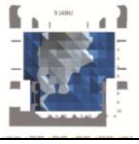	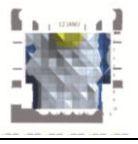	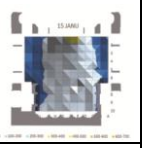		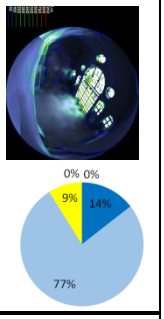
		21 June	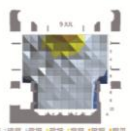	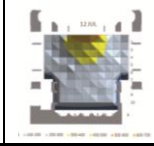	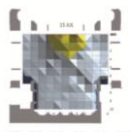		
5- No colure glass	 No colour glass	21 Jan	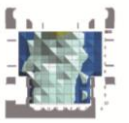	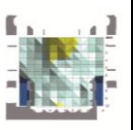	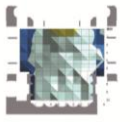		
		21 June					

Table 1: Study results of the room changes (Lux)

Room changes			Illumination distribution on the working plane of the room			Yearly UDI levels on the working plane area of the room	
			morning	noon	afternoon	9am-12pm-15pm	yearly
6- No mesh no colour glass	 No mesh - No colour glass	21 Jan	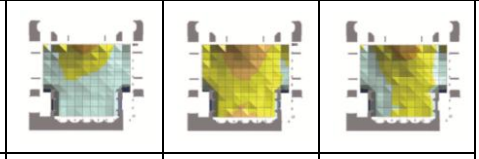			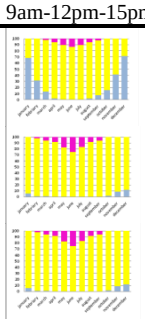	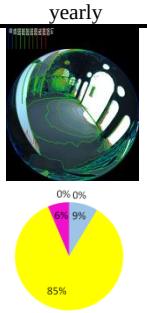
		21 June	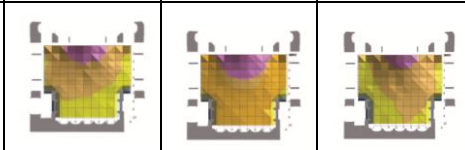				
7- Flat ceiling 4 meters height	Flat ceiling 4 meters height 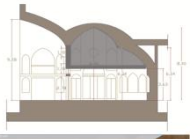 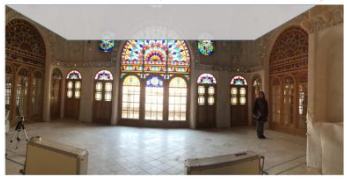	21 Jan	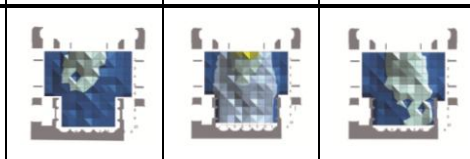			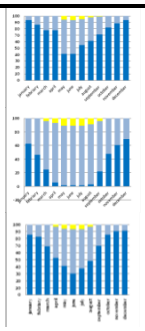	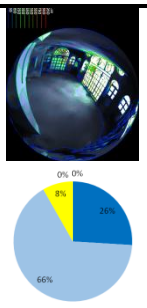
		21 June	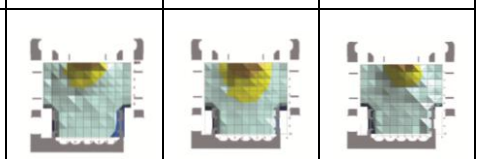				
8- Flat ceiling no mesh no color	 Flat ceiling, no side window, no crescent window, transverse window with single glass	21 Jan	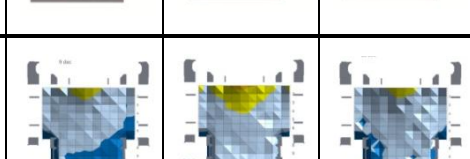			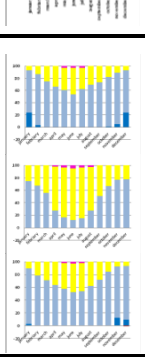	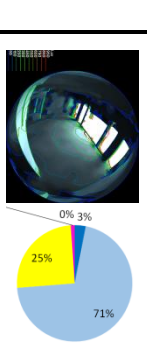
		21 June	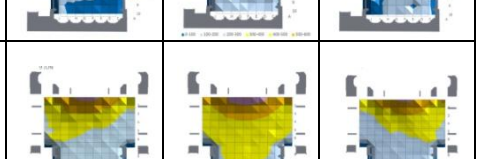				
9- Flat ceiling - no balcony	No balcony, flat ceiling, no side window, no crescent window, transverse window with single glass 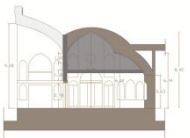 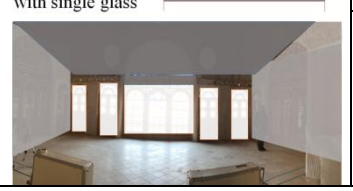	21 Jan	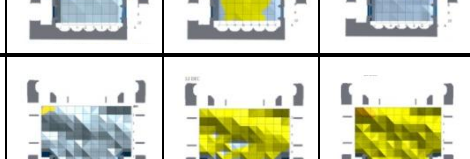			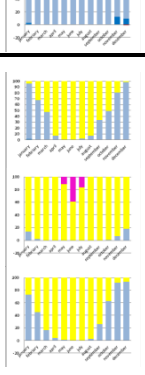	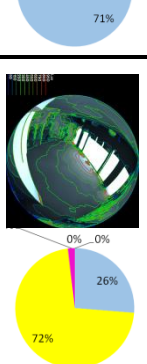
		21 June	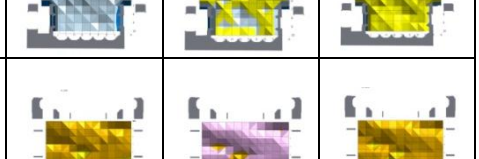				

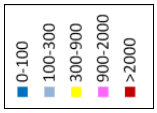

Table 1: (continued)

CONCLUSION

The results of this research show that in the historical house of Ameriha in Kashan, the original details of the studied room are designed for the best daylight distribution in all seasons and hours. It will create a delightful daylighting quality with coloured beautiful sun patches (Fig. 3). The mirror parts on the wall and ceiling with high curved ceiling help for better uniformity and adjust illumination in most parts of the room. The high crescent colour glass above the Orosi window is for enough illumination in the depth of the room, Shahneshin (VIP sitting place). This study also shows that with the same sky view and room dimension,

changing the detail design has great effect on illumination level and distribution inside the room. Therefore, in some cases, it is possible to modify the daylight condition of a room just by deliberate detail changes in architectural design.

Figure 3: sunlit position of the room in summer morning

REFERENCES

1. Tahbaz, Mansoureh and Fatemeh Moosavi: Daylighting Methods in Iranian Traditional Architecture (Green Lighting). CISBAT 2009 Proceedings, Lausanne, 2-3 SEP, pp. 273-278, 2009.
2. Ameriha house : http://adamakebaran.blogsky.com/1389/03/19/post-289/
3. Tahbaz, M., Jalilian, Sh., Moosavi, F. and Kazemzadeh, M.: Analyzing Daylighting of Door-Windows in Some Traditional Houses of Kashan. Research Project, Research and Technology Commission, Shahid Beheshti University, Tehran, 2012.
4. Tahbaz, M., Jalilian, Sh., Moosavi, F. and Kazemzadeh, M.: The Effect of Kashan Traditional Windows on indoor daylighting. (Research Project), Researchers' supporting finance of presidency institution, Tehran, 2014.
5. Lighting Guide 10: Daylighting and Window Design. London. The Society of Light and Lighting, CIBSE, 1999.
6. Lighting Guide 5: Lighting for Education. London. The Society of Light and Lighting, CIBSE, 2011.
7. BS 8206-2: Lighting for buildings. Code of practice for daylighting. London: British Standards Institution (BSI), 2008.
8. The SLL lighting Handbook: London: The Society of Light and Lighting. CIBSE, 2009.
9. The SLL Code for lighting: London: The Society of Light and Lighting. CIBSE, 2012.
10. Mardaljevic, John: Climate-Based Daylight Modelling –IESD, 2010. Retrieved from: http://climate-based-daylighting.com/doku.php?id=academic:climate-based-daylight-modelling date: 15/01/2014
11. Nabil, A. and J. Mardaljevic: Useful daylight illuminate: A new paradigm for assessing, daylight in buildings. Lighting Research and Technology, Vol. 37, No. 1. 2005.

OPTIMIZATION OF ENERGY EFFICIENT LUMINAIRE LAYOUT DESIGN IN WORKSPACES

I.E. Uygun; Z.T. Kazanasmaz; S.Kale

Department of Architecture, Izmir Institute of Technology, 35340, Urla, İzmir, Turkey

ABSTRACT

There are several methods used in lighting design. The realistic methods have been developed by computer graphics such as DIALux, VELUX, Radiance etc. These methods use the engineering computational tools and architectural rendering together. Although lighting designers would design an accurate lighting system which provides desired illuminance levels through computer graphics, it is still necessary to propose optimal and alternative solutions by maximizing comfort conditions and minimizing energy consumption by practical techniques. Researchers continue developing and using different methods to find optimum solutions for visual comfort of occupants; to get uniform illuminance, to prevent glare, to control daylight and artificial light by considering the energy performance of buildings. Thus, the purpose of this study is to estimate the most accurate locations of light sources according to visual comfort conditions by applying an optimization model through Excel Spreadsheet and Evolver. It is considered that such a new proposed optimization model would be beneficial, less time consuming, effective and dynamic, if integrated in the early design phase. The optimization model is employed for an office by obtaining photometric data of an energy efficient luminaire from the simulation tool s DIALux. Its performance is also tested by the DIALux models to explore its applicability and validity.

Keywords: optimization, luminaire layout, energy efficiency, workspace

INTRODUCTION

Lighting design of a workspace is a complicated task that includes multiple criteria based on many physical and psychological aspects. Occupants spend a large part of their time at their workspaces. So, they need to work in comfortable and healthy environments [1]. Appropriate lighting conserves eye health, increases the work performance, and provides visual comfort [2]. Besides, a properly-designed lighting system helps to balance the lighting, heating and cooling loads by decreasing the energy consumption. Energy consumption of workspaces is taken into consideration because a significant amount of buildings' energy consumption is due to artificial lighting [3]. The planning of artificial lighting systems involves consideration of the metrics of lighting quality and quantity [1]. The basic metric for the quantity of lighting design is illuminance. Illuminance depends on the features of visual tasks, room surfaces, photometric data of the lighting sources (the lamp/and the luminaire) and their location [4]. It is necessary to distribute illuminance uniformly in the indoor environment, since non-uniform light distribution causes glare. One metric to determine the uniformity is the light distribution curve of the luminaire which is unique for each of them [5]. The light distribution curve of the luminaire consist of information about the power of the light source on different angles of x, y and z plane. Illuminance is calculated according to this information. The other metric is the location of luminaires. It is necessary to determine the correct position of the luminaire to avoid unbalanced illuminance distribution while selecting the accurate light source.

Lighting designers select and decide on the types of lamps and luminaires according to these metrics. Simulations are the assisting tools in their decision process. They present many design alternatives. However, they do not have the power to show the most accurate or optimum position of light sources according to candle power distributions [6]. Simulation tools are helpful in proposing lighting design decisions in general; however, they are not the decision maker to propose the best solution. Potential solutions/designers' assumptions for better performance cannot be confirmed or rejected through effective search mechanism.

Lighting design alternatives may present some bright or dark regions in the horizontal plane due to the overlap or gap of the candle power distribution curve. Non-uniform light distribution results in glare when one region in the interior space is brighter than the general brightness [5]. Thus, it is necessary to determine the correct position of the lighting fixture. The effective and dynamic search mechanism to find optimum solutions should be integrated in the lighting design process. It is worth to study optimization techniques in this sense.

Although optimization techniques have been widely used in the field of engineering [7], [8], [9] i.e. chemical, industrial, and mechanical engineering etc., they are not a well-known technique in the field of architecture. It is necessary to make a contribution to literature in this sense.

Lighting designers make decisions about the locations of luminaires by estimating illuminance levels through simulations. However, by employing optimization techniques, combinations of different design (layout, lamp and luminaire selection) alternatives would be tested together in one model to obtain the most accurate locations of light sources according to defined comfort and efficiency constraints. That optimum solution provides the optimal illuminance on the work plane and of the luminous power.

Thus, it is necessary to find the optimal solution for lighting design which may be achieved by maximizing comfort conditions, and minimizing the energy-consumption of the lighting scheme.

METHOD

The main objective of this study is to estimate the most accurate locations of light sources according to visual comfort conditions by proposing a mathematical model. The other objective is to validate the model by a simulation tool; DIALux [10]. In this section, the procedure of the research is introduced to achieve these objectives.

Firstly, a problem case has been selected to build the phases and to practice the mathematical model. The room was intended to represent a small cellular office and measured 5.80 m in the x-direction and 4.20m in the y-direction. The ceiling height was 3.3 m. The measurement plane was 0.80 m above the floor. Calculation points were placed at least 0.5m away from the surface of the walls. There were 81 calculation points by giving spaces 0.6 m between them in the x-direction and 0.4 m in the y-direction (Figure 1). Locations of light source were constructed out based on ceiling tiles of size 600x600 mm. Recessed mounted modular luminaires have been selected according to architectural qualities of the space. There were 54 different points to estimate location of light source (Figure 1). Location points of luminaires and calculation points are not aligned to capture the distribution angles of the luminaire extensively and to obtain dissimilar illuminance levels at each calculation points. Non-aligned location grids were used in previous studies [6,13].

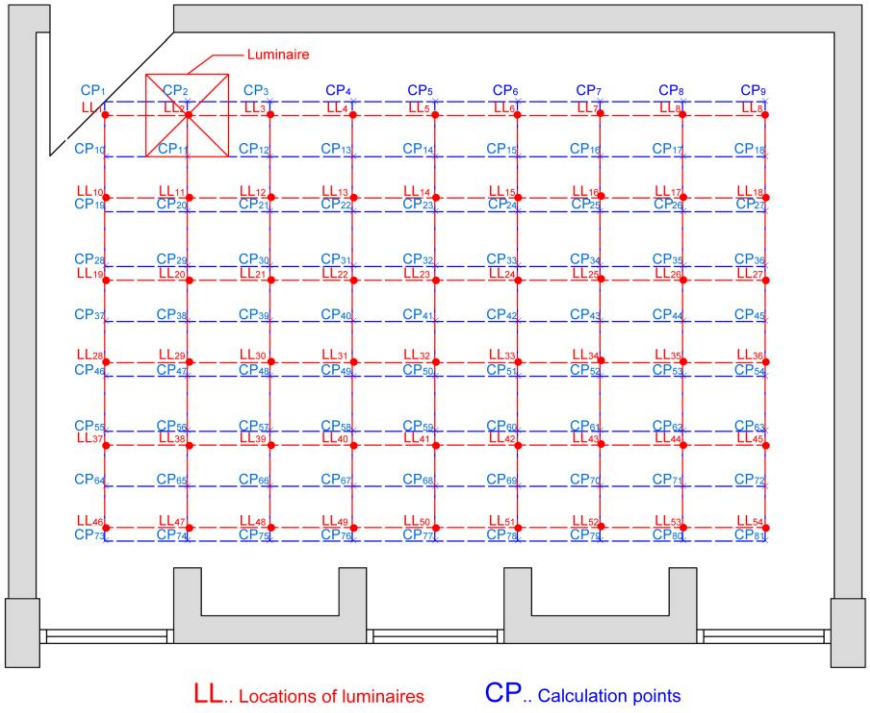

Figure 1. Location points of luminaire in model case and calculation points.

Spreadsheet Steps

A mathematical model was created and developed for this optimization problem. An Excel spreadsheet was used as a base of the model because of its simpler and transparent approach to modelling. This spreadsheet included 5 steps.

Step 1. The first step of this model was the construction of the locations of points on the working plane and ceiling. Their co-ordinates on x, y and z plane were entered to the model according to point of 0, 0, 0 on left and bottom side of the room. C and gamma angles between calculation points of model case and location points of light source were calculated. C angle is the resulting angle on horizontal plane. Likely, Gamma angle is the resulting angle on vertical plane.

Step2. Luminous intensity of luminaires which varies according to C and Gamma angles composes photometric data. DIALux provided such data to be imported in this model.

Step 3. This step included composing information about total luminous flux of selected luminaire, data about room dimensions (height, width and length), and reflectance of wall, ceiling and floor. This type of data is interchangeable easily to create different lighting scenarios for the same room. For this reference room reflectance of wall, ceiling and floor are 0.50, 0.70 and 0.20 respectively.

Step 4. This step is the calculation process. The model calculates total illuminance of the points (the summation of reflected and direct illuminance), which varies according to the light source location scenario. The point method has been used to calculate illuminance at calculation points on the working plane.

Step 5. Based on recommendations about working places, the average illuminance level is 300-500 lx. According to the illuminance level at calculation points, the average illuminance level on the working plane was calculated by the division of total illuminance by the number of points. On the other hand, the main goal of the study, after having desired light intensity, is to provide uniform illuminance on the working plane. The mean relative deviation (MRD)

was used for this problem to calculate relative deviation of illuminance level at the point from average level of whole space [11].

The validation process involves the formulation of a linear regression line to compare the simulation and mathematical model illuminance levels at each calculation points for two luminaire locations and observe the strength of their relationship. Coefficient of determination (R^2), root mean square error (RMSE), normalized root mean square error (NRMSE) and coefficient of variation (CV) are calculated for two luminaire locations. A scatter diagram is developed to figure out whether the mathematical model fits the simulation model or not.

Problem Formulation

The design variables of the study were the positions of selected luminaires on the x plane. The luminaire is recessed mounted type (4 x 14 W – 64.6W) which is 600 x 600 mm in dimension. The problem involves two scenarios; one including two luminaires and the other including three luminaires. There are a total of 54 different positions to locate the luminaires and 81 horizontal calculation points which are on the working plane. The illuminance levels resulting from these two scenarios were analysed to define their optimal positions.

The primary objective of the research is to get illuminance uniformity (1) on the working plane with two constraints (2, 3). I_{avg} is the average illuminance level of working place. I_i is the illuminance level at one calculation point, and I_m is the mean of illuminance level at all these points.

Minimize: $MRD = \frac{\sum_{i=1}^{N} -|I_i - I_m|}{NI}$ (1) [11]. Subject to: $I_{avg} \geq 300$ (2), $I_{avg} \leq 500$ (3)

To solve this optimization problem, Evolver 6 was used as optimizer in this study. Evolver applies genetic algorithm-based optimization techniques to find optimal solutions for standard linear and non-linear problems. This program is used as an add-in to Microsoft Excel spreadsheet program to solve problems set up in spreadsheets (Evolver 6) [12].

RESULTS

Before the optimization process, the mathematical model was evaluated due to DIALux findings. Considering the photometric data, the luminous intensity of luminaire is 4264 lm. Model was performed at two different specific luminaire locations. The illuminance level at calculation points on the work plane was calculated for one luminaire at LL_{23} and LL_{32}. The luminaire was located at similar positions in the DIALux model. Outputs of the mathematical model were higher than the ones in the simulation. To compare them quantitatively, R^2 was almost 88 % at for all results, showing the high accuracy of the mathematical model. This meant that knowing the illuminance at points by the mathematical model gives an almost 88% chance of predicting their values on the simulation model (Figure 2). To observe differences between outputs and model results at two luminaire locations, RMSE was 42.82 and 43.09 respectively. NRMSE and CV were 0.14 and 0.26.

After the validation step, the optimizer tool employs to solve this optimization problem while using the same luminaires. According to results of the first scenario, which was to identify the best position of these two luminaires meeting recommended horizontal illuminance requirements, the average illuminance (E_{avg}) is 306.71 lx and uniformity (MRD) is 0.31. Locations of this optimization problem were simulated in DIALux and their average illuminance is 224 lx and E_{min}/E_{avg} is 0.28(Figure 3). The second scenario, which was to identify the best position of three luminaires, resulted in better uniformity with higher illuminance level. E_{avg} is 363.87 lx and uniformity (MRD) is 0.13. By conducting the

simulation for the second scenario, E_{avg} increased to 283 lx and better uniformity with E_{min}/E_m is 0.436 was obtained (Figure 3)

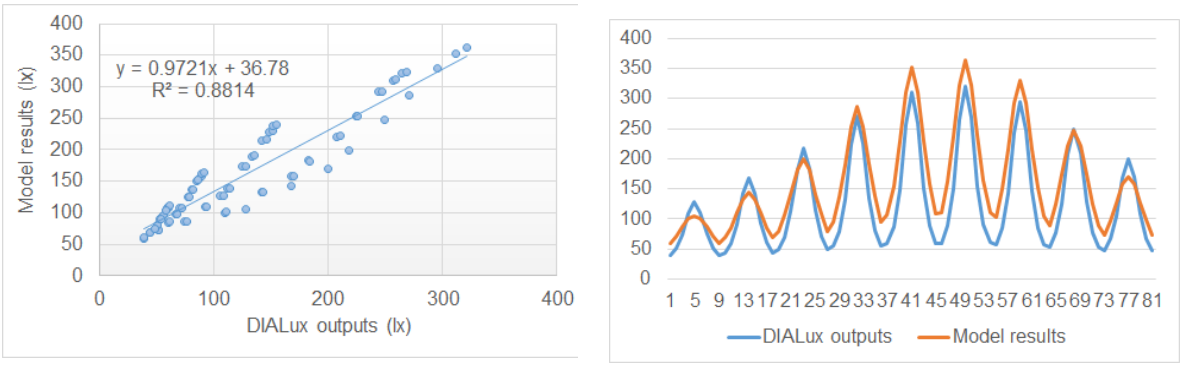

Figure 2. Scatter diagram and comparison of illuminance distribution at calculation points.

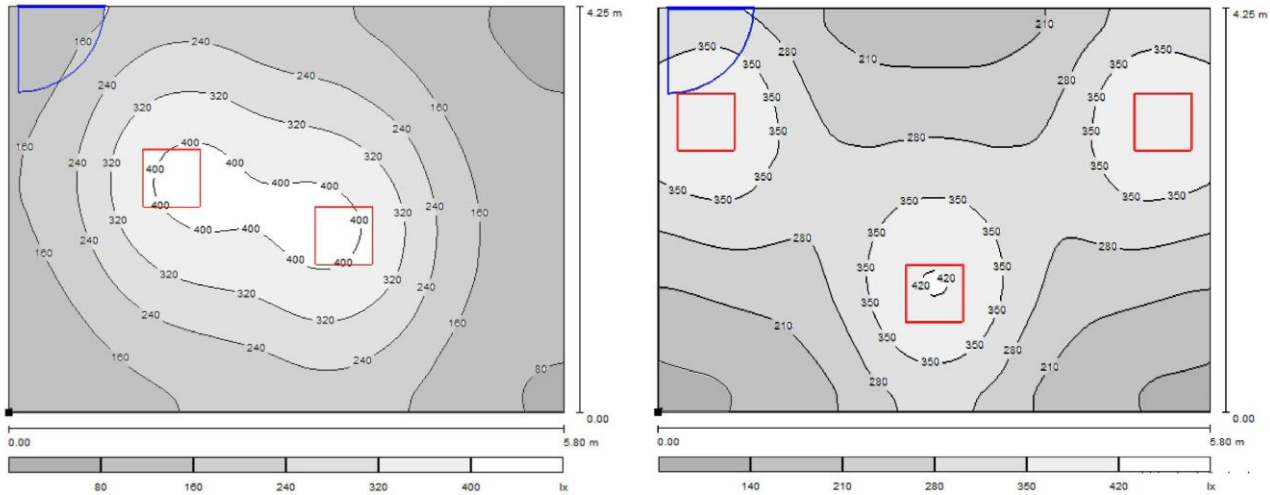

Figure 3. Illuminance distribution and location of luminaires in the first scenario and second scenario.

DISCUSSION AND CONCLUSION

This study proposes a mathematical model to find the optimum position for luminaires by providing visual comfort requirements. Two different scenarios for a selected test case were conducted to obtain sufficient illuminance levels by using different numbers of luminaires. At the same time, by minimizing the differences between illuminance of calculation points and the average illuminance level, maximum uniformity of light distribution was tried to achieve.

This proposed method is a new and alternative approach of applying a mathematical model with an optimization process in architectural research. It is considered that this model would be beneficial, less time consuming, effective and dynamic if integrated in the early design phase. In an earlier study [14], researchers tried to find optimum positions for two different luminaires in two identified and smaller/limited areas. Apart from that study, the optimization study focused on finding the optimum positions of two luminaires in Scenario 1 and three luminaires in Scenario 2 in one identified and determinate area. Thus, their mutual impact while calculating the illuminance and uniformity is integrated in the optimization model. The optimization model in this case performs well in locating and determining the luminaire positions. It presents a high accuracy with the outputs of the DIALux model.

As this is an ongoing research, this model can be developed by integrating different objectives to achieve best positions for luminaires by regarding energy efficiency in further steps. For instance, adding constraints about distances between luminaires would be a good solution to reduce glare on walls and darker spaces between luminaires. Since the simulation, bright spots on walls were observed in Scenario 2 (with three luminaires). To add the distance constraint in the optimization problem, this inefficient and unbalanced light distribution will be eliminated. Also, the problem could be developed by integrating different types of luminaires with different luminous flux and distribution. Luminance efficacy (lumens per watt) would be a good objective for this problem to consider energy consumption. Such objectives would be helpful to estimate positions and numbers of different types of luminaire in designing energy efficient luminaire layout.

REFERENCES

1. Bal, A.: Ofis mekanlarında aydınlatma tekniklerinin değerlendirilmesi ve yorumlanması, Thesis of Master of Science Mimar Sinan Fine Arts University, 2005.
2. Apaydin, S.: Ofislerde aydinlatma tasariminin sürdürülebilirlik açisindan mekan tasarimina etkileri, Thesis of Master of Science, Haliç University, 2012.
3. Dubois, M.C. and Blomsterberg, Å. : Energy saving potential and strategies for electric lighting in future North European, low energy office buildings: A literature review Energy and Buildings 43, pp 2572–2582, 2011.
4. IES. : The Lighting Handbook, 10th edition. Illuminating Engineering Society of North America, 2011.
5. CIBSE.: Code for lightıng, Oxford, Butterworth- Heinemann, 2002.
6. Mourshed, M. et al.: Phi-array: A novel method for fitness visualization and decision making in evolutionary design optimization Advanced Engineering Informatics 25, pp 676–687, 2011.
7. Ravindran, A., Ragsdell K. M. and Reklaitis G. V.: Engineering Optimization: Methods and Applications, Second Edition, John Wiley & Sons, Inc, 2006.
8. Wright, J. and Loosemore, H.: The multi-criterion optimization of building thermal design and control. Proc. of the 7-Th IBPSA Conference, (Dm), pp 873–880, 2001.
9. Magnier, L. and Haghigha, F.: Multiobjective optimization of building design using TRNSYS simulations, genetic algorithm, and artificial neural network, Building and Environment 45 (3), pp 739–746, 2010.
10. DIALux version 4.11. User manual. Software standard for calculating lighting layouts, Lüdenscheid; 2014. Retrieved from:http://www.dial.de/DIAL/en/dialux-international-download/tuerkce.html, 2014.
11. Ferentinos, K. P., & Albright, L. D.: Optimal design of plant lighting system by genetic algorithms. Engineering Applications of Artificial Intelligence, 18(4), pp 473–484, 2005.
12. Evolver 6.: The Desicion Tools Suite, Palisade Europe UK Ltd, Retrieved from http://www.palisade.com/cart/products_EN.asp?cat=51&panel=0, 2015.
13. Shikder S.H. and Mourshed, M.M.: Price ADF. Luminaire position optimisation using radiance based simulation : a test case of a senior living room, Proceedings of the International Conference on Computing in Civil and Building Engineering, 2010.

Indoor Environment Quality

USING PASSIVE HEATING AND COOLING STRATEGIES TO IMPROVE THERMAL COMFORT AND REDUCE ENERGY CONSUMPTION IN HOT ARID REGIONS

García Chávez J. R.[1]; Fernández, F.[2]
1: Universidad Autónoma Metropolitana-Azcapotzalco.
División de Ciencias y Artes para el Diseño
Departamento de Medio Ambiente
Área de Arquitectura Bioclimática
Posgrado en Diseño. Arquitectura Bioclimática
San Pablo 180. Colonia Reynosa Tamaulipas.
C.P. 02200, México, D.F. Tel. 52 55 5318-9110
e-mail: joserobertogsol@gmail.com

2: Universidad Autónoma Metropolitana-Azcapotzalco
División de Ciencias y Artes para el Diseño
Posgrado en Diseño. Arquitectura Bioclimática
San Pablo 180. Colonia Reynosa Tamaulipas.
C.P. 02200, México, D.F. Tel. 52 55 5318-9110
e-mail: pancheiro181@hotmail.com

ABSTRACT

Hot arid climates are characterized by prevailing high temperatures and high solar radiation, with large diurnal temperature differential, often larger than 20 K. In Mexico, hot arid regions cover more than seventy-five percent of the country, with severe climate conditions in winter and summer. Most buildings located in these climates present large energy consumption patterns due to their high dependence on air conditioning systems (AC) for providing comfort to occupants, which in turns provokes the emission of huge amounts of greenhouse gasses (GHG), severely affecting the environment. For those people who cannot afford AC in their buildings, the situation is even worse, as it severely affects their health. This research deals with the investigation of several passive cooling and heating strategies in experimental modules aimed at achieving hygrothermal comfort whilst reducing energy consumption. The cooling techniques involved the four environmental heat sinks, and included: Ground cooling, solar control, natural ventilation, direct evaporative cooling, night sky infrared radiation and thermal insulation. During the underheating season, direct and indirect heat gain techniques along with infiltration control and thermal insulation were also implemented and investigated. The systems were built in the modules and their performance monitored during the prevailing overheating and underheating periods. The results showed that the combined effect of the strategies provided better results than their single influence. During the underheating period, the minimum temperature was 15°C, and the maximum during the overheating season was 25°C. As a result of this research, it is suggested to implement the combined action of the passive cooling and heating techniques in buildings located in prevailing hot arid regions, to improve hygrothermal comfort and to reduce the energy consumption for AC and this would eventually reduce also the emission of pollutants to the atmosphere and promote a favorable sustainable approach.

Keywords: Passive cooling and heating; thermal comfort; hot arid regions; health; energy consumption.

INTRODUCTION

The main characteristics of hot arid regions are the high summer daytime temperatures, large diurnal temperature range, and high solar radiation. Direct solar radiation is as intense as the radiation reflected from the light-coloured and bare ground. The sky is clear most of the year, with high heat loss patterns by long infrared radiation during the nights and mostly during winter season, requiring heating. Horizontal global radiation can approach 1000 W/m^2 and continuous net long-wave radiation loss can be about 100W/m^2. The result is a large diurnal temperature that reach in extreme cases up to 50°C although in many hot-arid regions the typical maximum dry bulb temperature is about 35°C-45°C. Minimum temperatures in summer are about 25°C to 30°C. The round surface temperature in summer may reach up to 70° C. Sunlight reflection for the bare, often light-coloured ground may produce intense glare which, together with reflection from building's walls and external surface obstructions, may cause visual discomfort and significant radiant heat load for buildings through the envelope mainly from windows and walls [Figure 1]. Certainly, in hot-dry regions the summer is the more demanding season. Therefore the design of buildings and exteriors should aim mainly to minimise indoor stress and maximise hygrothermal comfort during the overheating period, whilst minimizing the heat gains from the external heat sources and maximizing the dissipation of heat gains load from interior spaces. However, these regions, which are hot in summer, may also experience uncomfortable winters due to low temperatures that in some cases maybe well below freezing and the lower limit of the comfort range for buildings occupants. On the other hand, cold winds and dust/sandstorms prevail in winter. The air humidity is low. Therefore, in such regions, winter performance should also be considered carefully in the design of buildings and external urban spaces, consequently, the buildings in these climate regions should be carefully designed to consider both overheating and underheating periods.

Figure 1. Typical Building Typology in Hot Arid Regions

RESEARCH OBJECTIVES

The objective of this work focused on investigating the hygrothermal performance of several passive cooling and heating strategies implemented in experimental modules aimed at achieving hygrothermal comfort for building occupants. Pervious research has identified the favorable performance and potential these systems [1, 2, 3, and 4]. The passive cooling techniques involved the four environmental heat sinks, and included these strategies which were implemented in the experimental modules: Ground cooling, solar control, natural ventilation, direct evaporative cooling, night sky infrared radiation and thermal insulation.

The premise of passive cooling focuses on heat gain control from external heat sources (heat gain prevention) and heat dissipation of internal heat gains load (removing heat). It is aimed at improving and maximizing the indoor hygrothermal comfort with the minimal energy consumption. Therefore, this approach works either by preventing heat from entering the interior (heat gain prevention) or by removing heat from the building (passive or hybrid cooling). Natural cooling utilizes on-site energy, that is, heat sinks, which are energy ambient storage components, available from the natural environment, combined with the architectural design of building components of the envelope, rather than using mechanical systems to dissipate heat. Therefore, natural cooling depends not only on the architectural design of the building but how it uses the local site natural resources as heat sinks: earth, water, air and sky (Figure 2). The research was conducted using experimental modules located in Mexico City Metropolitan Area (MCMA) (Figure 3), built with lightweight polystyrene panels with the dimensions: 2.44 meters length, 1.22 meters width, and 0.051meters thickness, on a slab of reinforced concrete foundation (Figure 4). One of the modules served as a control or reference unit and the other modules were where the bioclimatic strategies were implemented and investigated. Results will be extrapolated and applied in typical hot arid regions of the country. A solar shading analysis was conducted to orient the experimental modules towards true south and to select the most suitable location to prevent self-shading among them and to make sure that any external obstruction could not block solar irradiation on the modules (Figure 3).

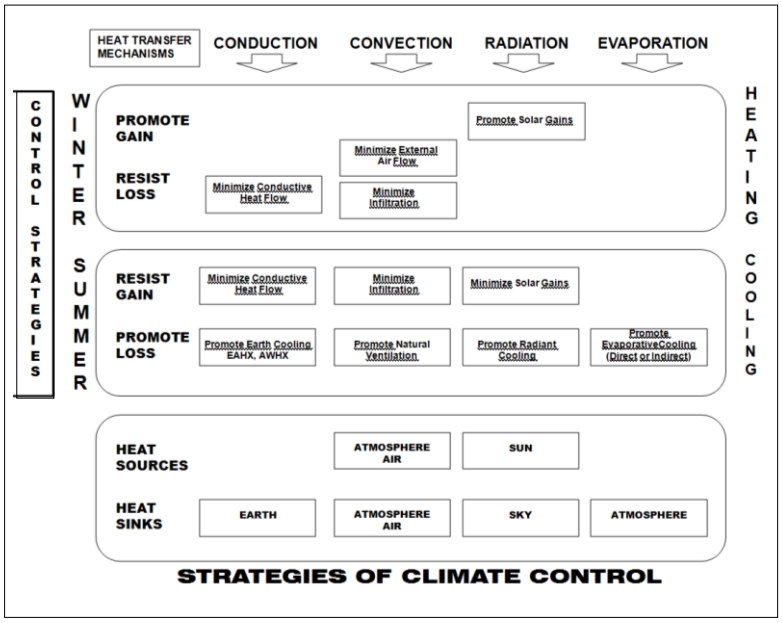

Figure 2. Strategies of Climate Control. Heat Sinks

CLIMATE CONDITIONS

The climate conditions on the experimental site indicate that the average annual temperature is 16.8°C; the maximum annual average is 24.8°C and the minimum 8.8 °C. During the overheating period, maximum average temperatures occur in March, April, May and June, of 27.0° C, 27.9°C, 27.7°C, and 25.9°C, respectively. During overheating period the lower temperatures occur in November, December, January, February and March, of: 6.8°C, 4.9°C, 4.1°C, 5.3°C and 7.5°C, respectively. Annual temperature differential is 16.0 K. Annual rainfall is 608.2 mm. Prevailing wind direction most of the year, comes from the NE with an average annual rate of 1.9 meters/second and a maximum of 2.4 meters/second The average annual solar radiation is 18.01 MJ/m^2, which is equivalent to 5.0 kWh/m^2 [5].

METHODOLOGY OF THE RESEARCH

Monitoring of the test and control modules took place during representative underheating and overheating periods, using data loggers to measure the temperatures in the middle of the experimental modules, as well as on surface temperatures of the interiors, on the plafond, and walls. External temperatures and relative humidities were concurrently registered using a weather station, located sixty meters from the experimental site. To calibrate the experimental arrangement, and to make sure all the modules have the same conditions and configuration, the internal temperatures and relative humidity of all the modules were monitored during fifteen consecutive days. Results were similar, indicating the validation of the experimental procedure.

Figure 3. Experimental modules investigated. Site Plan

Figure 4. Experimental Modules. Construction process and arrangement

RESULTS. ANALYSIS AND INTERPRETATION

From all the strategies investigated, the most promising was the Earth-to-Air-Heat Exchanger (EAHX), for both heating and cooling. This strategy consisted of earth tubes implemented in the test module and the results were compared with those of the control module, without any strategy applied. The experimental arrangement consisted of 100 mm polyvinyl chloride (PVC) underground pipes, located in a depth of 1.60 meters and 24 meters length. The tubes enter the test module for the lower northern side and are linked with a low energy fan to move and transfer in the air passing through. Data loggers were located in the experimental module to measure dry bulb temperature (DBT) and relative humidity (RH). The monitoring period covered the typical underheating and overheating seasons of the location and was conducted during ten representative days and are summarized in Table 1. The EAHX module showed an increase of 3.32 K maximum DBT; 2.84 K minimum DBT; and 3.10 K average DBT, relative to the control module. The temperature difference between the outside DBT and the EAHX module were: 6.76 K maximum DBT; 13.32 K minimum DBT; and 3.7 K average DBT. These results demonstrated the effectiveness of using the earth tubes for reducing the temperature differential between the external temperatures and those registered inside the EAHX module during the typical underheating period and to increase the indoor temperature to get closer to the lower limit of the comfort zone for this location.

During the overheating period (February 26.March 7), the EAHX showed a decrease of 7.13 K maximum DBT; 1.14 K minimum DBT; and 3.12 K average DBT, relative to the control module. The temperature difference between the outside DBT and the EAHX module were: 5.3 K maximum DBT; 6.01 K minimum DBT; and 1.22 K average BDT. These results demonstrated the effectiveness of using the earth tubes for reducing the temperature differential between the external temperatures and those registered inside the EAHX module during the typical overheating period and to reduce the indoor temperature to get into the comfort zone for this location.

Other strategy evaluated was the conductive thermal insulation located on West wall and the roof of the test module, evaluated during the typical overheating period for 10 days, from May 4th to May 13th. The results of the temperature inside the control module and experimental test module had a slightly lower variation relative to the previous system, with a temperature differential of about one degree at the maximum DBT temperature and slightly half a degree above the minimum DBT. Throughout the monitoring period the DBT of the test module temperature presented a lower temperature differential relative to the control module (Table 1). The results of the monitoring process showed that the thermal insulation applied in the test module provided an important reduction of maximum DBT of 31.77º C to 24.29 ºC, that is, a 7. 48 K temperature differential. This strategy was more effective during the overheating period.

Other strategy evaluated was direct evaporative cooling, consisted of a geotextile material forming a wet curtain positioned on the west opening of the test module. The monitoring period of this system run for 12 consecutive days, from May 16-27. However, on May 21 and 22, the evaporative cooling process was not applied and then data from these days were excluded, During the monitoring process, one liter of water was added daily to the geotextile, by means of a sprinkler every 1.30 hours at which time the volume of water evaporated completely. The DBT inside the experimental modules varied little, but remained within the comfort range. The results of this system are summarized in Table 1.

BIOCLIMATIC STRATEGIES INVESTIGATED SUMMARY					
Testing Period			Temperatures (ºC)		
Underheating Period December 4-13	**EAHX**		Exterior	Control Module	Test Module
		Maximum DBT	24.58	14.50	17.82
		Minimum DBT	-2.98	7.50	10.34
		Average DBT	10.88	11.48	14.58
Overheating Period March 10-23	**EAHX**	Maximum DBT	29.17	31.00	23.87
		Minimum DBT	3.35	10.50	9.36
		Average DBT	16.90	21.24	18.12
Overheating Period February 26 to March 7	**Tower Collector for Natural Ventilation**	Maximum DBT	29.41	21.00	22.01
		Minimum DBT	17.26	17.73	17.62
		Average DBT	3.46	14.00	12.24
Overheating Period May 4-13	**Thermal Insulation West Wall and Roof**	Maximum DBT	31.77	25.00	24.90
		Minimum DBT	7.70	15.50	16.08
		Average DBT	20.87	21.02	20.99
Overheating Period May 16-27	**Direct Evaporative Cooling**	Maximum DBT	34.68	27.00	27.16
		Minimum DBT	11.71	19.00	18.79
		Average DBT	22.58	22.86	22.75

Table 1. Summary of Experimental Results of Investigated Passive Cooling and Heating Strategies

CONCLUSIONS

The results of this research work indicate that the bioclimatic systems evaluated are a promising alternative to reduce energy consumption whilst providing hygrothermal comfort conditions for the building occupants. The subsequent work of this research is aimed at transferring and extrapolating the results to be applied in buildings located in hot arid regions, where due to the severe climate conditions; the results can be even more improved. Additionally, the results of this research can be even improved with the integration in a synergic action of all the bioclimatic systems, evaluated individually in this work, aimed at being implemented in both new and existing buildings. The application of this approach can eventually reduce the emission of GHG and improve the environment, which hopefully promote a more sustainable attitude in the application of bioclimatic architecture at regional and global levels for the wellbeing of people.

REFERENCES

1. Givoni, Baruch. Passive and Low Energy Cooling of Buildings (1st Ed.). 605 Third Avenue, New York, NY 10158-0012, USA: John Wiley & Sons, Inc. ISBN 0-471-28473-4. 1994
2. Santamouris, M.; Asimakoupolos, D. (1996). Passive Cooling of Buildings (1st Ed.). 35-37 William Road, London NW1 3ER, UK: James & James (Science Publishers) Ltd. ISBN 1-873936-47-8. 1996
3. Brown, G.Z.; DeKay, Mark. Sun, Wind, and Light: Architectural Design Strategies (3rd ed.). 605 Third Avenue, New York, NY 10158-0012, USA: John Wiley & Sons, Inc. ISBN 0-471-34877-5. 2014
4. Kwok, Alison G.; Grondzik, Walter T. The Green Studio Handbook. Environmental Strategies for Schematic Design (2nd Ed.). 30 Corporate Drive, Suite 400, Burlington, MA 01803, USA: Architectural Press. ISBN 978-0-08-089052-4. 2013.
5. Matsumoto, Y. et al. Global Solar Irradiation in North Mexico City and Some Comparisons with the South. 2013 ISES Solar World Congress. Cancun, Mexico, ISBN 57 (2014) 1179-1188. 2014.

INVESTIGATING THE EFFECT OF CO_2 CONCENTRATION ON REPORTED THERMAL COMFORT

S. Gauthier[1]; B. Liu[2]; G. Huebner[2]; D. Shipworth[2]

1: University of Southampton, Highfield, Southampton, SO17 1BJ, UK.

2: UCL Energy Institute, Central House, 14 Upper Woburn Place, London, WC1H 0NN, UK.

ABSTRACT

The need to predict occupants' perception of thermal discomfort has become one of the priorities in the quest to reduce energy demand in buildings. Drawn from physical and physiological principles, the current thermal comfort models have long been associated with environmental and personal variables. Research has shown that there is often gap between modelled and perceived thermal comfort sensation. One of the reasons may be additional parameters playing a role which are not currently accounted for in the models. One plausible candidate and causal pathway is elevated CO_2 levels stimulating the human respiratory system resulting in increased metabolic rate and heat exchange with the environment. The hypothesis is that people may feel warmer when indoor CO_2 concentration increases. To investigate this hypothesis, two empirical studies were carried out in London; the first one was undertaken in a climate chamber over the summer of 2014, and the second one in an office setting over the winter of 2015. Findings from the first experiment showed that participants felt on average warmer as CO_2 concentration increased but ambient temperature remained constant. However the relationship between reported comfort and CO_2 concentration was not significant. One may suggest that heating setpoint may be adjusted at lower temperature in winter while keeping CO_2 concentration low enough not to affect cognitive performance. This conjecture initiated the study design of the second experiment. As ambient temperature decreased by 3.1±0.5°C, CO_2 concentration increased by 297±45ppm. In this instance, participants felt slightly colder at the end of the sessions; however a modest relationship between CO_2 was found. Thus future studies may chose to increase the variation in CO_2 concentration, and decrease the variation in operative temperature. To conclude the picture that is emerging from this research shows that there is no significant relationship between reported thermal comfort and CO_2 concentration; although this may be due to the relatively small sample size in the first study, and the relatively small variation in CO_2 concentration in the second study. This finding may support building operation strategies that optimise fresh-air level independently of the provision of thermal comfort.

Keywords: Occupant thermal comfort, Indoor CO_2 concentration, Mixed-methods.

INTRODUCTION

In UK, buildings account for nearly half of the carbon emissions; of which heating, ventilation and air conditioning (HVAC) systems represent the largest part [8]. Thus reducing the demand from these systems while keeping occupants comfortable is considered an important component in the quest to reduce carbon emissions. As described in BS EN 15251:2007 [2], thermal comfort is dependent upon external temperature in the adaptive model, and upon four environmental factors (ambient air temperature (Ta), mean radiant temperature (Tr), mean air velocity (Va) and relative humidity (RH)) and two personal factors (metabolic rate [M] and clothing insulation [Icl]) in the predictive model. Research has shown that there is often a gap between modelled and perceived thermal comfort sensation [1]. One of the reasons may be additional parameters) playing a role, which are not currently accounted

for in the models. Persily [9] has shown that indoor CO_2 concentration from 600 ppm to 1000 ppm or higher is linked to occupants' perceptions of stuffiness and discomfort. Results of the study by Kavgic et al. [4] suggests that cold discomfort complaints increased when indoor spaces are over-ventilated with a lower CO_2 concentration level. Additionally, high CO_2 concentrations in internal environments are associated with poor indoor air quality, increased symptoms of health response, poor cognitive performance [7]. Human respiration is one of the important sources of indoor CO_2 [3]. During the respiration process, the human body inhales oxygen (O_2), and exhales CO_2. As metabolic rate increases, the breathing rate increases, and more CO_2 is generated by human respiration [12]. Besides, an increase in indoor CO_2 concentration stimulates the breathing rate [10], and a decrease in indoor CO_2 concentration results in a decrease in breathing rate [11]. Indoor CO_2 concentration stimulates human respiratory system, which will in turn increase human metabolic rate and heat exchange with the surrounding environment. Hence, the hypothesis is that people may feel warmer when indoor CO_2 concentration increases, and people may feel cooler when indoor CO_2 concentration decreases. The two empirical studies presented in this paper aim to test this hypothesis, and to investigate the potential effect of CO_2 concentration on thermal comfort perception.

METHOD

Experiment in climate chamber

The first empirical study was carried out in a climate chamber over the summer of 2014. While the six independent variables of the predictive thermal comfort model were kept constant, eighteen participants were each exposed to three consecutive conditions: an increase (Stage 1), then a decrease (Stage 2), and finally a constant exposure (Stage 3) in CO_2 concentration. Six experimental sessions were carried out with three participants taking part in each session. This was a convenience sample, participants were recruited through a call for participation sent out to friends and colleagues. The age range was 22 to 25 years old. The sample consisted of N = 18 participants, only four were male. During Stage 1, the participants were exposed to a gradual increase in CO_2 concentration for a period of 30-minutes. The source of CO_2 was the product of four occupants' respiration (including the researcher) in the fully closed climate chamber. During the next stage (Stage 2), participants were exposed a gradual decrease in CO_2 concentration by partly opening two vents and the chamber's door, for a period of 30-minutes. Finally during Stage 3, participants were exposed to constant and low level of CO_2 concentration by fully opening two vents and the climate chamber door, for a period of 30-minutes. In the climate chamber (Ta) was set at 24°C, and (RH) at 50% [3]. Upon arrival, the participants were given information sheets, a consent form, and had to fill in a background survey about their age, gender, clothing, activity prior to testing, etc. This pre-testing period of about 15 minutes ensured a somewhat comparable rate of metabolic activity, i.e. 15 minutes of sitting still. During the experiment all participants remained seated. Using ISO 7730:2005 Annex B [6], participants' activity level was estimated as 1 met or 58 W/m^2, and constant throughout the experiment. With regards to (Icl), participants were asked not to change their clothing insulation level during the experiment. Using ISO 7730:2005 Annex C [6], (Icl) was estimated at 0.78 ±0.2 clo.

During the experiment, four Eltek datalogger GD-47 were used to monitor (Ta), (RH) and CO_2 concentration at 1-min interval. Three datalogger were located in the climate chamber at the height of 1.2 m, which is regarded as the breathing zone height of seated participants. The fourth datalogger was located outside the climate chamber. Additionally, an anemometer was placed inside the chamber to monitor (Va) during the experiments. Concurrently to the environmental monitoring, participants were required to complete thermal comfort surveys at

10-minutes interval. These aimed to assess participants' thermal perception or actual mean vote (AMV); which was evaluated using the 7-points scale, from -3 ("cold") to +3 ("hot") [2].

Experiment in office setting

To follow the experiments in the controlled environment, a second study was carried out in an office setting over the winter of 2015. While ambient air temperature was decreasing, participants were exposed to an increase in CO_2 concentration for a period of 40-minutes. CO_2 concentration increased due to breathing of the participant and the research assistant in a relatively small space of about $8m^2$. Participants were recruited through the online subject data pool of the University College London (UCL). The age range was limited to 18 to 35 years. The sample consisted of N = 30 participants, only two were male. For the purpose of a separate research question, participants had been split up into a control (N = 12) and an intervention group (N=18), with the only difference that in the intervention group participants had control over the light setting in the room. To reflect any potential impacts of this manipulation, group membership (control = 0; intervention = 1) was included as a dummy predictor in subsequent analysis. During recruitment, participants were told what to wear during the experimental session in order to keep the (Icl) identical across participants. This was specified as '*a long-sleeve top, long trousers, shoes and socks*', resulting in (Icl) of about at 0.7 clo [6]. Similar to the first experiment, a pre-testing period of about 15 minutes ensured comparable rate of metabolic activity. During the experiment participants remained seated, with an estimated (M) of 1 met or 58 W/m^2.

During the experiment, one Eltek datalogger GD-47 was used to monitor CO_2 concentration, one anemometer monitored (Va), and four HOBO datalogger U12-012 were used to monitor (Ta) and (RH) at four heights - 0.1m, 0.6m, 1.1 and 1.7m [5]. The sampling rate was set at 1-min interval. Concurrently, participants were asked to complete thermal comfort surveys at 10-minutes intervals, these were similar to the one used in Experiment 1.

RESULTS

Experiment in climate chamber

This study in controlled environment intended to keep the six predicted factors associated with thermal comfort constant. Clothing insulation and metabolic rate were controlled for. With regard to the environmental variables, (Ta) varied slightly with a mean of 22.9±0.4°C, (RH) also varied slightly with a mean of 60±3%. From the output of the anemometer, (Va) was maintained at 0.05 m/s during the six sessions. As this result is lower than 0.15 m/s,

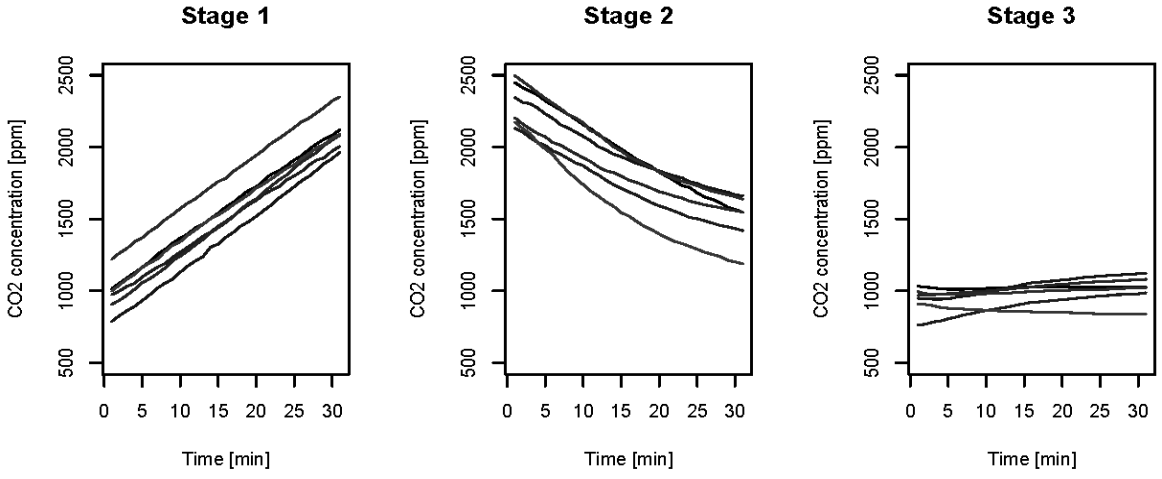

Figure 1: Variation in CO_2 concentration, during Stage 1 to 3, for the six experiments.

(Tr) was regarded as equal to (Ta) (ISO 7726:2001, Table 3 [5]). With regards to variation in CO_2 concentration, results are illustrated in Figure 1. During Stage 1, CO_2 concentration increased on average by 1,118 ±55 ppm; during Stage 2, it decreased on average by 799 ±135 ppm; and during Stage 3, it remained relatively constant with an average of 78 ±113 ppm.

With regards to thermal perception, the mean AMV for the eighteen participants at each survey time is shown in Figure 2. The results show that AMV varied slightly around the "*Neutral*" rating. During Stage 1, AMV increased on average by 0.23 points; during Stage 2 it decreased on average by 0.22 points; and during Stage 3 it remained relatively constant with an average decrease of 0.06 points.

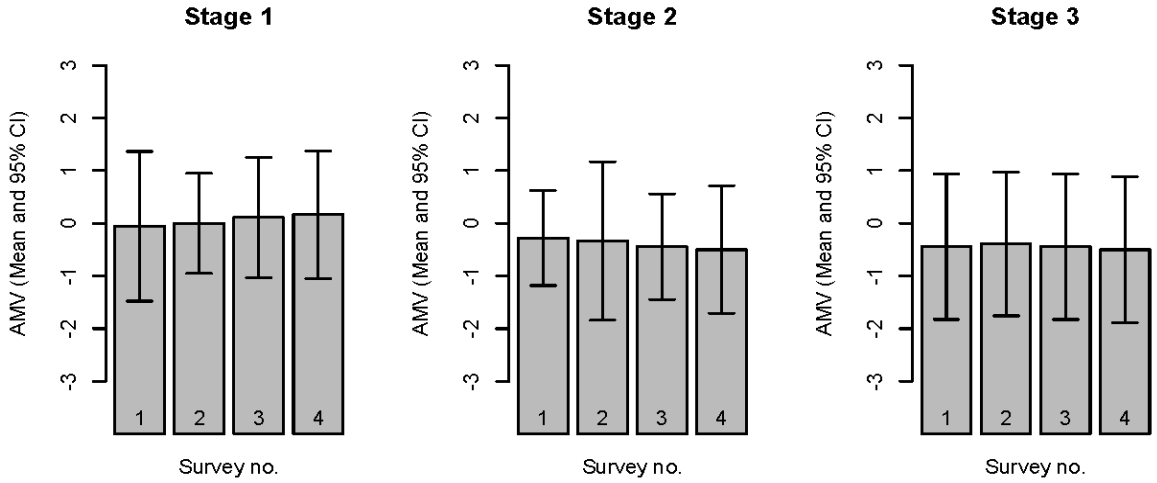

Figure 2: Variation in AMV, during Stage 1 to 3, for the eighteen participants.

To investigate the relationship between CO_2 concentration and thermal perception, repeated measures ANOVA for each Stage were carried out. Although participants felt warmer on average when CO_2 concentration increased, there was no statistically significant effect of CO_2 concentration on AMV, $F(1, 68) = 0.51$, $p = 0.479$. In Stage 2, participants felt on average colder when CO_2 concentration decreased, but there was no statistically significant effect of CO_2 concentration on AMV, $F(1, 68) = 0.01$, $p = 0.921$. Finally, participants' individual AMV was compared at the start and the end of Stage 3 using Wilcoxon paired test. Results showed that AMV is not significantly different at the start and the end of the experiment ($Z = 0.33$, $p = 1$), therefore participants' thermal perception did not change when CO_2 concentration remained constant.

Experiment in office setting

This study in office environment intended to keep five predicted factors associated with predictive thermal comfort constant. Clothing insulation and metabolic rate were controlled for. With regard to the environmental variables, (RH) varied slightly with a mean of 35±3%, and (Va) was maintained below 0.1 m/s. As this result is lower than 0.15 m/s, (Tr) was regarded as equal to (Ta) [5]. With regards to (Ta), a review of the monitoring output using z-score revealed three outliers, where (Ta) did not varied significantly during the course of the session, and where (Ta) level was set at a significantly higher level at the start of the session. These three outliers were not included in the subsequent analysis. With regards to variation in (Ta) and CO_2 concentration, results are illustrated in Figure 3. During the course of the 27-sessions, (Ta) decreased on average by 3.1±0.5°C, and CO_2 concentration increased on average by 297±45ppm.

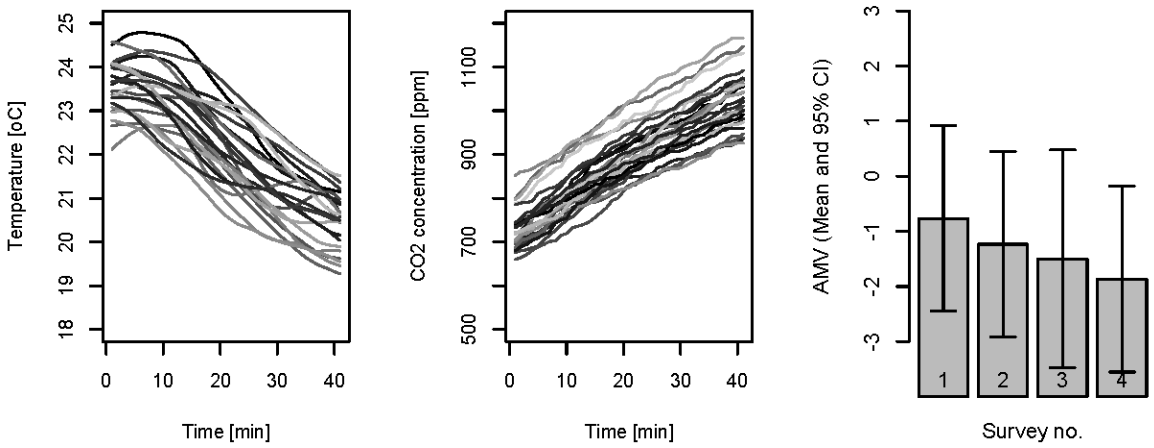

Figure 3: Experiment 2 - variation in (Ta), CO_2 concentration and AMV.

With regards to thermal perception, the mean AMV for the twenty-seven participants at each survey time is shown in Figure 3. The results show that AMV decreased on average by 1.1 points; on average participants felt slightly colder at the end of the session.

To investigate the relationship between CO_2 concentration and thermal perception, cross-sectional regression analysis between mean AMV and mean CO_2 concentration at each survey time were carried out, with AMV as dependent variable and CO_2 and condition as predictors. Results showed weak relationships, with Survey 1 (Adj. R^2=0.08, p=0.08, β=-0.33), Survey 2 (Adj. R^2=0.02, p=0.55, β=-0.11), Survey 3 (Adj. R^2=0.04, p=0.91, β=0.02) and Survey 4 (Adj. R^2=0.03, p=0.82, β=-0.04). Further analysis need to take the longitudinal character of the study into account, building a hierarchical model with the repeated measures of comfort as dependent variable; and with time-varying covariates (CO_2, Ta) and time-constant predictors (e.g. Body-Mass-Index) as predictors.

DISCUSSION

With regards to the first study, the sample size was relatively small, with N=18. Using the results of the experiment to determine the expected effect size, a power calculation was undertaken to determine how many participants you be required to obtain a significant numerical difference. The desired statistical power was assumed to be 80% and alpha level was set at 5%. Results show that for Stage 1, 75 participants would be required, and for Stage 2, 50 participants would be required. Future research may also consider varying the sequencing of the exposure to CO_2 concentration, as there might be a 'lag' in thermal sensation between stages. This will require the use of a climate chamber with control over fresh-air intake, and rising CO_2 concentration using gas bottle. Ethical consideration should be reviewed. With regards to internal validity and study design, one limitation of the second study might be the CO_2 concentration range considered, which was relatively low. A larger effect on AMV may be observed when increasing CO_2 concentration further. Finally, the analysis methods considered AMV as a continuous variable, however studies using the adaptive approach have considered AMV as a discrete variable [1]. Further analysis may employ logistic regression to review the monitoring results.

CONCLUSION

Our study used two experimental designs to investigate the relationship between indoor CO_2 concentration and reported thermal comfort. Results of the first experiment in climate chamber show that when reviewing the mean comfort vote at each survey time, participants felt warmer when CO_2 concentration increased, colder when it decreased, and reported no

change when it remained constant. However the results were not satistically significant. A post-hoc sample size calculation has shown, that the study would have required substantially larger number of participants (75) to reveal a satistically significant effect. To follow from this study, a second experiment in office environment was carried out. As operative temperature decreased, CO_2 concentration increased. Results of this experiment showed that participants felt slightly colder at the end of the session. This may be due to the fact that (Ta) may have a greater impact on AMV than CO_2 concentration. In addition the variation in CO_2 concentration was relatively modest compare to the first experiment, with a mean decrease of 297±45ppm. Thus future studies may chose to increase the variation in CO_2 concentration, while minimising the impact on cognitive performance. To conclude this paper shows that there is no significant relationship between reported thermal comfort and CO_2 concentration, therefore there is no basis for concern when controlling for CO_2 concentration having adverse effect on occupants' perception of thermal comfort. In winter, heating and ventilation systems should provide fresh-air and thermally comfortable environments. This will be a challenge; as thriving for energy conservation, buildings are becoming more airtight with lower infiltration rate and fine-tuning of fresh air intake.

REFERENCES

1. Brager, G. and de Dear, R.: Thermal adaptation in the built environment: a literaturereview. Energy and Buildings, 27, 83–96, 1998.
2. CEN: Standard BS EN 15251, Indoor environmental input parameters for design and assessment of energy performance of buildings addressing indoor air quality, thermal environment, lighting and acoustics. ECS, Brussels, Belgium, 2007.
3. CIBSE: Guide A - Environmental Design. The Chartered Institution of Building Services Engineers, London, UK, 2007.
4. Kavgic, M. et al.: Analysis of thermal comfort and indoor air quality in a mechanically ventilated theatre. Energy And Buildings, 40, 1334-1343, 2008.
5. BS EN ISO 7726:2001 Ergonomics of the thermal environment - Instruments for measuring physical quantities. ISO, Geneva, Switzerland, 2001.
6. BS EN ISO 7730:2005: Ergonomics of the thermal environment - Analytical determination and interpretation of thermal comfort using calculation of the PMV and PPD indices and local thermal comfort criteria. ISO, Geneva, Switzerland, 2005.
7. Liu, B: Empirical study: investigating the effect of CO_2 concentration on reported thermal comfort and perceived concentration level. MSc Dissertation. UCL, UK, 2014.
8. Perez-Lombard, L., Ortiz, J. and Pout, C.: A review on buildings energy consumption information. Energy And Buildings, 40**,** 394-398, 2008.
9. Persily, A.: Evaluating building IAQ and ventilation with indoor carbon dioxide. ASHRAE Transactions, Vol. 103, No. 2, 1997.
10. Rice, S.: Health effects of acute and prolonged CO_2 exposure in normal and sensitive populations, In proceedings: Second Annual Conference on Carbon Sequestration, Alexandria, Virginia, USA, 2003.
11. Sircar, S: Principles of Medical Physiology. Georg Thieme Verlag, 353-355, 2008.
12. Weissman, C. et al.: Effect Of Routine Intensive-Care Interactions on Metabolic-Rate. Chest, 86, 815-818, 1984.

PERSONAL COOLING USING THERMAL CONDUCTION ON THE DESK

J. Verhaart[1]; R. Keune[1]; M. Veselý[1]; R. Li[1], W. Zeiler[1].

1: Dep. of the Built Environment, Rondom 70, 5612 AP, P.O. Box 513, 5600 MB Eindhoven, The Netherlands. Email corresponding author: J.C.G.Verhaart@tue.nl

ABSTRACT

In order to reduce the energy load on buildings, the indoor climate will not be maintained within narrow boundaries in the future. With the application of local conditioning systems that offer individual building occupants the possibility to increase their personal comfort level, a narrow boundary is no longer necessary. In uniform conditions, the comfort level is directly related to the heat balance of a person. However, even before the heat balance is restored from a slightly uncomfortable environment, a thermal stimulus in the right direction can give a person a pleasant feeling. This effect is called alliesthesia. In this study positive alliesthesia in a warm environment was tested by offering cooling via a plate on top of a desk.

Tests were conducted in the climate chamber in a slightly warm environment (PMV = 1.0, operative temperature of 28ºC, clo = 0.6). Six subjects were recruited to test the three cooling settings. The plate temperature was maintained by running water through the integrated water pipes. The first ('passive') test was conducted without cooling water. The second test was 'cold' with a water temperature of 26 ºC, in the third ('warm') test, the water temperature was maintained at 28 ºC.

Alliesthesia was found in all tests. The alliesthesia in the 'passive' and the 'warm' tests were positive, in the 'cold' test, two groups formed. People who initially felt comfortable with the cooling and people who felt uncomfortable. People who voted neutral in the beginning of the test, moved to either comfortable or uncomfortable. The comfort level in the 'passive' test was maintained, unlike the level in the 'warm' tests, because of the increasing temperature of the plate. The cooling plate was unable to effect the heat balance and improve the overall thermal sensation (TS).

Keywords: personal cooling, alliesthesia, thermal comfort

INTRODUCTION

Currently, building indoor environment are maintained within a narrow boundary. Two setpoints are used in building operations, one for heating in winter, and a higher setpoint for cooling in summer. The setpoints can be found in standards [1] and are different depending on the quality class of the building. However, in previous studies [2] it was shown that applying a narrow boundary does not increase the comfort level of the building occupants, even though this is what could be expected based on the relation between predicted mean vote (PMV) and predicted percentage dissatisfied (PPD).

Maintaining the indoor temperatures within these narrow boundaries needs a big energy consumption. This means that there is a large opportunity to reduce the energy demand of a building when a more flexible temperature control strategy can be applied [3]. The application of a localised conditioning systems such as a personal heating or cooling system comes naturally to a less strictly controlled indoor environment [4][5]. A personal conditioning system (PCS) offers individuals the possibility to increase their personal comfort level above that in traditional buildings. Alliesthesia is the effect that a thermal stimulus has on the body. Small thermal stimuli can cause a pleasant or unpleasant feeling in people who are near the border of their comfort zone. A stimulus in the right direction (so a warm stimulus when near the cold

side) will feel pleasant, while a cold stimulus (a breeze for example) will feel unpleasant. [6] [7] [8]. Understanding the phenomenon of alliesthesia is therefore essential to control PCS in dynamic temperature regimes. Understanding the alliesthesia effect in relation to thermal comfort will enable us to design a better, active and stimulating indoor environment and help us to apply personal conditioning systems in an effective and energy efficient manner.

We studied positive alliesthesia in a slightly warm environment with the application of local cooling. The study is performed using human subject experiments in the climate chamber. The cooling effect is reached by using a cooling plate that cools the subject locally when he touches the plate with his hands and forearms.

METHOD

The cooling plate that was used in this experiment is 0.6 m by 1.0 m. It's an aluminium plate integrated with water channels. Figure 1 shows the plate with the positions of temperature sensors indicated. The temperature sensors were placed on the bottom side of the plate, in between the water channels.

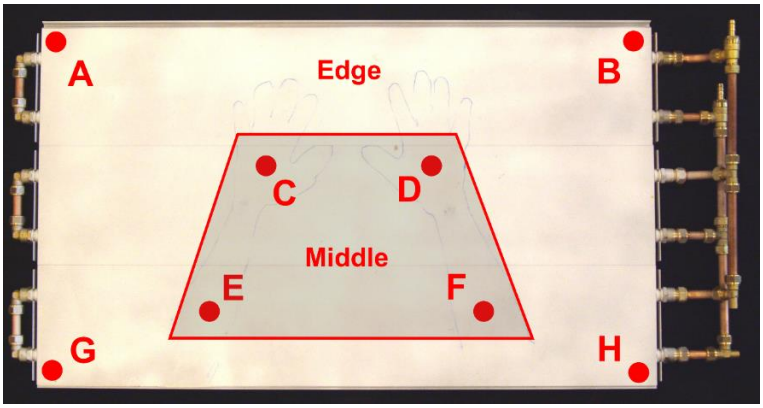

Figure 1: Position of the temperature sensors underneath the aluminium plate. The sensors in the middle are in the area where the subjects would place their forearms.

The tests were performed in the climate chamber at Eindhoven University of Technology. During the tests, the air temperature, speed and humidity of the air in the climate chamber were controlled. The environmental conditions during all tests were selected to reflect a PMV of 1.0 operative temperature of 28°C and an airspeed below 0.15 m/s. The subjects were instructed to wear clothes to a level of 0.6 clo.

During the tests, the subjects were exposed to three different levels of local cooling. In the first series of tests, the aluminium plate was used without water. The cooling effect during these 'passive' tests relies totally on the effusivity of the aluminium. During the second series of tests, the plate is actively cooled to 26°C. These tests are called the 'cold' tests. In the third series, the plate was kept at 28°C. In this 'warm' series, the plate temperature is the same as the wall and air temperature, and the same as in the passive tests initially. In the passive test, the temperature slowly increases. There is still a net cooling effect in both cases because of the effusivity of the aluminium and the plate temperature that is lower than the skin temperature.

For the experiment, six male, college-age students were recruited. Their physical characteristics are listed in Table 1. All three series of tests were performed with all six subjects, making a total of eighteen.

Before the start of a test, a short (five minutes) explanation was given and the subject would enter the climate chamber to acclimatize for 20 minutes. After that, the test would start and the subject would place their hands and forearms on the cooling plate. The subject was asked not

to take their arms off the plate, except for filling out the questionnaires. The test would last for 30 minutes and is followed by a short interview.

Subject	Age [yr]	Height [m]	Weight [kg]	BMI [kg/m²]	Skin area [m²]
A	24	1.87	84	24	2.09
B	27	1.97	75	19	2.07
C	24	1.88	72	20	1.97
D	24	1.86	78	23	2.02
E	23	1.72	67	23	1.79
F	24	1.78	78	25	1.95

Table 1: Physical characteristics of the test subjects

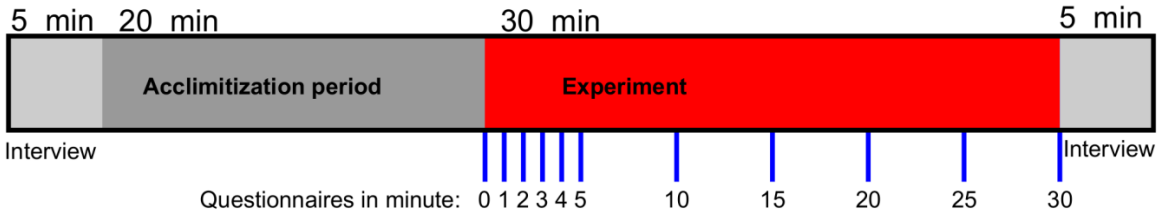

Figure 2: Schedule for the experiments: After the initial interview and acclimatization the 30 minute test started in which eleven questionnaires were done at the indicated times

Questionnaires were used to determine the thermal sensation (TS) and comfort level of the subjects during the tests. To capture the alliesthesia effect, especially in the beginning of the test, a high frequency was chosen. The first five minutes, the subject was asked to fill out the questions every minute. During the remainder of the test this was reduced to every five minutes. In the questionnaires, we asked for the TS of the hands, arms and the head specifically and for the TS and comfort of the whole body. To ensure that the subject would not spend too much time filling out the questionnaires, he only had to indicate the TS per body part on a continuous line from -3 (Cold) to +3 (Hot) in correspondence with the ASHRAE 7-point scale and indicate the comfort level by selecting the most appropriate smiley. A part of the questionnaire is shown in Figure 4.

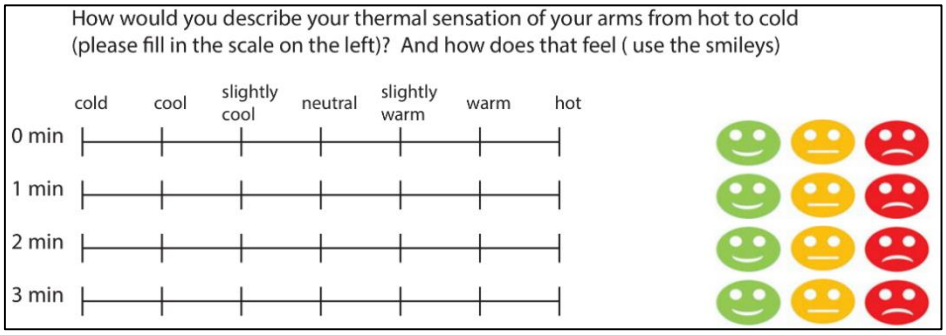

Figure 3: Part of the questionnaire used in the experiments.

The skin temperature was measured on the top side of the ring finger, the hand, the wrist and the forearm, both on the left and the right arm.

RESULTS

The test was started after the subject has acclimatized to the warm environment. This means that the TS overall is close to the PMV. During the test, this remains the same on average as can be seen in Figure 6, 8 and 10. In these figures, the TS votes from all tests within one series

are combined with the average PMV calculated from the environmental conditions, not taking into account the local cooling. The TS of the body parts that were exposed to the aluminium is much lower.

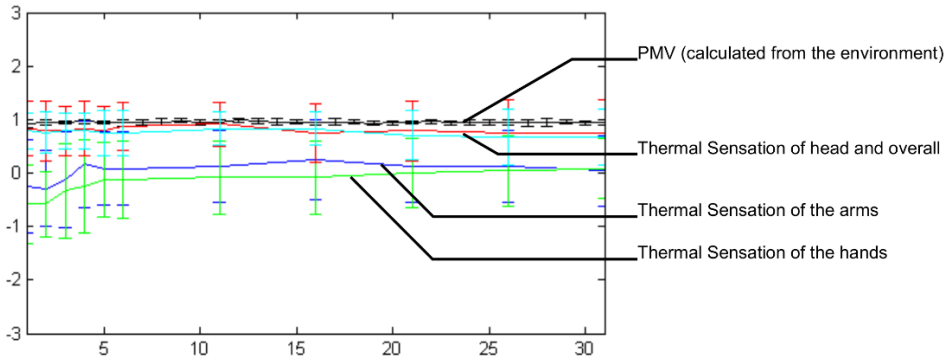

Figure 4: TS of the different body parts compared to the calculated PMV from the environmental conditions in the climate chamber during the 'passive' tests. The error bars mark the standard deviation.

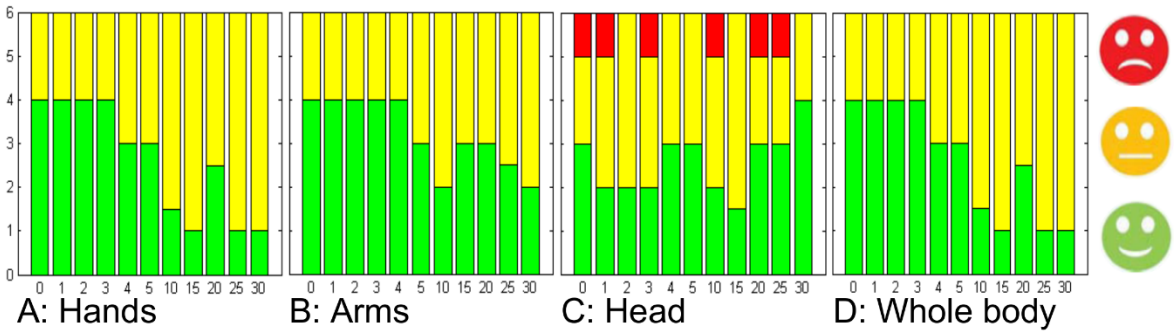

Figure 5: Comfort votes of the subjects in the 'passive' test, separated in three body parts and an overall vote. The height of the bar shows the number of votes per questionnaire. The time of the questionnaire is shown on the horizontal axis.

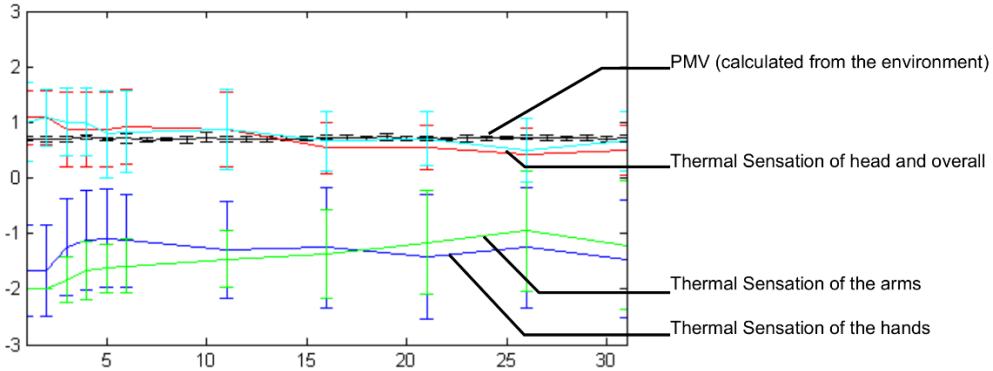

Figure 6: TS of the different body parts compared to the calculated PMV from the environmental conditions in the climate chamber during the 'cold' tests. The error bars mark the standard deviation.

In Figure 8 and 10, a similar trend can be seen, the TS overall and the TS of the head are close to the PMV, but the TS of the hands and arms are significantly lower compared within the series. During the 'cold' tests, the TS of the arms and hands are lower than in the other two series, showing the effect of a 2 degree lower surface temperature. The TS and comfort levels

of the ‘passive’ (Figure 6 and 7) and the ‘warm’ tests (Figure 10 and 11) are comparable for the exposed areas in the beginning of the test. However, when the test progresses, the comfort level of both the exposed areas and overall in the ‘passive’ series goes to neutral, some of the subjects get uncomfortable in the ‘warm’ series. The difference between the ‘passive’ and the ‘warm’ series is that the plate temperature increased during the ‘passive’ tests, reducing the cooling effect.

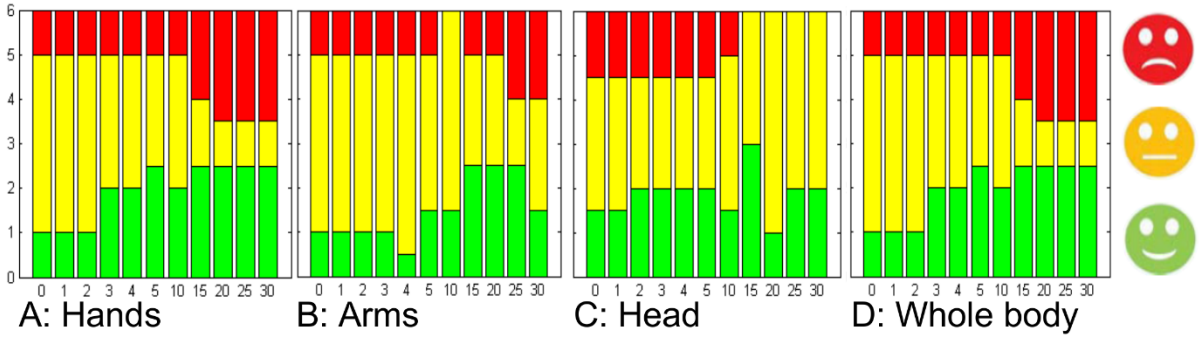

Figure 7: Comfort votes of the subjects in the ‘cold’ test, separated in three body parts and an overall vote. The height of the bar shows the number of votes per questionnaire. The time of the questionnaire is shown on the horizontal axis.

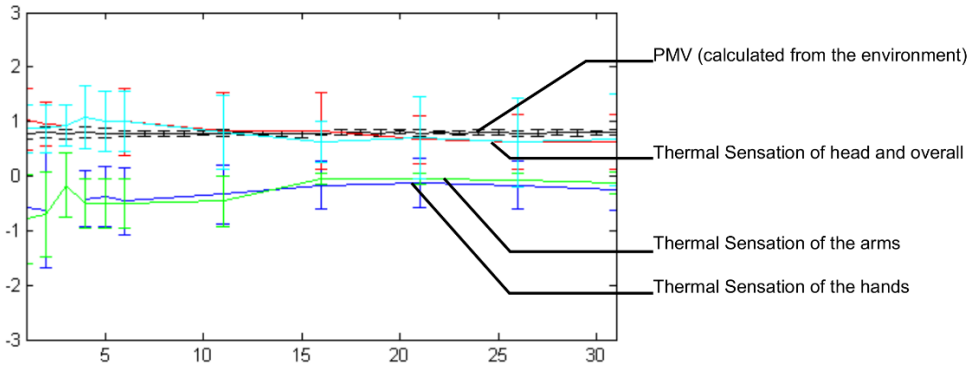

Figure 8: TS of the different body parts compared to the calculated PMV from the environmental conditions in the climate chamber during the ‘warm’ tests. The error bars mark the standard deviation.

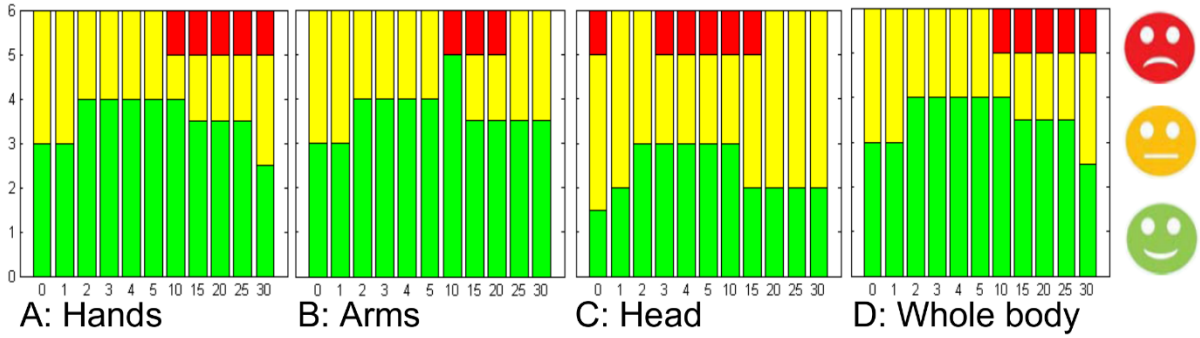

Figure 9: Comfort votes of the subjects in the ‘warm’ test, separated in three body parts and an overall vote. The height of the bar shows the number of votes per questionnaire. The time of the questionnaire is shown on the horizontal axis.

The comfort level of the test subjects during the ‘cold’ test is clearly divided in two sides and when the test progresses, both sides increase in size. Closer inspection of the individual votes

show that no subjects crossed over from uncomfortable to comfortable and vice versa. The increase of both sides come from the people that initially votes neutral.

DISCUSSION

The alliesthesia effect can be seen in the development of both the TS and comfort votes for the exposed body parts during the test. Initially, the TS is lower than later on while the comfort votes show a reverse trend: comfortable at first and more neutral towards the end. The comfort level of the head is lower than on the other regions, this is in line with the findings of Arens et al. [9], that the head is the most sensitive body part in a warm environment.

The trend in the 'cold' test is different. The low temperature caused a much larger cooling effect, divided the subjects. This division could be a similar trend as found by Parkinson [8]. The initial state of discomfort determines how the stimulus effects the person. Habituation later in the test causes more people to vote either uncomfortable or comfortable rather than neutral.

In none of the tests, the heat balance of the subject could be changed. The overall TS remained close to the PMV. The effect of the plate on the comfort level, especially in the 'cold' series suggests that the cooling effect cannot be increased much further. This makes the cooling plate insufficient to provide locally thermal comfort. However, a combination with other local cooling systems such as personal ventilation might be suitable as a local cooling system.

The six subjects were all male and quite similar, this caused the small deviations between the tests. This number however is not sufficient to show significant results, the trend described in this paper is a starting point for future research.

CONCLUSION

The alliesthesia effect could be seen in the tests by looking at the TS and the comfort levels at the body areas exposed to the local cooling.

The cooling system however was not able to effect the heat balance of the person, making it hard to apply alone as a long term solution.

REFERENCES

[1] B. W. Olesen, O. Seppanen, and A. Boerstra, "Criteria for the indoor environment for energy performance of buildings: A new European standard," *Facilities*, vol. 24, no. 11/12, pp. 445–457, 2006.

[2] E. Arens, M. a. Humphreys, R. de Dear, and H. Zhang, "Are 'class A' temperature requirements realistic or desirable?," *Build. Environ.*, vol. 45, no. 1, pp. 4–10, Jan. 2010.

[3] T. Hoyt, K. Lee, H. Zhang, E. A. Arens, and T. Webster, "Energy savings from extended air temperature setpoints and reductions in room air mixing," 2009.

[4] J. Verhaart, M. Veselý, and W. Zeiler, "Personal heating: effectiveness and energy use," *Build. Res. Inf.*, vol. 43, no. 3, pp. 346–354, 2015.

[5] M. Veselý and W. Zeiler, "Personalized conditioning and its impact on thermal comfort and energy performance – A review," *Renew. Sustain. Energy Rev.*, vol. 34, pp. 401–408, Jun. 2014.

[6] R. J. de Dear, "Revisiting an old hypothesis of human thermal perception: alliesthesia," *Build. Res. Inf.*, vol. 39, no. 2, pp. 108–117, Apr. 2011.

[7] M. Cabanac, "Physiological role of pleasure," *Science (80-.).*, no. September, 1971.

[8] T. Parkinson, R. De Dear, and C. Candido, "Experimental Study of Thermal Response to Local Stimulation: Converting Local Discomfort into Thermal Pleasure," in *13th international Conference on Indoor Air Quality and Climate*, 2014.

[9] E. A. Arens, H. Zhang, and C. Huizenga, "Partial- and whole-body thermal sensation and comfort, Part I : Uniform environmental conditions," 2005.

INDOOR COMFORT EVALUATION OF A SUSTAINABLE WOODEN HOUSE WITH A NOVEL VAPOR-OPEN ENVELOPE SYSTEM IN SUBTROPICAL CLIMATE

Y. Goto[1]; Y. Ostermeyer[1]; H. Wallbaum,[1]

1: Chalmers University of Technology, Sven Hultins gata 8, SE-41296 Gothenburg, Sweden

ABSTRACT

Concerning the resource depletion and global warming, the realization of sustainable constructions is crucial because the building industry has a big impact on the greenhouse gas emission. Recently the interest in the buildings in subtropical regions has been growing due to the high growth rate of their urbanized areas. From the view point of building physics, those regions are very challenging because they have both heating and cooling demand. Also the prediction of indoor air humidity is acquiring a greater interest concerning the envelope durability, the comfort and the energy consumption, which is very relevant to such regions. Meanwhile, there is a need of developing a new construction system and its design method for subtropical regions since it is inappropriate to simply use the established construction systems for cold regions which have only heating demand.

Based on the transient hydrothermal model of the envelope and the whole building heat and moisture balance model taking into account the moisture buffering by hygroscopic interior materials, the authors have developed an envelope system and its insulation optimization scheme which considers lifetime environmental impact, lifetime cost, durability, users' behaviour and local climate. The envelope consists of natural materials such as wood and clay and thus allows the moderate transfer of the water vapour in both directions i.e. from exterior to interior and from interior to exterior. A detached house with this system was realized in Ohmihachiman (central Japan) in June 2013 and the indoor temperature and humidity have been monitored at several points.

The measured indoor climate was analysed and it was revealed that 1. the indoor climate in summer has a certain improvement potential and 2. the indoor climate in winter is satisfying. As the monitoring of electricity generation by the photovoltaic panels and the electricity consumption of the whole house has showed a positive balance (more generation than consumption), it is suggested to either use the cooling radiator more actively or install an active dehumidifier into the mechanical ventilation system to provide a more agreeable indoor cli-mate in the summer. The former recommendation will be implemented in summer 2015 and its impact on the comfort and energy consumption will be further analysed.

Keywords: vapour-open envelope, subtropical climate, indoor comfort, wooden building

INTRODUCTION

Concerning the resource depletion and global warming, the realization of sustainable constructions is crucial because the building industry has a big impact on the greenhouse gas (GHG) emission. The rapid economic development and urbanization in subtropical regions is a major issue with regard to the reduction of GHG emission and the mitigation to global warming. As the construction industry plays a significant role, there is a need for innovations on building technologies in those regions [1]. From the view point of building physics, those regions are very challenging because they have both heating and cooling demand. Also the prediction of indoor air humidity is acquiring a greater interest concerning the envelope

durability, the comfort and the energy consumption, which is very relevant to such regions. Meanwhile it is crucial to take into account that there is an enormous socio-cultural diversity and different economic situations among the regions, which needs to be thoroughly taken into account when applying and developing new technologies to and for these regions.

The authors have developed a vapour-open wooden building envelope system and the optimization method of its insulation layer for central Japan, which has typical subtropical climate conditions, and evaluated its sustainability aspect from environmental, economic and building physics perspective with a sound consideration of the local socio-cultural context [2, 3, 4]. This study presents the evaluation of indoor comfort of a test house which was realized using this envelope system in Ohmihachiman (central Japan) in June 2013.

METHOD

Vapour-open wooden building envelope for subtropical regions

A new building envelope system was developed within the research team led by the authors. This envelope system mainly consists of major layers with natural materials, namely the external insulation layer with wood fiber board, the structural layer with cross laminated wooden panel and the interior finishing layer with the composite of wood and clay. The illustration of the envelope system and the materials for each layer is shown in Figure 1. The basic design philosophy of this system is that the envelope consists of hygroscopic materials with moderate vapor permeability. This system allows the moisture flux to move through the wall in both directions. By defining the appropriate thickness to each layer, it is possible to avoid moisture related problems inside the wall by humidity buffering.

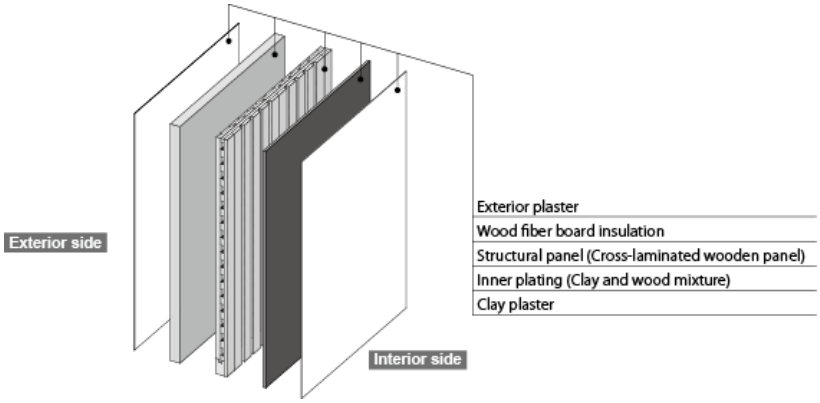

Figure 1: Layered structure of the vapour-open envelope for subtropical regions.

The test house and the measurement setup

In June 2013, a residential building with the envelope system was realized in Ohmihachiman (central Japan) which has a typical subtropical climate with hot-humid summer and cold-dry winter. The general design of the building was done by local architects and the technical supervision was done by the research team. The building is a detached residential building where two to four persons (two adults and up to two children) are supposed to reside. Apart from the basic layered design presented in Figure 1, the surface of the insulation was covered with vapour-open water-tight membrane. Air-tight membrane was applied between the insulation and the structural panel. The concrete foundation was designed to have a flat surface and to be covered with asphalt sheet so that the control of heat and moisture transfer through it becomes the least intricate. The roof was based on the conventional design with air venting layer. Figure 2 shows the plan and elevation of the test house.

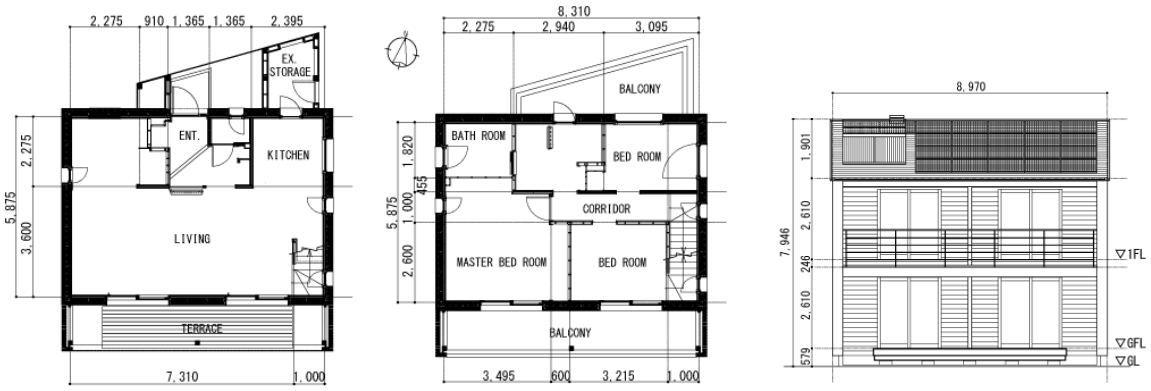

(a) *(b)* *(c)*

Figure 2: Plan and elevation of the test house. (a: the floor plan of the ground floor, b: the floor plan of 1st floor, c: the elevation of south façade)

Based on LCA, LCCA and hygrothermal analysis considering the specific design conditions [2, 3, 4], the insulation (thermal conductivity lamda: 0.038 W/mK) thickness was decided to be 18 cm. The other solid components of the envelope were 90 mm thick cross laminated timber panel with air gaps (lamda: 0.110 W/mK considering the effect of the air gap), For the openings air-tight and triple grazing windows (0.7 W/m^{2}K), 14 mm thick clay board (lamda 0.299 W/mK) and 4mm thick clay plaster (lamda: 0.590 W/mK). The U-value of the wall was thus 0.158 W/m^{2}K. Photovoltaic (PV) panels cover the south roof (4.18 kWp) combined with solar water heater panels for domestic hot water supply. The building orientation and the shading of the openings were carefully decided considering the balance of solar gain in summer and winter. As for HVAC system, radiators for heating and cooling-dehumidification and mechanical ventilation with heat exchanger were employed. The façade consists of cladding with ventilation gap.

Figure 3 shows the finished house. In order to measure the indoor climate and the conditions inside the external walls, 21 temperature and humidity sensors were installed. Figure 4 shows the sensor and sensor node. The measuring points are; northern side wall on the ground floor (5 points across the wall from the living room to the exterior), living room, kitchen, northern side wall on the 1st floor (5 points from the bathroom to the exterior), west side wall on the 1st floor (5 points from the master bedroom to the exterior), northern side roof (4 points from the attic to the exterior). The measurement started in September 2013. The data logging interval is set at 10 minutes. The preliminary validation investigation on the heat and moisture transfer across the envelope was reported in [5].

Figure 3: The completed house. (left: east side façade, right: living room on the ground floor)

Figure 4: The installation of sensors. (left: an sensor inserted between air-tight membrane and insulation, right: a sensor node box)

RESULTS

Figure 5 shows the exterior condition (temperature and humidity in the ventilation gap under the façade cladding) on the north side in the first floor of the building. The measurement was interrupted in February due to a technical reason (a battery problem). Figure 6 shows the measured temperature and relative humidity of the living room on the ground floor and that of the master bedroom on the first floor in 2014.

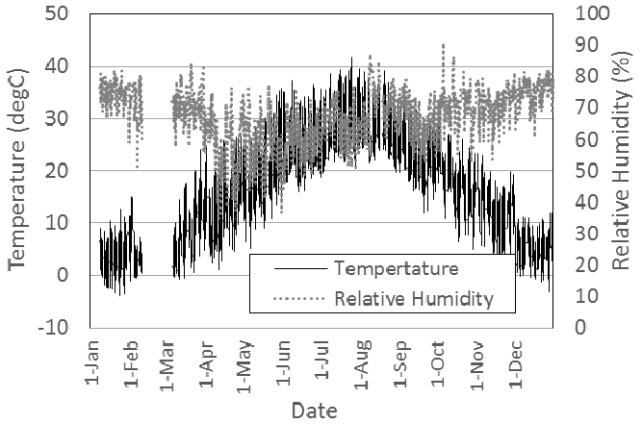

Figure 5: Temperature and relative humidity in the ventilation gap in the north wall

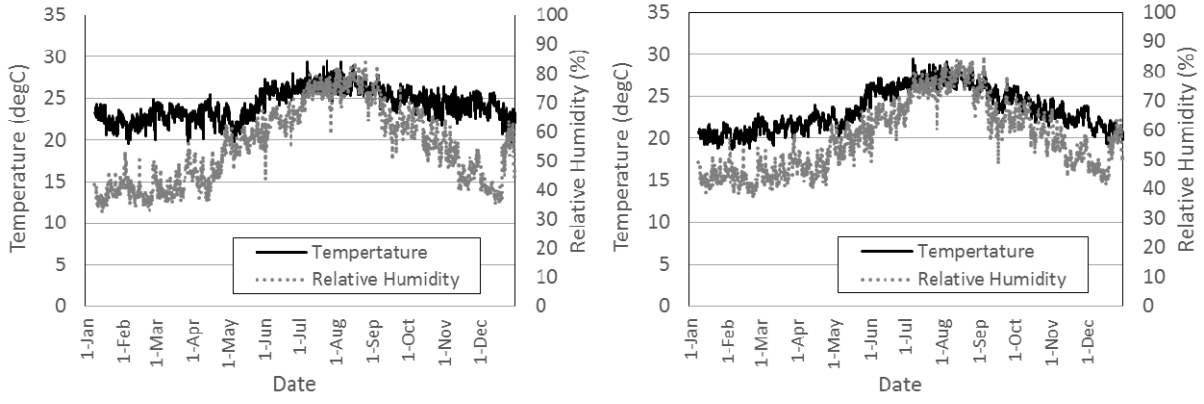

(a) *(b)*

Figure 6: Measured indoor temperature and relative humidity. (a: living room on the ground floor, b: master bedroom on the first floor)

As these two different rooms in different locations in the building showed a similar condition, the following discussion focuses only on the condition of the living room.

In order to evaluate the indoor comfort, the acceptability-index (Acc.) proposed by Fang et al. was applied [6]. By this method, the indoor air quality can be defined based on the air temperature, humidity and the pollution level. Acc. Is given between 1.0 and –1.0. The higher the value, the more comfortable is the air. Figure 7 shows the acceptability-index in the living room throughout 2014 disregarding the effect of neither CO_2 concentration nor contamination by hazardous gasses.

Table 1 lists the measured electricity supply by the PV panel and electricity grid and its consumption by the cooling unit and the entire household (the whole electricity demand including the consumption by the cooling unit).

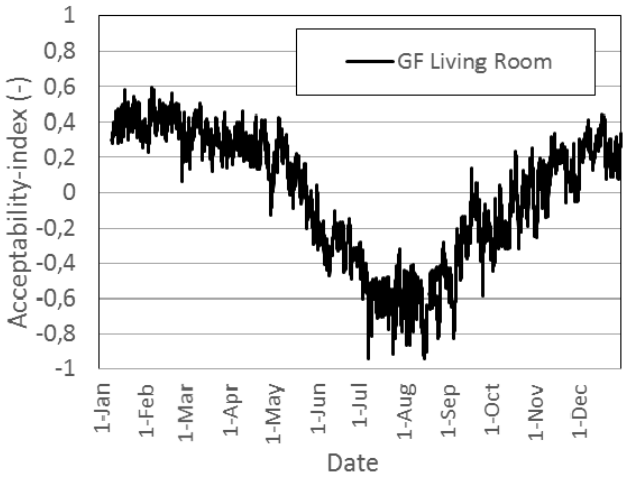

Figure 7: Acceptability-index of the living room based on the measured values.

	Energy (kWh)											
	Jan	Feb	Mar	Apr	May	Jun	Jul	Aug	Sep	Oct	Nov	Dec
Consumption by heating/cooling unit	246.6	182.3	163.7	84.4	98	0	61.8	78.3	0	28.2	55.8	204.4
Production by PV panel	371.3	360.9	453.3	555.7	576.7	506.3	536.5	417.2	501.2	430.2	211.7	315.9
Electricity sold	209.8	207.8	298.4	420.0	421.1	421.1	371.4	266.0	413.4	338.7	148.2	190.4
Electricity bought	417.9	309.7	269.7	149.4	75.2	70.9	137.8	167.0	85.1	124.7	112.7	344.0
Electricity demand	579.4	462.8	424.7	285.1	162.3	156.2	302.9	318.1	172.9	216.1	176.2	469.5

Table 1: Electricity supply and consumption in summer 2014

DISCUSSION

Figure 7 shows that the indoor climate in the winter was satisfying while the energy (electricity) consumption for heating was low (11.0 kWh/m^{2}a in which the electricity was partly supplied by the PV panel). Regarding the summer, it reached uncomfortable level (lower than Acc. value of -0.4) for about three months (June-August). The reason for this was obviously high level of both temperature and relative humidity. This implies that the cooling radiator which works by electricity and as dehumidifier as well did not contribute to create a comfortable indoor environment. The reason is either reduced use of the cooling unit or its insufficient capacity. It shows a positive balance (more production than consumption), which

means that the electricity production by the PV panel was large enough to allow more cooling throughout the summer period. In fact, as the first year experience, the inhabitants tried to live in the house with the least energy consumption with a certain sacrifice on the comfort. Therefore it is recommended to use the cooling unit more actively in order to reach better comfort level in the summer.

CONCLUSION

In this study, the indoor comfort of a residential building in Japan with a vapour-open wooden building envelope system for subtropical climate is analysed. The indoor climate measurements showed that the comfort level in the summer has the potential to be improved while the winter condition was satisfying with low energy consumption. The energy consumption for cooling and dehumidification showed that it had significant surplus of energy by the PV panel throughout the cooling season. Therefore it is recommended to use the cooling system more actively in order to acquire better comfort. This will be implemented in summer 2015 and its impact on the comfort and energy consumption will be further analysed.

ACKOWLEDGEMENT

The authors would like to express the gratitude to EIT Climate-KIC flagship program Building Technology Accelerator for the grant, Dr. Karim Ghazi Wakili and Roger Vonbank of Empa for the support of the measurement and Mr. and Mrs. Iida for providing the possibility to carry out the project and measurements in the house in Ohmihachiman.

REFERENCES

1. CIB & UNEP-IETC: Agenda 21 for Sustainable Construction in Developing Countries, 2002.
2. Goto, Y., Ghazi Wakili, K., Ostermeyer, Y., Frank, T., Ando, N., Wallbaum, H.: Preliminary investigation of a vapor-open envelope tailored for subtropical climate. Building and Environment, Vol 46, pp 719–728, 2011.
3. Goto, Y., Ghazi Wakili, K., Frank, T., Stahl, T., Ostermeyer, Y., Ando, N., Wallbaum, H.: Heat and moisture balance simulation of a building with vapor-open envelope system for subtropical regions. Building Simulation, Vol 5, pp 301–314, 2012.
4. Goto, Y., Ostermeyer, Y., Ghazi Wakili, K., Wallbaum, H.: Economic, ecological and thermo-hygric optimization of a vapor-open envelope for subtropical climate. Energy and Buildings, Vol 46, pp 719-728, 2012.
5. Goto, Y., Ostermeyer, Y., Ghazi Wakili, K., Frangi, A., Ando, N., Wallbaum, H.: Sustainable wooden envelope for subtropical regions - The realization and validation in Japan. WCTE 2014, Quebec City, Canada, 2014.
6. Fang, L., Clausen, G., Fanger, P.O.: Impact of temperature and Humidity on the Perception of Indoor Air Quality. Indoor Air, Vol 8, pp 80-90, 1998.

DESIGN, SIMULATION AND TESTING OF A HYBRID LIQUID DESICCANT FOR INDEPENDENT CONTROL OF TEMPERATURE AND HUMIDITY

L. Alonso[1], X. Peña[1], C. Pascual[1], J. Prieto[2], J. Ortiga[2], K. Gommed[3]

1: Tecnalia Research & Innovation, Thermal Energy Area, Energy and Environment Division. Area Anardi 5, 20730 Azpeitia (Gipuzkoa), Spain

2: Universitat Rovira i Virgili, CREVER, Mechanical Engineering Department. Avda Països Catalans 26, 43007 Tarragona, Spain

3: Technion – Israel Institute of Technology, Faculty of Mechanical Engineering. Haifa 32000 Israel

ABSTRACT

In this paper the design, simulation and testing of a hybrid liquid desiccant system for a case study in Taiwan is presented, in the scope of the European project nanoCOOL. The designed system has been constructed and is being tested at laboratory scale. After the set-up of the system, it will be sent to Taipei for demonstration in real scale conditions, in the Taiwan Building Technology Center. The demonstration site comprises two locker rooms in a swimming pool of the university, with high internal humidity generation, low sensible heat ratio, and high external humidity levels due to sub-tropical humid climate present in Taiwan.

Keywords: hybrid liquid desiccant system, simulation, temperature and humidity control

INTRODUCTION

The treatment of humidity on HVAC systems is crucial when a satisfactory indoor air quality needs to be reached. Traditional HVAC systems meet the latent cooling load by reducing the air temperature until its dew point, heating subsequently the air in order to reach the supply temperature for user comfort, with the energy waste this entails. Hybrid liquid desiccant systems (HLDS) combine the liquid desiccant technology for dehumidification of air with conventional compression cycle technology for cooling.

The demo site comprises two locker rooms in a swimming pool of the National Taiwan University of Science and Technology, with high internal humidity generation, low sensible heat ratio, and high external humidity levels due to sub-tropical humid climate present in Taiwan. Based on the design conditions, the internal sensible and latent heat generation, and the ventilation requirements according to international standards; the design conditions and the cooling and dehumidification loads have been calculated:

Outdoor design conditions	30ºC / 21,5 g/kg dry air
Comfort design conditions	24ºC / 7,5 g/kg dry air
Ventilation rate	2.500 m^3/h
Internal sensible heat load	3,5 kW
Ventilation sensible heat load	5 kW
Total sensible heat load	8,5 kW
Internal latent heat load	8,8 kW
Ventilation latent heat load	21,3 kW
Total latent heat load	30,1 kW

Table 1: Design conditions and cooling/dehumidification loads

DESIGN AND SIMULATION

The designed hybrid liquid desiccant system (HLDS) is comprised by a liquid desiccant system (LDS) whose main components are the absorber, regenerator and liquid-liquid heat exchanger; and a conventional Air Handling Unit (AHU) with a cooling coil and a cross-plate heat exchanger for ventilation heat recovery. A polyvalent unit able to simultaneously provide cooling and heating, feeds the absorber and the cooling coil with cold water at 15ºC, and the regenerator with hot water at 55ºC.

Models of the individual components of the Liquid Desiccant System (absorber, regenerator and liquid-liquid heat exchanger) and the Air Handling Unit (cooling coil, air-air plates heat exchanger) have been implemented in EES (Engineering Equation Solver) [1]. By combining the separate models of each component, a versatile mathematical model has been developed, which can be used for both the design and simulation of the HLDS.

Liquid Desiccant System

The absorber and the regenerator are falling film type, internally cooled and heated respectively. They are comprised by a polypropylene tube bundle, a liquid distributor system with spray nozzles, and a demister inside a fiber glass tower. Tube bundles are formed of individual modules of 97 tubes, which are linked horizontally in threes, and then vertically to form 14 passes, with a total area of 53,2 m^2. A proper wettability of the tubes is key for obtaining good performance in the liquid desiccant cycle, for that reason the polypropylene tubes have received a plasma treatment in order to improve their wettability [2]. The air flows from bottom to top getting in contact with the descendent lithium chloride solution, which forms a falling film outside the tubes. The rich LiCl solution absorbs humidity from air in the absorber, and the poor LiCl solution desorbs humidity enriching the solution in the regenerator. Cold water (15ºC) and hot water (55ºC) flows inside the tubes, cooling the solution and the air in the absorber, and heating the solution and the air in the regenerator.

Models for the absorber and regenerator are based on the theoretical model described by Gommed and Grossman [3]. Water and salt mass balances, energy balances, thermodynamic equilibrium and heat and mass transfer equations are included in the model.

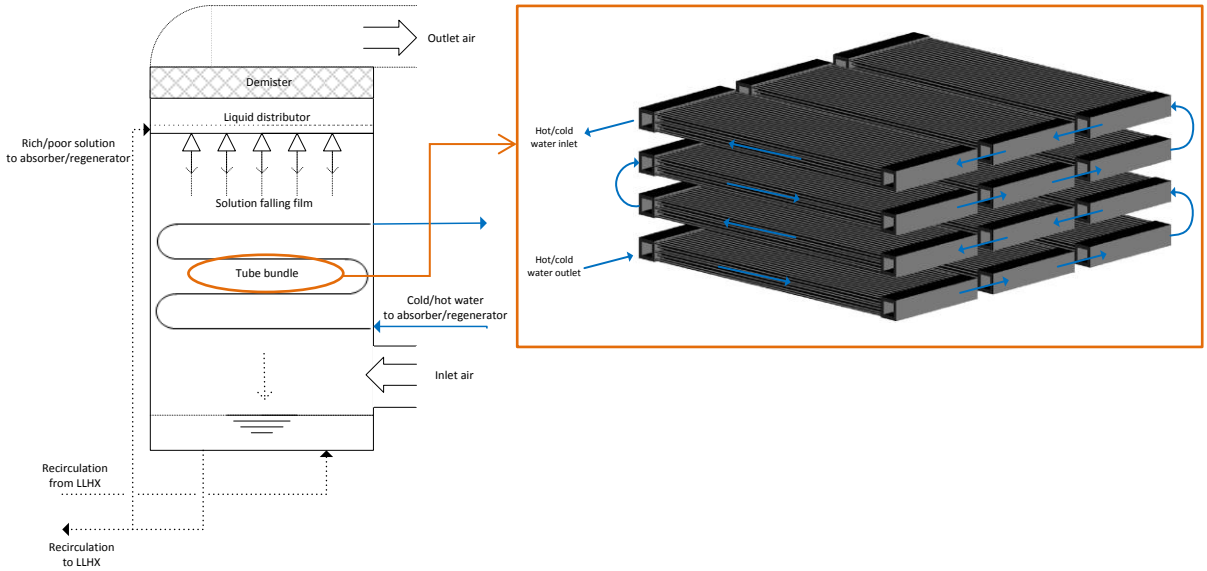

Figure 1: Scheme of the absorber/regenerator units, and the tube bundle layout.

Heat and mass transfer coefficients involved in the modelling are the global heat transfer coefficient between external medium and the solution (U), the heat and mass transfer coefficients between air-solution interface and the air stream (σ_a, β_a), and the heat and mass transfer coefficients between air-solution interface and the solution stream (σ_s, β_s).

The heat transfer coefficient between external medium and solution stream is calculated as:

$$U = \frac{1}{\frac{\emptyset_{ext}}{\emptyset_{int}}\frac{1}{h_{wt}} + R_t + \frac{1}{h_{ts}}} \quad (1)$$

The water-tube heat transfer coefficient (h_{wt}) has been calculated depending on the flow regime by using correlations described by Nellis & Klein [4]; using the following correlation for Re<2300,

$$Nu = \frac{\left[0{,}1156 + \frac{0{,}08569}{Pr^{0{,}4}}\right] Gz}{[1 + 0{,}1158 Gz^{0{,}6}]} \quad (2)$$

The Gnielinski equation for fully developed flow for 2300<Re<10000,

$$Nu = \frac{\left(\frac{f_{fd}}{8}\right)(Re - 1000)Pr}{1 + 12{,}7(Pr^{2/3} - 1)\sqrt{\frac{f_{fd}}{8}}} \quad (3)$$

$$Nu = \frac{1}{[0{,}790 \ln(Re) - 1{,}64]^2} \quad (4)$$

And the Dittus-Boelter equation for Re>10000,

$$Nu = 0{,}023 Re^{0{,}8} Pr^n \quad (5)$$

N=0,4 for heating of the fluid (absorber)

N=0,3 for cooling of the fluid (regenerator)

The tube-solution heat transfer coefficient (h_{ts}) and the mass transfer coefficient between air-solution interface and the air stream (β_a) have been obtained from experimental results of the field tests developed in Technion (Israel Institute of Technology) in Haifa [5]. In the field tests a Liquid Desiccant System was experimentally tested using different types of tubes in absorber mode. The performance with plastic tubes, which showed poor wettability, was lower than with the titanium tubes, which presented good wettability. The designed HLDS will be using polypropylene tubes which have received a plasma treatment in order to increase their wettability [2]. Therefore, the experimental values used for the modelling correspond to the experiments carried out with titanium tubes.

Assumption of a Lewis factor equal to one is considered, which is applicable for air.

$$Le = \frac{\sigma_a}{\beta_a Cp_{air}} \quad (6)$$

The liquid-liquid heat exchanger is a plate heat exchanger made of a polymeric matrix composite including graphene nanoparticles, from SGL company. It is used to precool the solution going to the absorber, and to preheat the solution going to the regenerator. Its model is based on the ε-NTU method with correlations for heat transfer in plate heat exchangers described by H. Martin [6]. The model has been contrasted with the design data from SGL. Heat exchanger effectiveness for design working conditions is 0,85.

Air Handling Unit and polyvalent unit

The air handling unit comprises the air plate heat exchanger for heat recovery of ventilation, the cooling coil, and the corresponding fans, dampers and filters for the system. The casing and the arrangement of the different elements is specially designed for its optimal connection with the LDS.

The air heat exchanger is a compact plate heat exchanger, with cross-flow configuration, made of aluminum and with internal fins to increase the heat transfer between both air streams. The use of such equipment enables considerable savings to be achieved in the operating costs of air-conditioning plants, and thus the saving of energy that would otherwise be lost. In the HLDS it is used for preheating the air entering the regenerator. It is modelled by using the ε-NTU method.

The cooling coil has been modelled by using the model described in [7]. This model is based on epsilon-NTU and LMTD and LMHD equations and uses Braun's hypothesis to simulate the behaviour of the cooling coil in an AHU (air handling unit). Normally, cooling coils in Air Handling Units deal with sensible and latent cooling loads, condensing water from air in the surface of the tubes. In this case, the cooling coil serves for dealing only with sensible cooling loads; no condensation will occur in the surface of the tubes, so in theory the dry cooling coil approach could be used for the modelling. However, the model includes also the wet coil approach, in case the cooling coil may be used for dehumidification as well. In that case, the cooling coil should be oversized respect to the actual size. For the air side the correlation proposed by Wang et al.[8] is selected and the HTC validated against a reference HX calculation software; on the other hand for the calculation of the tube side coefficient the correlation proposed by Gnielinski [9] for turbulent region and the described on Nellis & Klein [4] for the laminar one as in the case of the absorber and regenerator have been used.

The polyvalent unit is a heat pump able to provide heating and cooling simultaneously, by recovering heat from a water condenser when the machine is working on dual mode, and by condensing with air when the machine is working on cooling mode. Therefore, it will be used in cooling mode when the LDS is only dehumidifying and cooling (regenerator off), or in dual mode when the system is regenerating LiCl solution as well, with no need from another external source of heat.

WHOLE CYCLE MODELLING AND RESULTS

The individual models of the LDS and the AHU have been combined to develop the complete model of the HLDS. A split system is included at the solution outlet of the absorber and regenerator, so that the amount of solution which is recirculated to the absorber and regenerator from the bottom of each tower is set to 0,9 of the outlet solution from each component; sending 10% of the solution through the liquid-liquid heat exchanger. The figure below shows the results from the modelling of the whole HLDS.

Calculated impulsion air conditions are 19,8ºC and a humidity ratio of 6,8 g/kg dry air. In order to achieve these conditions, the required capacity of the absorber and regenerator is 40,3 kW and 40,8 kW respectively, with a 13,5 kW capacity liquid-liquid heat exchanger. The air plate heat exchanger has a capacity of 13,3 kW. The cooling coil needs to provide 1,4 kW in the design conditions, however for the construction of the prototype it will be oversized in order to be able to deliver the necessary cooling to meet the sensible cooling load, which leads to 8,5 kW. Considering the electrical consumption of the polyvalent unit, the HLDS has a COP of 2,7.

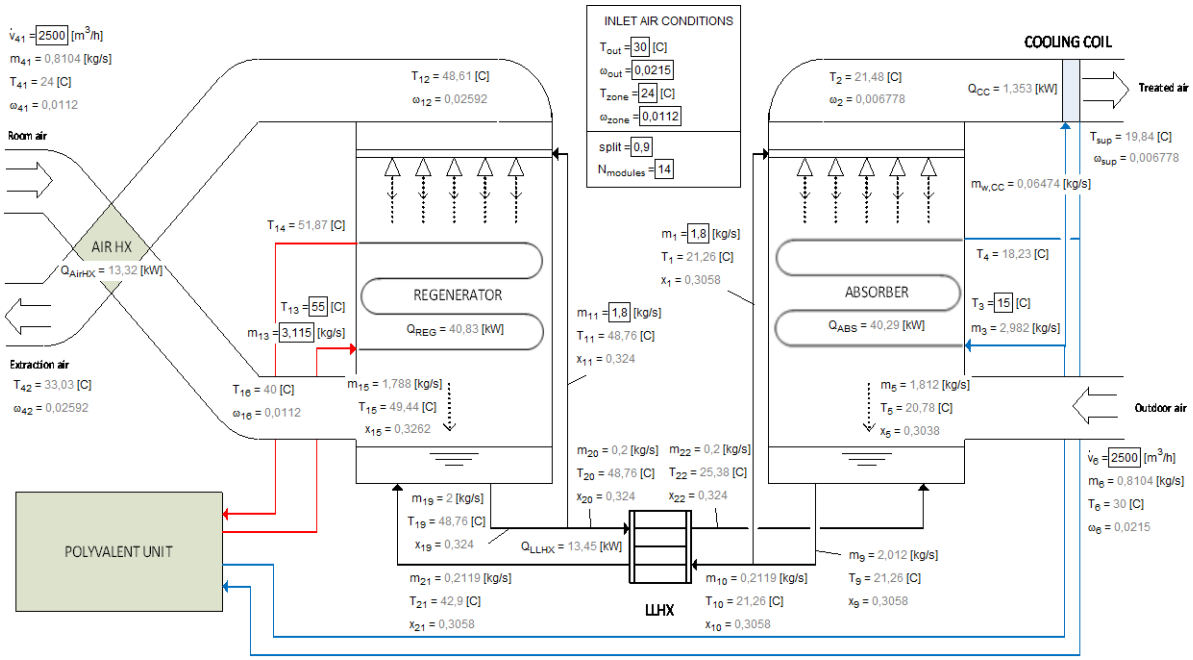

Figure 2: Results from simulation of the HLDS

COP of the HLDS and conventional system are calculated as:

$$COP_{HLDS} = \frac{Cooling\ effect}{Energy\ consumed\ by\ polivalent\ unit} \quad (7)$$

$$COP_{conv} \frac{Cooling\ effect}{\frac{Q_{cc}}{COP_{heat\ pump}} + Q_{reheat}} \quad (8)$$

A representation of the HLDS process in a psychrometric chart is shown below, as well as the corresponding process to the treatment of air with a conventional system. In the conventional system, the air needs to be cooled down to a high extent in the cooling coil to reach the required dehumidification. In order to achieve comfort indoor conditions, the air needs to be reheated in a reheating coil. With the HLDS process, the need for reheating is eliminated, which leads to important energy savings. Taking into account the reheating consumption in the conventional system, an improvement of around 45% in COP is achieved.

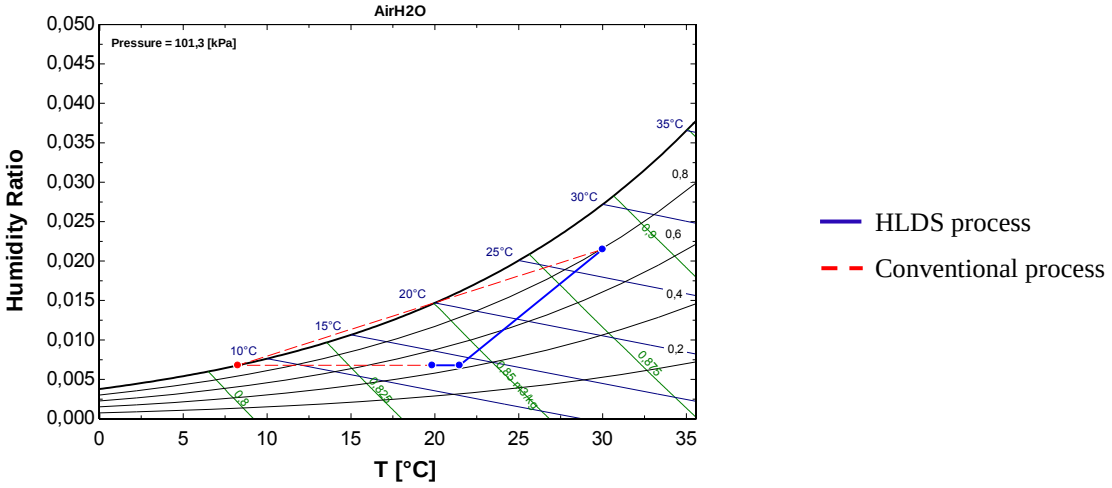

Figure 3: Air treatment processes in the HLDS and in a conventional cooling system represented in the psychrometric chart

CONCLUSION

Based on the cooling loads calculation, a hybrid liquid desiccant system has been designed and simulated for a case study in Taiwan, sizing every component to match the sensible and latent cooling loads. The system achieves a reduction in energy consumption; as unlike conventional systems it does not need to reach the dew point to remove humidity, with the consequent improvement in the COP. The designed system has been constructed and is at the setting-up phase in the laboratory, in order to define the best control strategies for the system. Future work focuses on its performance monitoring in the real-site demonstration in Taiwan.

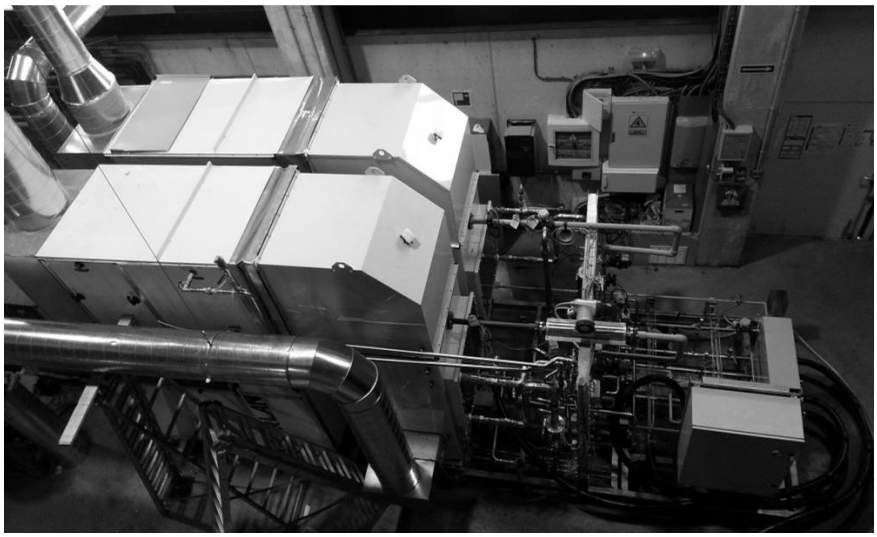

Figure 4: Nanocool system

REFERENCES

1. Engineering Equation Solver. F-Chart Software. http://www.fchart.com
2. A. Fina, A. Guerriero, S. Colonna, F. Carosio and G. Saracco. Polymer-based materials for the application in Liquid Dessicant heat exchangers. *V Congreso Iberoamericano de Ciencias y Técnicas del frío*. Tarragona, June 18-20 (2014).
3. K. Gommed, G. Grossman. Improved Simulation Model for Air-Liquid Contactors in Open Absorption Air Conditioning Systems. *Proceedings, the International Sorption Heat Pump Conference*, College Park, MD, USA, March 31-April 3 (2014).
4. G. Nellis, S. Klein. Heat Transfer. *Cambridge University Press* (2009), 661-671.
5. K. Gommed, G. Grossman, J. Prieto, J. Ortiga, A. Coronas. Experimental Comparison between Internally and Externally Cooled Air-Solution Contactors. *Proceedings, the International Sorption Heat Pump Conference*, College Park, MD, USA, March 31-April 3 (2014).
6. Holger Martin. Pressure Drop and Heat Transfer in Plate Heat Exchangers. *VDI Heat Atlas* (2010), 1515-1521.
7. Air-Braun, J.E., Klein, S.A., Mitchell, P.E., Effectiveness models for cooling towers and cooling coils. *ASHRAE Transactions Vol.92 part 2* (1989), p.164-174.
8. C. Wang, Y. Hsieh, Y. Lin. Performance of Plate finned Tube Heat Exchangers Under Dehumidifying Conditions, *Journal of Heat Transfer*. Vol.119 nº1 (1997), p109-117
9. V. Gnielinski, New equation for heat and mass transfer in turbulent pipe and channel flow, *International chemical engineering*, vol. 16 (1976) pp.359-368.

A SOCIO-TECHNICAL APPROACH TO THERMAL COMFORT AND HEATING BEHAVIOUR IN UK HOMES

H. Ben[1]; M. Sunikka-Blank[1]

1: Department of Architecture, University of Cambridge, 1-5 Scroope Terrace, Trumpington Road, Cambridge CB2 1PX

ABSTRACT

Understanding thermal comfort and heating behaviour is crucial for energy policy and practice on sustainable buildings. This paper proposes a socio-technical systems (STS) approach to analyse and compare occupant heating behaviour and thermal comfort at home. The domestic sector accounts for nearly one third of total UK energy use, and building energy demand per household in this sector remains flat despite large increases in energy efficiency. The main reason may lie in occupants' increased level of comfort. The research analyses empirical evidence collected from a sample of households living in Cambridge, UK. Adopting a STS approach, the paper uses both qualitative and quantitative methods to collect household data on comfort and heating patterns. It incorporates a series of observations, photo records, diary records, data logger monitoring, questionnaire surveys and interviews. The results show significant gap between heating behaviour and thermal comfort, and that the provision of heating does not necessarily lead to high level of thermal comfort satisfaction. An analysis using STS identifies the gap with the elements of technology, occupant, activity, composition, indicating the link between thermal comfort and home performance.

Key words: socio-technical systems, thermal comfort, heating behaviour

INTRODUCTION

Occupant daily domestic interactions account for one-third of UK energy consumption, and the main part of this relates to maintaining a comfortable indoor environment [1, 2]. The Government has mainly focused on energy-efficient buildings and technologies over the past decades. However, the predicted energy savings associated with energy efficient technologies frequently exceed actual savings made upon behavioural factors [3, 4, 5, 6]. Heating behaviour has the highest impact on domestic energy use [7]. This paper focuses on how occupants regulate their heating towards thermal comfort at home and it proposes a socio-technical approach for understanding why they act as they do. It also shows how social-technical systems strongly shape household thermal behaviour and comfort.

Thermal comfort has been studied for many decades. There have been two main approaches to thermal comfort: the steady-state model and the adaptive model [8]. Fanger developed PMV/PPD model based on heat balance equations [9], which treats all occupants the same and disregards location and adaptation to the thermal environment. Nicol and Humphreys later argued that humans can adapt to their indoor and outdoor environment [10], and proposed adaptive model which has been incorporated into internationally used standards such as ANSI/ASHRAE 55 [11] and EN 15251 [12]. Researches in thermal comfort have mainly adopted engineering and physiology-based approaches; studies on social and cultural aspects of thermal comfort are yet relatively unexplored.

An emerging focus on the subject of social and cultural aspects of comfort can be found in special issues of *Building Research & Information* and *Energy and Buildings*. Shove et al. suggested that indoor thermal expectations are historically and socially specific, and thus also

likely to change in response to the society and technologies [13]. Similarly, Kempton and Lutzenhiser described and analysed how culture and technology influence what temperatures are considered as comfortable at different times and places [14]. Parkhurst and Parnaby argued that consumer comfort expectations are tempered by the relationship between production and consumption [15]. Furthermore, Healy addressed the questions on how thermal comfort standards shape both the built environment and lifestyles [16]. These studies provided details on how people regulate and use domestic technologies and systems, and how cultural myths guide people's daily comfort habits and thus energy consumption [17].

Much research on sustainable buildings with a socio-technical perspective has been focusing on overall user comfort (e.g. [3, 13, 15, 16, 18, 19]). Influential examples can be found in many recent works such as Shove's idea on how comfort preferences have changed within a socio-technical boundary [20], and Wilhite et al.'s view on how cultural and technological variations influence occupants' indoor practices [21]. While comfort has received increased attention within the field of sustainable buildings, thermal comfort has not been fully investigated with a holistic socio-technical systems (STS) approach.

This paper therefore proposes a holistic socio-technical systems (STS) approach to examine thermal comfort and heating behaviour at home, focusing on household as a system unit. It asks for what influences occupant heating behaviour has and how it impacts upon thermal comfort. It also identifies the parameters that have an impact on thermal comfort within the STS framework, so that they can be further tested with respect to their interrelationships, and then be implemented in policy and design strategies to increase both domestic comfort and energy savings.

Hence, while the research of this paper is set within a socio-technical framework, it does not examine societal and technological aspects of thermal comfort and behaviour with a top-down view. Rather, it frames household as a single unit for STS analysis with a bottom-up view. This study uses STS primarily as a way of framing heating behaviour in order to uncover the link between thermal comfort and home performance. It seeks to understand how heating behaviour within STS framework influences thermal comfort on an individual level, such as occupant, household composition, activity, and technology.

The next section outlines the methodology developed for the research. This is followed by the results, presented as empirical analyses with a detailed focus on occupant thermal behaviour and comfort from a socio-technical perspective. Finally, based on the findings, different heat-comfort factors are interpreted and the potential benefits from the use of socio-technical systems considered.

METHOD

The study uses qualitative, holistic approach in a sample of in-depth case studies in Cambridge, UK, including a study of households' comfort practices and their relation to daily activities and energy use behaviour. Empirical data is collected from 14 domestic case studies, including personal observations, photo records, daily activity diary-log records, data logger monitorings, questionnaire surveys, and semi-structured interviews. The selection of a sample is not aiming for representativeness or other forms of statistical extrapolation, but to understand the variety and complexity of occupant heating behaviour towards thermal comfort and to develop a sound base for the next research step. Within the dataset, there were several dimensions of variability among the participants, such as household composition, built form and dwelling type, as well as variations in terms of heating system and energy bill type.

Fourteen households were interviewed and monitored for this study, between January and March 2014 in Cambridge, UK. The interviews were carried out in all participants' homes

respectively, with each lasted about 2 to 3 hours. Interviewees were briefed about the research topic before the interviews. A set of predesigned questions was used to guide the interviews, alongside spontaneous queries allowing new ideas for exploration during the interview. The surveys were carried out along with the interviews, after which the data loggers were planted inside participants' homes. The number of data loggers was determined according to the number of main rooms occupied by each household. During the one-week data-logger monitoring period, participant filled in their diary-logs respectively.

RESULTS

This section presents the results and analysis of the case study research. The general results are discussed in relation to the theoretical framework concepts developed from STS theory: occupant, composition, activity, and technology. As guided by the ethical conduct of the research, all the case studies have been depersonalized and their names have been changed in this paper.

Occupant

Personal lifestyle, attitudes, preferences have impacts on how occupants would like to heat their house and how comfortable they would feel thermally. These individual differences may be attributed to occupants' socio-demographic background such as age, education level, working status, income, etc. A variety of definitions on comfort from the interviewees' views elaborate the intangible construct of comfort, providing the context for thermal comfort evaluation. A majority of the respondents were, for example, relating comfort with environmental aspects, such as reasonable warmth, appropriate lighting, fresh air, cleanliness, lack of noise and bad smell, easily accessible toilet and shower, isolated room and feeling protected.

> *Comfort seems to be a mental state where you would not be distracted from the adversity of environment, unawareness of the surrounding* (Interview N).

Furthermore, interviewees perceived comfort from physical, psychological and social aspects, such as a sense of security, coziness and homeliness, feeling relaxed, life quality, fulfillment from work, physical activity, social life, wellbeing, feeling secure and at ease, intellectually stimulating environment, having a peace of mind and equanimity, and meaningful relationships with family and friends. Leo (interview L), for example, felt privacy is very important as a major component of comfort, thus he kept all of the window blinds down during the day even though this shuts out the daylight. In this circumstance, privacy and daylight both comprised the meaning of comfort in Leo's view, and the motivation of Leo's action (i.e. keeping the blinds down) was to gain privacy instead of daylight.

Therefore, comfort can contain several meanings simultaneously to an individual, such as financial comfort, freedom, control, flexibility or a pleasant environment. It means that when some aspects of their comfort needs have been meet, occupants feel satisfied irrespective of other aspects (i.e. low temperature, low lighting level). These various factors involved in the notion of comfort would impact on how occupants feel about thermal comfort, which may not necessarily be justified only by heat balance equation and physiology theories.

Composition

The interviewees are comprised of various household types, sizes, and tenure types. Household types include single, couple, family with children, single with children, extended family, and non-family household. In addition, household sizes range from 1 person to 5 persons or above. Meanwhile, tenure types are categorized into owner occupied, private

rented, rented from local authorities, and rented from housing association. These various compositions of a household have influence on occupants' thermal behaviour such as how the heating is used and controlled, and how different rooms are occupied with different household members. For example, Natalia (Interview N) lived in a single private rented room in a shared Victorian house; her landlord controlled the heating system of the house. Nevertheless, she could open her windows, adjust room radiators, and use secondary heating. Other non-family household members regulated their individual rooms through room thermostats; and the overall energy performance of the home was influenced by each individual's thermal preferences and behaviour. Jessica (Interview J), on the other hand, lived in a modern apartment with her husband and children. Her room temperature was regulated subject to both the parents and children's preferences. The priority was given to her children as Jessica considered that a warmer temperature was good for the babies. Such compromise exists in a social setting where household members live together and prioritize different thermal preferences. Different tenure types also have an influence on thermal behaviour, such as whether the energy bill is included in the rental and how the dwelling is controlled.

Activity

The interviewees perform different activities in different places and times. These include the length of time spent at home, and on different activities in various spaces. It is therefore important to see how these variations link to heating behaviour in each room with different thermal sensations. From the monitoring results of all the interviewees, some of the temperatures in different rooms and times varied relating to occupant activities. Patterns can be found such as the temperature in bedrooms went higher in the evenings comparing with the daytimes, and living rooms peaked in the early evenings while cooking and dinner took place. For example, in a normal weekday, Alex (Interview A) worked at home office from 9am to 12am and 2pm to 7pm, and slept in the main bedroom with his wife between 11pm and 7am, spending the rest of time in other rooms (e.g. living room, exercise room) or out for work or leisure purpose. He turned heating on at 5-7am (23^{o}C) and 5-8pm (23^{o}C) for the whole house. The measured temperature varied with peaks in the evening in the living room (21^{o}C), and bottoms during night in the living room and office (15-16^{o}C). Here discrepancies existed between the set temperatures and measured temperatures. Nevertheless, Alex felt very satisfied about his thermal comfort at home.

Technology

The technologies, or building physical characteristics, shape the way occupants behave at home as well as thermal comfort. These include the arrangement of space, floor area, room orientation, dwelling type and age, energy and environmental performance of the dwelling and its individual elements (i.e. walls, roofs, floors, windows, heating and controls, hot water and lighting), heating system, user control, lighting, and appliances. Taking heating system for example, Ethan (Interview E) lived in a flat located in an old poorly insulated house built in 1960s. He shared the central heating control (in the kitchen) with 3 other housemates, and could not control heating temperature in his own room due to the unavailability of an individual programmer and his thermostat valve not working; he had to keep the windows open at night to cool down the indoor temperature. However, he still felt thermally dissatisfied due to high temperature at night.

DISCUSSION - CONCLUSION

This research proposes a STS approach to evaluate occupants' thermal comfort and heating behaviour at home. A combination of quantitative measurements and qualitative interviews

has shown how different usage patterns of houses might relate to occupant comfort and home performance. A detailed analysis using STS was employed to identify the gap between heating behaviour and thermal comfort. Inspired by recent theoretical approaches, this analysis was used to explain differences within a socio-technical homogeneous group rather than by changes across time, space or culture.

The inclusion of socio-technical system theory into the study of thermal comfort and home performance provides insights. Compared with other theoretical approaches in the assessment of thermal comfort, the advantage of STS theory as presented here is therefore twofold: it combines the different elements that are relevant in the understanding of the theory and it focuses on the structural nature of thermal behaviour and comfort. The aim of this paper was to identify the socio-technical parameters influencing household thermal comfort and to compare thermal behaviour and comfort satisfaction. We investigated the applicability of socio-technical approach to thermal comfort and behaviour. The results have the potential to be used for improving future house design and retrofit. In conclusion, we were able to understand thermal behaviour and comfort at home and to identify the gap between the two using a socio-technical approach.

This study also has implications for socio-technical theory. STS theory has been critically developed since 1980s, drawing attention to the mutual formation of society and technology that influence each other at all levels. Four main elements of STS and how they relate to domestic thermal behaviour and comfort were presented. The advantage of these elements is that they provide a holistic framework to sustain STS structure in individual households, and thus illustrate at a micro level on the complexity of regulating indoor thermal comfort. These four aspects of STS not only display the collective structure of the system, but also show the interconnections among the parameters holding STS structure. To draw more general conclusions, the way ahead is to quantify the parameters relating to thermal comfort using STS framework in a broader material.

ACKNOWLEDGEMENTS

The authors would like to thank Prof. K. Steemers and Prof. K. Gram-Hanssen for their advices. The financial support of the Cambridge Trust, CSC, and Wolfson College Cambridge is also gratefully acknowledged.

REFERENCES

1. Department for Energy and Climate Change (DECC) : Energy consumption in the UK. Department for Energy and Climate Change, London, 2011.
2. Department of Trade and Industry (DTI): Meeting the Energy Challenge - A White Paper on Energy. Department of Trade and Industry, London, 2007.
3. Cole, R.J., Robinson, J., Brown, Z., O'Shea, M.: Re-contextualizing the notion of comfort. Building Research and Information, Vol 36, No 4, pp 323-336, 2008.
4. Blom, I., Itard, L., Meijer, A.: Environmental impact of building-related and user-related energy consumption in dwellings. Building and Environment, Vol 46, pp 1657-1669, 2011.
5. Gram-Hanssen, K., Christensen, T.H., Petersen, P.E.: Air-to-air heat pumps in real-life use - Are potential savings achieved or are they transformed into increased comfort. Energy and Buildings, Vol 53, pp 64-73, 2012.

6. Galvin, R., Sunikka-Blank, M.: A Critical Appraisal of Germany's Thermal Retrofit Policy. Springer, London, 2013.
7. Ben, H., Steemers, K.: Energy retrofit and occupant behaviour in protected housing: A case study of the Brunswick Centre in London. Energy and Buildings, Vol 80, pp 120–130, 2014.
8. Taleghani, M., Tenpierik, M., Kurvers, S., Dobbelsteen, A. : A review into thermal comfort in buildings. Renewable and Sustainable Energy Reviews, Vol 26, pp 201-215, 2013.
9. Fanger, P. O.: Thermal Comfort: Analysis and applications in environmental engineering. Danish Technical Press, Copenhagen, 1970.
10. Nicol J.F., Humphreys, M.A. : Adaptive thermal comfort and sustainable thermal standards for buildings. Energy and Buildings, Vol 34, pp 563-572, 2002.
11. ANSI/ASHRAE Standard 55, Thermal Environmental Conditions for Human Occupancy, ASHRAE Inc., Atlanta, 2010.
12. CEN EN 15251, Indoor Environmental Input Parameters for Design and Assessment of Energy Performance of Buildings Addressing Indoor Air Quality, Thermal Environment, Lighting and Acoustics, European Committee for Standardization, Brussels, Belgium, 2007.
13. Shove, E., Chappells, H., Lutzenhiser, L., Hackett, B. : Comfort in a lower carbon society. Building Research & Information, Vol 36, No 4, pp 307-311, 2008.
14. Kempton, W. and Lutzenhiser, L. : Introduction. Energy and Buildings, Vol 18, pp 171–176, 1992.
15. Parkhurst, G. and Parnaby, R. : Growth in mobile airconditioning: a socio-technical research agenda. Building Research & Information, Vol 36, No 4, pp 351–362, 2008.
16. Healy, S. : Air-conditioning and the 'homogenization' of people and the built environments. Building Research & Information, Vol 36, No 4, pp 312–322, 2008.
17. Gram-Hanssen, K. : Residential heat comfort practices – understanding users. Building Research & Information, Vol 38, No 2, pp 175-186, 2010.
18. Strengers, Y. : Comfort expectations : the impact of demand-management strategies in Australia. Building Research & Information, Vol 36, No 4, pp 381-391, 2008.
19. Hinton, E. : Review of the literature relating to comfort practices and socio-technical systems. Environment, Politics and Development Working Paper Series (35). King's College London, 2010.
20. Shove, E. : Comfort, Cleanliness and Convenience. The social organization of normality, Berg, Oxford, 2003.
21. Wilhite, H., Nagakami, H., Masuda, T., Yamaga, Y. and Haneda, H. : A cross-cultural analysis of household energy use behaviour in Japan and Norway. Energy Policy, Vol 24, No 9, pp 795–803, 1996.

TRANSITION STUDIES IN RURAL BUILDING TYPOLOGIES: A CASE-STUDY

Kumari Moothedath Chandran[1]; Nallaval Chinnaswamy Balaji[2]; Monto Mani[2]

1: Centre for Product Design and Manufacturing, Indian Institute of Science, Bangalore 560 012, India.

2: Centre for Sustainable Technologies, Indian Institute of Science, Bangalore 560 012, India.

ABSTRACT

Influences of development and rapid modernization (technology, lifestyle) are increasingly evident in countries such as India and China housing nearly two billion rural population. The built-environment typology of rural settlements in India are undergoing rapid transitions from vernacular passive dwellings which adopt local material and skill to standardised cement based constructions. There are but, intermediate transitions phases which involves a typology involving both traditional and modern materials. A case study of Bommanahalli village near Bangalore, India is presented in this paper where authors examine one such typology adopting random rubble masonry and burnt brick walls with mud-plaster in the interior (traditional materials) and cement plaster in the exterior (modern material) with a gable clay-tiled roof. The results of this study will throw light into how combining traditional and modern construction materials are giving rise to new building typologies and how this combination performs thermally.

Keywords: rural – urban transitions, rural building typology

INTRODUCTION

India's urban areas recorded an absolute increase in population by 1 million in 2001-2011 decade which is for the first time more than its population increase in rural areas [1]. While urban growth rate was +0.3%, rural population growth rate has recorded -5.95% in the last decade [1]. Bangalore, a major city in South India, alone recorded a population growth rate of 46% in the last decade with a population of 11 million in 2011 [1]. Large scale construction activities, have been taking place to accommodate such rapid increase in population and to build infrastructure for the growing economic activities from the IT and allied sectors. Reinforced cement concrete (RCC) based construction is widely used in high rise and mid-rise apartment complexes (high & middle income) and in high density low-rise housing (low income) in Bangalore's residential sectors. The predominantly rural area of Kunigal (in Tumkur District) adjacent to Bangalore (70.5 km from Kunigal), is undergoing transitions in its rural-urban population distribution. Kunigal recorded 12.55% increase in urban population and 6.88 % decrease in rural population in 2011[1, 2]. However, 84.87% of its population still lives in the rural areas of this district. Movement of people between Kunigal and the nearby metropolitan for employment and an urbanising rural population might be influencing its building construction styles. Building typology similar to that of Bangalore's low-rise housing (low income) can be found in new constructions of the rural areas in Kunigal. Such a trend of transition from traditional styles to modern urban style can be seen in the choice of materials in newly built houses as well as in refurbishments, modifications and additions in the houses of this rural area. Therefore, there are houses which are neither entirely traditional, nor entirely modern, but has elements from both. One can see a palette of materials in the houses of these villages which are in intermediate phases of transition towards an urban-like style. A

village, Bommanahalli (12° 48' 13.31"N, 76° 58' 55.35"E), of Kunigal is chosen for a case study to understand how the building typologies are in transition here.

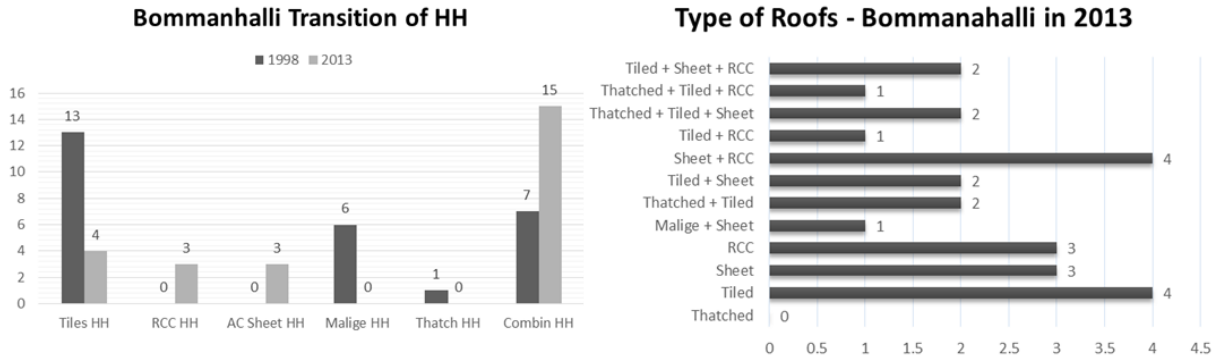

Figure 1: Transition of houses by roof types in Bommanahalli from 1998-2013 (left) and houses by type of roofs in Bommanahalli in 2013 (right).

TRANSITION OF BUILDING TYPOLOGIES

Kunigal has hot and humid climate and temperatures can go up to 40°C in the month of May. Traditional construction practices involve use of locally sourced random rubble masonry and locally made burnt brick masonry for walls, and straw or coconut leaves thatch or Mangalore Tiles for roof. Local masons or people themselves built their houses. From the interviews conducted in Bommanahalli and 2 other adjacent villages, it was learnt that these are no longer practised in new constructions and people prefer modern materials due to their aspirations of having a house similar to those in Bangalore. [2]. New constructions are widely built with cement plastered and painted brick masonry walls, and RCC roofs. This transition is evident when the number of households (HH) by roof types in 1998 and 2013 are compared (Figure 1). Compared to 1998, in 2013, RCC and Sheet (Galvanised Iron/Tin/Asbestos Corrugated roofing sheets) roof types have increased as well as Combination roof types. Combination roof types are those which involve two or more of different roof types in one house. Figure 1 (right) shows the distribution of houses in Bommanahalli by roof types including different combination roofs. The existing traditional constructions which are undergoing additions and partial refurbishments, have combination wall types as well. From the data obtained from Bommanahalli and 2 adjacent villages in Kunigal, it was observed that these transitions seem to follow a trend of direction in terms of the choice of materials for

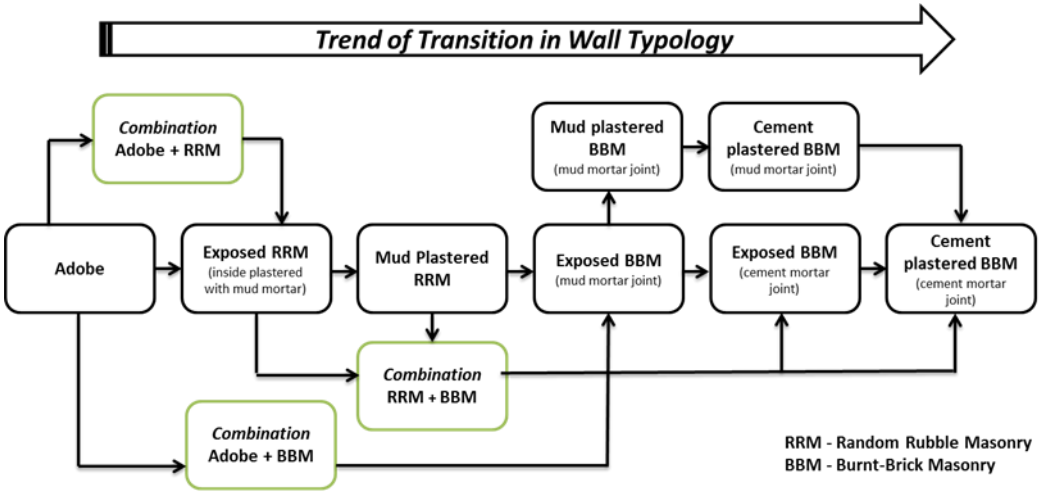

Figure 2: Trend of transition in Wall typology

walls and roofs [2] (see figure 2). One can see in these villages a variety of building typologies with different combination wall and roof types which are at intermediate phases of transition. A house with one such intermediate typology in Bommanahalli is chosen in this study to compare and understand its combination walls and thermal performance in this climate.

CHARACTERISATION OF BUILDING TYPOLOGIES

Since, the existing typologies of Thatched house, Tiled house and RCC house were insufficient to name the kind of typologies which are now prevalent in this village, the authors arrived at a new building typology characterisation based on a matrix of prevalent wall and roof types. The matrix has the change of direction of roof types in columns, and wall types in rows (Figure 3). We then documented all the houses of Bommanahalli based on its wall and roof types in this matrix. The number of houses in each typology are entered in the corresponding cells. This helped in situating the typology of the house the authors chose for further study, by highlighting it with a tick mark in the field. Therefore, the case study house has a combination of tiled and thatched roof, and a combination of Random Rubble Masonry (RRM) and Burnt Brick Masonry (BBM) walls (Figure 4). This matrix will help in classifying and documenting rural houses of other Indian villages as well.

		Roofs													
		Thatched	Tiled	Sheet	RCC	Thatched + Tiled	Thatched+ Sheet	Tiled + Sheet	Tiled + RCC	Sheet + RCC	Thatched + Tiled + Sheet	Thatched + Tiled + RCC	Thatched + Sheet + RCC	Tiled + Sheet + RCC	Thatched + Tiled + Sheet + RCC
Walls	Adobe		2		1	1		1							
	RRM e														
	RRM p							1							
	BBM e														
	BBM p		1	2	3					3			1	3	
	Adobe + RRM e		1												
	Adobe + RRM p									1					
	Adobe + BBM e														
	RRM e +RRM p														
	RRM e + BBM e		1												
	RRM e + BBM p														1
	RRM p + BBM p										1				
	BBM e + BBM p			1				1							
	Adobe + RRM e + BBM e		1												
	RRM e + RRM p + BBM p											1			
	RRM e + BBM e + BBM p					✓ 1									

Figure 3: Matrix for characterising new building typologies

INFRARED THERMOGRAPHY BASED ANALYSIS

Infrared Thermography (IRT) is used for non-destructive testing of building elements where thermal cameras measure the surface radiation [4, 5]. Passive thermography by walk-through surveys were done capturing both internal and external walls of the case study house. The IRT device used was FLUKE TiR32 IR imaging camera with wide-angle lens from Fluke Thermography (camera characteristics: IR sensor size of 320x240 IR resolution; 76,800 total IR pixels; instrument calibration range -10 °C to 170 °C; software used for post processing is SmartView 3.2.639.0). The advantages of using IRT was that it is portable, and it eliminated the need to leave the device at site without supervision. The residents were apprehensive on installation of temperature data loggers, and such devices were often tampered with or discarded by them soon after installation while not under supervision.

The plan of the house is shown in figure 4 (left) and we measured the indoor and outdoor surface temperatures of each of the walls named in the plan. The images were taken on April 24, 2015 between 12.40 and 13.10 hours (30 minutes) IST (Indian Standard Time) were shadows on walls were minimal. Indoor and outdoor IR image of West wall 1 is shown in

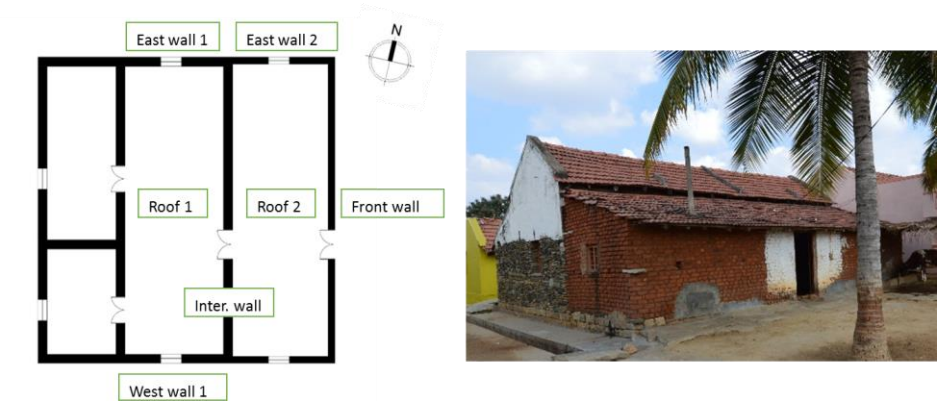

Figure 4: Plan of case study house (left) and image taken at site (right)

figure 5. In this wall, the internal surface temperature was 3.83°C lower than its external surface temperature on the RRM portion. Because IR thermography gives the instantaneous temperature, the indoor-outdoor temperature differences discussed here are not instantaneous measurements, but from the images taken within a 30 minute time span. Similar imaging was done for 7 portions on all external walls with different wall material and surface finish. The results of IR imaging are tabulated in Table 1. Here, exposed BBM has internal surface temperatures which are approximately 4.5°C lower than that of its external surface temperatures. The exposed RRM wall portion in East wall 1 has a much lower internal surface temperature that is 6°C less than that of its external surface temperature, and also it has the lowest internal surface temperature in the East wall 1 and West wall 1 compared to other wall types.

Figure 5: IRT of West wall 1- Indoor surface (top) and outdoor surface (bottom)

Walls	BBM - Exposed			BBM- Plastered & Painted		RRM - Exposed	
	East wall 2	East wall 2a	Front wall	East wall 1	West wall 1	East wall 1	West wall 1
Internal surface temp. (°C)	33.35	33.05	32.12	35.76	35.06	32.2	32.73
External surface temp. (°C)	37.51	37.53	36.86	35.4	33.39	38.85	36.56
Difference in surface temp. (°C)	-4.16	-4.48	-4.74	0.36	1.67	-6.65	-3.83

Table 1: Surface temperatures from IRT

The external surface temperatures of cement plastered and painted BBM portion is the lowest compared to other wall types on East, West and Front walls. However, it has the highest internal surface temperatures compared to all other wall types on all sides. This wall type also has higher internal surface temperatures than its corresponding external surface temperatures.

In the East side, there is a reduction (2°C) in external surface temperature of BBM walls when it is plastered and painted (whitewashed). This is further demonstrated in figure 6 in the thermal image of West Wall 1. Here again, the BBM plastered and painted portion has 3.9°C lesser external surface temperature than the exposed one. The average values of wall surface temperatures for each wall type in West Wall 1 is given in Table 2. In the thermal image of Front wall (Figure 7) in exposed BBM, the painted BBM portion has 2.73°C lower external surface temperatures than the non-painted portion. However, both portions have similar internal surface temperatures.

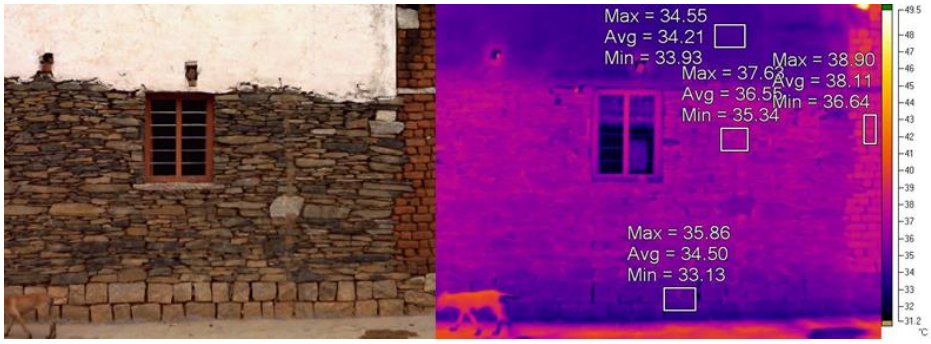

Figure 6: IRT of West wall 1 outdoor surface with 4 different wall types

West Wall	Surface Temperature (°C)
Plastered BBM white-washed	34.21
Exposed BBM in mud mortar	38.11
RRM in mud mortar	36.55
SSM plinth in mud mortar	34.5

Table 2: Surface temperatures from IRT of West Wall 1

Figure 7: IRT of front wall- Indoor surface (top) and outdoor surface (bottom)

DISCUSSIONS

For houses with new building typologies in intermediate transition phases, further study should be done to see how each combination of roofs and walls performs thermally in its climatic condition in order to understand if this trend of transition are in the direction of improved thermal comfort. Shastry et al (2012) in a study done in Sugganahalli (adjacent village of Bommanahalli) showed that traditional buildings have indoor temperatures 7-10°C lower than that of modern RCC houses in the summer months [6]. Cost of construction and non-availability of local masons have been stated as the reasons for adopting new construction practices apart from the aspirations to build modern houses in an interview done in our previous study [3]. Cement plastering and painting seem to be done for the aesthetic aspirations of the people and it does not appear to change indoor wall temperatures from our IRT study. The transition trend also seem to be towards building houses which are more rigid and durable. The transition of building typologies are also found shaping the rural-scape at street-level and village level [2, 3]. For example, reduced interaction with neighbours and street by the prevalence of compound walls in new houses.

CONCLUSIONS

Building construction in rural areas near Bangalore is transitioning from traditional to a more urban style. People combine traditional materials and new materials for construction based on socio-economic reasons (availability of masons and resources), as well as emotional reasons (aspirations). Rapidly transitioning fast paced constructions in this village leaves climatic considerations behind. Standardisation of building design and styles across rural areas of India is a serious concern in a country with varied climatic zones and high rural population. Thermal performance of new building typologies with combination of materials should be studied in depth, so that effective integration of these combinations can help in designing buildings for better thermal performance and comfort. Houses in this intermediate phases of transition are learning grounds for understanding evolution of building designs and for arriving at new typologies of climate friendly designs with available resources.

REFERENCES

1. Government of India: Census of India, 2011. http://censusindia.gov.in/2011-prov-results/paper2/data_files/india/Rural_Urban_2011.pdf <accessed 30 April, 2015>
2. Chandran, K.M., Balaji, N.C., Mani, M.: Well-being and sustainable design: A case study of building typology transition in a rural settlement in India. Design for Sustainable Well-being Conference. June 2014. In Mani, M., and Kandachar, P., Design for Sustainable Well-being and Empowerment, IISc Press and TU Delft, 207-226.
3. Chandran, K.M., Balaji, N.C., Mani, M.: Rural-Urban Transition and Well-Being: A case study of a rural settlement in India. Current Science (Forthcoming article in Special Section, September 2015).
4. Barreira, E., de Freitas, V.P.: Evaluation of building materials using infrared thermography. Construction and Building Materials. Vol 21, pp 218-224, 2007.
5. Matthew, F., Coley, D., Goodhew, S., de Wilde, P.: Thermography methodologies for detecting energy related building defects. Renewable and Sustainable Energy Reviews, Vol 40, pp 296-310, 2014.
6. Shastry,V., Mani, M., Tenorio, R.: Impacts of Modern Transitions on Thermal Comfort in Vernacular Dwellings in Warm-Humid climate of Sugganahalli (India). Journal of Indoor and Built Environment. October, 2012. doi:10.1177/1420326XI2461801

INDOOR PERFORMANCES OF LIVING WALL SYSTEMS: TOOLS AND REQUIREMENTS

Roberto Giordano, Elena Montacchini, Silvia Tedesco

Politecnico di Torino – Department of Architecture and Design – Viale Pier Andrea Mattioli, 39 – 10125 –Turin (TO), Italy

ABSTRACT

The benefits of the use of vegetation in indoor environment, and in particular the use of Living Wall Systems (LWSs), are demonstrated by the international scientific literature. Such benefits can be listed as follows: acoustic comfort, indoor air quality and dilution of pollutants, thermo hygrometric comfort, psycho-emotional well-being (improvement of cognitive skills, stress reduction, user satisfaction).

During the last years the LWS' spread is confirmed by the increasing number of building featured by vegetation both on façades and partitioning.

Despite their diffusion there is a lack of data concerning the LWS' indoor performances as well as on properties and featuring about materials and products they are made-up.

With regards to outlined constraints the paper deals with a research focused on studies and on an indoor LWS project. Two tools are described: the Indoor LWS' datasheet and the Indoor Agronomic database. Further a methodological approach concerning the technologies and the materials selection is also illustrated. Such approach was finally adopted in designing and prototyping an advanced indoor LWS.

The Indoor LWS' datasheet was developed in order give to designers and enterprises information concerning the indoor LWS' featuring with regards to those available on the construction market. Every datasheet was developed on a common format in order to make them comparable. The information refer to: general data (e.g. manufacturing site); technical performances (e.g. size, weight, use of environmentally friendly materials); indoor featuring (e.g. acoustic comfort, air quality and thermo-hygrometric comfort).

The Indoor Agronomic database was addressed to select proper species fit for indoor use. The database was divided in two parts: the former provides information about botanical aspects; the latter compares the plant species hygro-thermal comfort to human comfort. Such comparison was carried out by the adoption of bioclimatic Olgyay chart on humidity and temperature data.

The effectiveness of mentioned tools was confirmed in further research tasks. The information available were used to define a proper set of technological and agronomical requirements to be included in a new indoor LWS design. Indoor requirements were divided according to LWS life cycle. They were adopted in order to fulfil the largest numbers of indoor environmental goals.

Keywords: Living Wall Systems (LWS), indoor performances, environment requirements

INTRODUCTION

The international scientific research is now interested in studying the many ecological benefits of Living Wall Systems (LWSs): vegetated wall with plants on pre-assembled panels using a growing medium as root support. Such benefits can be listed as follows: heat island

effect mitigation, noise pollution insulation, heating and cooling energy demand reduction, enhancement of urban biodiversity [1].

Recently to indoor LWSs have been recognized other functions summarised as follows:

- Air purification and absorption of particulate matters as well as of Volatile Organic Compounds (VOCs). Some plants have the ability to absorb from 50 to 90% of the polluting substances present in the air [2].
- Psycho-emotional well-being (improvement of cognitive skills, stress reduction, user satisfaction). Studies have shown that simply having a view of greenery increases workplace productivity and patient recovery rates in hospitals [3, 4].
- Acoustic comfort and noise reduction. The acoustic benefit derived from green walls varies according to their construction and level of vegetation cover. Substrate effectively reduces sound at low to middle frequencies. A relatively smaller reduction is achieved at higher frequencies due to the scattering effect of the foliage. As the level of vegetation cover increases, the sound absorption properties of a green wall also increase [5].

Finally vegetated surfaces are generally considered aesthetically pleasing.

During the last years, several indoor and outdoor LWS patents have been developed but much more for improving their performances might be done. Both the technological and the agronomic aspects such as the structure, the materials, the irrigation system, the choice of plants, and the substrate or growing medium, may be improved.

On the whole few studies focus their attention on materials used in LWS manufacturing as well as on materials connections and to those ecological requirements usually taken into account in an environmentally friendly design approach. Thus the research here presented was focused on indoor LWS featuring and it was a step in the direction of the development of a new sustainable and performing modular indoor LWS. The paper deal with the outcomes and the outlooks of a research methodology based on the following tasks: development of the Indoor LWS' datasheet and the Indoor Agronomic database. Environmental requirements have been identified and prototyping activities carried out in order to develop an advanced indoor LWS.

ANALYTICAL TOOLS

Indoor LWS' datasheet

The Indoor LWS' datasheet was developed to give to designers and enterprises information concerning the indoor LWS' featuring with regards to those available on the construction market.

In order to make possible a comparison among several indoor LWSs a format-datasheet was developed to collect a wide range of information. The datasheet is an informative tool by means of designers might be conscious about technological and environmental performances and they might select the right one according to the needs to be matched.

The datasheet was divided in two parts. The first one includes the technical and performance data, providing information about technical characteristics, materials and products performance. Such part may be assumed as the core of the datasheet. The second one contains general information related to architectural design solutions, executive drawings and pictures taken from selected buildings, useful for a better understanding of formal and morphological aspects.

According to the above remarks the technical data filling concerns the following records: sizing, weighting, water consumption, plant species, plants number per square meter, type of substrate. Records on the location were also included, providing information about the manufacturing site (Italy, Europe, non European Countries).

A checklist was developed encompassing a number of parameters commonly used in the design process. The parameters may be quantitative or qualitative. Records were implemented on the datasheet as follows:

- Materials record: description concerning the materials and product performances used in a LWS (e.g. the growing medium, the plants, the frameworks, the insulation and the finish work).
- Connections record: description concerning the system assembly (e.g. bolting, gluing, screwing, etc.).
- Indoor environmental performances record: description concerning the acoustic comfort, air quality and thermo-hygrometric comfort.

On the whole the total number of filled datasheets reached 20.

Figure 1 shows an example of datasheet implemented. Above the LWS' name and the corresponding code (a); (b). From the top left a summery of the LWS featuring (c), a table including the records used for gathering the technological data (d), detailed drawings, renders, pictures and photos of built projects are even included (e).

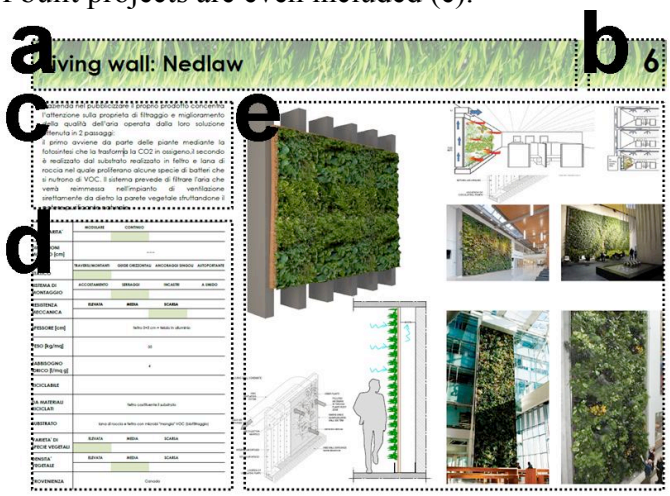

Figure 1: Example of Indoor LWS' datasheet: (a) product name and manufacturer; (b) progressive datasheet code number; (c) technology description; (d) performances assessment; (e) details and pictures.

Indoor Agronomic database

The Indoor Agronomic database was addressed to select proper species fit for indoor use and particularly for indoor living walls (based on available literature, internet sources, preview researches).

International research has clearly demonstrated that indoor plants can be used to reduce indoor concentrations of VOCs and CO_2, two classes of contaminants often in higher concentrations indoors than outside [6]. Two criteria were basically assumed for plants selection procedure:

- Plant species suitable for the indoor vertical installations.

- Plant species able to improve air quality.

The database was divided in: Part 1: botanical and ecological data; Part 2: hygro-thermal and comfort data. The former provides botanical data (e.g. species name, group and family, height, type, habit, leaf, root system) and ecological data (e.g. conditions of growth, watering, lighting, maintenance). The latter gives information on comfort requirements through a superimposition on bioclimatic chart of plant needs on bioclimatic chart of human needs. Such analysis was allowed to assess the plants effectiveness use with specific indoor conditions and their correlation with human comfort zone. It was carried out by the adoption of Olgyay chart with regards to a range of climatic variables. Indoor air temperature and relative humidity were assumed as climatic variables for plants comfort (see grey dashed area). Human requirements and comfort zone are featured with a ticked black line. The intersection between the total comfort zone area and vertical lines set up a perimeter of best comfort conditions. The human comfort zone is featured to a range of variables including indoor air temperature, relative humidity, solar radiation absorbed and internal air movement as well. On the whole 28 plants were analysed and assessed as suitable for indoor uses and compatible in terms of comfort needs.

Olgyay's bioclimatic chart specify different zones at different combinations of relative humidity and dry bulb temperatures; the level of comfort is applicable to indoor spaces according to a indoor level of clothing. Figure 2 displays an example of plant specie analysed (Scindapus). The percentage was obtained by dividing the human comfort zone by the plant comfort zone. Percentage calculated for plant specie shown in figure 2 was 54%. Such value was assumed as "good compatibility". Thirty-five percent was the limit value assumed as acceptable for considering the zones as each other compatible.

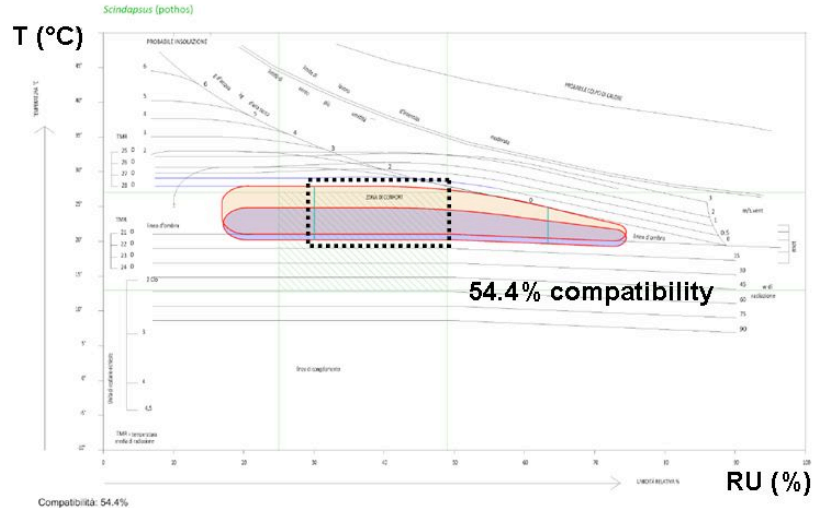

Figure 2: Olgyay's chart: superimposition between the human comfort zone and the Scindapsus (plant specie) one. The dotted line area shows the compatibility between the analysed zones.

The Indoor Agronomic database was finally completed collecting and assessing information concerning the 28 plants VOCs potential removal or dilution.

METHOD

The tools developed were used to define an appropriate set of ecological requirements to be included in a new indoor LWS design and prototyping. Such analytic approach was crucial for characterise the indoor LWS requirements and overcome those requirements usually

implemented in the design process (e.g. LEED®: Leadership in Energy and Environmental Design) not properly fit for making an environmentally friendly LWS.

Indoor environmental requirements

The requirements were adopted in order to fulfil the largest numbers of indoor environment requirements over the LWS life cycle (manufacturing, on site assembling, use and maintenance as well as final disposal).

An Italian Technical Specification (TS) was used as general framework to implement the requirements (Environmental sustainability of construction works - Operational tools for sustainability assessment: part 1 and part 2).

Matching the technological and agronomical data - collected in the mentioned databases - with the TS requirements a selected and adapted number of requirements was set up. Such requirements were gathered, classified and arranged in a tabular format. Each requirement "fiche" includes: the life cycle stage (e.g. manufacturing, maintenance, etc.), the category impact (e.g. non-renewable source depletion, carbon dioxide emissions, etc.), the corresponding requirement (e.g. minimizing the water need and giving priority to organic fertilizer) and the indicator (qualitative and quantitative), and finally, the assessment method for the requirement characterization.

The requirement fiches were subsequently tested. The LWSs featured in the technological database were assessed through the indoor environmental requirements. Each requirement was converted into a quantitative score used to calculate strengths and weaknesses.

Such procedure therefore was provided to:

- Categorizing the recurring building systems or assembling processes used in the LWSs technologies (e.g. lightweight systems vs. heavyweight systems, modular box systems vs. green walls or bolted materials vs. welded materials).
- Categorizing the recurring sizes and thickness used in the LWSs technologies (e.g. square modular box vs. panel systems).
- Categorizing the recurring materials used in the LWSs technologies (e.g. plastic based materials vs. metal alloys).

Every category was then assessed. For instance, if a system or a material belonging to a category fulfills an indoor environmental requirement it gets a positive score (from 1 to 3). The more a system (or a material) implements its score, the more is assumed as best solution to be used in indoor LWS.

The procedure was enabled to improve the LWS' design process as well as the prototyping stage enhancing strengths and minimizing weaknesses.

Designing an advanced indoor LWS

Environmental requirements provide both a broad knowledge about the technological connections and information about suitable materials to be used for designing an ecological indoor LWS.

The advanced modular LWS was designed with the following technological solutions here listed:

- Structural system: freestanding stick system.
- Panel size: 0,6 x 0,6 m: easy assembling and handling.

- Growing medium: recycled felt fabric. To improve water retention felt fabric should be integrated with sphagnum
- Fertirrigation plant: integrated in the stick system, with water harvesting system.
- Framework: recycled aluminium
- Lighting: led tubes.
- System assembly: screws, fast and reverse connection.

CONCLUSION AND OUTLOOKS

The method described was extremely effective for the research purposes. The LWS design was carried out through a preliminary assessment procedure based on environmental requirements developed according to LWSs featuring. Databases were necessary to enhancing the strengths of those materials, connections and plant species analyzed.

Further research activities will be planned. For instance, some environmental aspects to be investigated concerns: the effects on VOC in the indoor environment due to the number of plants per square meter; VOC's absorption will be monitored (according to CEN/TC 350 scenario) in a chamber test and in an indoor installation. With regards to acoustic performance, sound absorption coefficient will be measured according to the ISO 354 standard in a reverberation room to test the properties of plant species with the change characteristics such as density of the leaves, shape, etc.

However the tools described are an open issue source allowing the implementation and integration of data. It may carry in effect the optimization of indoor LWS design.

Acknowledgments

The research was developed in the framework of DOUBLE_FAÇE project developed by Politecnico di Torino, Department of Architecture and Design. Authors thank Massimo Consolandi for his technical advice.

REFERENCES

1. Weinmaster, M. (2009). Are Green Wall as Green as they look? An introduction to the various technologies and ecological benefits of Green Wall. Journal of Green Building, vol. 4, pp. 3-5.
2. Wolverton, B. C., Douglas, W. L., Bounds, K. (1989). A study of interior landscape plants for indoor air pollution abatement. NASA techdocs.
3. Bringslimark, T., Hartig, T., Patil, G. G. (2009). Psychological benefits of indoor plants in workplaces: putting experimental results into context. HortScience, vol. 42, pp. 581-587.
4. Bringslimark, T., Hartig, T., Patil, G. G. (2006). The associations between indoor plants and perceived stress, sick leave and performance. Proceedings of the 26th International Horticulural Congress, Seoul, Korea, pp. 117-121.
5. Wong, N., Tan, A., Tan, P., Chian, K., Wong, N. (2010). Acoustics evaluation of vertical greenery systems for building walls. Building and Environment, vol. 45, pp. 411-420.
6. Burchett , M. et al. (2010). Greening the Great Indoors for Human Health and Wellbeing. Final Report to Horticolture Australia Ltd, online available: http://www.ngia.com.au.

THERMAL COMFORT FOR OLDER ADULTS. AN EXPERIMENTAL STUDY ON THE THERMAL REQUIREMENTS FOR OLDER ADULTS

Matteo Iommi[1]; Eduardo Barbera[2]

1: University of Camerino (UNICAM), School of Architecture of Ascoli Piceno. matteo.iommi@unicam.it

2: University of Camerino (UNICAM), School of Architecture of Ascoli Piceno. edoardo.barbera@unicam.it

ABSTRACT

In this paper is presented an experimental study about thermal comfort requirements for older adults, trying to establish a specific range of parameters for optimal thermal conditions in residential indoor environments. One of the most important reasons for this study is the constant growth in the number of older people all the world, that wish to live in health and to continue their life style. Today, in most industrialized countries, people are living longer, thanks to technological and economic progress, with an average life expectancy of about 80 years, and it is estimated that in the future the population constituted by older adults, over 65 years, will continue to grow. In this context, is important to understand how older adults feel thermal comfort as the home environment plays an important role to provide healthy and comfortable life styles. To evaluate the thermal environmental conditions for human occupancy, in moderate indoor environments with mechanical heating or cooling systems, the PMV/PPD method is still used, also to evaluate thermal comfort of older adults. There is a wide literature and research activity about indoor thermal comfort, but most of the studies and references, like also the current standards, offer only general and overall approaches, with no differences with regard to age. In order to relate the conditions of thermal comfort to older people, more specific considerations and evaluations are necessary.

The purpose of this study is to define some specific thermal comfort requirements for older adults, with specific profiles and a range of related parameters, using software and virtual test rooms according to current evaluation methods. To perform this study, analyses and simulations are performed, using tools such as CBE Thermal Comfort Tools, Ashrae Thermal Comfort Tool and Perla Pmv. With these tools are simulated some situations in real conditions, such as rooms with different floor areas, different activities and clothings, and different internal gains. All the simulations and analyses are based on investigations on older adults behaviors. The results yeld specific values and indices, related to thermal comfort, able to represent the ranges of older adults thermal parameters and to define some daily profiles.

Keywords: thermal comfort, pmv/ppd method, older adults.

INTRODUCTION

Today in Europe, the average life expectancy is over 80 years, and it is estimated that in 2020, about 25% of the population will be over 65 years old [1]. This growing population of older people involves a great challenge about residential indoor environments with appropriate solutions and conditions. The home environment plays an important role to offer healthy and comfortable spaces. In 2025, there will be 360 million people aged over 60 years, in the industrialized countries of the world [2]. In Italy, in the last 50 years, aging of the population has been one of the fastest and it is estimated that in 2050 the people over 65 years will amount to 32% of the total population, with an average life expectancy of 83.6 years for men and 88.8 for women [3]. If the increase of longevity is certainly a great achievement, that

evidences the growing improvement of living conditions and health progress, it will also be a major issue to be resolved in the future, in terms of the potentially growing number of sick people, an increases demand for assistance, reduction of well-being for older people and also the demographic transition towards the third age, with related modification of households, which involves large increases in energy demand.

Older adults are subjected to sensory changes, involving sight, hearing, feeling, smell and peripheral nervous system that result in different demand and requirements in terms of environmental comfort. In fact, these changes modify the physical and metabolic abilities and are caused by physiological deterioration of the human body but could also be caused by accidents or illness and can vary over time. In particular, the effects of aging on the perception of thermal comfort and on the body temperature control have recently been revaluated, according to Van Hoof *et al.* [4]. Until a few years ago, studies supported the hypothesis that the older adults do not perceive thermal comfort different from younger adults. Any differences about thermal requirements, related to sex or age, is evaluated and calculated as parameters by metabolic rate and by clothing insulation in PMV/PPD model. It has been shown that, the capability to regulate body temperature decreases with age, as basal metabolism decreases with age and leads to lower body temperatures. According to recent studies, older adults feel comfortable higher temperatures and perceive local thermal discomfort as very annoying. Lower metabolic rate and lower levels of physical activity, involve the demand of a warmer environment and higher temperatures. Also, the perspiration mechanisms, in people over 60 years, are less active than in younger people and the temperature threshold for the appearance of sweating increase progressively [5]. In older adults and in people with disabilities, there is a reduction in muscle strength, work capacity, and in the capability to transport heat from the internal organs to the skin surface, with decreased levels of hydration and vascular reactivity. All these phenomena, confirmed by many studies, represent a general framework of conditions for all older adults, although depending on sex, age and specific characteristics there may be sensitive differences.

One of the most important aspects in the perception of quality and satisfaction of the indoor environment is the thermal comfort, which contributes to the well-being and overall health. The current method for the evaluation of thermal comfort is the PMV/PPD model (Predicted Percentage of Dissatisfied and Predicted Mean Vote) derived from the Fanger model, which is adopted in the International Standards ISO-7730 and ANSI/ASHRAE Standard-55 [6-7]. The indoor thermal comfort analysis is a field study, belonging to Building Science, with a very large literature and many research activities, but most of the studies, knowledge and predictive methods are developed for healthy occupants between 20 and 60 years old. In order to differentiate thermal comfort requirements for older adults, more specific considerations and evaluations are necessar. A better understanding of the optimal thermal comfort requirements for older adults can afford to design more appropriate equipments, insulations performances and technical solutions.

METHOD

In this paper, starting from a previous recent survey, which tried to define some typological daily profiles about life-style of older adults in Italy, an experimental study is proposed, simulating and evaluating thermal comfort requirements for older adults. This study, which uses some existing data about older adults life-styles, establishes some real common conditions about indoor residential environments and uses international calculation models for thermal comfort evaluation, integrates all these aspects and runs simulations with the purpose to meet more specific thermal comfort requirements and to recognize closer ranges of thermal parameters for older adults. A fundamental starting point was a previous survey, named PASS (Private Assisted House), developed in 2014 by University of Camerino, Regione Marche and

INRCA, that monitored fifty older adults, from 60 years old to 80 years old, recording information about their life-styles: daily times, activities, alimentation, types of clothing, sleep duration, etc. Based on all these data, were defined three main average profiles, able to represent, in general, the most probable behaviors of older adults. These three profiles are used to set personal factors of thermal comfort: metabolic rate coefficients and clothing insulation coefficients (Figures 1-2-3). The three profiles show three average daily trends about clothing index (clo) and metabolic index (met).

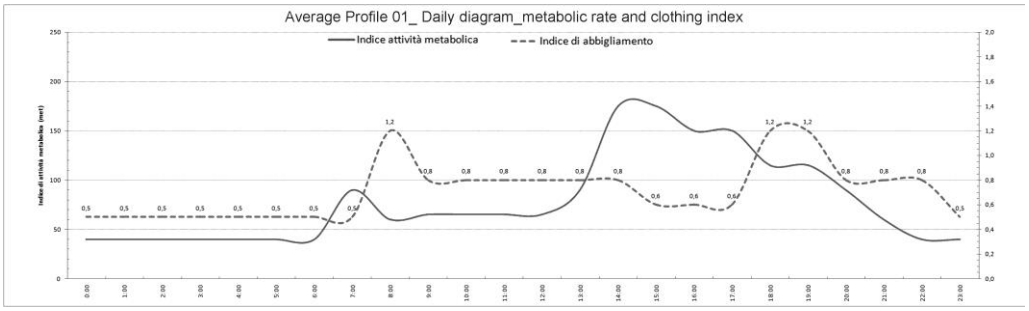

Figure 1: Average daily profile older adult 01. Diagram of profile of metabolic rates and clothing indices. The diagram shows trends, in Met and Clo, extracted from PASS survey, for a reference older adults (male, height 170cm, BSA 1,85 m^2, weight 70 kg, age 60 years old).

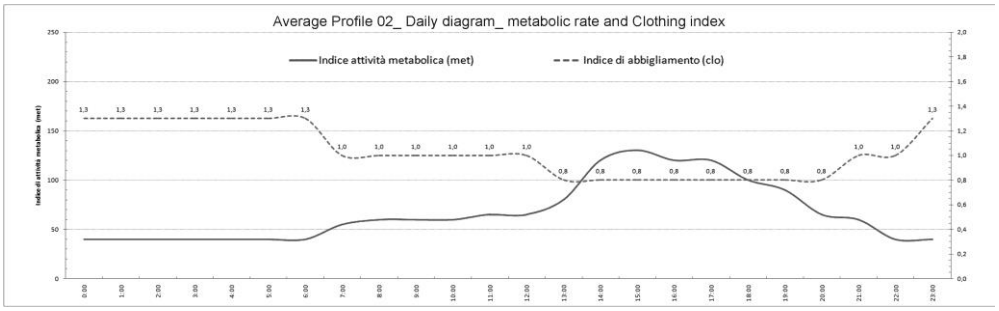

Figure 2: Average daily profile older adult 02. Diagram of profile of metabolic rates and clothing indices. The diagram shows trends, in Met and Clo, extracted from PASS survey, for a reference older adults (male, height 160cm, BSA 1,72 m^2, weight 70 kg, age 70 years old).

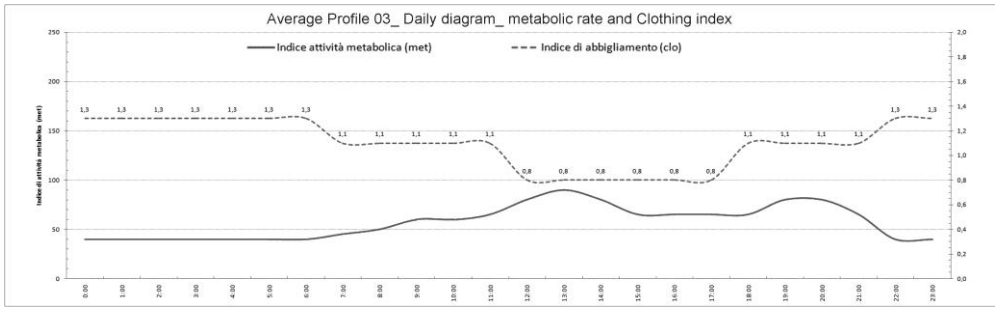

Figure 3: Average daily profile older adult 03. Diagram of profile of metabolic rates and clothing indices. The diagram shows trends, in Met and Clo, extracted from PASS survey, for a reference older adults (male, height 165cm, BSA 1,81 m^2, weight 75 kg, age 80 years old).

Before performing simulations and analyses, with the aim to represent conditions closer to the real current indoor residential environments, a building scenario is defined, like a virtual test room. The building scenario tries to represent a typical indoor environment, like a living-room, with which it is possible to detail some important features that mainly affect on mean

radiant temperature of surfaces, like the existence of a window or the dimensions of envelope surfaces (Table 1).

Reference Test Room				
Architectural dimensions			Environmental features	
	Room	Window	Type of ventilation	natural
Width	4,00 m	1,50 m	R.H. control	no
Height	2,80 m	1,20 m	Cooling system	no
Depth	4,60 m		Heating system	radiators
Surface	18,4 m^2	1,80 m^2	R.H. range	40% - 60%
Volume	51,5 m^3		Air speed range	0,1 m/s – 0,3 m/s

Table 1: Default parameters of reference test room. The table shows geometric and other features of the virtual indoor environment, used to run pmv/ppd calculations.

With these conditions, the thermal comfort analysis process simulates and calculates the pmv and ppd index, for all the hours of the three average profiles with some default parameters, like clothing insulation indices, metabolic rates and indoor environment dimensions. In this process, only some parameters can be changed, like the air temperature, the mean radiant temperature and, within a restricted range, the air speed and the relative humidity. The adopted method is related to the target of the research, that does not want to recognize if and how the thermal comfort is felt, but on the contrary, as a function of an optimal comfort range, tries to know what levels of some manageable environmental factors should be necessary.

RESULTS

The study calculated PMV and PPD indices for 72 different configurations, 24 configurations, like 24 daily hours, for each of the 3 average profiles of older adults. In each single calculation are included personal factors, like not editable default parameters, and environmental factors, which are managed to reach near zero heat balance, enclosed in a optimal PMV range +0,5 and -0,5. Different tools are used to calculate pmv and ppd indices to confirm the accuracy of results. In particular, at first, calculations are made with the Ashrae Thermal Comfort Tool and the CBE Thermal Comfort Tool, then with the Perla pmv tool, an Italian software product which provides the ability to model a virtual room with specific dimensions and features, and at the end, indices given by different tools are compared to verify equality of results. The output of the analysis are three diagrams, one for each profile, where trends about pmv and ppd during the 24 hours are displayed (Figures 4-5-6).

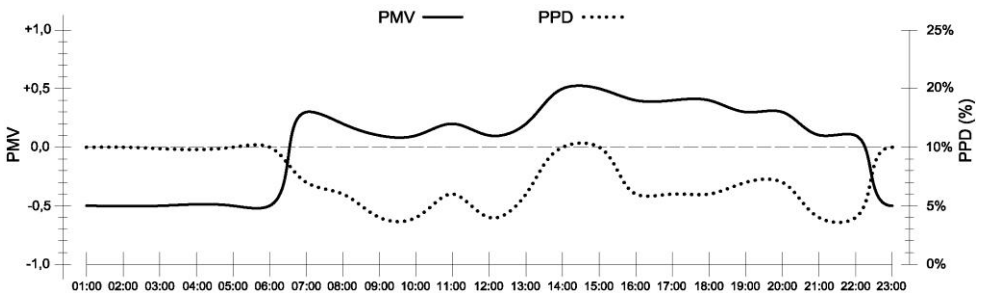

Figure 4: PMV/PPD diagram for average older adult profile 01. Diagram represents the trends of pmv/ppd indices, calculated as functions of personal and environmental factors, to achieve optimal thermal comfort levels.

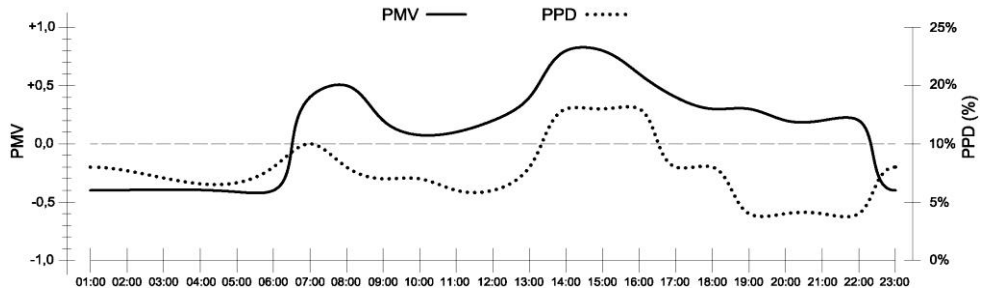

Figure 5: PMV/PPD diagram for average older adult profile 01. Diagram represents the trends of pmv/ppd indices, calculated as functions of personal and environmental factors, to achieve optimal thermal comfort levels.

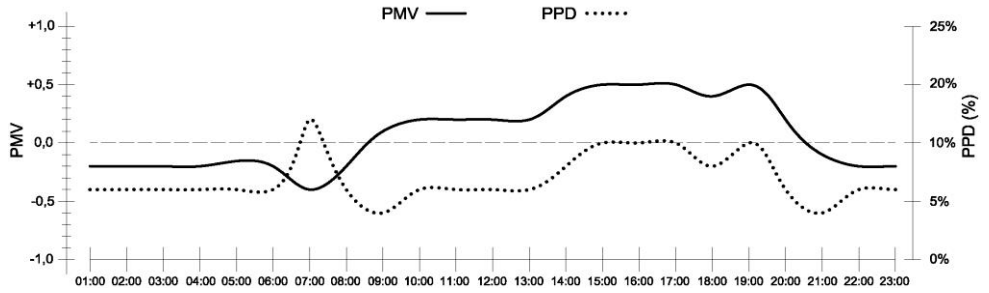

Figure 6: PMV/PPD diagram for average older adult profile 03. Diagram represents the trends of pmv/ppd indices, calculated as functions of personal and environmental factors, to achieve optimal thermal comfort levels.

The results are average daily pmv/ppd trends, obtained by using personal factors, that are predefined, and environmental factors that are managed, within restricted ranges, to achieve indices within an optimal thermal comfort range. To achieve these comfort levels, the necessary values of environmental factors are very reduced: air temperatures range from 20C° to 24C° and often over 22C°, radiant temperatures of surfaces need to be constant and homogeneous with air temperatures, relative humidity always within 40% and 60% and air speed steadily within a range from 0,1m/s to 0,3m/s (Figure 7). These values about environmental factors, could give back specific information about how energy performances are necessary to reach and maintain thermal comfort for different types of older adults. These values are theoretical and, in real conditions, are very difficult to obtain and to maintain without an integration of all building systems, with mechanical systems and equipments, controlled by a building automation system.

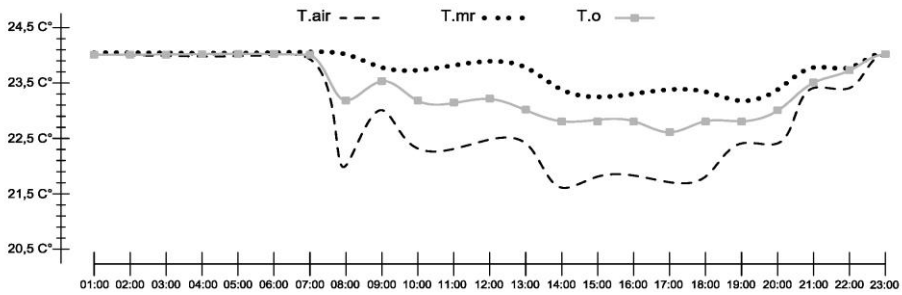

Figure 7: Indoor temperatures diagram for profile 01. Diagram represents the trends of air temperatures (T.air), mean radiant temperatures (T.mr) and operative temperatures (T.o) required to achieve and maintain pmv/ppd levels for average older adults profile 01, shown in figure 4.

DISCUSSION

This experimental study includes some restrictions and limitations, like: no differences between underheated and overheated periods, diseases or disabilities that affected thermoregulation in many older adults are not evaluated, starting data about survey on life-styles of older adults are not entirely useful and the ANSI/ASHRAE Standard-55 method, that is an overall evaluation system, could not give back a specific satisfaction assessment of older adults with the thermal environment. However, this experimental study, based on real behaviors of some older adults, examines the energy performances that residential indoor environments could have, highlighting some conditions as higher air temperatures are required, environmental factors need to be more stable, and also small variations can involve important reduction on thermal satisfaction of older adults.

CONCLUSION

Starting from the above discussion, is possible to accept that indoor residential environments, where older adults live, need a very high control of indoor climate conditions, so heating and cooling mechanical systems and other equipments, are required, involving important considerations about energy saving and energy building design solutions, because the achievement of thermal comfort for older adults need integrated and advanced strategies, like thermal mass, high insulation, no local discomfort phenomena and control systems for air speed, relative humidity and air quality. In this sense, building automation could be a very important support to obtain and maintain high indoor thermal performances. Further researches are planned, to continue the studies in this sector, targeting developments of building automation and integrated management of indoor thermal comfort for older adults. This study has been carried out, based on a previous work, named PASS, made with Regione Marche and INRCA.

REFERENCES

1. Scano, R.: Libro bianco. Tecnologie per la disabilità. Commissione interministeriale sullo sviluppo e l'impiego delle tecnologie dell'informazione per le categorie deboli. Ministero Italiano per l'innovazione e le Tecnologie, Roma, 2003
2. Van Hoof, J. Hensen J.L.M.: Thermal comfort and older adults. Gerentchnology 4(4), 2006
3. ISTAT: Il futuro demografico del paese. Ufficio Stampa Istat, Roma, 2011
4. Van Hoof, J. Kort, H.S.M. Hensen, J.L.M.: Thermal comfort and the integrated design of homes for older people with dementia. Build Environ 45 (2), 2010
5. Blatteis C.M.: Age dependent changes in temperature regulation. Gerentology 58(4), 2012
6. ASHRAE, ANSI/ASHRAE Standard 55-2003 : Thermal environmental conditions for human occupancy. Atlanta, 2013
7. ISO EN 7730 2005, Moderate Thermal Environments. Determination of the PMV and PPD indices, ISO International Standards Organizations, Geneva, 2005
8. Peeters, L. De Dear, R. Hensen, J. : Thermal comfort in residential buildings: Comfort values and scales for building energy simulations. Appl Energy 86 (5), 2009

EFFECT OF DIFFERENT DESIGN PARAMETERS ON THE VISUAL AND NON-VISUAL ASSESSMENT CRITERIA IN OFFICE SPACES

P. Khademagha[1]; J.F.L. Diepens[1]; M.B.C. Aries[1]; A.L.P. Rosemann[1]; E.J. van Loenen[1,2]

1: Building Physics and Services Unit, Department of the Built Environment / Intelligent Lighting Institute, Eindhoven University of Technology, Eindhoven, The Netherlands

2: Philips Research, Eindhoven, The Netherlands

ABSTRACT

Light entering the human eye does not only enable the performance of visual tasks, but also influences the health and well-being of humans via non-visual effects. A substantial amount of people in the Western society spends the majority of their work time indoors. Well-designed lighting positively impacts the visual comfort and well-being of people working in offices.

Current standards for office lighting design are solely based on enabling the visual tasks via recommendations for photometric quantities such as the maintained illuminance on the task and surrounding areas and/or the glare limitation. The luminous radiation that contributes to the health related non-visual effects is not addressed in these recommendations at all. It is therefore essential to include the impact of effective luminous radiation in the lighting design process.

This paper discusses the necessary distinction between photometric quantities on one side and effective luminous radiation on the other side. It investigates the effect of design parameters such as ‘window size’, ‘exterior ground plane color and luminous reflectance’ on the visual and non-visual effects for different view directions. Simulations have been conducted for the IEA Task 27 reference office using the light software tool Radiance

The findings show reverse influence of the exterior ground plane color and luminous reflectance on the visual and non-visual effects of light. While the exterior ground plane luminous reflectance plays an important role on the visual evaluations, its color is the most influential design parameter for the non-visual evaluations. For the optimal health related non-visual effects of light, findings suggest using bluish exterior ground plane and placing the work plane facing the window.

Keywords: lighting recommendations, window size, exterior ground plane color and luminous reflectance, view direction

INTRODUCTION

Light is essential not only for its visual effects but also for its health-related non-visual effects. Visual effects of light can be categorized into ‘visual performance’ and ‘visual comfort’. Current standards and lighting recommendations are solely based on the visual effects of light. In the standards, visual performance is addressed by recommendations with regard to the maintained horizontal illuminance on the task and surrounding areas. The required maintained illuminance varies depending on the type of task; for typical office work this is usually 500 lx on the (horizontal) work plane. Visual comfort is addressed by recommendations with regard to glare limitations/prevention, which is related to the luminance distribution in the visual field. All these standards have been defined based on solely photometric quantities such as illuminance and luminance, in which the spectral sensitivity of the human eye for photopic vision V(λ) has been taken into account. The

luminous radiation that contributes to the non-visual effects is not addressed in these recommendations.

The discovery of a third photoreceptor in the human eye, called intrinsically photosensitive Retinal Ganglion Cells (ipRGCs), has highlighted the health-related non-visual effects of light. The spectral sensitivity of the ipRGCs, indicated with C(λ) [1], varies from that of a photopic vision and is blue shifted [2, 3]. Recently, a definition of new terminology has been proposed by the Commission Internationale d l'Eclairage (CIE) for the photobiological quantities [4]. According to CIE, photo-biological quantities are to be defined in purely physical terms (radiant quantities) weighted by their spectral sensitivity curve. For instance, when non-visual effects of light are concerned, the vertical effective irradiance with respect to the C(λ) ($E_{e,c}$) is the quantity to address/measure, instead of the vertical illuminance at the eye.

In western societies, a substantial amount of people spends approximately 80-90% of their (work) time indoors. A lighting design, incorporating both visual and non-visual effects of light, not only positively impacts the visual performance and comfort of people working in the offices, but also influences their health and well-being. The effect of design decisions on visual and non-visual lighting demands is not fully comparable .

This paper investigates the influence of the design parameters 'window size', 'exterior ground plane (GP_{ex}) color', and 'GP_{ex} luminous reflectance' on the visual and the non-visual light effects for different view directions.

METHOD

Modelling protocol

The (backward) ray-tracing lighting simulation software Radiance [5] was used to investigate the effect of different design parameters on visual and non-visual light effects. Via its spectral distribution and dynamic character daylight is believed to contribute most positively to the well-being of humans. Therefore, it was used as the primary source of light. A standard CIE overcast sky model with a horizontal illuminance in the unobstructed field of 10000 lx was used for the quantitative analysis as it represents a worst-case daylighting condition.

Simulations were carried out for the IEA task 27 reference office room [6]. This reference office (dimensions 3.6 x 5.4 x 2.7 m) has a facade with a single daylight opening containing double pane low E glazing (with normal luminous reflectance of 0.1). The window is located at the south wall and is placed at the center of the wall in order to maintain a view to outside. The window size varies from 10% to 100% Window to Wall Ratio (WWR) with 10% increments. This paper presents the results related to three window sizes of 10%, 50%, and 100%.

In order to study the influence of the GP_{ex} color and luminous reflectance on evaluation criteria (see evaluation criteria section), a GP_{ex} was placed below the modeled room. First, the influence of the GP_{ex} color was studied. Doing so, the GP_{ex} luminance reflectance (ρ) was assumed equal to 20% as a typical ground plane reflectance while its color was changed into pure blue (mimicking sky or sea), pure green (mimicking nature), and grey (mimicking asphalt). Secondly, the influence of the GP_{ex} luminous reflectance was investigated for two extremes of 0% (no light reflection) and 85% (mimicking snow). For comparison purposes, grey colored GP_{ex} is assumed as the base case. Table 1 shows the properties of the different materials used for the GP_{ex} in RGB values.

	R	G	B	Luminous reflectance (ρ)
Pure green	0.000	0.299	0.000	20%
Pure blue	0.000	0.000	3.086	20%
Grey	0.200	0.200	0.200	20%
White	0.850	0.850	0.850	85%
Black	0	0	0	0%

Table 1: Properties of the GP_{ex} materials in RGB values and their luminous reflectance.

Assessment protocol

The horizontal illuminance on the work plane (at the height of 0.80 m from the floor) and the $E_{e,c}$ at the occupants eyes in the sitting position (height of 1.20 m from the floor) were assessed in every design scenario. The $E_{e,c}$ was measured for the four cardinal directions (N, E, S, and W). Horizontal illuminance and the $E_{e,c}$ data were collected on 216 reference points (0.30 m apart in x and y directions).

In Radiance, irradiance is assessed spectrally for three primary RGB channels. In order to convert the spectral irradiance triad (I_R, I_G, and I_B) to irradiance, every spectral irradiance value is multiplied to a coefficient as shown in the following formula [5]:

$$E_e = 0.265\, I_R + 0.670\, I_G + 0.065\, I_B$$

To implement the sensitivity of the human eyes for photometric measurements, e.g., illuminance, in Radiance the irradiance is multiplied by a conversion factor of K_R = 179 lm/W which is Radiance's own value for the luminous efficacy as shown in the following formula [7]:

$$E = 179 \frac{lm}{W} \cdot (0.265\, I_R + 0.670\, I_G + 0.065\, I_B)$$

To derive the $E_{e,c}$, the coefficients were adjusted as shown in the following formula [7]:

$$E_{e,c} = -0.034\, I_R + 0.323\, I_G + 0.558\, I_B$$

In addition to the illuminance and the $E_{e,c}$, glare discomfort was assessed using the Daylight Glare Probability (DGP) as a glare index that gives the most plausible results when daylight is concerned [8]. Glare assessment was carried out for two positions (midline point P1 at 1.2 m distance from the façade, and P2 at 1.2 m from the back wall) facing towards the window.

Evaluation criteria

The visual and non-visual effects of light were assessed based on the following evaluation criteria:

1) Space availability (%A) [9] as the percentage of the work plane area with either E > 500 lx or $E_{e,c}$[1] > 5 W/m^2,
2) $R_{1,2}$ as the ratio between the illuminance or the $E_{e,c}$ of two control points (P1 and P2) in the room,
3) DGP as the index with which the probability of discomfort glare assessed using the criteria defined in [8].

[1] The value for the $E_{e,c}$ is preliminary for comparison purposes only, since there is no assessment value available yet.

RESULTS AND DISCUSSION

Table 2 shows the influence of the design parameters, i.e. window size, GP_{ex} color and luminous reflectance on the visual evaluation criteria. In general, increasing the window size increases the space availability for the visual tasks and improves the illuminance ratio in the room. The GP_{ex} color does not influence the visual space availability, but its luminous reflectance does. For instance in the design with 50% WWR, compared to the base case (ρ = 20% grey) the visual space availability decreases by 29% for the black GP_{ex} (ρ = 0%) and increases by 55% for the white GP_{ex} (ρ = 85%). The influence of GP_{ex} color on the illuminance ratio is less than 2% while the influence of its luminous reflectance reaches up to 37% in the design with 10% WWR (GP_{ex} white).

WWR	**Ground plane**									
	Blue		**Green**		**Grey**		**Black**		**White**	
	%A	**$R_{1,2}$**	**%A**	**$R_{1,2}$**	**%A**	**$R_{1,2}$**	**%A**	**$R_{1,2}$**	**%A**	**$R_{1,2}$**
10% WWR	4%	9.6	4%	9.7	4%	9.7	4%	12.3	5%	6.1
50% WWR	29%	6.0	29%	5.9	29%	5.9	21%	7.4	45%	4.2
100% WWR	49%	4.9	49%	4.8	49%	4.9	42%	5.7	81%	3.8

Table 2: Influence of window size, GP_{ex} color, and luminous reflectance on the visual evaluation criteria

Figure 1 shows the distribution of $E_{e,c}$ over the floor plan for the four cardinal directions (room with 50% WWR; GP_{ex} white). The results show that the $E_{e,c}$ is lowest when the observer is facing the back wall and highest when facing the window. Data from the East and the West view directions are mirrored. In this paper, results related to the South view direction are presented as they show the highest influence.

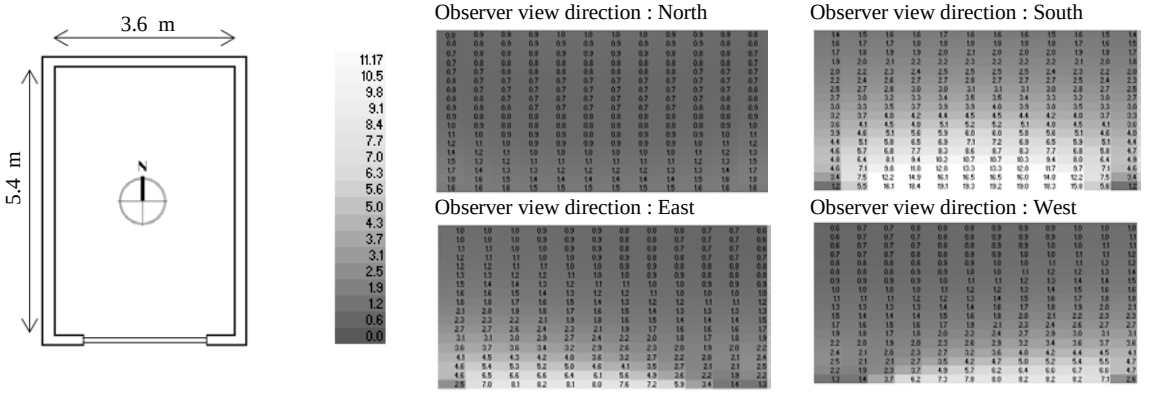

Figure 1: The distribution of $E_{e,c}$ over the floor plan of the reference office room with 50% WWR for the four cardinal directions (GP_{ex} white).

Table 3 shows the influence of the design parameters, i.e. window size, GP_{ex} color, and reflectance on the non-visual evaluation criteria. In general, increasing the window size increases the non-visual space availability and improves the $E_{e,c}$ distribution in the office room.

WWR	Ground plane									
	Blue		Green		Grey		Black		White	
	%A	$R_{c,1,2}$	%A	$R_{c,1,2}$	%A	$R_{c,1,2}$	%A	$R_{c,1,2}$	%A	$R_{c,1,2}$
10% WWR	7%	8.8	3%	10.0	3%	8.6	2%	7.9	4%	9.1
50% WWR	67 %	4.5	15%	5.4	17%	5.3	13%	5.4	33%	4.7
100% WWR	100%	3.0	35%	3.9	41%	3.8	31%	4.0	65%	3.6

Table 3: Influence of window size, GP_{ex} color, and luminous reflectance on the non-visual evaluation criteria for the South view direction.

The GP_{ex} color has a more pronounced influence on the non-visual evaluation criteria compared to its luminous reflectance. The influence of the GP_{ex} color on the non-visual space availability is higher than the $E_{e,c}$ ratio. Compared to the base case, the non-visual space availability decreases when the GP_{ex} is black and green, and increases when the GP_{ex} is blue and white. The highest influence on the non-visual space availability is observed when the GP_{ex} color is blue. Although the white GP_{ex} (ρ=85%) comparing to the base case resulted in a higher space availability, the magnitude of effects is not as high as compared to the blue GP_{ex} (ρ=20%). For instance, in the design with 50% WWR, the influence of the blue GP_{ex} on the space availability is 2 times higher compared to the white GP_{ex}. Compared to the base case, the largest increase on the non-visual space availability is observed in designs with 50% WWR.

Table 4 shows the influence of the window size, the GP_{ex} color, and luminous reflectance on the discomfort glare assessment for the reference points P1 and P2. As expected, changing GP_{ex} color, and luminous reflectance did not influence the DGP values a lot for overcast sky conditions. Most DGP values are within the imperceptible range (<0,30).

WWR	Reference points	Ground plane			
		Blue	Green	Grey	White
10% WWR	**P1**	0.19	0.19	0.19	0.20
	P2	0.03	0.03	0.02	0.05
50% WWR	**P1**	0.25	0.25	0.25	0.30
	P2	0.20	0.20	0.20	0.19
100% WWR	**P1**	0.28	0.20	0.28	0.36
	P2	0.20	0.25	0.20	0.22

Table 4: Influence of window size, GP_{ex} color, and luminous reflectance on discomfort glare assessed by DGP.

CONCLUSION

The influences of design parameters 'window size', 'GP_{ex} color', and 'GP_{ex} luminous reflectance' on (non)visual effects for different view directions have been investigated with respect to the three evaluation criteria: 'space availability', 'illuminance or $E_{e,c}$ ratio', and 'discomfort glare'.

In general, increasing the window size increases the *visual* and *non-visual* space availability and improves the illuminance and $E_{e,c}$ distribution in the office room. Although increasing window size increases the DGP values, most of the DGP values are within the imperceptible range.

View direction plays a critical role with regard to the *non-visual* effects on the observer. Facing the window tends to increase the chance of receiving sufficient $E_{e,c}$ at the eye.

Comparisons show reverse influence of the GP_{ex} color and luminous reflectance on the *visual* and *non-visual* effects of light. The highest influence on the *visual* space availability was observed when the white GP_{ex} (ρ=85%) was used. However, with regards to the *non-visu*al space availability, the color of the GP_{ex} (resulting from the spectral reflectance) shows a more pronounced influence compared to its luminous reflectance. Findings show that the *non-visual* space availability is highest when the GP_{ex} is blue. Such findings could lead to a suggestion of using bluish GP_{ex} and placing the work plane facing the window for the optimal non-visual effects of light at no expense to the visual effects.

REFERENCES

1. Gall, D.: Circadiane Lichtgrößen und deren meßtechnische Ermittlung. Proc. Of the Licht 54, pp 1292-1297, 2002.
2. Brainard G., Hanifin J., Greeson J., Byrne B., Glinkman G., Gerner E., Rolling M.: Action Spectrum for Melatonin Regulation in Humans: Evidence for a Novel Circadian Photoreceptor. Neuroscience, Vol 21(16), pp 6405-6412, 2001.
3. Thapan K., Arendt J., Skene D.: An action spectrum for melatonin suppression, evidence for a novel non-rode, non-cone photoreceptor system in humans. Physiology. Vol 535, pp 261-267, 2001.
4. Blattner, P.: Relating photochemical and photobiological quantities to photometric quantities. CIE TN 002:2014. Austria. 2014.
5. Ward G., Shakespeare R.: Rendering with Radiance: The Art and Science of Lighting Visualization, Morgan Kaufman Publishers, San Francisco, 1998.
6. van Dijk, D. and Platzer, W.: Reference office for thermal, solar and lighting calculations. swift-wp3-tno-dvd-030416, 2003.
7. Geisler-Moroder, D. and Dür, A.: Estimating melatonin suppression and photosynthesis activity in real-world scenes from computer generated images. Proc. of the CGIV 2010/MCS'10 5th European Conference and 12th International Symposium, pp 346-352, Joensuu, Finland. 2010.
8. Jakubiec J., Reinhart C.: The 'adaptive zone' - A concept for assessing discomfort glare throughout daylit spaces. Lighting Research and Technology, Vol 44, pp 149-170, 2012.
9. Mangkuto R., Aries M., van Loenen E., Hensen J.: Modelling and simulation of virtual natural lighting solution with complex views. Building Simulation, Vol 7, pp 563-578, 2014.

INDOOR AIR QUALITY INVESTIGATION IN A NATURALLY VENTILATED UNIVERSITY BUILDING, AIR CHANGE MEASUREMENT AND CALCULATION CASE STUDY

Alžběta Kohoutková[1]; Karel Kabele[2]

1: University Centre for Energy Efficient Buildings (UCEEB), Czech Technical University (CTU) Třinecká 1024, 273 43 Buštěhrad

2: Department of Microenvironmental and Building Services Engineering, Faculty of Civil Engineering, CTU in Prague, Thákurova 7, 166 29 Prague 6 - Dejvice

ABSTRACT

Indoor environment quality is characterized by thermal comfort, indoor air quality, lighting and many other parameters. According to the last trends of energy savings for building services operation and building envelope insulating, the minimum air change rate is evaluated and calculated. Ventilation system control is usually based on the CO_2 measured concentration. The air change rate is dependent on occupant behaviour. When occupants have just natural ventilation in the room then they are not able to control the air change rate. A pilot study was performed in order to figure out a main environmental pollutant during unoccupied time. This study was performed to identify the main IAQ pollutant which may be used to specify a minimum ventilation rate for office buildings and school buildings. How should ventilation system control work – based on which pollutant? The study continues and develops the Clear–up project carried out at the CTU during years 2008 – 2012. The indoor air quality is analysed and evaluated in an office building of a university based on concentration measurements of chemical pollutants: formaldehyde, carbon dioxide and total volatile organic compounds (TVOC). The office building envelope has been retrofitted recently. The paper is focused on the question how the IAQ in an office is influenced by a natural ventilation rate and by the newly retrofitted facade. This paper is focused on experimental description of investigated pollutants in a naturally ventilated room without occupants. The aim of the paper is to determine the most important pollutant to specify ventilation requirements. The measurement was carried out during a weekend period without occupant presence. The ventilation rate was calculated from measured concentrations of a tracer gas SF_6. The air change was calculated as 0,108 [1/h]. The measured pollutant values are presented in charts. The main results are expressed by percentage frequency of measured concentrations divided by permissible exposure limits (PELs). In order to save energy, infiltration through the building envelope is negligible. The office is not equipped with a ventilation system, which has a negative impact on IAQ in the room. The user's personal belongings can also cause higher pollutants concentration and can cause health problems. The conclusion is to find a way to ventilate a room during unoccupied hours.

Keywords: air change, indoor air quality, IAQ measurement, IAQ evaluation, natural ventilation

INTRODUCTION

According to the last trends of energy savings in building services operation and building envelope insulation, the minimum air change rate is calculated considering heat retention. Ventilation system control is usually based on the CO_2 measured concentration. When there is just natural ventilation in a room, it is not always possible to control the air change rate. The

air change rate is dependent on the occupant behavior. This paper is focused on experimental description of the investigated pollutants in a naturally ventilated room during unoccupied hours. The aim of the paper is to determine the most important pollutant to specify ventilation requirements.

IAQ VENTILATION RATE AND MEASUREMENT CASE STUDY

Measurement of pollutants and tracer gas concentrations

The measurement was carried out by Innova 1412 (Innova, Denmark). This device works on the photoacoustic spectroscopy principle. The following gases were selected as IAQ parameters and were measured: formaldehyde, carbon dioxide and TVOC (total volatile organic compounds). (Fig. 1, 2).

Tracer gas selection, dosing and measurement

Tracer gas techniques are typically based on active dosing of tracer gas into the tested zone which is not convenient in occupied dwellings. Another possibility is the use of carbon dioxide as a tracer gas. Unfortunately the office was occupied during the a. m. hours and the CO_2 concentration would be dependent on that. Carbon dioxide is not usually used to measure direct ventilation rate. [1] The tracer gas SF_6 was dosed into the investigated office on Friday in the afternoon hours. The concentration uniformity was provided by the use of mixing fan. The tracer gas concentrations were measured. (Fig. 2) According to the EU directive [2], it is forbidden to sell SF_6 gas to unauthorized users and labs and use it. This measurement was carried out before this directive became effective.

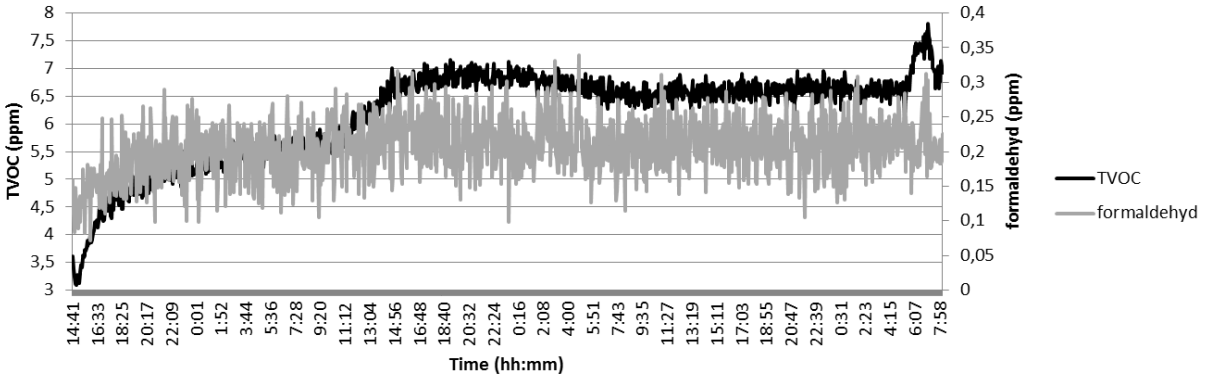

Figure 1: Measured concentrations of formaldehyde and TVOC (total volatile organic compounds).

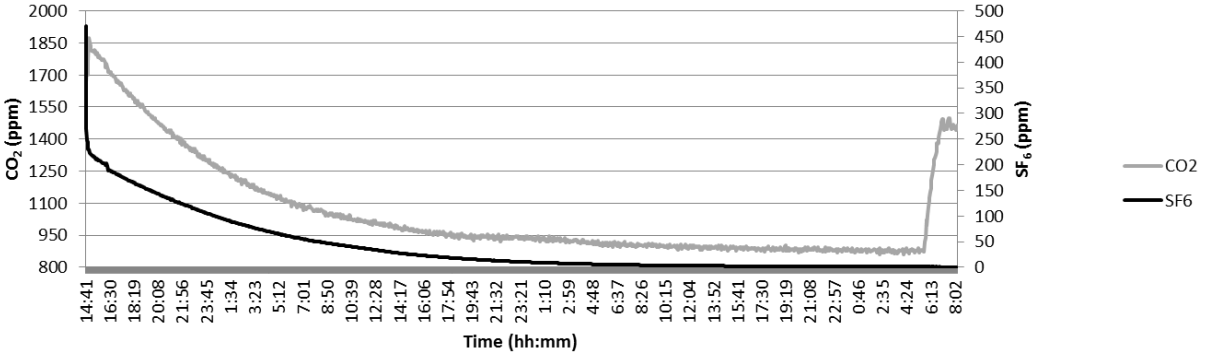

Figure 2: Measured concentrations of carbon dioxide and SF_6 tracer gas.

VENTILATION RATE CALCULATION

The building envelope was recently retrofitted. New air – tight windows were installed together with the thermal insulation. The investigated office is naturally ventilated and the question was if the minimum ventilation rate requirement for unoccupied hours is fulfilled. The required value is according to the standard [3] 0, 1 (1/h). The ventilation rate through the building envelope was calculated by the concentration decay method. This method is one of the so called Age-of-Air methods. According to [4] the used Age-of-Air measurement equation was:

$$AC = \frac{\int_0^{\infty} C(\tau) d\tau}{C(0)} \left[\frac{1}{h}\right] \quad (1)$$

where

AC air change rate [1/h]

C (τ) measured concentration at τ = ∞ [ppm]

C (0) measured concentration at τ = 0 [ppm]

τ time of measurement [h]

The air change rate through the envelope was calculated as 0,108 (1/h) which meets the requirements.

IAQ EVALUATION

In the working environment different risk factors may be present, which also include chemical pollutants. In the Czech Republic, the concentration limits of pollutants are mandatorily prescribed in the working environment. [5] The following equation represents how IAQ can be evaluated [6]:

$$\frac{C_{HCHO}}{PEL_{HCHO}} + \frac{C_{CO}}{PEL_{CO}} + \frac{C_{TVOC}}{PEL_{TVOC}} \leq 1 \quad (2)$$

where

C measured gas concentration [ppm]

PEL permissible exposure limit [ppm]

The Evaluation of IAQ can vary from country to country. In the following Tab. 1, different PEL and STEL values are given for different averaging times. World Health Organization also has guidelines applicable for Europe. [7], [8]

Table 1: Occupational exposure limits for Germany, Czech Republic and Europe (WHO).

			Czech Gov. Regulation no. 93/2012			
OELs for Germany			**PEL**	**PEL**	**STEL (NPK)**	**STEL (NPK)**
substance	**OEL value mg/m^3**	**Averaging time**	**mg/m^3**	**ppm**	**mg/m^3**	**ppm**
formaldehyde	0.12	Not determined	0.5	0.37	1	0.747
TVOC (total volatile organic compound)	0.2 – 0.3	Not determined	-	-	-	-
WHO Air Quality Guidelines for Europe (2010)	**Guideline values for individual substances**		**PEL**	**PEL**	**STEL (NPK)**	**STEL (NPK)**
substance	**Time – weighted average value mg/m^3**	**Averaging time**	**mg/m^3**	**ppm**	**mg/m^3**	**ppm**
Carbon monoxide	7	24 h	-	-	-	-
Carbon monoxide	10	8 h	30	24	150	120
Carbon monoxide	35	1 h	30	24	150	120
Carbon monoxide	100	15 min	30	24	150	120
formaldehyde	0.1	30 min	0.5	0.37	1	0.747

RESULTS

In the Table 1 there is a comparison of obtained results. The air changes for CO_2, TVOC and formaldehyde were calculated. The air change through the building envelope was higher than the air change to get rid of CO_2 concentration and TVOC concentration. The air change for formaldehyde is a negative value. That means the volume should not be ventilated because of outside concentration is higher than inside concentration.

DISCUSSION

This measurement was taken just for the above mentioned pollutants. Therefore we cannot predict other possible pollutants concentration. The whole measurement was carried out with completely closed windows however modern air-tight windows also have the "micro – ventilation" possibility which would change the air change rate significantly. The measurement was influenced by an unexpected occupant presence before the end of it. Therefore there are peaks for some values in the measurement. In the investigated office there was not a single flower. It would be interesting to solve this problem for the new passive houses standard.

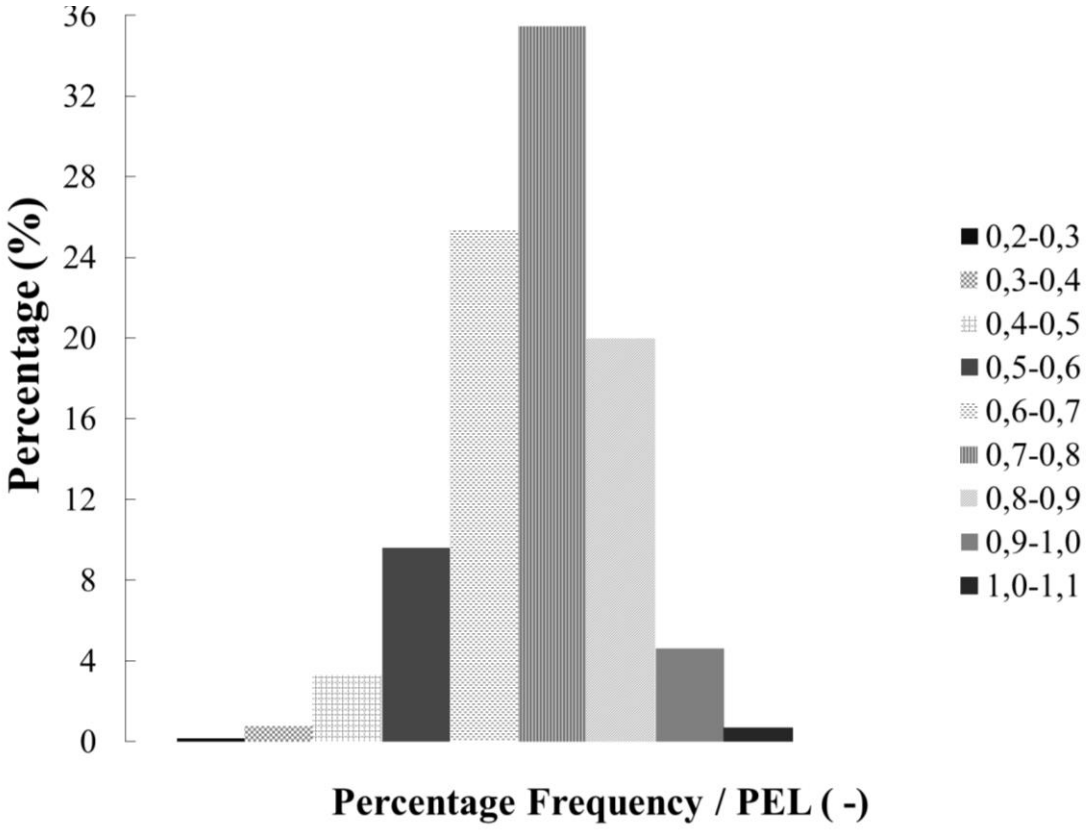

Figure 3: Percentage frequency of values present in the above mentioned ranges.

CONCLUSION

The aim of the experiment was to find a crucial IAQ pollutant for room ventilation without occupant presence. It is a complicated problem with many changing boundary conditions. Which pollutant should be the most important? According to the measurements and calculations the air change was calculated as 0,108 (1/h). The other air changes to ventilate the whole investigated office and get rid of pollutants were: 0,015 1/h (to get rid of the CO_2 concentration), 0,021 (TVOC) and, -0,012 (formaldehyde) which says that the outdoor concentration is higher than the indoor concentration. That brings the dilemma if ventilating is indicated or not. The changing outdoor boundary conditions (location of the building close to highways, city centre during rush hours) are the main deciding factors for ventilation of the office during unoccupied time.

ACKNOWLEDGEMENT

The authors wish to thank for financial support the following grants: student grant SGS15/130/OHK1/2T/11 and European grant OP VaVpl no. CZ.1.05/2.1.00/03.0091 – University Centre for Energy Efficient Buildings.

REFERENCES

1. Štávová, P.: Experimental Evaluation of Ventilation in Dwellings by Tracer Gas CO_2, Dissertation thesis, CTU in Prague, 2011.
2. Regulation on fluorinated greenhouse gases. Regulation (EU) No. 517/2014 of the European Parliament and of the Council of 16 April 2014. Brussels: Official Journal of the European Union, 2014.
3. CSN 73 0540:2002. [Thermal protection of buildings] in Czech. Prague: Czech Standards Institute, 2002.
4. Innova Air Tech Instruments. Ventilation Measurements And Other Tracer – gas Applications, Appendix A, Age of Air Measurement Equations, Concentration decay method: Innova booklet. p. 29, 1997.
5. Government directive no. 93/2012. Occupational Health Conditions. Prague: Czech Standards Institute, 2012.
6. Drkal, F.; Zmrhal, V.: [Ventilation] in Czech. Faculty of Mechanical Engineering. CTU in Prague, p. 31. ISBN 978-80-01-05181-8. Prague: CTU Publisher, 2013.
7. EN 14412:2004. Indoor Air Quality, Diffusive samplers the determination of concentrations of gases and vapours: Guide for selection, use and maintenance. London: British Standard Institute, 2004.
8. WHO Guidelines for Indoor Air Quality: Selected pollutants [online]. World Health Organization. Regional Office For Europe. Copenhagen, 2010. ISBN 978-92-890-0213-4. http://www.euro.who.int/__data/assets/pdf_file/0009/128169/e94535.pdf (accessed Jun 8, 2015)

ACOUSTIC FALSE CEILING IN WIDE ROOMS, REALIZED BY AN INNOVATIVE TEXTILE SYSTEM

F. Leccese[1], V. Palla[1], M. Rocca[1], G. Munafo'[2], M. Martino[2], S. Lapouge[3]

1: Dept. of Energy engineering, Systems, Territory and Constructions (DESTeC), University of Pisa, 56122 Pisa, Italy.

2: Dept. of Civil and Industrial engineering (DICI), University of Pisa, 56122 Pisa, Italy

3: Profil Tensions System Europ Ltd, 1203 Geneve, Switzerland.

ABSTRACT

The aim of this article is the study of wide rooms' acoustic false ceilings. In order to improve indoor acoustic comfort, it is possible to install an acoustic false ceiling. Many technical solutions are used to improve the inner room quality in terms of reverberation time and speech intelligibility. Restaurants and dining halls often can have acoustic problems caused by uncontrolled background disturbing noise. Indoor comfort can be seriously impaired in crowded rooms with many speakers, such as in restaurants and dining halls: the background noise produced by people talking damages the speech intelligibility level. If the speaker cannot be heard by his listener, he will speak louder. The speaker's increasing voice power will gradually intensify the background noise producing a domino effect (cocktail party effect).

In this case study we show the use of a brand new textile false ceiling system. This solution has just been installed in the Centre Hospitalier Universitaire Vaudois (Lausanne) new restaurant (1800 m^2) that can host 800 people. The innovative textile system, designed for this project, is composed of an aluminium structure within a shaped rock wool panel, enfolded by stretched EPS "acoustically transparent" fabric. This system, suspended from the ceiling and held by metallic lateral supports, improves the room acoustic quality, creating a nice dynamic effect as well. The installation of this system began in July 2014 and was completed in April 2015. We used the CATT-Acoustic software to analyse the room acoustic behaviour, the reverberation time and speech intelligibility.

Keywords: acoustic false ceiling, textile false ceiling systems, indoor acoustic comfort, speech intelligibility, reverberation time.

INTRODUCTION

Crowded rooms, such as restaurants and dining halls, often can have a low acoustic indoor quality. Disturbing noise produced in these rooms compromises customers' relaxing moment and the main room function. The acoustic issue of a workspace must be studied during project planning and design, in the same way as function and aesthetic tasks.

A comfortable environment gives to employees an optimum performance and makes them feel more predisposed to work. Workspace and relaxing places comfort is given by indoor environmental and acoustics quality. The interaction between the people, the room and the activity decides the room acoustic comfort, which contributes to the human well-being [1-3]. The room bigger and crowded the room, the more it could have acoustic problems: the size of the room and the number of the people inside threaten the indoor quality. One solution can be to install an acoustic false ceiling that absorbs the sound waves, reducing the reverberation in the room. There are many acoustic systems that can work as porous material or vibrant

membrane; it depends on the material origin and the way that it is installed. The best system to choose is the one which absorbs the most, but , the solution's appeal is also important, especially in wide places [4-5].

In this research we want to study in deep the indoor acoustic comfort in wide rooms, based on a "case study", in which the indoor quality has been improved using an innovative textile system. In order to improve uncomfortable wide room acoustics, in terms of reverberation time and speech intelligibility, we can act on the ceiling, installing some kind of acoustic false ceiling.

CASE STUDY

In this case study we show a brand new textile false ceiling system. This solution has just been installed in the Centre Hospitalier Universitaire Vaudois (CHUV- Lausanne) new restaurant, see Figure 1. The project is part of a general renovation of the Centre Hospitalier Universitaire Vaudois, incorporated in a new local cantonal planning, called "PAC315", that includes eight big projects for the "Cité Hospitalière".

Figure 1: Google earth view of the CHUV (left); CHUV main entrance (centre); CHUV back side entrance (right).

The CHUV's Technical Direction's main purpose has been to give employers a comfortable relaxing place in terms of natural lighting and acoustic comfort. Natural light it is very important for human beings; the restaurant has three glass curtain walls that have a low indoor acoustic performance and low soundproofing. The 1800 m^2 (8100 m^3) restaurant can contain 800 people. The ceiling was the only surface that could be acted on, using a false ceiling system, with a good acoustic performance and pleasing appearance.

The Hospital Direction needed a false ceiling solution that could absorb as much as possible the sound waves. A traditional "plane" false ceiling placed in a wide and flat (around 4m) room can produce an oppressive feeling to customers. For these reasons the CHUV Main Direction called for tenders for the executive project and installation of an acoustic false ceiling solution. The project winning concept was to realize a well designed and dynamic structure, which would change its aspect on the restaurant width, length and height, in order to give customers a nice place to eat and relax.

The installation of the system began in July 2014 and was completed at the end of April 2015 (Figure 2).

Figure 2: Exterior view of CHUV installation (left); Indoor view at the end of the first step of the installation (right).

INNOVATIVE TEXTILE ACOUSTIC SYSTEM AND ITS APPLICATION

A very important parameter in the workplaces is the comfort, so it was important to project a system that could reduce the room reverberation time, considering the size and the crowding of the room. This innovative textile system (designed by Profil Tension System Europ Ltd and "Meier + associés architectes", Genève) is formed by an aluminum structure, called "sail", within shaped rock wool panel; everything is enfolded by a stretched EPS "acoustically transparent" fabric (Figure 3). These "sails" are suspended from the ceiling and held by metallic lateral supports. These structures have a different shape, in order to create a dynamic effect in the room and improve the room acoustic quality. Four "sail" types have been designed (Figure 4): the "V0", the "V30", the "V50" and the "V80". The number following the "V" means the angle degrees between the sail and the horizontal plan.

Figure 3: Sail prototype covered with fabric (left); Sail prototype without fabric (centre); photorealistic view of the restaurant (right).

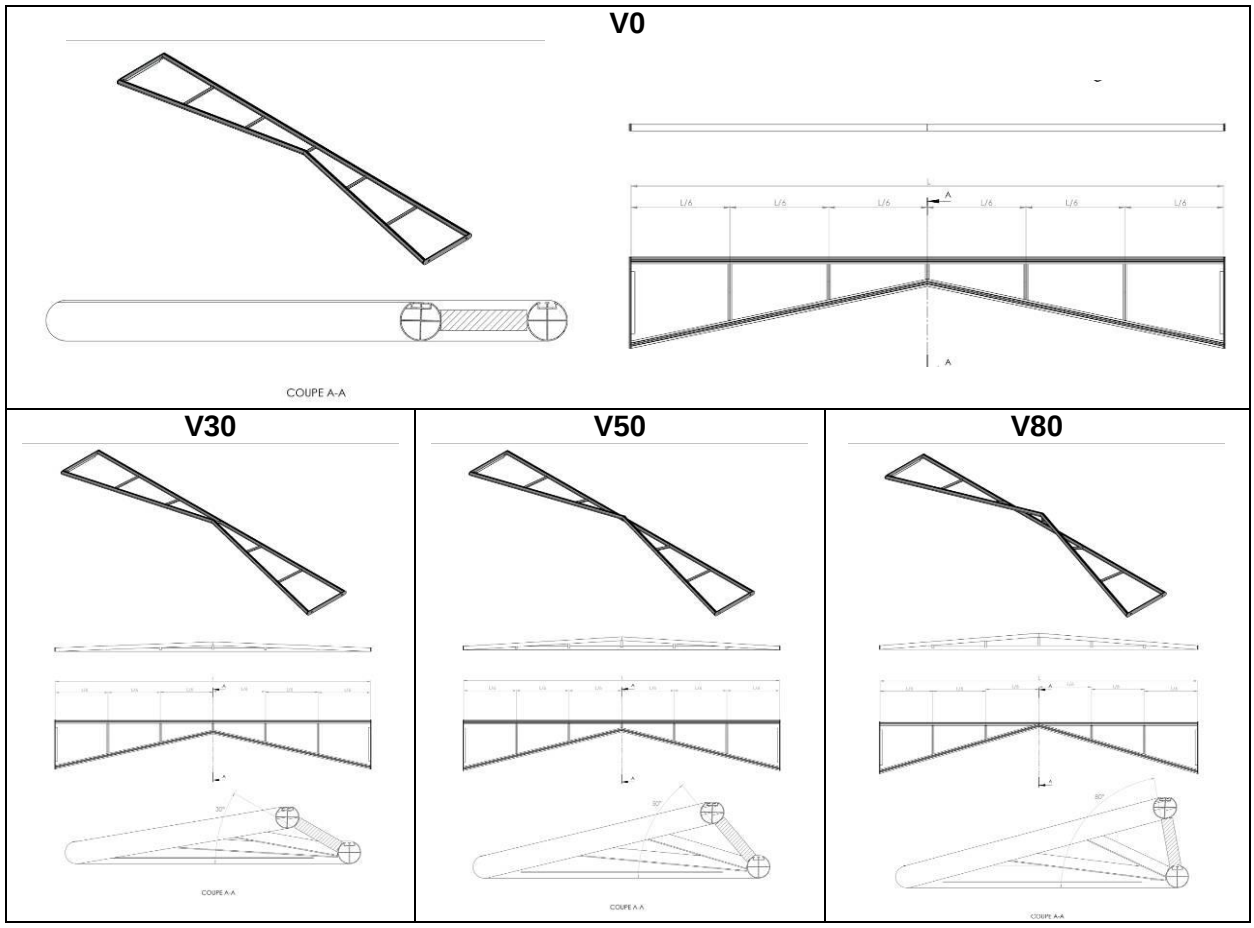

Figure 4: "V0"sail details (upper); "V30"sail details (down left); "V50"sail details (down centre); "V80"sail details (down right).

To fit the entire ceiling surface the "Sails" were designed with different lengths. The aluminum structure shape has an almost circular hollow section, to which are welded "T" profiles, necessary to hold rock wool panels. In the circular section there are two metallic stiffenings, which hold two PVC grips, called "Sollto Grip" (patented by Profil Tension System). These grips can induce tension in the fabric, giving the panel a uniform finishing (Figure 5). Rock wool soundproofing shaped panels (Figure 6) are fitted in the aluminum frame.

The "Sails" have a double exposed absorption surface giving a high acoustic performance (Figure 6). "Sails" are covered by an acoustically transparent fabric, extensible and can model itself on the shaped panel, hiding what is inside.

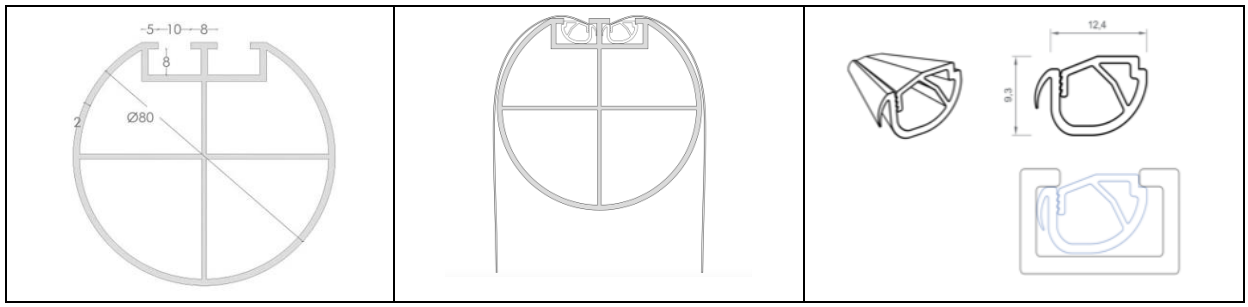

Figure5: Details of the aluminium structure and "Sollto Grip".

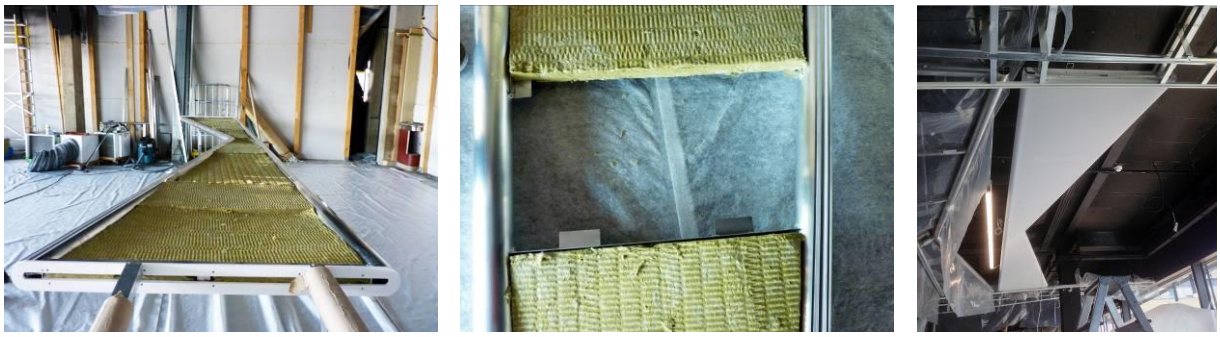

Figure 6: Views of the shaped rock wool panels (left and centre); sail covered with EPS fabric (right).

The false ceiling system is made of 237 "sails", different in dimension and type, suspended by lateral metallic rails, connected to the structural columns. The dynamic effect was created putting the less sloping ones in the restaurant perimeter and the most sloping ones in the middle. There were installed: 85 elements type "V0", 40 type "V30", 52 type "V50" and 60 type "V80" (Figure 7). This project was integrated with lighting and air emission systems.

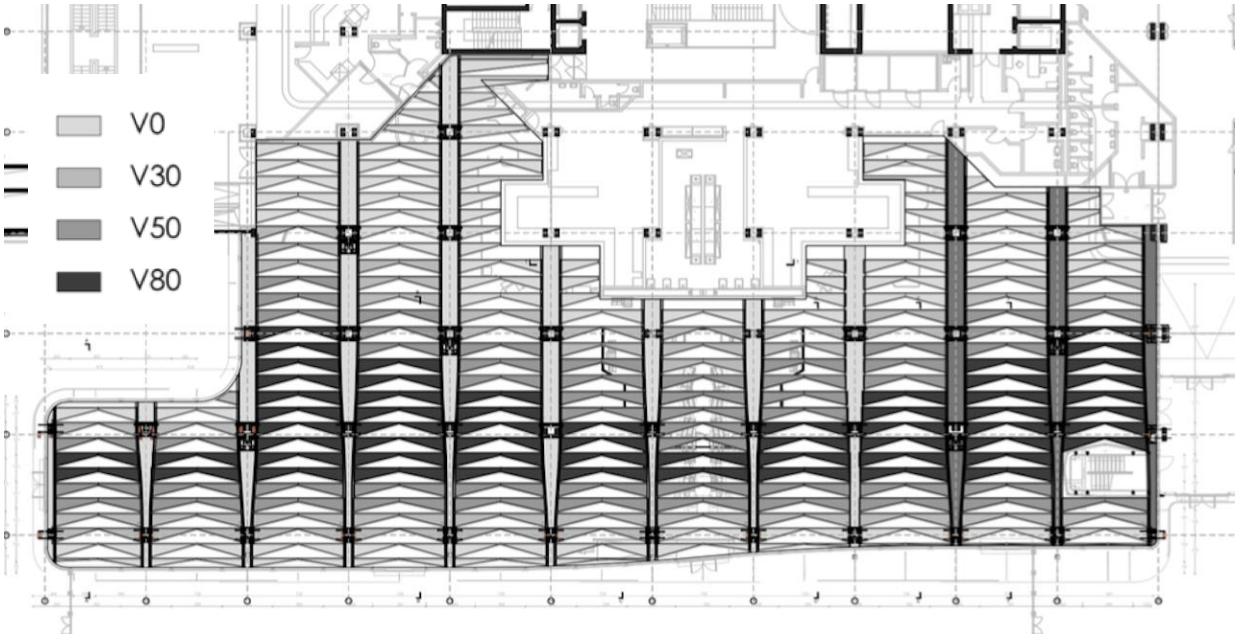

Figure 7: Plan of the restaurant and distribution of the sails in the room.

ACOUSTIC ANALYSIS

The main purpose of the acoustic design was to make the room the most absorbent on the ceiling as we could, in order to have a low reverberation time and a good speech intelligibility. Table 1 (left) shows sound absorption coefficients of the materials in the restaurant. We studied the room acoustic behavior with CATT-Acoustics software, and we verified that the sound field in the room, using the textile system, satisfied the reverberation time optimal value, according to the Sabine, Eyring and Arau-Puchades' formulas and the Ray tracing method. We checked also the speech intelligibility. The reverberation time limit value, depending on the volume and the destination use (speech), is around 1.1 sec. Table 1 (right) shows the acoustic analysis results. The system is very performing and can improve the indoor comfort, reducing the reverberation time below the limit value. In order to analyze the room speech intelligibility, we used the software. We placed one speaker (male voice with normal vocal effort) and one receiver per table, far each other 0.7 m and at a height of a 1.2

m. We evaluated the speech intelligibility index (STI) in three different percentage of people sitting in the dining hall: 30%, 50%, and 70%. The simulation results show that for each percentage of occupation, the medium values of STI achieves an appropriate levels of intelligibility (STI>0.45). In particular: for an occupation of 30% (222 people, 37 speakers) we obtained STI=0.67; for an occupation of 50% (360 people, 60 speakers) we obtained STI=0.58; for an occupation of 70% (528 people, 88 speakers) we obtained STI=0.54.

Absorption	**Frequency (Hz)**							**RT**	**Frequency (Hz)**						**θm**
Materials	**m^2**	**125**	**250**	**500**	**1000**	**2000**	**4000**	**Methods**	**125**	**250**	**500**	**1000**	**2000**	**4000**	
Linoleum	1800	0.02	0.02	0.03	0.03	0.04	0.04	Sabine(1)	1.77	0.56	0.43	0.39	0.41	0.41	0.66
Plaster	561	0.02	0.02	0.03	0.03	0.03	0.03	Arau-Puchades(1)	1.67	0.6	0.44	0.41	0.45	0.44	0.67
Mineral wool	1800	0.18	0.63	0.85	0.97	0.93	0.96	Sabine(2)	1.85	0.61	0.46	0.43	0.44	0.41	0.70
Glass	605	0.18	0.06	0.04	0.03	0.02	0.02	Eyring(2)	1.74	0.49	0.34	0.31	0.32	0.30	0.58
Rock wool	1422	0.18	0.77	1.01	1.04	0.97	0.97	Ray tracing(2)	2.31	1.09	0.49	0.56	0.48	0.44	0.90
(1) results of the hand calculation; (2) results of the software simulations.															

Table 1:Sound absorption coefficient of the materials (left) Values of reverberation time (RT) according to the Sabine, Eyring and Arau-Puchades' formulas and the Ray tracing method (right).

CONCLUSIVE REMARKS

In this research an innovative false ceiling system has been studied. This kind of system, adaptable for design and acoustic performances, has been used for the false ceiling installation in the Centre Hospitalier Universitaire Vaudois restaurant. It is very important to have comfortable working places, so it is important as well to design a system that could reduce the room reverberation time. The system, designed for the "case study", is made of suspended shaped panels and is high performing because of its double exposed surface. We have studied in depth the restaurant acoustics with CATT-Acoustic software simulation in order to see how the system worked in terms of reduction of reverberation time, using the Sabine, Eyring and Arau-Puchades' formulas and Ray tracing simulation. Results show that the system, in addition to having a nice and unusual appeal, can really improve the indoor comfort, reducing the reverberation time, even if the room is crowed and characterized by reflective surfaces.

REFERENCES

1. Egan M.D.: Architectural Acoustics, J.Ross, Plantation FL (USA), 2007.
2. Leccese F., Tuoni G., Silipo M.: The "cocktail party effect" and the acoustic of restaurants. A case study. Proc. of the 34° National Congress of the Italian Association of Acoustic (AIA), Florence (I), 2007, (in Italian).
3. Leccese F., Salvadori G., Francesconi M.: Analysis of acoustic requirements of a small hall of a theatre according to the coupling factor with the stage. Proc. of the Acoustics 2012 Conference, pp. 931-936, Nantes (F), 2012.
4. Palla V.: Innovative textile system for false ceilings realization in wide rooms. Analysis of acoustics, technological and safety skills: The case study of the Centre Hospitalier Universitaire Vaudois restaurant (Lausanne, Switzerland), Master Thesis in Building Engineering (Tutors: F. Leccese, G. Munafò, M. Martino, S. Lapouge), Faculty of Engineering, University of Pisa (I), 2014.
5. Leccese F., Palla V., Rocca M., Munafò M., Martino M., Lapouge S.: On the choice of acoustic false ceiling in wide rooms based on value analysis. 22th International Congress of Sound and Vibration, Florence (I), July 2015.

EVALUATION OF DIFFERENT ENERGY-EFFICIENT REFURBISHMENTS

Tanja Osterhage, Davide Calì, Rita Streblow and Dirk Müller

RWTH Aachen University, E.ON Energy Research Center, Institute for Energy Efficient Buildings and Indoor Climate, Mathieustraße 10, 52074 Aachen

Corresponding email: tosterhage@eonerc.rwth-aachen.de

ABSTRACT

In Germany, three-quarters of all existing buildings were built before 1979 and have mostly only been minimally retrofitted. Despite numerous policy incentives the annual retrofitting quota remains at a low 1.1%. In refurbished buildings often predicted energy consumption is lower than the real energy consumption: this phenomenon is known in literature as energy performance gap. The occupants' behaviour is considered to be the main cause for it. To validate the efficiency of advanced energy efficient retrofitting, three residential buildings built in South Germany in the 1950s were retrofitted and monitored, to qualitative and quantitative evaluate the energy performance gap. The refurbishment included structural as well as engineering system aspects. Seven different retrofit designs were implemented. A high time resolution monitoring system provides information about the occupants' behaviour, the technical functioning of the engineering systems and allowing faults' detection.

Initial results from the field test support the findings by other research institutes that occupants who were in badly insulated buildings prior to the retrofits behave much more economically and energy aware than those in energy efficient buildings.

Further evaluation of the energy consumption levels shows clear discrepancies between the buildings retrofitted with different layouts. Two of the seven retrofit layouts consume less heating energy than expected while the other layouts need more heating energy than expected. The different occupants' behaviour regarding the floor heating seems to be the driver of this discrepancy. For all retrofit layouts, hot water consumption as well as the distribution and storage losses remains almost constant throughout the year. While the consumption of domestic hot water, measured at apartment level, is very similar for all the retrofit layouts, huge differences are identified for the distribution losses.

Keywords: renovation, field test, energy saving ordinance, user behaviour, rebound effect

INTRODUCTION

About 40% of final energy consumption in Germany accounts for households. About 70% of the buildings in Germany were built before 1979 and therefore before the first heat insulation ordinance [1]. The potential of this sector in terms of primary energy savings is correspondingly high. Therefore, the adopted "Aktionsprogramm Klimaschutz" (Action Program Save the Climate) of the federal government focuses on the renovation of buildings. In conjunction with the "Nationaler Aktionsplan Energieeffizienz" (NAPE, National action plan for energy efficiency) the energy efficiency in buildings is regarded as an important basic point to achieve climate change targets by 2020 [2]. To exploit the potential in the building sector, the federal government provides incentives to implement energy efficiency measures in order to double the annual rate of renovation of narrow 1.1% to 2% [1]. The analysis of various central and decentralized domestic hot water systems, heating and ventilation systems,

in terms of energy consumption and user behaviour, after an extensive renovation process is the focus of the here presented ongoing research project.

METHOD

In the study area three blocks from the 1950/60th were refurbished. Each block has three entrances with five floors. Over the five floors 10 apartments are located built specular to the stairs. The roof and the cellar of the buildings are not heated. For the comparison of different renovation strategies, seven retrofit layouts are implemented (see *figure 1* left). While block 1 has only one retrofit layout for all entrances, one layout per entrance is implemented for block 2 and 3.

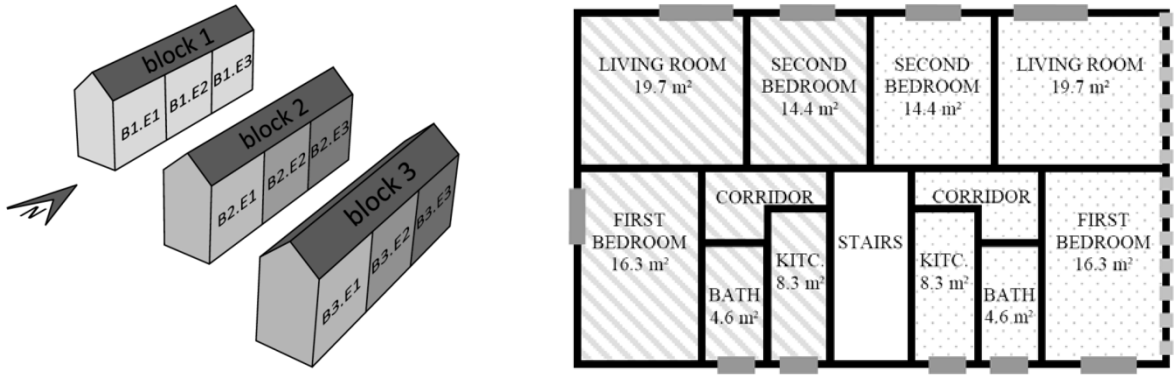

Figure 1: Overview of the situation and different refurbishments plus qualitative layout of one floor of the first building of each block (KITC. is the Kitchen)

For block 1 the external wall is equipped with 16 cm thermal insulation (thermal conductivity 035 means WLG 035), plastic windows with double glazing (U_w = 1.3 W/(m²K)), an insulation (WLG 035) of the top floor ceiling (16 cm) and the basement ceiling (7 cm). Block 1 is connected to the district heating network (primary energy factor 0.49 [3]). The domestic hot water is produced centralized (with circulation). Exhaust ventilation has been built as following: moist-controlled slots for fresh air supply are installed in the window frame. The exhaust air is extracted in kitchen and bathroom.

In block 2 (E1 to E3) a retrofit layout per block entrance was realized. The building construction refurbishment for B2.E1 and B2.E3 do not differ from each other. B2.E2 has passive house windows with a triple-insulating glazing, thereby resulting an u-value of 0.8 W/(m²K) for the window (so called “passive house windows”). The outer walls are provided with 16 cm insulation (WLG 022), the top floor ceiling is covered with 16 cm and the basement ceiling with 8 cm of insulation (WLG 024). District heating is also planned for the heating of the block 2. B2.E1 disposes of radiators with decentralized heating pumps. The domestic hot water is provided by decentralized fresh water stations. B2.E1 has also decentralized window ventilation systems with heat recovery. For kitchen and bathroom an air exhaust system is provided, and opening slots are installed on the windows’ frames. For B2.E2 a central hot water system with buffer storage is installed. The needed fresh air is done through central exhaust ventilation system in kitchen and bathroom. The decentralized supply air comes over the window frame slots. The rooms are heated via compact radiators with small heating pump installed in each radiator. In B2.E3 floor heating was provided for the rooms. The domestic hot water production and ventilation does not change compared to B2.E2 except for the manufacturers' of the installed products.

The constructional renovation for B3 has the same average U-value of 0.165 W/(m²K) as for B2. The redevelopment is based on the renovation of the exterior walls of a sandwich

construction with vacuum insulation panels (WLG 008). The top floor ceiling and the basement ceiling are retrofitted as in B2. B3.E1 and B3.E2 have passive house windows and B3.E3 standard double glazing windows. For B3 different heat pump systems are used. In B3.E1 and B3.E2 heat pumps with CO_2 probes are installed. In B3.E3 an air source heat pump in combination with an exhaust air heat pump is used. In B3.E1 a floor heating, in B3.E2 an air heating and in B3.E3 a ceiling heating deliver the heat to the rooms. The necessary exchange of air in B3.E1 is generated by centralized ventilation with heat recovery devices installed in each apartment. For B3.E2 the ventilation is done in combination with the air heater. In B3.E3 demand-controlled supply air elements in the window frames, in combination with exhaust elements in kitchen and bath, supply the rooms with the necessary exchange of air. The domestic hot water is produced locally via freshwater stations (produced by different manufactures) for each entrance. [4, 5]

To verify the real achieved energy savings, a high-resolution monitoring system for rooms, apartments and engineering system has been installed. The monitoring includes the recording of the indoor air quality, indoor air temperature, relative humidity, window position and daylight in each room of block 2 and block 3. The energy flows of the installed engineering system (heating, domestic hot water, ventilation) from generation, storage and distribution are recorded. The monitoring system collect the data with an interval of one minute, for a total of ca. 6 million data point collected each day.

RESULTS

Study of thermal offsets inside the building and across the thermal envelope

With each amendment of the energy-saving ordinance [6] more stringent requirements for thermal insulation of buildings are demanded. In the case of a building renovation, the maximum heat transfer coefficient of the outer walls is fixed at 0.24 W/(m²K). Generally the internal walls of two adjacent apartments do not get any insulation. This raises the question whether the heat losses or gains of an apartment for the neighbouring apartment will have a significant impact on the total heating requirement of each apartment. For the analysis of the thermal offset within and across the thermal envelope a dynamically computing program language Modelica® is used to generate the buildings' dynamic models.

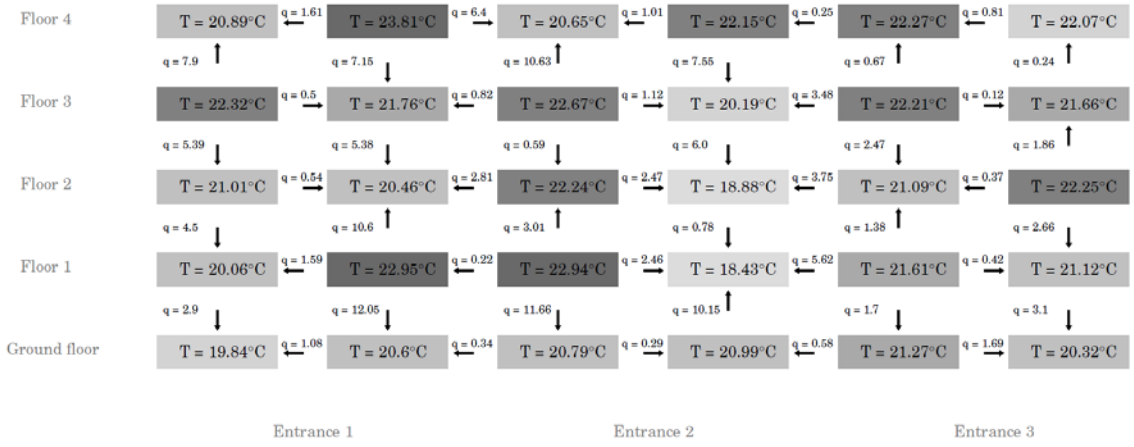

Figure 2: Heat transfers between the apartments in block 2

Due to the temperature difference of two adjacent apartments (or between apartment and other confining zones such as the staircase, the cellar or the roof) a heat shift can occur inside the thermal envelope of a building. In *figure 2* the level and direction of the transmitted heat between the apartments, for the heating season, is shown for one of the blocks (to guarantee the privacy of the tenants the block number and the year of the heating season are omitted).

The apartments are represented by colored rectangles. The color of the rectangle is determined by the measured average interior room temperature during the heating period. Dark gray stands for high, medium gray for medium and light gray for low average indoor temperatures. The black arrows indicate the heat-flow in kWh per square meter of living space and its corresponding direction.

Due to the larger transfer surface, at approximately same temperature difference, the heat flows transmitted between the different floors are larger than between the two adjacent apartments on the same floor. It is noticeable that, as expected, there are apartments (with relatively high indoor temperature) that only lose their heat, giving this to the neighbors. At the same time some apartments (low indoor temperature) collect the heat of all the neighboring apartments. In *figure 2* the heat shifts between the apartments and the staircase are not shown. The staircase is parameterized in the simulations with a constant temperature of 17 °C. In this way, the temperature of the housing space is always higher than the selected temperature of the staircase: Due to this temperature gradient, the staircase collects the heat from all the apartments.

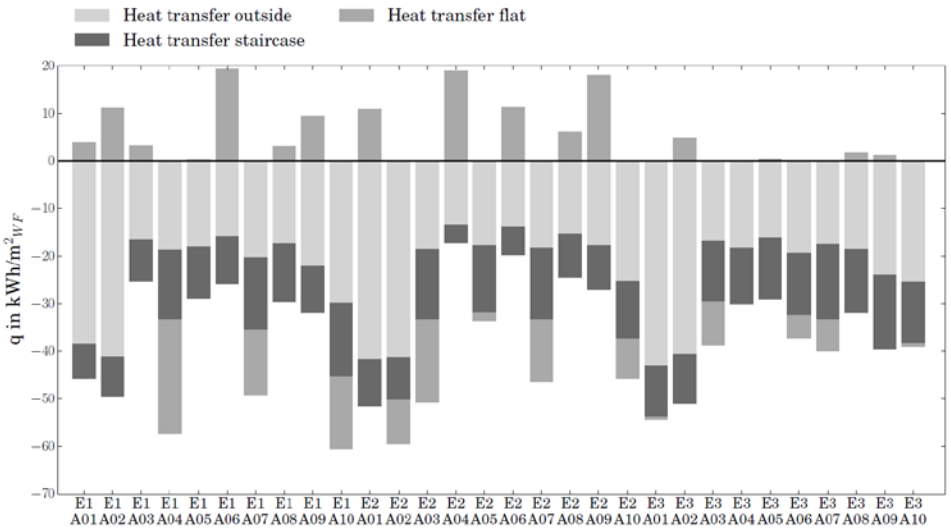

Figure 3: Comparison of the heat transmission per apartment based on the living space for block 2

In *figure 3* the specific heat shifts in kWh/m²$_{\text{floor space}}$ per apartment, compared to the living space, are covered for B2. The light gray bars indicate the heat transmitted over the external surfaces; the medium gray columns show the heat transmitted to the neighboring apartments and the dark gray columns indicates the heat transmission to the staircase. In comparison with the other apartments an increased heat loss to the ground floor (A01 and A02) and to the roof (A09 and A10) is evident. The reason for this is the larger heat-transferring surface to the outside. The heat shift over the walls to the neighboring apartment is not equally distributed. Some users will benefit significantly from the heating characteristics of adjacent apartments, while other users have high losses to their neighbors. In some cases, the thermal displacements to neighboring dwellings are negligible.

The analysis of the thermal shift within the building shows that the heat gains by the neighboring dwellings may compensate partially the losses by transmission to the outside and into the staircase. On the other hand, the heat shifts to neighboring apartments can make up more than 40% of the total transmission heat loss of each apartment. It can be then concluded that the heating behavior of the adjacent dwelling and the associated heat shift within the building have a high influence on the heat demand of each apartment.

Comparison between expected and observed consumption

In the comparison of expected and observed consumption, the measured raw data cannot be directly used because the expected consumption has been identified using a standard weather data set. The observed consumption should therefore first be weather adjusted. Weather adjustment means that the proportion of heat consumption dependent on the weather is multiplied by a climate correction factor. Recognized method are described in the VDI 2067 [7] and VDI 3807 [8] and could be used for the determination of these climate correction factors. The difference between the average outdoor air temperature and average room temperature forms the basis for the determination of heating days. Heating days number those days when the heating temperature limit is below 15 °C. The normative procedure provides a good opportunity for the comparability of the consumption of buildings in different locations.

But in reality it is to known that in addition to the temperatures inside and outside, the solar radiation has a big influence on the consumption. Therefore, for this work, instead of adjusting the consumption energy figures, the expected energy figures have been calculated with real, observed weather patterns including not only the outdoor temperature, but also the solar radiation. The expected consumption values have been calculated for each monitored year, and the expected and observed consumption energy figures are compared with each other. A tool for the "weather adjustment of expected consumption data" has been therefore developed at the institute.

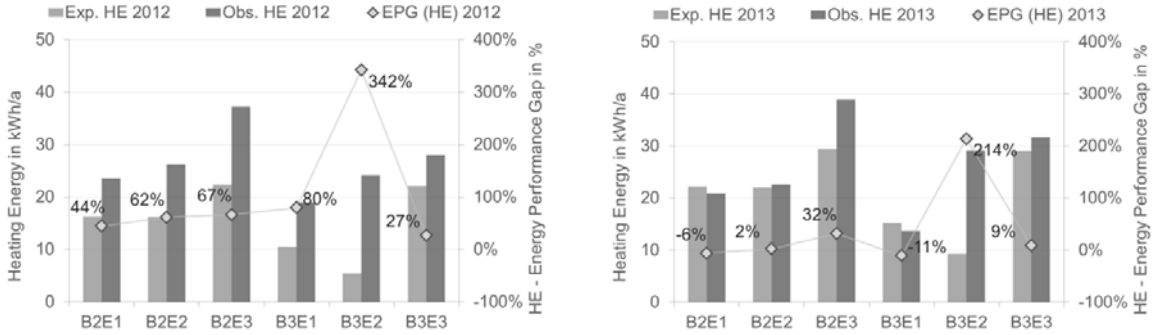

Figure 4: Energy performance gap, related to the heating energy, of block 2 and block 3, in the year 2012 (left) and 2013 (right)

Figure 4 shows the comparison of the expected heating consumption (light gray) and the observed heating consumption (dark-gray) for the years 2012 and 2013. In all cases a discrepancy between the expected and observed consumption data is revealed. The Energy Performance Gap (EPG), which is plotted on the right scale, between observed and expected consumption and the expected consumption (is defined in equation (1).

$$EPG = \frac{(Q_{obs} - Q_{exp})}{Q_{exp}} \quad (1)$$

The values shown in *figure 4* reflect only the heating energy [9]. The comparison of this value illustrates the user behavior (heating and ventilation) without taking into account the resulting losses for transport, storage and conversion. The EPG varies between 27% and 342% for B3.E1 and B3.E2 in 2012, and between -11% and 214% for B3.E1 and B3.E2 in 2013. In 2013 there are significantly lower values than in 2012. The repeated explanation about the use of the engineering system for the tenants at the beginning of the heating season and the accompanying interviews and surveys counts to the reasons for these results. As part of the study the correct use of the heating and ventilation system and the basic features of the ventilation are mediated to the tenants. In spite of the educational explanation the gap between

consumption and demand values is still too large. A reason for this gap could be that the tenants do not use as expected the mechanical ventilation system with heat recovery.

CONCLUSION

Future analyses will show whether the trends described here will be confirmed or a further reduction of consumption (especially for block 3) is possible through training courses for tenants and continuous maintenance of the engineering systems.

The presented research project offers the possibility of a systematic and scientific basis for the analysis of different renovation strategies. For evaluation and detailed consumption data of the residential building over several heating periods are available. Despite the not fully achieved conservation objectives it can be shown that an energy efficiency of buildings can reduce greenhouse gas emissions, energy consumption and, consequently, contributes to the energy costs.

ACKNOWLEDGEMENTS

We gratefully acknowledge the financial support of BMWi (03ET1105A) and of E.ON New Build and Technology.

REFERENCES

1. Bundesregierung: Energiekonzept für eine umweltschonende, zuverlässige und bezahlbare Energieversorgung. http://www.bundesregierung.de/ContentArchiv/DE/Archiv17/_Anlagen/2012/02/energiekonzept-final.pdf?__blob=publicationFile&v=5. Version: 2010.
2. BMWi Bundesministerium für Wirtschaft und Energie; BMWI Bundesministerium für Wirtschaft und Energie (Hrsg.): Nationaler Aktionsplan Energieeffizienz (NAPE). Berlin, Dezember 2014.
3. MiRO Mineralölraffinerie Oberrhein GmbH & CO. KG: Raffinerieabwärme für noch mehr Karlsruher Wohnungen: MiRO und Stadtwerke bauen Wärmeauskopplung zur Nutzung von Prozessabwärme für die Fernwärmeversorgung weiter aus. http://www.miro-ka.de/de/presse/ presse-informationen-2014_153.htm. Version: 2014.
4. Calì, D., Osterhage, T. and Mueller, D.: Field study of different retrofit solutions for residential housing. Proceedings of Clima 2010.
5. Calì, D., Osterhage, T. and Mueller, D.: Retrofit Solutions for Residential Buildings. International Journal of Sustainable Building Technology and Urban Development, vol. 2, no. 2, pp. 131–136, 2011.
6. Energieeinsparverordnung EnEV 2014, Verordnung über energiesparenden Wärmeschutz und energiesparende Anlagentechnik bei Gebäuden - Energy saving ordinance for buildings.
7. Verein Deutscher Ingenieure: VDI-Richtlinie VDI 2067 - Wirtschaftlichkeit gebäudetechnischer Anlagen. 09/2012.
8. Verein Deutscher Ingenieure: VDI-Richtlinie VDI 3807 – Blatt 1 - Verbrauchskennwerte für Gebäude - Grundlagen. 06/2013.
9. DIN Deutsches Institut für Normung e. V : DIN V 4108-6: Wärmeschutz und Energie-Einsparung Vornorm in Gebäuden. Teil 6: Berechnung des Jahresheizwärme- und des Jahresheizenergiebedarf. 02/2013.

A GLOBAL APPROACH TO EVALUATE IAQ AND THERMAL COMFORT IN A HEALTHY BUILDING PERSPECTIVE

F. Sicurella[1]; P. Colamesta[2];

1: Planair SA; fabio.sicurella@planair.ch

2: Planair SA; perla.colamesta@planair.ch

ABSTRACT

In recent years many progress have been made in the knowledge of Indoor Air Quality (IAQ), ventilation, and building-related health problems in schools, offices and other workplaces. Ensuring the IAQ inside these kinds of buildings is very important since people spend about 90% of their time indoors. Currently new buildings are the most affected by indoor pollutants (CO_2, VOC, formaldehyde etc.) since they are characterized by a very high air tightness that significantly reduces the inlet of fresh air through infiltrations. For this reason the ventilation (natural and mechanical) is becoming a very important topic for the health in new buildings. In this study the concentration of indoor pollutants was evaluated for different envelope air tightness and ventilation strategies. The simulations were run on EnergyPlus. The methodology proposed in the present paper includes a parametric multi-objective analysis that takes into account not only IAQ but also thermal comfort; this approach allows to propose optimised solutions during the concept and the design of new "healthy" buildings.

Keywords: IAQ and thermal comfort, healthy buildings, ventilation strategies

INTRODUCTION

Problems of IAQ are recognized as important risk factors for human's health worldwide. IAQ is also important because people spend a substantial proportion of their time in buildings. In residences, day-care centres, retirement homes and other special environments, indoor air pollution affects population groups that are particularly vulnerable owing to their health status or age. The World Health Organization (WHO) indicate a number of chemicals commonly present in indoor air that can cause momentary troubles [1]. In [2] it is suggested that when 20% of a single building's occupant suffers such troubles, the structure is suffering from sick building syndrome (SBS).

Guarantee the IAQ means also sparing the discomfort caused by these pollutants. In this paper, for brevity, only two pollutants were simulated to analyse IAQ and thermal comfort: Formaldehyde and CO_2; the first usually linked to furniture the latter to metabolic activity.

INDOOR POLLUTANTS IN BUILDINGS: FORMALDEYDE AND CARBON DIOXIDE

Indoor sources of formaldehyde may be combustion processes such as smoking, heating, cooking, candle or incense burning. However, major sources in non-smoking environments appear to be building materials and consumer products that emit formaldehyde [3]. Predominant signs of short-term exposure to formaldehyde in humans are irritation of the eyes, nose and throat; with higher concentration, lachrymation, sneezing, coughing, nausea, etc. (Figure 1, left). Symptoms are often more severe at the start of exposure than after minutes or hours, when they gradually diminish.

Concerning CO_2, the indoor primary source is human metabolism. An average person, in fact through the natural process of breathing, produces approximately 1 kg of carbon dioxide per

day, even though it strongly depends on the person's activity level [4]. Many researches have shown that high CO_2 concentration are associated with perceptions of poor air quality and may increase prevalence of acute health symptoms (e.g., headache, mucosal irritation), slower work performance and absence. Even a moderately high indoor concentration of CO_2 can significantly impair people's decision-making performance [5] (Figure 1, right).

Concentration range or average (mg/m³)	Time range or average	Health effects in general population
0.03	Repeated exposure	Odour detection threshold (10th percentile) [a]
0.18	Repeated exposure	Odour detection threshold (50th percentile) [a]
0.6	Repeated exposure	Odour detection threshold (90th percentile) [a]
0.1 – 3.1	Single and repeated exposure	Throat and nose irritation threshold
0.6–1.2	Single and repeated exposure	Eye irritation threshold
0.5 – 2	3–5 hours	Decreased nasal mucus flow rate
2.4	40 minutes on 2 successive days with 10 minutes of moderate exercise on second day	Post-exposure (up to 24 hours) headache
2.5 – 3.7	~ [b]	Biting sensation in eyes and nose
3.7	Single and repeated exposure	Decreased pulmonary function only at heavy exercise
5 – 6.2	30 minutes	Tolerable for 30 minutes with lachrymation
12 – 25	~ [b]	Strong lachrymation, lasting for 1 hour
37 – 60	~ [b]	Pulmonary oedema, pneumonia, danger to life
60 – 125	~ [b]	Death

[a] Frequency of effect in population.

[b] Time range or average unspecified.

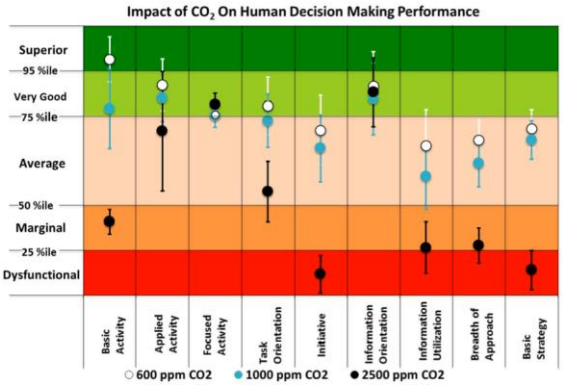

Figure 1(left): Effects of formaldehyde in human after short-term exposure. Source: [1]
Figure 1(right): Impact of CO_2 on Human Decision-Making Performance. Source: [5]

FORMALDEHYDE AND CARBON DIOXIDE GENERATION RATE AND LIMITS

In the present study formaldehyde class E1 (release equal to 3.5 $mg \cdot m^{-2}h^{-1}$, [6]) was considered for indoor furniture.

In technical standards and literature it is possible to find different values of suitable formaldehyde concentration inside a building. The authors have analysed the limits imposed by the WHO, the OFSB (Office fédéral de la santé publique en Suisse), the Leed and Minergie-ECO standards and have chosen the more restrictive, the Leed limit, equal to 27ppb.

The contaminant generation rate in an office building is equivalent to the combination of the constant coefficient model defined in the sources and sinks element types of CONTAM 3.0. The basic equation used to calculate formaldehyde source and sink for the constant model is given below:

$$S_f(t) = G_f(t) - R_f(t)C_f(t)10^{-6} \quad (1)$$

where:

S_f : Formaldehyde source strength $[m^3s^{-1}]$

G_f : Formaldehyde generation rate $[m^3s^{-1}]$

R_f : Formaldehyde effective removal rate $[m^3s^{-1}]$

C_f : Formaldehyde concentration value at a given previous time step [ppm]

In urban environments, outdoor formaldehyde concentrations is considered as 20 $\mu g \cdot m^{-3}$[1, 7]. Concerning Carbone dioxide, only CO_2 emitted by people was considered in this study.

In literature and technical standards it is possible to find different values of suitable CO_2 concentration inside a building. Following the ASHRAE Standard 62 [8], this limit can be set at 1000 ppm even though the standard revision [9], suggests as upper limit 700 ppm above the outdoor concentration. According to [10] the outdoor CO_2 concentration is 400 ppm. As a consequence the authors decided to choose the more restrictive of these rate values for CO_2 concentration, which in this case study was set at 1000 ppm.

The basic equation used to calculate carbon dioxide source and sink for model is given below:

$$Sc(t) = N_n\, S_n(t) A_n(t)\, G_c(t) \quad (2)$$

where:

Sc : carbon dioxide source strength [m^3s^{-1}]

N_p : Number of People [dimensionless]

S_p : People Schedule [dimensionless]

A_p : People Activity [$Wperson^{-1}$]

G_c : Carbon Dioxide Generation Rate [$m^3s^{-1}W^{-1}$]; (equal to $3.82 \cdot 10^8 m^3s^{-1}W^{-1}$, following [11]).

EVALUATION OF VENTILATION AIR FLOW RATE AND THERMAL COMFORT

The calculation model used for simulating the ventilation air flow rate is a function of wind speed and thermal stack affect, combined with the infiltration effect.

The equation used to calculate the ventilation rate driven by wind is:

$$Q_w = C_w A_o F_s V \quad (3)$$

where:

Q_w : Volumetric air flow rate driven by wind [m^3s^{-1}]

C_w : Opening effectiveness [dimensionless]

A_o : Opening area [m^2]

F_s : Open are fraction [dimensionless]

V : Local wind speed [ms^{-1}]

The equation used to calculate the ventilation rate due to stack effect is:

$$Qs = C_d A_o F \sqrt{(2g\Delta H_{NPL}\, (|T_{zone} - T_{odb}| / T_{zone})} \quad (4)$$

where:

Q_s : Volumetric air flow rate driven by wind [m^3s^{-1}]

C_d : Discharge coefficient for opening [dimensionless]

A_o : Opening area [m^2]

Fs : Open are fraction [dimensionless]

ΔHNPL : Height from midpoint of lower opening to the neutral pressure level [m]

T_{zone} : Zone air dry-bulb temperature [K]

T_{odb} :Local outdoor air dry-bulb temperature [K]

The total ventilation rate is given by:

$$\text{Ventilation}_{\text{Wind and Stack}} = \sqrt{Q_w^{\,2} + Q_s^{\,2}} \quad (5)$$

The equation used to calculate infiltration in the effective leakage area is based on LBNL model [7,12] where:

$$Infiltration = \frac{A_L T}{1000} \sqrt{C_S \Delta T + C_w U^2} \quad (6)$$

where:

A_L : Effective Air Leakage Area at 4 Pa [cm^2]

C_S : Stack Coefficient [$(Ls^{-1})^2(cm^4K)^{-1}$]

ΔT : average difference between zone air temperature and the outdoor air

C_W : wind coefficient [$(Ls^{-1})^2(cm^4(ms^{-1})^{-2})$]

U : average wind speed [ms^{-1}]

The Effective Air Leakage Area is function of the n_{50} that is a variable parameter in this study.

Concerning thermal comfort, it was evaluated following the SIA 180:2014 [13]. The approach used to evaluate IAQ and thermal comfort simultaneously is presented in [14, 15].

THE CASE STUDY

The results presented in this work refer to a south-oriented meeting room of a new office building in Courtelary (Switzerland) (Figure 2). It is 3.65 m large, 6.80 m length and 2.8 m high, and it is occupied by six people (following [16]) from 9 am to 12 am et from 2 pm to 5 pm. The floor and all furnishing are considered made by formaldehyde class E1 (74 m^2). The glazing area is 8.8m^2, only 2.2 m^2 is an openable area in bottom hung mode. The simulations were presented in a typical day (21.09).

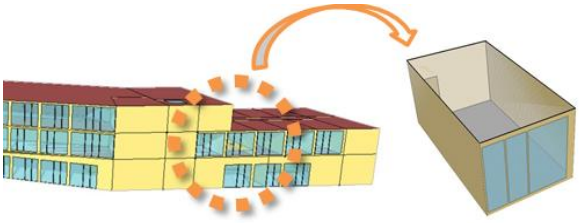

Figure 2: Southern view of the building with in evidence the analysed office

AIR TIGHTNESS AND VENTILATION STRATEGIES

In order to understand the impact of the envelope air tightness and the ventilation strategies on IAQ and thermal comfort, the following simulations were run (Table 1):
Case 1: standard air tightness, without ventilation; ***Case 2***: high air tightness (Standard Minergie), without ventilation; ***Case 3***: very high air tightness (Standard Minergie-P), without ventilation, ***Case 4, 5, 6***: Standard Minergie-P with different mechanical ventilation rates (activated only during occupation); ***Case 7***: Standard Minergie-P with natural ventilation.

	n_{50} [h^{-1}]	Natural ventilation	Mechanical ventilation
Case 1	2	/	/
Case 2	1	/	/
Case 3	0.6	/	/
Case 4	0.6	/	36 $m^3(h\cdot person)^{-1}$ [23]
Case 5	0.6	/	12 $m^3(m^2h)^{-1}$ [23]
Case 6	0.6	/	0.5 h^{-1}
Case 7	0.6	Bottom hung mode	/

Table 1: Simulations.

THE RESULTS

On the basis of the results shown in Figures 2, 3 and 4 one can observe that:

- a high envelope air-tightness without adequate ventilation entails relevant IAQ problems. Figures 2 and 3 show that, without ventilation, formaldehyde and CO_2 concentration exceed standard limits. The ventilation becomes necessary for high performance buildings. For buildings with higher infiltration rate (case 1) these concentrations are significantly lower and could be enough for formaldehyde dilution but not for CO_2;
- for new high performance buildings (e.g. Minergie, Minergie-P) an intense mechanical or natural ventilation rate is usually enough for IAQ purposes; nevertheless, for this case study, the rate of 0.5ACH (case 6) revealed to be insufficient for IAQ during occupation;
- a natural ventilation strategy (case 7) implies from one hand a higher reduction of pollutant concentration, but from another hand a higher fluctuation in terms of indoor temperature than a mechanical ventilation strategy (Figure 4 left); as a consequence a higher thermal discomfort for cold can occur (Figure 4 right) as well as local discomfort (drafts).

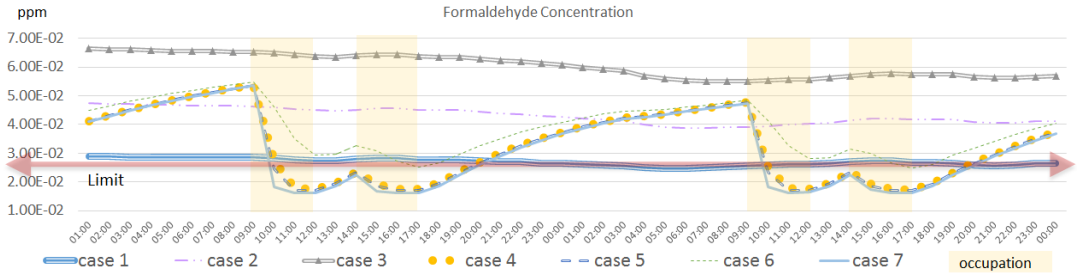

Figure 2: Simulation results: Formaldehyde concentration

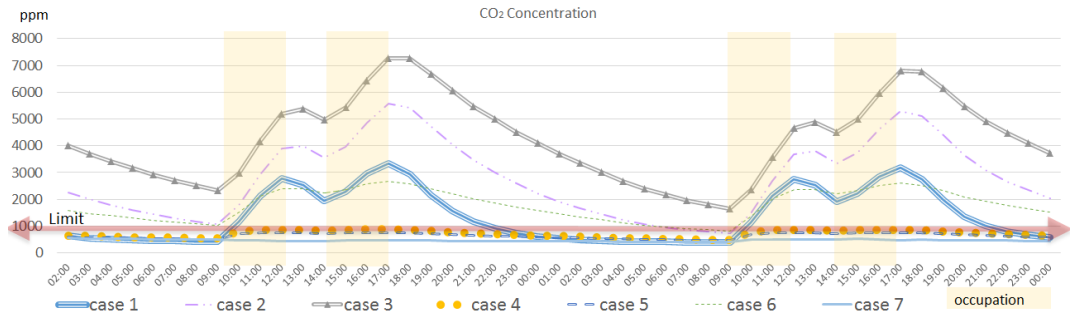

Figure 3: Simulation results: Carbon dioxide concentration

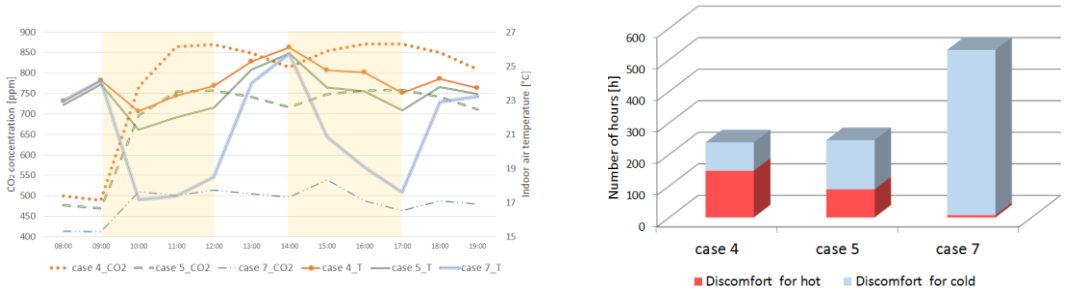

Figure 4 (left): Comparison between ventilation strategies for IAQ and thermal comfort
Figure 4 (right): Comparison between ventilation strategies for thermal discomfort (case 4 and 5 analysed with SIA 180 model for conditioned room, case 7 with SIA 180 model for non-conditioned room; analysed period: 15.05-15.10 [13])

CONCLUSIONS

Achieving IAQ and thermal comfort for new high performance buildings characterised by a very high air-tightness is a real challenge. For these buildings, dynamic simulations show an actual risk in terms of concentration of indoor pollutants that only an adequate ventilation (natural or mechanical) can overcome. Both (natural and mechanical ventilation) are very effective to dilute pollutants. Natural ventilation can be even more effective than mechanical ventilation but strongly depends on the occupant's behaviour and can easily entail thermal discomfort and drafts. In any case for new high performance buildings a ventilation strategy becomes primordial and should be defined during the preliminary phases of the building design.

REFERENCES

1. WHO: guidelines for indoor air quality: selected pollutants. 2010
2. Rask, D.: Indoor air quality and the bottom line. Heating, Piping and Air Conditioning. 1988
3. Salthammer, T., Mentese, S., Marutzky, R.: Formaldehyde in the indoor environment. Chemical Reviews, 2010
4. Carbon Dioxide Information Analysis Center. Frequently Asked Global Change Questions http://web.archive.org/web/20110410142100/http://cdiac.ornl.gov/pns/faq.html. 2011
5. Satish, U., Mendell, M.J., Shekhar, K., Hotchi, T., Sullivan, D., Streufert, S., Fisk, W.J.: Is CO2 an Indoor Pollutant? Direct Effects of Low-to Moderate CO2 Concentrations on Human Decision-Making Performance. 2012
6. EN 13986: Wood-based panels for use in construction - Characteristics, evaluation of conformity and marking. Annex B, 2004
7. ASHRAE: Fundamentals Handbook . Chapiter 26,2001
8. ASHRAE: Standard 62. Ventilation for acceptable Indoor Air Quality. 1989
9. ASHRAE: Standard 62. Ventilation for acceptable Indoor Air Quality. 1999
10. National Oceanic & Atmospheric Administration (NOAA), Earth System Research Laboratory (ESRL): Trends in Carbon Dioxide http://www.esrl.noaa.gov/gmd/ccgg/trends. 2015
11. ASHRAE: Standard 62.1. Ventilation for Acceptable Indoor Air Quality. 2007
12. Sherman, M.H., D.T Grimsrud.: Infiltrationpressurization correlation: Simplified physical modelling. 1980.
13. SIA 180: Protection thermique, protection contre l'humidité et climat intérieur dans les bâtiments. 2014
14. Sicurella, F., Colamesta, P.: Passive solutions for the optimizations of indoor environmental quality: a case study. 2nd IBPSA-Italy Conference, Bolzano, 2015
15. Sicurella, F., Evola, G., Wurtz, E.: A statistical approach for the evaluation of thermal and visual comfort in free-running buildings. Energy and buildings. 2011
16. SIA 2024: Conditions d'utilisation standard pour l'énergie et les installations du bâtiment. 2006.

LOW COST INFRARED ARRAY AS A THERMAL COMFORT SENSOR

M. Veselý[1]; A. Cieszczyk[1]; Y. Zhao[1]; W. Zeiler[1]

1: Department of Built Environment, Eindhoven University of Technology, P.O. Box 513, 5600 MB Eindhoven, the Netherlands

ABSTRACT

Energy in buildings has to be deployed in a more effective way, bearing in mind a comfortable indoor climate and full occupant satisfaction. Recent developments show that heating or cooling locally can improve both, the thermal comfort and energy effectiveness. Personalized conditioning systems are in principle able to satisfy the individual thermal comfort requirements, and at the same time they are conditioning only a small space around a single user and are thus more energy effective.

However, personalized conditioning systems are still controlled only by direct user interaction, which can lead to problems such as temperature overshoots or energy wastes. For automation of the control process it is necessary to look into individual parameters that can predict thermal discomfort. It has been shown that the fingertip temperature is a good predictor of cold discomfort. Therefore, it has a potential to be used as a control signal for automatic personalized heating. For practical use it is necessary to develop a low cost sensor that can sense the fingertip temperature without direct interfering with the user.

In this paper the initial tests of low cost infrared arrays are presented that can be used for this application. Two infrared arrays of resolution 4x4 and 16x4 pixels were tested in terms of their accuracy and feasibility for skin temperature measurement. The static tests proved these sensors to be adequate for the intended purpose. One of the infrared arrays was then combined with a visual camera allowing a real-time tracking of the hand movement. Development of this integrated visual and infrared sensor and their relation to thermal comfort are presented in this paper.

Keywords: Image processing, Infrared thermography, Thermal comfort, Tracking

INTRODUCTION

Currently building sector accounts for approx. 40% of total energy consumption in EU and US [1]. Most of this energy is used to keep the indoor climate in a narrow range of conditions prescribed by thermal comfort standards. However, narrowing this range still does not ensure that the building occupants are thermally comfortable [2]. These issues led in recent years to development of personalized conditioning systems, which allow users to adapt their microenvironment to their desires [3]. Personalized conditioning systems can also help to decrease building energy consumption by higher effectiveness [3], [4].

Personalized conditioning systems are nowadays controlled just by user interaction. This can lead to certain problems. For instance personalized heating controlled by user interaction will be only turned on when the user experiences cool discomfort, and turned off when warm discomfort will occur. Incorporating automated or semi-automated control can improve overall satisfaction and performance of the system. Therefore, there is a need for a parameter that can predict thermal discomfort.

Wang et al. [5] identified distal skin temperature, particularly finger and hand temperature, as a good predictor of cold discomfort under cool uniform conditions. In order to use distal skin temperatures as a control signal it is needed to measure them in a way that does not negatively affect overall user comfort. Recent tests show that infrared thermography is a feasible method for this application [6]. However, only an expensive and sophisticated thermocamera was used in these tests.

This paper describes the development of a low cost sensor that integrates temperature measurement by infrared thermography and tracking of hand movement.

METHODS

Static tests of accuracy of infrared arrays

At a first stage two low cost infrared arrays, OMRON D6T 44L [7] and Melexis MLX90620 [8] (see Table 1), were tested for their accuracy and repeatability of measurements in a static setting. Both sensors were connected to a PC via an Arduino microcontroller [9].

	OMRON D6T 44L 	**MELEXIS MLX 90620** 
Matrix	4x4	16x4
Frame rate	4 FPS	0.5 to 512 FPS
Temperature resolution	0.14 K	0.08 K
Accuracy (by manufacturer)	± 1.5 K	± 1.0 K
Range	5÷50 °C	-20÷300 °C
Field of view	44.2° x 45.7°	40° x 10.4°

Table 1 Tested sensors

The measurement setup is shown in Figure 1. A carousel with six heated surfaces with different emmissivity simulated a measured object. One of three plates with a cut-off opening in a shape of a finger (finger negative) was placed in front of the heated surface. A thermal image of this setup was captured by the infrared arrays for all combinations of heated surface and plate in front. The temperature of the heated surface was at the same time measured also by a thermistor that can be taken as a reference. The distance and position of an infrared array from the measured object were varied in order to get different placement and size of the "finger" according Figure 2.

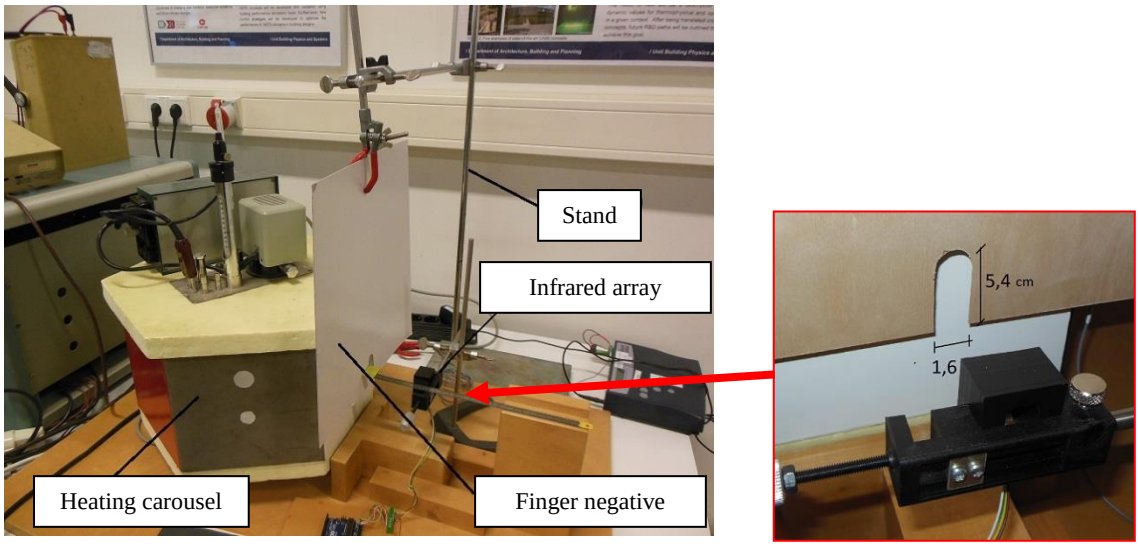

Figure 1 Static tests - measurement setup

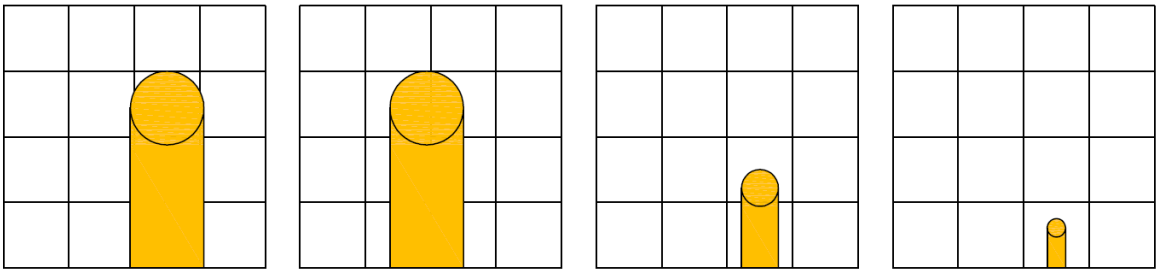

Figure 2 Finger placement on 4x4 pixel matrix – different positions and distance of the sensors

Movement tracking in visual spectrum

Figure 3 shows a principle of coupling an infrared array and an optical tracking. A Pixy CMUcam5 [10] is used in this case for tracking in the visual spectrum. It is a camera with integrated circuit for image processing that allows tracking of a particular colour in an image. A hand can thus be tracked by skin colour, if a proper background is used. The position of the hand identified in a visual image can then be used to point a temperature value from an infrared image (infrared and visual image are de facto overlaid).

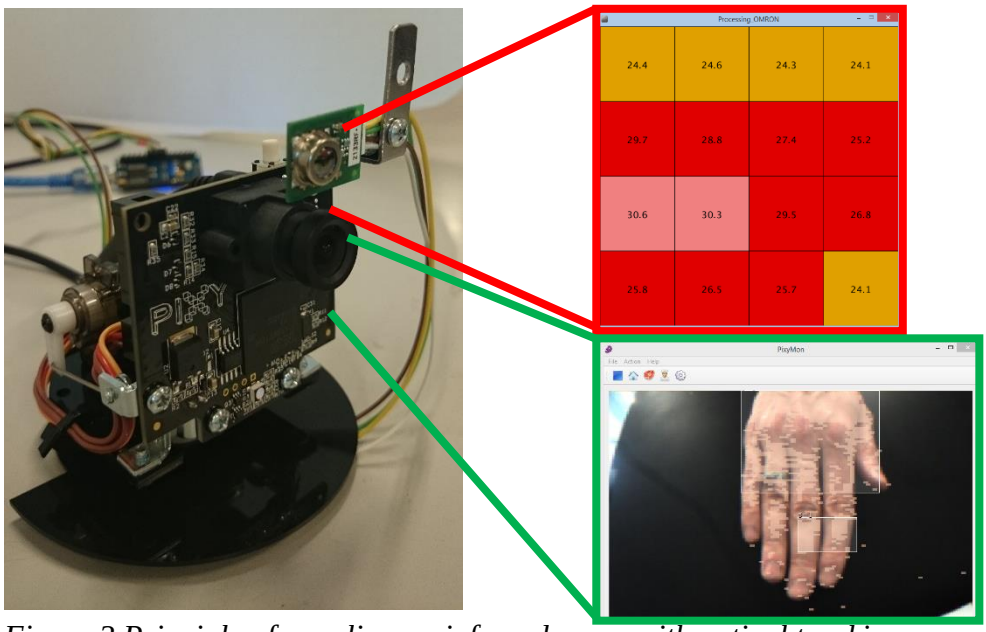

Figure 3 Principle of coupling an infrared array with optical tracking

RESULTS & DISCUSSION

Static tests of accuracy of infrared arrays

Figure 4 shows two tests of OMRON D6T 44L. These tests represent a first case of Figure 2, so the measured object fully filled three pixels. The black heated surface has an emissivity close to human skin (0.98) and wooden and white backgrounds are surfaces that commonly occur as an office desk top layer. From the charts it is clear that the sensor accuracy is even better that the value given by the manufacturer (± 1.5 K) and in most cases falls under ± 0.5 K. Considering that the temperature drop related to a change in comfort reaches about 10 to 15 K [5], this accuracy is good enough for the intended application. The accuracy of Melexis MLX90620 under our tests was considerably lower. Therefore, we decided to use OMRON D6T 44L in our further tests.

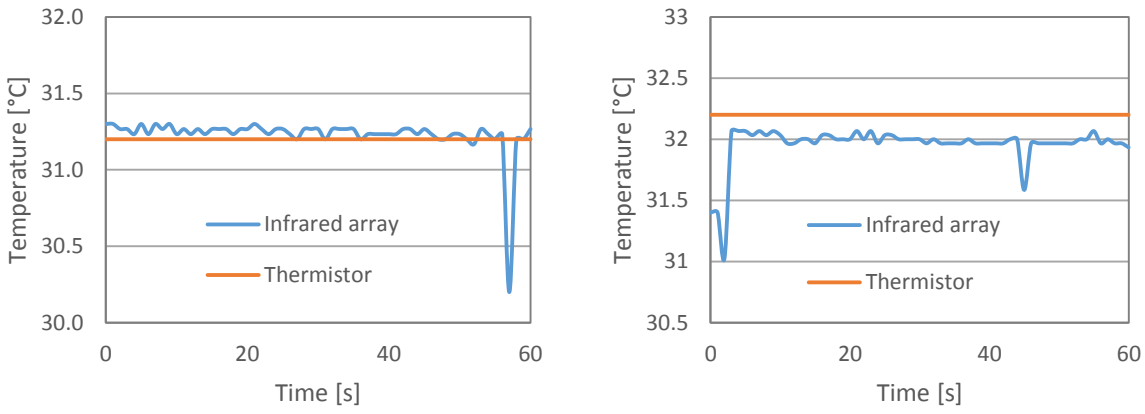

Figure 4 Average object temperature (3 pixels) corresponding to the first case of Figure 2, OMRON D6T 44L, black heated surface, wooden background (left), white paper background (right)

Temperature values of pixels that are not fully filled with the measured object would require an extrapolation using known background temperature. However, in our application we expect pixels nearly fully filled and we will adjust the sensor position accordingly.

Movement tracking in visual spectrum

In our previous study we have used a pattern matching algorithm to search for the shape of a finger in a high resolution infrared image [11]. This is only possible as long as there is a temperature difference between the skin temperature and the background. However, under mild cool conditions the fingertip temperature comes close to the environmental temperature, which causes a lack of contrast in an infrared image and the pattern matching algorithm fails. Tracking in a visual spectrum can overcome this problem and opens a possibility to use a low resolution infrared array. It is also not possible to use the pattern matching with a low image resolution of low cost infrared arrays.

Because of the above mentioned reasons we will test hand tracking using a Pixy CMUcam5 [10]. This a camera with integrated image processing that can track a particular colour. This allows tracking for a skin colour on a proper background and using the spotted object as a pointer for a temperature value from an infrared image.

Future tests

It is necessary to test the new integrated sensor for its reliability and accuracy. This should be done in comparison with contact methods of measuring skin temperature, such as using wireless temperature loggers iButtons [12]. At the moment it is also not clear how reliable tracking a hand based on skin temperature is. This has to be tested using different background surfaces.

As already mentioned Wang et al. [5] found a relation between distal skin temperature and thermal sensation. However, their experiments were conducted under uniform and steady state conditions. Our recent, yet unpublished, tests imply that relating skin temperature and thermal sensation is becoming more complex in a non-uniform thermal environment. After applying personalized heating under mild cool conditions we have observed a significant increase in thermal sensation, but only a slight change in distal skin temperatures. This does not disqualify distal skin temperature as a possible control signal for personalized heating. However, a combination with other parameters might be necessary. This should be tested also in comparison with control based solely on user interaction.

CONCLUSIONS

Development of a new sensor is described in this paper. This sensor integrates a temperature measurement by low cost infrared array and movement tracking in visual spectrum. The intended application is remote measurement of hand skin temperature that can be used as control signal for personalized heating.

The future tests will focus on accuracy and reliability of this new sensor and the application with personalized heating.

REFERENCES

[1] L. Pérez-Lombard, J. Ortiz, and C. Pout, “A review on buildings energy consumption information,” *Energy Build.*, vol. 40, no. 3, pp. 394–398, Jan. 2008.

[2] E. Arens, M. A. Humphreys, R. de Dear, and H. Zhang, “Are ‘class A’ temperature requirements realistic or desirable?,” *Build. Environ.*, vol. 45, no. 1, pp. 4–10, Jan. 2010.

[3] M. Veselý and W. Zeiler, “Personalized conditioning and its impact on thermal comfort and energy performance – A review,” *Renew. Sustain. Energy Rev.*, vol. 34, pp. 401–408, Jun. 2014.

[4] J. Verhaart, M. Veselý, and W. Zeiler, “Personal heating: effectiveness and energy use,” *Build. Res. Inf.*, vol. 43, no. 3, pp. 346–354, 2015.

[5] D. Wang, H. Zhang, E. Arens, and C. Huizenga, “Observations of upper-extremity skin temperature and corresponding overall-body thermal sensations and comfort,” *Build. Environ.*, vol. 42, no. 12, pp. 3933–3943, Dec. 2007.

[6] M. Veselý and W. Zeiler, “Fingertip temperature as a control signal for personalized heating,” in *Proceedings of Indoor Air*, 2014, no. 2007.

[7] OMRON, “D6T MEMS Thermal Sensors,” 2015. [Online]. Available: http://www.omron.com/ecb/products/pdf/en-d6t.pdf. [Accessed: 29-Apr-2015].

[8] Melexis, “No TitleMLX90620 FIRray:16X4 Far InfraRed Array,” 2015. [Online]. Available: http://www.melexis.com/Infrared-Thermometer-Sensors/Infrared-Thermometer-Sensors/MLX90620-776.aspx. [Accessed: 29-Apr-2015].

[9] Arduino, “Arduino,” 2015. [Online]. Available: http://www.arduino.cc. [Accessed: 29-Apr-2015].

[10] CMUcam, “Pixy CMUcam5,” 2015. [Online]. Available: http://www.cmucam.org/projects/cmucam5. [Accessed: 29-Apr-2015].

[11] M. Veselý and W. Zeiler, “Tracking hand movement in an infrared image,” in *Proceedings of 8th Windsor Conference: Counting the Cost of Comfort in a changing world*, 2014, no. April.

[12] W. D. van Marken Lichtenbelt, H. a M. Daanen, L. Wouters, R. Fronczek, R. J. E. M. Raymann, N. M. W. Severens, and E. J. W. Van Someren, “Evaluation of wireless determination of skin temperature using iButtons.,” *Physiol. Behav.*, vol. 88, no. 4–5, pp. 489–97, Jul. 2006.

Model Predictive Control

DR-ADVISOR: A DATA-DRIVEN DEMAND RESPONSE RECOMMENDER SYSTEM

Madhur Behl[1], Truong X. Nghiem[2]; Rahul Mangahram[1]

[1]*Electrical and Systems Engineering, University of Pennsylvania, USA.,* {*mbehl,rahulm*}*@seas.upenn.edu*

[2]*Laboratoire d' Automatique, École Polytechnique Fédérale de Lausanne, Switzerland, xuan.nghiem@epfl.ch*

ABSTRACT

A data-driven method for demand response baselining and strategy evaluation is presented. Using meter and weather data along with set-point schedule information, we use an ensemble of regression trees to learn non-parametric data-driven models for predicting the power consumption of the building. This model can be used for evaluating demand response strategies in real-time, without having to learn complex models of the building. The methods have been integrated in an open-source tool called DR-Advisor, which acts as a recommender system for the building's facilities manager by advising on which control actions should be during a demand response event. We provide a case study using data from a large commercial vistural test-bed building to evaluate the performance of the DR-Advisor tool. *Keywords: demand response, regression trees, machine learning*

INTRODUCTION

In 2013, a report by the National Climate Assessment provided evidence that the most recent decade was the nations warmest on record [1] and experts predict that temperatures are only going to rise. Every year an overstressed electric grid faces increasing challenges to operate homes and buildings. Heat waves in summer and polar vortexes in winter are growing longer in duration which could result in energy shortages and blackouts.

To improve reliability of the electricity grid, across the United States, electric utilities and independent system operators (ISOs) are devoting increasing attention and resources to demand response (DR) [2]. While energy efficiency is a prominent component of growing efforts to supply affordable, reliable and clean electric power; most utilities and system operators are increasingly turning to demand response as a cost effective and environmentally responsible way to serve peak load. Potential peak reduction from demand response markets in U.S. increased by $2,451$ MW or 9.3 percent to a total of $28,503$ MW from 2012 to 2013 [3]. The estimated revenue for economic and load management DR markets with PJM alone is about $700 million [4].

Buildings, particularly large commercial buildings, are large consumers of electricity and a significant contributor to peak load conditions in the grid. Their electricity demands are often sensitive to weather conditions, which can results in peaks in their power consumption on an extremely hot or an extremely cold day. Such customers are also increasingly looking to DR programs to help manage energy costs.

Demand response programs are designed to elicit changes in customers electric usage patterns. Some types of demand response, implemented through approved utility tariffs or through contractual arrangements, vary the price of electricity over time to motivate customers to change their consumption patterns; this approach is termed price-based demand response.

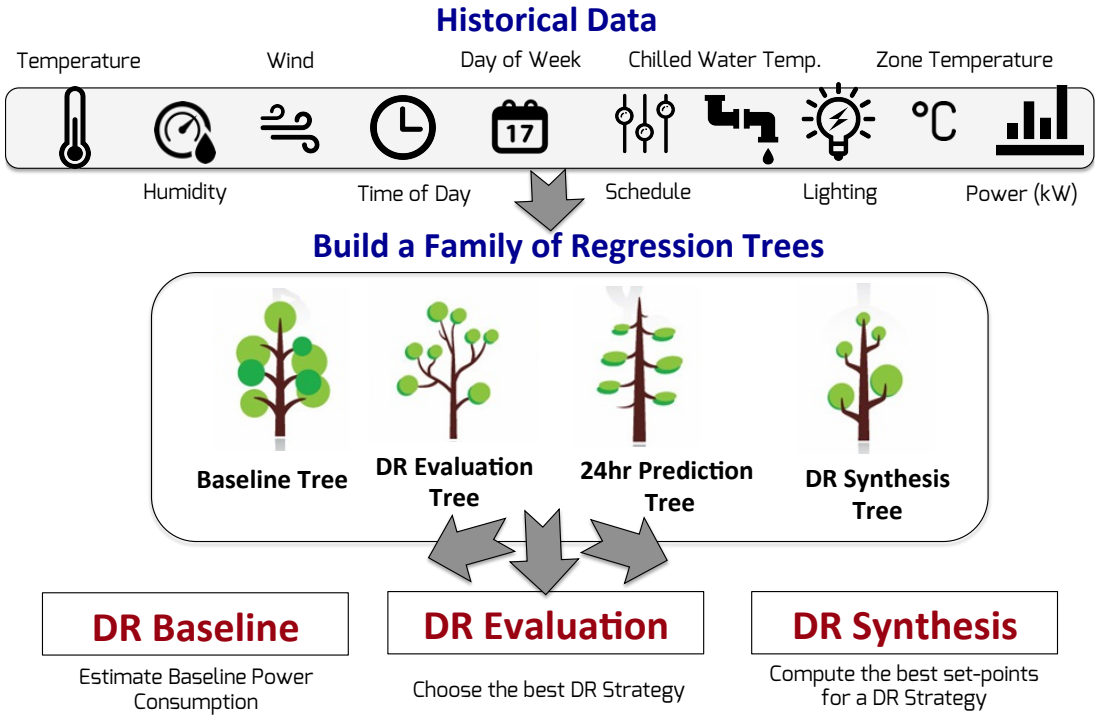

Figure 1: DR-Advisor Architecture

DR-Advisor is a data-driven tool for demand response baselining, strategy evaluation and synthesis. Using meter and weather data along with set-point and schedule information, it uses a family of regression trees to learn non-parametric data-driven models for predicting the power consumption of the building (Figure 1). These models can be used for real-time demand response strategy evaluation, without having to learn complex models of the building. DR-Advisor acts as a recommender system for the building's facilities manager by advising on which control actions should be taken during a DR event.

1. We demonstrate the benefit of using regression trees based methods for estimating demand response baseline power consumption and for evaluating pre-determined demand response strategies in real time. The use of such methods for demand response problems is novel.
2. We evaluate and compare the performance of several tree based methods on a Department of Energy's (DoE) Large Commercial Reference Building using actual meteorological data.
3. The biggest contribution of this work is the fusion of a family of regression trees into DR-Advisor, a simple and highly interpretable open source tool. It eliminates the cost of time and effort required to build and tune high fidelity models of buildings for DR.

Problem Definition

The two most popular approaches to respond to a demand response event include rule based and model based DR strategies. In a rule based demand response strategy, different levels of curtailment are achieved by following a pre-programmed strategy. Such a DR strategy can include fixed setbacks for thermostat set-points, pre-determined dimming of lights and temporarily switching off large equipment e.g., elevators. Model based design

for DR involves explicitly mathematically modeling the building and its equipment in order to predict the overall power consumption. However, creating and learning such high fidelity models is both cost and time prohibitive. This is because the user expertise, time, and associated costs required to develop a software model of a single building is quite large.

In this paper, we focus on two challenging problems of demand response

1. **DR baseline prediction**: A baseline is an estimate of the electricity that would have been consumed by a customer in the absence of a demand response event. The measurement and verification of demand response is the most critical component of any DR program since any curtailment can only be measured relative to the estimate of the demand response baseline.
2. **Real-time DR strategy evaluation**: This is the problem of choosing good DR strategies from a pre-determined set of strategies, in real-time. During a DR event notification, there are several options available to a buildings facilities manager in the form of a control actions. These may include setbacks in the zone temperature set-point, increasing supply air temperature and chilled water temperature set-point, dimming or turning off lights, decreasing duct pressure set-points and switching off no-essential electrical load. However, there could be several such fixed rules or strategies. With our tree based models, we can predict the response of the building due to any strategy, and hence, choose the best action during the DR event.

In key to solving both the problems is the ability to predict the power consumption of the building in real-time.

DR-ADVISOR: DATA-DRIVEN DEMAND RESPONSE

Regression trees are decision tress which predict responses to data. Regression trees belong to the class of recursive partitioning algorithms. At each node of the tree, we check the value of one the inputs (or features) X_i and depending of the (binary) answer we continue to the left or to the right subbranch. When we reach a leaf we will obtain the prediction of the response Y. The seminal algorithm for learning regression trees from data is the CART algorithm as described in [5]. Contrary to linear or polynomial regression which are global models (the predictive formula is supposed to hold in the entire data space), trees try to partition the data space into small enough parts where we can apply a simple different model on each part. They are conceptually simple yet powerful. Regression trees offer several advantages in addition to being simple, which make them suitable for solving the challenges of demand response and building modeling. We list some of these advantages here:

1. Trees require very low computation power, both running time and storage requirements.
2. Trees can easily handle the case where the data has lots of features which interact in complicated and nonlinear ways. the predictor variables themselves can be of any combination of continuous, discrete and categorical variables.
3. Sometimes, data has missing predictor values in some or all of the predictor variables. This is especially true for buildings, where sensor data streams fail frequently due to faulty sensors or faulty communication links. By design, regression trees can handle missing data better than most algorithms through the use of surrogate variables.
4. Tree based models are generally not affected by outliers but regression based models are.

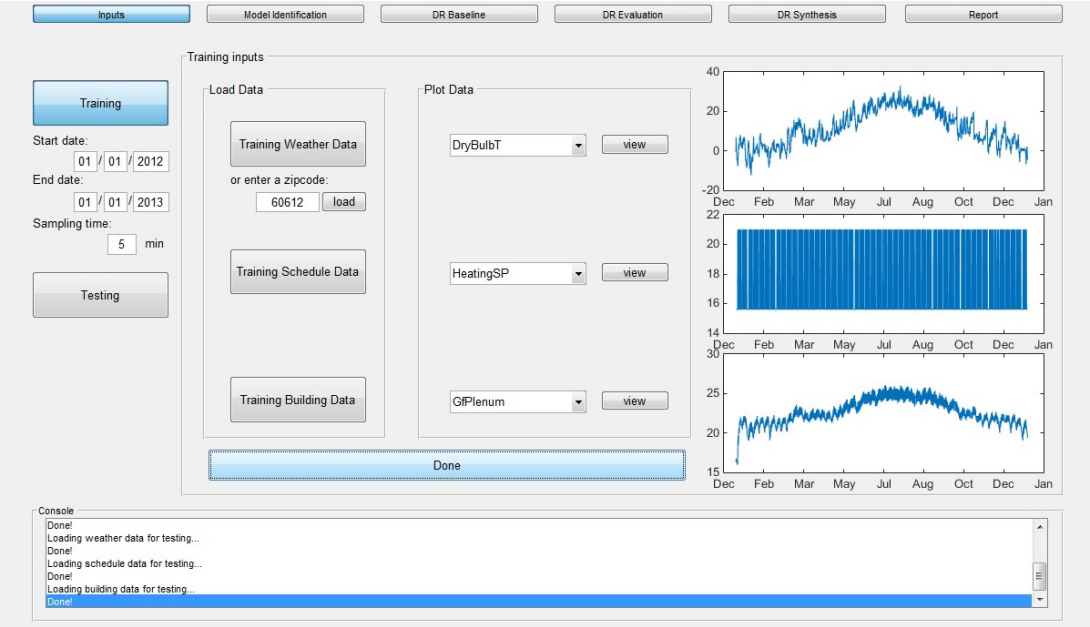

Figure 2: DR-Advisor graphical user interface

5. Trees are highly interpretable algorithms. Complex building models go through a long calculation routine and involve too many factors. It is not easy for a human engineer to judge if the operation/decision is correct or not or how it was generated in the first place. Trees only involve simple *if this then that* rules which are very easy to understand.

Ensemble Methods

The problem with trees is their high variance and that they can over fit the data. It is the price to be paid for estimating a simple, tree-based structure from the data. While pruning and cross validation can help reduce over fitting, in DR-Advisor,we use ensemble methods for growing more stable trees. The goal of ensemble methods is to combine the predictions of several base estimators built with a given learning algorithm in order to improve generalizability and robustness over a single estimator. Two families of ensemble methods are usually distinguished: (a) In averaging methods, the driving principle is to build several estimators independently and then to average their predictions. On average, the combined estimator is usually better than any of the single base estimator because its variance is reduced. (b) By contrast, in boosting methods, base estimators are built sequentially and one tries to reduce the bias of the combined estimator. The motivation is to combine several weak models to produce a powerful ensemble. The DR-advisor tool used a combination of cross validated trees, random forest and boosted regression trees as the underlying ensemble methods. For a more comprehensive review we refer the reader to [6].

CASE STUDY

The building under consideration is the DOE Commercial Reference Building simulated in EnergyPlus [7] This virtual test-bed is a large 12 story office building consisting of 73 zones with a total area of $500,000$ sq ft. There are upto $2,397$ people in the building during peak occupancy. The building has 2 electric water-cooled chillers, variable air volume (VAV) supply air terminals with reheat and plenum zones and a single gas based boiler. During peak load conditions the building can consume up to 1.6 MW of power. EnergyPlus

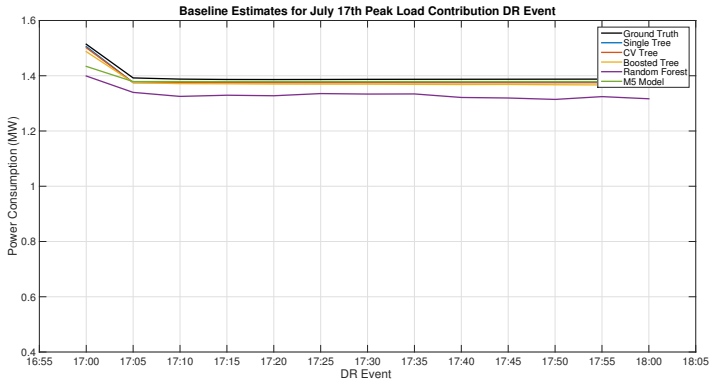

Figure 3: Comparison between the actual power consumption and the baseline prediction for July 17th, 2013; a peak load contribution day. The DR event is from 1700-1800 hrs.

provides typical meteorological year data files for many sites which are generated as averages of different weather characteristics across the past 15-30 years. However, for the purposes of the simulation we use `Actual Meteorological Year` (AMY) data from Chicago for the years 2012 and 2013.

The data that we use can be divided into three different categories as described below:

1. Weather data, which includes measurements of the dry bulb temperature, wet bulb temperature, relative humidity and wind conditions.
2. Schedule data, which includes fixed temperature set-points schedules of chilled water supply, supply air temperature and zone air temperature on the HVAC side and lighting schedules.
3. Building data, which includes the measurements of zone temperature, lighting, supply air and water temperatures, power consumption etc.

   In addition to these data sets we also train on engineered features like the time of day and the day of week.

DR Baseline

On July 17, 2013 a demand response event occurred across the PJM ISO from 1700 hrs to 1600 hrs. We estimate the baseline power consumption of the office building for the DR event for July 17, 2013. The result of this comparison is shown in Figure 3. In addition to evaluating a single regression tree, we implement and evaluate the performance of cross validated trees and the random forest and the boosted regression tree ensemble methods as well. The lowest root mean square error obtained in this case is only 12 kW on an average consumption of 0.62 MW, which corresponds to a normalised root mean square (NRMSE) of only 2.01%. Using the ensemble methods, the DR-Advisor is able to accurately predict the baseline consumption of the building using just weather and schedule data, which require little to no sensor installations at the building site.

DR Strategy Evaluation

As stated earlier, the challenge is DR strategy evaluation is to predict the power consumption profile of the building in real-time due to a fixed policy. The following demand response strategy is evaluated. Upon receiving the notification of the DR event at 1600 hrs, the zone air temperature set-point for all the zones is increased from a nominal value of 24°C by 2° to 26°C. The chilled water supply temperature set-point is increased from 6.7°C by 1.5° to 7.2°C. At the beginning of the event at 1700 hrs, the zone air temperature set-point is further increased by 2° and the chilled water supply temperature set-point

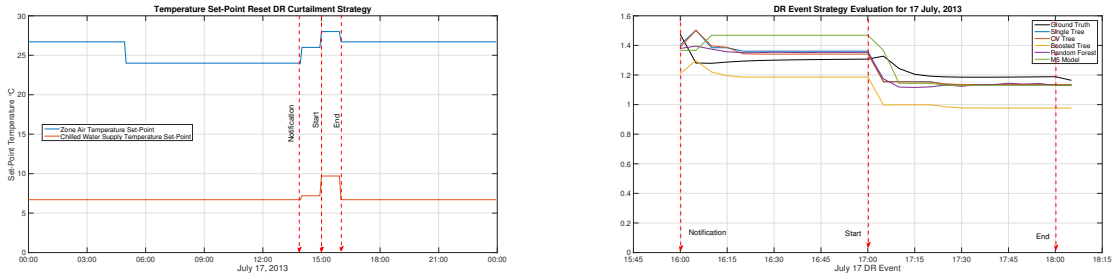

Figure 4: Left:Rule based demand response temperature set-point reset strategy executed for July 17, 2013. Right: Comparison between the actual power consumption and the predicted power for July 17th, 2013; There is a DR event from 1700-1800 hrs.

is increased by another 1.5°. This fixed, rule-based strategy is shown in Figure 4(left). The predicted response of the building compared to the actual response due to the fixed strategy is shown in Figure 4(right). We obtain an error of 6.23% for predicting the power consumption of the building in real time during a demand response event.

DISCUSSION

We presented DR-Advisor, a data-driven tool which acts as a recommender system for demand response baselining and strategy evaluation. We evaluate the performance of DR-ADvisor on a large scale DOE reference commercial building , using actual meteorological year data. We show how the tree based methods can achieve a good prediction accuracy of $3-6\%$ on average for all the cases. The biggest advantage of DR-Advisor is that it completely bypasses the need to build high fidelity models of buildings e.g., with EnergyPlus or with RC networks. Another major advantage of DR-Advisor is that the models it builds are highly interpretable and simple, an attribute which is often completely neglected in the design of such algorithms. These advantages combines with the fact that the tree based methods can achieve high prediction accuracies, make DR-Advisor a very alluring tool for evaluating and planning DR curtailment responses. DR-Advisor (Figure 2) is being developed into a free and open source tool. Since DR-Advisor is a data-driven approach, it can be easily scaled to multiple buildings and can be used for campus-wide demand response which is a part of our on-going work.

REFERENCES

1. Melillo, J. M., Richmond, T., and Yohe, G. W.: Climate change impacts in the united states: the third national climate assessment. *US Global change research program*, 841, 2014.
2. Goldman, C.: Coordination of energy efficiency and demand response. *Lawrence Berkeley National Laboratory*, 2010.
3. Commission, F. E. R.: Assessment of demand response and advanced metering. 2008.
4. pjm interconnection: 2014 demand response operations markets activity report. 2014.
5. Breiman, L., Friedman, J., Stone, C. J., and Olshen, R. A.: *Classification and regression trees*. CRC press, 1984.
6. Breiman, L.: Random forests. *Machine learning*, 45(1):5–32, 2001.
7. Deru, M., Field, K., Studer, D., et al.: U.s. department of energy commercial reference building models of the national building stock. 2010.

A PRINCIPAL COMPONENT ANALYSIS-BASED APPROACH FOR THE ONGOING COMMISSIONING OF CENTRIFUGAL CHILLERS

N. Cotrufo; R. Zmeureanu

Department of Building, Civil and Environmental Engineering, Centre for Zero Energy Building Studies, Concordia University, 1455 de Maisonneuve West, Montréal, Québec, Canada H3G 1M8

ABSTRACT

Ongoing commissioning (OCx) of HVAC systems aims to continuously monitor and analyse the building systems operation to detect faults and performance degradation in terms of operation costs, energy use and demand as well as quality of indoor environment. A huge amount of relevant operation data are collected and stored by the Building Automated System (BAS). Hence the extraction of information through data mining is a challenging aspect. Anomaly detection, clustering, classification and regression analysis are examples of data mining techniques. Regression techniques are probably the most used to identify relationships between measured data, and between indices of performance and data. Artificial Neural Network (ANN) models and Support Vector Method (SVM) are other examples of statistical learning techniques. This paper presents the use of Principal Component Analysis (PCA) for the OCx of chillers in a large cooling plant. PCA allows to drastically reduce the number of variables, preserving most of the information included in the original data set. A PCA based commissioning approach has been applied in this study to highlight changes in chiller operation level through the years, detect unexpected measurement values and address commissioning effort to solve them. Measurements have been collected by the BAS from two centrifugal chillers, of 3165 kW (900 tons) cooling capacity each, over six cooling seasons (May to September, from 2009 to 2014). The Principal Components (PCs) visualization have allowed to identify different operation patterns, supporting clustering and classification techniques implementation. The effectiveness of PC visualization is due to the PCA capability to reduce the number of variables to be used as regressors, and to represent, in a 2-D PC-based space, a data set made of several inter-correlated variables. Visualization techniques are considered very important to increase awareness and knowledge of building operators about equipment operation.

Keywords: Principal Component Analysis, Ongoing Commissioning, HVAC systems

INTRODUCTION

The use of Principal Component Analysis (PCA) for OCx of HVAC systems was not exploited enough in the recent past. PCA based detection and diagnosis methods have been developed for AHUs and AHU sensor faults, Wang and Xiao [1] and Li and Wen [2]. In [3] a PCA based linear regression model has been developed to predict electricity consumption in an office building. All the above cited studies highlight the PCA capability to reduce large number of variables to few new components while maintaining most of the information. In this paper, PCA is applied to the BAS trend data from a cooling plant to identify patterns, implement OCx and visualize variations in chiller operation performance over the years.

METHOD

PCA transformation, applied to a data set X of j inter-correlated variables and i observations, produces a new set F of j independent variables, the Principal Components (PCs), which contains the same original data set information. F elements ($f_{i,j}$), named *scores*, are the

coordinates of the original data along the PCs, and are given by linear combination (1) of the $x_{i,j}$ Original Variables (OVs) with the *coefficient matrix Q*, made of $q_{j,j}$ elements [4]. *Q* is evaluated by PCA transformation.

$$f_{i,j} = x_{i,1} \cdot q_{1,j} + x_{i,2} \cdot q_{2,j} + \ldots + x_{i,j-1} \cdot q_{j-1,j} + x_{i,j} \cdot q_{j,j} \quad (1)$$

Dealing with variables of different units and range of variation, some sort of data normalization is needed [5]. Here, given a data set X = [*i* x *j*], of *i* observations and *j* variables, normalization goes through the average column values (m_j), and the *j* columns standard deviations (σ_j):

$$zx_i = \frac{x_i - m_i}{\sigma_i} \quad (2)$$

Variables reduction results from the distribution of explained variance along the PCs *(figure 1)*. The first 2-3 PCs account together for the most of the original data set variance. Chiller #2 operation data from 2010 to 2014 have been compared against a 2009 data based threshold. Data sets have been normalized (3), and projected into a 2-D PCs based space (4), with reference to 2009 data PCA transformation:

$$zX_{2010} = \frac{X_{2010} - mX_{i,2009}}{\sigma X_{i,2009}} \quad (3)$$

$$F_{2010} = zX_{2010} \text{ x } Q_{2009} \quad (4)$$

where: zX_{2010} is the 2010 normalized data set; X_{2010} is the original 2010 data set; $mX_{i,2009}$ is the 2009 data set mean value vector; $\sigma X_{i,2009}$ is the 2009 data set standard deviation vector; F_{2010} is the 2010 matrix of scores; Q_{2009} is the 2009 matrix of PCA coefficients.

An elliptical threshold condition has been formulated (5), based on the Gaussian approximation of *scores* distribution along PCs. Hence, around 95% of *scores* is expected to be within the interval $[-2 \cdot \sigma_{pc} ; 2 \cdot \sigma_{pc}]$ around the mean value.

$$|y| < \sqrt{b^2 \cdot \left(1 - \frac{x^2}{a^2}\right)} \; ; \; a = 2 \cdot \sigma_{pc1} \; ; \; b = 2 \cdot \sigma_{pc2} \quad (5)$$

RESULTS

This study focuses on a cooling plant installed in a University Campus in Montreal, QC. It consists of two centrifugal chillers (CH-1 and CH-2) of 3165 kW (900 tons) cooling capacity each. When one chiller is not sufficient to match the thermal load, the second one starts, working simultaneously with the first chiller. Chilled water is circulated by constant speed pumps of around 86.5 L/s [6]. The BAS collected measurements each 15 minutes. Data set includes 9,408 measurements per cooling season, over 14 weeks, for four different operation modes: *a*) both the chillers (CH-1 and CH-2) work at the same time; *b*) only CH-1 works; *c*) only CH-2 works; *d*) no chiller. We considered nine variables at plant level: chilled water flow rate from the central plant, $\dot{m}_{chw}$; difference of return – supply chilled water temperature, ΔT_{CP}; electrical power input to CH-1 and CH-2, E_{CH-1} and E_{CH-2}; water temperature difference at the evaporator of CH-1 and CH-2, ΔT_{CHW}^{CH-1} and ΔT_{CHW}^{CH-2}; water temperature difference at the condenser of CH-1 and CH-2, ΔT_{CND}^{CH-1} and ΔT_{CND}^{CH-2}; outdoor air temperature, T_{OA}. A preliminary PCA based analysis has been conducted at plant level. *Coefficient* matrix *Q* with the projection coefficients for the first two PCs are given in (6). Equation (7) gives an example of *i* score calculation for PC #1.

$$Q = \begin{array}{c} \begin{array}{cccccccc} PC\#1 & PC\#2 & PC\#3 & PC\#4 & & PC\#8 & PC\#9 \end{array} \\ \begin{pmatrix} +0.401 & +0.152 & +0.631 & +0.287 & \cdots\cdots & -0.163 & -0.021 \\ +0.421 & -0.001 & -0.436 & -0.605 & \cdots\cdots & -0.127 & +0.026 \\ +0.359 & -0.320 & +0.157 & -0.023 & \cdots\cdots & +0.257 & -0.656 \\ +0.176 & +0.486 & +0.058 & -0.701 & & +0.747 & +0.124 \\ +0.367 & -0.305 & +0.167 & -0.053 & \cdots\cdots & -0.002 & +0.720 \\ +0.167 & +0.484 & +0.098 & -0.101 & \cdots\cdots & -0.574 & -0.149 \\ -0.371 & +0.298 & -0.056 & +0.150 & & +0.004 & +0.112 \\ -0.196 & -0.474 & -0.008 & +0.150 & \cdots\cdots & -0.038 & +0.032 \\ +0.404 & +0.070 & -0.585 & +0.698 & \cdots\cdots & -0.035 & +0.0073 \end{pmatrix} \end{array} \quad (6)$$

$$f_{i,1} = x_{i,1} \cdot 0.401 + x_{i,2} \cdot 0.421 + \ldots + x_{i,j-1} \cdot (-0.196) + x_{i,j} \cdot 0.404 \quad (7)$$

Figure 1 shows the cumulative original data set variance explained by PCs. The first two PCs account together for about 93% of the original data set information. *Figure 2* shows the scores from 2009 data set represented in a 2-D PCs based space. It is worth to notice that PCA distinguishes different operation modes through well-defined point clouds, which can be useful to identify normal operation modes and detect abnormal situations. The case of CH-2 working alone have been considered for a PCA-based analysis. A threshold condition, developed based on 2009 data set, has been applied to data over six cooling seasons to highlight changes in CH-2 operation level. A separate five OVs list has been considered for chiller analysis: electrical power input, $E_{CH\text{-}2}$ [kW]; outdoor air temperature, T_{OA} [ºC]; difference of water temperature across the evaporator and condenser, ΔT_{CHW}^{CH-2} and ΔT_{CND}^{CH-2} [ºC]; chilled water flow rate, $\dot{m}_{\text{chw}}$ [L/s] (*table 1*).

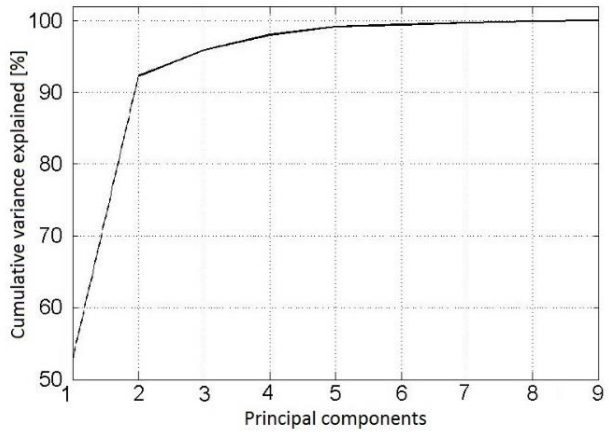

Figure 1: Cumulative variance explained by PCs, cooling plant data set from summer 2009.

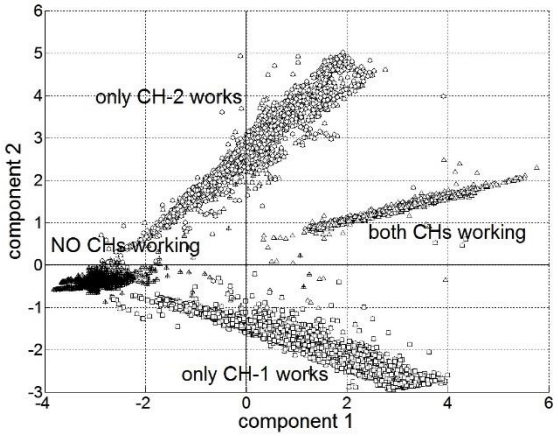

Figure 2: Cooling plant 2009 data set scores plotted in a 2-D PC based space.

	$E_{CH\text{-}2}$ [kW]	T_{OA} [°C]	ΔT_{CHW}^{CH-2} [°C]	ΔT_{CND}^{CH-2} [°C]	$\dot{m}_{chw}$[L/s]
Range of variation	71 - 530	11.9 – 39.8	0 – 13.5	-9.6 - 0	69.4 – 95.7
Mean value	297	21.5	4.1	-4.6	84.7
Standard deviation	96.4	4.54	1.53	1.79	4.99

Table 1. Selected original variables of summer 2009 for the PCA of chiller CH-2

PC #1 and PC #2 together account for about 92% of information in the original CH-2 data set. In *Figure 3* are represented the OV axes in a 2-D PC based space, given plotting the first two column of the *coefficient* matrix. 2009 data scores for PC #1 and #2 are represented in *Figure*

4. Any interpretation of *scores* distribution should be based on OV axes orientation. Assuming a Gaussian distribution of *scores* along PC axes, around 95% of *scores* are expected to be within the range [-2·σ; 2·σ]. For PC #1, 97% of the *scores* is in the range [-2·σ_1; 2·σ_1] while, for PC #2, 98% of the *scores* is within the range [-2·σ_2; 2·σ_2]. *Figure 5* shows results from applying 2009 threshold condition to following cooling season data sets. Results are given in terms of percentage of data points per year, which comply with 2009 threshold. Over six years, the percentage of data points within the threshold decreases from 93.3% (2009) to 83.7% (2014). The annual mean values of the PC #1 and PC #2 through the years (*Figure 6*) moved from the origin, which could indicate the change of annual mean operation data.

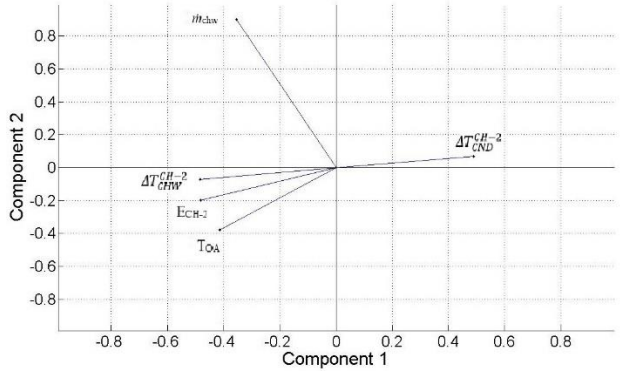

Figure 3. CH-2 OV axes projected on a 2-D principal component based space.

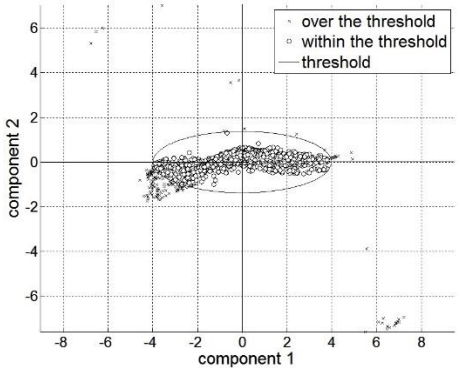

Figure 4. 2009 data sample plotted against the threshold in a 2-D PCs based space.

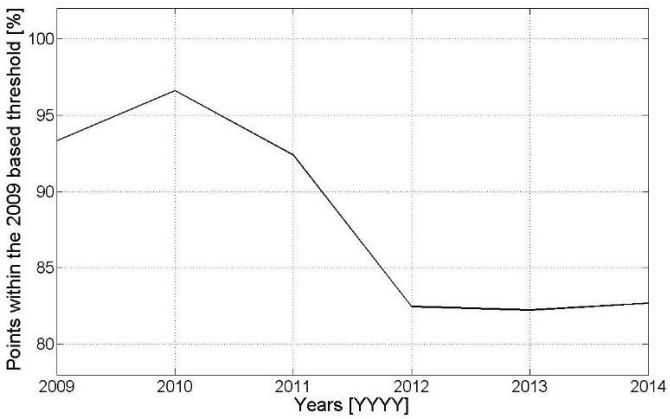

Figure 5. Percentage of data points per year which comply with the 2009 based threshold condition.

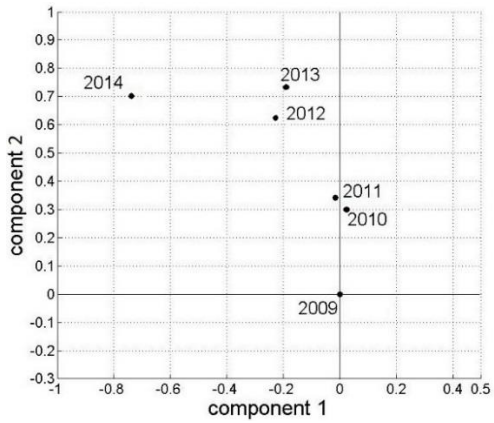

Figure 6. Variation of annual mean values of PC #1 and #2, 2009 to 2014.

DISCUSSION

The threshold condition can give information about quantitative aspects in operation changes. The trend of percentage of outliers per year highlights that some change in operation occurred (*figure 5*), although it is not necessary to be considered as *degradation*. We name this phase "*detection*". Otherwise, in order to understand the causes of operation changes, we have to deal with the OV axes orientation (*figure 3*). The more a point is located far from the *zero-*

value of the *j*-variable axis, the more an unexpected *j*-variable value characterizes that point. For each outliers, the distance from the *zero*-value of each variable axis has been evaluated. *Table 2* gives, for 2014 *scores*, the statistics of the most influential OV per outlier.

	Variables	Count [-]	Percent [%]
1	Electrical power input	0	0.0
2	Outdoor air temperature	621	97.2
3	Difference of water temperature across the evaporator	0	0.0
4	Difference of water temperature across the condenser	0	0.0
5	Chilled water flow rate after the two chillers	18	2.8

Table 2. Frequency of the most influential original variables of 2014 data set

Over 639 outliers have been detected for 2014 data set. According to *table 2*, the outdoor air temperature and the chilled water flow rate are the outliers most influential OVs. The outdoor air temperature is accountable for 97.2% of the outliers, while the remaining 2.8% are due to the chilled water flow rate. In this case, the commissioning efforts focus on those two OVs variables. A detailed investigation revealed that the outdoor air temperature measurements had fast and abnormal temperature variation within one time step (15 minutes). That was due to two elements: the difference in outdoor air temperature between 2009 and 2014, and the need for re-calibration and re-location of the air temperature sensor. PCA showed to be effective in the detection of abnormal values.

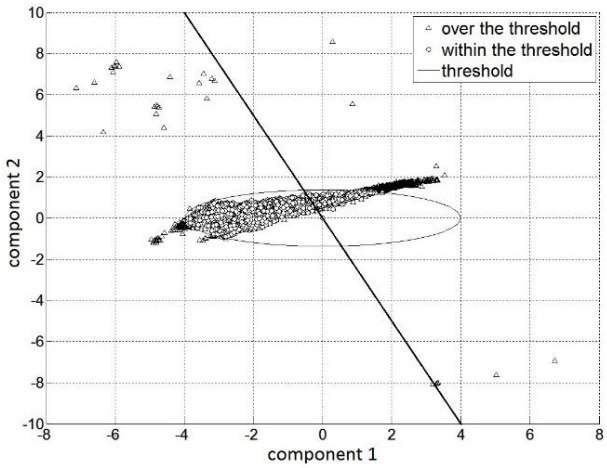

Figure 7. 2014 data set in a 2-D PC based space against the reference threshold. The axis of chilled water flow rate is showed.

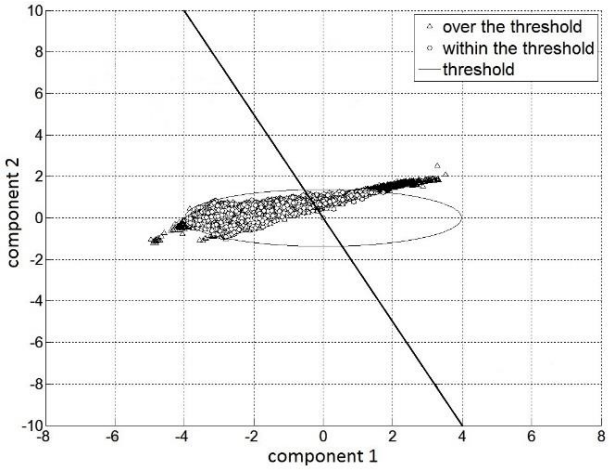

Figure 8. 2014 modified data set in a 2-D PC based space against the reference threshold. The axis of chilled water flow rate is showed.

The expected chilled water flow rate, for only one chiller works, is around 86.5 L/s. Several times during the summer of 2014, some isolated, unexpected values, have been recorded (*figure 7*). A test is simulated by excluding the unexpected chilled flow rate measurements from the data set. PCA applied to modified data set shows that $\dot{m}_{chw}$ is not anymore responsible for any of the remaining outliers (*figure 8*). Again, the PCA based approach correctly detected abnormal values and addressed efforts in the right direction.

CONCLUSION

PCA has been used to study a cooling plant and its changes in performance through six consecutively summer seasons. A threshold definition has been given based on 2009 reference data set, and changes in the equipment performance have been highlighted in terms of outliers from the threshold, which is intended as representative of proper chiller operation. The proposed approach proved to effectively capture the variation in percentage of points which comply with the threshold condition, from 93.3 % in 2009 to 83.7 % in 2014. The chiller's performance seems to change, although the change is not qualified as a system degradation. Also, the proposed method allowed to identify the influential OVs for outliers in 2014, effectively addressing efforts to identify faults in chiller operation. The possibility to reduce to two principal components a bigger number of original variables allows to display 2-D representations of the equipment performance. This would increase building operator's awareness and knowledge in HVAC system operation.

ACKNOWLEDGEMENT

The authors acknowledge the support from the NSERC Smart Net Zero Energy Buildings Network and from the Faculty of Engineering and Computer Science, Concordia University, Montreal Canada.

REFERENCES

1. Wang, S., & Xiao, F.: Detection and diagnosis of AHU sensor faults using principal component analysis method. *Energy Conversion and Management, 45*(17), 2667-2686, 2004;
2. Li, S., & Wen, J.: A model-based fault detection and diagnostic methodology based on PCA method and wavelet transform. *Energy and Buildings, 68*, 63-71, 2014;
3. Lam, J. C., Wan, K. K., Cheung, K., & Yang, L.: Principal component analysis of electricity use in office buildings. *Energy and Buildings, 40*(5), 828-836, 2008;
4. Abdi, H., & Williams, L. J.: Principal component analysis. *Wiley Interdisciplinary Reviews: Computational Statistics, 2*(4), 433-459, 2010;
5. Reddy, T. A.: *Applied data analysis and modeling for energy engineers and scientists* Springer Science & Business Media, 2011;
6. Monfet, D.: *New Ongoing Commissioning Approach of Central Plants: Methodology and Case Study*, PhD Thesis, Concordia University, Montreal, QC, 2011.

FIELD TESTS OF AN ADAPTIVE MODEL-PREDICTIVE HEATING CONTROL SYSTEM

D. Lindelöf[1], H. Afshari[1], M. Alisafaee[1], J. Biswas[1], P. Borsò[1], X. Mocellin[1], J. Viaene[1]

[1]*Neurobat AG, Research and Development, Rue de Veyrot 9, 1217 Meyrin, Switzerland*

ABSTRACT

Model-predictive control (MPC) has shown in the past great potential for optimising the operation of heating control systems in buildings, but the major drawback has always been the automatic identification of the system itself. In this work we report on field tests of a heating control system derived from previous research work at EPFL, implementing MPC with an adaptive model, i.e. a model that identifies automatically its parameters. These field tests involved 10 sites, most of them single-family houses. By alternating on a regular basis (typically every two weeks) between the original control system and the model-predictive one, we have derived estimates for the possible energy savings; these estimates range from 10% to 40%, with a marked improvement in the stability of the indoor temperature.

INTRODUCTION

Space heating is one of the largest consumers of energy in buildings, but even professional heating installers find it remarkably difficult to properly configure a central heating installation. Furthermore, there is little economic incentive for them to do so: few customers will be able to prove that a building could use less energy if it were better parameterised. This is especially true for smaller installations such as single-family dwellings. With little information at their disposal, most end-users are satisfied provided that the indoor comfort is maintained. Consequently, the energy demand of much of the existing building stock is significantly higher than needed, although there is little research on the subject.

A solution is the so-called *Model-Predictive Control* (MPC) class of algorithms, where a mathematical representation of the building, together with a model of the future climate conditions, let the system compute the flow temperature that minimises the consumed energy while preserving thermal comfort. MPC has attracted much interest because, provided the model is accurate and provided the prediction of future perturbations is correct, it is not possible to significantly outperform such a system. Furthermore, by choosing a suitable formulation of the objective function, it is possible to incorporate desirable attributes such as time-varying tariffs; future changes in setpoint; night-setback; constraints on control variables; and constraints on the rate of change of control variables. There is no significant additional computational cost for including such constraints.

The present work traces its roots to the NEUROBAT swiss research project [1, 2, 3, 4, 5], an early proposal for a so-called *adaptive model-predictive control* of heating systems. The algorithms enabled an efficient MPC for HVAC without requiring the user to provide an identified model; the model itself, being provided with sensor data, was capable of identifying its own parameters while running. However, computing costs at that time made its commercial implementation impractical.

In this paper we report on experimental tests carried out during the 2013–2014 heating season on ten test sites with a recently introduced commercial model-predictive heating controller that features a adaptive model. As will be seen, the controller achieved an average of 25% energy savings without requiring any major intervention on the building itself. A more complete description of the present work can be found in [6].

THE MODEL-PREDICTIVE HEATING CONTROLLER

Our building model is based on the adaptive model described in [1, 2, 3, 4, 5], and implemented in a commercial product called the NiQ. The NiQ samples its sensors always simultaneously and at regular intervals (every 900 s). The current and past sensor values are used by the model to predict the indoor temperature at the same instant. The actual, measured value of the indoor temperature is compared to the predicted value, resulting in some error. The self-learning algorithm uses this error to update the parameters of the building model. Thus, over time, the building model adjusts its internal parameters and reduces the prediction error. Similarly, a climate model is trained for the short-term prediction of local weather conditions.

The optimal control strategy consists in finding the sequence of hot water temperature values that results in the best trade-off between energy consumption and discomfort. We form a cost function that is to be minimised, taking as arguments the controlled values, as follows. Let t_{setpoint} be the normal indoor temperature setpoint (chosen by the user), t_{reduced} be the reduced indoor temperature setpoint (the minimum indoor temperature that must be maintained at all times), and t_{flowmax} the highest allowed flow temperature (detected by the NiQ from historic data). Furthermore, let $\sigma[i]$ be a vector of zeroes and ones, indicating whether normal or reduced comfort should apply at time i.

Then the problem can be stated as:

$$\begin{aligned} \text{minimize} \quad & \sum_{i=1}^{N} \sigma[i](t_{\text{indoor}}[i] - t_{\text{setpoint}})^2 + \lambda \sum_{i=1}^{N} t_{\text{flow}}[i] \\ \text{subject to} \quad & \begin{cases} t_{\text{indoor}}[i] \geq t_{\text{reduced}}, & i = 1, \ldots, N \\ t_{\text{indoor}}[i] \leq t_{\text{flow}}[i] \leq t_{\text{flowmax}}, & i = 1, \ldots, N \end{cases} \end{aligned}$$

Here it is understood that the $t_{\text{indoor}}[i]$ values are predicted by the building model from the future flow temperatures $t_{\text{flow}}[i]$, the future outdoor temperatures $t_{\text{out}}[i]$ and the future solar irradiance $e[i]$. The $t_{\text{flow}}[i]$ values are the N optimization variables of the problem; the control horizon being 24 hours at 900 s intervals, we have $N = 24 \times 3600/900 = 96$. The problem is a constrained minimization problem with 96 variables. λ is a parameter that controls the relative trade-off between discomfort and energy consumption.

When the problem is solved, $t_{\text{flow}}[1]$ is returned as the optimal flow temperature that is to be applied for the next 900 s, after which the process is repeated, in a classic receding horizon control strategy. The NiQ manipulates the outdoor temperature measured by the heating controller in order to keep the flow temperature close to this optimal value.

METHODOLOGY

We have tested the performance of this system during the 2013–2014 heating season on eight single-family houses and two appartments. The NiQ uses PT1000 temperature sensors to measure the forward and return flow temperatures, the indoor temperature, and the outdoor temperature. The solar irradiance is measured with a GBS01 irradiance sensor [7]. A laptop was connected to the NiQ, sampling the sensor values every 5 minutes through a serial port, and copied to a database every hour.

The NiQ features a mode where it merely copies the real outdoor temperature to the temperature "seen" by the heating controller. When in this so-called *bypass mode*, the original controller runs as if no NiQ had been installed. We alternated between the two modes (bypass and normal) at periodic intervals, letting each mode run for at least two weeks before switching again.

For each day of the experiment, we derive:

- The date;
- The mode, i.e. bypass or normal;
- The daily mean outdoor temperature;
- The daily mean indoor temperature;
- The daily mean temperature of the heating fluid;
- The daily mean solar irradiance;
- The energy consumption of the space heating.

RESULTS

The energy requirements for space heating in a residential building should be a linear function of the difference between the indoor and the outdoor temperature. If the indoor temperature is kept constant (as is usually the case in homes), then the energy requirement for space heating becomes an affine function of the outdoor temperature.

For each day of the field tests, and for each site, we plot in Fig. 1 the daily space heating energy against the mean daily outdoor temperature, together with a regression line. A separate regression is carried out for the NiQ and for the reference controller. The difference between the slopes of these regression lines yields the relative energy savings of one controller against another.

The estimated relative energy savings with their standard errors are given in Table 1 and shown graphically in Fig. 2.

From this sample of buildings, the mean energy savings can be estimated. We take into account the uncertainties surrounding the estimates for each site by forming a weighted average, taking as weights the inverse of the estimated variances (the squares of the estimated standard errors). We obtain a mean energy savings of 0.254 ± 0.034. In other words, installing the NiQ system on a large population of buildings can be expected to achieve about 25% heating energy savings.

We conclude by evaluating the resulting thermal comfort. We will use a metric commonly used by heating professionals: the proportion of daytime during which the indoor temper-

Site	$\alpha_{\text{Ref.}}$	$\Delta\alpha_{\text{NiQ}}$	Savings	Setpoint [°C]	$\text{RMSE}_{\text{Ref.}}$	RMSE_{NiQ}
Luedenscheid	-3.72 ± 0.69	1.88 ± 0.95	0.505 ± 0.20	22.00	1.86	1.73
Ruswil	-6.66 ± 0.31	2.71 ± 0.47	0.408 ± 0.06	21.00	4.00	2.12
Ihmert	-6.21 ± 4.97	2.24 ± 5.04	0.361 ± 0.53	23.00	1.49	0.76
Sprockhoevel	-11.1 ± 1.40	3.7 ± 1.62	0.332 ± 0.11	21.50	1.20	0.34
Brugg	-7.19 ± 0.23	2.23 ± 0.90	0.311 ± 0.12	22.00	1.24	0.38
Remscheid	-9.65 ± 0.48	1.59 ± 1.08	0.165 ± 0.11	21.00	0.48	0.30
Fey	-6.29 ± 1.64	0.715 ± 1.71	0.114 ± 0.24	23.00	1.32	0.25
Unterengstringen	-6.3 ± 0.55	0.711 ± 0.80	0.113 ± 0.12	21.00	0.87	0.21
Lausanne	-17.2 ± 0.76	1.04 ± 1.27	0.0603 ± 0.07	22.50	0.42	0.29
Hedingen	-4.62 ± 1.09	0.154 ± 1.20	0.0334 ± 0.25	23.50	0.29	0.17
Mean			$\mathbf{0.254 \pm 0.034}$			

Table 1: Slope of the regression line (α) for all test sites, mean energy savings, indoor temperature setpoint, and root mean square error between indoor temperature and setpoint. The sites are sorted by decreasing energy savings.

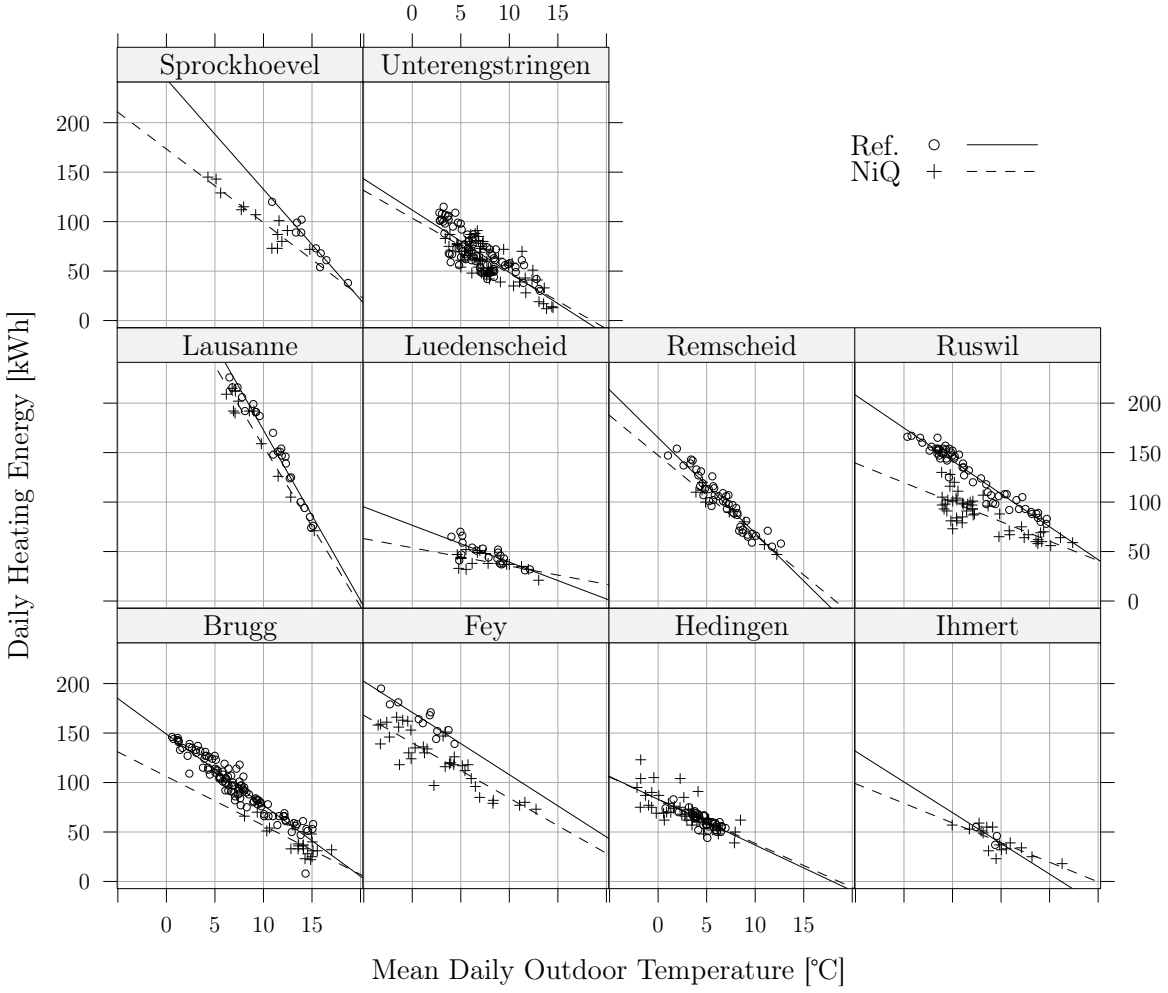

Figure 1: Energy signatures for all test sites, for both control systems.

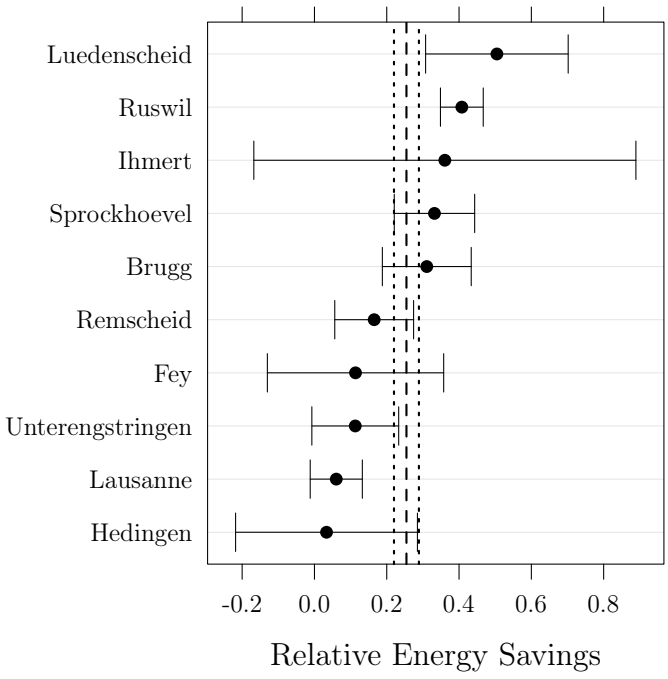

Figure 2: Estimated relative energy savings (with standard error) on all test sites. The dashed lines show the estimated average with its standard error.

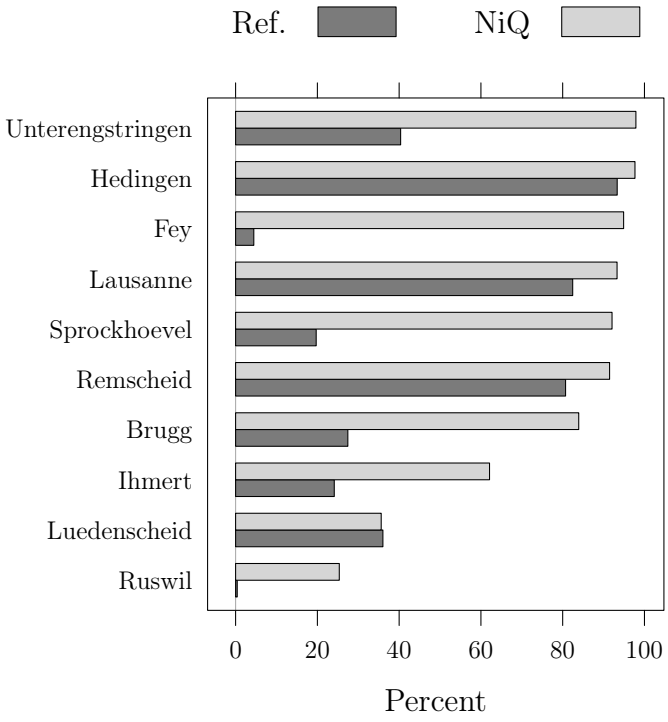

Figure 3: Percentage of time within half a degree of the indoor temperature setpoint, for both control systems. The sites are sorted by decreasing comfort with the NiQ.

ature is within half a degree of the desired setpoint. That fraction is shown, in percent, in Fig. 3 for all test sites and for both controllers. The comfort improvement with the NiQ is evident for all sites.

CONCLUSION

Conventional weather-compensated heating controllers are by nature open-loop controllers. Their efficiency depends on the correctness of their parameterization, and they are unable to take into account future climate conditions. This results in wasted energy and a less than optimal thermal comfort.

One solution to this problem is believed to be the adaptive model-predictive class of controllers. Such a controller has been proposed for the heating control of residential buildings by the NEUROBAT swiss research project, which we have implemented in an embedded controller.

We have tested this sytem against existing heating controllers during the 2013–2014 heating season on ten different test sites. All test sites have yielded positive relative energy savings, with a mean and standard error of 0.254 ± 0.034.

Adaptive model-predictive control has therefore been shown to be a viable solution to achieve significant energy savings on the heating of residential buildings, at a fraction of the cost usually required for more invasive procedures.

References

1. Bauer, M. *Gestion Biomimétique de l'Energie dans le Bâtiment*. PhD thesis, Ecole Polytechnique Fédérale de Lausanne, 1998.
2. Bichsel, J., Krauss, J., and Bauer, M. Neurobat - Neuronaler Heizungsregler Schlussbericht Phase II. Technical report, 2000.
3. Krauss, J., Bauer, M., Bichsel, J., and Morel, N.: Energy and HVAC: NEUROBAT—a Self-Commissioned Heating Control System Using Neural Networks. In *Sensors Applications*, pages 63–83. 2008.
4. Morel, N., Bauer, M., El-Khoury, M., and Krauss, J.: Neurobat, a predictive and adaptive heating control system using artificial neural networks. *International Journal of Solar Energy*, 21(2-3):161–202, 2001.
5. Neurobat Final Report to Swiss Federal Office of Energy. LESO-PB/EPFL, Lausanne, Switzerland. A predictive neuro-fuzzy building control system. Technical report, 1998.
6. Lindelöf, D., Afshari, H., Alisafaee, M., Biswas, J., Caban, M., Mocellin, X., and Viaene, J.: Field tests of an adaptive, model-predictive heating controller for residential buildings. *Energy and Buildings*, 99:292–302, 2015.
7. Technische Alternative. Radiation sensor. `http://www.ta.co.at/en/products/sensors/radiation-sensor.html`, 2014. accessed 13-June-2014.

A NOVEL OCCUPANT-ADAPTED AND FUZZY LOGIC-READY VISUAL COMFORT MODELLING APPROACH USING MACHINE LEARNING ALGORITHMS

N. Zarkadis; N. Morel; J.-L. Scartezzini

Solar Energy and Building Physics Laboratory (LESO-PB), Ecole Polytechnique Fédérale de Lausanne (EPFL), Station 18, CH-1015 Lausanne /Switzerland

ABSTRACT

In this article we present a novel approach to model visual comfort based on supervised state-based machine learning with Hidden Markov Models and one easy-to-obtain variable (illuminance measurements at the horizontal work-plane; E_{desk}). Data mining was performed on sensor data recorded for two years in a single-occupant office room and the developed model classifies workplane illuminances into 3 states: comfort; discomfort because of low light; discomfort because of excessive light.

Results show that a training period of 4 to 8 months of recorded data leads to a visual comfort identification (classification) accuracy of 100%. When training the model using 4-month data, an overall 92% accuracy can be achieved (75% for the 'discomfort because of low light' state). Following further analysis of this occupant-adapted model, we discuss the confidence ('normalised relative likelihood') with which the model classifies illuminances in one of three different states as a function of the E_{desk}. We argue that the resulting metrics are an ideal input which can be readily used into automatic lighting controllers based on fuzzy logic. Last, the model's performance is compared and validated against state-of-the art classifiers such as Bayesian and k-Nearest Neighbors.

Keywords: visual comfort, machine learning, Hidden Markov Models, fuzzy logic, lighting control

INTRODUCTION

Light has important visual and non-visual effects on humans so the provision of good lighting conditions inside buildings is central in shaping a healthy and productive indoor environment [1; 2]. The estimation of the lighting quality in buildings has been the subject of continuous research since the 1950s and since then methods and indices have been developed focusing on the estimation of discomfort glare due to daylight [3 pp. 108-112]. However, no one method is accepted as a standard internationally. Further, most of them suffer from inherent limitations: they require detailed information on the occupant's field-of-view which is usually acquired by means of extensive hardware and software equipment; they address an "average user" without taking into account individual needs and preferences; they often output numbers that are non-intuitive and are difficult to interpret; they only estimate discomfort glare without addressing discomfort caused by insufficient or excessive lighting conditions. In the presented research we attempt to tackle these limitations by using machine learning techniques such as Hidden Markov Models (HMM).

HMM are state-based stochastic approaches that can be used for modelling of complex systems via machine learning. They find applications in domains such as speech and handwriting recognition, biometric authentication and financial time series analysis [4; 5]. More recently they have been used in building control in the fields of occupant pattern detection [6; 7] and appliance identification [8]. In HMM, the system being modelled is

assumed to be a Markov process with hidden states but with visible output tokens which depend on the (hidden) state. For instance, when modelling the visual comfort variable we "cannot see" the state in which the variable is in (comfort, discomfort, etc.) but the parameters of the model (also known as *observations*) are visible and known (e.g. desktop illuminance or user actions with the blinds). To the best of our knowledge, this is the first attempt to model visual comfort using HMM.

METHODS

In this paper we use the HMM Matlab toolbox built in the framework of the Green-Mod research project and described by Ridi et al. [9 pp. 4-5]. The data used for the machine learning and the development of the model were collected in the LESO solar experimental building from 2001 to 2008 and recorded in a MySql database [10]. Data mining was performed on sensor data recorded for two years in a single-occupant LESO office room (1347 user actions were considered out of a total 736695 database entries).

Model's description

The model is consisted of (and classifies workplane illuminances into) three hidden states: *Comfort*, *Discomfort-L* (Discomfort because of Low illuminances) and *Discomfort-H* (Discomfort because of High illuminances). As with other generative algorithms, HMM perform the classification task by learning one model per class (state). In the presented implementation each state of the models corresponds to one of the 3 states above.

The model's topology is considered as *ergodic*, meaning that every state of the model can be followed or preceded by any of the other two. The training and the testing of the model is based on observations containing only one visible output token (the illuminance value at the horizontal work-plane: E_{desk}). For the training phase, observations are labelled as one of the 3 states above (supervised training). The labelling task is based on previous research performed at the LESO solar experimental building [11]. The $\mathrm{E_{desk}}$ immediately preceding a user action resulting in a modification of the workplane illuminance (i.e. actions on the electric lighting or on the blinds) is labelled either *Discomfort-L* or *Discomfort-H*, depending whether the action resulted in an increase or in a decrease of $\mathrm{E_{desk}}$, respectively, while the $\mathrm{E_{desk}}$ recorded immediately after the action is labelled *Comfort*. Depending on the observation data distribution, the considered number of Gaussians per state varies, as it is shown in the Results Section.

Regarding the datasets, it should be noted that although the unprocessed illuminance measurements pulled from the database are continuous temporal signals ranging from 0 to about 3,500 lux, the filtering out and labelling processes above result in discrete, non-continuous illuminance values recorded immediately before or after a user action. Thus, between two consecutive values in the observations dataset there is an unknown number of values filtered out. Likewise, the elapsed time between two consecutive values can be anything from a few minutes to hours or days.

State identification I: Classification

Once these observations datasets are prepared, their sequence is decoded and the most probable sequence of states is recovered with the use of the *Viterbi* algorithm. The Viterbi algorithm is a dynamic programming algorithm which computes the best state sequence (among the hidden states) that results in a sequence of observations (our training data). The algorithm tests every observation separately against each of the 3 possible hidden states and finds the most likely state that this observation sequence belongs into. It then computes and

outputs the *alignment* (the state sequence) and the associated probability (*likelihood*). As Rabiner [12] explains, if $Q = \{q_1, q_2, \dots, q_T\}$ is the best state sequence for a given observation sequence $O = \{O_1, O_2, \dots, O_T\}$, we define for the model λ the best score $\delta_\tau(i)$ along a single path at step *t* (which accounts for the first *t* observations) and ends in state $S_{i,}$, as follows:

$$\delta_t(i) = \max_{q_1, q_2, \dots, q_{t-1}} P\ [q_1 q_2 \cdots q_t = i, O_1 O_2 \cdots O_t | \lambda] \quad (1)$$

Where by induction:

$$\delta_{t+1}(j) = [\max_i\ \delta_t(i) a_{ij}] \cdot b_j(O_{t+1}) \quad (2)$$

In the above equations, a_{ij} denotes the state transition probability between states *i* and *j* and b_j represents the emission probabilities of state *j*. To get the actual state sequence, we keep track of the argument which maximised (2), for every *t* and *j*. This information is used by the HMM to classify the given observations into the three hidden states. The classification accuracy, which is the percentage of the correctly identified test sets, is presented in the *Confusion matrices.*

State identification II: Confidence of identified states

In the classification phase, the HMM-based model processes a given set of illuminance observations and outputs the best state that matches them. In this phase we move beyond the crisp answer and explore the confidence with which the model decides on one state over the other two.

For this, the *likelihood* scores of the Viterbi algorithm are employed. In the HMM toolbox used, the scores are obtained via a log-likelihood and, as shown above in (1), are computed on a one-to-one basis (each observation against each state), so they are not directly comparable. To enable comparisons, a normalisation of the acquired log-likelihoods of the 3 states is performed. If X_i is the log likelihood for the state i, then the normalised relative likelihood for this state is calculated as follows:

$$\text{Normalised likelihood}_i = e^{X_i} \Big/ \sum_{i=1}^{3} e^{X_i} \quad (3)$$

By applying the above equation for each of the 3 identified states, we obtain for every observation set the confidence with which is classified in a state.

RESULTS

This section presents the results acquired during the development of a Visual Comfort model using HMM approaches and based on horizontal plane illuminance measurements.

HMM Identification accuracy

The results presented in Table 1 demonstrate that 100% identification accuracy is achieved when the developed models are tested against real data collected from the same office room. Several training/testing cycles were performed, where we varied the number *k* of Gaussian mixtures (GMMs) and each time the observation data sets were randomly separated into either training or testing data to minimize bias. Multiple tests revealed that a training period of 4 to 8 months of recorded data is necessary to maintain the model's accuracy at this percentage, even when using a relatively low number of k (1 to 10). Table 2 shows the best results achieved when reducing the training period (down to 4-month data). For a k=13, 92% overall identification accuracy is attained (75% for the 'Discomfort-L' state). Higher values of k were

tested but the reduced size of the training tests resulted in non-convergence of the algorithms after a finite number of iterations.

k: 1-10	Discomfort-L	Comfort	Discomfort-H
Discomfort-L	100	0	0
Comfort	0	100	0
Discomfort-H	0	0	100

Table 1: Confusion matrix showing accuracy per state (in percentages). Results were obtained using training data corresponding to 8-20 months of observations for the GMMs with 1-10 mixtures (k).

k: 13	Discomfort-L	Comfort	Discomfort-H
Discomfort-L	75	25	0
Comfort	0	100	0
Discomfort-H	0	0	100

Table 2: Confusion matrix showing accuracy per state (in percentages) with reduced training data (equivalent to about 4 months of observations) for the GMMs with 13 mixtures (k).

Classification

The results presented in this section show the response of the developed model as a classifier of workplane illuminance values (E_{desk}). We considered HMM trained with all the available observation data (24-month long) and tested against synthetic illuminance values that ranged from 0 to 3500 lux and for different GMM mixtures *k* ranging from 1 to 40. For k>5, the *Comfort* state identification pattern is stabilised in the region between 500 and 1300 lux while illuminances below and above this zone are consistently classified as *Discomfort-L* and *Discomfort-H*, respectively (Figure 1). Models with k>15 produce more fine results and reveal subtleties that include a visual comfort zone on and slightly past the 1500 lux mark. However, these subtleties do not prevail among all the tested models hence they do not appear on the mean classification results of all the models illustrated in Figure 1, which summarizes the outcome of the 1400 testing cycles[1].

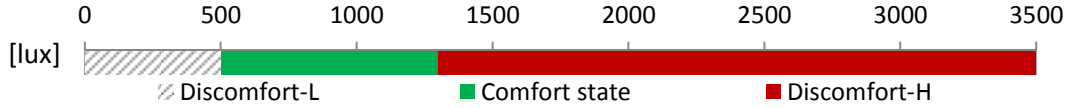

Figure 1: Visual comfort classification of E_{desk} values for 35 different HMM with a k ranging from 1 to 40 (results do not include HMM with k equal to 24-26, 34 and 40 because of non-convergence).

DISCUSSION

The results presented herein are very promising as they demonstrate that high-accuracy personalised visual comfort modelling can be achieved after a relatively short period of data acquisition using HMM. This, along with the classification capabilities makes the proposed approach a worthy candidate for lighting-related control applications in buildings. To validate our results, we compared our model against established, state-of-the-art classifiers.

Using the same data sets, a simplified Bayesian approach was applied as detailed by Zarkadis [3 pp. 119-122]. Assuming equal priors and choosing a decision rule (threshold) of 0.4 for the visual comfort[2], the *Comfort* state is established between the 450 and 1600 lux region, with an additional "comfort island" at around 1800 lux. By comparing this to the HMM developed (Figure 1), we notice the similarities with the principal 500–1300 lux comfort zone, as well as with the narrower one at 1500–1600 lux of several high-k HMM (k>15). In addition, similar comfort patterns were reported by Lindelöf [11 p. 100] who had also used the rule of Bayes on the same data. Comparison with k-Nearest Neighbor (k-NN) classifiers was also

[1] In every test cycle, each model (40 in total) classified a set of 10 illuminance values randomly generated within a specific illuminance zone. The spectrum of 0-3500 lux was evenly distributed into 35 zones of 100 lux each. Hence, 40 $models\ x\ 35\ illuminance\ zones\ =\ 1400\ test\ cycles$.

[2] We consider E_{desk} values resulting in discomfort probability equal or lower than 0.4 as part of *Comfort* state.

attempted. For Euclidean computation distance and priors of 0.5, 0.32 & 0.18 for the *Comfort*, *Discomfort-L* and *Discomfort-H* classes respectively (chosen according to each class' data representation), 40 different k-NN classifiers (with a *k* from 1 to 40) were trained and tested. Models with k>20 attribute a much broader spectrum to the "Comfort" class (300–2000 lux) as compared to the HMM (500–1300 lux). One can argue that this broader identified comfort zone is generally considered as a region where most people can perform their tasks comfortably, especially if the illuminances are due to natural daylight [13; 14]. On the other hand, one should also be cautious regarding the k-NN classifier: in our analysis, classification for k<20 is much less stable, while is on the borderline of being erratic for k<10 (as revealed by Resubstitution & Cross-validation loss analysis). In addition, k-NN accuracy was always below 70%, while the HMM-based model had an accuracy of 92% even when training with a fraction of the available data.

Confidence of identified states: Fuzzy logic-ready inputs

The merits of the proposed approach become even more evident when we attempt to "look under the hood" of the HMM algorithms and compute the confidence levels of the identified states as explained in the Methods Section. Figure 2 presents the normalised relative likelihoods for each identified state of the 35 different HMM and their means as a function of E_{desk}. While classifiers normally output crisp decisions, it becomes immediately apparent that the process behind the decision of the model does not always resemble a binary process (especially between 100–2000 lux). The notion that an observation can "**belong**" e.g. 85% in the *Comfort* state, 15% in the *Discomfort-L* and 0% in the *Discomfort-H* is exactly the same behind the fuzzy logic where a variable (i.e. E_{desk}) does not take a binary value (i.e. *Comfort* or *Discomfort-L*) but instead has a truth value that ranges between 0 and 1, dictated by the so called **membership** functions (i.e. the means of the normalised relative likelihoods for every hidden state). As such, the outputs of this analysis can directly be implemented as the membership functions of a fuzzy inference input i.e. for the control of electric lighting.

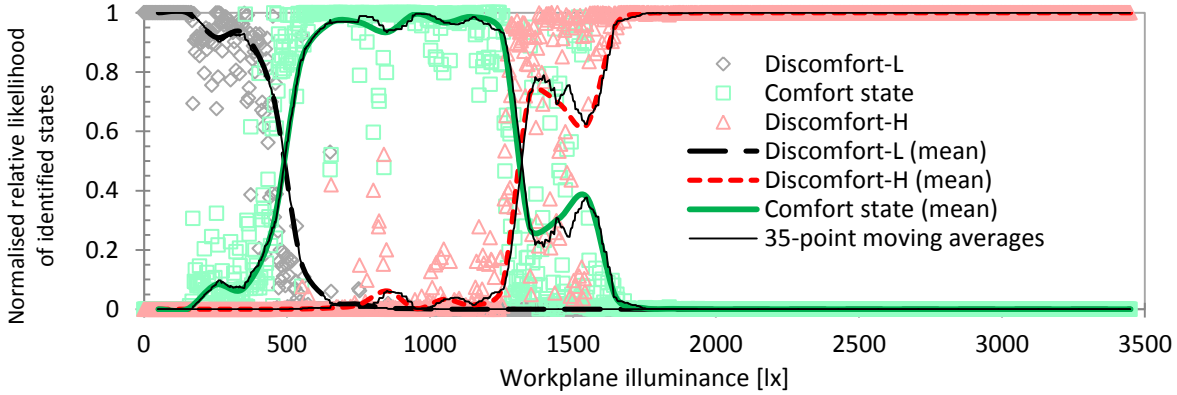

Figure 2: Normalised relative likelihoods of the identified states in all the 35 different HMM (scattered points) and their means (lines) as a function of the horizontal workplane illuminance.

CONCLUSION

This paper presents the development of a novel model based on HMM for the estimation of visual comfort in an office room. As demonstrated, the proposed approach overcomes some of the limitations of the current visual comfort metrics and exhibits some strong advantages. In specific, our approach does not require a detailed knowledge of the user's visual environment (it only uses data from sensors and actuators of a standard building control system); yet the model reflects the individual preferences and behaviour of the user. The model's accuracy remains remarkably high (92%) when compared with other state-of-the art classifiers, even

when limited to a 4-month period of learning data. Also, since it's a machine learning based approach, it can be applied in new or unseen building configurations as soon as observation data become available. Last, following the analysis concerning the normalised relative likelihoods of the identified states, we argue that this modelling approach and the resulting metrics could be an ideal input to building automation systems based on fuzzy logic.

Future work will focus on incorporating into the model the pupilar plane illuminance (which bibliography suggests correlates much better with the visual comfort [15]) and on field implementation of the model's output into an electric lighting and blinds controller based on fuzzy logic.

AKNOWLEDGEMENTS

The presented work has been supported by the Hasler Foundation in Switzerland through the research project Green-Mod.

REFERENCES

[1]. **Fisk, W.J. and Rosenfeld, A.H.** Estimates of Improved Productivity and Health from Better Indoor Environments. *Indoor Air.* 1997, Vol. 7, 3, pp. 158-172.

[2]. **Knez, Igor.** Effects of indoor lighting on mood and cognition. *Journal of Environmental Psychology.* 1995, Vol. 15, 1, pp. 39-51.

[3]. **Zarkadis, N.** *Novel models towards predictive control of advanced building systems and occupant comfort in buildings.* PhD thesis no. 6440, EPFL. 2015.

[4]. **Rabiner, L. R. and Juang, B. H.** Fundamentals of speech recognition. *Englewood Cliffs: PTR Prentice Hall.* 1993.

[5]. **Hennebert, J.** *Hidden Markov models and artificial neural networks for speech and speaker recognition.* PhD thesis no. 1860, EPFL. 1998.

[6]. **Dong, B., Lam, K.P. and Neuman, C.** Integrated building control based on occupant behavior pattern detection and local weather forecasting. *Twelfth International IBPSA Conference. Sydney: IBPSA Australia.* 2011, pp. 14-17.

[7]. **Lu, J., et al.** The smart thermostat: using occupancy sensors to save energy in homes. *Proceedings of the 8th ACM Conference on Embedded Networked Sensor Systems.* 2010, pp. 211-224.

[8]. **Ridi, A., Gisler, C. and Hennebert, J.** Automatic identification of electrical appliances using smart plugs. *Systems, Signal Processing and their Applications (WoSSPA), 2013 8th International Workshop on.* pp. 301-305.

[9]. —. Appliance and state recognition using Hidden Markov Models. *Data Science and Advanced Analytics (DSAA), 2014 International Conference on.* 2014, pp. 270-276.

[10]. **Zarkadis, N., Ridi, A. and Morel, N.** A multi-sensor office-building database for experimental validation and advanced control algorithm development. *Procedia Computer Science.* 2014, Vol. 32, The 5th International Conference on Ambient Systems, Networks and Technologies (ANT-2014), the 4th International Conference on Sustainable Energy Information Technology (SEIT-2014), pp. 1003-1009.

[11]. **Lindelöf, D.** *Bayesian optimization of visual comfort.* PhD thesis no. 3918, EPFL. 2007.

[12]. **Rabiner, L.** A tutorial on hidden Markov models and selected applications in speech recognition. *Proceedings of the IEEE.* February 1989, Vol. 77, 2, pp. 257-286.

[13]. **Haldi, F.** *Towards a Unified Model of Occupants' Behaviour and Comfort for Building Energy Simulation.* PhD thesis no. 4587, EPFL. 2010.

[14]. **Nabil, A., & Mardaljevic, J.** Useful daylight illuminance: a new paradigm for assessing daylight in buildings. *Lighting Research and Technology.* March 2005, Vol. 37, 1, pp. 41-57.

[15]. **Wienold, J. and Christoffersen, J.** Evaluation methods and development of a new glare prediction model for daylight environments with the use of CCD cameras. *Energy and buildings.* July 2006, Vol. 38, 7, pp. 743-757.

A NEW INTELLIGENT PREDICTIVE SOLAR-GAS TRIGENERATION SYSTEM FOR AIR CONDITIONING INDUSTRIAL SPACES

Y. Boukhris[1]; Y. Allani[2]; N. Al-Azri[3]; Z. A. Saâd[4]

1: Industrial Engineering Departement, National school of engineers of Tunis, Tunis El Manar University, Tunisia.
2: Allani Sunlife Holding SA, Suisse.
3: Department of Mechanical and Industrial Engineering, College of Engineering, Sultan Qaboos University, Oman.
4: Responsible Energy, Alimentary Group, Tunisia.

ABSTRACT

The Tunisian strategy for energy transition 2014-2030 is a large scale deployment of renewable energy (30%) and energy efficiency (30% energy savings). Cogeneration and trigeneration technologies in the industry and the commercial sector are the most recommended ways to optimize fuel and electrical savings and thus to achieve energy efficiency. Moreover, the benefits of the trigeneration are not limited to the country, especially in the regularization of the load curve which is increasingly affected by the emergence of a new peak due to the cooling of industrial buildings and the increasing demand for industrial refrigeration. Moreover, such installation provides a significant net economic impact for industrial companies. The implementation of an intelligent management system for solar-gas contribution is thus important to maximize the air conditioning predictive control in industrial buildings. This work deals with the retrofitting of an existing industrial cogeneration plant to an intelligent trigeneration system which combines a thermal solar energy contribution through solar collectors integrated into the roof of an industrial building located in the North of Tunis, Tunisia. Indeed, the industry in question plans to generate industrial cold production mode with the principle of trigeneration wich is considered as a new approach in Tunisia.

Keywords: Smart building, predictive model, HVAC, solar-gas trigeneration, industrial building cooling

INTRODUCTION

One of the proposed solutions for the case described in the abstract is to use an absorption refrigeration unit and Organic Rankine Cycle (ORC) arranged in cascade with energy cogeneration unit and solar thermal installation. This refrigeration unit is expected to replace, wholly or partially, an existing compression refrigeration unit and, thus, improve the overall energy efficiency through optimal energy integration. In this paper, we also present the results of an experimental study that we conducted on the existing cogeneration unit. The tests carried out have allowed us to characterize the performance parameters and the structure of a new parametric model associated with the cogeneration part. The experimental study revealed the existence of original correlations between the various operating parameters, such as ambient temperature.

Due to the obtained experimental results and the conceptual analysis involving coverage of chilling requirements and structure, we succeeded in simulating the installation behavior of the projected solar-gas tri-generation according to two possible conceptual variants. The installation should be managed intelligently, taking into account the level of sunlight, ambient

temperature, the occupancy rate in staff and the rate of production and storage of industrial products. Our principal goal is to offer the optimal design and predict energy performance in order to allow to best plan achievement of the industry in question.

DEVELOPED CONFIGURATION

In this work, the configuration of the thermal power, the solar energy captured at the collectors and steam generated from the heat recovered from the hot gases coming from the heat engine, are supplied to the Organic Rankine Cycle (ORC) via a buffer tank. The cooling effect is produced by two cycles: firstly, using vapor-compression cycle which is powered by the ORC or an electrical generator when solar gain is low and the second source is the absorption cycle which works on the heat discharged by the ORC [1, 6] or directly from the hot gases coming from the heat engine based on the operation mode. The heat that comes from the ORC to the absorption cycle is either stored or used immediately.

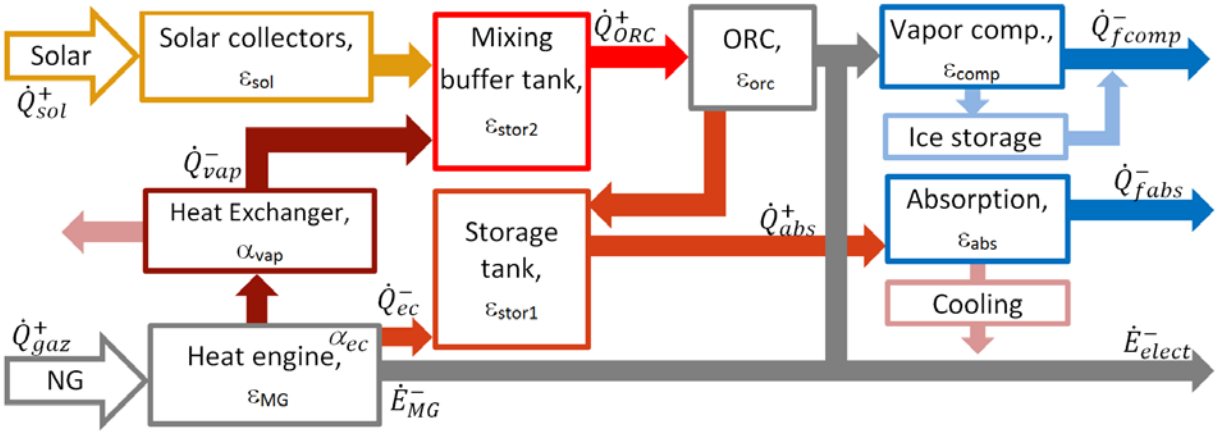

Figure 1 : *A schematic disgram for the principle of type Sunlife 3 installation.*

A NEW PREDICTIVE MODEL

The change in internal energy is assumed to be zero. The system is therefore evolving in quasi-stationary operating conditions.

Overall Efficiency Model: Type Sunlife3

The ratios, shown below, are used to simulate energy balance and the overall efficiency of trigeneration under the different assumptions.

The solar contribution, (τ_{sol}) is the ratio of the solar gain at the solar collectors to the total heat input of solar gain and the primary heat from natural gas:

$$\tau_{sol} = \frac{\dot{Q}^{+}_{sol}}{\dot{Q}^{+}_{sol}+\dot{Q}^{+}_{gaz}} \quad (1)$$

The ratio of the net electrical utility produced to the sum of the electrical power produced by the ORC and the heat engine is given by:

$$\tau_{elect} = \frac{\dot{E}^{-}_{elect}}{\dot{E}^{+}_{MG}+\varepsilon_{orc}.\dot{Q}^{+}_{ORC}} \quad (2)$$

The overall efficiency of the given configuration (dual input solar-gas with the heat engine cogeneration) is based on two assumptions:

Assumption 1 : The system is considered to mainly produce both cooling and electricity and for which the following expression is developed :

$$\varepsilon_{g-cog.trigen} = \frac{\dot{Q}^{-}_{fabs} + \dot{Q}^{-}_{fcomp} + \dot{E}^{-}_{elect}}{\dot{Q}^{+}_{sol} + \dot{Q}^{+}_{gaz}}$$

$$= \varepsilon_{abs}.\varepsilon_{stor1}.\varepsilon_{stor2}(1-\varepsilon_{orc}).\left(\tau_{sol}.\varepsilon_{sol} + \alpha_{vap}.(1-\tau_{sol})\right)$$
$$+(1-\tau_{sol}).\left(\varepsilon_{abs}.\varepsilon_{stor1}.\alpha_{ec} + \tau_{elect}.\left(\varepsilon_{MG} + \varepsilon_{stor2}.\varepsilon_{orc}.\alpha_{vap}\right)\right)$$
$$+\varepsilon_{comp}.(1-\tau_{elect}).\left(\tau_{sol}.\varepsilon_{orc}.\varepsilon_{sol}.\varepsilon_{stor2} + \left(\varepsilon_{stor2}.\alpha_{vap}.\varepsilon_{orc} + \varepsilon_{MG}\right).(1-\tau_{sol})\right)$$
$$+\tau_{elect}.\tau_{sol}.\varepsilon_{orc}.\varepsilon_{sol}.\varepsilon_{stor2} \quad (3)$$

Assumption 2: The system is assumed to mainly provide both cooling and electricity with the cooling is the only recognized final output. The following expression is given for this scenario:

$$\varepsilon'_{g-cog.trigen} = \frac{\dot{Q}^{-}_{fabs} + \dot{Q}^{-}_{fcomp}}{\dot{Q}^{+}_{sol} + \dot{Q}^{+}_{gaz}}$$

$$= \varepsilon_{abs}.\varepsilon_{stor1}.\varepsilon_{stor2}(1-\varepsilon_{orc}).\left(\tau_{sol}.\varepsilon_{sol} + \alpha_{vap}.(1-\tau_{sol})\right) + (1-\tau_{sol}).(\varepsilon_{abs}.\varepsilon_{stor1}.\alpha_{ec})$$
$$+\varepsilon_{comp}.(1-\tau_{elect}).\left(\tau_{sol}.\varepsilon_{orc}.\varepsilon_{sol}.\varepsilon_{stor2} + \left(\varepsilon_{stor2}.\alpha_{vap}.\varepsilon_{orc} + \varepsilon_{MG}\right).(1-\tau_{sol})\right) \quad (4)$$

Both models have the advantage which is not involving any performance parameters other than those used for the energy component in the considered configuration. However, the feasibility and the optimization of such configuration must be validated at the design phase using process integration methods such as pinch technology [2, 3, 5, 6 ,7]. The goal here is to verify the consistency of the heat exchange surfaces used [3, 4].

Parametric Representation Model of Power Outputs

By identifying the following terms:

$$\dot{Q}^{+}_{ORC} = \varepsilon_{stor}.\left(\dot{Q}^{+}_{sol}.\varepsilon_{sol} + \dot{Q}^{-}_{vap}\right) \quad (5)$$

$$\dot{Q}^{+}_{gaz} = \dot{Q}^{+}_{sol}.\left(\frac{1-\tau_{sol}}{\tau_{sol}}\right) \quad (6)$$

$$\dot{Q}^{-}_{vap} = \alpha_{vap}.\dot{Q}^{+}_{gaz} \quad (7)$$

$$\dot{Q}^{-}_{ec} = \alpha_{ec}.\dot{Q}^{+}_{gaz} \quad (8)$$

$$\dot{E}^{-}_{MG} = \varepsilon_{MG}.\dot{Q}^{+}_{gaz} \quad (9)$$

In this work, the following parametric presentation has been developed :

$$\dot{Q}^{-}_{fabs} = \varepsilon_{abs}.\left(\varepsilon_{stor1}.\varepsilon_{stor2}.\tau_{sol}.\varepsilon_{sol}.(1-\varepsilon_{orc}) + \varepsilon_{stor2}.\alpha_{vap}.(1-\tau_{sol}).(1-\varepsilon_{orc}) + \varepsilon_{stor1}.\alpha_{ec}.(1-\tau_{sol})\right).\left(\frac{\dot{Q}^{+}_{sol}}{\tau_{sol}}\right) \quad (10)$$

$$\dot{Q}^{-}_{fcomp} = \varepsilon_{comp}.\left(\tau_{sol}.\varepsilon_{orc}.\varepsilon_{sol}.\varepsilon_{stor2}.(1-\tau_{elect}) + \left(\varepsilon_{stor2}.\alpha_{vap}.\varepsilon_{orc} + \varepsilon_{MG}\right).(1-\tau_{sol}).(1-\tau_{elect})\right).\left(\frac{\dot{Q}^{+}_{sol}}{\tau_{sol}}\right) \quad (11)$$

$$\dot{E}^{-}_{elect} = \left(\tau_{elect}.(1-\tau_{sol}).\left(\varepsilon_{MG} + \varepsilon_{stor2}.\varepsilon_{orc}.\alpha_{vap}\right) + \tau_{elect}.\tau_{sol}.\varepsilon_{orc}.\varepsilon_{sol}.\varepsilon_{stor2}\right).\left(\frac{\dot{Q}^{+}_{sol}}{\tau_{sol}}\right) \quad (12)$$

Experimental Model Representing Heat Engine with Cogeneration

For the considered experimental model, the following expression is used based on the electrical power generated by the cogenerative heat engine:

$$\varepsilon_{MG} = \frac{\dot{E}_{MG}^{-} + \dot{Q}_{ec}^{+} + \dot{Q}_{vap}^{+}}{\dot{Q}_{gaz}^{+}} = \varepsilon_e + \alpha_{ec} + \alpha_{vap} \quad (13)$$

The hourly experimental measurements were taken for one year from the cogeneration heat engine at a food processing plant in Tunisia. The results obtained has yielded the following correlations for α_{ec} and α_{vap}:

$$\alpha_{ec} = -0.0006\ \dot{E}_{MG}^{-} + 19.978 \quad (14)$$

$$\alpha_{vap} = -0.0042\ \dot{E}_{MG}^{-} + 17.533 \quad (15)$$

For a typical day, the following values are considered in the simulation:

$$\varepsilon_{MG} = 41\%;\ \varepsilon_{cogen} = 74\%;\ \alpha_{ec} = 22\%;\ \alpha_{vap} = 17\%$$

Experimental Model Representing the Efficiency of the Absorption Machine

The absorption refrigerator exchanges heat with three sources given by three levels of temperatures denoted by T_{m0}, T_{m1} and T_{m2}, which are those of the evaporator, the cooling tower and the generator.

We propose an empirical model that has been widely validated using both dimensional and dimensionless analysis and it was inspired by two basic expressions of COP.

$$\varepsilon_{abs} = c_{0.}\left(\frac{T_{m0}}{T_{m2}}\right)^{c1}.\left(\frac{T_{m2} - T_{m1}}{T_{m1} - T_{m0}}\right)^{c2} \quad (16)$$

The empirical model we developed has been validated through an experimental study in 2015; with our experience in the field, we were able to identify its parameters c_o, c_1 (explaned in the appendix). The experiments were conducted on the absorption chiller (dual solar-gas) with an output of 175 kW used to cool the industrial premises in one of our agro-industry partners in Tunisia.

Experimental Model Representating the ORC Efficiency

The structure of the cycle has a single volumetric turbine stage involving an organic fluid with the high temperature kept constant while the lower temperature is variable. The condensation of the organic fluid does not take place at ambient temperature but at a temperature higher than that required by the absorption machine [1, 3, 4, 5] and it is also subject to the average ΔT_{pinch}. The efficiency can be expressed by the following model where parameters d_o and d_1 are determined experimentally.

$$\varepsilon_{ORC} = d_0.(T_{ORC} - T_{m2})^{d1}.(T_{ORC})^{-1} \quad (17)$$

The Efficiency Model of The Solar Field

After a thorough analysis of the most appropriate solar collectors and the selected temperature ranges, we selected the following model:

$$\varepsilon_{sol} = F'.(\tau\alpha) - \frac{F'.U_{L0}}{E_n}.(T_{m-sol} - T_a) - \frac{F'.U_{L1}}{E_n}.(T_{m-sol} - T_a)^2 \quad (18)$$

This model has been extensively validated in numerous studies involving several experimental works [1, 8].

SIMULATING TYPE 3 SUNLIFE CONFIGURATION

Power Simulation

For $\tau_{sol} = 0.3$, the solar collector surface is 1200 m^2 using vacuum tube collectors.

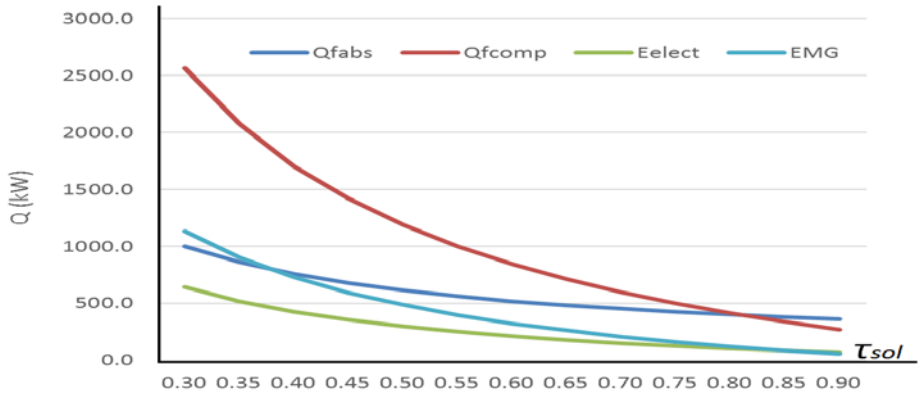

Figure 2: Simulation for the different refrigeration and electrical outputs (Type Sunlife 3).

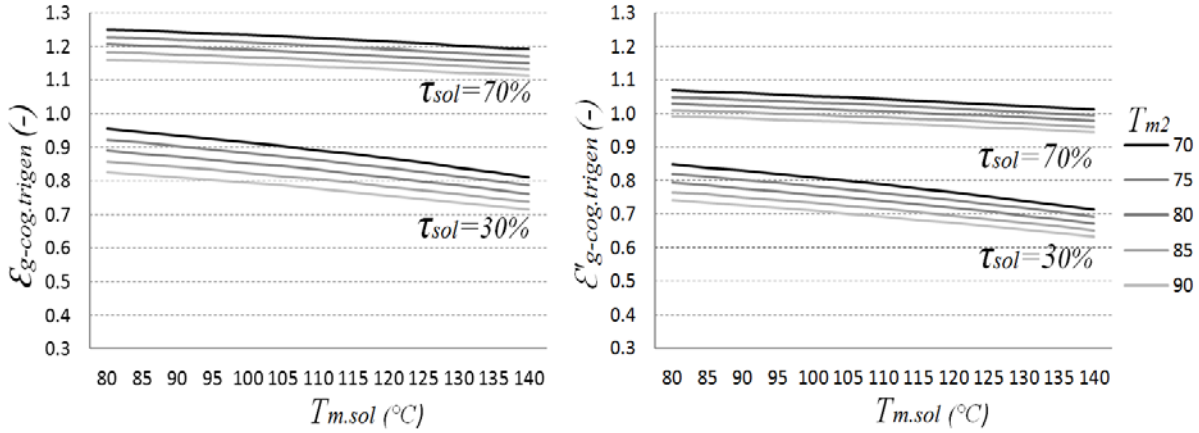

Figure 3: Simulation at Different Effciency Levels around the Nominal Design Point.

MAIN RESULTS

The performance of the trigeneration system (based on the field of solar collectors, heat engine cogeneration and ORC cycle which derives its heat from the hot gases released by the engine) is very sensitive to the temperature variation at the solar collector and the generator of the absorption system and also to the changes in solar radiation. For solar contribution of 30% and 70%, the overall efficiency considering both cooling and electricity is 115% and 75% while the overall efficiency when considering cooling only is 98% and 68% respectively. These results were achieved for the following conditions:

T_{m-sol}= 140 °C; T_{m2} = 80 °C (Type 1 and 2); E_n = 900 W/m^2, T_a = 25 °C.

Notice that for a nominal rate $\tau_{sol} = 0.3$, the surface of the solar collectors is 1,200 m^2 with $\dot{E}_{MG}^{-} = 1100\ kWe$.

CONCLUSION

We have demonstrated that the possibility of improving the nouriously power consuming cooling systems through the combination of solar energy and natural gas which has significant advantages, using a design solar contribution between 30% and 70%. Trigeneration system improves energy efficiency in refrigeration systems and can also guarantee supply of cooling, heating and electricity with the operation being reliably adaptable to the condition when the system is in use. By involving thermal storage in the refrigeration process, it is possible to use this new autonomous dual-fuel energy configuration to ensure an intelligent cooling and power supply for industrial buildings with efficiency exceeding 100%.

SYMBOLS

Symbol	Designation	Unit	Symbol	Designation	Unit
$\dot{Q}^{+}_{sol}$	Heat from solar collectors	kW	τ_{sol}	Nominal solar contribution	(-)
$\dot{Q}^{+}_{gaz}$	Primary heat from natural gas fuel	kW	τ_{elect}	Ratio of net electricity produced	(-)
$\dot{Q}^{+}_{ORC}$	Useful thermal power input to ORC	kW	$\varepsilon_{stor1,2}$	Storage tank effciency,1, 2	(-)
$\dot{Q}^{+}_{abs}$	Thermal power provided to the absorption machine	kW	ε_{MG}	Electrical efficiency of the cogeneration heat engine	(-)
$\dot{Q}^{-}_{fabs}$	The cooling load of the absorption machine	kW	ε_{sol}	efficiency of solar collectors	(-)
$\dot{Q}^{-}_{fcomp}$	The cooling load of the vapor compression machine	kW	α_{vap}	efficiency of vapor recovery at heat engine	(-)
$\dot{E}^{-}_{MG}$	Power produced by heat engine	kW	ε_{ORC}	Effciency of ORC	(-)
$\dot{E}^{-}_{elect}$	Net electrical power produced	kW	α_{ec}	Effciency of steam generation at heat engine	(-)
E_n	Solar radiation	W/m^2	ε_{abs}	absorption machine COP	(-)
T_a	Ambient temperature	°C	ε_{comp}	Vapor compression COP	(-)
T_{m-sol}	Average temperature (solar collectors)	°C	ε_{cogen}	Overall effciency of the cogeneration heat engine	(-)
T_{m0}	Temperature (evaporator)	°C	$\varepsilon_{g-cog.triger}$	Trigeneration system overall effciency (assummption 1)	(-)
T_{m1}	Temperature (cooling tower)	°C	$\varepsilon'_{g-cog.trige}$	Trigeneration system overall effciency (assummption 2)	(-)
T_{m2}	Temperature (generator)	°C	$F'.(\tau\alpha)$	Loss factor	(-)
T_{ORC}	High temperature of the ORC	°C	U_{L0}, U_{L1}	Conductivity of solar collectors	W/m^2/°C
T_{e0}, T_{s0}	Inlet, outlet temp. of the evaporator	°C	c_0, c_1, c_2	Absorption machine coffcients	(-)
T_{e2}, T_{s2}	Inlet, outlet temp. of the generator	°C	d_0, d_1	ORC Coeffcients	(-)
$\dot{m}_0, \dot{m}_2$	Mass flow, evaporator & generator	Kg/s	C_{p0}, C_{p2}	Specific heats	J/kg/°C

REFERENCES

1. Henchoz, S., Buchter, F., Favrat, D., Morandin, M., Mercangoez, M.: Thermoeconomic analysais of a solar enhanced Energy storage concept based on thermodynamics cycles. Energy. Vol. 45 (1), PP 358-36, 2012.
2. Alllani, Y., Favrat, D., Von Spakovsky, M.: *CO2*, mitigationtrough The Use Of Hybride Solar-Combined Cycles. Energy Conversion and Management. Vol. 38, PP S661-S667, 1997.
3. Kane, M., Favrat, D., Larrin, D., Allani, Y.: Small hybrid solar power system. Energy. Vol. 28 (14), PP 1247-1443, 2003.
4. Kane, M., Favrat, D., Allani, Y., Larrin, D.: Thermoeconomic Analysis of Advanced Solar-Fossil Combined Power Plants. Int. Journal of Applied Thermodynamics, Vol. 3 (4), PP 191-198, 2000.
5. Kane, M., Zanelli, T., Favrat, D., Allani Y., Glauser, E.: Conception d'une mini-centrale electro-thermo-solaire hybride adaptée aux pays en voie de développement. Proc. of The Inetrnational Conference on Solar Energy and Buildings (CISBAT'99), PP 103-108, Lussane, 1999.
6. Al-Azri, N., Al-Rawahi, N., Allani, Y.: Solar Power Generation and Solar Cooling Cogeneration. Project Report, The RESEARCH COUNCIL (TRC) Sultanate of Oman, 2012.
7. Al-Azri, N., Al-Thubaiti, M., El-Halwagi, M.: An algorithmic approach to the optimization of process cogeneration. Clean Technologies and Environmental Polices, Vol. 11(3), PP.329-338, 2009.
8. Allani, Y.: Caractérisation des convertisseurs héliothermiques par couplage entre modèles physiques et de représentations. Thèse de doctorat, Ecole Polytechnique Fédérale de Lausanne, 1993.

ENERGY POSITIVE NEIGHBOURHOODS - NEW TOOLS FOR THEIR COST EFFECTIVE AND INCREMENTAL IMPLEMENTATION

P. Brassier[1], K. Bäckström[2]

1: NOBATEK, 67 rue de Mirambeau, 64600 ANGLET, France

2: Posintra Oy, Krämaregatan 4A, 06100 BORGÅ, Finland

ABSTRACT

IDEAS, "Intelligent Neighbourhood Energy Allocation & Supervision", is a R&D project, focused on the development and operation of energy positive neighbourhoods. IDEAS aims at illustrating how communities, public authorities and utility companies across the EU can be engaged in this context. In addition, IDEAS focuses on the economic and environmental benefits of doing so.

In this framework, IDEAS develops and validates different tools and business models needed for demonstrating the cost effective and incremental implementation of an energy positive neighbourhood.

Energy Positive Neighbourhoods (EPNs) are those in which the annual energy demand is lower than annual energy supply from local renewable energy sources. The project includes two pilot sites: one in Bordeaux, France and another in Porvoo, Finland.

The Finnish site makes extensive use of a local bio-CHP power plant. The CHP energy production power is, as typically, controlled according to district heat demand. IDEAS will demonstrate how the heat demand could be time shifted by interacting with the household heat controls for a residential neighbourhood, in order to function as a temporary heat buffer for the ESCo. This enables a more favourable energy production, which can be adapted to favour stochastic renewables as well, since the advantageous CHP energy is not as much bound to the real heat demand anymore. The Finnish pilot site includes a simulated wind turbine, a simulated battery and a simulated heat storage connected to the same Energy Management System (EMS).

The French site is specific in terms of occupancy and energy usages. The IDEAS tools aims at providing real time information to the facility manager related to energy consumptions both at site and building level as well as energy production predictions so that he can optimise the energy functioning of the site. Moreover awareness tools are also developed to be used at different levels: tools dedicated to end-users' awareness as well as pedagogical tool supporting the teaching staff in explaining and disseminating concepts underpinning the energy positive neighbourhood approach to the students or to people external to the site.

The different tools have been deployed in the Finnish and French pilot sites and will be operated until autumn 2015.

The work presented is part of the IDEAS Collaborative Project which is co-funded by the European Commission, Information Society and Media Directorate-General, under the Seventh Framework Programme (FP7).

Keywords: neighbourhood, energy positive, Energy Management System, decision support, renewable energy, predictions, simulation.

INTRODUCTION

The IDEAS project aims at contributing to the European Energy-Efficient Buildings Initiative by developing management and control systems, and decision-support systems addressing the dynamics of energy supply and demand in neighbourhoods and extended urban/rural communities. This project aims at demonstrating how energy positive neighbourhoods can be cost effectively and incrementally implemented. IDEAS project aims at creating, testing, demonstrating and validating a real-time optimization and decision support system for the management of energy production and consumption within a neighbourhood. The tools will be tested in two demonstration pilots: a university campus in France and a newly built residential area in Finland.

The focus of this paper is to report the different tools which have been developed as part of the IDEAS project and the objectives underlying these tools for each pilot site.

DEMONSTRATION SITES OF THE PROJECT

The primary objective is to provide empirical evidence of the benefits of the internet based infrastructure and decision support system for control management in terms of energy positivity, total cost of operation, CO_2 reduction and improved services for users; provide evidence for the potential for scaling up the demonstration scenarios and test various aspects of the business models that have been identified.

The Finnish pilot site

The Finnish demonstration site of IDEAS, Omenatarha, is part of the Skaftkärr area in Porvoo [1]. The Skaftkärr development project aims to create an energy efficient, safe, personal and cosy area that offers different living alternatives. Omenatarha is a newly built area in Skaftkärr, and is situated near the centre of the city, about 3 kilometres from the market square. Omenatarha is a residential area with predominantly single family houses and a nursery school. The city planning processes in Porvoo is being developed to improve the way energy efficiency is addressed.

Figure 1: Finnish pilot site – Omenatarha, Porvoo, FINLAND

The Finnish site makes extensive use of a local bio-CHP power plant. The CHP energy production power is, as typically, controlled according to district heat demand. One of the IDEAS objectives is to demonstrate how the heat demand could be time shifted by interacting with the household heat controls for a residential neighbourhood, in order to function as a temporary heat buffer for the ESCo.

The project also simulates heat storage for the district heating and simulates electricity battery for the power grid. The objective is to provide the ESCO with valuable information to base future investment decisions on.

Another major objective is to reduce and or time shift the energy consumption by improving the energy awareness of citizens, and by continuously providing them with relevant advices based on actual conditions.

The French pilot site

The French pilot site selected for the demonstration of the IDEAS project is the Institute of Technology (IUT Bordeaux 1) located on the Bordeaux campus 5 km southwest of the centre of the city of Bordeaux. The institute provides teaching and office facilities for some 2000 students and 500 staff (teachers-researchers; technicians, maintenance workers and administrative staff) in 11 buildings. The total area of the site is 80000 m^2 with around 40000 m^2 of buildings [1]. Almost all of the buildings are used for teaching, although some of them also house offices, workshops, computer laboratories, research laboratories, cafeterias, but also dwellings.

Figure 2: French pilot site – IUT Bordeaux1, Gradignan, FRANCE

The use of the site is highly variable with many parts of the buildings occupied only occasionally. Some researchers-teachers working on energy and ICT issues are key contacts for pedagogical purposes and for getting in touch with students. Similarly, the facilities energy management team on the site is really committed to improving energy efficiency and they constitute key actors for the IDEAS demonstration.

The IDEAS project aims at providing tools enabling the end-users and Energy Manager of the IUT site to better understand how the site consumes and can produce energy and to visualise the output of the energy optimization process. The purpose of these tools is to increase occupants' awareness about energy and induce changings in occupants' behaviours. The major objective is to reduce and optimise the energy consumption by improving and raising the energy awareness of students and IUT staff inducing reactions at the occupants' level. Another major objective is to take into account the occupancy of the site in the energy optimisation process.

The project also aims at simulating PV production based on real irradiation conditions on site and simulates electricity storage so that optimisation of the use of electricity energy can be done by the Energy Manager of the site.

OVERVIEW OF THE GENERAL ARCHITECTURE OF THE ENERGY MANAGEMENT SYSTEM DEVELOPED WITHIN IDEAS

In order to comply with the objectives mentioned above, an Internet based ICT infrastructure has been developed to support all the required functionalities. A high-level overview of the inter-relationships and functionalities of the two main demonstration sites has been specified and is shown on the following figure along with the wider contextual domains of a smarter energy grid and smarter city. Within this global infrastructure, the IOC (IBM®Intelligent Operations Centre), a software solution that is designed to facilitate effective supervision and coordination of operations, is used in IDEAS to provide a central control centre to implement the Energy Management System (EMS) of IDEAS including database and data management, geographical information systems, web hosting and internet interfaces, performance metrics/analytical engines and optimization tools.

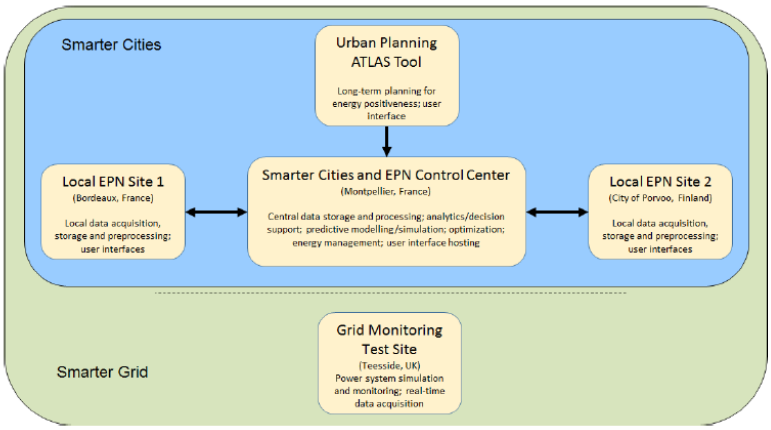

Figure 3: High-level overview of demonstration sites, IT tools and functionalities in the IDEAS project

The IT systems in Finland and France are described in figure 4 and are based on a metering system installed in each pilot site, on an EMS including optimisation algorithms and collecting also external information such as weather forecast and real-time energy prices.

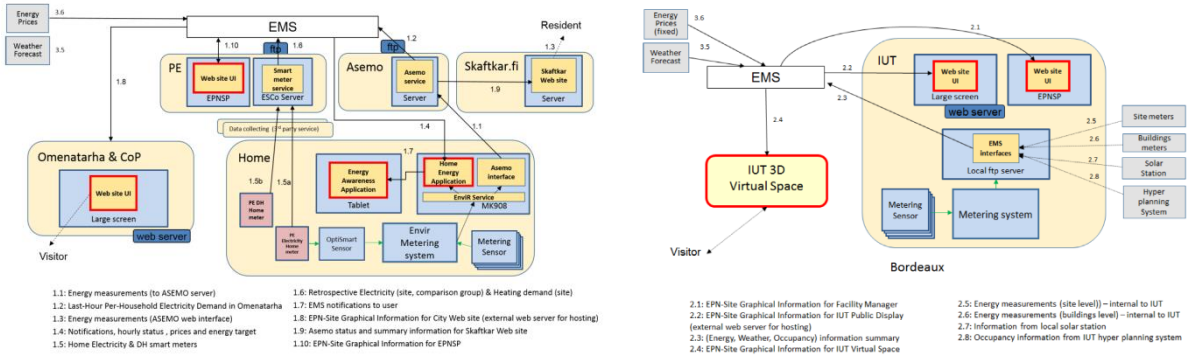

Figure 4: IT systems in Finland (left) and in France (right)

TOOLS DEVELOPED FOR END-USERS' AWARENESS AND NEIGHBOURHOOD ENERGY MANAGEMENT

End-users awareness tools

- **Advising the residents – HEAA (Home Energy Awareness Application)**

The IDEAS project has developed a Home Energy Awareness Application, in order to both improve the energy awareness of the residents by making the consumption visible, but also in order to send energy related advises or co-operation requests based on measured or forecasted data that typically is invisible for the users.

The bleeding edge image recognition technology from IBM has been included to regular Android tablets. The augmented reality is displaying an overlay with the real time consumption of a device that has been recognized by the tablet camera. The Finnish pilot is demonstrating this in 23 private single family households, with at least 6 measured devices in each household (z-wave based solution).

Instead of having automated control over the household electrical equipment and heating system, the impact is supposed to be achieved by sending notifications to the residents, who is requested to act upon the received notification (triggered by the decision support system of the neighbourhood level Energy Management System).

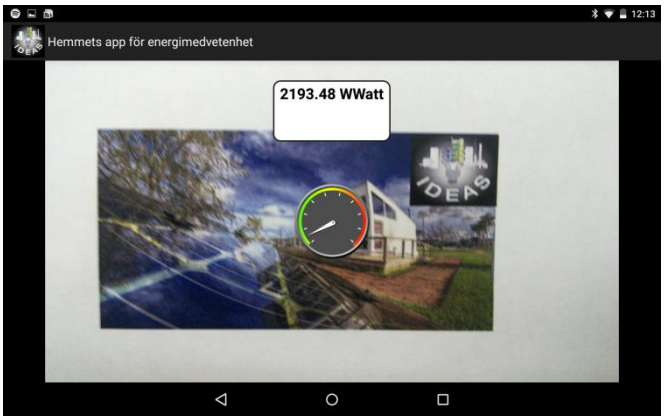

Figure 5: HEAA (Home Energy Awareness Application) interface

- **Raising end-users' awareness - Public screens interface**

The IDEAS project has also developed an "energy awareness" user interface (figure 6) which has been installed on wide screens in public spaces within the French pilot site (5 large screens have been installed in relevant locations) and the Finnish pilot site (3 interactive screens have been installed in the nursery school of Omenatarha and one in the City of Porvoo citizen service point, in the city centre). This interface is displaying general information related to energy efficiency of the surrounding environment and related to the impact the neighbourhood occupants have on their own neighbourhood. The interface zooms from the big picture of the national level down to the neighbourhood detail level, including measured data of energy consumption of the whole site.

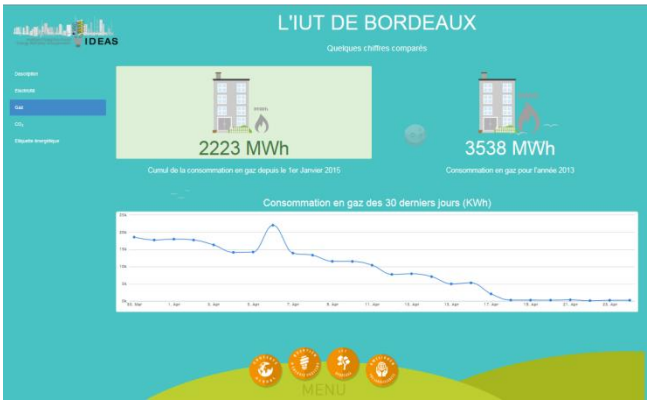

Figure 6: Public screens interface – Electrical consumptions at the French site

Energy manager interface

The Energy Manager interface provides energy related professional information that enables managing the EPN. The primary intended user of the tools developed in the IDEAS project is a new type of actor, the Energy Positive Neighborhood Service Provider (EPNSP, described in [2]). The developed interfaces are hosted by the IBM® WebSphere Portal embedded by the Intelligent Operations Center ® (IBM® IOC) as part of the EMS. The main view of the EPNSP interface is a manager dashboard (Figure 7) which summarizes most relevant data in real time: for instance, the current solar irradiation measured on site and the associated simulated energy production, the energy consumption of the whole site but also at building level.

Figure 7: Energy Manager interface – Dashboard for the French site

This tool constitutes a decision support interface for the energy service company (ESCO) which is involved in the project (Porvoon Energia, Finland). This interface includes abilities for (i) visualization of estimated future energy supply, demand and pricing, plus the optimal plan for buying, selling and/or storing energy and (ii) functionality for configuring the optimization and decision support tools. This tool can help the Energy Manager in the coordination and optimization of demand side management (DSM) and supply side management (SSM) which are the two key goals of the EPN service provider.

CONCLUSION

In order to support the development of EPNs, ICT tools are required for energy awareness and management. This includes user interfaces that raise awareness and enable the visualisation of all the energy aspects within the neighbourhoods.

The pilots are currently running and will be operated until autumn 2015. Some promising results are already visible in the French pilot site in which energy savings opportunities have already been detected thanks to the IDEAS tools.

ACKNOWLEDGEMENTS

This work is part of the “IDEAS - Intelligent NeighbourhooD Energy Allocation & Supervision” project (Grant Agreement No. 600071) which is co-funded by the European Commission, Information Society and Media Directorate General, under the Seventh Framework Programme (FP7), Cooperation theme three, “Information and Communication Technologies”. Project partners are acknowledged.

REFERENCES

1. Ala-Juusela M. and al.: D3.1 Case study scoping, IDEAS project, 2014.
2. Shvadron U. and al.: D3.3 Specifications for the user interfaces, IDEAS project, 2013.
3. Crosbie, T. and al.: D2.2 Specific business models for demo cases, IDEAS project, 2014.

A MODEL-PREDICTIVE CONTROLLER FOR AIR HANDLING UNITS

Y. Stauffer[1], L. Von Allmen[1], E. Onillon[1], S. Arberet[1], E. Olivero[1], D. Lindelöf[2]

1: CSEM SA, Jaquet-Droz 1, 2002 Neuchatel, Switzerland

2: Neurobat AG, Rue de Veyrot 9, 1217 Meyrin, Switzerland

ABSTRACT

Heating and cooling for thermal comfort are the main consumers of energy in buildings, and there is a growing need to improve the energy efficiency (and thereby reduce CO_2 emissions) of these building services. The regular increase in energy tariffs only exacerbates the problem.

Building owners are seldom willing to invest in a deep retrofit that may lower their energy consumption, but are instead willing to replace their outdated HVAC systems. Indeed, off-the-shelf controllers are often based on (only) the outdoor temperature, and occasionally take into account the indoor temperature. In particular, practically no commercial systems take into account weather forecasts. Consequently, these control systems lead to poor comfort and sub-optimal energy efficiency.

In this paper, a novel model-predictive control (MPC) algorithm for fan coil units (FCU) is presented, which aims at reducing the operational costs while guaranteeing thermal comfort. It is planned to be deployed on a test site in Greece within the second half of 2015.

The simulation results are presented and compared to a standard PI controller. For the MPC based controller, the trade-off between the user comfort and the energy consumption of the will be presented and commented. Simulations have demonstrated energy savings of up to 57% compared with the reference controller. Results from field tests are expected by the end of 2015.

Keywords: thermal regulation, MPC

INTRODUCTION

Thermal comfort regulation, linked to Heating, Ventilating and Air Conditioning (HVAC), is one of the main energetic expenditure in buildings. In order to reduce that consumption, without degrading user comfort, two distinct, yet complementary paths can be taken. First, retrofit can be carried out. Extra insulation can be added to the walls and roof and the windows can be upgraded. Second, the means of controlling the temperature within the building can be changed. In this work, the second option was chosen.

It is shown in [1] that available control systems in buildings rely mostly on conventional techniques such as cooling curves, classical Proportional Integral Derivative (PID) controllers and fuzzy controllers. These are the most widely used controllers in the industry [2]. While PID controllers are an improvement compared to thermostats, they still have several issues, mainly due to the difficulty to choose the gain values [3]. To address this problem, self-tuning adaptive PID controllers based on recursive least-squares [4] and fuzzy control [5] have been developed. Other strategies include adaptive controllers, which have the ability to adapt according to climate conditions and building properties. Adaptive systems can include parameters estimation methods using Recursive Least-Squares (RLS) algorithms [6], genetic algorithms (GA) [7], nonlinear disturbance rejection controllers with thermal load estimation and fuzzy controllers [8]. In order to achieve simultaneous and often contradictory energetic and comfort objectives, model predictive control (MPC) strategies have been developed.

Ruano et al. [9] have used a multi-objective genetic algorithm (MOGA) for designing an off-line radial basis function (RBF) neural network (NN) model. When compared to a simple on-off control strategy the authors claimed a 27% reduction in the use of the air conditioner for a better thermal control. Ferreira et al [10] also used a predictive model implemented by RBF NN identified by a multi-objective genetic algorithm to minimize energy consumption while achieving a desired thermal comfort level.

In the present article, a Model-Predictive Control (MPC) algorithm applied for heating and cooling is presented. While the developed algorithm is meant to be used to control a Fan Coil Unit (FCU), it can easily be adapted for other devices, i.e. more generally an air handling unit (AHU), however for clarity reasons and given the test site specificities, the term FCU will be used throughout the article. The developed MPC controller is benchmarked against a PI controller.

The document is organized in four main sections. First the simulation environment, the model-predictive control (MPC) algorithm and the test case are presented. Second, the simulation results are presented. Third, the results are analysed and discussed. Finally, the works is summarized and an outlook is provided.

METHOD

Simulation environment

In order to develop and validate our MPC algorithm, a simulation environment had to be developed. Naturally, the various elements available on the test site had to be modelled with enough accuracy, so as to allow the porting of the work to the test site. The chosen simulation platform was MATLAB and Simulink. The main blocks are:

- Heater chiller[1]: simulates the heating/cooling of the water which is delivered to the fan coil units;
- Room[1]: simulates the thermal behaviour of the room (including the FCU);
- Controller: a PI and our MPC controller;
- Simulation inputs: weather, temperature set points and energy tariffs.

MPC controller

The MPC controller aims at guaranteeing user comfort while minimizing energy expenditure. Accordingly, the objective function is a weighted sum of the two following terms:

- Temperature error (comfort): its role is to penalize deviations between the indoor temperature and its setpoint
- Power consumption: its role is to penalize the cost of the energy consumption.

The formulation of the objective function is shown below (equation (1)):

[1] The work was performed in the framework of the European project AMBASSADOR (Seventh Framework Programme Grant Agreement No. 314175) and is meant to be deployed on a test site in Lavrion (Greece) in the second half of 2015. The heater/chiller as well as simulated room model were developed by members of the AMBASSADOR consortium.

$$\underset{P_t,\forall t}{\text{minimize}} \sum_{t=1}^{N}\left[K_E \cdot C_t^2(P_t) + Occ_t \cdot K_C \cdot \left(T_t - \hat{T}_t(P_t, weather)\right)^2\right] \quad (1)$$

With: $C_t(P_t) = K_{heat} \cdot \max(P_t,0) + K_{cool} \cdot \min(P_t,0)$ (2)

Where:

- P_t: power applied during the interval t
- K_C: weighting coefficient for the comfort term
- K_E: weighting coefficient for the energetic term (K_E = 1 - K_c)
- C_t: cost of using the FCU (€) at interval $\hat{T}_t$
- T_t: temperature set-point
- $\hat{T}_t$: temperature given by the building temperature prediction model
- Occ_t: binary variable used to discard the discomfort computation when there is no occupancy in the room (i.e. when Occ_t is set to zero)
- K_{heat}: the "cost" of heating (€/W)
- K_{cool}: the "cost" of cooling (€/W)
- N: number of time intervals over the prediction horizon

Beside the objective function, two additional functions are required:

- The **building temperature prediction model**: It is based on an ARMAX model and takes as inputs: the FCU power, the outdoor temperature and the solar irradiance. This model is used to predict the evolution of the room temperature over the prediction horizon.
- The **FCU cost model**: It predicts the power needed to process the air. The model is based on the physics of the heater/chiller and essentially computes the cost associated with treating the air.

Simulation conditions and simulation cases

The following boundary conditions were used for all the simulations:

- Weather data: Neuchâtel (Switzerland)
- Temperature set points: 2 scenarios (see Figure 1):
    - scenario 1 (full occupancy: Occ = 1): 20°C during daytime, 22°C during night-time;
    - scenario 2 (partial occupancy: Occ = 0): 20°C during daytime, no occupancy (i.e. occupancy parameter Occ_t = 0) during night-time (i.e. free set point).
- Daytime: 9 am to 6 pm, night-time: 6 pm to 9 am).

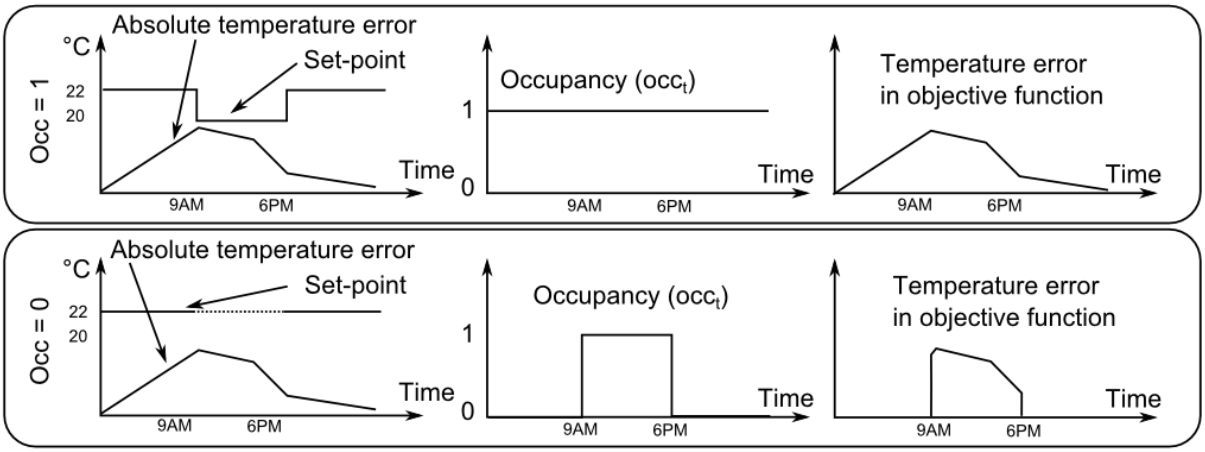

Figure 1: Illustration of the effect of Occ = 1 or 0 in the objective function. In the top line, comfort is to be achieved all the time (even during the night). In the bottom line, the temperature error is not computed during periods without occupancy.

First a series of short simulations (~60 days) were performed in different conditions. The following settings were tested: full (Occ = 1) vs partial occupancy (Occ = 0) scenarios, summer versus winter external conditions and various values of the comfort-energetic trade-off, i.e. parameter K_c taking values between 0 and 1.

Finally, one year simulations were undertaken to assess the algorithm over long durations.

All the simulation cases and associated results are summarized in Table 1. In addition, for a specific simulation with high comfort (i.e. K_C = 1 and Occ = 1) an illustration of the measured and desired room temperature is depicted in Figure 2.

RESULTS

The simulation results are provided in Table 1. Note that the mean temperature error is defined as the average over the simulation of the absolute value between the desired room temperature and the measured room temperature.

Simulation parameters				Simulation results	
Duration	**Season**	**K_c**	**Occ**	**Mean T. error [K]**	**Energy [kWh]**
60 days	Summer	1	1	0.112	2.25E+03
60 days	Summer	1	0	0.186	9.96E+02
60 days	Winter	1	1	0.089	5.60E+03
60 days	Winter	1	0	0.351	3.40E+03
1 year	All	1	1	0.093	2.78E+04
1 year	All	1	0	0.216	1.48E+04
60 days	Summer	0.9999	1	0.128	2.13E+03
60 days	Summer	0.9995	1	0.343	1.85E+03
60 days	Summer	0.999	1	0.607	1.57E+03
60 days	Summer	0.9985	1	0.896	1.28E+03
60 days	Winter	0.9999	1	0.110	5.39E+03
60 days	Winter	0.9995	1	0.268	5.32E+03
60 days	Winter	0.999	1	0.521	5.23E+03
60 days	Winter	0.9985	1	0.777	5.14E+03
60 days	Summer	0.999	0	0.953	5.23E+02
60 days	Winter	0.999	0	1.022	3.02E+03
1 year	All	0.999	0	0.871	1.16E+04

			Energy	
Duration	**Season**	**K_c**	**Occ = 0**	**Occ = 1**
60 days	Summer	1	9.96E+02	2.25E+03
60 days	Winter	1	3.40E+03	5.40E+03
1 year	All	1	1.48E+04	2.78E+04
60 days	Summer	0.999	5.23E+02	1.57E+03
60 days	Winter	0.999	3.02E+03	5.23E+03

Table 1: Test cases with associated simulation parameters and simulation results (left). Focus on the effect of Occ on the energy expenditure (right)

DISCUSSION

The effect of the comfort-energy trade-off parameters K_c, K_E, and the effect of taking into account non-occupancy by discarding the comfort term in the objective function when there is

partial occupancy (scenario Occ = 0) versus assigning another set point temperature during the same period (Occ = 1), are presented below.

First, the effect of K_c is highlighted in Figure 2. We can notice an almost linear relationship between the mean temperature error and the consumed energy. It can also be observed that our MPC algorithm consumes less than the PI controller (MPC: 2130 kWh, PI: 2200 kWh), for a better comfort level (mean temperature error MPC: 0.12°C, PI: 0.18°C).

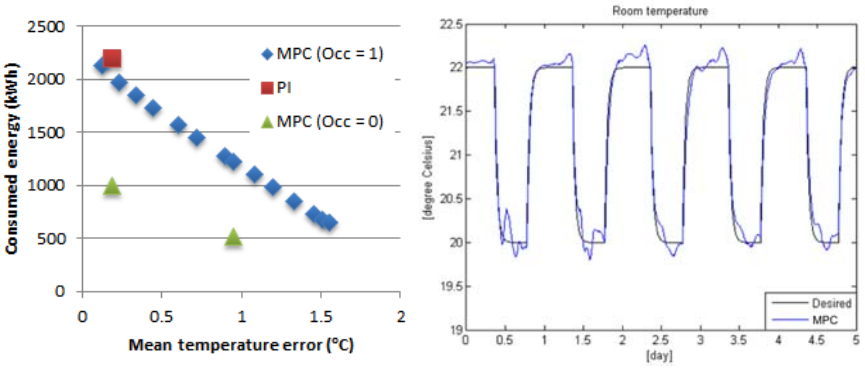

Figure 2: Total energy consumption as a function of the mean temperature error, obtained by changing the K_c parameter (left). Desired and measured room temperature for a high comfort (K_c = 1) simulation (right).

Second, the effect of the occupancy parameter Occ is shown in Table 1 and compared with our reference PI controller in Figure 2. It can be observed that letting the system free when there is partial occupancy (Occ = 0) reduces the energy consumption almost by a factor two for a similar comfort value (during the occupancy periods). It is to be noted that the MPC anticipates the heating and cooling needs before the transition from un-occupied to occupied, which maintains an acceptable level of comfort. The PI controller is unable to perform such preemptive actions.

It can be seen that as expected, the K_c and Occ parameters affect the comfort and energy expenditure. In addition, the MPC algorithm achieves a better comfort for a lower energy expenditure, especially in the partial occupancy scenario (Occ = 0), i.e. when non-occupancy is exploited in the optimization. Finally, a similar behaviour was observed when starting the algorithm at various times of the year or during all-year simulations.

CONCLUSION AND OUTLOOK

This article presented an MPC algorithm developed for FCU control. The optimization is based on an objective function, which includes a comfort and an energetic/cost term. The user has the possibility to adjust the trade-off between these two terms with a single and simple parameter, ranging between 0 (only energy/cost optimization) and 1 (only comfort optimization). In addition, the system can take advantage of unoccupied periods. Simulation results have shown that, by taking into account the energy/cost in the optimization and/or by exploiting the unoccupied periods, the energy consumption could be drastically reduced while maintaining user comfort.

The algorithms will be deployed in the test site in Lavrion (Greece) during the second half of 2015.

ACKNOWLEDGMENT

The work has been developed under the project AMBASSADOR, that receives funding from the European Union Seventh Framework Programme Grant Agreement No. 314175.

REFERENCES

1. F. Behrooz & al.: A survey on applying different control methods approach in building automation systems to obtain more energy efficiency, International Journal of the Physical Sciences Vol. 6(9), pp. 2308-2314, 4 May, 2011
2. D. S Naidu, C. G. Rieger, Advanced control strategies for heating, ventilation, air-conditioning and refrigeration systems – An overview: Part I: Hard control, HVAC&R Research, 17:1, pp 2-21.
3. A. I. Dounis, C. Caraiscos, Advanced control systems engineering for energy and comfort management in a building environment – A review, Renewable and sustainable Energy Reviews 13 (2009) pp 1246-1261.
4. C. G. Nesler, Adaptive control of thermal processes in buildings, American control conference, Boston, MA, June 19-21 1985.
5. B. Moshiri, F. Rashidi, Self-tuning based fuzzy PID controllers: application to control of nonlinear HVAC systems, Intelligent Data Engineering and Automated Learning – IDEAL 2004, LNCS 3177, pp 437-442.
6. S. I. Chaudhry, M. Das, Adaptive Control of Indoor temperature in a building, IEEE International Conference on Electro/Information Technology (EIT), 2012, pp 1-6.
7. G. Wang, L. Song, Air handling unit supply air temperature optimal control during economizer cycles, Energy and Buildings 49 (2012) pp 310-316.
8. H. B. Kuntze, T. Bernard, A New Fuzzy-based Supervisory Control Concept for the demand-repsonsive Optimization of HVAC Control Systems, Decision and Control, 1998. Proceedings of the 37th IEEE Conference on, pp 4258-4263 vol 4.
9. A. E. Ruano, E. M. Crispim et al, Prediction of building's temperature using neural networks models, Energy and Buildings 38 (2006), pp 682-694.
10. P. M. Ferreira, A. E. Ruano et al, Neural networks based predictive control for thermal comfort and energy savings in public buildings, Energy and buildings 53 (2012) pp 238-251

ACTIVE LOADS IN OFFICE BUILDINGS AS A DEMAND SIDE RESOURCE TOWARDS THE SMART GRID

Wim Zeiler; Kennedy Aduda; Kevin de Bont

Faculty of the Built Environment, TU Eindhoven, Eindhoven, Netherlands

ABSTRACT

A key characteristic of the smart grid is its multi-directional flow of power and information and hence transformation of the demand side management to demand side integration philosophy at low level voltage. This implies that buildings must also provide service to the electrical smart grid in as much as it is also serviced by the latter. Consequently the phenomenon of active loads has become evident in form of using Building Services components like cooling machines, heat pumps and others to service the utility grid. Taking cue from tests performed in the United States and the United Kingdom, experiments were conducted at an existing office building in Breda, Netherlands. Additional metering was installed to be able to measure rather detailed the energy flows within the building. The potential and possible effects on recommended comfort levels were investigated in this case study building. The electrical steam humidifier and the air handlings units were used as an active load to see to what extent they could support the Smart Grid. The effects of the different contributions towards the Smart Grid were determined. Specifically the steam humidifier and ventilators were operated on modulated mode and reduced capacity all within corresponding comfort conditions monitored. Results indicated that whereas potentials existed for such uses, care had to be taken to determine critical operational boundaries of the equipment. Depending on the level of responsiveness and the control strategy, the main energy uses of the building, the steam humidifier and air handlings unit, can be used as active loads.

Keywords: Active loads, SmartGrid

INTRODUCTION

The subject of energy has become increasingly contentious with current strict emissions targets for the future [CIBSE 2012]. Recently these environmental issues along with the rapid growing surge in fuel cost have drawn particular attention to distributed renewable energy resources (DRES) [Brahman et al 2015]. With the expected increase of renewable generated energy with its stochastic behaviour in the total generated energy mix, the energy management of the grid will change in the future. This forms a challenge for the grid stability and as well as efficiency, reliability, availability, controllability and security. As commercial office buildings are more sophisticated and better equipped for more flexible control and actuation possibilities, dynamic control of building's Heating, Ventilation and Air-Conditioning (HVAC) systems in relation to actual perceived occupancy comfort presents an opportunity for more efficient use of these systems as active loads towards the Smart Grid. In the Netherlands there are around 78.000 office buildings which use in total around 225 PJ/year compared to around 370 PJ/year for households in the Netherlands [RVO 2014]. So overall the energy use of offices is around 60% of the total energy use of the households, so quite substantial. The energy consumption of office buildings is increasing slightly, despite the 2020 targets set by the EU, which calls for a 20% reduction in energy use by the year 2020. Therefore our focus was on the energy efficiency as well as the possible use of active loads in office buildings as a demand side resource towards the Smart Grid.

METHOD

Buildings offer unexpected possibilities. Without knowing people sit 90% of their time in a vast energy storage device. The heat or cold storage in buildings is an enormous resource for providing regulation services [Cui et al 2015]. Buildings can play an important role in DR programs by actively reducing their power consumption during peak hours. The heating, ventilation and air conditioning (HVAC) systems, which account for 50% or more of the whole building power consumption on average, are the main contributor for demand response in buildings. HVAC systems can be an excellent demand response resource to supply ancillary reserves [Motegi et al 2005]; HVAC systems contribute the largest portion of consumption in buildings. And the operation of HVAC systems can be curtailed or the equipment can be partially shut down without producing serious impact on building occupants [Eto et al 2007]. This DR does not have ramping time, minimum on or off time limits that constrain many generators {Cui 2015}. The curtailment can be nearly instantaneous, which is much faster than the 10 min allowed for generators to fully respond [Kirby et al 2008].

Two main categories of DR strategies for HVAC systems were summarized by Watson et al. [2006], which are global temperature adjustment plus system adjustment. Global temperature adjustment is done by increasing building zone temperature set-points during the active intervention. System adjustment includes duct static pressure setpoint reduction, fan quantity
Hao et al. [2012] described how ancillary services could be achieved by reducing the power consumption of HVAC systems. The numerical experiments showed that for this HVAC system, 15% of fan power capacity could be provided for regulation, while maintaining indoor temperature deviation to no more than ±0.2 °C. Based on these results, they concluded that the HVAC systems in all the commercial buildings in the U.S. can provide about 70% of the current regulation capacity needed in the United States.
Energy management system (EMS) are a promising mean to optimally coordinate all generation, consumption and energy storage resources of buildings connected to the SG both economic and technical facets [Brahman et al 2015] Chen et al [2011] presented a smart EMS, which incorporates a power forecasting module, ESS, and an optimization module to achieve a great coordination between power production of DRES units and SG [Brahman et al 2015].
At the core of dynamic energy management is the concept of active load. Active loads are unique in their ability to reliably deliver resources to the power system whilst also maintaining quality primary service to end users [Callaway and Hiskens 2011] In essence, this can be any load that has a form of thermal storage capacity such as HVAC systems, refrigeration and driers [Trudnowsk et al 2006]. To be relevant, active loads must be both competitive in comparison to generators that provide the same service whilst also ensuring that they have an almost negligible effect on quality of service rendered to the end user [Callaway and Hiskens 2011]. A number of advantages make active loads preferable. However, these differ from one piece of equipment to the other and are specific to both equipment and operational boundary conditions; past studies have not fully specified operational boundaries or quantified process specific advantages associated with active load concept [Pratt 2004]. As part of a wider experiment in building control within SG some experiments with active load based dynamic energy management were conducted in the Netherlands to evaluate the potential and operational boundaries for using HVAC-systems as active loads as demand resources to the power system.

CASE STUDY OFFICE BUILDING

The Kropman Breda office was built in 1992 and revised in 2009. It is a three story high building with around 1400 m² floor space and 50 employees. The office building is connected to a mid-voltage transformer station by two main connections and main power systems

connected were measured. Fig. 1 shows the major electricity load groups of the office building: a mechanical ventilation system with heat recovery wheel (no recirculation of air); central cooling; electrical steam humidifier; heating by ventilation and two radiator groups.

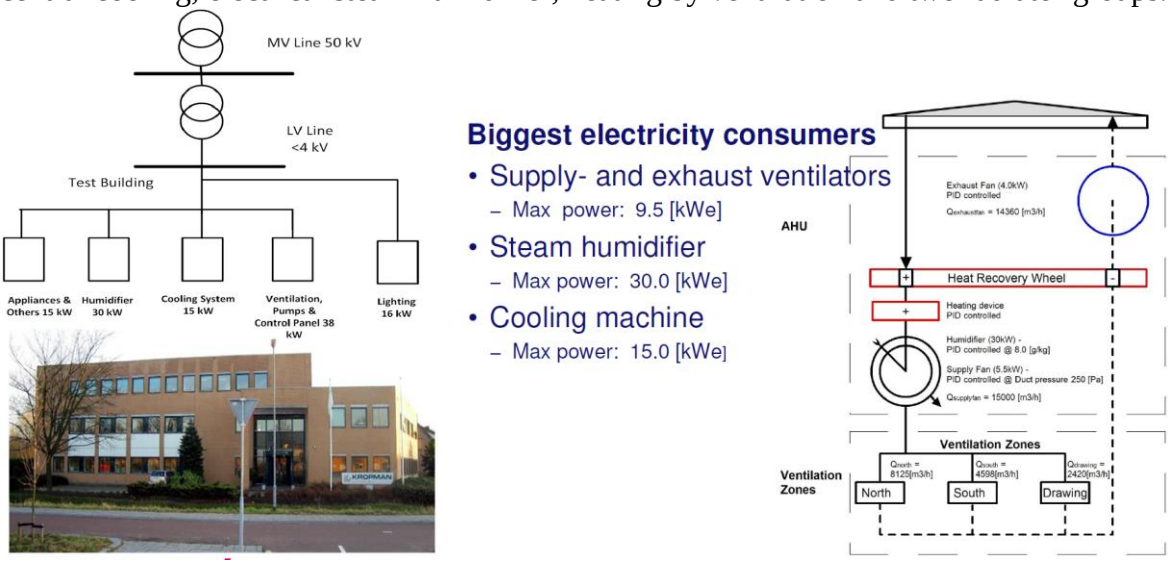

Figure 1. The electrical connections from Mid Voltage grid to building and its major electricity consumers.

The first floor, see Fig. 2, was chosen for more detailed measurements because it was the most regularly occupied floor. In each room the temperature, CO_2 concentration, humidity and average airspeeds were measured during the project in accordance to ISO 7726 [ISO 1998] and the ASHRAE Performance Measurement Protocol [ASHRAE 2010].

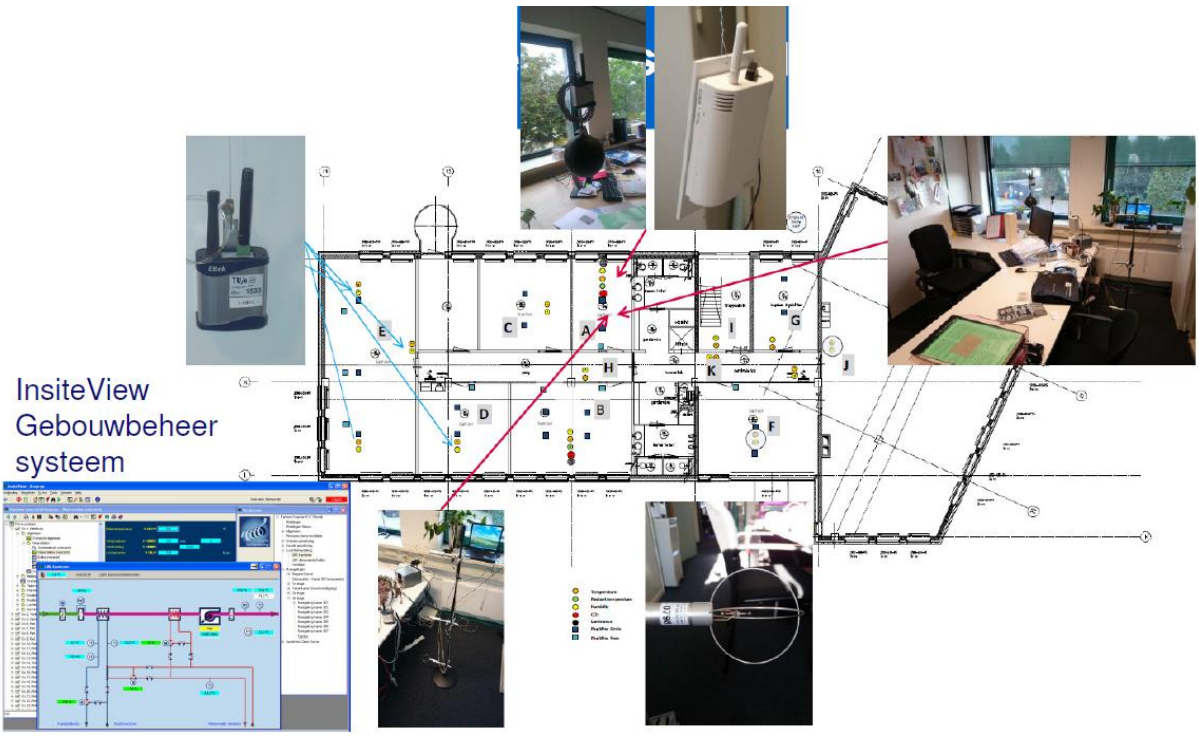

Figure 2. Test case office building Kropman Breda

The biggest controllable electrical energy consumer is the Air Handling Unit during wintertime with its steam humidifier, see Fig. 3. The installed VAPAC VP30 power consumption peaks at 30 kW.

Figure 3. Air Handling Unit and steam pipe

The biggest controllable electrical energy consumers in the AHU during wintertime are the supply and exhaust fans and the steam humidifier with an installed capacity of 5.5, 4.0 and 30 [kW]. The actual power usage is usually lower than the maximum rated power. For both fans together the actual consumption during normal operations is 4 – 5 [kW]. The humidifier operates at start in the early morning near its peak to 28 [kW], but then dependent on the out- and indoor conditions the power consumption reduces from usually 6 – 20 [kW].Two experiments were done for active load purposes: Experiment I: during the steam humidifier power reduction interval of 15 minutes, approx. 14 [kW] power was saved, during the 30 minutes interval 9 – 14 [kW] and during the 60 minutes interval about 12 [kW] was saved. To avoid peaks after switching to normal set point, the interval set point should be slightly higher than the minimum demand of the humidifier. Experiment II: during the fan power reduction interval of 15 and 30 minutes a total of 7 [kW] was saved, at the 60 minute interval 6 – 7 [kW] was saved.

RESULTS

The energy reduction statement is tested by two experiments namely: Exp. I: steam humidifier power reduction and Exp.2: supply- and exhaust fan power reduction.

The experiment I took place at the 20th of December. The power savings in [kW] during this experiment day were at interval time: I (15min), II (30min), III (60min): 14, 9 – 14 & 12. This energy saving is generated by changing the humidifier absolute humidity set point from 8.0 to 6.0 [g/kg], at 21.5 [˚C], this correspond respectively to a supplied RH of 51 [%] and 37.5 [%], see Fig. 4.

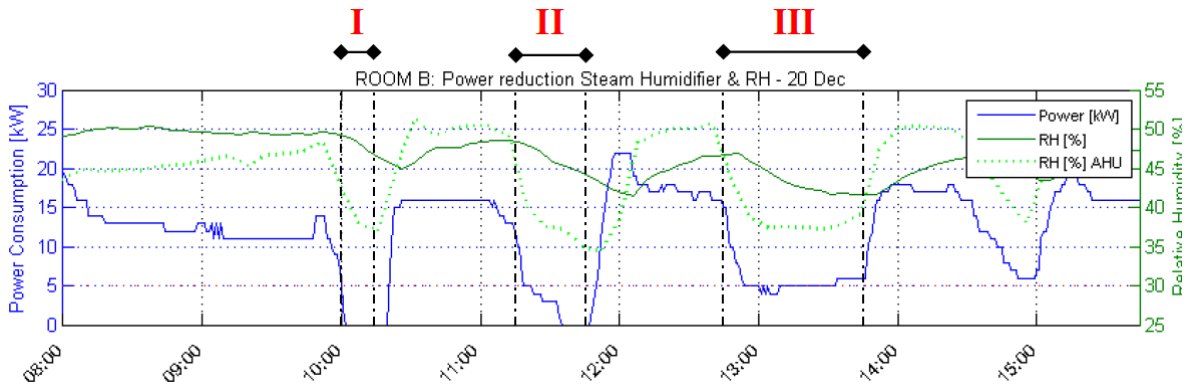

Figure 4. Results room B relative humidity, relative humidity AHU and power consumption

At the second experiment the fan supply- and exhaust rates are reduced to 25% of the normal conditions. This results in 2 [kW] energy savings from the fans for all three interval times, but at the same moment the power consumption of the steam humidifier also decreased with 5 [kW]. The relative humidity concentration in all rooms remains stable since the set point of

the absolute humidity stays 8.0 [g/kg]. The indoor carbon dioxide concentration [ppm] did not exceed the comfort boundary condition of 800 [ppm]. Approximately 7 [kW] is saved during the 14th of January with 25% flow reduction. This is a proper flexible energy saving source derived by the AHU, without exceeding set comfort boundary conditions.

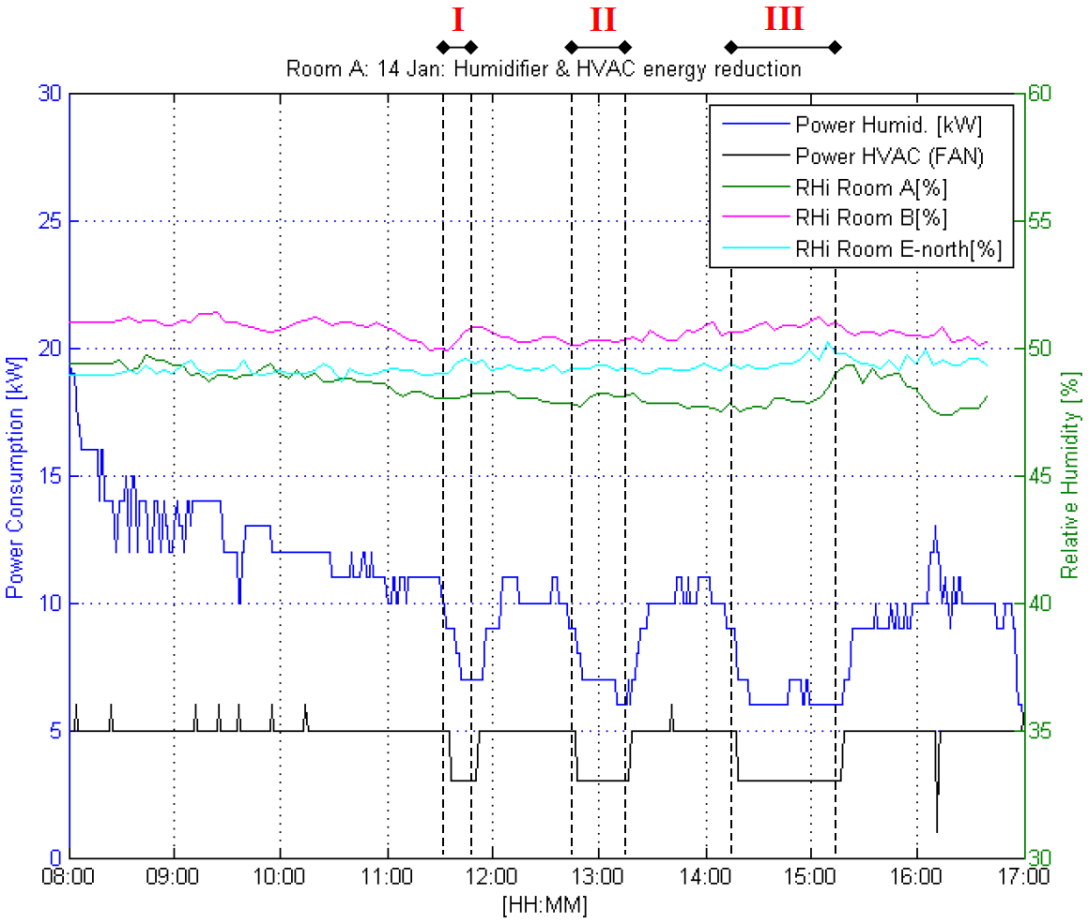

Figure 5. Energy consumption fans and humidifier during experiment II, interval times are black dashed

Below table 1 shows the potential yearly energy savings based on the data gathered during the experiments.

Table 1: Yearly energy savings with energy data found at 3rd interval experiment I & II

	Expected operation time during a year:	*Expected saving:*
Exp 1. Humidifier	1392 hours	13920 [kWh] (10kW saving /h)
Exp 2. Fans	2739 hours	5487 [kWh] (2kW saving /h)
Exp 2. Side effect fan reduction → humidifier power reduction	1392 hours	6960 [kWh] (5kW saving /h)

DISCUSSION AND CONCLUSIONS

The energy saving and active load experiments were only done at two particular winter days to show energy savings from the AHU. More test days are preferred to understand the energy reduction at different outdoor conditions. Short time (15 – 60 minutes) energy savings from the (AHU) steam humidifier and fans as active loads can be derived within comfort

boundaries during wintertime. This energy saving regulation could be used for future smart-grid integration. The humidifier is slow responding because of the control time delay, this can be adjusted to faster responding times for better interaction to the grid. The fan reduction has a fast responding time, since a fast time delay is set in the BMS control. It has a good potential for future frequency demand control service. Active loads in office buildings can offer as a demand side resource benefits towards the Smart Grid.

REFERENCES

1. CISBSE, 2012, Mind the performance gap: regulated vs unregulated, CIBSE conference, London
2. Brahman F., Honarmand M., Jadid S., 2015, Optimal electrical and thermal energy management of a residential energy hub, integrating demand response and energy storage system, Energy and Buildings 90: 65-75
3. RVO, 2014, Monitor Energiebesparing Gebouwde Omgeving 2013, November 2014
4. Cui B., Wang S., Yan C., Xue X., 2015, Evaluation of a fast power demand response strategy using active and passive building cold storages for smart grid applications, Energy Convers Manage, http://dx.doi.org/10.1016/j.enconman.2014.12.025
5. Motegi N., Piette M.A., Watson D.S., Kiliccote S., Xu P., 2005, Introduction to commercial building control strategies and techniques for demand response. Berkeley:Lawrence Berkeley National Laboratory LBNL-59975
6. Eto J., Nelson-Hoffman J., Torres C., Hirth S., Yinger B., Kueck J., Kirby B., Bernier .C, Wright R., Barat A., Watson D., 2007, Demand response spinning reserve demonstration. Berkeley: Lawrence Berkeley National Laboratory LBNL- 62761.
7. Kirby B., Kueck J., Laughner T., Morris K., 2008, Spinning reserve from hotel load response. Electricity J 21(10):59–66.
8. Watson D.S., Kiliccote S., Motegi N., Piette M.A., 2006, Strategies for demand response in commercial buildings. In: Proceedings ACEEE Summer Study on Energy Efficiency in Buildings, Pacific Grove, USA.
9. Hao Y.H., Middelkoop T., Barooah P., Meyn S., 2012, How demand response from commercial buildings will provide the regulation needs of the grid, Proceedings 50th Annual Conference on Communication, Control and Computing Allerton.
10. Chen C. , S. Duan, T. Cai, B. Liu, G. Hu, Smart energy management system for opti-mal microgrid economic operation, Renew. Power Gener. IET 5 (2011) 258–267.
11. Callaway D.S., Hiskens I.A.., 2011, Achieving controllability of electric loads, Proceedings of the IEEE 2011; 99: 184-199.
12. Trudnowski D., Matt D., Eric L, 2006, Power-system frequency and stability control using decentralized intelligent loads. In 2005/2006 IEEE PES Transmission and Distribution Conference and Exhibition, IEEE,
13. Pratt R.G., 2004, Transforming the US electricity system. In IEEE PES Power Systems Conference and Exposition 2004, IEEE, 2004.
14. ISO 7726, 1998, Ergonomics of the thermal environment -- Instruments for measuring physical quantities
15. ASHRAE, 2010, Performance Measurement Protocols for Commercial Buildings.

BUILDINGS' ENERGY FLEXIBILITY: STARTING FROM THE USER TO SUPPORT THE SMART GRID

Wim Zeiler; Kennedy Aduda

Faculty of the Built Environment, TU Eindhoven, Eindhoven, Netherlands

ABSTRACT

Using the flexibility within energy generation, distribution infrastructure, renewable energy sources and the built environment is the ultimate sustainable strategy within the Built Environment. However, at the moment this flexibility on building level is still to be defined. The new IEA Annex 67 is just starting work to define this specific flexibility.
Our research is aimed at developing, implementing and evaluating new process control strategies for improving the energy interaction within the building, its environment and the energy infrastructure by effectively incorporating the occupants' behaviour. An integral approach based on the Open Building strategy is used which divides the whole system in different layers from user up to centralized power generation and as a results offers new possibilities for buildings' energy flexibility towards the Smart Grid.

Keywords: energy flexibility, user, Smart Grid

INTRODUCTION

Energy infrastructures form the back bone of modern society as energy is needed for nearly all necessary services[1]. The built environment is currently a major consumer of fossil energy with nearly 40% [2] but it also has huge potential to contribute to the supply and management of renewable energy. The built environment is the most complex distributed technical system with its energy infrastructures for electricity, gas, heat- and cold on utility level as well as all the ducts, pipes and cables within the buildings. As concerns grow about the environmental cost and limited supply of fossil energy resources, so does the importance to society of carefully managing the energy resources available and of developing and implementing alternative renewable energy sources. As the future cannot be predicted there is a need for flexibility of the energy infrastructure. The current electricity system already uses many sources of flexibility to run efficiently such as: demand-side response, energy storage, distributed generation, demand change, time-shifting demand, embedded generation, fuel substitution, and efficiency schemes. However, new sources of flexibility are likely to be required to deal with the changing operation of the system. There is a need to take a more holistic approach to system flexibility, which looks at the potential interactions between new and traditional sources of flexibility and how these sources are used by different parties [3]. This paper presents an integral approach to optimize the flexible interaction between buildings, renewable energy sources and their energy infrastructure, especially the Smart Grid.

THE GRID

Electricity is traditionally generated in large central plants and distributed throughout the country. However, the last decades have seen the beginning of some change in this trend. More and more decentralized electricity production is now achieved using wind turbines, geothermal heat pumps and photovoltaic systems. Smart adaptive control of energy consumption and generation inside (nano Grid) and around buildings (micro Grid) can

provide major contributions to address the imminent energy problems within the total energy infrastructure (Electricity as well as the Gas distribution). The stochastic nature of renewable production has a negative impact on system balancing. Further changes of the whole distribution system are expected from a strictly top down to a more bottom-up system; this will be capped by ability of the user to supply electricity to the distribution grid on different levels. Coping with complex and unpredictable factors related to DRES and the Grid requires a more flexible approach in the design process that is increasingly bottom up rather than top down. As a result the influence of the building's design and its users' interactions becomes more important. Buildings, building services systems and energy infrastructure must be designed for more flexibility. It is widely recognized that increasing flexibility is key for the reliable operation of future power systems with very high penetration levels of DRES [4]. To model flexibility in energy systems there are several approaches: using heuristics, sector-specific highly detailed models or combining models [5]. However, currently available models do not seem to be able of capturing flexibility issues properly. New holistic approaches are needed in energy system modelling [5]. Besides the flexibility in energy systems there is also the flexibility in the demand: the energy flexibility of a building. This energy flexibility of a building is not yet defined but a working definition of the IEA Annex 67 Energy Flexible Buildings is its ability to manage energy demand and generation according to local climatic conditions, occupant needs and energy grid requirements [2]. New integral approaches are needed to increase buildings' flexibility towards the Smart Grid.

METHOD

In facing uncertainty in design, common practice in systems engineering is to optimize a system that satisfies a given set of parameters. Such an optimized solution is rigid and will not perform well when uncertainty is high [1]. This calls for a new approach that design systems can be easily changed to adapt and adjust to changing conditions. Flexibility in design is needed to cope with the effects of uncertainty [1,6]. To optimize the energy infrastructure in the built environment, an integral approach based on general systems theory developed by von Bertalanffy [7] is proposed [8,9]. This system engineering like method uses functional decomposition and different levels of abstraction to cope with the complexity of the energy infrastructure of the built environment, see Fig. 1:

- building level (possible energy supply from micro Grid, nano Grid and RES),
- floor level (distribution of occupancy and the necessary energy flows)
- room level (energy need depends on outside environmental conditions and internal heat load),
- workplace level (workplace conditions and energy needs from appliances), and
- human level (different comfort needs of individuals).

Traditionally the energy approach towards the built environment is top-down (centralized energy generation/distribution through the Smart grid). We want to use instead a middle-out (control on building level by the Building Energy Management Systems BEMS) as well as a bottom-up approach (demand driven by the human behaviour).

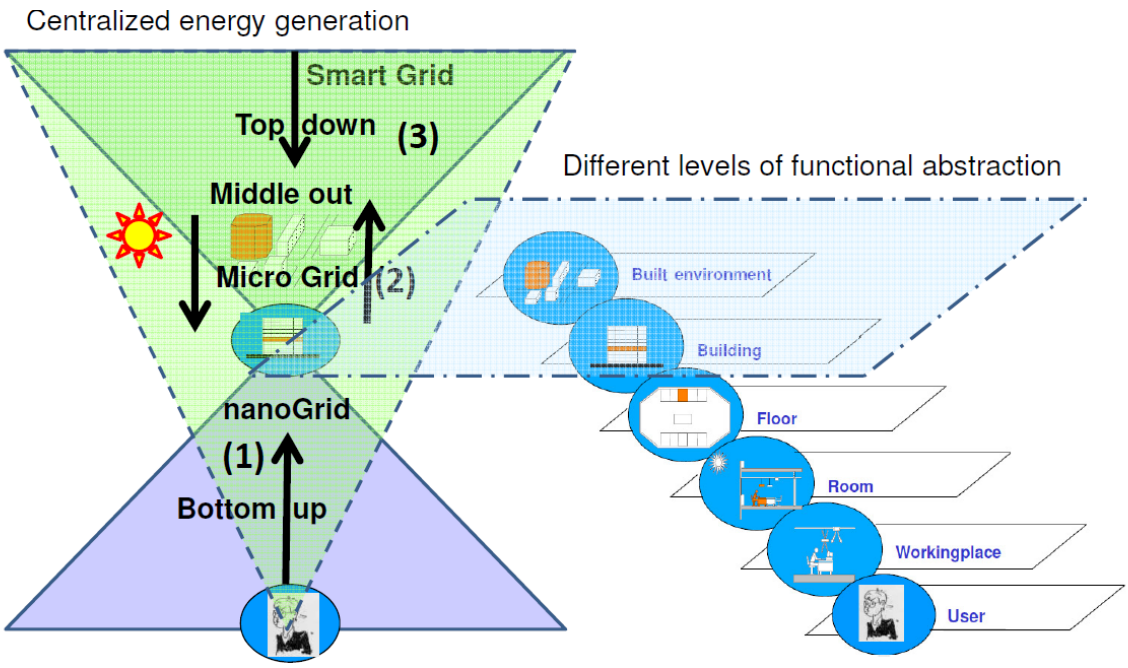

Figure 1. Representation of the approaches for optimizing building interaction with the Smart Grid, complementary to the traditional top-down approach.

The open building concept developed by Habraken [10] approached the built environment as a constantly changing product caused by human activity, with the central features of the environment resulting from decisions made at various levels which is also typically the case with the energy infrastructure of the built environment. During the design process participants and their decisions were structured at several levels of decision-making the infill-level; the support-level; and the tissue-level. On each level a balance has to be made between the performances of supply and demand for buildings during the life-cycle. The levels of city structure, urban tissue, support, space and infill were usually distinguished. Open Building lends formal structure to traditionally and inherent levels of environmental decision making [11,12]. The principal tool used by those working in an open building way is the organization of the process of designing and building on environmental levels. Open building entailed the idea that the need for change at a lower level such as the dwelling, emerged faster than at upper levels, such as the support. The "thinking in levels" approach of Open Building was introduced to improve the design and decision making process by structuring them at different levels of abstraction. Different decisions have to be taken at each level in the energy infrastructure of the built environment. One of those decisions is the application of sustainable energy systems and components. However, this is rather complex to integrate in the early stages of building design as many aspects still have to be taken into account. Applying the principles of Open Building design to the optimization of the energy infrastructure of a building makes it possible to integrate in a flexible way the energy flows connected to heating, cooling, ventilation, lighting, and power demand, within a building and between buildings and the built environment. This leads to flexibility of energy exchange between different energy requirements and sustainable energy supply on the different levels of abstraction in the built environment. There is a close similarity between the highly abstract approach of Integral Design with the hierarchical abstraction used within Open Building, see Fig. 2.

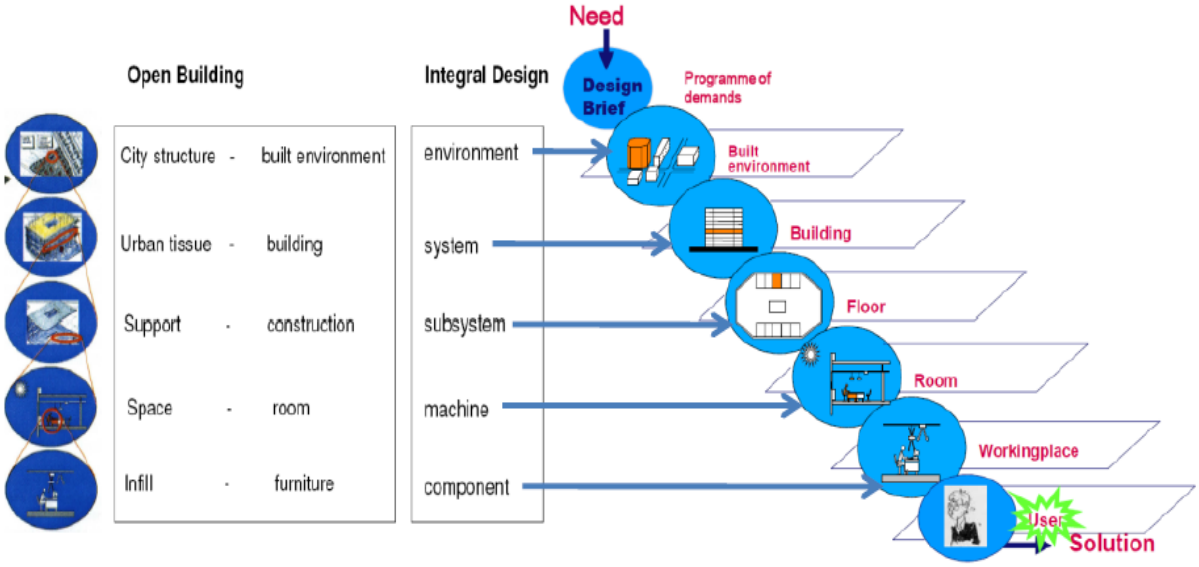

Figure 2. Comparison hierarchical abstraction Open Building and Integral Design approach.

RESULTS

There is a different focus on the processes that occur in the building, which also depends on the strategy that is leading: bottom-up (user orientated), middle out (building services systems orientated) and top-down (Smart Grid). As mentioned by Bloem and Strachan [13] a top-down approach gives mainly the boundaries for energy consumption related to occupancy behaviour. The bottom-up approach is able to estimate the individual energy consumption and then aggregate it to predict the total building energy demand, which is highly desirable despite the uncertainties in end-user's behaviours in time and space.

Based on each of these approaches the results and insights are used to specify specific functionalities for the level below and the level above. In this way flexibility enables the developers to gain from upside opportunities and minimize downside risks [1,6]. Taking cue from the required dynamism and flexible operations, we adapt the framework of Kofler et al. [14] as ideal for realization of the pervasive control envisioned by Kolokotsa et al.[151] with a central role for Building Automation (BEMS) and Multi Agent System (MAS), see Fig. 3.
In general two kinds of flexibilities can be distinguished in energy infrastructures [1];
- architectural, enables with relative ease to modify configurations or layouts of the system to future uncertainty
- operational, which allows energy modification of operating strategies without major changes.

Energy infrastructure's functionalities boil down to energy management making use of the flexibilities of all grid connected systems which will lead to a better balanced and controlled network at all levels [16-19]. The energy demand characteristics of buildings available in Building Automation Systems represent crucial information for grid optimisation [20] to activate participation of buildings in the grid. For an optimal SG from a system of systems point of view, the BEMS has to be coupled with the management platform of the grid [17

DISCUSSION AND CONCLUSION

The responsiveness of SG to changing uncertainties & requirements can be realized through the intrinsic flexibility measures embedded in energy infrastructures design processes. A methodological design framework based on a unified theoretical system engineering concept related to Open Building gives the designers the opportunity to systematically integrate architectural and operational flexibility early on in the conceptual design phase of energy infrastructures of the built environment. This hierarchical design framework aims at providing support for integrating flexibility at the early stage of the conceptual designs of infrastructure

systems. The manner of description of a system influences the identification of the possible changes that may take place and the interpretation of their demands for flexibility. In this paper the focus was on operational flexibility for which the integration of the end-user through a bottom-up approach is essential for BEMS.

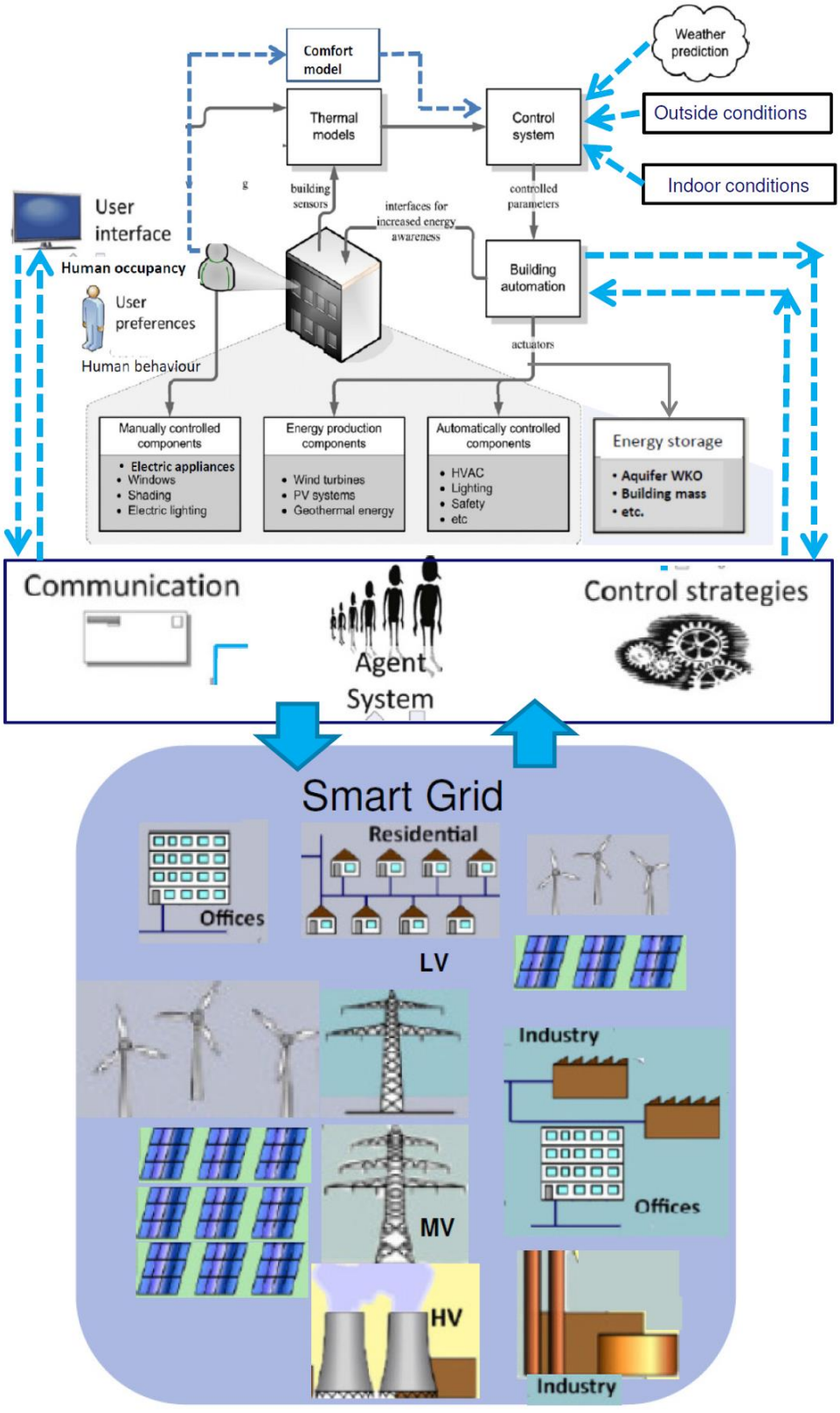

Figure 3. SG and User Interaction, based on Kolokotsa et al. [15] and Kofler et al[14]

REFERENCES

1.Melese Y.G., Heijnen P.W., Stikkelman R.M., 2014, Designing Networked Energy Infrastructure with Architectural Flexibility, Procedia Computer Science 28: 179-186.

2. IEA 2015, International Energy Agency, Energy in Buildings and Communities programme, EBC Annual Report 2014

3. Frerk M., 2015, Open letter: facilitating efficient use of flexibility sources in the GB electricity system, OFGEM, The Office of Gas and Electricity Markets, 28 January 2015

4. Papaefthymiou G., Grave K., Dragoon K., 2014, Flexibility options in electricity systems, Project number: POWDE14426, Ecofys 2014 by order of: European Copper Institute

5. Hidalgo Gonzalez I., Pablo Ruiz Castello P., Sgobbi A., Nijs W., Quolin S., Zucker A., Thiel C., 2015, Addressing flexibility in energy system models, European Commission Joint Research Centre, Institute for Energy and Transport, Report EUR 27183 EN

6. Neufville R.de, Scholtes S., 2011, Flexibility in Engineering Design, MIT Press, Cambridge, MA, USA

7. Blanchard B.S., Fabrycky W.J., 2005, Systems Engineering and Analysis, fourth Edition

8. Savanović P., 2009, Integral design method in the context of sustainable building design, PhD thesis, Technische Universiteit Eindhoven.

9. Zeiler W., Savanović P., 2009, General Systems Theory based Integral Design Method, Proceedings ICED'09, Stanford, USA.

10. Habraken N.J., 1961, De dragers en de mensen, Haarlem (Dutch)

11. Kendall S., Open Building Concepts, CIB W104,www.open-building.org/ob/concepts.html

12. Kendall S., Teicher, J., 2000, Residential Open Building, E & FN SPON, London

13. Bloem J.J.,Strachan P., 2012, Evaluating and Modelling Near-Zero Energy Buildings; Are we ready for 2018?, Expert Meeting 30-31 January 2012 Glasgow, JRC Technical report

14. Kofler M.J., Reinisch C., Kastner W., 2012, A semantic representation of energy-related information in future smart homes, Energy and Buildings 47:169-79.

15. Kolokotsa D, Rovas D, Kosmatopoulos E, Kalaitzakis K., 2011, A roadmap towards intelligent net zero- and positive-energy buildings. Solar Energy 85: 3067–3084

16. Lo C., Ansari N., 2011, The Progressive Smart Grid System from Both Power and Communications Aspects, Communications Surveys & Tutorials, IEEE PP(99): 1-23.

17. Dave S., Sooriyabandara M., Yearworth M., 2011, A Systems Approach to the Smart Grid, The First International Conference on Smart Grids, Green Communications and IT Energy-aware Technologies.

18. Lopes A. J., Lezama R., Pineda R., 2011, Model Based Systems Engineering for Smart Grids as Systems of Systems, Procedia Computer Science 6: 441-450.

19. Acevedo S., Molinas M., 2012, Identifying Unstable Region of Operation in a Micro-grid System, Energy Procedia 20: 237-246.

20. Wang S., 2013, Intelligent Building Electricity Demand Management and Interactions with Smart Grid, Proceedings Clima 2013, Prague

Urban Ecology and Metabolism

ASSESSING THE ENVIRONMENTAL IMPACT OF FUTURE URBAN DEVELOPMENTS AT NEIGHBOURHOOD SCALE

J. A. Fonseca[1]; A. Willmann[1]; C. Moser[3]; M. Stauffacher[2]; A. Schlueter[1]

1: Architecture and Building Systems – Institute of Technology in Architecture – ETH Zurich. John-von-Neumann Weg 9. 8093 Zurich; 2: Transdisciplinarity Lab - Department of environmental systems science – ETH Zurich, Sonneggstrasse 33, 8092 Zurich; 3: Institute of Sustainable Development – School of Engineering – ZHAW. Technoparkstrasse 2, 8400 Winterthur

ABSTRACT

This paper presents the results of a two-year trans-disciplinary research project investigating opportunities and limitations of the Swiss 2000-Watt/1-ton CO_2 society vision for the transformation of industrial sites into liveable neighbourhoods. By involving local stakeholders we elaborated four plausible scenarios for the transformation of an industrial area in the city of Zug, Switzerland. Based on life cycle analysis methods and urban energy modelling, we estimated the carbon and energy footprint of every scenario due to construction, operation, retrofit and dismantling of buildings, production processes and logistics, commuting, and business flights. The results of our research present a comprehensive description of focal points of environmental impact in future forms of urban development and a description of the role of industry in a transition towards more sustainable urban environments. These are topics of high interest for decision makers involved in initiatives for the sustainable transformation of neighbourhoods such as the 2000-Watt Areale or alike.

Keywords: Urban transformation, environmental impact in neighbourhoods, 2000-Watt/1-ton CO2 society.

1. INTRODUCTION

New patterns of urbanization and population growth have induced the renewal and expansion of urban areas across the globe. A rising awareness on climate change and its effects on cities have suggested processes of urbanization focusing on improving the social, economic and especially the environmental performance of cities. In Switzerland, an environmental vision known as the 2000-Watt/1-ton CO_2 society calls for the reduction of 1/4 of every inhabitant's carbon foot-print by 2050. By acknowledging a direct relation between these targets and the environmental impacts of the built environment, a set of acupunctural projects at neighbourhood scale (2000-Watt Areale) have recently risen as part of physical initiatives to assess the implementation of this concept as potential role-model for sustainable development in Switzerland.

The concept of the 2000-Watt Areale has been widely analysed for residential and commercial areas in Switzerland [1]. For industrial areas there is a need for a congruent knowledge base that serves decision makers to understand the role of industry in the process of revitalization of urban areas and the applicability of the 2000-Watt/1-ton CO_2 society vision for this endeavour. The key question is: what are the opportunities and limitations of the 2000-Watt/1-ton CO2 society vision for the transformation of industrial sites into liveable neighbourhoods?

This question is analysed by means of a case study in the Swiss city of Zug. It consists of an industrial site of around 25ha undergoing a process of urban transformation. Siemens Building Technologies (SBT), a large manufacturer in the light industry sector, owns and predominately occupies the site along with several companies in the services sector. At the moment, there is no residential use on site.

In this paper, we present an assessment of the environmental impact of scenarios of urban transformation for this former industrial area. In section 2 we present key information about data collection, scenarios construction, and life cycle assessment (LCA) methods. In section 3 we present a comparison among scenarios and discuss the implications of these trajectories of development in relation to the 2000-Watt/1-ton CO_2 society vision and areas with industrial uses.

2. METHOD

2.1. Data collection and processing

We collected data of buildings, infrastructure, industrial processes, users and mobility patterns on site in order to set-up a baseline. Figure 1 presents a visual representation of this baseline or Status Quo scenario.

For buildings and infrastructure, we collected information regarding energy consumption and energy systems along with key characteristics of buildings (e.g. dimension, program and thermal properties). We evaluated retrofit options for existing energy infrastructure and buildings along with the potential for integration of renewable energy and waste heat [2].

For industrial processes, we gathered data about the production chain of two characteristic products of SBT and evaluated potential energy efficiency strategies [3].

For mobility, we conducted a postal survey in SBT (N = 1085, response rate 62%) and received data about users, distances, frequency, transport means, and willingness to relocate to the site [4].

2.2. Scenario construction

In order to assess the environmental impact of future states of urban development, we constructed plausible urban scenarios for the area of study in an interdisciplinary process. This processes consisted in a series of workshops including researchers from architecture, engineering, sociology, and psychology and representatives of SBT.

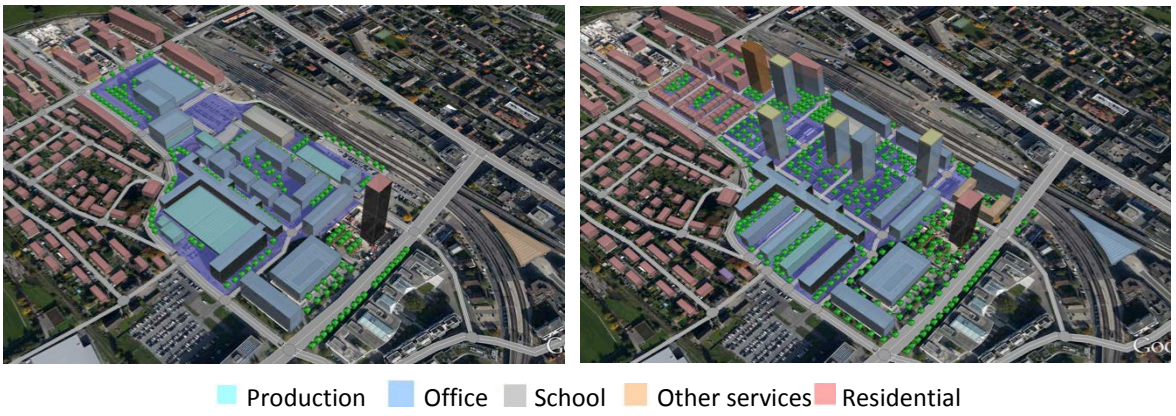

Figure 1 Status Quo and example of urban scenario, left: Status-Quo, right: High-End and Business. Image elaborated with CLM [5]

Following the approach of [6], four scenarios were developed from the combination of a top-down vision and different levels of variables such as mixed-use, building typology, target groups etc. The four scenarios are: **Business-as-usual** (**BAU**) (isolated development; no activities in the evening/during the night; little social life; a few new buildings; existing industrial production is kept; more office space); **Campus** (**CAMP**) (Innovation park; student housing; collaboration between science, little industry, and education; existing industrial production on site is kept; shopping possibilities for students; priced restaurants; nightlife); **High-End Business (HEB)** (Research and development; global companies; densification and high buildings; business hotel; luxury apartments; little industry; restaurants and nightclubs); **Urban Condenser (UC)** (lively city quarter, markets, family friendly, pedestrians and bikes, urban farming, small and local businesses; little industry; more residential areas). In Figure 1 we present a visual example of the HEB scenario.

2.3. Carbon footprint assessment

The carbon footprint of the area is assessed accounting to the shares of buildings and energy infrastructure, production processes and logistics and finally, commuting and business flights.

Buildings and energy infrastructure

The emissions due to construction, retrofit and dismantling of buildings in a scenario basis were computed by relating statistical data of the Swiss building stock [7] to the building's geometry [8]. For new scenarios, the emissions due to operation of buildings and related infrastructure were calculated with the multi-objective optimization approach of [9] assuming an equal balance between costs, emissions and efficiency.

Production processes and logistics

The emissions due to production processes and logistics of SBT are calculated for the supply chain of two representative products. For this we considered the life cycle of components, and processes of fabrication and distribution. We used SimaPro and ReCiPe Midpoint to carry out a detailed energy demand and a reduction potential analysis dissecting three main impact factors: transport distance, weight of product, and means of transportation. The emissions of other types of industry on site were calculated by correlating statistical data to the built area [3], [10], [11].

Commuting and business flights

We calculated the carbon footprint due to commuting and business flights following the recommendations of the standard SIA 2039. For this we took into consideration the data gathered in section 2.1 and estimated future states of trip generation of every target group (i.e. students, expats and families) considering both private and public transportation modes (i.e. Bicycle, pedestrian, public transport, aircraft). We considered only one-way trips to attribute 50% of the total emissions to the area. All factors relating the carbon foot print of a target group and transportation mode were obtained from [12]–[14] and the Ecoinvent database.

3. RESULTS AND DISCUSSION

Based on the approach of [14] we calculated target values of the 2000-Watt-society vision for the year of 2050. These target values are obtained for the dimensions of embodied energy, operation of buildings and mobility. As shown in Figure 2a, both, grey emissions and embodied energy in buildings will increase for every possible scenario at a maximum of 180% from today's levels. For the area of interest this level is still below its target values. For the Swiss average, we might assume that an urban transformation in this direction will tremendously increase its carbon footprint due to embodied energy.

For operation of buildings and industry, we found the expected performance of each scenario (Figure 2b) to slightly exceed its target values. The same statement is valid for the total emissions of the area (Figure 2d). We found this behaviour to be strongly related to technology efficiency rather than to industry operation, whose share is negligible in comparison to building operation (Figure 3). In consequence, we foresee that an increase from today's 14% to 20% efficiency of photovoltaic technology (considered the most optimal for every scenario in section 2.3) would allow the CAMP, HEB and UC scenarios to attain the target value of total emissions for the area.

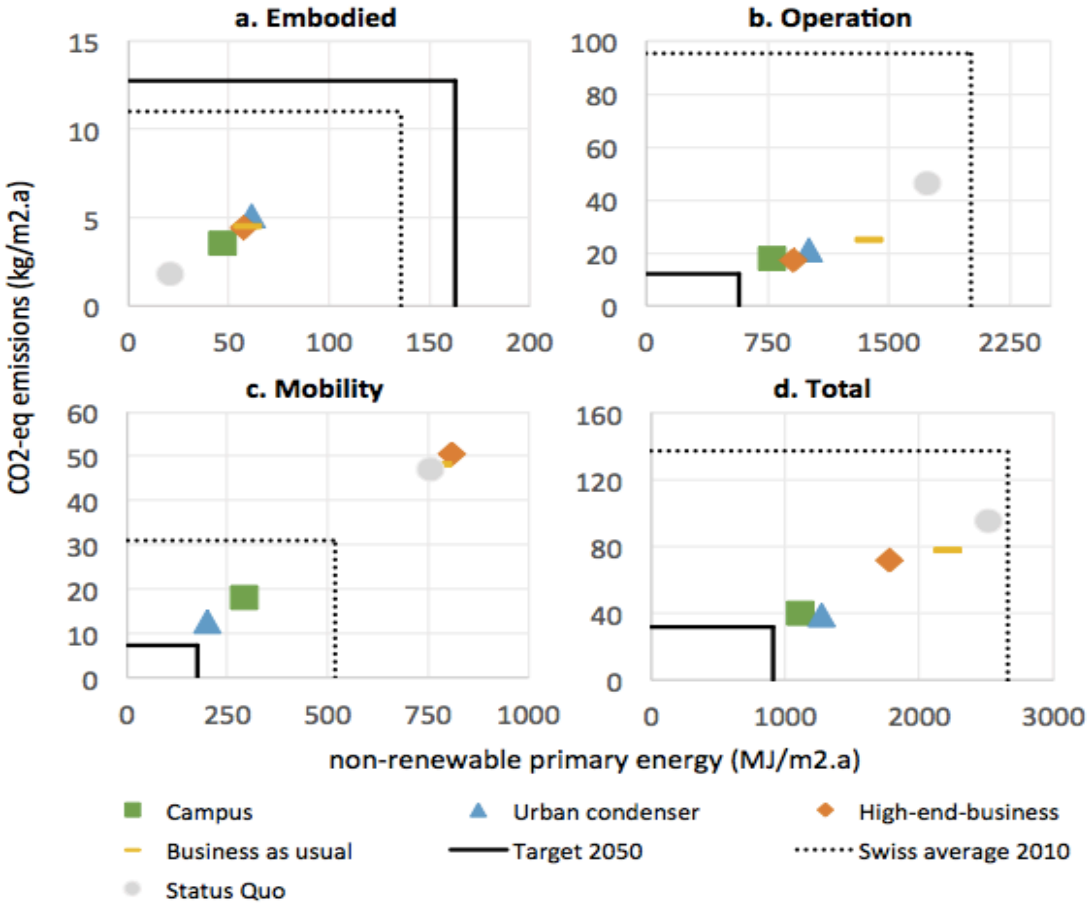

Figure 2 Comparison to short and medium term 2000-Watt/1-ton CO_2 society goals due to: a. embodied energy, b. building operation, c. mobility and d. total for the area

In terms of emissions due to mobility the panorama can highly change from scenario to scenario. In general SQ, BAU and HEB scenarios could potentially generate up to four times more emissions due to mobility than the other (Figure 2c). This behaviour is driven by top-level management positions and related business flights, which correspond to the highest share of total emissions in the area (Figure 3). As a consequence the Scenario HEB will be the most polluting one with 32% more emissions than today (SQ).

As shown Figure 3 the CO_2-eq emissions per scenario will decrease by 20% to 63%, the later coming close to the 2000-Watt/1-ton CO_2 benchmark of 75% (2 ton/p.a). As stated above, the highest leverage to attain this benchmark for the area of concern exists in the building sector, where despite the grey emissions of new buildings and infrastructure, energy and building technology allows to drastically reduce emissions. As in the total values of Figure 3, the predominant share remains in business flights whereas the lowest lie in logistics and industrial processes. The total emissions in the area can decrease up to 48% for a scenario with low business flights, or increase in 32% for the most demanding one.

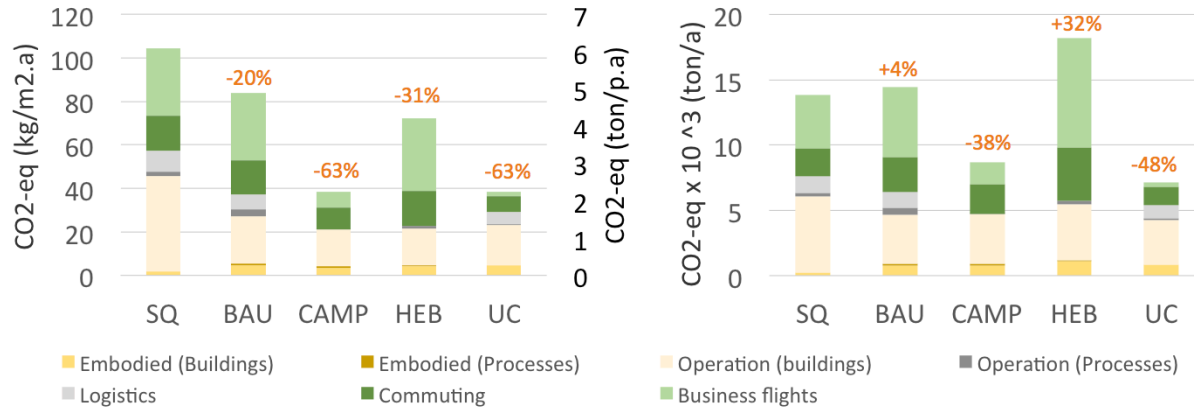

Figure 3 Variation in percentage of CO_2-eq emissions per scenario with respect to Status Quo, a. Left: Relative b. Right: Total

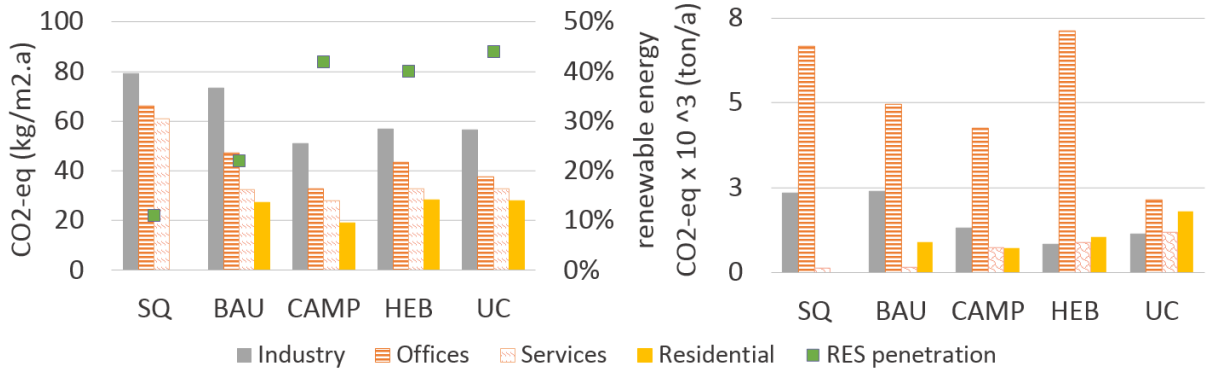

Figure 4 CO_2-eq emissions per building sector. a. Left: Relative values and penetration of renewable energy b. Right: Total

As depicted by the relative values of Figure 4, the CO_2-eq emissions of each sector decreases proportionally to the penetration of renewable energy resources in site. The highest leverage is found in residential, offices and services sectors while the lowest in industry. This behaviour is due to the relatively few energy efficiency alternatives found for industry on site in comparison to the other building categories [8]. In terms of total values, offices uses could predominantly increase the total carbon footprint of the area, what we found to be in line with current trends of high penetration of services uses in cities.

4. CONCLUSIONS

We presented a case study of urban transformation and assessed the expected carbon footprint of plausible urban scenarios. We compared their cross-sectorial (industry, buildings and transportation) and multi-dimensional (during construction and operation) environmental impact. We presented a comprehensive description of focal points of environmental impact as well as a description of the role of industry in a transition towards more sustainable urban environments.

For the case study of Zug, we described how, in relation to the different scenarios, the shares of embodied energy in buildings and operation of industrial sectors have the potential to generate the lowest emissions, whereas mobility in the service sector (business flights) potentially generates the highest. The existence of light industry itself does not jeopardize the future environmental performance of the area, but instead, it brings positive effects as a potential source of waste energy. In contrast top-management levels creates the highest share

of emissions due to business flights. Technological advances in energy and building technology will represent a critical factor to attain the 2000-Watt/1-ton society goals.

In general, the series of assessment methods here before introduced are applicable to studies in any urban area with or without industrial use, as benchmarks can be easily changed. Further work could consider sensitivity analysis techniques for more detailed intra and inter scenario comparison.

5. ACKNOWLEDGEMENTS

We would like to thank our project partners Martin Schaer and Benno Moser from Siemens Building Technologies, Christian Wirz, Sandra Moebus, Stefan Hofstetter, and Ariane Staeubli from UMTECH/WERZ institute. We also thank Zoltan Nagy for reviewing and proof reading. This research was financed by the Swiss Commission for Technology and Innovation (CTI)

6. REFERENCES

[1] D. Kellenberger, M. Menard, S. Chneider, M. Org, K. Victor, and S. Lenel, “Areal-entwicklung fur die 2000-Watt gesellschaft: Leitfaden und Fallbeispiele,” Bern, 2012.

[2] J. A. Fonseca and A. Schlueter, “Method and data analysis for assessment of local energy potentials for urban transformation: case study of a mixed use city quarter,” in CISBAT 2013, 2013, pp. 649–654.

[3] W. Huber, “Effiziente Druckluft- und Stickstoffversorgung für den Neubau BT@Zug der Siemens Schweiz,” 2013.

[4] A. Kollros, Reduktion der CO2-Emissionen bei Geschäftsflügen: Das Beispiel Siemens Building Technologies. Zürich: ETH-UNS TdLab, 2014.

[5] Siemens Corporate Technology, “City Life Management Tool (CLM),” City in a Digital Nutshell, 2012.

[6] J. Gausemeier, A. Fink, and O. Schlake, “Scenario ManagementAn Approach to Develop Future Potentials,” Technol. Forecast. Soc. Change, vol. 59, no. 2, pp. 111–130, 1998.

[7] E. Thoma, J. A. Fonseca, and A. Schlueter, “Estimation of base-values for Grey Energy, Primary Energy, Global Warming Potential (GWP 100A) and Umweltbelastungspunkte (UBP 2006) for Swiss constructions from before 1920 until today,” in Contemporary Urban Issues ’14, 2014, no. Ubp, p. 17.

[8] A. Schlueter, J. A. Fonseca, A. Willmann, C. Wirz, S. Moebus, S. Hofstetter, M. Stauffacher, C. Moser, N. Muggli, M. Schaer, and T. Gruenewald, “Nachhaltige, softwaregestützte Arealtransformation vom Industriestandort zum Stadtquartier,” Zurich, 2015.

[9] S. Fazlollahi, “Decomposition optimization strategy for the design and operation of district energy systems,” 2014.

[10] S. Bachmann, R. Scherer, P. A. Salamin, M. Ferster, and J. Gulden, “Energieverbrauch in der Industrie und im Dienstleistungssektor Resultate 2012,” Bern, 2013.

[11] MIBAG property + Facility Management AG, “Beschreibung der Medien Siemens Areal in Zug,” Zug, 2011.

[12] Oikos, Der CO2-Fussabdruck der HSG. St. Gallen: oikos Carbon Neutral Campus.

[13] C. Heye and S. Fahrlaender, “Nachfragesegmente im Wohnungsmarkt,” AKZENT, Zuerich, pp. 55–58, Jul-2007.

[14] D. Kellenberger, M. Ménard, S. Schneider, M. Hänger, M. Org, K. Victor, and S. Lenel, Arealentwicklung für die 2000-Watt-Gesellschaft: Beurteilungsmethode in Anlehnung an den SIA-Effizienzpfad Energie. Bern: Bundesamt für Energie, 2012.

ENERGY RETROFITS OF RESIDENTIAL BUILDINGS IN BRUSSELS: WHAT IMPACTS ON STOCKS AND MATERIAL FLOWS?

Gobbo Emilie R., Trachte Sophie

Architecture et Climat, Université catholique de Louvain (UCL),
Place du Levant, 1, B-1348, Louvain-la-Neuve, Belgium.
E-mail : emilie.gobbo@uclouvain.be
Phone: +32/10.47.26.36

ABSTRACT

One of European Union's main goals is to promote efficient resource management via conservation and preservation of these natural resources. Waste reduction and recovery improvements are key components as well. Moreover, within the context of present energy efficiency, the renovation of the old and energy-consuming housing stock has become a major issue. Although the renovation process generates energy gains during the operation phase of the building, it also leads to resource consumption and waste production that are rarely taken into account in the design process. Therefore, the initiatives essentially based on energy efficiency alone have to be extended in order to incorporate the future value of recyclable and recoverable materials. In this way, the research proposal is to consider buildings as a bank of materials that could constitute local resources on a medium or long-term basis?

Considering the context and issues mentioned above, the present contribution aims to answer the followed question: what impact will the energy-retrofit of buildings have on material stocks and flows? The data in this field is currently non-existent or incomplete. Our proposal is to analyse case studies in terms of intervention trends of sustainable retrofit on the one hand - considering demolition and insulation - and in terms of *material balances* on the other. Particularly, we considered the energy retrofit operation in metabolic terms: the purpose is to identify and quantify the material stocks and flows created before, during, and after the renovation process. Because it is one of the most important elements of the building that has to be upgraded to achieve energy efficiency, this contribution focused on the building envelope.

Keywords: material stocks & flows, energy retrofit, construction material, construction & demolition waste

INTRODUCTION

The European economy requires a significant amount of resources for operations: material use is estimated at 16 tons per capita per year. It also produces a huge amount of waste: about 6 tons per capita per year. Despite management that is more and more efficient, this level continues to grow with devastating consequences for our ecosystems.

The construction sector plays a major role in this context. The sector is responsible for 40% of the raw depletion and energy consumption, and 35% of the European waste generation. Existing building stock represents about 25 billion square meters with a high percentage of dwellings built before 1960.

These ratios are similar in the Brussels Capital Region (BCR). The housing stock is important (almost two thirds of developed areas), as well as being old and energy-consuming. The

construction sector is responsible for a large part of waste generation and material consumption. Indeed, it represents more than a third of the non-domestic waste of the region.

Therefore, the challenges facing the sector in the reduction of energy and raw material consumption, as well as waste production, are monumental.

As players in the construction sector, the architect's primary concern relates to reducing energy consumption during the use phase of the building. Actually, this concern is greatly influenced by the implementation of new energy efficiency regulations, and the many financial incentives making the energy retrofit of buildings more cost effective. New concepts and certifications have appeared, such as passive houses, and Nearly Zero Energy Building. What about the reduction of material consumption and waste generation of the construction projects? These considerations are little known and rarely taken into account by designers and other actors in the sector.

METHOD

Goal and scope of the research

In light of the fore going, the research has enlightened some questions and assumptions:

- First, why not consider waste as material resources? This could be an answer to the waste and resource challenges cited above
- Applied to the construction sector, the building could be considered as a material deposit. In other words, a source of potential reusable materials. In a wider scale, our existing environment may represent a bank of local resources. To achieve this objective, end of life must be introduced and considered in the design stage of a project, and not after construction. When we currently design a building, we rarely think about its end of life. By doing so, we compromise the opportunities of recovery.
- As energy retrofits of buildings have become absolutely necessary from an energy perspective, what impact will these upgrades have on material stocks & flows?

This contribution highlights the impact of sustainable renovation not only on the energy side but also in terms of materials. The proposal is presented in the figure below:

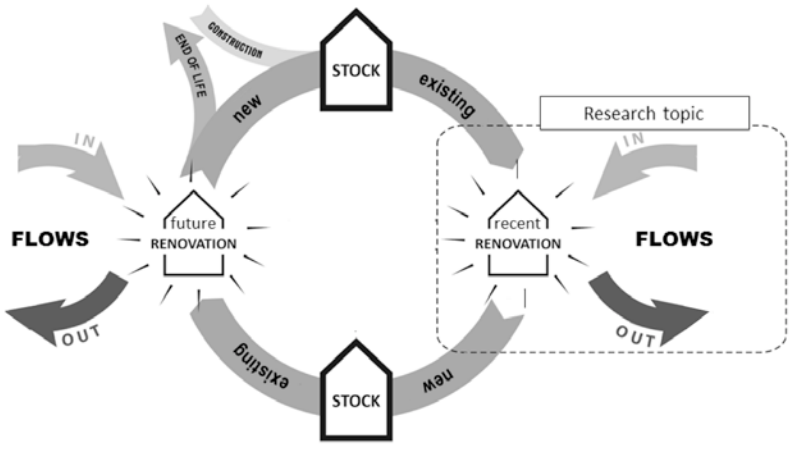

Figure 1: Proposal of the research

Globally, we illustrate the building life cycle with its initial construction phase, its end-of-life and intermediate upgrading processes. We have particularly focused on the analysis of what currently happens during retrofit operations in terms of material:

- What material stock does the building contain prior to an energy retrofit?
- What materials flows (in / out) are involved in this operation?
- What influence will the renovation have on the existing material stock (new stock)?

The present contribution intends to identify and quantify all these material stocks and flows.

Structuring

We chose a subject sufficiently representative at a regional scale considering the Brussels Capital Region.

We focused on dwellings built before 1945 and renovated with high criteria of sustainability and energy efficiency. Specifically, this analysis has been based on the competition « Bâtiments Exemplaires ». A competition developed by the Brussels Environment Administration to support sustainable construction & renovation in Brussels. Actually, this kind of renovation represents one of the primary objectives of the Region in terms of sustainable construction: 23 projects met these specifications.

Then, to provide a systematic approach, we propose to categorize the building in systems (envelope, interior space limits, and equipment), components (roof, façade, and floor) and layers (external, internal and structural). We specifically focused on the envelope, due to having the most effect on the energy efficiency of buildings.

The analysis is developed in 2 steps:

- Intervention trends of the sustainable energy retrofit: 10 on 23 retrofitting projects were analysed.
- Material balances to identify & quantify material stocks & flows: 1 retrofitting project was analysed.

RESULTS

Intervention trends

The following figure illustrates the renovation trends on the envelope in terms of demolition.

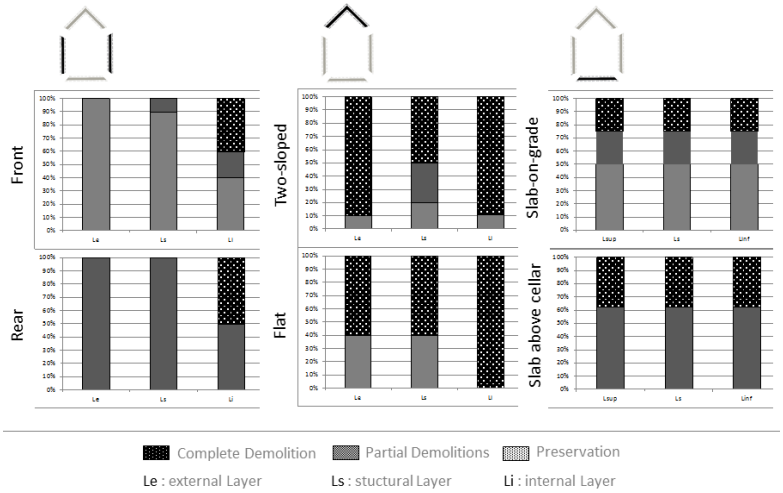

Figure 2: Intervention Trends in term of demolition

Results show that demolition rates differ between components and layers considered. The roof is commonly the component for which the most important demolition is conducted. Primarily on its internal layers while the structural layer is more preserved than the others. Regarding the front façade, preservation is commonly applied, except for its internal layer. Unlike the front façade, the rear one is usually subject to partial demolition (Le & Ls) or complete demolition (Li). Concerning Floors, all layers show the same conclusions: this means that when a demolition occurs, it will be on the total floor thickness.

The third figure below illustrates the trends in terms of an insulated envelope.

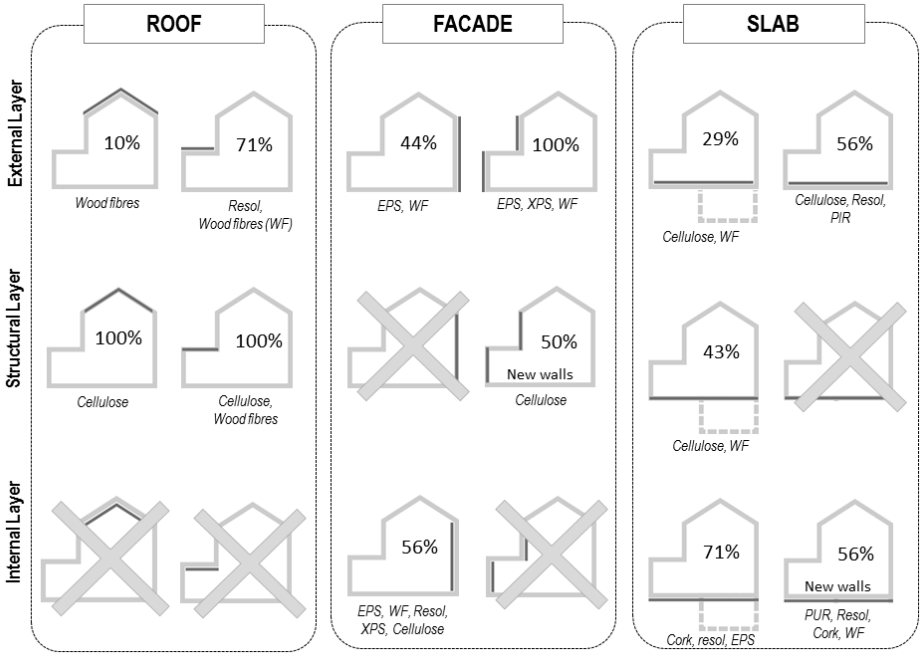

Figure 3: Intervention Trends in term of insulation

Insulation opportunities depend on the components and how they are built. Insulation in the external layer is usually preferred to avoid thermal bridges and some indoor moisture disease. Some exceptions do exist: when the structure allows the insulation in the structural thickness (in the case of existing or new wood structure especially for roofs), when some planning regulations require the preservation of the component appearance (for example, concerning the front façade), or the external layer is not accessible (existing slab-on-grade). Sometimes, insulation is made at the level of two different layers in a simultaneous and complementary way (for example in flat and two-sloped roofs).

Material balances

We focused the *material balances* analysis on one project. We identified and quantified the different fractions of materials contained in the building, before and after the energy retrofit operation. We also analysed inflows and outflows generated by the renovation process. We considered two distinct measurement units: weight and volume. The results of these *material balances* are showed below.

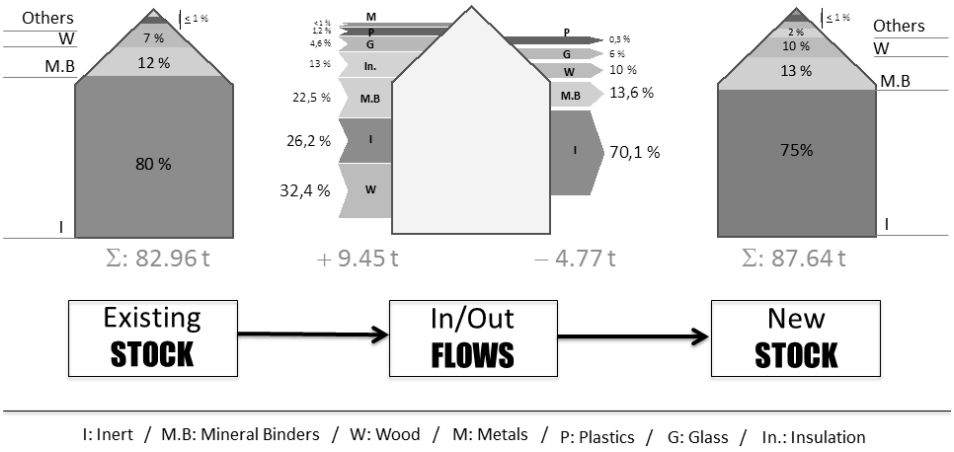

Figure 4: Material Balance in term of weight (tons)

In terms of weight, the findings confirm that inert represents a major part of the construction materials total weight. This tendency is similar after renovation. Inert waste also have a dominant place in the outflows. While inflows are more widely distributed with fractions of wood, inert, mineral binders, insulation etc.

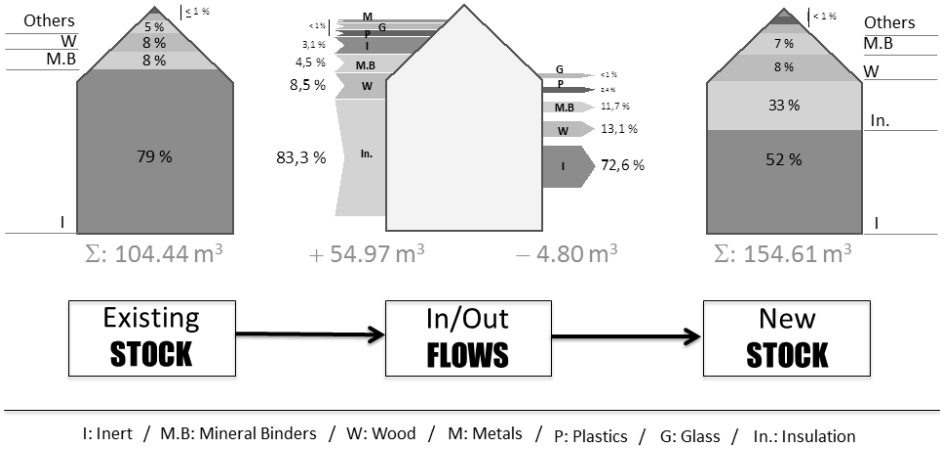

Figure 5: Material Balance in term of volume (m³)

In terms of volume, the comparison with the previous findings is quite interesting:

Before refurbishment, inert materials are still the dominant part of the construction. This trend changes after energy retrofitting. Insulation accounts for a third of the entire volume of the materials contained in the construction. That is quite significant. We can also see the huge impact of insulation on the inflows during renovation: 83% of the volume of the new materials. In the future, insulation may represent a key fraction to handle.

Obviously, the differences with the previous results are due to the disparate densities of all these materials: inert has a considerably higher mass to volume ratio when compared to insulation. Even if weight is the reference unit in the waste sector (except for evacuation on worksite), we believe that these two measurement units must be considered in flows and stock analysis. Or, we may « miss » some future key fractions, such as insulation.

DISCUSSION & CONCLUSION

This study contributes to:

- Introduce material (considering its 'value') into renovation processes mainly turned toward energy efficiency of buildings. By 'value', we mean the potential of possible resources the materials used in building can represent.
- Provide previously lacking data concerning material deposit. Developing a method and applying it on a case study to identify and quantify stocks and flows generated by energy retrofit operations.

The *materials balances* and renovation trends allow us to establish some key fractions and material ratios per square meters. The study of these ratios, could lead the region to a useful planning tool for a better waste and resource management. We don't currently have enough case studies to offer such a reliable tool. But, we believe they can positively affect our material deposit knowledge, and optimal valorisation. By considering the urban renovation policy, they could help the region to anticipate material flows and to reach an integrated resource and waste management.

Outside the scope of this research, it could certainly be interesting to extend the proposed analysis to other case studies, other building types, and other systems (like equipment). We could also develop demonstration or pilot projects involving waste and material for their possible value, and as potential resources in an integrated approach, considering end-of-life. Furthermore, in a long term vision, an improved understanding of the material stocks contained in our cities could lead us to a better resource & waste management... Including positive impacts on our dependency for supply & waste treatment. In this way, we are joining currents as urban metabolism, urban mining, and lending momentum to a more circular economy.

REFERENCES

1. BARLES S. : *L'invention des déchets urbains : France 1790-1970*, Champ Vallon, collection milieux, Seyssel, France, 2005
2. BRAUNGART M., MCDONOUGH W.: *Cradle to Cradle, créer et recycler à l'infini*, Alternatives Manifestô, Paris, France, 2011
3. ERKMAN S.: *Vers une écologie industrielle* (2ème édition), Charles Leopold Mayer, Paris, France, 2004
4. HUYGEN J-M.: La poubelle et l'architecte: vers le réemploi des matériaux, Actes Sud, Arles, France, 2008
5. NORDBY A.S.: Salvageability of building materials: Reasons, criteria and consequences regarding architectural design that facilitate reuse and recycling, PhD thesis, NTNU, Trondheim, Norway, 2009
6. PADUART A.: *Re-design for change: a 4 dimensional renovation approach towards a dynamic and sustainable building stock*, PhD thesis, VUB, VUBPRESS, Brussels, Belgium, 2012
7. TRACHTE S.: Matériau, matière d'architecture soutenable : Choix responsable des matériaux de construction, pour une conception globale de l'architecture soutenable, PhD thesis, UCL, Presses Universitaires de Louvain, Louvain-la-Neuve, Belgium, 2012

EVALUATION OF MICROCLIMATIC CONDITIONS IN URBAN ENVIRONMENT FROM THE HUMAN COMFORT PERSPECTIVE

Katarzyna Klemm[1]

1: Technical University of Lodz, Department of Geodesy, Environmental Cartography and Descriptive Geometry, Division of Urban Planning

Al. Politechniki 6, 90-924 Lodz, Poland

ABSTRACT

The paper presents a new assessment method for microclimatic conditions in the urban environment. The proposed model defines quantitative and qualitative features of the study area from the human comfort aspect. Two main elements of the urban environment, weather conditions and urban development are evaluated.

To determine whether the environment is comfortable for inhabitants, a simple criterion of comfort has to be established. This criterion must take into account the complex nature of heat exchange between a man and environment. In the light of extensive research carried out in many countries it can be demonstrated that there is a correlation between the intensity of heat fluxes with air temperature and wind speed, which allows approximations to be applied. This parameter can be used for the relative comparison of different environmental conditions. Taking into account the efficiency ranges of the thermoregulatory systems (applied in thermophysiology), criteria for thermal comfort can be established.

For the assessment of weather conditions, a weather typology is proposed. Human thermal sensation caused by the reaction of the thermoregulatory system to atmospheric stimuli (air temperature, wind speed) are related to the specific type.

The second important element affecting the final assessment of microclimatic conditions is the structure of the urban area i.e. participation of the various urban structures, tall vegetation and open area in the total surface as well as zones with wind comfort and discomfort. The above estimation is carried out using numerical simulations, assuming wind speed 4m/s and by simultaneously taking into account frequencies of wind flow occurring from 8 or 12 directions and related air temperature.

The proposed method in its current version constitutes an approximation only. Many parameters, such as land profile, shadow fall, or heat loss by the external surfaces of the building, are not included. However further future developments and incorporation of other parameters are possible.

Keywords: microclimate, human comfort, CFD

INTRODUCTION

Dense urban structures in city areas affect unique microclimatic conditions and hence greatly influence residents' comfort. In some situations, local problems associated with excessive airflow in the vicinity of buildings or formation of strong turbulences, may arise. At the same time, tall, concentrated buildings may significantly decrease urban ventilation thus resulting in deterioration of hygienic conditions and potential local accumulations of snow or pollution. The degree of urban areas ventilation also depends on the climatic conditions of individual residential districts, as these may enhance or counteract the influence of urban development. The assessment of environmental impacts on human presence is a complex issue, as the

consideration of a great number of variables that characterise individual occurrences, are necessary. The descriptive method and the model method are the most frequently used for these purposes. The quantitative and qualitative structure of the external environment should be considered in the assessment of microclimatic conditions. For this purpose two models: an exponential function model and a model analogous to Ohm's law can be used. In the exponential function model, the function base characterises quantitative features of the environment $y = x^z$, while the index exponent – its qualitative features. The value of the function y ranges between 0 and 1. No favourable features of the environment occur for $y = 0$, and the ideal state is recorded for $y = 1$. Values x fall within the range of variable between 0 and 1 whereas z may range between 0 and $+\infty$. For the most favourable qualitative features $z = 0$ the function y equals 1, [1]. The second model can be described by:

$$y_i = \frac{P_i}{R_i} \tag{1}$$

where:

y_i – value of a given parameter

P_i – potential, treated as favourable features of the environment

R_i – resistance, treated as the conditions that make long-term human occupation difficult or impossible

Finally, the proposed model is a combination of two above mentioned models and has the following form:

$$y = \left(\frac{P_x}{R_x} \right)^{\frac{R_z}{P_z}} \tag{2}$$

where:

P_x, R_x – potential and resistance of quantitative features

P_z, R_z – potential and resistance of qualitative features

HUMAN COMFORT CRITERIA

The comfort sensation is associated with changes in body temperature caused by an increase or decrease in ambient temperature, the cooling effect of wind, and the convective and the radiative heat loss from the body. There are a number of factors which affect the heat exchange between man and the external environment. The most important physical parameters include: air temperature, wind speed, solar radiation, relative humidity and radiation temperature. Equally important are the parameters related to the individual person, such as the activity, exposure time, clothing thermal insulation and finally the psychological factors associated with the level of adaptation, expectations or previous experiences, [2,3]. The inclusion of so many factors requires the application of complex models and detailed meteorological and physiological data, which in practice are difficult to obtain. As a result there is a need for a more simplified method of determining criteria for human comfort in open areas.

In the light of extensive research carried out in many countries described by [4] it can be demonstrated that there is a correlation between the intensity of heat fluxes with air temperature and wind speed, which allows approximations to be applied. In order to identify thermal criteria based on heat balance equations, some assumptions have been made:

Metabolism M – 70W/m^2

Thermal insulation of the cloths 1 clo

Solar radiations absorption R – 30W/m^2

Heat exchange through evaporation Q_E – 8W/m^2 for T_a < +5^{o}C, 20W/m^2 for $T_a \geq$+5^{o}C

Heat exchange through conduction Q_K is not taken into account

Heat loss caused by respiration Q_R - 8W/m^2

Furthermore heat transfer by convection and long wave radiation, based on temperature and wind speed, are specified thus:

For weather conditions where wind speed U≤4m/s and temperature $T_a \geq$+5^{o}C

$$Q_C + Q_L = 3{,}4T_a + 0{,}2\overline{U} - 118{,}8 \quad (3)$$

Where the wind speed U≤4m/s and temperature T_a<+5^{o}C

$$Q_C + Q_L = 1{,}7T_a + 6{,}0\overline{U} - 101{,}4 \quad (4)$$

Where the wind speed U>4m/s and temperature $T_a \geq$+5oC

$$Q_C + Q_L = 3{,}3T_a + 0{,}2\overline{U} - 127{,}8 \quad (5)$$

Where the wind speed U>4m/s and temperature T_a<+5^{o}C

$$Q_C + Q_L = -1{,}5T_a + 0{,}3\overline{U} - 126 \quad (6)$$

By applying the above to the heat balance equation, thermal loads on the body were derived.. The parameter can be used for the relative comparison of different environmental conditions.

In weather conditions where wind speed U≤4m/s and temperature $T_a \geq$+5^{o}C

$$\Delta Q = 2{,}8T_a - 4{,}8\overline{U} - 29{,}8 \quad (7)$$

Where the wind speed U≤4m/s and temperature T_a<+5^{o}C

$$\Delta Q = 1{,}7T_a - 6{,}0\overline{U} - 23{,}0 \quad (8)$$

Where the wind speed U>4m/s and temperature $T_a \geq$+5^{o}C

$$\Delta Q = 2{,}3T_a - 3{,}5\overline{U} - 35{,}4 \quad (9)$$

Where the wind speed U>4m/s and temperature T_a<+5^{o}C

$$\Delta Q = 1{,}5T_a - 3{,}0\overline{U} - 34{,}0 \quad (10)$$

Taking into account the efficiency ranges of the thermoregulatory systems, which are applied in thermophysiology, the criteria for thermal comfort were established based on the following thresholds for heat loads on the body ΔQ.

$|\Delta Q|$ < 20W/m^2 - comfortable condition

$|\Delta Q|$ in ranges 20 – 40 W/m^2 – unfavourable loads on the body,

$|\Delta Q|$ in ranges 40 - 80 W/m^2 – strong unfavourable loads on the body

$|\Delta Q|$ > 80W/m^2 - dangerous loads on the body

ASSESSMENT OF WEATHER CONDITIONS

For the purpose of the study, a weather typology was proposed. As the basic feature of the weather type, human thermal sensation caused by the reaction of the thermoregulatory system to atmospheric stimuli (air temperature, wind speed) were used. Three types of weather conditions and twenty groups were determined.

In the assessment of weather conditions, quantitative features are represented by the occurrence of favourable and unfavourable weather types from a human comfort point of view. Qualitative features of weather conditions may be described by the parameters of the intensity of wind speed, wind direction and air temperature changes. Intensity changes were defined as the relation of a standard deviation to mean value.

$$K_w = \left[\frac{cA_1 + cA_2 + cA_3 + cA_4 + cA_5}{1 + \left(cC_1 + cC_2 + cC_3 + ...cC_8 \right)} \right]^{\left[\frac{\left(1+I_U^C\right)\left(1+I_k^C\right)\left(1+I_T^C\right)}{\left(1+I_U^A\right)\left(1+I_k^A\right)\left(1+I_T^A\right)} \right]} \tag{11}$$

where:

cA_1, cA_2, cA_3, cA_4, cA_5 – occurrence frequency of favourable weather conditions, defined by groups A_1, A_2, A_3, A_4, A_5,

cC_1, cC_2, ...cC_8 – occurrence frequency of unfavourable weather conditions, defined by groups C_1, C_2, ...C_8,

I_U^A, I_U^C - intensity of wind speed changes in *A* and *C* weather groups, I_k^A, I_k^C - intensity of wind direction changes in *A* and *C* weather groups,

I_T^A, I_T^C - intensity of air temperature changes in *A* and *C* weather groups.

ASSESSMENT OF URBAN DEVELOPMENT

The second important element having an effect on the final assessment of microclimatic conditions is the structure of the urban area i.e. participation of the various urban structures, tall vegetation and open area in the total surface as well as zones with wind comfort and discomfort. The above estimation is carried out using numerical simulations, assuming wind speed 4m/s and by simultaneously taking into account frequencies of wind flow occurring from 8 or 12 directions and also it's related temperature.

The participation of the open area Z_w in the total surface was considered to be the potential of quantitative features of the land development coefficient Z_t and the participation of various urban structures and green areas in relation to the study area was considered to be their resistance (Z_m). The quantitative features may be described by:

$$x = \frac{Z_w}{1 + Z_m} \tag{12}$$

The qualitative features z may be described by:

$$z = \left[\frac{1+Z_1^C}{1+Z_1^A} \cdot \frac{1+Z_2^C}{1+Z_2^A} ..... \frac{1+Z_8^C}{1+Z_8^A} \right] \tag{13}$$

From the human sensation point of view, uncomfortable conditions are influenced by wind flow and air temperature. Weak air flow in built-up areas is leading to deterioration of hygienic conditions and encourage local accumulation of pollution whereas increased speeds can trigger dynamic loads. Simultaneously even at moderate wind conditions the local

discomfort may appear, due to low or high temperature. This fact was considered in proposed qualitative features.

The resistance of qualitative features was determined from the equation

$$Z_k^C = Z_k^{C(U)} + Z_k^{C(T)} \tag{14}$$

The first element in the equation describes situations in which, due to low wind speed ventilation of the area, is problematic (U<1m/s) and situations in which high wind speed can cause discomfort (U>4m/s). In order to assess wind flow conditions around buildings and determine size of zones in which wind speed reaches values lower than 1m/s and over 4m/s numerical simulations can be used.

$$Z_k^{C(U)} = \left[\frac{S_k^{U<1}}{S_{Lg}} + \frac{S_k^{U>4}}{S_{Lg}} \right] \cdot f_k^{U=4} \tag{15}$$

where: $\frac{S_k^{U<1}}{S_{Lg}}$ and $\frac{S_k^{U>4}}{S_{Lg}}$ - ratios of the areas of zones in which wind speed U < 1 m/s and U > 4 m/s to the surface S_{Lg}, which is characterised by clear fluctuations in wind speed caused by buildings. Surface size S_{Lg} is determined on the basis of principle pro-posed by Bottema [5]. The length L_g is specified using the formula

$$L_g / H = \frac{W/H}{1 + 0{,}5W/H} \tag{16}$$

where:

L_g – geometrical influence scale [m],

W – building width [m],

H – building height [m].

Since the wind speed U_{ref} = 4 m/s (wind speed measured at the meteorological station at a height of 10m) assumed in the numerical simulation as the inflow wind speed occurs with different probability on different directions, it was necessary to introduce weighting coefficient , resulting from meteorological data analysis.

The second element in eq. 14 refers to conditions when de-spite comfortable wind speed thermal loads of human body exceeded 40W/m^2.

$$Z_k^{C(T)} = \left(\frac{S_k^{1 \le U \le 4}}{S_{Lg}} \right) \cdot f_k^{U=4} f_k^{U=4,\Delta Q>40} \tag{17}$$

where:

$f_k^{U=4,\Delta Q>40}$ - weighting coefficient taking into account the thermal conditions on the direction of k, when the heat loss of the body exceeds 40 W/m^2, and the inflow wind speed is at the level of 4 m/s.

The potential of qualitative features describes situations in which human comfort is achieved through moderate wind speed ($1 \le U \le 4$) and temperature which guarantee thermal loads $\Delta Q \le 20$W/m^2.

$$Z_k^A = \left(\frac{S_k^{1 \le U \le 4}}{S_{Lg}} \right) f_k^{U=4} f_k^{U=4,\Delta Q \le 20} \tag{18}$$

where:

$f_k^{U=4,\Delta Q\leq 20}$ - weighting coefficient taking into account the thermal conditions considered as comfortable on the direction of k, when the thermal loads $\Delta Q \leq 20 W/m^2$ and the inflow wind speed is at the level of 4m/s.

The above mentioned qualitative features were determined by use of numerical simulation of wind flow around buildings and analysis of meteorological data.

After all the urban development coefficient was described by:

$$Z_t = \left(\frac{Z_w}{1+Z_m} \right)^{\left[\frac{1+Z_1^C \;\; 1+Z_2^C \;\; \cdots \;\; 1+Z_8^C}{1+Z_1^A \;\; 1+Z_2^A \;\; \cdots \;\; 1+Z_8^A} \right]} \tag{19}$$

After all the urban development coefficient was described by:

$$B_k = \left[0{,}2K_w + 0{,}8Z_t \right] \tag{19}$$

CONCLUSION

The paper presents a proposition of an assessment method for microclimatic conditions in the urban environment. An assessment model defines quantitative and qualitative features of the study area from the human comfort aspect. Two main elements of the urban environment, local climate and urban development are evaluated. The proposed method constitutes a certain approximation due to many unincluded parameters, such as the lay of the land, shadow fall, or heat lost by the external surfaces of the building. Construction of the model also allows the taking into account of other elements. Knowledge of environmental conditions, as well as the appropriate application of the assessment results, greatly contributes to increasing the quality of resident's living conditions.

REFERENCES

1. Klemm, K.: The complex assessment of microclimatic conditions in well-spaced and dense urban structures. Studia z Zakresu Inżynierii PAN, Warszawa, 2011 [in polish]
2. Koss, H., Sahlmen J.: Method in pedestrian wind comfort assessment; Theoretical and practical comparisons. Proc. of COST Action C14 Workshop, Nantes, 2002
3. Nikolopoulou, M., Steemers K.: Thermal comfort and psychological adaptation as a guide for designing urban spaces. Energy and Building, vol.35, 2003 95-101
4. Błażejczyk, K.: Heat exchange between man and his surroundings in different kinds of geographical environment. Institute of Geography and Spatial Organization, Polish Academy of Sciences, Geographical Studies, 159, 1993 [in polish]
5. Bottema, M. : Wind climate and urban geometry, Ph.D. Thesis, FAGO, Technical University of Eindhoven, 1993

EXPANSION AND DENSIFICATION OF CITIES: LINKING URBAN FORM TO URBAN ECOLOGY

Nahid Mohajeri[1*], Agust Gudmundsson[2], Jean-Louis Scartezzini[1]

[1]*Solar Energy and Building Physics Laboratory (LESO-PB), Ecole Polytechnique Fédérale de Lausanne (EPFL), 1015 Lausanne, Switzerland, e-mails: nahid.mohajeri@epfl.ch; jean-louis.scartezzini@epfl.ch*

[2]*Department of Earth Sciences, Queen's Building, Royal Holloway University of London, Egham TW 20 0EX, UK. E-mail: a.gudmundsson@es.rhul.ac.uk*

**Corresponding author. E-mail: nahid.mohajeri@epfl.ch*

ABSTRACT

Despite much research on the ecological impacts of urbanization, we still do not know what development patterns are most effective in supporting ecological function. In particular, it is as yet unclear if compact urban forms are ecologically more favourable than dispersed forms. Using historical data from the city of Geneva in Switzerland, we present results on its growth from 1841 to 2005, or for 165 years. We first show that the main street orientations have been maintained since the initiation of the city, which implies that the Shannon-Gibbs orientation entropy has been essentially constant during this period. We also show that the length-size distributions of the streets follow power laws and that the length entropy has, in contrast to the orientation entropy, gradually increased during the 165-year evolution of the city. This means that the maximum length and the average length of the street network has increased as the network has expanded. This study suggests that the city of Geneva has grown through two processes: expansion and densification. In Geneva, expansion has dominated during the entire period, but there has also been densification, particularly in the second half of the period. City expansion means that the land used for human activities increases over time. The urban area covered by Geneva increased from about 0.6 km^2 in 1841 to about 16 km^2 today, so that the area covered by fields and woodlands and available to plants and animals has reduced by more than 15 km^2 during this period. Similarly, densification normally (but not always) implies that the green areas available for plants and animal inside the city reduce in size. Densification results in less average human-travel distances, less fuel consumption for transportation, and less land being urbanized; it is also favourable to certain aspects of the ecosystem. Densification may thus be a viable planning scenario for the future growth of many cities, in Switzerland and elsewhere. However, expansion appears to favour other aspects of the ecosystem, and further studies are needed to assess ecologically the overall pros and cons of city densification versus expansion.

Keywords: Urban Ecology, Size, Scaling, Spatial distribution, Urban growth

INTRODUCTION

Rapid urban expansion and associated land cover changes have strong impact on the ecosystem (e.g., biodiversity). In Switzerland, urban growth has been rapid. In 1930, less than 36% of its population was urban (the majority being rural), whereas by 2011 74% of the

population was living in urban areas. The forecast is that by 2050 more than 83% of the Switzerland population will be urban [1].

Given the current high rate of growth of cities worldwide, it is of great importance to minimise the negative ecological effects of the growth. This means that we should design city growth so as to make efficient use of land and aim at sustaining the ecosystem and promote biodiversity. To accommodate increasing urban population, cities can grow primarily through two processes or mechanisms: densification and expansion. Densification means adding build-up areas, primarily streets but also houses, within the existing boundaries of the city. By contrast, expansion means adding new urban areas at the margin, that is, at the present boundary, of the city.

These two different mechanisms of growth have different urban and ecological implications which are here explored with reference to the evolution of the city of Geneva, Switzerland, during the past 165 years. In particular, we show that both mechanisms have operated during this period, but one has been the more dominating. We put the results from Geneva into a wider context of city growth and discuss the implication of the results for further growth of cities in general, and those in Switzerland in particular.

The purpose of this paper is to present new data on how cities grow, with a particular focus on the evolution of the street network of the city of Geneva over the past 165 years. The results as to the street network are then related to the general population growth during the same period, as well as the mechanisms of expansion and densification. These mechanisms are then discussed in the context of their ecological implications with a view of suggesting viable designs for further urban expansion in Switzerland and elsewhere.

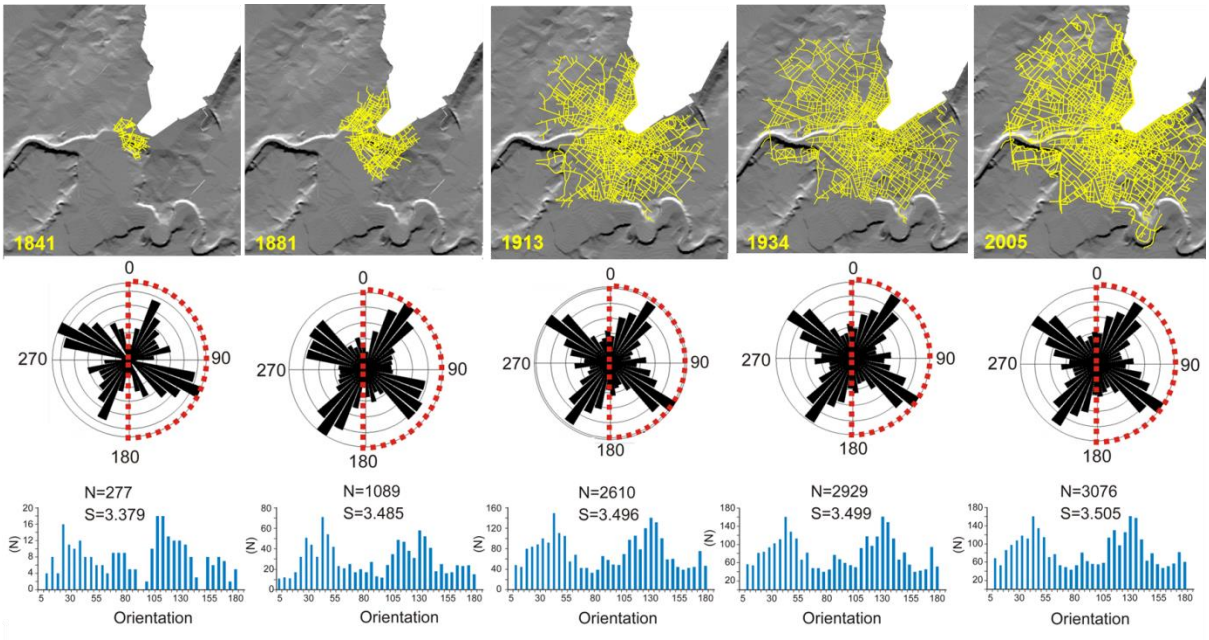

Figure 1: Growth of the street network of Geneva from 1841 to 2005. Rose diagrams and histograms show the orientation of the streets. N = number of streets; S = orientation entropy.

THE STREET NETWOKR OF GENEVA

Over a period of 165 years, the street network of Geneva has greatly expanded (Figure 1). In 1841 the total street network comprised 277 streets, whereas in 2005 (the last update) the network comprised 3076 streets. Thus, during this period the number of streets increased by a factor of about 11. During the same period, the area covered by the street network and the city increased from about 0.6 km^2 to about 16 km^2, showing that the area has grown by a factor of about 27, that is much more than the number of streets.

The street network has certain remarkable characteristics (Figure 1). First, at its initiation (in 1841) the streets had two main orientations or directions, a NW-direction and an ENE-direction. These two main directions have been maintained through the city development for 165 years. This is seen in the rose diagrams and histograms in Figure 1. As a consequence, the street-orientation entropy – a measure of dispersal or spreading in orientation or azimuth – has been essentially the same during the enormous growth of the city over the 165 years.

Second, all the length-size distributions of the streets during this period are power laws (Figure 2). This means that most of the streets are comparatively short while a few are comparatively long. As the street network has grown, the length of the longest streets has increases, and so has the length range of the streets. This means that while the shortest streets of the network at any time are of similar length, the longest streets have become gradually longer as the network evolved. Thus, in contrast with the street-orientation entropy which has remained essentially constant during the network evolution (Figure 1), the street-length entropy, a measure of the length range and thus the average length, has gradually increased during the growth of the network (Figure 2). This implies that as the street network grew, the average length of the streets, hence the length-entropy, increased.

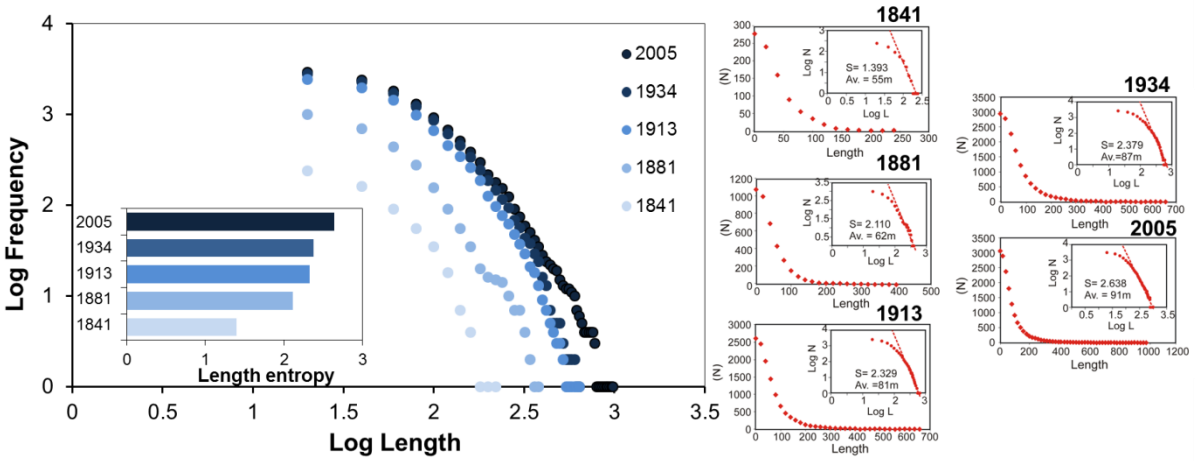

Figure 2: Power-law length-size distribution of streets in Geneva during the period 1841-2005. The length distributions are shown on log-log (log-transformed) plots (left) and ordinary plots (right). The length entropy increase over the period is indicated on the inset.

The third remarkable feature of the street network evolution is that its growth has not always gone hand in hand with the population growth. For Geneva the population growth during the 165-year period has been rather steady whereas the street network has grown more irregularly (in steps) as indicated by the cumulative length of the network (Figure 3). In particular, there

was a very rapid growth in the cumulative length of the street network from 1881 to 1913, and to a lesser extent from 1913 to 1934. Since that time the cumulative street length has grown at a slower rate than the population. One reason for this difference in the growth rate of the street network and the associated population is that a street network must reach a certain minimum size, here measured as the cumulative street length, to interconnect the entire city. The network grows in steps for this interconnection to be possible. After the rapid growth from 1881 to 1934, the network was very large in relation to the population, and thus far from used to its full transport capacity. From then on the rate of population growth has been faster than that of the street network, simply because the capacity of the network was so large after 1934 that it could, theoretically, serve a much larger population. So gradually, the population is 'catching up' with the street network.

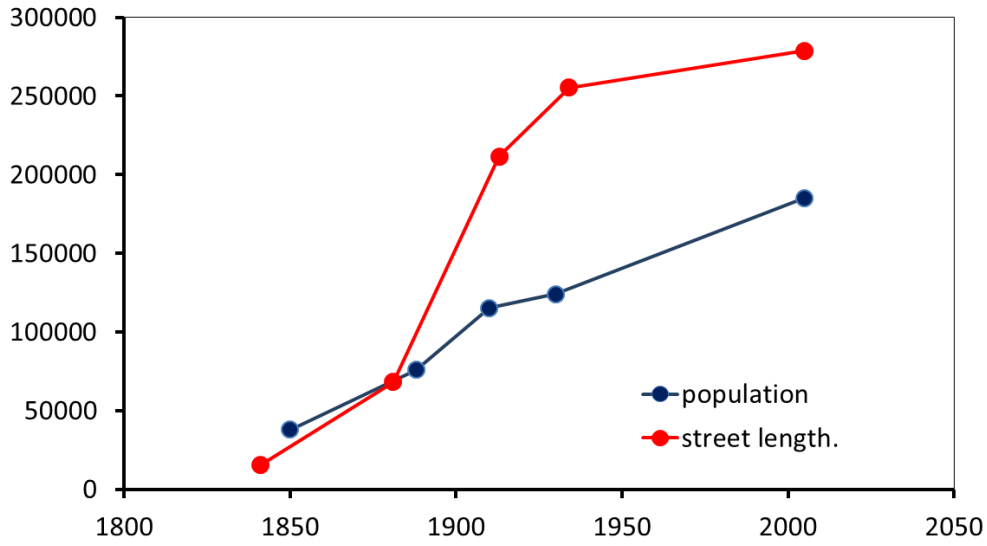

Figure 3: Population growth (number of people, blue curve) and cumulative street length growth (in metres, red curve) in Geneva from 1841-2005.

DENSIFICATION AND EXPANSION – ECOLOGICAL IMPACT

The street network of Geneva has grown through two main mechanisms during the 165-year period: expansion and densification. The results (Figure 4) show that in all the measured periods expansion has dominated. However, in the past 100 years, the contribution of densification is clearly greater than earlier in the history of the city. Expansion means that the land covered by the network and almost entirely used for human activities gradually increases, as is reflected in the area covered by the city increasing from 0.6 km^2 to about 16 km^2 over the 165-year period. It follows that the area covered by fields and woodlands and available to plants and animals has reduced by nearly 15 km^2 during this period.

Densification have different ecological effects in that less fraction of the rural area, with fields and woodlands, is made urban (and thus covered by streets and buildings). Normally, densification implies that the green areas available for plants and animal inside the city reduce in size. However, a densified or compact city commonly has shorter average transport distances for its inhabitants, so that there may be less fuel demand and normally less CO_2 emissions per capita than in more dispersed or spread cities [2].

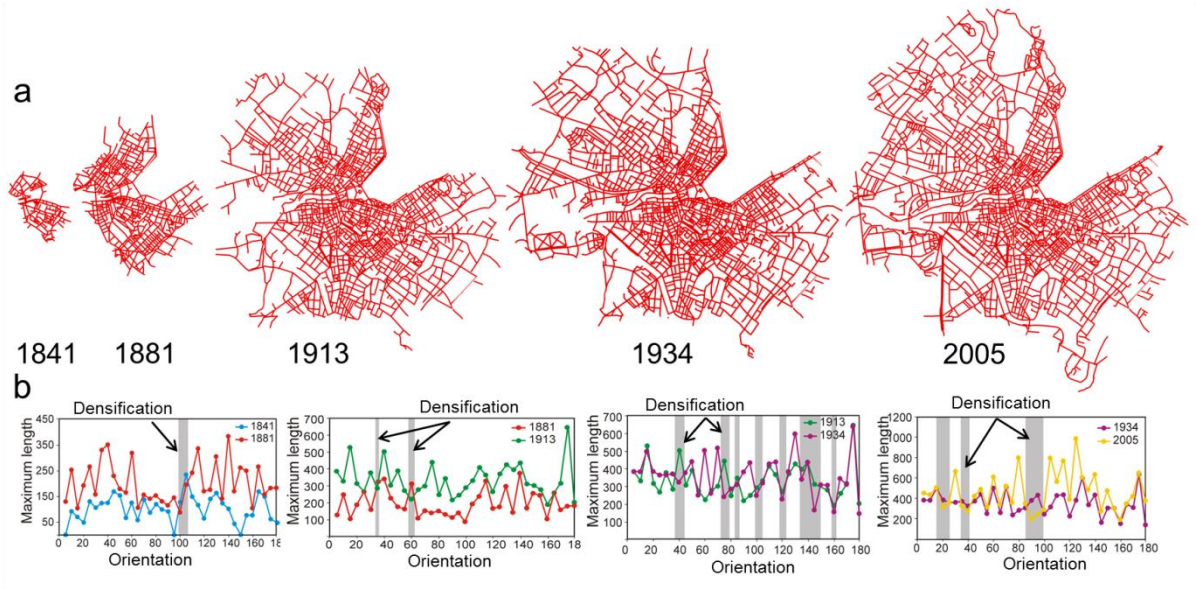

Figure 4: (a) Evolution of the street network of Geneva from 1841 to 2005. (b) Densification (grey zones) and expansion (white zones) during the evolution of the street network.

Compact cities are commonly thought to be marked by biodiversity decrease [3, 4]. There is, however, also some evidence for biodiversity increase. For example, in a study of cities in Switzerland, Home et al. [5] conclude that cities are the sites of high biodiversity. Their conclusion is partly based on the ecological effects of heat islands (the city temperatures being higher than in the surrounding rural areas), and partly on the fact that cities provide the sites for a variety of imported exotic plants and animals that can thrive in the urban ecosystem but could not do so in its rural surroundings. This conclusion applies particularly to various thermophilous plants and animals that prefer urban systems. More general studies suggest that biodiversity reaches its peak at 'medium' or moderate urbanization, that is, in suburban areas (and thus not in very compact areas). By contrast, the biomass may be highest in the highly urbanized, that is, compact areas [6]. Clearly more quantitative studies are needed so as to explore not only the exact ecological impacts of different urban forms and densities (urban compactness) but also how the impact may change from one place to another, within cities and between cities.

DISCUSSION AND CONCLUSIONS

The effects of densification (resulting in city compactness) and expansion (resulting in city dispersal or spreading) have been the principal mechanisms of the growth of the city of Geneva during the past 165 years (Figures 1 and 4). The same mechanisms and street-network structures have been identified in many other cities in countries such as the Britain and Iran [7]. Like in Geneva, expansion is the most common mechanism of growth in these cities, but during certain periods densification may dominate. The results from Geneva, however, show some aspects of city growth that have not been identified before. One of these is the observation that the rate of population increase may 'lag behind' the rate of street-network increase (Figure 3). While there may be clear reasons for such rate differences, they are presumably costly and avoidable to a large degree with proper modern planning.

Given that densification results in more compact cities, with less average human-travel distances and less land being urbanized, making cities more compact may be a viable planning scenario for city growth in various countries, including Switzerland. Compact cities may also be generally more energy efficient than disperse cities [8]. One major issue, however, is the impact of urban densification in comparison with expansion on the urban ecosystem. Increasing land fragmentation and less green areas within compact cities may have negative impact on habitats and biodiversity. Biodiversity loss is widely regarded as making the ecosystem more vulnerable [4]. Also, there are indications that the greatest biodiversity occurs at the margins of the urban areas, where the suburbs and the rural areas meet and where many heat-seeking plants and animals may live (heat-island effects) while being unable to survive in the rural areas themselves. Since such areas are generally proportionally larger the more spread (less compact) the city, this indication would favour city growth through expansion. In addition, it has been suggested that the urban biodiversity reaches its peak at a 'medium' or moderate urbanism, and then declines with higher urbanism or more compact cities [6].

In conclusion, efficient use of energy and land may favour densification and compact cities. Densification may also favour some aspects of the general ecosystem, while other aspects of the ecosystem are better served through expansion as the main mechanism of city growth.

ACKNOWLEDGEMENT

This research has been financially supported by CTI within SCCER FEEB&D (CT.2014.0119).

REFERENCES

1. Swiss Federal Statistical Office (SFSO). Neuchâtel, Switzerland, 2013.
2. Makido, Y., Dhakal, S., Yamagata, Y.: Relationship between urban form and CO_2 emissions: Evidence from fifty Japanese cities. Urban Climate 2, 55–67, 2012.
3. Grimm, N.B., Faeth, S.H., Golubiewski, N.E., Redman, C.L., Wu, J., Bai, X., Briggs, J.M.: Global change and the ecology of cities. Science 319, 756-760, 2008.
4. MacDougall, A.S., McCann1, K. S. Gellner, G., Turkington, R.: Diversity loss with persistent human disturbance increases vulnerability to ecosystem collapse. Nature 494, 86- 90, 2013.
5. Home, R., Moretti, M., Sattler, T. Bauer, N., Hunziker, M.: BiodiverCity, A transdisciplinary approach to urban ecology, in Macias, A. & Mizgajski, A., (eds.) Implementation of landscape knowledge in practice, Wydawnictwo Naukowe UAM, Poznan, pp. 134-140, 2010.
6. Adler, F.R., Tanner, C.J.: Urban ecosystems. Cambridge University Press, Cambridge, 2013.
7. Mohajeri, N., Gudmundsson, A.: The evolution and complexity of urban street networks. Geographical Analysis 46, 345–367, 2014.
8. Mohajeri, N., Gudmundsson, A., Scartezzini, J.L. Statistical-thermodynamics modelling of the built environment in relation to urban ecology. Ecological Modelling 307, 32-47, 2015.

IMPROVEMENT OF URBAN WATER METABOLISM AT THE DISTRICT LEVEL FOR A MEDITERRANEAN COMPACT CITY

Federica Paolini[1]; Carlo Cecere[1].

1: Civil, Constructional and Environmental Engineering (DICEA) - Sapienza University of Rome, Via Eudossiana 18, 00184 Rome, Italy. Email: federica.paolini@uniroma1.it

ABSTRACT

Cities are under constant and increasing pressure because of global changes, fast urbanization and growing resources demand. Those threats force urban systems to find development opportunities and solutions to minimize the demand and to shift from linear to circular economy, in which recycling and reusing are key activities [1]. Urban Metabolism (UM) analysis has become an important tool for the study of urban ecosystems. The problems of large metabolic throughput, low metabolic efficiency and disordered metabolic processes are a major cause of unhealthy urban systems. Nowadays, the most critical urban resource flow is water, followed by energy and materials: water is vital for our survival and the largest component in terms of sheer mass [2]. Furthermore, climate change increases geo-hydrological risks (landslides, floods and sinkholes), especially in Italy, causing damages and threats to the population, requiring a better management of the water cycle. However, due to the complexity of contemporary urban phenomena, it is difficult to understand what happens within those urban systems and to answer to these current pressures. Applying the UM at the city level presents some limitations due to the lack of data and the generalizations required at this scale. The traditional approach considers the city as a "black box", quantifying in-flows and out-flows. Indeed, resources availability depends strongly on local context characteristics that enable the reduction of input water flows, maximizing the reuse of wastewaters and closing water loops. Along with the new challenges of sustainable design, it is possible to define different scenarios and roadmaps for compact cities, developing decision support systems that follows the principles of urban metabolism at the local scale. This research presents a project to evaluate the local water potential in a portion of the compact city of Rome in order to improve the local metabolism through a more efficient use of the resource. The innovative methodology will enable sustainable actions through the identification and assessment of a set of green projects to suggest pathways that enhance the modification of water metabolic flows.

Keywords: urban water metabolism, water sensitive cities, sustainable development, city district, water cycle, resilience, circular economy

INTRODUCTION

Urban water systems play an important role in sustainable development and in urban metabolism flows, dealing with a fundamental human need: access to drinking water, sanitation, water quality and health. According to the European Environment Agency (2006), approximately 75 percent of the population in Europe lives in urban areas and forecasts show an increase between 80 to 90 percent by 2020. Cities exploit resources, producing wastes in a linear way; the high rate of resource consumption and massive disposal of waste stress the resources availability by depletion, causing pollution. Projections [3] for the near future show that scarcity of water will have more of a limiting effect on human activities than either energy or capital. Furthermore, as growing urban communities seek to minimize their impact

on already stressed water resources, an emerging challenge is to design for resilience to reduce the impacts of climate change, ensuring secure water supplies and the protection of environments.
Despite considerable progress over the past ten years, the forecasting of natural water cycle variability and extreme weather events in the short and medium term still suffers from severe limitations. Improved understanding of the impacts of climate change on the hydrological cycle is necessary to better inform decision-makers and ensure sustainable water supply, management of water systems and quality of water bodies. This strong trend creates an enhanced need to understand water flows through and within the urban boundary, meeting the needs of water planners but without considering the hydrological performance of a system [4]. In the Mediterranean regions, the risk of water shortage is significant and the demand is growing despite limited renewable water resources, mainly irregular and of unequal quality as for the European Commission Mediterranean water scarcity and drought report in 2007. In the last 50 years, many cities faced increasing vulnerability to water stress, especially in Italy, where extreme weather events increased geo-hydrological risks (landslides, floods and sinkholes), causing damages to the population and requiring an accurate management of the water cycle to increase the resilience of cities. Those threats depend on climate changes, on the rapid growth in the urban population, on the pollution and the depletion of groundwater, increasing per capita water use, soil sealing and the aging of traditional drainage systems, having a discernible impact on the aquifers' level variation below urban systems and on the water cycle integrity [5].

The transition to water centric cities: closing water cycles at the district level

The study of the water metabolism is crucial for the future of sustainable cities and of high relevance to the water industry [6]. To solve current urban water problems it is necessary to solve their metabolic processes and to organize water flows in a sustainable way, reducing their metabolism and reusing the resource according to the quality of the demand. In this perspective, the reuse of remaining qualities should match with lower quality demanding purposes. Reducing flows through cities while improving human livability and overall ecosystem well-being represents both a clear sustainability pathway and a challenge [4, 6]. In a circular model, water is reused several times, retaining full value for a "circular economy".
Optimal regulation of an urban metabolic system starts with research on the mechanisms that govern interactions among the components of the system's structure and the functioning of the system [7]. Without a change in the paradigm of water management, urban water demand will eventually keep increasing, water supplies will diminish and the population pressure will cause the decay of the infrastructures [8]. As an example, Agudelo-Vera and colleagues [9] illustrate an innovating water resilience strategy including demand, output minimization and multisourcing, the Urban Harvest Approach.
Over the past decade, the green/sustainable building industry attended significant progress in tracking energy and material flows at the building scale, but there is arguably a need to step to higher level. The incorporation of sustainability principles in neighborhood design is important because many of the problems encountered at the macro-city scale are cumulative consequences of poor planning at the micro-neighborhood level. This is particularly evident in the historical reliance on large-scale, centralized urban infrastructure projects. Neighborhood-scale analysis is necessary to evaluate and develop more sustainable local infrastructure, including buildings, transportation, urban vegetation and water systems [10]. Today, studies of resource flows at the city scale become an increasing practice but present some serious and recurring deficiencies like accounting problems, lack of available, reliable and updated data, lack of knowledge on the use of these data (if present), absence of a clear

and well-funded methodology. However, the most important limitation of the majority of current UM studies is the black box approach, which means that all the different studies show only macroscopic inputs and outputs of an urban system. Neighborhoods and intermediate to large-scale mixed-use development projects offer interesting advantages and opportunities. Neighborhoods have a mix of uses, which makes it easier to balance loads and match the intermittent supply of resources, with larger flows to treat that can generate the critical mass to enable sustainable intervention. The urban landscape becomes an infrastructure that can play a role to temper the climate, absorb carbon, clean stormwater and sewer effluent. The challenge is to redesign the UM of cities, downscaling results from urban planning and upscaling household models to a relevant scale.

Cities need to make a transition towards a more Sustainable Urban Water Management (SUWM) with a strong need to compare and analyze their performances [11]. How can we achieve these objectives? Researchers emphasize the need for the integration and decentralization of water supply, wastewater, stormwater systems and their assessment of social and economic impacts while neighborhood design features, such as lot size and street layout, have a large impact on the performance of water systems. Only a systemic approach will result in a reduction of local water use, wastewater generation and stormwater runoff, in a socially and economically acceptable way [10]. A critical barrier to progress is the lack of decision support systems to develop of long-term policy for SUWM. While there has been significant progress in many cities, particularly related to the innovation of more sustainable technologies and shifts in community values around the environment and waterways, numerous commentators argue that current progress is still too slow [12]. More recently, some cities used a distributed "green infrastructure" strategy through the Water Sensitive Urban Design (WSUD) approach to urban planning and design [13]. This method integrates the management of the total water cycle into the urban development process, including:

- integrated management of groundwater, surface runoff (including stormwater), drinking water and wastewater to protect water related environmental, recreational and cultural values;
- storage, treatment and beneficial use of runoff;
- treatment and reuse of wastewater, using vegetation, water efficient landscaping and enhancing biodiversity;
- water saving measures within and outside domestic, commercial, industrial and institutional premises to minimize requirements for drinking and non-drinking water supplies.

The WSUD techniques are considered as "best practice level" which means that we still have little information on their technical effectiveness under different types of climate. It is also desirable to decentralize the water system by promoting multiple spatial scales. This could include rainwater harvesting and local water reuse/treatment that might increase the flexibility, transformation and resilience of the whole system in the face of external shocks, including those resulting from climate change [14].

METHOD

Today, the scientific literature shows that WSUD methodologies help to reach these objectives but the effects of the integration of water-sensitive design strategies for a specific urban morphology and for a particular climate are still unknown. This is what the SOS_Urbanlab (Engineering Laboratory for Construction and Environmental Sustainability, "Sapienza" University of Rome) is trying to explore, focusing on the Mediterranean climate and on the compact city of Rome. This network reshaping rests on one side on part of the principles of the Urban Harvesting Approach like estimation of the local demand-supply and

wastewater's recovery potential. On the other side, the study follows the Urban Water Metabolism of the city of Brussels [15] for some city water indicators and for correlations with climate factors. The methodology of flow reshaping will act as follows:

- Calculating the local water demand: after the identification of a roman neighborhood and its different urban functions (residential, shopping+horeca, public services, sport facilities etc), the demand results as a weighted sum of the average requirements per function (demand inventory in m^3/ha – year for every function).
- Calculating in-flows (local water supply, rainwater and waterways): data of the supply inventory arise from the roman municipality, considering network leakages. In 2005, the supply of the case study's district is 499.736 m^3/year. For rainwaters, we consider data coming from the nearest weather stations. Waterways data comes from the average annual flow values for the Tevere and the Aniene rivers (Tevere: 240 m^3/s – year; Aniene: 31 m^3/s - year).
- Calculating internal flows (infiltration, runoff and stock): the infiltration and the runoff change the destination of the rainwater in-flows towards out-flows, depending on the sum of pervious and sealed surfaces within the urban tissue. The stock of water (surface water, groundwater and accumulation systems) is the amount of water remaining in the urban system, without generating a flow in output.
- Calculating out-flows (wastewaters, evapotranspiration, waterways): like the local water demand, wastewater data arise from the specific urban tissue, its inner functions and the average wastewater per function. Another part of wastewaters comes from the runoff, estimated by the sum of the sealed surfaces of the specific urban tissue. The evapotranspiration depends on the sum of green surfaces within the urban tissue. Like the in-flow waterways, out-flow waterways data arises from the average annual flow values for the Tevere and the Aniene rivers (similar in and out discharge).
- Coupling water demand and supply: deriving from the Mass Flow Analysis (MFA) and adapting to the water flows in figure 1, the general water mass balance WMB (water storage) at any specific instant in time (t) becomes:

$$WMB(t) = \sum Water\ inputs\ I(t) - \sum Water\ outputs\ O(t) - \sum Consumptions\ C(t)$$

$$I(t) = S(t) + W(t) + R(t) \quad \text{and} \quad O(t) = W_w(t) + W(t) + E(t)$$

S = Supply; W = Waterways; R = Rainwaters; W_w = Wastewaters; E = Evapotranspiration

Consumption is a fraction of the demand that cannot be reused or recycled (e.g. diminished by decay). The goal is trying to satisfy the demand with the water mass stored into the system and wastewaters in out-flow. The challenge is to manage these flows, using internal and out-flows to reduce the in-flow, which means reducing the resource's use through its reuse.

- Calculating wastewater's and rainwater's recovery potential: by studying the urban tissue, it is possible to calculate the potential resource to capture and transform into new sources to remain within the urban area. The urban tissue will display the spatial distribution of flows, hierarchy of activities and uses to improve water management and providing guidelines for urban planning. Wastewaters have different levels of quality: some wastewaters can become in-flows to fulfill some of the demand. The total sum of rainwaters and wastewaters is the maximum value of the reuse potential. The real reuse potential derives from the assessment of the level of quality of the maximum potential, on the distribution of the system functions and on the level of quality required by these functions.

- Select the WSUD to reshape flows: the next step is to reorganize and reshape those flows to achieve the faster closure of water cycles and a greater autonomy of the urban cells. The reorganization of water flows within the local context, with consequent benefits on the water balance at the larger scale, aims at matching the demand with the recovery potential with the help of WSUD techniques that enable this possibility. Once identified the resource's recovery potential, the implementation of WSUD allows transforming both stock and out-flows in lower quality in-flows, reshaping the actual linear water management in a circular water cycle.

The methodology can support stakeholders in decision-making, considering WSUD in terms of delta-flows based on the current and the future water-flow scenarios. The combination of the different categories of WSUD generates a set of possible interventions with a high level of flexibility to reach many different targets of sustainability, characteristics of the local urban system, to maximize its degree of independence.

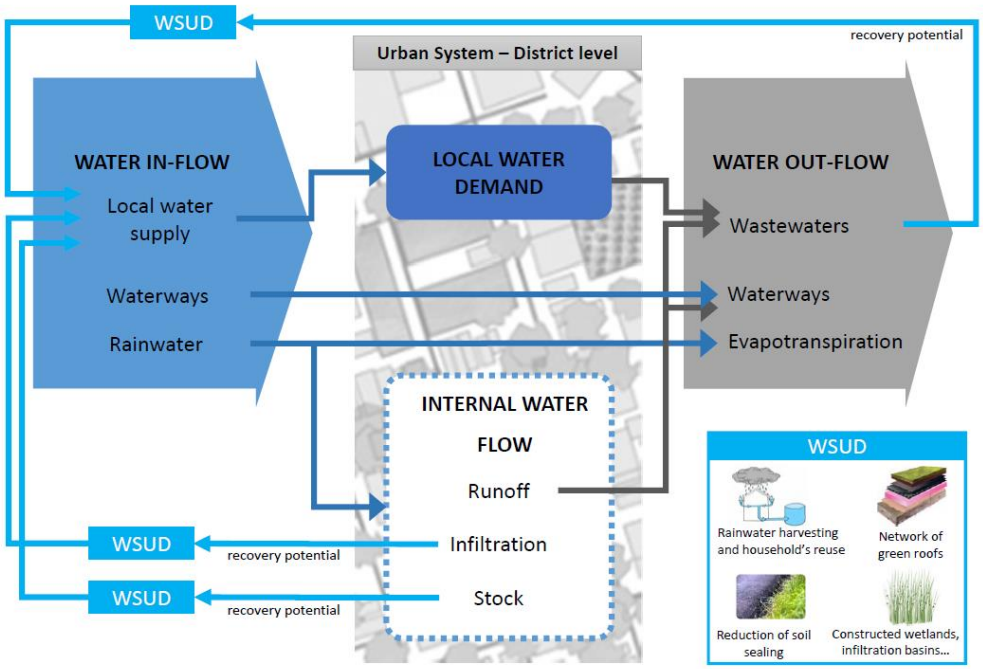

Figure 1: Urban water metabolism of a sustainable district

RESULTS

The research is an ongoing project that analyses three urban tissues within the third municipality of Rome, in the northeast area of the city, with an extension of 97.818 km^2. The total population amounts to 204.623 with a density of 2.103,1 inhabitants per km^2 (2013). The whole municipality shows many dissimilar built regions related to different historical construction periods, ranging from the beginning of the 20th century to the "eco-monsters" public housing, characteristics of the 60's and the 70's. Given the heterogeneity of the whole district, the study will consider different types of areas with different density (calculated through the FAR index - Floor Area Ratio), with particular attention to more compact regions. Considering the difficulties in finding data at the local scale for the city of Rome, a bottom-up approach is necessary to avoid the lack of information and macro approximations. The study sets three regions (approximatively 1 ha each) within the municipality and identified the amount of the urban functions (residential, commercial and industrial) to evaluate the local water demand. After this step, the study will calculate the water in-flows, out-flows and internal flows to determine the water mass balance and the recovery potential of wastewaters and rainwaters to evaluate the possibility of water reuse. The choice of the typologies of

WSUD will depend on the local characteristics of the built environment and the local flows structure. For example, the rainwater collected by roofs can partly fulfill the water demand. The standard Roman rooftop is flat, with more than 20 thousand rooftops that cover the city. This value represents almost 400 hectares of potential green lung in terms of rainwater harvesting, reduction of pollution, caption of particulate matter and reduction of the heat island effect and flooding.

CONCLUSION AND DISCUSSION

Reordering land use, layout of neighborhoods and design of buildings helps to reshape the environmental profile of the resource's use, to compare different territorial potentials and to identify strategies that could allow urban regeneration, supporting competitiveness and sustainable development. However, the urban system's sustainability depends on the sustainability of each of its internal cells and the connections among all the parts, in this way we can talk about cities as organisms, with their own metabolic systems, balanced by the equilibrium of all its parts. This study tries to fill this gap, proposing a methodology that appropriately downscales urban metabolism principles to drive current sustainability challenges. Optimize urban metabolic networks by regulating their processes to increase their efficiency: on the results of this research, it will be possible to identify and regulate key water issues and their related processes, as well as the relations between these local water issues and the fluxes in each process.

REFERENCES

1. Girardet, H. (2004). The Metabolism of Cities. In S.M. Wheeler, & T. Beatley (Eds.). *The sustainable urban development reader* (pp. 125-133). London: Routledge.
2. Kennedy, C., Cuddihy, J., Engel-Yan, J. (2007). The changing metabolism of cities. Journal of Industrial Ecology, 11, 43-59.
3. Brawn, K. (2002). Water scarcity forecasting the future with spotty data. Science, 297, 926-927
4. Kennedy, C., Pincetl, S., Bunje, P. (2011). The study of urban metabolism and its applications to urban planning and design. Environmental Pollution, 159, 1965-1973.
5. Kennedy, C., Baker, L., Dhakal, S., Ramaswami, A. (2012). Sustainable Urban Systems. An Integrated Approach. Journal of Industrial Ecology, 16 (6), 775-779.
6. Pamminger, F., Kenway, S. J. (2008). Urban metabolism - improving the sustainability of urban water systems. Water, 35, (1), 28-29.
7. Zhang, Y. (2013). Urban metabolism: A review of research methodologies. Environmental Pollution, 178, 463-473.
8. Fattahi, P., Fayyaz, S. (2010). A compromise-programming model to integrated urban water management. Water resources management, 24 (6), 1211-1227.
9. Agudelo-Vera, C., Leduc, W., Mels, A.R., Rijnaarts H. (2012). Harvesting urban resources towards more resilient cities. Resources, Conservation and Recycling, 64, 3-12.
10. Engel-Yan, J., Kennedy, C., Saiz. S., Pressnail, K. (2005). Toward sustainable neighbourhoods: the need to consider infrastructure interactions. Journal of Civil Engineering, 32, 45-57.
11. Kenway, S., Gregory, A., McMahon, J. (2011). UrbanWater Mass Balance Analysis. Journal of Industrial Ecology, 15 (5), 693-706.
12. Brown, R.R., Farrelly, M.A., Keath, N. (2007). Summary Report: Perceptions of Institutional Drivers and Barriers to Sustainable Urban Water Management in Australia. Report NO. 07/06, National Urban Water
13. Water Sensitive Urban Design Technical Manual (2009) Manual for the Greater Adelaide Region, Government of South Australia, Adelaide
14. Delgado-Ramos, G.C. (2014). Water and the political ecology of urban metabolism: the case of Mexico City. Journal of Political Ecology, 22, 98-114.
15. Bruxelles Environnement, ULB-BATir, Ecores (2015). Métabolisme de la Région de Bruxelles-Capitale. In press.

SMART STABILITY – MARKET-ECONOMIC INTERACTION OF SMART HOMES FOR IMPROVED POWER NETWORK STABILITY

Nicola Schulz[1]; Jürg Bichsel[2]; Holger Wache[3]; Abdul Atisam Farooq[1]; Caroline Hofmann[2]; Benjamin Lammel[3]; Fabian Mettler[3]

1: Fachhochschule Nordwestschweiz, Hochschule für Technik, Klosterzelgstrasse 2, CH-5210 Windisch, Switzerland

2: Fachhochschule Nordwestschweiz, Hochschule für Architektur, Bau und Geomatik, St. Jakobs-Strasse 84, CH-4132 Muttenz, Switzerland

3: Fachhochschule Nordwestschweiz, Hochschule für Wirtschaft, Riggenbachstrasse 16, CH-4600 Olten, Switzerland

ABSTRACT

In this article, the "SmartStability" concept is introduced and first results are shown. The concept is based on the exchange of electrical energy within a network of households that possess temporal flexibilities in consuming or providing energy from or to the network. The exchange is governed by a market-economic negotiation principle between the households.

Temporal flexibility is achieved by exploiting thermal capacities of the buildings themselves and those of warm water storages, and by allowing certain temperature bands. Electric and thermal energy forms are coupled by means of heat pumps and electric water boilers. The physical energy exchange takes place via the electrical grid.

The behaviour of a SmartStability network has been simulated, based on physical models of the energetic resources within each network unit, and by interlinking the individual units to form the entire SmartStability network within a multi-agent environment.

Goal of several simulation scenarios was the adaptation of the time-dependent power consumption profile of the network to a given schedule. Networks consisting of 5 to 100 houses have been simulated. The simulation results show that deviations from schedule can be reduced by approx. 50% by the market-economics-based self-optimization and the resulting intelligent operation of resources. By additionally using battery storages, the deviation from schedule can be further significantly reduced.

Keywords: smart grid, market-economic interaction, thermal storage, flexibility

INTRODUCTION

The implementation of renewable energy sources on a large scale imposes (a) technical and (b) economic challenges: (a) the fluctuating energy production needs to be handled, i.e., power needs to be consumed and stored when it is produced, and for times of little energy production storages have to be exploited. (b) Renewable energy sources and in particular energy storages are often only profitable when using federal subsidies due to the required high capital investments.

The "SmartStability" concept approaches both, technical and economic issues by establishing an interaction for the exchange of electrical energy between a number of small energy units (e.g., households) based on a market economical negotiation principle. Therefore, a distributed (or local) network of individual energy units is formed with the ability to

communicate and to exchange energy via the electrical grid, similar as in [1]. The network will be able to adapt its power consumption profile *P(t)* to given boundary conditions.

The behaviour of such a network has been modelled, based on the physical behaviour of the energetic resources within the individual houses, and by interlinking the individual units within a multi-agent environment.

METHOD

For a realistic simulation of the entire SmartStability network, the individual units have to be physically correctly represented. To achieve a temporal flexibility in power consumption, the thermal capacitances and resulting time constants of selected elements within the units are exploited, and certain temperature bands are allowed. The surplus power consumption (e.g. for lighting etc.) is approximated by using standardized electric power consumption profiles.

Thermal building model

In order to represent the main part of the Swiss building stock the most common building type was chosen: a single-family dwelling with two storeys (Figure 1).

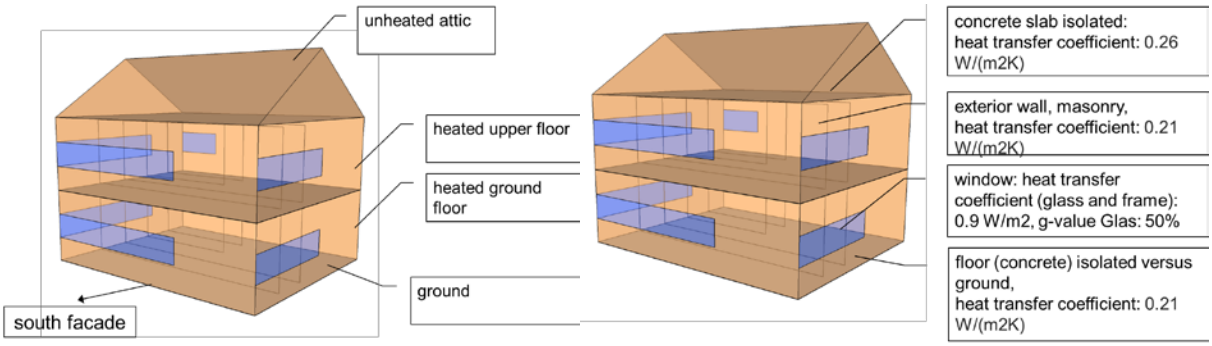

Figure 1: Building model. Left: zones; right: U values of the building envelope.

Ideally, to integrate the building model as a component within the SmartStability network the building should be reduced to a single formula. Although possible, this leads to a very simplified model and consequently to a loss of accuracy. A compromise would be to reduce the thermal behavior to several functions.

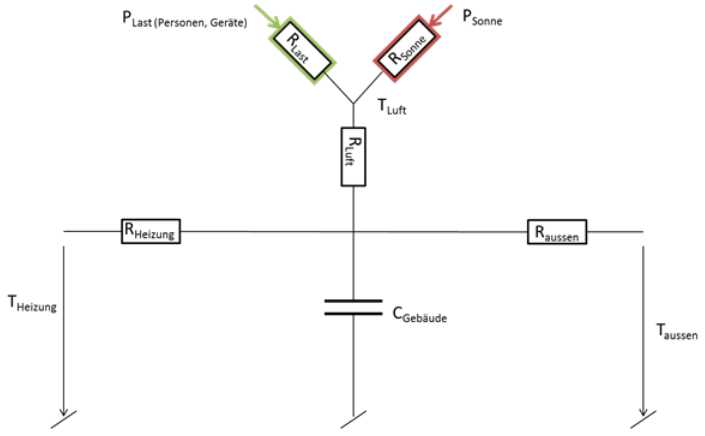

Figure 2: simplified R-C model following ISO 13790.

Therefore, some boundary conditions (e.g. temperature and radiation bins instead of weather data, no internal loads, ACH 0.7 h-1) were simplified. Our interest in the building as a thermal storage raised two questions: Firstly, how long is the heating-up time for the building from

20°C to 26°C (heat being provided by floor heating)? Secondly, how long is the cool-down time from 26° to 0°C without any heating? With these results and the heat storage capacity according to EN ISO 13786 [157 Wh/(m^{2}K)] a mathematical model has been developed.

A simplified analytical model corresponding to ISO 13790 (Figure 2) was used. The parameters were identified with the simulation data from ESP-r using the step responses for heating up (20°C to 26°C) and for cooling down (26° to 0°C). With the thermal resistance of the ground floor ($R_{Heizung}$), and of the outside walls (R_{aussen}) and thermal capacity ($C_{Gebäude}$) the dynamic behaviour of the building is described. Figure 3 below shows selected results.

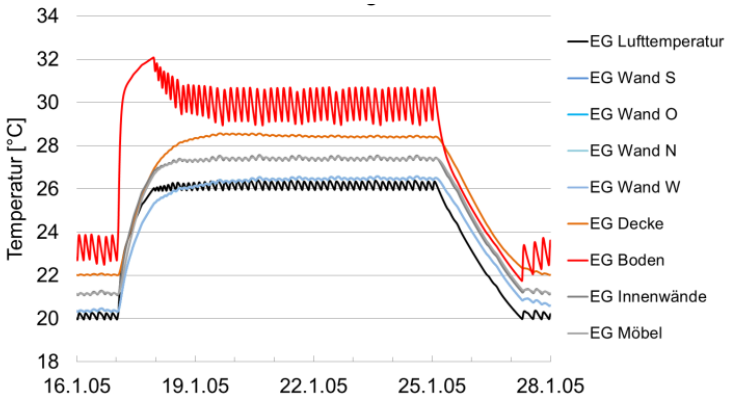

Figure 3: temperature profiles for the ground floor: air temperature, surface temperature of building elements (outside temperature: -5°C; average global irradiation < 25 W/m^2). For this example the heating-up time is 14 h, the cooling down time is 80 h.

Besides the thermal resistances and capacities, a heat-pump model transforming outdoor air-temperature into water temperature of the ground-floor heating system by using electrical power is needed. To describe a heat pump the heating curve and the coefficient of power (COP) are required. The heating curve describes the relation between outdoor and water temperature of the heating system: Lower outdoor temperatures correspond with higher water-temperatures of the ground-floor heating system. The COP = $P_{thermal}$ / $P_{electric}$ is the major parameter describing the relation between electrical input power versus thermal output power. By knowing the outdoor air temperature and the heating curve, the COP can be determined by using data from the heat-pump manufacturer.

The thermal resistances, the capacity, the heating curve and the functional description of the COP are used as parameters in the SmartStability network.

Physical modelling of energetic resources within the buildings

To develop the mathematical model of an electric water boiler, a test bed of a 3 kW, 300-liter domestic hot water boiler was chosen because such boilers are widely used. The physical boiler model on the one hand has to be simple in order to be processable in the SmartStability network simulation environment which contains a large number of individual boilers. On the other hand, the boiler model should yield precise figures regarding time constants for flexibility in turning it on or off. In the present case, a boiler model based on 8 coupled differential equations, based on heat transfer and neglecting convection, was used [2].

To verify the boiler model, a warm water boiler has been employed with temperature sensors, data logging and data measuring devices. Figure 4 shows time-resolved measurements of the water temperatures in 8 different layers, the bottom plot of Figure 4 shows the corresponding simulated temperature profiles. As can be seen, the behaviour of the real boiler and the simplified model are in an acceptable agreement.

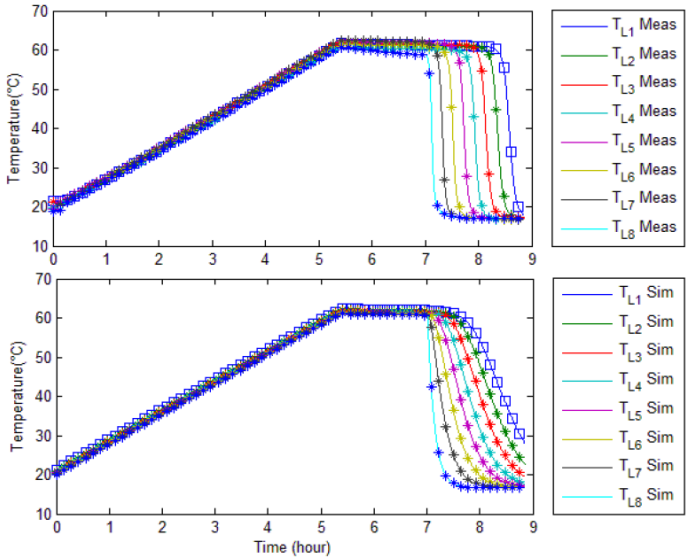

Figure 4: Measured (top) and simulated (bottom) water temperatures in different layers. The heater is on between t = 0 and 5.5 hrs; the water outflow is 0.09 l/s between t = 7 and 9 hrs.

A PV model yielding the power output of a solar panel, depending on its size, efficiency, angular orientation, geographic location, and weather conditions, has been also established. A comparison of the output of a real solar panel and the model is shown in Figure 5.

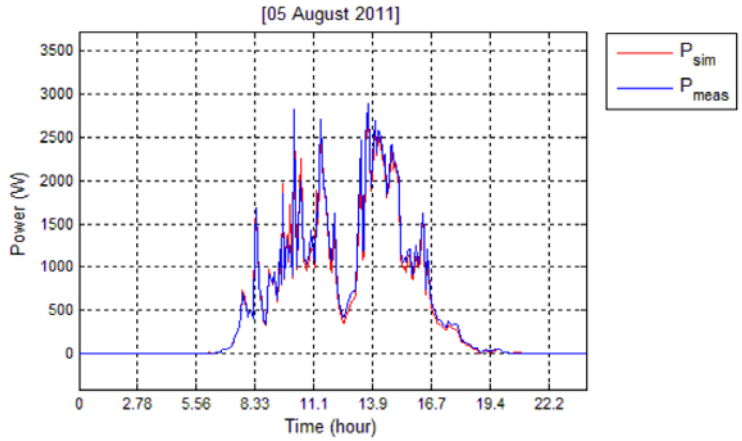

Figure 5: Measured (blue) vs. simulated (red) responses of a PV panel (3.3 kW peak power; location: Windisch, Switzerland) on a summer day with variable weather conditions.

Trading in the SmartStability network

To simulate the effects of the SmartStability network a multi-agent environment was developed. All agents in that environment are equal but two different roles are identified. All agents play the role “SmartStabilityHouse” which represents one power consumer. Each agent interprets the status of its boiler and heat pump and provides offers to the network. One agent in the network plays additionally the role of a “MarketPlaceCoordinator”. That agent is automatically determined out of the network. The coordinator receives all offers and decides which offers will be accepted and which not.

In contrast to other approaches [3, 4] the house agents offer capacity instead of power. For example, an agent offers to turn on its boiler and therefore consumes excessive power (positive capacity). Another agent may offer to turn off its heat pump and therefore does not consume power (negative capacity). Capacities are traded explicitly – not implicitly as in other approaches. Usually in other approaches, a coordinator distributes price signals and thus

tries to motivate houses to turn their resources on or off. Instead trading capacity explicitly, as being used in the present approach, provides the advantage that the coordinator is able to control the resources of the houses. Of course, accepted offers are paid to the offering houses.

The trading process consists of five phases; being initiated by the market place coordinator:

1. Requesting energy demand of all SmartStability houses;
2. Calculating the power deviation from the schedule;
3. Conducting the auction;
4. Calculating the penalty fee for not matching to the schedule;
5. Announcement of the next cycle.

Figure 6 shows a visualized simulation screenshot of a SmartStability network of 5 houses. The top graph shows the target consumption (green line), the actual consumption (red line) and the deviation (thin blue line). If the network includes resources such as batteries, the deviation can be reduced to a minimum, depending on the battery dimensions. The bottom graphics shows the numbers of given (red) and accepted offers (blue).

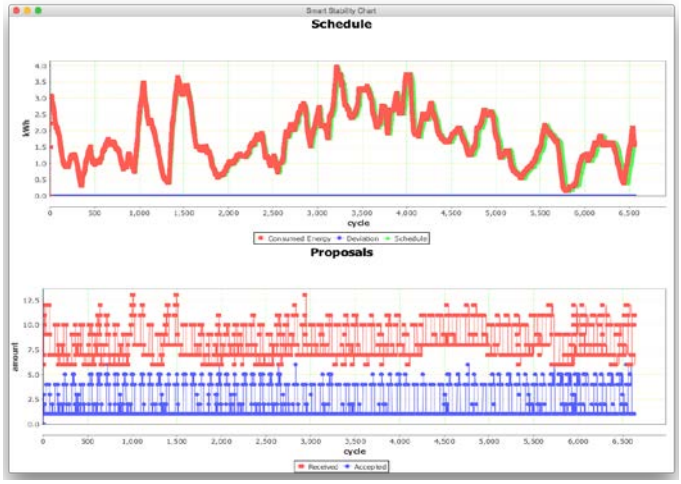

Figure 6: Screenshot of the simulation environment.

RESULTS

Figure 7 shows average deviations of the network from a given schedule for scenarios without batteries. It can be seen that reference scenarios (without trading) behave worse than with trading. Furthermore, Figure 7 relates the deviation to different network sizes. The deviation relatively decreases if more houses participate in the SmartStability network.

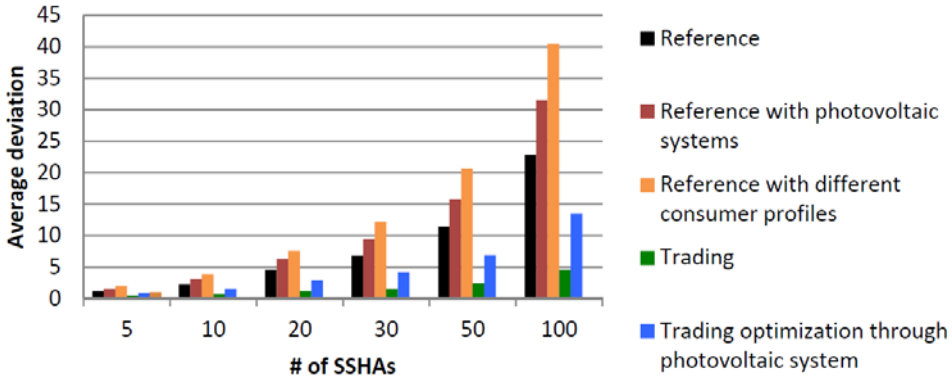

Figure 7: Average deviations from reference and trading scenarios.

Table 1 displays the deviations of several scenarios with different network sizes. In every scenario the aim was to minimize the deviation of consumed energy from a predefined schedule. In the simulation the average of 100 cycles (= 100 · 15 minutes) was chosen as a predefined schedule. The table shows that if a battery is traded then the deviation goes to zero. In those scenarios obviously the households possess enough capacity to store and shift power.

Scenario	Average deviation per cycle over a period of a year with # Households in kWh					
	5	10	20	30	50	100
Reference	1.141	2.283	4.566	6.850	11.416	22.832
Reference with photovoltaic systems	1.575	3.151	6.30	9.456	15.761	31.522
Reference with different consumer profiles	1.991	3.888	7.853	12.197	20.651	40.486
Trading	0.524	0.719	1.132	1.549	2.435	4.577
Trading optimization through PV system	0.907	1.559	2.892	4.229	6.886	13.513
Trading optimization through battery	0.0	0.0	0.0	0.0	0.0	0.0
Trading optimization through photovoltaic system and battery	0.0	0.0	0.0	0.0	0.0	0.0
Trading optimization with different consumer profiles	0.0	0.0	0.0	0.0	0.0	0.0

Table 1: Average deviation per cycle of a period of year in kWh

CONCLUSION AND ACKNOWLEDGMENT

In conclusion, it has been shown that a network of SmartStability houses is able to adapt its power consumption profile to a given schedule. Basis is the trading of capacities, based on a pure market-economic trading principle between the houses. In first instance, only the existing thermal capacities (i.e., those of the buildings themselves and of the warm water storages) have been exploited to generate capacities. Adding battery storage capacities significantly improves the adaptation of the consumption profile to a given schedule.

The authors acknowledge the funding by the Strategic Initiative Research Program of FHNW.

REFERENCES

1. R. Abe, H. Taoka, D. McQuilkin, *Digital grid: Communicative Electrical grids of the Future,* IEEE Transactions on Smart Grid, 2, 399-410, 2011.
2. A. Farooq, A. Afram, N. Schulz, F. Janabi-Sharifi, *Grey-box modeling of a low pressure electric boiler for domestic hot water system,* Appl. Therm. Eng., 84, 257-267, 2015.
3. Marqués, A., & Serrano, *M. et al., NOBEL – A neighborhood oriented brokerage electricity and monitoring system*. Energy-Efficient Computing and Networking, 54, 187-196, 2011.
4. Kok, J., Scheepers, M., & Kamphuis, I.: *Intelligence in electricity networks for embedding renewables and distributed generation*. Intelligent Infrastructures, 2010. Retrieved from http://link.springer.com/chapter/10.1007/978-90-481-3598-1_8

PRESERVING BRUSSELS IDENTITY: METHODOLOGICAL PRINCIPLES FOR THE RETROFITTING OF CITY BLOCKS

G.G.A. Galan Gonzalez Aránzazu[1,2]; D.Q. Deltenre Quentin[1,3]; Athanassiadis A.[1] ; Trachte S.[4] ; Evrard A.[4] ; Acha Román C.[2] ; Bouillard Ph.[1,5].

1: Building, Architecture and Town Planning (BATir), Université Libre de Bruxelles, Avenue F.D. Roosevelt 50 CP 192/4, 1050-Brussels, Belgium. Aranzazu.Galan.Gonzalez@ulb.ac.be

2: Construcción y Tecnología Arquitectónica, Escuela Técnica Superior de Arquitectura de Madrid, Spain (ETSAM)

3: Faculteit Ingenieurswetenschappen,Vrije Universiteit Brussel, Begium (VUB)

4: Architecture et Climat, Université Catholique du Louvain, Belgium

5: School of Engineering, Nazarbayev University, Kazakhstan (NU)

ABSTRACT

The form of Brussels Capital Region city blocks is part of the identity of the city. Preserving the built environment includes preserving the urban form while allowing them to adapt to the new necessities without losing this identity. The city block is not first defined as an architectural form but as a set of plots attached ensemble that acquire meaning because a dialectic relation with the surrounding roads grid [1] The urban block is formed by the complex dialogue between the distribution of properties, the constructions and the public spaces.

This paper aims to stress the role of the city blocks as a main contributor to the heritage value of the city and present a set of methodological principles to approach their retrofitting.

Under the scope of the project B³-Retrotool [2], several scenarios of retrofitting have been developed and assessed over three representative case studies. This research has pinpointed the importance of transforming the city-blocks as a basic unit of the urban matrix. Its originality is to identify new determinants in designing modern, economic and efficient city-blocks using a multi-criteria and multi-scale approach.

Using different mapping tools, a thorough and new classification of the city blocks is provided based in their morphology and urban function. A series of so-called “retrofitting sheets” divided in energy and morphological approach will be presented to illustrate the results.

The paper concludes by presenting these results integrated in a pre-assessment tool developed to provide a clear vision and comprehension of the city of Brussels from a bottom-up and top-down approach. It identifies priority city-blocks requiring an urgent retrofitting and proposes various retrofitting principles to enhance their energy and environmental performances while preserving its identity and cultural heritage.

Keywords: city-blocks, urban form, built environment, retrofitting guidelines, pre-assessment tool.

INTRODUCTION

In the last decades, energy has become one of the most popular topics in research. As a matter of fact, since the continuing increase of oil price starting in 1973, the scarcity of energy resources and the Kyoto Protocol adopted in 1997, energetic strategies emerged all around the world. The 27 Member States in Europe set an energy savings target of 20 percent as well as 20 percent of reduction in greenhouse gases (GHG) emissions by 2020.[3, 4]

In Europe, the dire need to reduce the energy demands and the GHG emissions concern every line of activity but it appears that the building sector is the most energy consumer.

The indicator for energy efficiency is heating demand, as it accounts for the largest percentage of energy consumption in residential buildings [5]. Namely, more than half of the final energy consumption of residential buildings in the EU is used for space heating, reaching up to 70% [4],. In terms of CO_2 emissions, buildings are responsible for around 36% in Europe [6]. Belgium emits around 70 Kg of CO_2 per m² of useful floor area [4]

There is so a big necessity to tackle the big tasks of renovating this old building stock to achieve the ambitious energy performance goals [5]. Till date, all the improvements have been done at the scale of the building. Due to the big number of interventions, it seems complicated to see important results in the planned date. Nevertheless, the hypothesis that big improvements could be perceived by working in the city-block scale is lately explored by several researches. The city-block is perceived as the first urban particle to have an influence at the city scale. This scale highlights the impact of urban geometry in the energy performance of the individual buildings and allows tackling biggest interventions with renewable techniques.

It is not an easy task, however, to work in this scale. Until now, the models created to analyze the energy performance tend to restraint their view at the building level, neglecting the effect of urban geometry acting on energy consumption. One of the reasons is probably the difficulty of modeling complex urban geometry. For instance, establishing the shadow pattern at the city block scale is extremely complex because of too much vectorial intricacy [6].

Nevertheless, there is an increasing interest in city-blocks. Collective equipment appears to perform better efficiency than equipment for each single house. Moreover, a number of community projects at the city-block scale have arosed in Europe: BedZED , Hammarby Sjötad (SE) or l'Espoir (BE).

Several classifications have also emerged, either theoretical or more practical, mixing morphological, typological, social, energetic and environmental indicators. No guidelines to retrofit the city-blocks in a sustainable manner have resulted, though, from these classifications. This increasing concern and interest in the retrofitting of the city-blocks, lead to the need of developing a framework that can help in the decision making from an early design stage to assure the expected results.

This research is one of these attempts: beginning from a brand-new classification of Brussels' city-blocks based in morphological and heritage indicators, a series of so-called "retrofitting sheets" have been developed. These take into account the current state of the city-block and propose a series of retrofitting guidelines for its renovation.

METHODOLOGY

City-blocks could be defined from different indicators: morphology, social and heritage value, energy consumption, urban function and so forth. In order to develop guidelines to retrofit the Brussels city-blocks, some main values had to be established as a starting point.

A few classifications have been done in recent years focusing in one or several of the aforementioned domains. These were twofold: theoretical and practical classifications. Theoretical classifications were achieved through literature studies, but not applied directly to the blocks, which makes them unusable to base the guidelines on. Practical classifications represented the ones which have been developed through the use of quantitative indicators that have been then applied physically to the blocks. The problem lies in the fact that none of these practical classifications were available.

Nonetheless, the conclusions of the previous studies provide very valuable data that helped to develop indicators at the city-block level that led to create a new classification. This classification, taking into account a larger number of indicators than the previous and the relation and impact of the selected among each other, is the strong base over which the retrofitting guidelines have been developed.

Classification of the City-Blocks

Two main data sources have been used during the research: the Brussels Capital Region cadastral matrix and the UrbIS maps. The first one is a database developed by the Federal Public Finance Department (Service Public Fédéral des Finances) in Belgium, which is responsible for the Real State inventory.. It provides for each plot and owner, information such as the year of construction, the number of stories, and the number of housings in the plot, the heated area, and so forth. The second one is a map database of Brussels in 2D and 3D.

The aforementioned data was treated with cartographic tools which allowed that more than 20 indicators could be calculated for each one of the 4500 city-blocks in Brussels.

The two main concerns regarding the retrofitting guidelines were focused in the energy performance and the morphology of the city-block. Therefore, the classification was mainly based on morphological indicators.

These indicators would show the potential to develop large renewable energy solutions, such as geothermic or solar farm, but also to emphasise the city-blocks in need of densification, heightening or construction of free plots. Very specific building-blocks of Brussels have been taking into account for the classification (e.g. garden city-blocks).

Several attempts were made in order to find the most suitable indicators to classify the blocks. As a result, eighteen block typologies have been developed and gathered in the catalogue where the most relevant information about each typology is presented. Figure 1 shows the seven chosen indicators and their value for one of the typologies and the map generated to illustrate each of them.

Blocks' Indicators	Unit	Values
Area	m²	>1000
Number of Plots		>1
(A) Average Height	m	>10
(B) Maximal Height	m	>1 & <30
(B) - (A) Height Diff.	m	-
Building type		2 facades
Built Density	%	>30

Figure 1: Indicators and value to enter in the traditional typology (left) and map of the blocks which categorise in this typology (right).

Case Study Analysis

Three case studies, among the most representatives of Brussels' stock, were selected to illustrate the retrofitting guidelines methodology. These case studies illustrate the most numerous typologies, namely the traditional city-blocks (2121 blocks), the traditional-high-rise city-blocks (384 blocks) and the traditional detached city blocks (412 blocks). The average-type block in each of these typologies was chosen according several indicators. Each indicator is divided into classes (e.g. built density has 4 classes: 0-10%, 11-30%, 31-70% and 71-100%) and the most representative one is kept. To finally have the selected case study, the average between the number of plots and the area is used.

Indicators	Most representative class	Number of blocks
Built density	30% – 70%	1411 (67%)
Functions	> 70% Residential	1416 (67%)
Year of construction	1850 - 1950	1377 (65%)
Empty plot	0%	1128 (54%)
Av. Height	10m – 20m	2082 (98%)

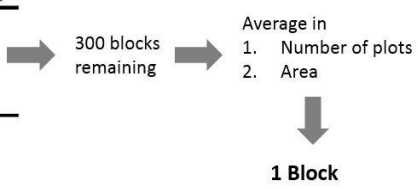

Figure 2: Selection process of the most representative block in the traditional typology

Each case study is then thoroughgoing analysed by means of pictures, plans and charts. (Figure 3).

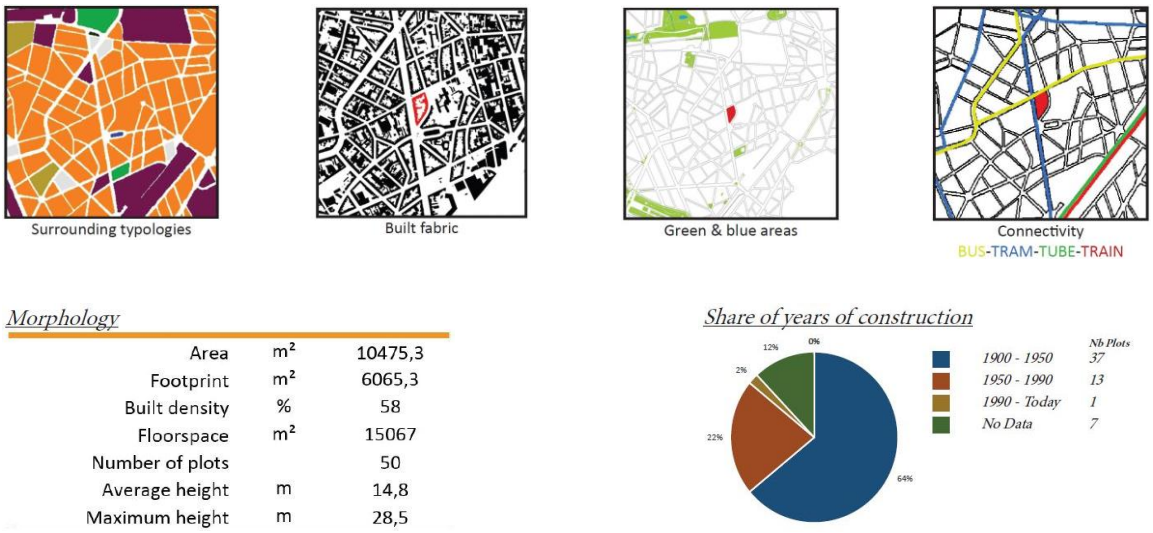

Figure 3: Part of the analysis of the chosen traditional city-block, representative of the typology.

Retrofitting Sheets

Based on the classification and on the City-Blocks' database, methodological principles to retrofit the Brussels' blocks have been developed by means of retrofitting sheets. These are twofold: energetic and morphological. Energetic retrofitting includes geothermic, solar and PV panels and biomass solutions, while the morphological retrofitting concerns heightening and densification concepts.

Each sheet follows a pre-established layout. Firstly, the current state of such retrofit is emphasised in Brussels and compared with the rest of the world. Secondly, guidelines to implement this retrofit to an entire block are highlighted and the most suitable typologies are extracted. As an example, the main results for the geothermic scenario are explained below.

The first part includes an introduction about the topic, what are the different systems used (hot-cold storage, extraction, drilling/storage, geothermal probes, etc.) and what the case of Brussels is so far. The pre-sizing section, based on a literature review, gives rules of thumb and tips depending on the chosen system. The references section shows between 4 to 6 existing projects in Brussels, Belgium and Europe that have been applied to city-blocks or buildings with more than 50 households. The legal framework is also discussed. *L'institut Bruxellois de la Gestion de l'Environnement*, *IBGE*, provides guidelines for open and closed systems. Both need an environmental permit to exploit the ground surface. As well, the potential of use in Brussels according to previous studies (As an example, VITO, an European independent research and technology organization developed two maps for open and closed systems at the Brussels' Region)

The second part highlights which city-block's typologies are most suitable for geothermic purposes according to the pre-sizing section and the developed database (Figure 2).

In a step forward, and thanks to satellites pictures, it was possible to approximate the amount of permeable surface, surface assumed favorable to install geothermal facility, in every city-block [7]. The Cadastre also provided the total heated surface for every house. It allowed approximating the total heating demand for every block, based on the average heating consumption per m² provided by Sibelga (grid manager of electricity and gas distribution in Brussels).. Figure 4 shows the final table with the percentage of city-blocks wherein the implementation of geothermic could sustain the entire block in heating.

Blocks' typologies	Number of Blocks	YES	NO	No Resid' Plot
BlockPlot	38	0%	18%	82%
Detached	166	78%	22%	0%
Empty Block	85	1%	4%	95%
Extremely low densification	83	61%	1%	37%
Garden City	109	48%	48%	5%
HighRise	357	17%	63%	20%
Hyb(BlockPlot-Highrise)	70	1%	17%	81%
Hyb(Green-Detached)	17	100%	0%	0%
Hyb(Green-Tradi-Detached)	11	100%	0%	0%
Hyb(Green-Traditional)	94	60%	40%	0%
Hyb(Traditional - Detached - Highrise)	1	100%	0%	0%
Hyb(Traditional - Detached)	414	35%	65%	0%
Hyb(Traditional-Highrise)	384	5%	95%	0%
Interregional Block	68	3%	35%	62%
Not classified	455	15%	61%	24%
Traditional	2121	1%	99%	0%

Figure 4: Percentage of blocks in each typology wherein vertical geothermic probes could provide enough heating energy for housings. Considering distance between probes: 10 meters

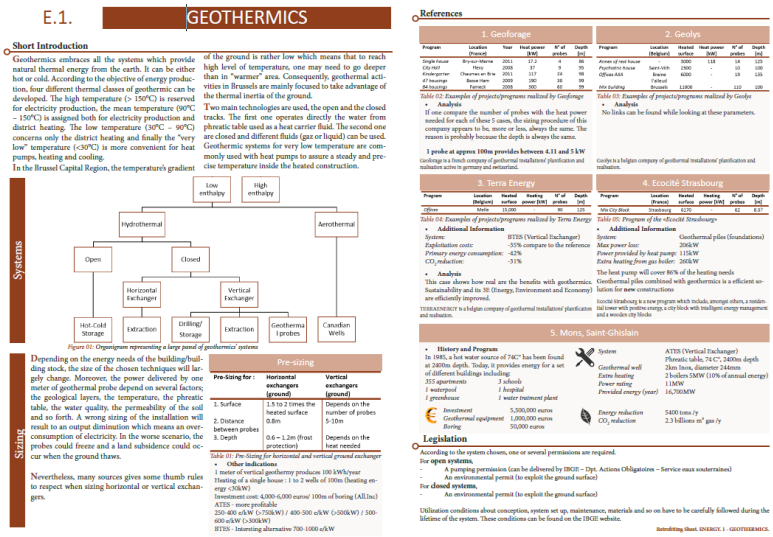

Figure 5: Retrofitting sheets consist in several different pages depending on the amount of data (e.g. Geothermic)

CONCLUSION

This research gives the Region and other interested parties a clearer insight of the City-Blocks in Brussels. For the first time, a database has been developed at this scale, giving information about diverse aspects such as the general morphology (average and maximal height, footprint, surfaces, facades …), main functions (Residential or non-residential), year of construction, and so forth. Insofar the purpose of this study was to create guidelines to retrofit the city-blocks' stock of Brussels. As a result, a set of 18 blocks' typologies have been created gathering the blocks with the same morphological aspects.

Based on a literature studies and the aforementioned database, retrofitting scenarios have been developed for several energy and morphological concerns such as densification (in height or on ground), and geothermic, solar and wind potential. These scenarios suppose a first approach to emphasise the best retrofitting solutions for each block typology in Brussels.

The possibilities to extend the research are manifold. First, the typologies' classification has been performed according to 7 morphological indicators. Other aspects such as social, economic or consumption indicators have not been implemented in this research. Either sub-classifications of the existing typologies or a new classification taking into account all these aspects could be foreseen.

The retrofitting scenarios have been developed with rules of thumb from literature review. It is likely that these numbers are far from reality. For instance, the geothermal potential is very dependent on the type of soil as well as on the system used and the depth of the probes. The values given in this research are focused on one specific system and give an approximate production of energy. For each system, precise production values could be calculated. Currently, the data for solar potential and land permeability is being refined. These new databases will allow providing accurate numbers of energy performance.

To conclude, the outcomes presented in this paper would be available in the Web Tool developed under the name B³ RetroTool. This project started in 2012, grant-aided by the Bxl-Retrofit platform. It was launched both by the Université Libre de Bruxelles and the Université Catholique de Louvain-la-Neuve. It concerns the retrofitting of the Brussels Region following three scales (city, city-blocks and houses) and three criteria (environment, energy and heritage) [2]. (Figure 6)

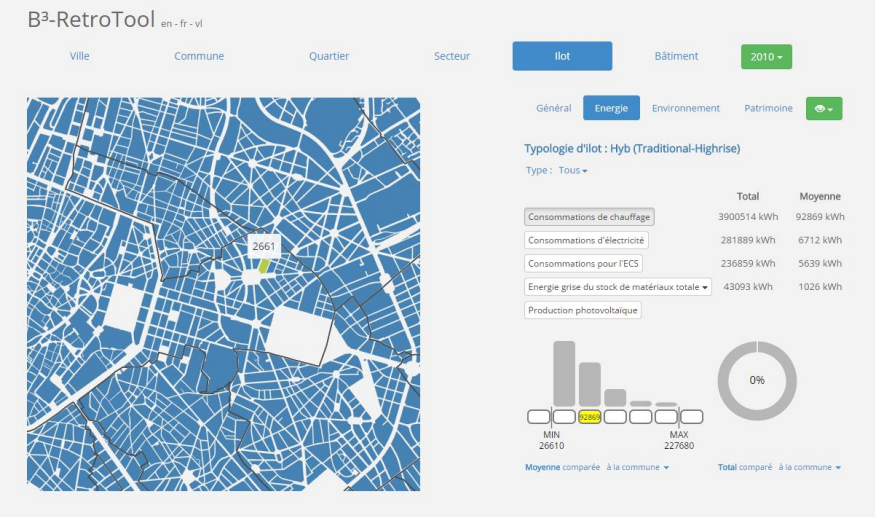

Figure 6: Screen shot of the Beta version of B³ RetroTool. It shows how the scale of the city-block would be visualised and the data available at each scale.

ACKNOWLEDGEMENTS

This research is funded by the Brussels Capital Region through the Innoviris Strategic Research Platform 2012 - Brussels Retrofit XL.

REFERENCES

1. Samuels, I., et al., *Urban Forms*. 2012: Routledge.
2. UCL-ULB. B³-RetroTool - Innoviris Strategic Research Platform 2012 - Brussels Retrofit XL. 2015.
3. Protocol, K., United Nations framework convention on climate change. Kyoto Protocol, Kyoto, 1997.
4. Economidou, M., et al., *Europe's buildings under the microscope.* A Country-by-country review of the energy performance of buildings, 2011: p. 131.
5. Konstantinou, T., *Facade Refurbishment Toolbox. Supporting the Design of Residential Energy Upgrades.* A+ BE| Architecture and the Built Environment, 2014. **4**(9): p. 1-420.
6. Energy., E.C.-. ec.europa.eu/energy/efficiency/buildings/buildings_en.htm. June 2011.
7. Stessens, P., Ecosystem Service Optimisation for Cities. ULB- BATir. On going Doctoral Thesis.

CATEGORIZATION OF THE HISTORIC ARCHITECTURE IN PALERMO FOR THE PURPOSE OF ENERGY ASSESSMENT

Enrico Genova[1]; Giovanni Fatta[1]; Tor Broström[2]

1: Università degli Studi di Palermo, Dipartimento di Architettura, viale delle Scienze, Edificio 8, 90128 Palermo, Italia

2: Uppsala Universitet, Konstvetenskapliga institutionen, Kulturvård, Visby, Sverige

ABSTRACT

The strategies to improve the energy performance of historic buildings can be compatible with their conservation if they are referred to material, construction, distribution features, strictly related to a local level. In the EU project EFFESUS, a method of categorization has been developed for historic districts and tested on the Swedish town of Visby. This approach aims at defining a manageable number of representative buildings, or archetypes, through which the energy performances of the district constructions, and their potential improvement, can be analysed. The present paper applies this categorization method to a representative part of the historic centre of Palermo, regulated by the urban plan "P.P.E. Centro storico". The study aims at relating the existing building typologies, defined in this plan, to the characteristics influencing the energy performance of the historic architecture of the town. This analysis has resulted in twelve building categories, proposed to detail the district typologies. The categorization of the historic architecture of Palermo and its integration with the current typologies are meant to facilitate guidelines for the improvement of its energy performances: for each category, several refurbishment measures can be analysed regarding their compatibility to the conservation restrictions; at the same time, their effectiveness can be assessed on the basis of geometric, distribution and construction features of the buildings.

Keywords: historic architecture, categorization, energy improvement, building typology

INTRODUCTION

The historic architecture is a relevant part of the European building stock. Therefore, its contribution to reduce the consumption of resources, notably energy, can be relevant in the construction sector. At the same time, the importance to preserve its material and aesthetic features highlights the risks related to an uncritical refurbishment, carried out through techniques now common, but suitable for modern constructions. For this reason, the Directive 2010/31/EU and the great part of its national implementations allow that officially protected buildings are exempted from minimum energy requirements. This decision excludes vernacular constructions, although their remarkable significance both as part of the landscape and as evidence of technical culture. On this subject, the scientific literature reports cases in which the energy efficiency of historic buildings has been improved in ways compatible neither to their conservation, nor to their hygrothermal function.

On the other side, there is a growing awareness of the question of energy use and indoor environmental quality in historic buildings, not only listed ones. Recent examples are the rating system *GBC Historic Buildings* and the *AICARR* Guidelines for the energy efficiency in historic buildings. Based on common conservation principles, these measures require an in-depth analysis of the building. Therefore, the reference to material, construction, typological features, strongly related to the local context, is necessary. From this point of view, in the European project EFFESUS [3, 5] a method of categorization has been developed to analyse

the energy performance and potential improvement of the building stock in historic districts. In the present paper, this method is applied to the heritage historic district of Palermo.

STATE OF THE ART

Several research projects have aimed at developing guidelines for the energy efficiency of the building stock. To analyse their performance and the possibilities of its enhancement, some studies follow a typological approach. In the French project BATAN [2], "thermal typologies" are used to describe the historic architectural heritage according to the aggregation of buildings and their material and construction features. The EU project TABULA [6] has described the European building stock by means of typologies, referred to the building size and age of construction. For each group, average values of several parameters identify archetypes or representative architectures. Through the selected constructions, the energy performance and the potential improvement have been calculated for each typology. The project, however, focuses more on modern constructions. Regarding historic districts, recent projects [1, 4] propose the analysis and simulation of case studies on the base of quick *in situ* inspections, through which relevant data are collected (about materials, construction techniques and envelope components, building size and distribution).

The European project EFFESUS has developed a method to categorize historic districts, which has been applied to the Swedish town of Visby. The historic district is categorized with respect to building size and aggregation, to construction and distribution features, to the technical systems for heating and cooling. Besides these characteristics, the cultural significance of the architectures and the legislative restrictions of protection are taken into account. Starting from the CityGML data model, the categories are defined according to the number of storeys and adjoining walls, the ground floor area and the volume. Further subcategories can be defined considering data such as the envelope construction and the systems used. As in TABULA, for each category a representative, real building or an archetype is defined. Therefore, a manageable number of representative buildings allow for an in-depth analysis of energy performances and the potential improvement of the historic district [3].

OBJECTIVE OF THE RESEARCH

The architectural heritage in the historic centre of Palermo is regulated by the urban plan "P.P.E. Centro storico" (1993), which is based on a typological approach. Its typologies are strictly related to the historical use of buildings: in the group "edifici speciali religiosi" the religious architectures (both convents and churches) are collected, in "edifici speciali civili" the public constructions (civilian and military), while the residential buildings are distributed in five typologies ("catoi semplici" and "catoi multipli" for the vernacular constructions, "palazzi" for aristocratic and monumental buildings, "palazzetti" and "palazzetti multifamiliari" for buildings reproducing the model of "palazzi" in a smaller size). Furthermore, for each typology the urban plan lists the elements to be preserved and the measures allowed, strictly connected to different conservation requirements. Hence, the categorization method developed in the EFFESUS project can be particularly useful in this context, where the aim is to relate the P.P.E. typologies to the features influencing the performances of the historic buildings, in order to integrate the energy improvement of the architectural heritage of Palermo with the conservation practices allowed by the urban plan. In order to limit the scope of the investigation, the following buildings are excluded: churches, constructions subsequent to the second world war (typology "Edilizia postbellica") and buildings not realised with traditional techniques.

METHODOLOGY: SELECTION AND COLLECTION OF DATA

This research applies the EFFESUS categorization to "mandamento Castellammare", one of the four parts which the historic centre of Palermo is traditionally divided in, comprising more than five hundred buildings. The main data sources were the urban map on a scale of 1:500 ("Carta tecnica", 1981) and the graphic documents of P.P.E. (1993). Since several building restorations have been carried out in the last two decades, these maps have been compared to more recent aerial photographs (*Bing Maps*, *Google Earth*; 2014) and checked through *in situ* inspections in some cases. For each building, the collected data regard mainly geometric features, notably the ground floor area and perimeter, the volume and the number of storeys. Furthermore, the typology the P.P.E. attributes to the building has been considered; for a small area not included in the plan, it has been assigned by analogy. The heating and cooling systems employed are not taken into account, because of the difficulties to find homogeneous and certain information. The data have been collected through the software *QUANTUM GIS* on the georeferred vectorial map of the historic centre, and processed in *Microsoft Office Excel*.

The boundaries considered for each construction are those, which the urban plan reports for the building units. Just in few cases, the limits have been modified, if relevant discrepancies exist with the current building state. The ground floor areas have been calculated referring to these boundaries, including outdoor spaces if covered by closed ones. However, the building size is expressed in terms of volume, while the number of storeys is not manageable. The historical development of Palermo's historic centre is based on the raising of existing constructions; consequently, the same number of floors refers to constructions very different in size, while some buildings can be connoted by more than one number of storeys. On the other hand, the urban map ("Carta tecnica", 1:500) describes the geometry of all roofs with their absolute heights, so it allows calculating the construction volumes in detail. Hence, each building unit has been divided in polygons, representing simple roof geometries. The corresponding relative heights have been obtained by subtracting the ground level reported in the map. Finally, outdoor covered spaces have been subtracted in the volume calculation.

The number of adjoining walls is not relevant to represent the aggregation of buildings in the fabric of the historic centre of Palermo: almost all the architectures are parts of urban blocks, generally characterised by irregular shape; at the same time, the buildings have often complex geometries, since they result from the historical union or division of previous constructions. Moreover, relevant distribution features such as the courtyard are specific to some typologies, as pointed out in the P.P.E. In this paper, only one parameter is introduced to consider synthetically these characteristics. This term is the ratio between the ground floor perimeter shared with the adjoining constructions and the total, and includes the courtyard when present. For the sake of simplicity, it has been assumed that the shared perimeter is common to the adjoining units for all their vertical extent. This hypothesis is acceptable because of the quite homogeneous distribution of heights in the analysed building stock.

As mentioned above, the study takes also into account the typology attributed to each unit by the urban plan. This information is important to guide the data analysis and connect the categories to the P.P.E. typological structure. At the same time, especially the residential typologies point out features concerning the inner distribution of buildings, but not their construction characteristics: the great part of the architectural heritage of Palermo results from centuries of building activities, where similar materials and techniques were used both in the vernacular and monumental architectures. Therefore, some evident differences, related to structural, spatial and decorative solutions peculiar to imposing architectures, are implicitly expressed in the current typologies. However, a distinction based on the age or techniques of construction would be hard, but also not relevant for the purpose of this research.

PROPOSAL OF CATEGORIZATION FOR THE HISTORIC ARCHITECTURE OF PALERMO

The categorization proposed in this study is based on the size of buildings, on their aggregation in the historic urban fabric and on the limits to intervention set by the urban plan. The thresholds for the aggregation and dimensional features have been defined by analysing the data of both each typology and the stock as a whole. The study does not aim at substituting the P.P.E. typologies, but at connecting them to the energy performance of the buildings. Nevertheless, starting from the existing typologies, the categorization would have resulted in a strong reliance on the characteristics of each group. The definition of common thresholds, on the opposite, leads to categories for which, given the geometric features, the strategies for energy improvement can be assessed on the base of different levels of protection.

Some relevant thresholds identify features specific to vernacular constructions. Concerning the aggregation, only "Catoi semplici" and "Catoi multipli" include buildings whose shared perimeter overcomes two thirds of the total: these constructions are generally in the middle of blocks and are not connected to inner courtyards. Moreover, the volume range for the vernacular buildings varies from 200 m^3 to 3500 m^3, while greater differences emerge in the other typologies: the volume ranges from 3500 m^3 and 40000 m^3 for the monumental residences, from 7000 m^3 and 80000 m^3 in the typology of convents and from 1000 m^3 to 10000 m^3 for "Palazzetti". Hence, a wide range marks notably the monumental buildings, whose peculiarities can not always be referred to typological characters. Two thresholds, consequently, have been identified for each of the analysed features. About the shared perimeter, the limit of two thirds (67%) is characteristic only to a part of the vernacular buildings; on the other side, a maximum value of 40% comprise the architectures, mainly monumental, where an inner courtyard is present. Considering the volume, the value of 3500 m^3 distinguishes both the vernacular buildings and the monumental ones, limiting the first at the top, the latter at the bottom. A second threshold, identified in the maximum volume of "palazzetti" (10000 m^3), has been introduced to highlight the buildings whose peculiarities overcome the typological features.

The seven groups of buildings defined through these thresholds have been subdivided according to the limits the urban plan sets to the intervention. For this purpose, three "levels of protection" have been introduced, referring to the distinction between "ristrutturazione" (renovation) and "restauro" (restoration). Derived from the national building regulations, this is the main difference among the measures allowed by the plan: restoration aims at preserving the architectural organism by respecting its aesthetic, typological and construction features; renovation allows a partial transformation of the building unit. Therefore, the possibility to substitute construction and technical elements and change the internal distribution of the space is higher in the latter than in the former. The urban plan for the historic centre of Palermo, while requires the restoration for the monumental buildings ("Palazzi", "Edifici speciali civili", "Edifici speciali religiosi"), allows renovation for the other typologies. However, a second specification has been considered necessary in this study: P.P.E. identifies indeed building elements to be preserved as characteristic to some typologies, so influencing the actual possibilities of refurbishment. Furthermore, although renovation is the way allowed for "Palazzetti", for some of these buildings and for many included in "Edilizia conseguente al piano regolatore Giarrusso" restoration is required. At the same time, also if subject to renovation, their formal and spatial features generally limit, compared to vernacular buildings, the possibilities of the intervention. Hence, while a level ("3") characterises the typologies for which restoration is required, two "levels of protection" are introduced when renovation is allowed: "level 1" for "Catoi semplici" and "Catoi multipli", "level 2" for "Palazzetti", "Palazzetti multifamiliari" and "Edilizia conseguente al piano regolatore Giarrusso".

Thereby, sixteen categories result from the seven groups based on geometric features. However, compared to the whole sample, four of them have been removed, since both the number of buildings and their total volume are less than 1% of the total. For each of the remaining twelve categories, the average values of ground floor area, volume and shared perimeter have been calculated, as reported in table 1. These values are meant to be used to identify representative buildings, or archetypes, through which the energy performance and the potential improvement of the architectural heritage of Palermo can be analysed.

Level 1	**1.I** Volume ≤ 3,500 m^3 Adjoining perimeter ≥ 67 %			**1.II** Volume ≤ 3,500 m^3 Adjoining perimeter 40÷67 %			**1.III** Volume ≤ 3500 m^3 Adjoining perimeter ≤ 40 %			
	96 buildings	17.3 % buildings 3.9 % volume		**147** buildings	26.5 % buildings 9.1 % volume		**46** buildings	8.3 % buildings 3.3 % volume		
	Average values	64 m^2 970 m^3 75.4 %		Average values	101 m^2 1,488 m^3 53.6 %		Average values	120 m^2 1,710 m^3 28.5 %		
Level 2	**2.I** Vol. ≤ 3,500 m^3 Adj. per. 40÷67 %		**2.II** Vol. ≤ 3,500 m^3 Adj. per. ≤ 40 %		**2.III** Vol. 3,500÷10,000 m^3 Adj. per. 40÷67 %		**2.IV** Vol. 3,500÷10,000 m^3 Adj. per. ≤ 40 %		**2.V** Vol. ≥ 10,000 m^3 Adj. per. ≤ 40 %	
	35	6.3 % buil. 3.0 % vol.	**41**	7.4 % buil. 4.2 % vol.	**29**	5.2 % buil. 5.8 % vol.	**43**	7.8 % buil. 9.4 % vol.	**10**	1.8 % buil. 7.3 % vol.
	Av. val.	135 m^2 2,055 m^3 52.4 %	Av. val.	167 m^2 2,468 m^3 29.3 %	Av. val.	265 m^2 4,756 m^3 49.2 %	Av. val.	297 m^2 5,242 m^3 24.6 %	Av. val.	834 m^2 17,571 m^3 14.1 %
Level 3	**3.I** Vol. 3,500÷10,000 m^3 Adj. per. 40÷67 %		**3.II** Vol. 3,500÷10,000 m^3 Adj. per. ≤ 40 %		**3.III** Vol. ≥ 10,000 m^3 Adj. per. 40÷67 %		**3.IV** Vol. ≥ 10,000 m^3 Adj. per. ≤ 40 %			
	17	3.1 % buil. 3.9 % vol.	**36**	6.5 % buil. 10.5 % vol.	**3**	0.5 % buil. 1.6 % vol.	**36**	6.5 % buil. 34.6 % vol.		
	Average values	337 m^2 5,520 m^3 48.4 %	Average values	425 m^2 6,967 m^3 25.8 %	Average values	762 m^2 12,911 m^3 45.5 %	Average values	1,284 m^2 23,027 m^3 18.0 %		

Table 1: Categories proposed for the historic centre of Palermo

CONCLUSIONS

This investigation has applied the categorization method, developed in the EU project EFFESUS, to the historic centre of Palermo. The geometric features of the buildings, which the method is based on, have been expressed by means of two parameters: the volume, to represent the dimensions of the building units; the ratio between the shared and total ground floor perimeter, for the aggregation in the urban fabric. Through these terms, and referring to the limits the current urban plan of Palermo sets to preserve its architectural heritage, twelve categories have been defined. They have been collected in three groups, on the base of "levels of protection": three categories comprise the vernacular buildings, where refurbishment is allowed and the restrictions to the intervention are less (level 1); five describe the constructions for which, though the same measures are generally permitted, more limits derive from the need of conservation (l. 2); four refer to the monumental architectures, where restoration is required (l. 3). Other four categories have been eliminated since negligible in respect to volume and number of buildings.

The number of categories could require corrections if all the district were subject to further analysis. Anyhow, in this study the EFFESUS categorization has been adapted to the features of the historic architecture of Palermo and to the available data. Thereby, the applicability of the method has been examined and its integration to the typological structure of the current

urban plan is proposed: for this purpose, the existing typologies are detailed through the defined categories, more directly related to the dimensional, distribution and aggregation features of buildings. In this way, the possible strategies for the energy improvement of the historic architecture of Palermo could be included in the current framework of regulations pertaining to their conservation.

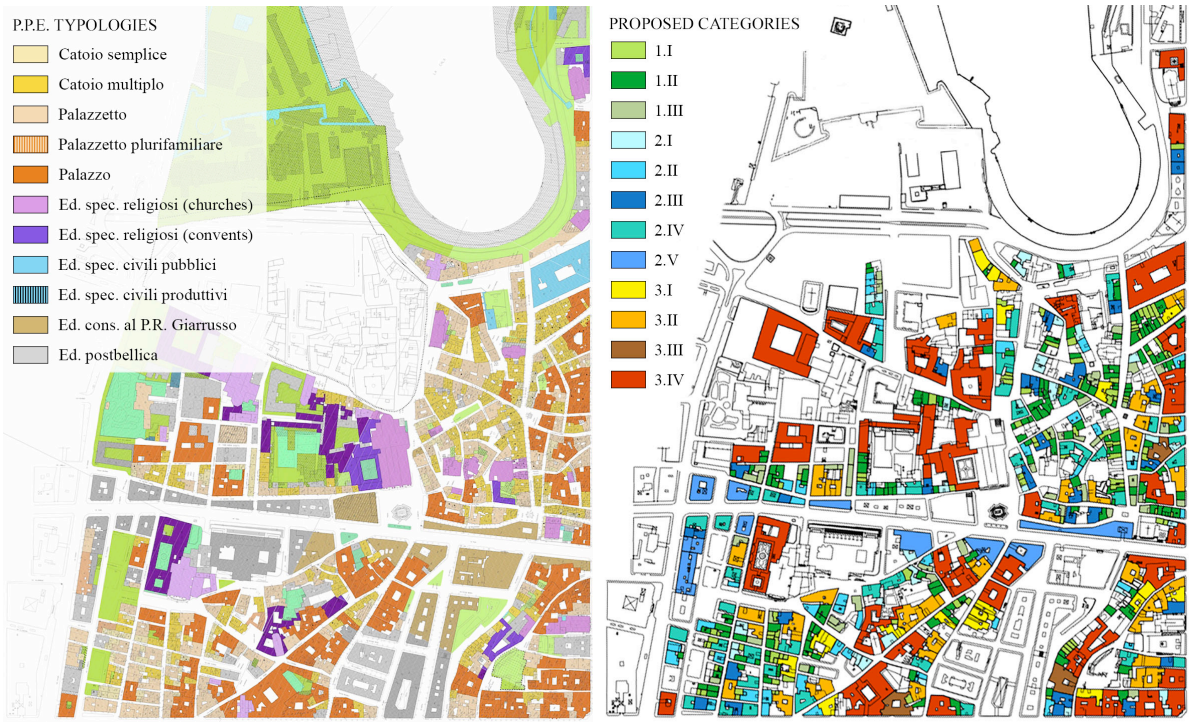

Figure 1: Comparison between the P.P.E. typologies (left) and the proposed categories (right)

AKNOWLEDGEMENTS

The present study has been supported by the European Commission under the project of the 7th Framework Program Energy Efficiency for the EU Historic Districts Sustainability (EFFESUS), No. 314678.e

REFERENCES

1. Ambrogio, K. and Zuppiroli, M.: Energia e restauro. Franco Angeli, Milano, 2013.
2. Modélisation du comportement thermique du bâtiment ancien avant 1948. Rapport de Synthèse. BATAN, 2011.
3. Berg, F.: Categorising a historic building stock - An interdisciplinary approach. Master Thesis in Integrated Conservation, Uppsala University, Department of Art History, 2015.
4. Boarin, P. and Davoli, P.: A systemic approach for preliminary proposals of sustainable retrofit in historic settlements. The case study of villages hit by earthquake. Proc. of the European Conference on Sustainability, Energy and the Environment 2013, 297-313, 2013.
5. Broström, T., Bernardi, A., Egusquiza, A.R., Frick, J. and Kahn, M.: A method for categorization of European historic districts and a multiscale data model for the assessment of energy interventions. Proc. of the 3rd European Workshop on Cultural Heritage Preservation, pp. 153-158, Bolzano, 2013.
6. Corrado, V., Ballarini, I., Corgnati, S. P. and Talà, N.: Fascicolo sulla Tipologia Edilizia Italiana. TABULA, 2011.

EVALUATING THE SENSITIVITY OF GRID INTEGRATION LEVEL FOR A MULTI ENERGY HUBS

A.T.D. Perera[1], V.M. Nik[2], D. Mauree[1], J.L. Scartezzini[1]

1:Solar Energy and Building Physics Laboratory (LESO-PB), EPFL, CH-1015 Lausanne, Switzerland

2:Division of Building Physics, Department of Building and Environmental Technology, Lund University, Lund, Sweden

ABSTRACT

Renewable energy integration into multi energy grids (MEG) is gradually getting popular due to the rapid depletion of fossil fuel resources and the global concern on GHG emissions through fossil fuel based energy conversion technologies. However, seasonal changes in solar and wind energy potentials make it challenging to increase the renewable energy capacity especially for urban applications where demand for energy services show a complex variation. According to recent literature, connecting multi energy hubs (MEHs) to a MEG can be a promising method to address the aforementioned challenge. However, a quantitative analysis of the improvement of system autonomy and renewable energy integration through multi energy hubs is missing.

In this work, Homer microgrid design tool is used to analyze the sensitivity of the grid integration level to the renewable energy integration process of a multi energy hub. Heating and electricity demand of the MEH and the energy flow through Solar PV panels, wind turbines, boiler and battery bank are evaluated on hourly basis. Homer, microgrid simulation tool is used to evaluate the sensitivity of electricity cost to renewable energy capacity and energy storage.

Key words: Multi Energy Hub (MEH); Multi Energy Grid (MEG); renewable energy integration

INTRODUCTION

Integrating renewable energy sources into current energy systems using fossil fuel resources and/or nuclear energy has been getting popular during last decade [1], [2]. However, designing such integrated energy systems combining renewable energy sources is challenging due to stochastic nature of renewable energy sources and demand [3], [4]. Therefore different methods have been introduced to optimize the system configuration for integrated poly-generation systems and real time control of these systems [5].

Identifying the capacity for renewable energy integration, energy storage and grid integration is a difficult research problem that needs to be addressed. Recent literature has been focused on designing such integrated energy systems for both grid connected and stand-alone operation [5]–[7]. Among these methods, the energy-hub (EH) concept is gradually getting popular integrated energy systems with multiple energy sources, storage methods, connected to multi energy grids are used to provide multiple energy services of users [8]–[11]. However, it is a challenging task to optimize such systems due to the complexity of the energy flow and extensive decision space created with a number of possible solutions.

Recently, number of groups has focused on implementing the energy hub concept at neighbourhood level where integration of non-dispatchable energy sources such as SPV and wind energy is given a priority. However, the limits for the integration of these energy sources and the requirement of energy storage in this process need to be analysed. This extends the design problem of these energy hubs from classical cost optimization.

OVERVIEW OF THE CONSIDERED ENERGY SYSTEMS

Energy storage and dispatchable energy sources are connected to renewable energy sources in order to absorb the fluctuations in renewable energy potential. This creates a complicated energy flow within the system with multiple options to be selected such as battery banks, H2-fuel cells and compressed air storage which can be used to absorb the fluctuations of renewable energy. In addition, dispatchable energy sources are used to generate electricity whenever renewable energy potential is not sufficient enough to provide the demand. In this study, an internal combustion generator, SPV panels and wind turbines are used to generate electricity. A battery bank is used as electricity storage. In addition, the hub is connected to the main grid in order to provide mismatch in demand. The electrical part consists of an AC bus and a DC bus. An internal Combustion Generator (ICG) and wind turbines are connected to the AC bus while SPV panels and a battery bank are connected to the DC bus. In this work only an AC load is considered. However, this can be extended considering a DC load such as vehicle charging as well. In addition, the thermal load is catered using a boiler. Interactions with a thermal grid in order to meet the thermal demand are not considered in this work.

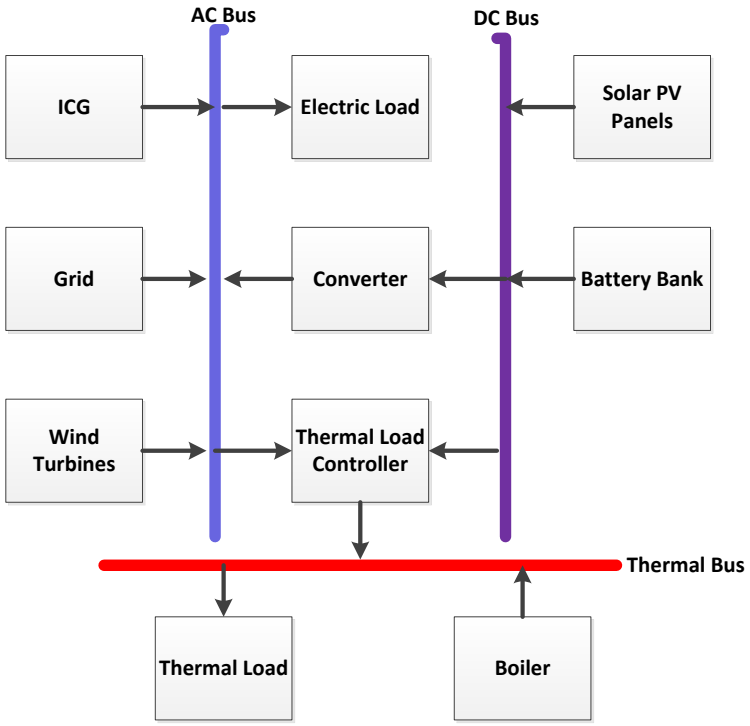

Figure 1 Overview of the energy hub

METHODOLOGY

Hourly solar irradiation and wind speed data need to be collected in order to determine the solar and wind energy potential. Subsequently, the energy conversion efficiency of SPV modules and wind turbines is calculated which helps to determine the power generation of non-dispatchable renewable energy sources. After determining the power generation from non-dispatchable energy sources, the operating state of the battery bank and ICG is determined using the dispatch strategy. This routine is used to simulate the system throughout the year considering a time step of one hour for 8760 time steps. The electrical and thermal demands for the application are taken according to Figure 2. Based on the simulation, the energy flow through system components is analysed for different COE in grid scenarios.

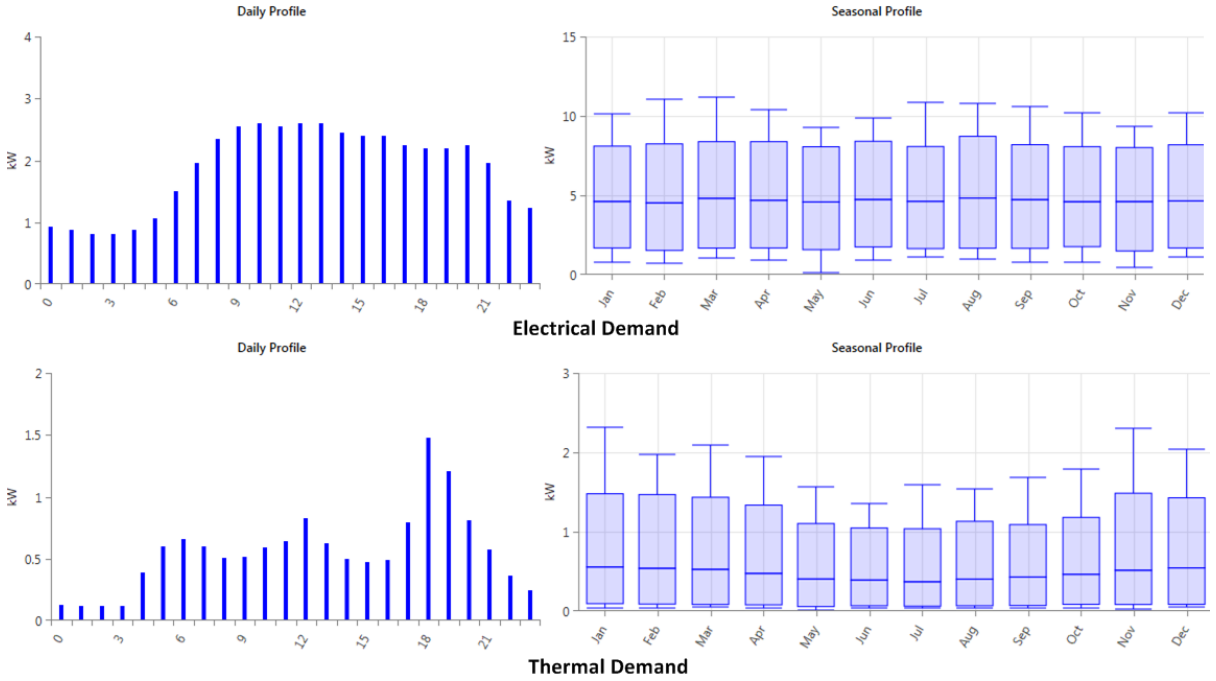

Figure 2 Thermal and electrical demand of the hub

The energy flow model used for this study is based on Homer micro grid simulation software. Monthly average global horizontal data, wind speed and ambient temperatures are taken from the NASA surface meteorology and solar energy data base. The power curve for the wind turbine is taken based on commercially available wind turbine (Figure 3). SPV panels are modelled considering an operating temperature to be 47 °C and temperature coefficient of -0.5. The cycle counting method is used to calculate the lifetime of the battery bank. The cycle charging strategy is used as the dispatch strategy [12]–[14]. Subsequently, hub is optimized considering life cycle cost as the objective function. A direct search method is used by Homer in optimizing energy hubs. All the possible combinations for system design are evaluated based on the objective function. For this case study, 4968 solutions are simulated and compared in the optimization algorithm.

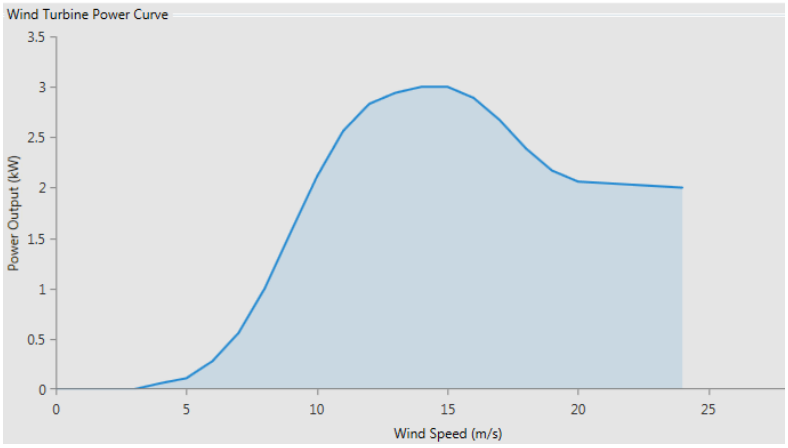

Figure 3 Power curve of the wind turbine

RESULTS AND DISCUSSION

Four different scenarios are taken into discussion in this work. Three scenarios are taken considering the grid connected operation mode. Finally, fourth considers the standalone operation mode which is taken as the reference case. The three grid connected cases are named Case A, Case B and Case C according to the ascending order of the grid price. Case D is based on the standalone application. Results of the optimized systems are illustrated in Table 1.

Table 1: Results of the case studies

Case	Case A	Case B	Case C	Case D
Renewable energy percentage (%)	60	65	72	63
SPV capacity (kW)	10	12	16	14
SPV contribution (%)	55	60	68	67
Wind turbine capacity (kW)	3	3	3	6
Wind turbine contribution (%)	5	5	4	23
Battery banks	0	0	0	23
Throughput of battery (kWh/year)	0	0	0	2161
Fuel consumption of ICG (l/yr)	0	0	0	1949
Units purchased from grid (kWh)	8717	8346	7821	0
Units sent to grid (KWh)	4485	6295	10130	0

The renewable energy level gradually increases when moving from Case A to Case C. This demonstrates that higher cost of the electricity grid encourages higher integration of renewable energy. SPV and wind energy generation increase from 60% to 72% with the increase of grid electricity prices. However, ICG and battery banks are not found in optimized design solutions for grid integrated designs. This clearly emphasizes that the grid has the capability to absorb the fluctuations of renewable energy without any support from dispatchable energy sources or storage. However, the battery bank size is 23 kWh for a standalone system which includes an ICG in addition to the battery bank. When considering the ICG for Case D, it operates during night at full load where SPV generation is not significant. At the same time the battery bank is charging during the daytime

and gets discharged during the night when the solar energy potential is not significant. The boiler is used to provide the heat demand of the application. Since the thermal grid or storage is not connected to the system, a significant change is not observed for the thermal part of the hub.

When analysing the standalone application it is clear that both ICG and battery bank are used to meet the demand quite often. Figure 4 clearly demonstrates that ICG is operated at full load throughout the year except for the daytime where SPV generates electricity. Similarly, the battery bank is charged during the daytime and is getting discharged during the night (Figure 5). This clearly demonstrates that both dispatchable energy source and storage play an important role in standalone applications which is performed by grid for grid connected applications.

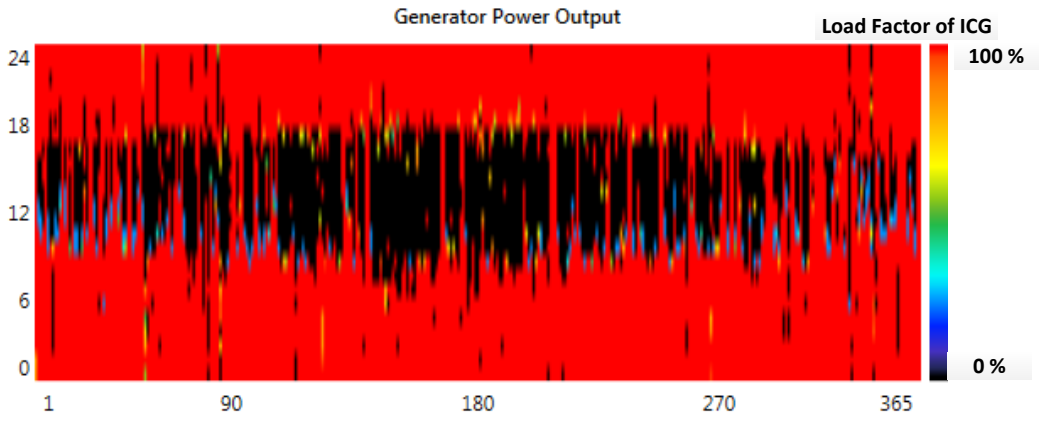

Figure 4 Operating conditions of ICG for Case D

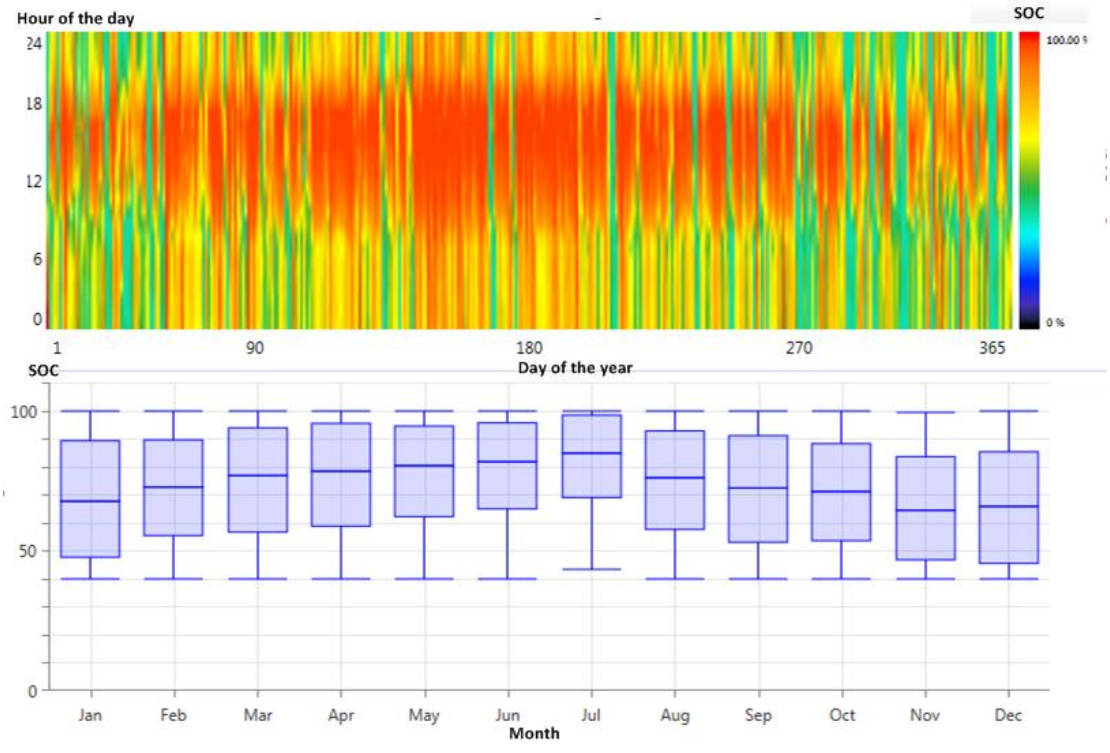

Figure 5 Operating conditions of the battery bank for Case D

CONCLUSIONS

This study focuses on integrating renewable energy sources through energy hubs to provide multiple energy services. The results obtained through the study shows that a higher level of non dispatchable renewable energy capacity can be handled with the support of the grid. However, it was demonstrated that both energy storage and a dispatchable energy source are required to achieve a 100% autonomy level.

References

[1] B. Ćosić, G. Krajačić, and N. Duić, "A 100% renewable energy system in the year 2050: The case of Macedonia," *Energy*, vol. 48, no. 1, pp. 80–87, Dec. 2012.

[2] G. Krajačić, N. Duić, Z. Zmijarević, B. V. Mathiesen, A. A. Vučinić, and M. da Graça Carvalho, "Planning for a 100% independent energy system based on smart energy storage for integration of renewables and CO2 emissions reduction," *Appl. Therm. Eng.*, vol. 31, no. 13, pp. 2073–2083, Sep. 2011.

[3] A. T. D. Perera, R. A. Attalage, K. K. C. K. Perera, and V. P. C. Dassanayake, "Converting existing Internal Combustion Generator (ICG) systems into HESs in standalone applications," *Energy Convers. Manag.*, vol. 74, pp. 237–248, Oct. 2013.

[4] A. T. D. Perera, R. A. Attalage, K. K. C. K. Perera, and V. P. C. Dassanayake, "Designing standalone hybrid energy systems minimizing initial investment, life cycle cost and pollutant emission," *Energy*, vol. 54, pp. 220–230, Jun. 2013.

[5] A. H. Fathima and K. Palanisamy, "Optimization in microgrids with hybrid energy systems – A review," *Renew. Sustain. Energy Rev.*, vol. 45, pp. 431–446, May 2015.

[6] S. Upadhyay and M. P. Sharma, "A review on configurations, control and sizing methodologies of hybrid energy systems," *Renew. Sustain. Energy Rev.*, vol. 38, pp. 47–63, Oct. 2014.

[7] D. Neves, C. A. Silva, and S. Connors, "Design and implementation of hybrid renewable energy systems on micro-communities: A review on case studies," *Renew. Sustain. Energy Rev.*, vol. 31, pp. 935–946, Mar. 2014.

[8] M. Geidl and G. Andersson, "Optimal Power Flow of Multiple Energy Carriers," *IEEE Trans. Power Syst.*, vol. 22, no. 1, pp. 145–155, Feb. 2007.

[9] R. Evins, K. Orehounig, V. Dorer, and J. Carmeliet, "New formulations of the 'energy hub' model to address operational constraints," *Energy*, vol. 73, pp. 387–398, Aug. 2014.

[10] K. Orehounig, R. Evins, and V. Dorer, "Integration of decentralized energy systems in neighbourhoods using the energy hub approach," *Appl. Energy*, vol. 154, pp. 277–289, Sep. 2015.

[11] F. Brahman, M. Honarmand, and S. Jadid, "Optimal electrical and thermal energy management of a residential energy hub, integrating demand response and energy storage system," *Energy Build.*, vol. 90, pp. 65–75, Mar. 2015.

[12] A. T. D. Perera, D. M. I. J. Wickremasinghe, D. V. S. Mahindarathna, R. A. Attalage, K. K. C. K. Perera, and E. M. Bartholameuz, "Sensitivity of internal combustion generator capacity in standalone hybrid energy systems," *Energy*, vol. 39, no. 1, pp. 403–411, Mar. 2012.

[13] A. T. D. Perera, R. A. Attalage, K. K. C. K. Perera, and V. P. C. Dassanayake, "A hybrid tool to combine multi-objective optimization and multi-criterion decision making in designing standalone hybrid energy systems," *Appl. Energy*, vol. 107, pp. 412–425, Jul. 2013.

[14] A. T. D. Perera, D. M. I. J. Wickremasinghe, D. V. S. Mahindarathna, R. A. Attalage, K. K. C. K. Perera, and E. M. Bartholameuz, "Determining wind turbine capacity for expansion of off grid Internal Combustion Generators (ICG) system; why it bec o mes challenging?," in *2010 IEEE International Conference on Sustainable Energy Technologies (ICSET)*, 2010, pp. 1–5.

A REVIEW ON REQUIREMENTS AND EXISTING QUALITATIVE TOOLS FOR DESIGNING SUSTAINABLE LARGE-SCALE HEALTHCARE FACILITIES: A CASE STUDY IN THE CONTEXT OF FLANDERS

Milena Stevanovic[1, 2], Karen Allacker[1], Stéphane Vermeulen[2]

[1] *Katholieke Universiteit Leuven, Faculty of Engineering Science, Department of Architecture, Kasteelpark Arenberg 1, 3001 Leuven, Belgium*

[2] *VK Studio, 210 Brugsesteenweg, 8800 Roeselare, Belgium. E-mail: milena.s@vkgroup.be, Tel:+32 (02) 414 07 77*

ABSTRACT

In the context of the increase in population and life expectancy of people, it is evident that the demand for healthcare facilities is growing. Not only the number of health-care buildings increases, but these facilities also enlarge in scale. Consequently, there is a trend to plan large-scale healthcare facilities on green-fields outside of the city boundaries, which requires large infrastructure works and induces a major impact on the surrounding environment. Moreover, the use of transport increases and so the CO_2 emissions proportionally grow. This research aims at developing a sustainability assessment method of large-scale healthcare buildings in Flanders. The research is based on a combination of a systematic scientific component at university, and an empirical approach gained in the industrial practice. This paper focuses on the first part of the study and provides an overview of current requirements for planning large-scale healthcare facilities in the context of the Flemish region and of available methods and tools for the sustainability assessment of healthcare facilities.

Keywords: healthcare facilities, early design phase, sustainability assessment, method development, environment

INTRODUCTION

With an increasing population worldwide, the large-scale healthcare facilities are becoming one of the most needed facilities for healing and well-being of people [Decker 2002]. Built for the community, they should be exemplary and fully integrated within their environment. Due to their constant operation 24 hours a day and seven days a week, high flow of people, intensive HVAC and lighting requirements, healthcare facilities are heavy users of energy and water. They also produce large amounts of waste. Furthermore, the healthcare sector accounts for more than 5% of the greenhouse gas emissions in Europe [Leetz, 2014]. The healthcare projects cover a range of characteristics of different common projects such as residential, offices and service buildings, and due to various complex project requirements, these buildings are not sufficiently designed and operated in a sustainable way [Castro et al, 2012]. Moreover, the quality of their planning and improvement depends largely on professionals' experiences in practice as well as guidelines provided by the local authorities. Most important decisions are made during the early design phase. These early design phase decisions are difficult to change afterwards and have a high impact on the life cycle environmental burdens and cost of the building. In order to reduce the life cycle impact and cost of healthcare facilities, designers and building practitioners hence need appropriate methods to support decision taking during the early design phase. Such methods are however not available to date and is the focus of this research. As a first research step current requirements and assessment methods have been analysed and are presented in this paper.

REQUIREMENTS AND SUSTAINABILITY INCENTIVES FOR HEALTHCARE FACILITIES IN THE FLEMISH REGION

Flemish Royal Decrees and specific standards for healthcare facilities

The notion *healthcare* in Belgium covers six types of healthcare facilities [Royal Decree of 10 July 2008 on law relating to the hospitals], each with a specific care, private infrastructure and operation as well as private financing. These types of facilities are listed as follows:

- hospitals
- psychiatric hospitals
- university hospitals
- nursing homes
- protected residential spaces and temporary residence homes
- small hospitals

As the focus of this study is on large-scale healthcare facilities, i.e. hospitals, psychiatric and university hospitals, we analysed the existing regulations for these facilities in the Flemish region. Each one of them is covered by a specific Royal Decree of the Flemish Government addressing the general, architectural and functional norms. Regarding the architectural norms for hospitals, a list of requirements has been provided by the Royal Decree laying down standards to which hospitals and their services must meet from October 1964. These requirements refer to:

- the general hygiene of the building standards (non-combustible materials, mitigation of humidity and prevention of infiltration, installations, lighting, ventilation, etc.);
- the hospitalisation standards (room size in m^2 per bed for sick people, location of the rooms within hospital, heating, lighting, etc.);
- the specific standards for each hospital department in terms of their surface and equipment necessity to function properly (specific rooms for medical treatment, operation rooms, m^2 per beds in single or multi-bed rooms, sanitary blocks, utility rooms, etc.).

By satisfying the described norms, the hospitals are approved by the government and are eligible to provide services to the patients. However, as these standards are almost five decades old, they do not provide any specific requirements regarding the sustainability of the hospital buildings. Most of the time, practitioners rely on the needs of a client, as well as their previous experiences when designing large-scale healthcare facilities.

Additionally to these norms, there are basic fire safety standards for new buildings [Royal Decree of 7 July 1994 on basic safety standards for the prevention of fire and explosion in new buildings, 1994] complemented with strict fire safety standards for healthcare facilities for: elderly services and centres for rehabilitation stay [Royal Decree of 9 December 2011 on the specific fire safety standards for older facilities and centres for rehabilitation residence, childcare facilities, 2011], childcare [Royal Decree of 22 November 2013 on the quality of family child care and group care for babies and toddlers, 2013], hospitals [Royal Decree of 6 November 1979 on protection against fire in hospitals, 1979] and nursing homes [Royal Decree of 15 March 1989 on fire safety in nursing homes, 1989]. For all other healthcare facilities there are no specific fire safety standards and it is usually necessary to involve specialists in the design process.

The VIPA sustainability requirements to obtain subsidies

Regarding the sustainability of the healthcare facilities, the Flemish Infrastructure Fund for Person-related Matters (VIPA) in collaboration with the Flemish Government published in 2009 a Ministerial Decree [Ministerial Decree determining the VIPA sustainability criteria, 2010] establishing a set of minimum requirements that projects need to fulfil to obtain VIPA

investment subsidies. These requirements rely on the principles and objectives included in the *Flemish Sustainable Development Strategy* [Flemish Government, department for sustainable development, 2006] and the *Flemish Climate Plan 2006-2012* [Heirman, J.P., 2006]. For each healthcare facility a specific requirement explanation is elaborated in the appendix of the Ministerial Decree as well as a checklist with five criteria as follows:

1. User comfort
2. Energy control
3. Sustainable material and renewable resource
4. Integrated approach
5. Building operation

5 building operation		Residential facilities	Offices and schools	Other specific facilities
5.1	basic quality monitoring	compulsory ☐	compulsory ☐	compulsory ☐
5.2	energy flows measuring			
5.2.1	counters	compulsory ☐	compulsory ☐	compulsory ☐
5.2.2	monitoring	compulsory ☐	compulsory ☐	compulsory ☐
5.3	training in management	free ☐	free ☐	free ☐
	minimum	3	3	3
	maximum	4	4	4
	score	☐	☐	☐

Table 1: Example of a building operation criteria checklist part for different facilities [Ministerial Decree determining the VIPA sustainability criteria, 2010]

Table 1 represents the building operation criteria and a list of compulsory and free sub-criteria for facilities with residential, office and educational or other specific character. However, with the new, recently published Flemish Climate plan and constant amendments of Royal Decrees regarding the healthcare facilities, the VIPA sustainability criteria have become out-dated.

SUSTAINABILITY ASSESSMENT METHODS FOR HEALTHCARE FACILITIES IN THE FLEMISH REGION

Many tools with various purposes, and dedicated to different users, have been developed in the most recent decades in order to assess the sustainability of buildings. These tools differ in scope as some focus on only one the three sustainability pillars while others combine two or three pillars. Some of these tools moreover assess building products, others building elements (e.g. outer walls, floors, roofs) or whole buildings [Haapio and Viitaniemi, 2008]. They furthermore differentiate in covering the spectrum of a building's emissions and/or energy usage and in a quantitative or qualitative approach.

Qualitative sustainability assessment methods

The VIPA started collaborating with the Department of Environment and Natural Energy (LNE), Royal Haskoning DHV and the Services for the General Government Policy (DAR) in order to develop a new certification system for healthcare facilities, adjusted for the context of the Flemish region. This tool, called Duurzaamheidsmeter (Sustainability meter) is largely based on the British BREEAM (Building Research Establishment Environmental Assessment Method) New Construction certification system; however it has been adapted for the Flemish region by relying on the VIPA sustainability criteria [Oosterbaan, 2014].

Building practitioners who had the opportunity of using it, and were involved in the development of this tool, claim that it is neither innovative, nor user-friendly and that the scoring system is subjective and thus leaves space for doubts for achieving real sustainable

buildings when using this tool (based on conversation with VK experts). The tool has moreover not yet been fully developed as the third (final) development phase has just begun. As it however is still the only qualitative sustainability assessment method available for the Flemish region, we present some of the most important available information in the subsequent paragraphs.

Similarly to the BREEAM New Construction, the VIPA Duurzaamheidsmeter is composed of three important parts: criteria, assessment indicators and credits. Figure 1 shows the criteria and their importance (in percentages) of both methods.

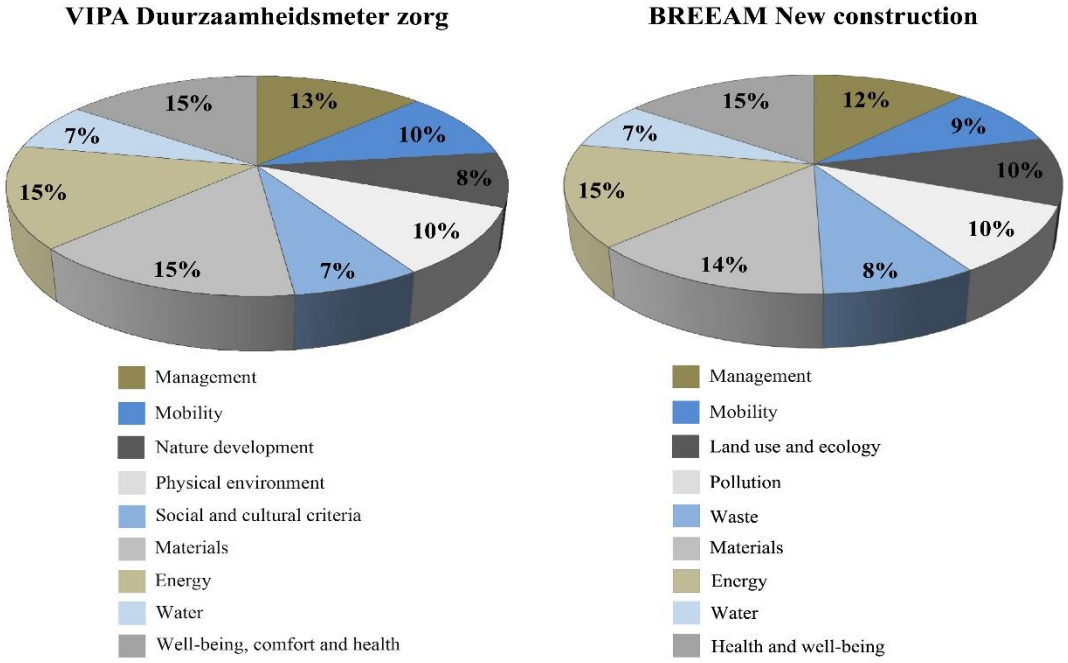

Figure 1: Criteria distribution in percentages for Duurzaamheidsmeter zorg and BREEAM New Construction sustainability assessment method [Oosterbaan, 2014]

Although the two tools are very similar, there are some difference between both. For instance, the VIPA Duurzaamheidsmeter zorg is specifically intended for healthcare facilities, covering buildings from nursery to home care and hospitals, whereas BREEAM New construction is used for all new non-domestic buildings. Another difference is the "pollution" criteria which exists as a separate one in BREEAM New construction, while it is included in *Physical environment* criteria of Duurzaamheidsmeter.

The main change introduced in the VIPA tool is that it includes the "social and cultural" criteria contrary to BREEAM. The indicators used for evaluation are as follows: (1) lively community; (2) inclusive community; (3) functional flexibility; (4) cultural value and (5) hospitality. Furthermore, the "management" criteria of Duurzaamheidsmeter has been complemented with the indicator *corporate social responsibility (CSR)* aiming at engaging institutions in Flanders to take a more active attitude towards sustainability.

The ranking in the VIPA Duurzaamheidsmeter is similar to the ranking in the BREEAM New Construction, with five qualitative sustainability performance levels provided by a star rating from 1 to 5 (Table 2).

	Performance levels				
	*	**	***	****	*****
Required relative score in order to achieve the performance level	≥ 30%	≥ 45%	≥ 55%	≥ 70%	≥ 85%

Table 2: Sustainability performance levels of VIPA Duurzaamheidsmeter [Oosterbaan, 2014]

DISCUSSIONS

This paper summarises the requirements for designing large-scale healthcare facilities (hospitals) complemented with the currently available methods and tools for healthcare sustainability assessment in the context of the Flemish region. Both VIPA Duurzaamheidsmeter zorg and BREEAM New construction belong to qualitative methods used to assess the sustainability in the construction sector. They present a list of criteria with indicators that can be used for either only healthcare facilities, or for all newly built non-domestic buildings. Although these qualitative methods have their strengths: they are easy to apply and are holistic, they also have important weaknesses. The two most fundamental ones are:

1) their subjectivity and hence the doubt that these lead to truly sustainable buildings and
2) their static character due to their approach of checking the application of a list of measures which does not allow to respond to the rapidly changing requirements and needs of healthcare buildings.

On the other hand, quantitative tools based on the life cycle thinking perspective, such as life cycle assessment (LCA), assess the environmental impact of a process or product, including a building, over its entire life cycle. This technique has become the recognized international approach to assess the comparative environmental merits of products or processes [Stephan, 2013]. The broad acceptance is amongst others reflected in the international standards ISO 14040 and ISO 14044 and in the European standards EN15804 [CEN 2012] and EN15978 [CEN 2011], focusing respectively on construction products and buildings. Besides the environmental impact, costs are an important issue in the sustainability context. This for two main reasons. Firstly, when measures are unaffordable, these will not be taken, even if these are beneficial for the environment. Secondly, considering the cost of environmentally beneficial measures, will allow to prioritize the most efficient measures within a limited budget. In terms of sustainability, it is important to, not only consider investment costs, but also life cycle costs as also affordability in future is important. The life cycle costing (LCC) approach is a well-known approach to estimate the life cycle costs of a building. It is therefore considered that the quantitative methods might hence be more appropriate to evaluate the sustainability of healthcare buildings and will be further investigated during this research.

CONCLUSIONS

There is clearly a lack of specific architectural and urban regulations for large-scale healthcare buildings in Flanders. Furthermore, with the constantly evolving sustainability concept and development of new Flemish climate plans, the current regulations in this regard are already outdated. On top of that, there is no comprehensive method to assess the sustainability of the projects supporting building practitioners.

As most important design decisions are taken in the early design phase, it is important to develop a reliable sustainability assessment method from a life cycle thinking perspective which allows practitioners to achieve the desired sustainability level. This method should moreover include the assessment of the integration of the building in its surroundings as the scale of healthcare facilities is increasing. In addition, such method could serve as a guide

towards establishing clear and comprehensive healthcare facilities regulations and to update the existing ones.

REFERENCES

1. Decker, S., *Disparities in Access to Health Care for Older Americans Before and After Medicare*, International Longevity Centre, USA 2002
2. Leetz,A. *Europe letter to President Barroso on 2030 climate and energy policy framework*, Brussels, Belgium 2014
3. Castro, M.F., Mateus, R., Bragança, L., *The importance of the hospital buildings to the sustainability of the built environment*, in T. Amoêda, R. Mateus, L. Bragança & C. Pinheiro (Eds.), *Proceedings of the BSA 2012 – 1st International Conference on building sustainability assessment*, Porto, Vol. 1, pp. 857-865
4. Flemish Government, *Royal Decree on the coordination of the law relating to hospitals and other care facilities*, Belgium 2008
5. Flemish Government, *Royal Decree laying down basic safety standards for the prevention of fire and explosion which new buildings must comply*, Belgium 1994
6. Flemish Government, *Royal Decree of the Flemish Government establishing the specific fire safety standards which older facilities and centres for rehabilitation residence must meet and determining the procedure for the award of the certificate of compliance with those standards*, Belgium 2011
7. Flemish Government, *Royal Decree of the Flemish Government establishing the license conditions and the quality of family child care and group care for babies and toddlers*, Belgium 2013
8. Flemish Government, *Royal Decree of the Flemish Government establishing the standards for protection against fire and panic which hospitals must meet*, Belgium 1979
9. Flemish Government, *Royal Decree of the Flemish Government, the specific safety which the nursing homes must satisfy to be recognized*, Belgium 1989
10. Flemish Government, *Ministerial Decree determining the VIPA sustainability criteria*, Belgium 2010
11. Flemish Government, Department for Sustainable Development, Belgium 2006
12. Heirman, J.P., *The climate is changing. Are you too? Flemish Climate Plan 2006 – 2012*, Flemish Government - Department of Environment, Nature and Energy, Belgium 2006
13. Haapio, A., Viitaniemi, P., *A critical review of building environmental assessment tools,* Environmental Impact Assessment Review 2008: 28 469–482
14. Oosterbaan, M., *Eindrapportage Duurzaamheidsmeter Zorg, Vlaanderen*, Royal Haskoning DHV Belgium in cooperation with VK Group, Belgium 2014
15. Stephan, A. Towards a comprehencive energy assessment of residential buildings, 2013, Presses Universitaires de Bruxelles: Brussels
16. EN 15804:2011 Sustainability of construction works — Environmental product declarations — Core rules for the product category of construction products, 2011
17. EN 15978:2011 Sustainability of construction works — Assessment of environmental performance of buildings — Calculation method, 2011

DYNAMIC ANALYSIS OF THE LOW-TEMPERATURE DISTRICT NETWORK "SUUSRTOFFI" THROUGH MONITORING

N. Vetterli[1]; M. Sulzer[2].

1, 2: Zentrum für Integrale Gebäudetechnik (ZIG), Technikumstrasse 21 CH-6048 Horw.

ABSTRACT

The Lucerne University of Applied Sciences has been analysing and monitoring the low-temperature district heating and cooling network (LTN) "Suurstoffi" since 2012. The analysis showed that heating demand was twice as high as expected. On the other hand, waste heat from free cooling was much lower than expected. The higher heating demand and the lower heat recovery combined resulted in a negative energy balance and hence in an average temperature decrease of the ground storage over the last two years. First of all, a pellet oven was installed as an interim solution in order to supply additional heat to the LTN. Secondly, direct electric heating was used to support the domestic hot water production in order to reduce the energy demand out of the LTN. These temporary measures were only set up until the first part of the planned hybrid solar panels (PVT) were taken into operation in summer 2014. The upcoming data of the monitored summer 2015 will help taking the decision if the temporary measures have to be extended and if additional PVT panels need to be installed.

So far, the measured electricity demand to operate the LTN and the connected heat pumps was more than twice as high as expected. This is mainly due to the high electricity demand for temporary electrical heating for domestic hot water, circulation pumps and heat pumps. Thanks to the monitoring, hydraulic shortcoming, which caused the high electrical consumption of the circulation pumps, could be identified. The heat pumps consumed more electricity than planned due to the excess space heating demand and domestic hot water of the consumers. If, in addition to the electricity demand for the heat pumps, the electricity demand of the circulation pumps is taken into account, the overall network efficiency (yearly COP measured = 4.6) is lower than expected (yearly COP planned = 6.8).

As a result of the monitoring analysis over the last two years, the following outputs and outcomes could be provided:

- The real efficiency of the thermal network has been calculated and benchmarked
- Design mistakes have been identified and guidelines for planning have been developed
- The energy efficiency has been improved by optimizing the system operation
- The accuracy of the monitoring has been improved
- The influence of the user on the energy efficiency has been quantified.

Keywords: Monitoring, low-temperature, district heating and cooling network.

INTRODUCTION

The low temperature district heating and cooling network (LTN) 'Suurstoffi' in Risch/Rotkreuz close to Zug has been in operation since 2012. The LTN connects residential buildings, offices and industrial buildings (= consumers and producers) to a borehole heat exchanger (215 pieces à 150 m depth), which acts as a geothermal storage. In its final state, the whole district will include approximately 165'000 m² energy reference area and the geothermal storage will have more than 700 boreholes down to 250 m depth. Heating and domestic hot water are produced by means of decentralised heat pumps, which are connected to the LTN. Waste heat deriving from cooling installations in the buildings is used to regenerate the geothermal storages. Conventional (PV) and hybrid solar panels (PVT)

installed on the roofs of the buildings shall cover the entire electricity demand for the buildings operation (heat pumps, circulating pumps, HVAC, public lighting, transport, building automation, etc.). In addition, the PVT panels shall supply additional heat to load the ground storage. This concept will reduce the non-renewable primary energy consumption and minimise the greenhouse gas emission during the operation.

Figure 1: Overview of the district "Suurstoffi", the red zone includes the building fields 2 (19'500 m², in operation since 2012) and 5 (27'000 m², in operation since 2013). Source: www.suurstoffi.ch

METHOD

In order to verify the objectives, the LTN "Suurstoffi" is being monitored for at least five years. Every heat and power flux as well as temperature change are measured in a 15 minute interval resulting in a total of about 400 data points over the building fields 2 and 5. The Lucerne University of Applied Sciences has been analysing the measured data since 2012.

The results have been regularly compared with the original calculations used for the network design. Some additional simulations have been executed in order to verify the gaps between the calculation results and the measurements. A comprehensive simulation model of the whole area is being developed to predict the energy balances in its final state. The measurements were used as a basis for the simulation models and hence improve the accuracy of the model. The simulation of different scenarios allowed to test the suitability of the concept and to generate suggestions for desirable improvements.

RESULTS

Figure 2 shows the comparison between the calculations for the first year of operation and the measurements for the period from October 1st, 2013 until September 30th, 2014 of the building fields 2 and 5.

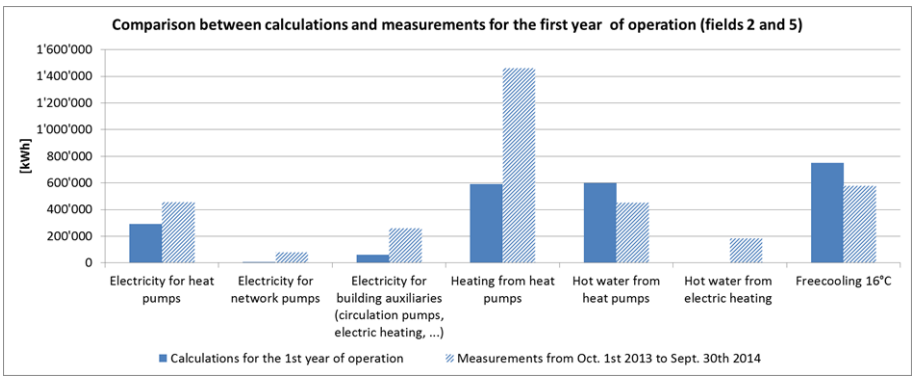

Figure 2: Comparison between calculations for the first year of operation and measurements for the period from October 1st 2013 until September 30th 2014 in the building fields 2 und 5.

The highest deviation was identified by the heat consumption. The results of the monitoring show a much higher heating demand than expected (590 MWh/a calculated and 1'460 MWh/a measured). The two main reasons for such a large gap between measurement and calculation are the overheating of rooms and the ineffective ventilation. The indoor air temperature measured during winter 2013 exceeded 22°C (design temperature: 20°C according to SIA) in more than 60% of the apartments in the building field 2. Furthermore, a majority of the rooms were ventilated by constantly opened windows, despite the mechanic ventilation system.

By means of dynamical simulations using the program IDA ICE it was proven that the higher indoor temperatures and the additional heat losses through natural and mechanical ventilation are the main reasons for the higher heat demand (see Figure 3).

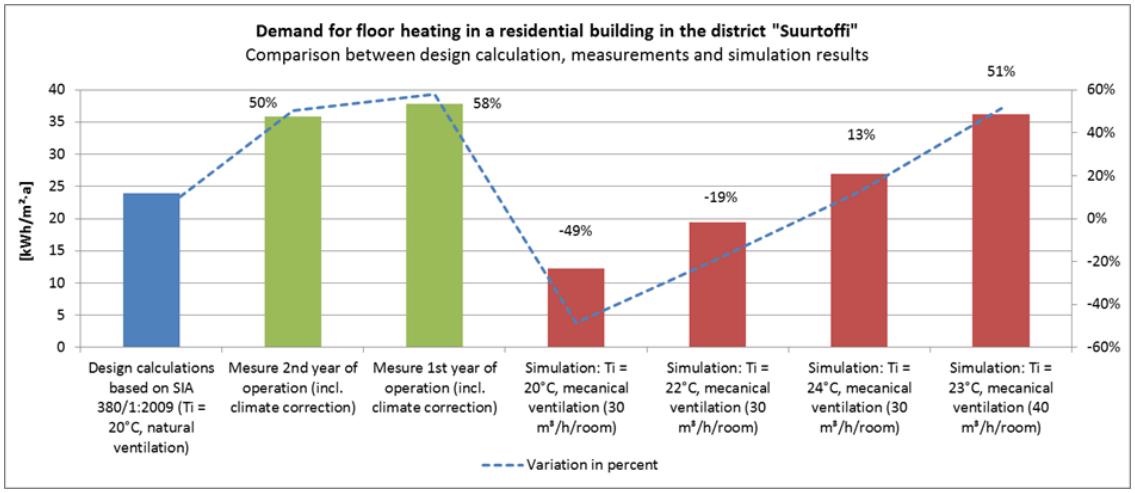

Figure 3: Comparison between design calculation, measurements and simulation results for the heat demand for floor heating in a residential building. [1]

Considering an indoor air temperature of 23°C and a mechanical ventilation with an increased air flow rate of 40 m³/h in each room (instead of 30 m³/h as planned), the simulated heating demand reached approximately the measured value.

The total electricity demand for the LTN (including the heat pumps, network pumps and building auxiliaries) was much higher than expected (360 MWh/a calculated and 800 MWh/a measured). The photovoltaic panels produced 346 MWh/a of electric power and could cover 43% of the total electricity demand for the network operation.

The total heat demand for space heating and domestic hot water was about 75% higher than expected (1.2 GWh/a calculated and 2.1 GWh/a measured). The total amount of heat extracted from the borehole heat exchangers to supply the heat pumps reached 1'600 MWh/a. Contrary to expectation, waste heat from the free cooling system was much lower than estimated (750 MWh/a expected and 580 MWh/a measured). One possible reason for the lower cooling demand is that the occupants were not well informed about the possibility of cooling their apartments.

The higher heating demand and the lower waste heat use both result in an overall decrease of the ground storage temperature. Figure 4 shows the network heat balance over the last two years (from January 2013 until December 2014). During summer season, the curve increases as a result of heat supply from free cooling, whereas in the winter, the curve decreases, due to the delivery of the heat pumps.

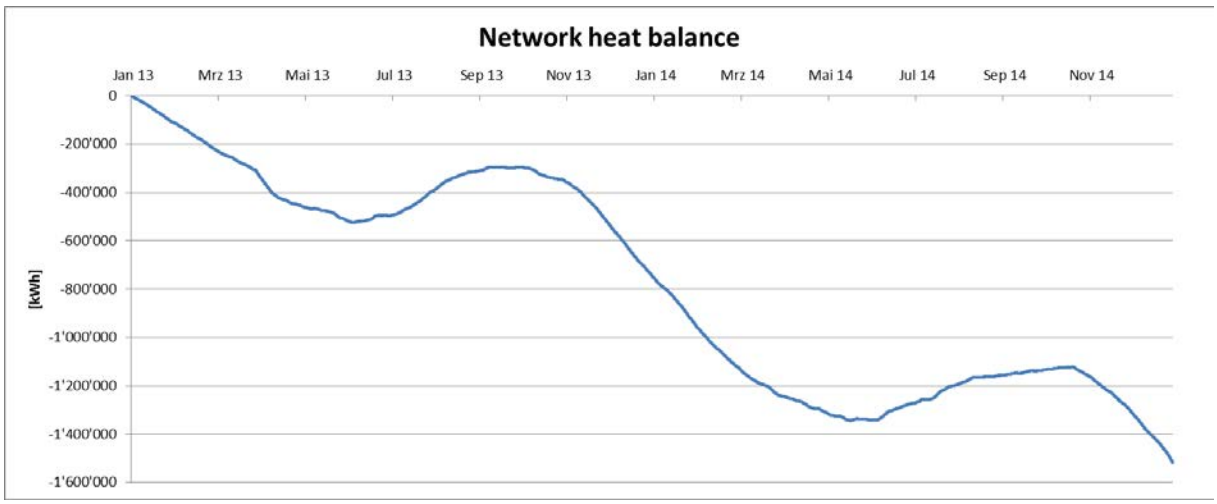

Figure 4: Network heat balance over the last two years (January 2013 – December 2014). Difference between heat demand of the heat pumps and heat supply of the free cooling in the building fields 2 and 5.

As an interim solution, a pellet oven was installed in order to supply additional heat to the LTN (640 MWh/a) until the hybrid solar panels were operational in summer 2014. Additionally, direct electric heating (184 MWh/a) was used to support the domestic hot water production in order to reduce additional heat withdrawal from the LTN. Despite the pellet oven, the annual heat deficit reached 380 MWh/a. The deficit results in a temperature decrease of the geothermal storage of about 0.6 K. The cooling tendency of the ground storage was verified through punctual measurements in one borehole heat exchanger a few meters under the ground. Figure 5 shows the measured water temperature in a borehole heat exchanger from May 2013 until December 2014. The comparison between the water temperature in May 2013 (11±0.3°C) and May 2014 (11±0.8°C) showed that the borehole heat exchanger field had almost recovered during that year. The network temperature will be locally higher because of the influence of the pellet oven. Considering the thermal inertia of the geothermal storage, the calculated temperature decrease should be observed in the upcoming months.

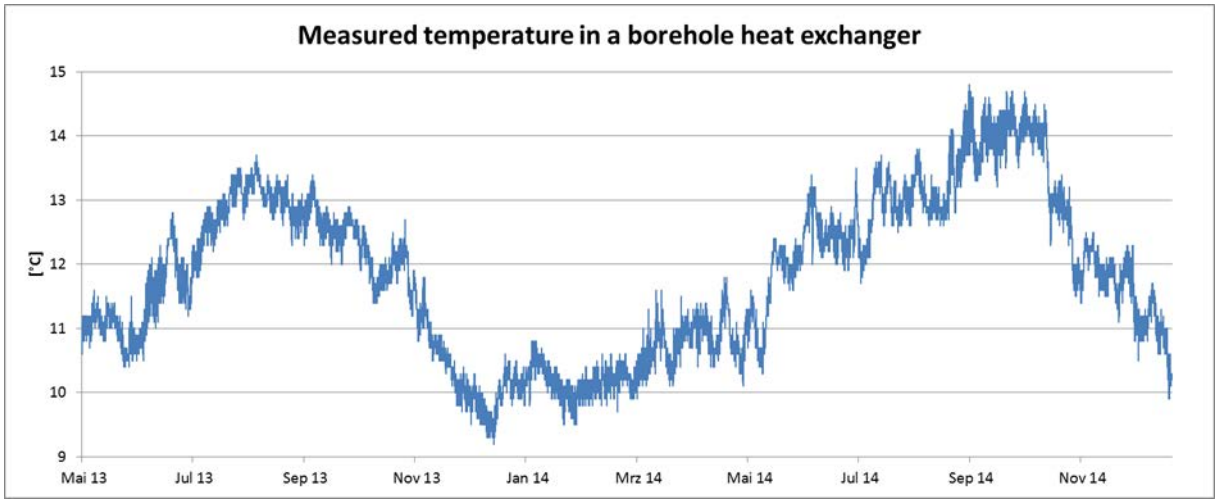

Figure 5: Measured water temperature in a borehole heat exchanger from May 2013 until December 2014.

Despite the heat deficit, the annual performance factor of the heat pumps was higher than expected (see Table 1). The main reason for the increase of the heat pumps efficiency was the partial production of the domestic hot water with the electric heating.

	Design calculations fields 2 and 5 (1st year of operation)			Measurements fields 2 and 5 (Oct. 1st 2013 - Sept. 30th 2014)		
Annual coefficient of performance heat pumps ($COP_{Heat\ pump}$)	Heating and hot water 4.1			Heating and hot water 4.2		
Annual coefficient of performance network ($COP_{Network}$)	Heating and hot water 4.1	Cooling 119.9	Heating + Cooling 6.8	Heating and hot water 3.8	Cooling 20.9	Heating + Cooling 4.3
Efficiency (Ɛ)						5.5

Table 1: Comparison between the calculated and the measured coefficients of performance and efficiency for the building fields 2 and 5.

The measured overall efficiency (yearly coefficient of performance) of the network reached 4.3 against 6.8 expected. The electricity demand for the district network pumps is included in this factor and shows the comprehensive efficiency of the LTN. The measured electricity consumption (81 MWh/a) of the network pumps was about eleven times higher than the calculated one (7 MWh/a). In such a case, a hydraulic analysis was recommended in order to identify problems as well as the possibilities of optimisation.

Figure 6 shows the difference between the measured energy consumption during the first and second years of operation in the building field 2. Despite the optimisation measures made during the second year of operation, the electricity consumption of the buildings auxiliaries had conspicuously increased. This is principally due to the use of electric heaters for the domestic hot water production. As a result, the heat pumps used less electricity during the second year of operation.

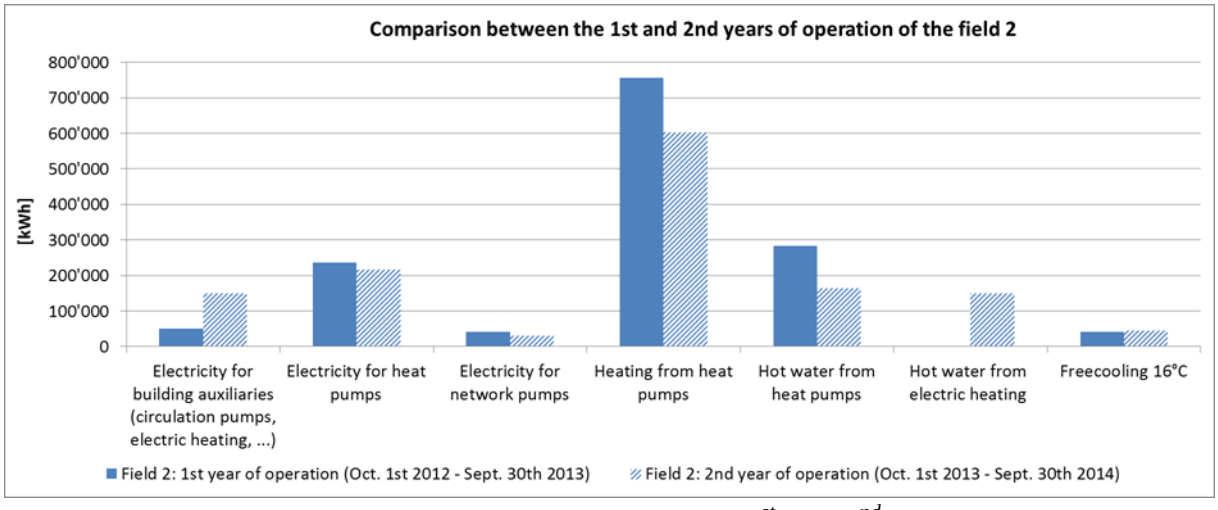

Figure 6: Comparison of the energy demand during the 1st and 2nd years of operation of the building field 2.

The overall heating consumption was reduced during the second year of operation. A major reason of the higher energy efficiency is due to warmer climate conditions as well as natural drying out of the building.

DISCUSSION

The importance of monitoring has been demonstrated once more in the project “Suurstoffi”.

- The measured values could be compared with the original planned values in order to the optimise processes and take early decisions in the planning sequence.
- Premature errors could be discovered and measures against them could be undertaken.
- The monitoring of the project constitutes an important data base and benchmark for future projects in the field of thermal networking.
- A simulation model of thermal networking could be calibrated with real data.

The monitoring of the project “Suurstoffi” is related to a significant amount of monitoring data points and some errors in measurements. Systematic data checks have to be performed in order to identify any inconsistency in the data logging and consequently to improve the monitoring accuracy. The data handling and verification is a crucial task in order to provide a solid database for formulating sound conclusions.

The monitoring analysis has been used for several studies since the area operation started. The measured data served as a basis for a multitude of simulations and benchmarks. For example, the future energy demand for the buildings in Suurstoffi East was estimated via measurements extrapolations and hence increased the accuracy of the SIA calculation due to consideration of the real user behaviour. Furthermore, simulations allowed quantifying the user influence on the energy efficiency (indoor air temperature, ventilation) and predicting the future energy demand.

By means of the monitoring and its analysis, the effective performance of the heat pumps and the low-temperature network has been calculated. Comparisons have been made with similar networks in order to identify optimisation potentials and design mistakes. The identified hydraulic problems by benchmarking the electricity consumption of the network pumps shows such a potential. Monitoring is an effective instrument commissioning an operation optimisation.

The analysis of changes in temperature in the borehole heat exchangers allows the ground storage to be supervised. In case of possible undercooling, appropriate actions can be implemented on time and hence prohibit damages on the technical equipment. By means of this detailed monitoring, the network undercooling in winter 2013 was avoided thanks to the operation of both the pellet oven and the electric heating for domestic hot water.

The major finding is the understanding of the dynamic performance of the LTN connected to various geothermal storages. This allows the development of a model predictive control system and hence an increase of the operational robustness of such systems. The complexity of LTN is high, but such concepts must not be susceptible. The key is to exploit synergies among the different elements by executing a comprehensive design process and implement predictive automation based on detailed monitoring data.

ACKNOWLEDGEMENTS

This work has been accomplished in the Efficient Buildings & Districts SCCER FEEB&D, funded by The Commission for Technology and Innovation of the Swiss Confederation.

REFERENCES

[1] Norm SIA 380/1, Thermische Energie im Hochbau, SIA Schweizerischer Ingenieuren und Architektenverband, 2009.
[2] Brücker S.; Vetterli N.; Sulzer M., Menti UP.: Monitoring Suurstoffi-Areal Risch/Rotkreuz - Dynamik und Optimierung eines Anergienetzes, Status-Seminar «Forschen für den Bau im Kontext von Energie und Umwelt», September 2014
[3] Kräuchi P., Kolb M., Gautschi T., Menti UP., Sulzer M.: Simulation thermischer Arealvernetzung mit IDA-ICE. Status-Seminar, Sept. 2014
[4] Gautschi T., Sulzer M.: ETH Zürich, Hönggerberg Masterplan Energie, Schweizerisches Status-Seminar Energie- und Umweltforschung im Bauwesen, September 2008

AUTHOR INDEX

Author Index

E

F

G

H

I

J

P

Q

R

S

T

ACKNOWLEDGEMENTS

CISBAT can only exist thanks to the patronage of the Swiss Federal Office of Energy and other donors. We are very grateful for their continuing support.

We also thank the Swiss Competence Center for Energy Research “Future Buildings and District”, supported by the Swiss Federal Commission for Technology and Innovation, for their partnership and funding of the Outreach Event.

Our scientific partners from Cambridge University, the Massachusetts Institute of Technology and the Swiss Chapter of the International Building Simulation Association as well as the members of the CISBAT scientific committee and the session chairs have enthusiastically supported the conference and ensured its quality. We would like to express our sincere thanks for the time and effort they have spent to make it a success.

Behind the scenes, we have received much competent support from the EPFL administration as well as from our caterers and diverse suppliers. We herewith express our sincere thanks for their efficient and friendly collaboration.

The active and uncomplicated help of all staff members of the Solar Energy and Building Physics Laboratory was much appreciated. Special thanks go to our technical and IT staff whose professionalism and excellent organisation was essential at every stage of preparation and during the conference.

Finally, we cordially thank all speakers, authors and participants who have brought CISBAT 2015 to life.

Prof. Dr J.-L. Scartezzini
Chairman of CISBAT 2015
Head of Solar Energy and Building Physics Laboratory (LESO-PB), Swiss Federal Institute of Technology Lausanne (EPFL)

Barbara Smith
CISBAT Conference Manager